UNIVERSITY OF QUEBEC AT CHICOUTIMI

DISSERTATION PRESENTED TO THE

UNIVERSITY OF QUEBEC AT CHICOUTIMI

IN PARTIAL FULFILLMENT OF THE REQUIREMENT FOR THE

DEGREE OF DOCTOR OF PHILOSOPHY IN ENGINEERING

BY

SHAHROOZ NAFISI

EFFECTS OF GRAIN REFINING AND MODIFICATION ON THE MICROSTRUCTURAL EVOLUTION OF SEMI-SOLID 356 ALLOY

APRIL 2006

Bibliothèque Paul-Émile-Boulet

UQAC Université du Québec à Chicoutimi

Mise en garde/Advice

Afin de rendre accessible au plus grand nombre le résultat des travaux de recherche menés par ses étudiants gradués et dans l'esprit des règles qui régissent le dépôt et la diffusion des mémoires et thèses produits dans cette Institution, **l'Université du Québec à Chicoutimi (UQAC)** est fière de rendre accessible une version complète et gratuite de cette œuvre.

Motivated by a desire to make the results of its graduate students' research accessible to all, and in accordance with the rules governing the acceptation and diffusion of dissertations and theses in this Institution, the **Université du Québec à Chicoutimi (UQAC)** is proud to make a complete version of this work available at no cost to the reader.

L'auteur conserve néanmoins la propriété du droit d'auteur qui protège ce mémoire ou cette thèse. Ni le mémoire ou la thèse ni des extraits substantiels de ceux-ci ne peuvent être imprimés ou autrement reproduits sans son autorisation.

The author retains ownership of the copyright of this dissertation or thesis. Neither the dissertation or thesis, nor substantial extracts from it, may be printed or otherwise reproduced without the author's permission.

UNIVERSITÉ DU QUÉBEC À CHICOUTIMI

THÉSE PRÉSENTÉ À

L'UNIVERSITÉ DU QUÉBEC À CHICOUTIMI

COMME EXIGENCE PARTIELLE

DU DOCTORAT EN INGÉNIERIE

PAR

SHAHROOZ NAFISI

EFFETS DE L'AFFINAGE DES GRAINS ET DE LA MODIFICATION SUR L'ÉVOLUTION MICROSTRUCTURALE DE L'ALLIAGE 356 SEMI-SOLIDE

AVRIL 2006

Dedicated to

My wife BITA who tolerated all the troubles

ABSTRACT

Semi-solid metal (SSM) processing is gaining momentum as an effective alternative to the classical manufacturing processes of casting and forging. This category takes advantages of both liquid and solid forming processes. In the absence of shear force, semi-solid slug is similar to a solid, self standing, while with the application of shear force, the viscosity is reduced appreciably and the material flows like a liquid; Thixotropic-"*dual characteristics where the SSM billet has solid-like characteristics, but flows like a liquid under shear stress*".

For SSM processing of Al-Si alloys, there are two important microstructural features which influence the properties of finished products. These are the size and morphology of the primary α-Al phase and the eutectic mixture which mainly consists of silicon.

The aim of the current study was to investigate the effects of inoculation and modification, individually and combined, on the microstructural evolution of Al-7%Si group of alloys with special emphasis on the 356 alloys in two different processes, i.e. conventional and rheocasting using the ALCAN patented process, Swirled Enthalpy Equilibration Device, SEED technology.

One binary and two commercial Al7%Si alloys have been used for the entire research plan. After melt preparation, different master alloys, depending on the objective, were added to the melt and the prepared alloy was poured and examined in two different setups to correlate a relation and highlight the differences between the conventional and SSM processes. Several techniques were used in order to characterize the obtained material. These techniques include thermal analysis, optical microscopy, quantitative metallography using image analysis technique, scanning electron microscopy, electron probe microanalysis, x-ray mapping, and rheological tests with a parallel plates compression machine.

Based on the SSM processing as a focal point, it is proposed that partitioning of the solidification range is also essential. Therefore the solidification range could be divided into two main intervals; the temperature range for the formation and growth of α-Al dendrites ($\Delta T\alpha$) and/or iron intermetallics and the temperature range for the main Al-Si eutectic and secondary-eutectic reactions including the formation of Mg_2Si and/or iron compounds. The main emphasis in this context is the α-Al solidification range since it has the paramount importance in the science of SSM processing.

The grain refiner results have shown that generally refiner increases the α-Al percentage due to the shifting of the cooling curve up and consequently a wider α-Al solidification range would be obtained. From SSM standpoint, a larger α-Al mushy zone

provides more flexibility for slurry production and control however side issues such as the risk of hot tearing, porosity formation, and segregation should be considered. Quantitative metallography on the samples prepared from billets reveals that by refining, the α-Al percentage increases and due to the higher number of efficient nuclei per unit area the globule size decreases. Improvement of sphericity and size reduction of globules are the main advantages of refiner addition. Limited rheological tests proved that smaller and rounder particles give better slurry flowability.

It has been shown that small addition of Sr in the range of 150-200ppm is quite adequate to change the silicon morphology from flakes to fibrous in both processes. By modification, α-Al solidification range increases due to the lowering of the main eutectic reaction temperature and interestingly by considering a constant total solidification range, eutectic solidification range decreases. In contrast to the SEED refined samples, by modification, the average globule diameter increases however the higher sphericity percentage is one of the main advantages of the Sr addition. It has been proposed that lowering the surface tension by Sr is the main reason for higher globularity. By decreasing the surface tension, wetability of α-Al particles by the remaining liquid is improved and this could be intensified by more flow around the α-Al particles and consequently better shaving causes rounder particles.

Combined treatment shows that α-Al solidification range increases more than sole treatments. This is due to the shifting of liquidus to the higher values from refiner side plus the added additional benefit of lowering the main eutectic reaction temperature due to the modification. In the SEED billets, grain refining efficiency is obvious through size reduction of globules and more primary particles, while modification effect could be detected in higher magnification by morphological changing of silicon particles from lamellar to fibrous. Besides, SSM microstructural investigations show that refiner efficacy always overshadows the modification outcome by increasing the number density of primary particles and lowering the average circular diameter.

Limited rheological tests by a parallel plate compression machine with a constant dead weight have shown that the highest and lowest rates of strain belong to refined and un-treated billets respectively. By refining, it is proved that billet has lesser particle size and more globularity and consequently deforms better while Sr lowers the surface tension of the liquid and as a result shows better deformability. Combined treatment has the added bonus of smaller particle size, more globularity, and lesser surface tension.

A new innovative concept is introduced for fluidity measurement by using the quantity of remaining liquid obtained from drainage step. It was deduced that by refiner and/or modifier, the percentage of the drainage increased. This is attributed to dendrite coherency point, DCP, where both stirring and refiner/or modifier postpone DCP and also the formation of smoother and greater number of channels within the semi-solid structure due to melt treatment.

RÉSUMÉ

Le traitement à l'état semi-solide des métaux (SSM) gagne du terrain en tant qu'alternative efficace aux procédés traditionnels de fabrication que sont la coulée et le forgeage. Ce développement tire profit des procédés de mise en forme liquide et solide. En l'absence d'effort de cisaillement, la masse semi-solide est semblable à un solide, autoporteur, alors qu'avec l'application d'effort de cisaillement, la viscosité est sensiblement réduite et le matériau coule comme un liquide; thixotrope- « caractéristique double où la billette possède des caractéristiques du solide, mais coule comme un liquide sous l'effort de cisaillement ».

Pour ce qui est du traitement SSM des alliages Al-Si, il existe deux caractéristiques des microstructures qui influencent les propriétés du produit fini, soit la taille et la morphologie de la phase α-Al primaire et le mélange eutectique, qui est constitué principalement de silicium.

L'objectif de la présente étude était d'étudier les effets de l'inoculation et de la modification, individuellement ou en combinaison, sur l'évolution des microstructures du groupe d'alliages Al-7%Si en portant une attention particulière aux alliages 356 pour deux procédés différents, soit le conventionnel et le « rhéomoulage » suivant le procédure brevetée de l'Alcan, la *Swirled Enthalpy Equilibration Device*, soit la technologie SEED.

Un alliage binaire et deux alliages commerciaux Al7%Si ont été utilisés tout au long du plan de recherche. Après la préparation du métal liquide, différents alliages mère, selon l'objectif, ont été ajoutés au liquide et l'alliage ainsi préparé a été versé et examiné à l'aide de deux montages différents afin d'obtenir une corrélation et d'identifier les différences entre les procédés conventionnel et SSM. Plusieurs techniques ont été utilisées afin de caractériser le matériau obtenu. Ces techniques incluent l'analyse thermique, la microscopie optique, la métallographie quantitative à l'aide de la technique d'analyse d'images, la microscopie électronique à balayage, l'analyse par microsonde, la cartographie par rayons X et les tests rhéologiques à l'aide d'un appareil de compression à plaques parallèles.

En se basant sur le traitement SSM, on propose qu'il soit également essentiel de procéder à un partitionnement de l'intervalle de solidification. Ainsi, l'intervalle de solidification pourrait être divisé en deux intervalles principaux, soit l'intervalle de températures pour la formation et la croissance des dendrites α-Al ($\Delta T\alpha$) et / ou des composés intermétalliques du fer, et l'intervalle de températures pour l'eutectique principal Al-Si et les réactions eutectiques secondaires, incluant la formation de Mg_2Si et / ou de composés de fer. Dans ce contexte-ci, l'accent est placé principalement sur

l'intervalle de solidification α-Al puisqu'il est d'importance capitale pour la science du traitement SSM.

Les résultats d'agents d'affinage du grain ont démontré que, généralement, les agents d'affinage augmentent le pourcentage α-Al en raison du décalage de la courbe de refroidissement vers le haut et, par conséquent, on pourrait obtenir un plus grand intervalle de solidification α-Al. Du point de vue SSM, une plus grande zone pâteuse α-Al donne une plus grande flexibilité pour la production de la pâte semi solide et son contrôle. Toutefois des questions secondaires comme les risques de déchirement à chaud, de formation de porosités et de ségrégation pourraient être considérées. La métallographie quantitative effectuée sur les échantillons préparés à partir de billettes démontre que l'affinage conduit à une augmentation du pourcentage α-Al et, en raison du plus grand nombre de sites de germination efficaces par surface unitaire, la taille des globules diminue. L'amélioration de la sphéricité et la diminution de la taille des globules sont les avantages principaux procurés par l'ajout d'agents d'affinage. Quelques tests rhéologiques ont prouvé que des particules plus petites et plus rondes mènent à une meilleure coulabilité de la pâte semi solide.

Il a été démontré que l'ajout d'un peu de Sr, entre 150-200 ppm, suffit pour changer la morphologie du silicium de floconnée à fibreuse dans les deux procédés. Par modification, l'intervalle de solidification α-Al augmente en raison de la diminution de la température de la réaction eutectique principale et, ce qui est intéressant, en considérant un intervalle de solidification constant, l'intervalle de solidification eutectique diminue. Par contraste avec les échantillons raffinés SEED, par modification, le diamètre moyen des globules augmente, mais le pourcentage plus élevé de sphéricité est l'un des avantages principaux de l'ajout de Sr. Il a été suggéré qu'une diminution de la tension superficielle à l'aide de Sr est la raison principale pour une globularité plus élevée. En diminuant la tension superficielle, la mouillabilité des particules par le liquide restant est améliorée, et ceci pourrait être intensifié par un écoulement plus important autour des particules α-Al, et par conséquent un meilleur façonnage conduit à des particules plus rondes.

L'augmentation de l'intervalle de solidification α-Al est plus importante avec le traitement combiné qu'avec les traitements uniques. Ceci est dû au décalage du liquidus vers des valeurs plus élevées du côté des agents d'affinage, en plus de l'avantage additionnel qu'est la diminution de la température de réaction eutectique due à la modification. Dans les billettes SEED, l'efficacité d'affinage des grains est évidente si l'on considère la diminution de la taille des globules et la formation accrue de particules primaires, alors que l'effet de la modification pourrait être détecté sous magnification plus élevée par le changement morphologique des particules de silicium de floconnées à fibreuses. D'ailleurs, des études microstructurales de SSM montrent que l'efficacité des agents d'affinage domine toujours le résultat de modification en augmentant la densité numérique des particules primaires et en diminuant leur diamètre circulaire moyen.

Des tests rhéologiques à l'aide d'un appareil de compression à plaques parallèles avec un poids mort constant ont montré que les vitesses de déformation les plus élevées et les plus basses appartenaient aux billettes affinées et aux billettes non traitées, respectivement. Il est prouvé que par l'affinage on obtient des billettes ayant de plus petites particules et une globularité plus importante et qui sont, par conséquent, mieux déformables, alors que le Sr diminue la tension superficielle du liquide et ainsi donne une meilleure déformabilité. Le traitement combiné donne les avantages supplémentaires de particules de plus petites dimensions, plus de globularité et une moindre tension de surface.

Un nouveau concept innovateur est présenté pour les mesures de fluidité en utilisant la quantité de liquide obtenue par drainage. Il a été déduit que des agents d'affinage et / ou des agents modifiants peuvent augmenter le pourcentage d'écoulement. Ceci est attribué au point de cohésion des dendrites, PCD, où les agents d'affinage et / ou les agents modifiants retardent le PCD et aussi la formation de canaux plus lisses et plus nombreux à l'intérieur de la structure semi-solide en raison du métal liquide.

Acknowledgments

This work was carried out with financial support of Natural Sciences and Engineering Research Council of Canada – NSERC, ALCAN International limited and Centre Québécois de Recherche et de Développement de l'Aluminium, CQRDA, through the NSERC-ALCAN-UQAC industrial research chair, Professors Reza Ghomashchi and Andre Charette, on the "Solidification and Metallurgy of Al-Alloys", grant No.IRCPJ268528-01.

I would like to take this opportunity to express my most sincere gratitude to my supervisors, Professor Reza Ghomashchi for his continued support, many technical discussions and suggestions and of course reading and editing my thesis and Professor Andre Charette, for his encouragement, support, and advice throughout this work.

I am also grateful to Mr. Joseph Langlais from ALCAN Arvida Research and Development Center, for his close collaboration, ideas, and permission for publications. Special thanks are also due to Dr. B. Kulunk and Mr. A. Lemieux from Societe des Technologies de l`Aluminium du Saguenay Inc., STAS, for industrial support, Dr.D.Emadi from CANMET-Materials Technology Laboratory for his helpful suggestions on thermal analysis technique, Professor F.Ajersch from Ecole polytechnique de Montreal for his great information and contribution on rheological experiments, Professor H.Vali, director of electron microscopy center at McGill University and all his colleagues specially Dr. S. Kelly Sears and Mrs. L. Mongeon, and Mr. Lang Shi of the microanalysis laboratory, earth and planetary science department.

I would also like to thank Mr.G.Lemire and Mr. M. Bouchard, technicians of the NSERC-ALCAN-UQAC Industrial Research Chair, for their assistance in casting operations, sample preparation, and construction of special devices.

I should also remember all of my friends who with their supports and encouragements gave me the strength to pass the hard time. Particularly, I would like to name Mr.O.Lashkari that without his collaboration, this work was impossible.

Finally, to my wife Bita, thank you for being so loving, supportive, patient, and all understandings in all good and "no good" situations.

List of publications

REFEREED JOURNALS

Due to the innovative nature of the current project and the fact that a comprehensive study was carried out, there are ample opportunities for numerous publications. However, due to confidentiality issues with ALCAN International limited, and prolonged submission time for journal publications, to date seven (7) Journal articles have been proposed for publication. Three have already been published and the others submitted for publication. In addition, there have been seven (7) conference (refereed) publications. The list of the publications is as follows:

1. Grain refining of Conventional and Semi-solid A356 Al-Si Alloy,
   Journal of Materials Processing Technology, 2006

2. Effects of Modification during Conventional and Semi-solid Metal Processing of A356 Al-Si Alloy,
   Journal of Materials Science & Engineering A, Vol.415, 2006, pp.273-285

3. Combined Grain Refining and Modification of Conventional & Rheo-Cast A356 Al-Si Alloy,
   Accepted for publication in Journal of Material Characterization, 2006

4. Semi-solid Metal Processing Routes; an Overview,
   Journal of Canadian Metallurgical Quarterly, Vol.44, No.3, 2005, pp.289-303

5. Laser Ablation ICP-MS Investigation of Solute Element Distributions during Al-Si Solidification,
   Journal of Alloys and Compounds, 2005

6. Microstructure and Rheological Behavior of Grain Refined and Modified Semi-solid A356 Al-Si Slurries
   Accepted for publication in Acta Materialia, Nov.2005

7. The Effect of Dissolved Titanium on the Primary α-Al Grain and Globule Size in the Conventional and Semi-solid Casting of 356 Al-Si Alloy,
   Accepted for publication in Journal of Material Science, 2005

CONFERENCE PROCEEDINGS

1. The SEED Technology: A New Generation in Rheocasting,
   CIM-Light Metals Conference, Calgary, Canada, Aug.2005, pp.359-371

2. Effects of Stirring on the Silicon Morphological Evolution in Hypoeutectic Al-Si Alloys,
   TMS-Light Metals Conference 2005, San Francisco, CA, Feb.2005, pp.1111-1116

3. Preliminary Results on the Effects of Modification during Semi-solid Processing of Al-7%Si Alloys,
   TMS-Light Metals Conference 2005, San Francisco, CA, Feb.2005, pp.1083-1088

4. Impact of swirling and superheat on microstructural evolution of 356 alloy in SEED slurry-on-demand process,
   CIM-Light Metals Conference, Hamilton, Canada, Aug.2004, pp.315-322

5. The Influence of Grain Refiner on the Microstructural Evolution of Al-7%Si and A356 in the Swirled Enthalpy Equilibration Device (SEED),
   8th International Conference on Semi-solid Processing of Alloys & Composites, Cyprus, September 2004

6. Semi-solid Processing of Al-Si Alloys: Effect of Stirring on Iron-Based Intermetallics,
   8th International Conference on Semi-solid Processing of Alloys & Composites, Cyprus, September 2004

7. Effects of Grain Refining on Morphological Evolution of Al-7%Si in the Swirled Enthalpy Equilibration Device (SEED),
   66th World Foundry Congress, Turkey, September 2004, pp.1253-1263

TABLE OF CONTENTS

LIST OF FIGURES

LIST OF TABLES

LIST OF ABBEREVIATIONS AND SYMBOLS

CET	Columnar to equiaxed transition
DAS	Dendritic arm spacing
DCP	Dendrite coherency point
EBSD	Electron backscattered diffraction
EMS	Electromagnetic stirring
EPMA	Electron probe micro analysis
FCC	Face center cubic
GRF	Growth restriction factor
IACS	International Annealed Copper Standard
IIT	Impurity Induced Twinning
LPP	Liquid peak parameter
MHD	Magneto hydro dynamic
NRC	New rheocasting process
OES	Optical emission spectroscopy
RPM	Revolutions per minute
SEM	Scanning electron microscopy
SoD	Slurry on demand
SSM	Semi-solid metal
SSR	Semi-solid rheocasting
TEM	Transmission electron microscopy
TPRE	Twin Plane Re-entrant Edge
UTS	Ultimate tensile strength, MPa
WDS	Wavelength dispersive spectroscopy
A_{SL}, A_{SM}	Areas of the solid/liquid and solid/mold interfaces, m^2
C	Concentration, at%, wt%
C_0	Initial alloy concentration, at%, wt%
C_p	Specific heat, $J.kg^{-1}.K^{-1}$
D	Diffusion coefficient in liquid, $m^2.s^{-1}$
D	Circular diameter, m
F	Force, $kg.m.s^{-2}$
G	Interface temperature gradient, dT/dz, $K.m^{-1}$
G_c	Interface concentration gradient, dC/dz, at%, wt%
G_V^S , G_V^L	Free energies per unit volume of solid and liquid respectively, $J.mol^{-1}$
Hz	Frequency unit, s^{-1}
I	Nucleation rate, $/m^3s$
K	Constant
K_b	Boltzmann's constant ($1.38x10^{-23}$), $J.K^{-1}$
N_n , N_l	Numbers of small crystalline clusters having n atoms per cluster and

	atoms in liquid respectively
N_V^P	Number of nucleant particles, /m^3
P_c	Solutal Peclet number
S_v	Specific volume surface of the particles, m^{-1}
T	Temperature, °C, K
T_{end}	Solidification termination, °C
T_f ,T_m	Equilibrium melting temperature, °C, K
Tg_{Al}	Recalescence of steady state growth temperature due to release of latent heat of primary α-Al dendrites, °C
T_i	Dendrite tip temperature during columnar growth, K
T_l	Alloy liquidus temperature, K
$Tmin_{Al}$	Newly nucleated crystals have grown to such an extent that the latent heat liberated balances the heat extracted from the sample, °C
$Tnuc_{Al}$	Start point of primary α-Al dendrites nucleation, °C
$Tmin_{eut}$ $Tmax_{eut}$	Minimum and maximum of eutectic temperatures respectively, °C
$Tnuc_{eut}$	Start of eutectic nucleation, °C
T_q	Measurable temperature, K
V	Rate of interface movement, m.s^{-1}
V_c	Growth rate of columnar dendritic growth front, m.s^{-1}
V_f	Entrapped liquid content, %
V_e	Radial growth rate of equiaxed dendrite, m.s^{-1}
V_L,V_S	Volume of solid and liquid respectively, m^3
V_x	Velocity of liquid in X direction, m
Y	Distance between plates, m
c	Volumetric specific heat, J/m^{3}K
k	Equilibrium distribution coefficient, C_s/C_l
m	Liquidus slope, dT_l/dC, K/wt%
n^o	Number of atoms in a nucleus
r	Radius, m
r^o	Critical nucleation radius, m
v'	Atomic volume, m^3
ΔC_0	Concentration difference between liquidus and solidus at solidus temperature of alloy, at%, wt%
ΔG	Gibbs free energy, J.mol^{-1}
$\Delta G°$	Activation energy for the nucleation of the cluster of critical radius, J
ΔG_n^0	Activation energy for the nucleation of a critical number of clustered atoms, J
ΔG_d	Activation free energy for diffusion across solid/liquid interface, J. mol^{-1}
ΔG_n	Free enthalpy change due to the formation of one nucleus containing n atoms, J

ΔG_V	Volume free energy change due to the formation of solid particles, $J.mol^{-1}$
Δh_f	Latent heat of fusion per mole, $J.mol^{-1}$
ΔT	Undercooling, °C, K
ΔT_n , ΔT_c	Undercooling responsible for columnar and equiaxed dendrites, °C, K
ΔT_c	Constitutional undercooling, K
ΔT_t	Thermal undercooling due to temperature difference in the melt, K
ΔT_r	Curvature undercooling, K
ΔT_k	Kinetic undercooling, K
ΔT_α	α-Al solidification range ($Tnuc_{Al}$ - $Tnuc_{eut}$), °C
ΔT_{eut}	Eutectic solidification range ($Tnuc_{eut}$ - T_{end}), °C
ΔT_{Rec}	Temperature difference between unsteady ($Tmin_{Al}$) and steady (Tg_{Al}) state growth temperatures of primary α-Al particles (recalescence), °C
$\Delta\theta$	Variation of eutectic undercooling ($Tmax_{eut}$ - $Tmin_{eut}$), °C
γ_{SL}, γ_{SM}, γ_{ML}	Surface tensions of the solid/liquid, solid/mold, and mold/liquid interfaces, $N.m^{-1}$
γ°	Shear rate, s^{-1}
θ	Angel, °
λ	Interlamellar spacing, m
μ	Constant of proportionality or dynamic viscosity, $N.s.m^{-2}$
τ	Shear stress, $N.m^{-2}$, Pa
δ_c	Solute boundary layer thickness, m
Ω	Dimensionless solutal supersaturation
Ω_t	Dimensionless thermal supersaturation

CHAPTER 1

INTRODUCTION

CHAPTER 1

INTRODUCTION

1.1 Overview

The recent Canadian roadmap on aluminum [1] identifies specific areas where research is urgently needed to bring aluminum to its full potential. Solidification and recycling, fabrication and finished products are particularly detailed. Prediction of microstructure, stress and strain, understanding of relationships between microstructure and materials performance, development of new manufacturing processes and forming techniques such as semi-solid casting are among the most important research avenues identified.

The aluminum foundry alloys, (Al-Si, Al-Cu, Al-Mg, Al-Zn, Al-Sn, Al-Si-Cu, Al-Si-Mg), constitute almost 20% of Al-alloys consumption worldwide with transport industry as its principle advocate. On the other hand, as the need for having readily useable components grew over the last two decades, casting became more attractive as one of the most economical near or net-shaped fabrication route amongst the many other metal forming processes. For aluminum foundry alloys, the most commonly used shaping route is a variety of casting processes such as sand and die castings. However, there are certain drawbacks for casting including the formation of defects such as porosity, hot tears, and segregation. They could be potential crack initiators during service operation [2,3]. Therefore, there have been considerable efforts to minimize such drawbacks and that have resulted in introducing more advanced casting routes such as rheocasting or squeeze casting

[4,5]. Parallel to such endeavor, efforts were also concentrated on developing new foundry alloys compatible with the new casting technologies.

In this context, rheocasting has come to play an increasing role as an alternative technique to minimize the drawbacks of the as-cast products in comparison to other more conventional casting routes. However, little investigative work has been carried out on the origin of resulted microstructure of rheocast products, both for wrought and foundry alloys, especially when modifiers and grain refiners are incorporated.

Semi-solid metal (SSM) forming is now in its thirty-third year. The original experiment leading to the invention of SSM was performed in early 1971 as part of a doctoral thesis [6]. This technology is different from the conventional forming processes which uses either solid or liquid metals as the starting material. This process deals with slurries, which in principle, can be produced in any material systems where liquid and solid phases coexist over a freezing range. The SSM process has advantages over other casting processes which is associated with less porosity and shrinkage voids, lower processing temperature and shorter time, less mold erosion, faster cycle time and longer die life [4,7,8].

Technologies for SSM processing can be generally divided into two basic groups:

- Rheo- routes
- Thixo-routes

The rheo-route involves preparation of SSM slurry from liquid phase and its direct transfer into a die or mold for component shaping. The term "Slurry-on-Demand", SoD, has recently been coined in industry to describe slurry making operations that take place in the cast shops, thus provide a constant supply of slurry for shaping operations.

The thixo-route is basically a three step process, involving preparation of a feedstock material having an equiaxed or globular/non-dendritic structure or indeed having the potential to transform into equiaxed structure on further processing. The second step is reheating of the feedstock material to temperatures between solidus and liquidus (mushy

zone) to generate a semi-solid structure. The final step is shaping of the mush that has thixotropic characteristics.

Semi-solid metal forming takes advantage of the unique flow behavior of specially prepared raw material slugs within the liquid-solid temperature range. The obtained globular structure allows the slug to be handled like a solid but switches to non-Newtonian fluid upon shearing during the forming step within a die casting or forging machine; *"dual characteristics where the SSM billet has solid-like characteristics, but flows like a liquid under shear stress"*.

One of the most appropriate alloys for SSM processes is aluminum alloys, e.g., Al-Si alloys. In this category hypoeutectic Al-Si gained a lot of attention due to its superior formability, better mechanical properties, higher strength to weight ratio, relative lower melting point, wider solidification range, etc. Generally, a desired structure in SSM processing is defined as a structure free of dendrites, preferably fully spherical primary particles, and minimum or no entrapped eutectic. Therefore globule morphology is the paramount concerned issue being sought while other variables are almost neglected. In the case of hypoeutectic Al-Si alloys, the primary α-Al particle size and eutectic silicon morphology are the main parameters that affect mechanical properties of the selected alloy. Addition of grain refining agents to molten aluminum is now a prerequisite for successful and economic casting. Grain refinement in conventional casting provides an equiaxed grain structure, uniform mechanical properties and better machinability. It also eliminates shrinkage porosity, increases resistance to hot tearing and improves feeding. On the other hand, mechanical properties of Al-Si alloys depend not only on the primary particles size and morphology, but also on the morphology of the eutectic Si particles. Therefore, the modification of Si morphology is the next important melt treatment during foundry operations. Sr is the most common modifier used for silicon modification in Al-Si alloys for a variety of casting methods.

In conventional diecasting, melt treatment, refining and modification, is rather uncommon. This can be explained by the nature of high cooling rate of the process and consequently finer microstructure. While for SSM processing, the process is divided into two different solidification categories, one with lower cooling rate to obtain globules and making slurries and the second step with faster cooling rates typical of conventional diecasting. This is the most important reason for using refiner and modifier in the SSM process.

For semi-solid metal processing, direct incorporation of grain refiners during the course of slurry processing and preparation has not been studied before. Most of the previous SSM studies were concentrated on the thixoforming of the pre-grain refined as-cast billets. As a result, the effect of grain refining was considered mainly during the post thermal treatment of conventionally cast and grain refined billets. In these methods, globular SSM slurries were obtained by simply reheating grain refined billets. It is reported that the optimum flow behavior for semi-solid metal processing is achieved if the raw material structure consists of very fine and globular grains [9-13]. Therefore, it has been the main objectives of SSM processing, with specific emphasis on Al-alloys, to obtain globular structure of primary phase to improve mechanical properties and thixotropic behavior of the alloy. As a result, there are not much works reported on the characteristics of other micro-constitutes which usually formed during solidification of Al alloys such as silicon morphology and implication of modification [14,15].

1.2 Objectives of the thesis

The main objectives of the current research study are to investigate the effects of grain refiners and modifiers on the microstructural evolution of semi-solid casting of Al-Si alloys, especially 356 alloying group.

For this purpose and according to the new strategies of the NSERC-ALCAN-UQAC industrial chair, the research is concentrated on the new ALCAN patented SSM process, the

so called Swirled Enthalpy Equilibration Device, "SEED process" [16]. Therefore the steps of this comprehensive research project were defined as follows:

1. Effect of process parameters on the resulting semi-solid metal structure

Since this process is totally new and different from other SSM processes, the first part of this research is focused on the effects of different process parameters such as rotation speed and time, melt superheat, melt drainage time and temperature, and mold temperature. A series of tests were carried out with one parameter changing at a time to identify the optimum conditions for which a specific SEED billet microstructure is resulted. The optimum conditions were then used for the rest of casting trials.

It should be mentioned that due to the confidentiality issues, the first part of the research is not included in this context and could only be found in industrial reports submitted to ARDC-ALCAN, Arvida research center [17-20].

2. Effects of grain refiners on the SSM structure

Different grain refiners are examined and the resulting microstructures are characterized for two alloys (356 alloys with and without Ti). The main points are the chemistry of grain refiner and its quantity.

3. Effects of Sr-modification on the SSM structure

Sr-modification is examined to achieve the optimum microstructures for two alloys (Al-7%Si and A356). The main points are the alloy constituents, chemistry, and the quantity of the modifier.

The effects of inoculation and modification parameters have been investigated on the optimum condition which achieved in 1.

4. Effects of combined addition of refiner and modifier

As mentioned before, refiner improves the morphology of the primary α-Al particles and modifier changes the eutectic silicon flakes morphology to fibrous. By optimizing the

addition rate of both refiner and modifier, a series of tests have been done to investigate the effect of simultaneous treatment on the resulting microstructure.

5. *Rheological tests to characterize the effect of grain refiners and Sr- modifier*

In the first definition of the project, investigation on the mechanical properties of the high pressure die cast billet was considered however due to the confidentiality issues, this step was changed to the rheological study which is performed in collaboration with another PhD candidate, Mr.O.Lashkari. The aim of this work is to differentiate the rheological properties of untreated and treated alloys.

1.3 Statement of originality

As mentioned earlier, SEED process is a new technology and basically there are few reports available in the literature on this process. Also as discussed later in the literature review, there are not much works reported on the direct incorporation of refiners and modifiers during the processing and preparation of SSM slurries and most of the published documents are related to thixocasting process. Therefore, the current research work contains a high degree of originality and references are provided where previous works are cited.

1.4 Outline of thesis structure

This dissertation discusses different aspects of refiner and modifier additions in the following order:

- Chapter 1 introduces the semi-solid metal processing and a brief description on the additions and effects of refiner and modifier
- Chapter 2 surveys the principles of solidification and focuses on the refining and modification of the aluminum alloys
- Chapter 3 explains different SSM processing and a brief review is given on the basic concepts of rheology
- Chapter 4 illustrates experimental procedures

- Chapters 5 and 6 provide the results and discussion on different refiner and modifier added separately
- Chapter 7 describes the effect of concurrent optimum addition of both grain refiner and modifier
- Chapter 8 gives some limited rheological tests on the results
- Chapter 9 shows complementary results based on the initial works and also some indirect researches obtained during the course of the main experiments
- Chapter 10 describes the conclusions and further suggestions for future studies

CHAPTER 2

LITERATURE REVIEW: PRINCIPLES OF SOLIDIFCATION, GRAIN REFINING, AND MODIFICATION

CHAPTER 2

LITERATURE REVIEW: PRINCIPLES OF SOLIDIFCATION, GRAIN REFINING AND MODIFICATION

There are many advantages in controlling the grain size and its distribution in the as-cast products including improved mechanical properties, superior surface finish, uniform distribution of second phases, better machinability and, so on [21]. This is only possible by close control of casting conditions to suppress columnar growth and promote the formation of equiaxed structure during solidification. An optimum condition is defined as where the presence of numerous potent nucleants is necessary to encourage heterogeneous nucleation and to provide adequate thermal and solutal conditions for nuclei to survive and form a fine and uniform network.

Therefore, in this part, for better understanding of the optimized condition, the principles of solidification including nucleation and growth processes will be discussed briefly.

2.1 Principles of Solidification

Solidification is governed by nucleation and growth of crystals from the melt, where nucleation controls the size of grains formed and growth determines the grain morphology and the distribution of alloying elements within the matrix. The driving force for nucleation is the degree of undercooling created during solidification and growth is controlled by the

temperature gradient in the liquid. Both are however affected by the rate of heat extraction from the melt. The rate of heat extraction controls the solidification rate.

Therefore, in order to characterize the solidification structure of cast aluminum alloys, a thorough understanding of the mechanisms of nucleation and growth is required as a function of casting conditions such as casting speed, melt superheat, alloy constitution and rate of heat extraction, as well as the influence of convection on those events.

2.1.1 Nucleation

If a liquid is cooled below its equilibrium melting temperature (T_f), it is expected to solidify spontaneously. However, this is not always the case. As pointed out by Porter and Easterling [22], under suitable conditions, it is possible to undercool liquid nickel by as much as 250K below its melting temperature and yet preserve its liquid state. The reason for such behavior is the fact that transformation only begins with the formation of energetically stable minute particles, nuclei, from unstable solid particles known as embryos. Consequently, a liquid-solid interface is formed and therefore the free energy of the system changes, and if sufficient undercooling is available, the embryo survives and will grow to form a nucleus. This large undercooling is not normal in a casting due to the existence of preferential nucleants such as the mold walls and impurities. In this case, heterogeneous nucleation starts at much lower undercoolings of ~1K. Unassisted nucleation, where the formation of nuclei is solely indigenous to the liquid is known as "homogenous nucleation" while the other case is "heterogeneous nucleation".

2.1.1.1 Homogenous nucleation

If in a given volume of undercooled liquid, some atoms clustered together to form an embryo of radius r, the free energy of the system is changed. This variation is associated with the decrease in the free energy resulting from the volume change from liquid to solid state and also increase in the free energy due to the newly created liquid-solid interface. For a sphere, the change in free energy is as follows:

$$\Delta G_{\text{hom}} = -V_s \Delta G_V + A_{SL}\gamma_{SL} = -\frac{4}{3}\pi r^3 \Delta G_V + 4\pi r^2 \gamma_{SL} \qquad (2.1)$$

Where V_s is the volume of solid formed, A_{SL} is the solid-liquid interfacial area, γ_{SL} is the surface energy associated with the newly formed solid particle.

This is graphically illustrated in Figure 2.1. The creation of a small solid particle is accompanied by increasing the interfacial term as r^2, whereas the volume free energy released increases as r^3. That is why the liquid is able to maintain a metastable state at temperatures below T_f. This behavior leads to the formation of a maximum value of ΔG when the melt is undercooled to a certain value. This is the maximum energy change in the system due to the formation of a critical sized crystal nucleus, r^o. To calculate the value of r^o, the first derivative of the equation 2.1 should be equaled to zero, $d\Delta G/dr = 0$ and therefore:

$$r^o = \frac{2\gamma_{SL}}{\Delta G_V} \quad \text{and} \quad \Delta G^o = \frac{16\pi\gamma_{SL}^3}{3\Delta G_V^2} \qquad (2.2)$$

If $r < r^o$, the system can lower its free energy by remelting of the solid, while when $r \geq r^0$ the free energy of the system decreases if the solid grows. Unstable solid particles with $r<r^o$ are referred as embryos while the stable particles are referred as nuclei and r^o is the critical nucleus size [22].

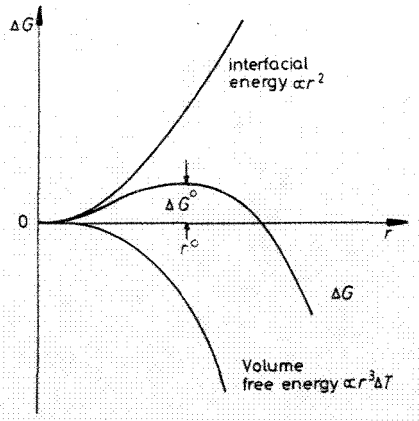

Figure 2.1: The free energy change in homogenous nucleation of a sphere [22]

2.1.1.2 Heterogeneous nucleation

When the melt contains pre-existing fragments of crystals or is in contact with a surface such as mold wall, nucleation is facilitated and the number of atoms per cluster or the activation energy is decreased. This is known as "heterogeneous nucleation".

While considering a solid embryo in contact with a perfectly flat mold (Figure 2.2), it can be shown that for a given volume of the solid, the total interfacial energy of the system is minimized if the embryo has the shape of spherical cap with a wetting angle of θ given by the following equation, see Figure 2.2:

$$\cos\theta = \frac{\gamma_{ML} - \gamma_{SM}}{\gamma_{SL}} \tag{2.3}$$

The free energy change due to the formation of a heterogeneous nucleus is given as:

$$\Delta G_{het} = -V_S \Delta G_V + A_{SL}\gamma_{SL} + A_{SM}\gamma_{SM} - A_{SM}\gamma_{ML} \tag{2.4}$$

Where V_S is the volume of spherical cap, A_{SL} and A_{SM} are the areas of the solid/liquid and solid/mold interfaces, and γ_{SL}, γ_{SM}, and γ_{ML} are the surface free energies of the solid/liquid, solid/mold, and mold/liquid interfaces respectively. Equation 2.4 may be re-written in terms of the wetting angle (θ) in the presence of the melt, between a growing spherical cap and a solid substrate as:

$$\Delta G_{het} = \left\{-\tfrac{4}{3}\pi r^3 \Delta G_v + 4\pi r^2 \gamma_{SL}\right\} f(\theta) = \Delta G_{\text{hom}} * f(\theta) \tag{2.5}$$

Where:

$$f(\theta) = \frac{(2+\cos\theta)(1-\cos\theta)^2}{4} \tag{2.6}$$

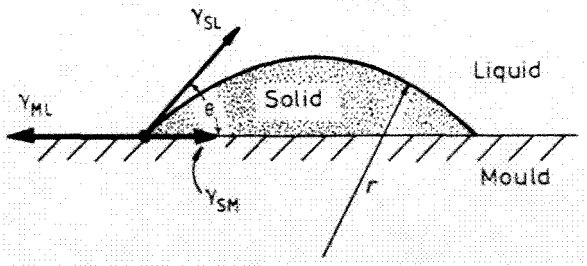

Figure 2.2: Schematic representation of spherical cap on a substrate

Table 2.1 shows the critical parameters for both homogenous and heterogeneous nucleations. Critical number of atoms (n^o) per nucleus in the heterogeneous nucleation is smaller than that of the homogenous nucleation by the shape factor $f(\theta)$ while the r^o value is not affected by shape factor, $f(\theta)$. This table shows that under appropriate solid/liquid wetting (small θ) condition, a large decrease in n^o, and ΔG_n^o can occur.

Table 2.1: Critical dimensions and activation energy for different nucleation conditions (v' is the atomic volume) [23]

	Homogenous nucleation	Heterogeneous nucleation
r^o	$\frac{2\gamma_{SL}}{\Delta G_V}$	$\frac{2\gamma_{SL}}{\Delta G_V}$
n^o	$-(\frac{32\pi}{3v'})(\frac{\gamma_{SL}}{\Delta G_V})^3$	$-(\frac{32\pi}{3v'})(\frac{\gamma_{SL}}{\Delta G_V})^3 f(\theta)$
ΔG_n^o	$\frac{16\pi\gamma_{SL}^3}{3\Delta G_V^2}$	$\frac{16\pi\gamma_{SL}^3}{3\Delta G_V^2} f(\theta)$

This is the basis of the current practice in foundries known as inoculation. In this method, a suitable material is added to the melt which has, for example, a higher melting point than the alloy. This effect is usually time dependent since the added substance tends to dissolve in the melt.

It is important to mention that not all the foreign particles in the melt are effective nucleants for solid formation. Generally at a given undercooling, these particles with the closest crystallographic similarity to that of the solidifying phase will become effective nucleants in the liquid as described later.

2.1.1.3 Nucleation rate

According to Kurz and Fisher [23], the number of grains nucleated within a given melt volume and time, the nucleation rate, can be calculated by considering an ideal mixture of small crystalline clusters and the liquid using the following equation:

$$\frac{N_n}{N_l} = \exp(-\frac{\Delta G_n}{K_B T}) \tag{2.7}$$

Where N_n and N_l are the numbers of small crystalline clusters having n atoms per cluster and atoms in liquid respectively, K_B is Boltzmann's constant, and ΔG_n is the free enthalpy change due to the formation of one nucleus containing n atoms. This equation shows that the number of clusters increases with decreasing the ΔG_n value.

In an undercooled melt, a maximum in ΔG_n as a function of n exists, over which clusters can escape and form the flux of nuclei, I. As it could be deduced from Table 2.1 ($\Delta G_V \propto \Delta T$), the ΔG_n^o varies with $\frac{1}{\Delta T^2}$ and hence N_n^0, the critical number of the cluster, nuclei, having n atoms is calculated as [23]:

$$N_n^0 = K_1 \exp(-\frac{K_2}{T\Delta T^2}) \tag{2.8}$$

Where K_1 and K_2 are constants. If the critical clusters concentration at equilibrium does not change, the steady state nucleation rate is given by;

$$I = K_3 N_l \exp(-\frac{\Delta G_n^0}{K_B T}) \tag{2.9}$$

Where K_3 is constant and I is the nucleation rate. As it was pointed out before [23], the formation of clusters require the transformation of atoms from liquid into the cluster and therefore an activation energy, ΔG_d ,exists for this transformation which must be added to the equation 2.9, giving:

$$I = I_0 \exp(-\frac{\Delta G_n^o + \Delta G_d}{K_B T}) \tag{2.10}$$

The equation 2.10 shows that the exponential term varies with two factors: ΔG_n^o which depends on $-\frac{1}{T\Delta T^2}$ and ΔG_d which is a diffusion term and hence varies with $-\frac{1}{T}$. An increase in undercooling, giving more and smaller nuclei whereas a decrease in T causes less transformation of atoms from liquid to nuclei due to lack of diffusion. These

opposing issues lead to a maximum in the nucleation rate between melting point ($\Delta T=0$) and the point where there is no longer any thermal activation (T= 0K). It is important to note that the presence of ΔG_d increases the temperature at which the maximum nucleation rate occurs.

At low values of ΔT, the term $\exp(-\frac{\Delta G_d}{K_B T})$ is approximately equal to 0.01 and I_0 is approximately equal to 10^{41} $m^{-3}s^{-1}$.Therefore, the nucleation rate becomes [23]:

$$I = 10^{39} \exp(-\frac{\Delta G_n^o}{K_B T}) \ (m^{-3}s^{-1}) \qquad (2.11)$$

A nucleation rate of one nucleus per cm^3 per second ($10^6 m^{-3}s^{-1}$) occurs when the value of exponential term is about 76. By changing this term by a factor of two, from 50 to 100, the nucleation rate also decreases by a factor of 10^{22}. This example shows that very slight changes in the solid/liquid interfacial energy can have considerable effect on the nucleation rate.

With the same nucleation rate ($1/cm^3s$) and with considering the contact angle, it becomes clear that for example by inoculation, the active surface area of the inoculants must also be taken into account in the pre-exponential factor (I_0) in equation 2.10. Table 2.2 illustrates the variation of undercooling with contact angle. This effect is relatively small in comparison with that caused by a change in activation energy and usually neglected [23]. However, when fine grained structures are required, a large number of particles with low interfacial energy should be introduced to the melt. This is best achieved by introducing particles having the same crystal structure as those of the solidifying phase, e.g. broken dendrites of Al. Since stirring can break up dendrites and thus may be regarded as a means to refine the structure. The addition of grain refiner with chemical reaction or precipitation within the melt having similar crystal structure to that of solidifying phase are quite effective in refining the cast structure.

Table 2.2: Absolute and relative undercoolings required to give one nucleus per second per cm^3 as a function of θ [23]

θ (°)	$\Delta T/T_f$	ΔT (T_f=1500K)
180	0.33	495
90	0.23	345
60	0.13	195
5	0.001	1
0	0.0	0

2.1.2 Columnar and equiaxed solidification

Grain structure is an important and readily observable feature in aluminum alloy castings. Depending on the heat flow and alloy chemistry, three distinct grain morphologies are possible, namely, equiaxed, columnar, and feathery or twin columnar grains. Feathery crystals are much less common than the other types but they occur at certain alloys with critical cooling rates [24].

At the mold/metal interface, the cooling rate is at its highest and therefore many randomly oriented small grains nucleate to form the outer equiaxed zone, i.e., chill zone. New grains form over the chilled zone rapidly become dendritic and grow along preferred crystallographic directions. Since these grains have higher growth rate, they become dominant morphology and finally leading to the formation of columnar zone. Finally, a coarse grained equiaxed zone forms at the center of the casting mainly as a result of secondary and tertiary dendrite arms detachment and subsequent flow towards the central part of the castings [23] (Figure 2.3).

Figure 2.4 shows the temperature fields in the various cast structures. The columnar grains grow out from the mold walls into the melt, i.e., in direction opposite to the heat flow. It means that the temperature gradient is positive. In this case, the liberated heat of fusion is transported through the growing solid. Thus, solute rejection should be considered for growth rate calculation.

On the other hand, the equiaxed grains grow in an undercooled melt and the generated heat during solidification must be extracted through the melt. Thus the equiaxed grains act as heat sink for each other and hence the direction of heat flow and growth are no longer unidirectional.

Figure 2.3: As-cast structure [25]

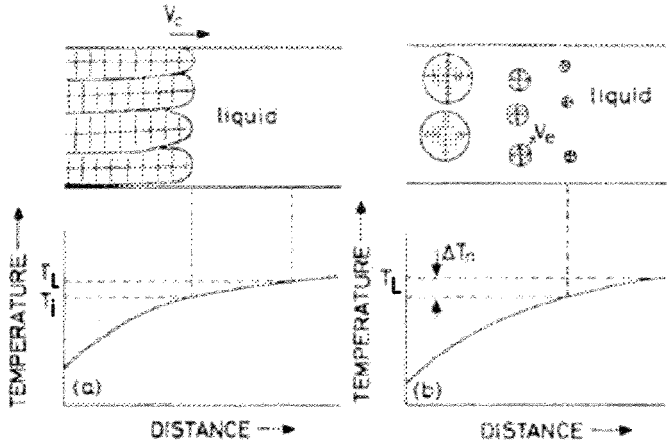

Figure 2.4: Solid/liquid interface morphologies and temperature distribution; (a) columnar growth, (b) equiaxed growth (T_l: liquidus temperature, T_i: growth front temperature, V_c: velocity, ΔT_n: undercooling, V_e: radial growth rate) [21]

From the morphological instability point of view, during columnar growth of a pure substance, the heat flow, Tq, increases in the Z direction, i.e., G is positive (Figure 2.5a). In this case, if any perturbation is formed, the temperature gradient in the liquid is higher than that of the solid (Figure 2.5a, with comparing full and dotted lines along section A-A). As a result, more heat flows into the tip of the perturbation and less flows out into the solid. As a result the perturbation melts back and planar interface is stabilized.

However, this is not the case for equiaxed solidification (Figure 2.5b). The equiaxed grains grow into an undercooled melt (cross-hatched) and the latent heat produced during growth also flows down the negative temperature gradient in the liquid. Any perturbation which forms on the sphere makes this gradient steeper (full line comparing to the dotted line) and permits the tip to reject more heat. As a result, the local growth rate is increased and the interface is always morphologically unstable.

Kurz and Fisher [23] stated that the equiaxed crystal morphology in alloys is almost indistinguishable from that in pure metals, although a difference exists in the scale. This is because the growth in pure metals is heat flow controlled while the growth in alloys is solute diffusion controlled.

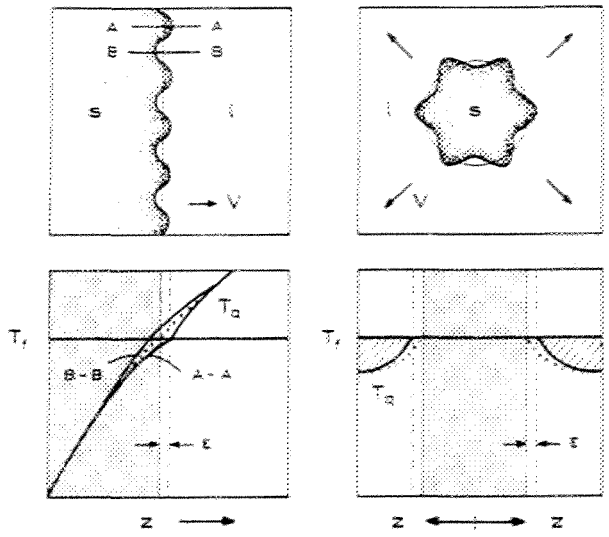

(a) (b)

Figure 2.5: Columnar and equiaxed solidification of a pure substance [23]

2.1.2.1 Constitutional undercooling

Solidification is governed by nucleation and growth of primary phase. In real applications, growth does not take place with complete mixing of solute elements within the solid phase resulting in what is called *"segregation"*. Thus the composition of liquid changes during solidification, and the last liquid has a different composition comparing to the first solidified liquid. The control of segregation in both micro and macro scales is one of the most challenging tasks for improving the soundness of the as-cast products including the mechanical properties.

Solidification in systems with a partition coefficient less than 1 ($k<1$) is accompanied by rejecting of solute atoms from the center to outside, layer by layer and this causes solute build up in the liquid adjacent to the solid (Figure 2.6a). Since mass diffusion is a slow process, solute atoms will pile up at the interface and consequently further growth

is retarded because of solute accumulation. According to Kurz and Fisher [23], the solute concentration in the boundary layer decreases exponentially, from C_0/k to C_0 given by:

$$C_l = C_0 + \Delta C_0 \exp(-\frac{V_z}{D}) \tag{2.12}$$

Where C_l and C_0 are liquid and initial alloy concentrations, V_z is the rate of interface movement and D is diffusion coefficient. Consequently, the equivalent boundary layer was given by:

$$\delta_c = \frac{2D}{V} \tag{2.13}$$

According to Figure 2.6b, this length is equal to the base length of a triangle having a height which is equal to the excess solute concentration in the interface, and an area which is the same as that under the exponential curve. It should be emphasized that the equation 2.13 reveals that the thickness of the boundary layer is inversely proportional to the growth rate.

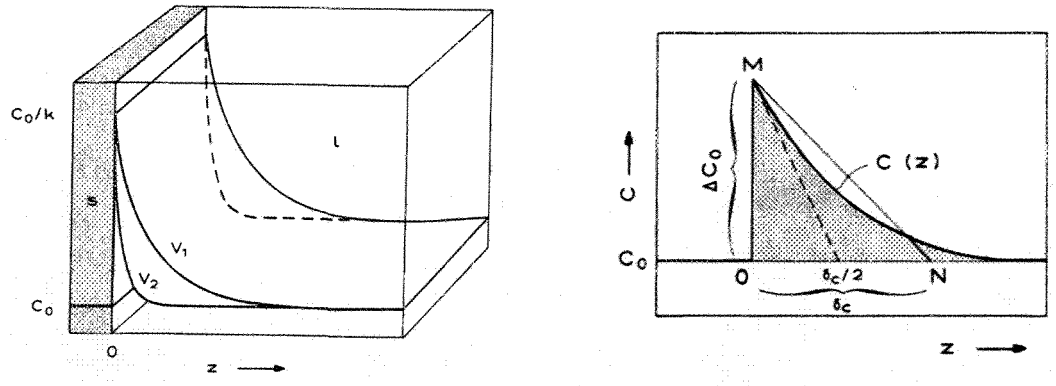

(a) (b)

Figure 2.6: (a) Steady state boundary layer at the planar interface (with considering two different growth rates, $V_2 > V_1$); (b) calculation of the equivalent boundary layer thickness [23]

This concentration difference will affect the local equilibrium solidification temperature of the liquid, T_l, which is related to the composition by:

$$T_l(C_0) - T_l = m(C_0 - C_l) \tag{2.14}$$

Where $T_l(C_0)$ is the liquidus temperature corresponding to the initial alloy composition. Figure 2.7 shows the correlation between concentration and temperature variation in the boundary layer.

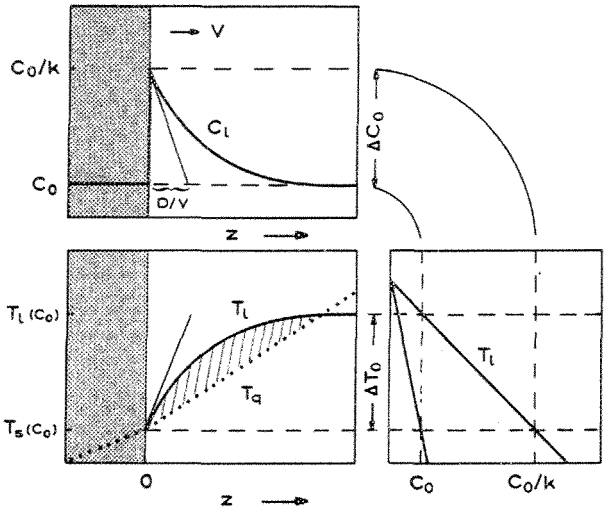

Figure 2.7: Constitutional undercooling in alloys for a given growth rate [23]

As the liquid concentration decreases with distance, Z, the liquidus temperature, T_l, of the alloy will increase as indicated by the related phase diagram. It means that the liquid at the various distances ahead of the solid/liquid interface has different freezing points. Now, considering the imposed temperature gradient arises from the heat flow in the casting, T_q, a volume of liquid may exist which is undercooled when the gradient of T_q is less than the gradient of T_l. This region (shown by cross hatched), was first called constitutional undercooling by Chalmers [25].

So, for achieving such a constitutional undercooled zone, the temperature gradient, G, at the interface in the liquid should be lower than the gradient of liquidus temperature change in the melt as follows:

$$G < mG_C \tag{2.15}$$

Where G is interface temperature gradient, G_c is interface concentration gradient in liquid, and m is liquidus slope.

2.1.2.2 Growth restriction factor

The effects of solute elements on reducing the grain size and consequently increasing mechanical properties of as-cast products goes back to Kissling and Wallace work in 1963 [26]. Normally, small addition of alloying or solute elements hinders the growth of grains and provides conditions required for new nuclei and consequently finer grains to form. The solutes form a zone ahead of the solidification front in which the actual temperature is lower than the solidification temperature, i.e., constitutional undercooling [25].

The number of effective nuclei together with alloying elements in the melt is the most important controlling parameters of growth process. Grain refinement is facilitated if growth of grain is restricted. The melt undercooling during solidification has four different components as [23]:

$$\Delta T = \Delta T_c + \Delta T_t + \Delta T_r + \Delta T_k \qquad (2.16)$$

Where ΔT_c, ΔT_t, ΔT_r, ΔT_k are undercoolings due to the concentration, temperature, curvature, and kinetic differences (K).

Under normal casting conditions, ΔT_c is the dominant term. The early stages of a grain formation may be assumed to be spherical. Kurz and Fisher [23] have shown that for a free hemi-spherical dendrite tip of radius r, the solute undercooling, ΔT_c, is given by:

$$\Delta T_C = m_l (C_0 - C_l^*) = mC_0 \left[1 - \frac{1}{1 - \Omega P}\right] \qquad (2.17)$$

Where: C_0 = initial alloy concentration (wt %)

C_l^*= concentration at the solid/liquid interface (wt %)

m_l = liquidus slope, dT_l/dc, (K/wt%)

Ω = Solutal supersaturation (which is approximately equal to Pc; Solutal Peclet number)

P=1-k, where k is equilibrium distribution coefficient ($k = \frac{C_s}{C_l}$)

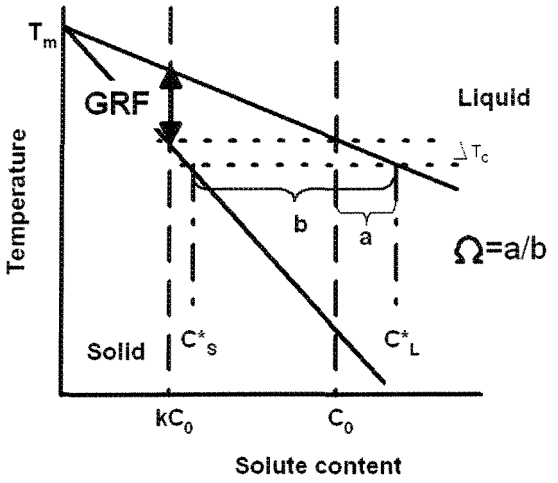

Figure 2.8: Different definitions in an alloying system [reproduced from 27]

This equation is valid for low supersaturations and much smaller than unity. Similarly, the thermal undercooling can be defined as:

$$\Delta T_t = \Omega_t \times \frac{\Delta h_f}{c} \tag{2.18}$$

Where: Ω_t = thermal supersaturation

Δh_f = latent heat of fusion per unit volume (J/mol)

c = volumetric specific heat (J/m^3K)

The growth of an equiaxed alloy dendrite is governed by both undercoolings. Thus, the growth rate and tip radius in the thermal case must be the same. Therefore, the only factor varying significantly with different alloy systems is constitutional undercooling, equation 2.17, which may be estimated to $m_lC_0(k-1)$ when the degree of partioning, $(C_l^*-C_s^*)$ is approximated to $C_0(1-k)$ with consideration of $\Delta T_C << (T_m - T_l)$ where T_m and T_l are the pure alloy melting point and the liquidus temperature at C_0 respectively. This parameter is known as Growth Restriction Factor (GRF) [27-29].

Table 2.3 shows some important factors in the calculation of GRF. From Table 2.3, it can be established that Ti has the largest GRF factor and apparently, the highest growth restriction effect on the aluminum. In hypoeutectic Al-Si foundry alloys, however, the high

Si content gives a higher GRF. For example for the alloy of 7%Si and 0.1%Ti, the GRF for silicon is 41.3 while that of Ti is 22.

Table 2.3: Data required for calculating the growth restriction factor, GRF [28,30,31]

Element	K	m_l	$(k-1)m_l$	Max C_0 (wt%)	System
Ti	7.8-9*	30.7-33.3	220-245.6	0.15	Peritectic
Ta	2.5	70	105	0.1	Peritectic
V	4	10	30	0.1	Peritectic
B	0.08	-18.2	16.7	0.022	Eutectic
Hf	2.4	8	11.2	0.5	Peritectic
Mo	2.5	5	7.5	0.1	Peritectic
Zr	2.5	4.5	6.8	0.11	Peritectic
Nb	1.5	13.3	6.6	0.15	Peritectic
Si	0.11	-6.6	5.9	12.6	Eutectic
Cr	2.0	3.5	3.5	0.4	Peritectic
Ni	0.007	-3.3	3.3	6	Eutectic
Mg	0.51	-6.2	3.0	34	Eutectic
Fe	0.02	-3	2.9	1.8	Eutectic
Cu	0.17	-3.4	2.8	33.2	Eutectic
Mn	0.94	-1.6	0.1	1.9	Eutectic

*depend on the reference

Backerud and Johnsson [30] conducted a number of grain refining experiments in the Al-Si system and found the results shown in Figure 2.9. In their experiments, the amount of boron was kept constant and the dissolved silicon and titanium were allowed to vary. As it could be seen, the grain size decreased to 2-3%Si after which further addition of silicon resulted in larger grain size.

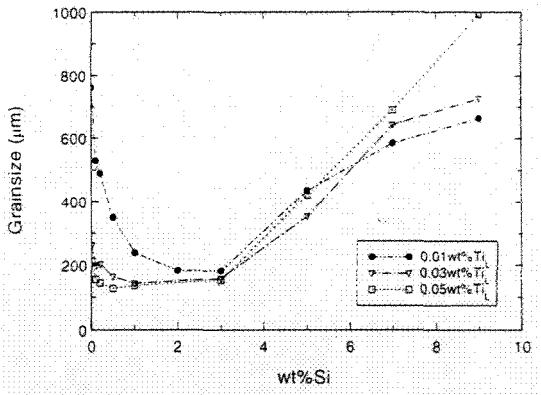

Figure 2.9: A grain refinement test in Al-Si alloys at $1°Cs^{-1}$ [30]

It was suggested that the growth restriction factor in an alloy would be the sum of GRFs for each alloying elements (assuming that there is no interaction between the solute phases) [21,30]:

$$GRF_{total} = \sum_i m_{l,i} (C_{0,i} - C_{l,i}^*) \qquad (2.19)$$

This factor is inversely proportional to the growth rate. Figure 2.10 shows the resulted total GRF plotted against the grain size for all experiments [30].

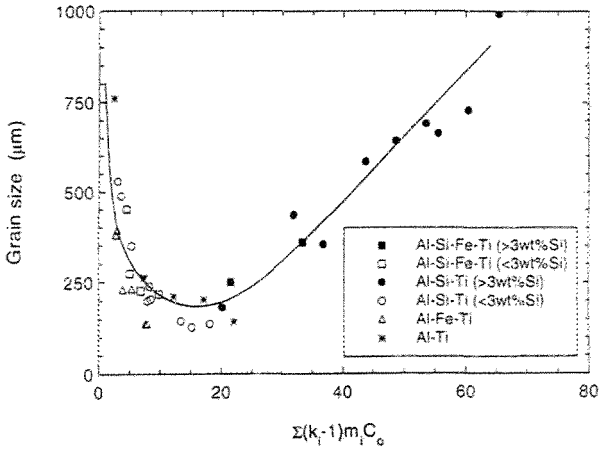

Figure 2.10: Average grain size vs. GRF for a number of alloy compositions [30]

Backerud et al. [30] suggested that the role of titanium depends on where the alloy is in Figure 2.10. On the left side, below the minimum in the curve, adding Ti causes smaller grains to form while on the right side, Ti addition results in larger grain size. Most of the alloying systems are located on the right hand side of the curve minimum and accordingly lower titanium levels should give better results.

As it could be seen in Figure 2.10, the data for hypoeutectic alloys are mainly located on the right hand side of the graph, which means the grain size should increase with increasing GRF value. In other words, the grain size should increase with increasing Ti concentration in solution. It seems that the correlation between grain size and total GRF value needs further clarification since the grain size decreases with higher percentages of Ti in solution.

2.1.2.3 Columnar to Equiaxed Transition (CET)

The as-cast structure normally has three distinct zones: chill, columnar and equiaxed zones. Depending on the casting condition, one of these zones may not be present but when a casting contains columnar and equiaxed grains, transition from columnar to equiaxed is usually narrow and occurs when the equiaxed grains are sufficient in size and number to change the columnar front.

An equiaxed zone forms when there are sufficient number of equiaxed grains in the bulk of liquid and grow rapidly enough to obstruct the columnar front. From a growth point of view, there is always a competition between equiaxed and columnar zones and the outcome depends on the degree and extent of the constitutional undercooling and the velocity of the columnar front. An equiaxed zone is promoted by a shallow temperature gradient in the bulk and depressed by increasing the superheat or reducing the natural convection [32].

There have been many experimental works carried out to understand the interrelationships amongst solidification parameters. Fredriksson and Olsson [33] stated that the columnar to equiaxed transition occurs when the bulk liquid temperature falls to a minimum prior to recalescence. They believed that recalescence increases the temperature difference between the solidification front and bulk liquid and causes greater convection to promote grain multiplication and acceleration of structural evolution. Hunt [34] analyzed the growth of equiaxed grains ahead of a columnar front during steady state directional solidification of binary Al-Cu alloys. In his model, the equiaxed grains are assumed to form by heterogeneous nucleation and the associated undercooling responsible for columnar and equiaxed dendrites are ΔT_c and ΔT_n respectively. He stated that if $\Delta T_n < \Delta T_c$, then equiaxed dendrites can grow. The predicted results for Al3%Cu are shown in Figure 2.11. As shown, columnar growth occurs at low velocities and high gradients. The mixed columnar and equiaxed structures only occur at high gradients (Figure 2.11a). In Figures 2.11b-d, only the transition to a fully equiaxed structure is shown. The effect of varying the heterogeneous nucleation temperature, alloy composition and number of heterogeneous nucleation sites are shown in Figure 2.11b-d respectively. This model predict a decreasing columnar range

with increasing parameters such as alloy content, number of nucleant particles (N_V^P), decreasing superheat and critical undercooling for heterogeneous nucleation (ΔT_n).

Casting geometry is also an important issue. Fredriksson and Olsson [33] showed that the columnar range increases with increasing height or width of the casting and the width factor is more important than the height. Flood and Hunt [32,34] also showed that flattening the thermal gradient in the bulk by convection reduces the columnar range by increasing the bulk undercooling and promoting equiaxed growth.

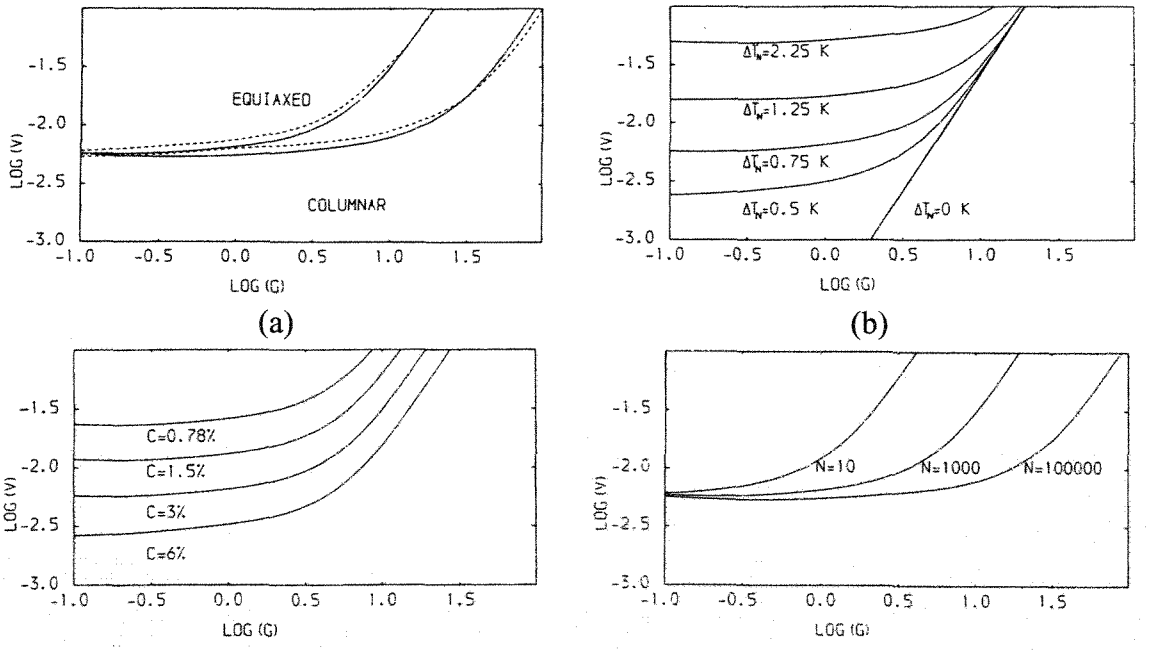

Figure 2.11: Plots of growth velocity (V) versus temperature gradient (G) for Al3%Cu to suppress the fully equiaxed growth [34]:
(a) N_V^P=1mm^{-3} and ΔT_n=0.75K showing columnar and equiaxed regions,
(b) N_V^P=1mm^{-3},(c) N_V^P=1mm^{-3},ΔT_n=0.75K, and (d) ΔT_n=0.75K

2.2 Grain refinement of Al-Si alloys, a review

Normally, aluminum alloys, form coarse, equiaxed and columnar crystals (grains) during solidification. The degree of coarseness or the length of columnar crystals depends on the solidification and casting parameters including pouring temperature, liquid thermal gradient in the mold, and alloying elements. It should be noted that all the common alloying elements added to aluminum reduce the grain size somewhat. Generally, the more soluble are the elements, the greater the refinement.

Close control of the as-cast structure is a major requirement in the production of premium quality aluminum products. A fine-grained structure provides a number of technical and economical advantages, including improved mechanical properties, increased casting speed, reduced cracking and better post solidification deformation characteristics (It should be pointed out that the properties in alloys which contain a large eutectic fraction, such as Al-Si alloys, are dependent on both the grain size and eutectic structure).

There are three principal methods for achieving grain refinement in Al alloys [26]:
a) Rapid cooling during solidification (chill grain refinement)
b) Agitation of the melt as for instance during semi-solid metal processing,
c) Addition of a grain refiner to the melt.

In the first method, a fine grain structure is formed by varying the solidification conditions such as cooling rate and temperature gradient in the casting. This is due to shortening of grain growth during the solidification process. In the second method, grain refinement is achieved by mechanical or electromagnetic agitation, forced convection, by breaking up the dendrites in the semi-solid state. The fragmented parts are transported into the bulk and become effective nucleants. This is the type of refinement mechanism when stirring is applied during the formation of the semi-solid structure. By far, the most successful method to control the grain size is to introduce into the melt particles that nucleate new crystals during solidification.

Each grain contains a family of aluminum dendrites originated from the same nucleus. Dendritic arm spacing (DAS) is determined by the cooling rate through the mushy zone, with slower cooling resulting in larger values of DAS. The grain size in aluminum foundry alloys varies between 1-10 mm, DAS values vary from 10 to 150 μm and the eutectic silicon may be found in plates up to 2 mm in length or spheres of less than 1 μm in diameter [24,35,36].

2.2.1 Principles of grain refinement

Generally molten aluminum foundry alloys contain a multitude of foreign particles and substrates ranging from oxides and other inclusions to the wall of the mold itself. It is well known that not all these particles in a melt are equally effective nucleants.

The basic requirements which must be fulfilled in order to obtain a good grain refining in aluminum alloys are as follows [32,36]:

- To promote the formation of crystals on a nucleant, the interface between the nucleant and the liquid should be of higher energy than that between the nucleant and the crystal solid (lattice compatibility). One way of maximizing this condition is to provide a nucleant-crystal relationship that is associated with a good crystallographic fit between the respective crystal lattices and this could be achieved if at least one atomic plane in the nucleus be similar to one in the nucleant. Then very close atomic matching can occur across the interface separating the two as shown in Figure 2.12.
- Minimizing the atomic mismatch will promote a low surface energy (lattice disregistry less than 10-12%) (Appendix A).
- Wettability of the nucleants by molten metal. As discussed in section 2.1.1.2, activation energy barrier (ΔG_n^o) and also critical number of atoms (n°) are highly dependent on the wetting angle and the smaller value is better. Therefore, a good grain refiner should have a low contact angle with the molten metal being refined.
- Particles must be stable in the melt and not undergo some other reaction that would destroy the active substrate.

- A high enough growth restriction factor (GRF)
- Grain refiners must be effective in small amounts and they should not impart any deleterious properties to the alloy being refined

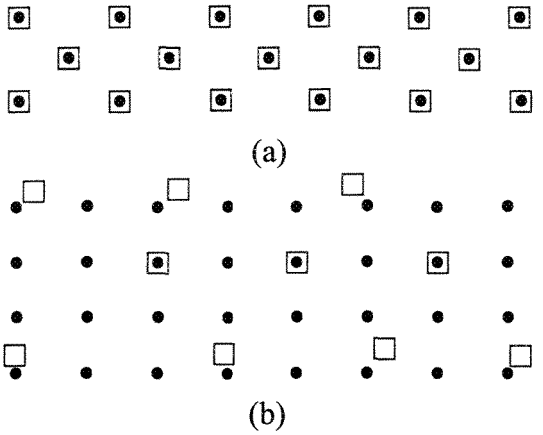

Figure 2.12: Two possible relationships between the atomic arrangements on a crystal plane of an aluminum nucleus □ and the atoms of a substrate ●. Case (a) is excellent grain refiner while in case (b) there is very poor nucleation due to a high interfacial energy between aluminum and the substrate [36]

2.2.2 Grain refining behavior

2.2.2.1 Nucleation without addition of grain refiner

Hypoeutectic Al-Si alloys have a large fraction of primary α-Al particles and the quality of the casting mainly depends on their size and distribution. In untreated alloy, there are limited numbers of nucleating particles having poor nucleation potency, need a high degree of undercooling (~3-4°C) before becoming active.

The first part of a cooling curve for pure aluminum alloy is shown in Figure 2.13a [24]. This figure clearly shows the melt needs to be undercooled before nucleation of new α-Al particles can occur. As the temperature decreases, the nucleation rate rises exponentially. Simultaneously, with temperature decreasing, growth will commence on each formed nucleus and the evolution of latent heat retards the cooling until a minimum temperature is reached, thereafter the temperature rises again to its normal growth temperature, i.e., recalescence. By the time recalescence ends, the nucleation process is

completed and no more new α-Al particles form. From this point on, solidification proceeds by growth of the primary particles leaving the unused nucleants redundant (Figure 2.13b). Yen et al. [37] by integration of the first derivative curve and magnifying and measuring the area above the base line (zero line), the positive segment of the derivative curve, obtained a correlation between this area and grain size and called it "liquid peak parameter, LPP". The larger is the area, the greater is the grain size.

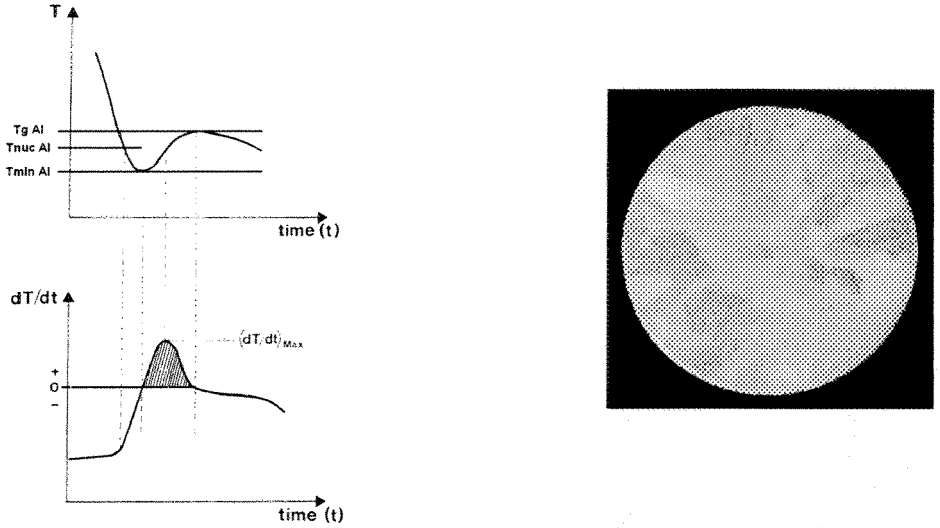

(a) (b)

Figure 2.13: (a) First part of a cooling curve and related derivation obtained from pure aluminum melt, (b) coarse-grained macrostructure with no addition of grain refiner [24]
$Tnuc_{Al}$: Start of nucleation. It is called the "potency" of the nucleating particles present in the melt.
$Tmin_{Al}$: At this point, the newly nucleated crystals have grown to such an extent that the latent heat liberated balances the heat extracted from the sample. After this moment the melt is actually heating up to the steady state growth temperature.
Tg_{Al}: Steady state growth temperature of the melt under the cooling conditions prevailing

2.2.2.2 Addition of grain refiner to a melt

As discussed above, nucleation on particles naturally present in the Al alloys needs ~3-4°C undercooling to become active which also results in a coarse grained structure in these alloys. If however, particles of high nucleating potency are added, like titanium-boride particles, a cooling curve such as Figure 2.14a will be resulted [24].

As seen in Figure 2.14a, nucleation starts above the steady state growth temperature. This means the new crystals can form, not only at the first contact of the melt with the cold walls of the mold, but also in the liquid ahead of the growing crystal across the bulk liquid from the walls to the center of the casting. Also the liquid peak area is less than that in Figure 2.13a which is an indication of lower grain size.

Grain refinement is now possible, provided that the liquid is constantly undercooled so that the new equiaxed crystals formed in the liquid can grow at such a rate that they impinge upon each other and form a continuous dendritic network. It is also important to note that due to the higher nucleation temperature, nucleation time is much longer than the previous condition and consequently more nuclei could form in the bulk. This was obviously the case in the sample shown in Figure 2.14b, to which an Al3Ti3B master alloy was added. The master alloy contains $TiAl_3$ and TiB_2 particles, which have effectively nucleated a great number of primary α-Al particles.

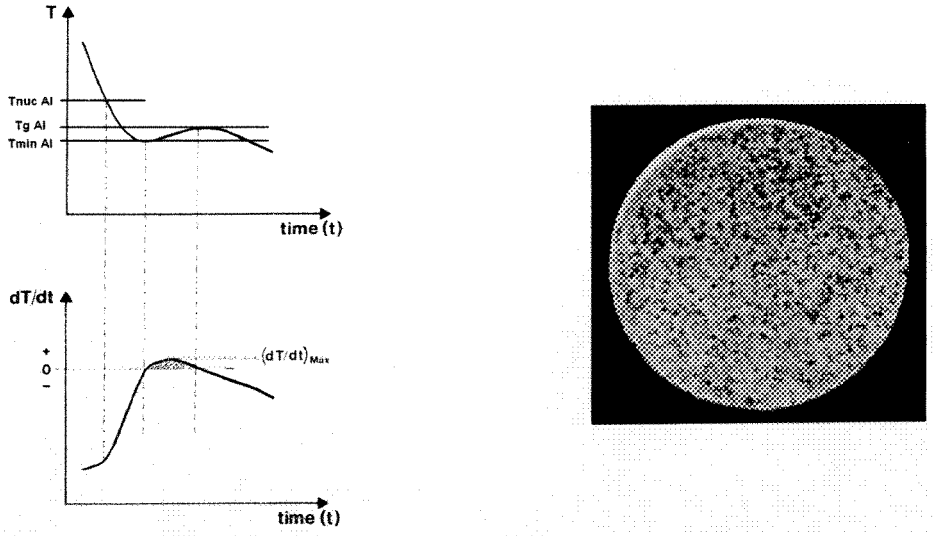

(a) (b)

Figure 2.14: (a) Cooling curve and its derivative from pure aluminum melt to which titanium boride particles have been added. The nucleation temperature ($Tnuc_{Al}$) here is above the actual growth temperature of the melt. Recalescence shows a low value of (dT/dt) Max, indicating a grain refined sample, (b) macrostructure of the sample after addition of titanium boron particles [24].

2.2.2.3 Addition of effective grain refiner

As shown in Figure 2.14a, the alloy still shows undercooling and since recalescence has a direct relation with grain size, it indicates for further refinement. Such alloys, still more effective nucleating particles, as is the case when using master alloys with an excess of titanium together with the boride particles. Figure 2.15a shows the cooling curve for an AA1000 type alloy after addition of Al5Ti1B master alloy [24].

As it could be seen, the nucleation temperature starts at higher temperatures compares to the Figures 2.13 and 2.14. Higher nucleation temperature means that more nucleants could be activated in the melt at the same time. Also there is no minimum and recalescence before the growth temperature and liquid peak area disappears. In this case nucleation occurs widely across the bulk of liquid, i.e. copious nucleation occurred. In another word, the mean free distance between the nuclei is reduced and the heat flow is no longer directional and finally equiaxed structure forms.

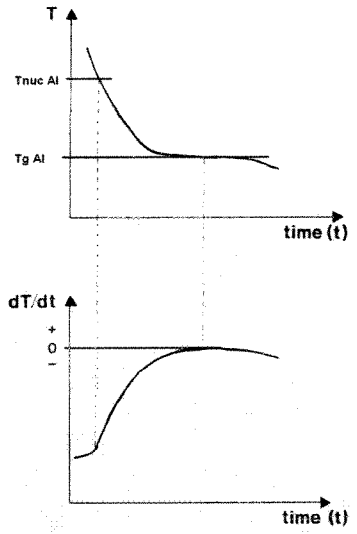

Figure 2.15: Cooling curve from the wall of a sample of alloy AA1050 after addition of 0.02% Ti in the form of Al5Ti1B [24]

2.2.3 Chilling refinement

If a melt is rapidly cooled (chilled), the rate of heat extraction can greatly exceed the rate of heat generated by the freezing process (latent heat of solidification). As a result, the liquid undercools as its temperature falls below the liquidus temperature. If this

undercooling is sufficient, the full range of heterogeneous nucleants present in the liquid can become active. This multiple nucleation results in a fine as-cast grain size.

According to Gruzleski [36], chilling can result in grain sizes in the 0.1-1000 μm range. The finest size is achieved by rapid cooling which is only possible in very thin sections by using rapid solidification techniques. While the range of grain sizes achievable by chilling is greater than with any other grain refinement technique, the method itself is of only limited applications in practice, since the rate of cooling is determined by the molding method used. This in turn is usually determined by considerations other than grain size; such as economics, casting size, number of castings to be produced, etc. Moreover, the rapid chilling of large castings produced by any method is usually impractical due to the amount of latent heat which must be removed. At best, some local control of grain size can be achieved by the insertion of chills in critical locations.

The mechanical properties of the as-cast alloy are improved with decreasing the dendrite arm spacing, DAS. Figure 2.16 illustrates the DAS values and resulting mechanical properties reported for 356 alloy [36,38]. A typical result is shown in Figure 2.17 [39]. The strength of the alloy is high near the chill, and the toughness is good. As the cooling rate is decreased (larger DAS values), the ultimate strength falls some what. Although this reduction is not disastrous, the fall continues until it reaches the yield stress. Thus failure is now sudden, without prior plastic deformation. The alloy is now brittle, as is confirmed by the elongation results which are close to zero [39].

Smaller DAS values are caused by faster solidification rates which are usually associated with finer as-cast grain sizes, but it was claimed that DAS is more effective than the grain size on the mechanical properties [36]. A smaller DAS also restricts nucleation and growth of interdendritic phases such as iron intermetallics. The highly deleterious effect of iron impurity in aluminum alloys is attributed to the extensive plate-like morphology of the iron-rich phases. Vorren et al. [40] have measured the length of iron-rich plates as a function of DAS. As expected, the two are closely related; as DAS reduces the plates become smaller (Figure 2.18). Also it can be seen that the strength and toughness are increased. In Al-Si alloys, chilling can cause partial modification of the silicon phase and

this effect can contribute to the increase in mechanical properties (quench modification which will be described later) [36].

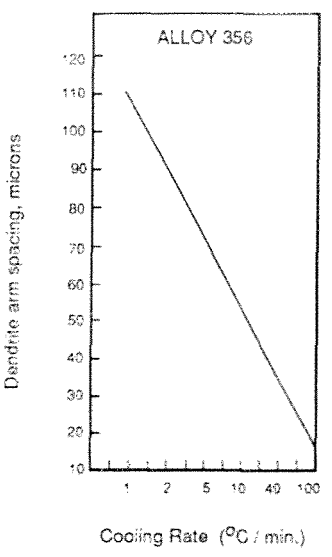

(a)

Figure 2.16: Variation of the DAS of a 356 alloy with cooling rate and its mechanical properties [38]

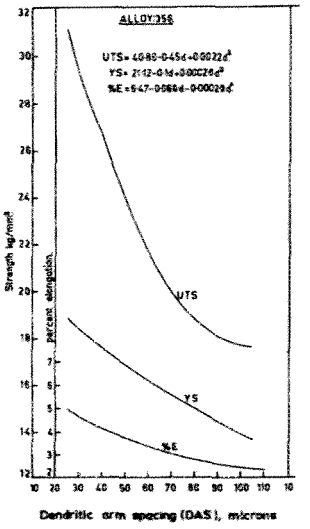

(b)

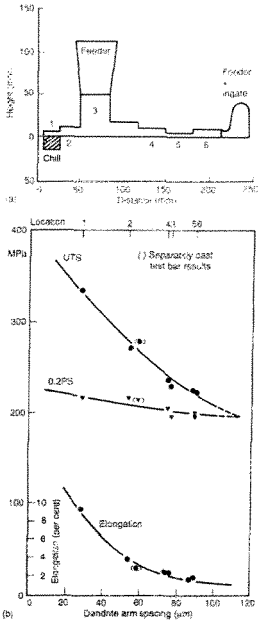

Figure 2.17: Variation of mechanical properties with DAS, Al7Si0.4Mg alloy [39]

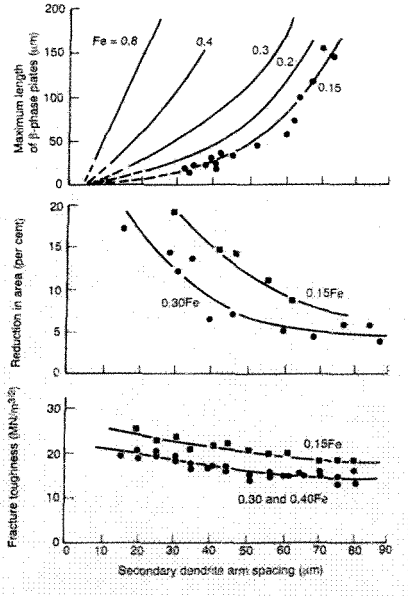

Figure 2.18: Properties of Al7Si0.4Mg alloy as a function of dendrite arm spacing [reproduced from 40]

2.2.4 Chemical grain refinement

As mentioned, in most cases, it is not possible to remove the heat content rapidly. Medium to large size castings can not be significantly refined by means of chilling, and therefore other form of grain refinement is essential.

Chemical grain refinement involves the addition of special substrates to act as nucleants or react with other elements in the melt to form solid nucleant particles. A fine grain size is promoted by the presence of an enhanced number of nuclei, with solidification proceeding at very small undercooling. Furthermore, chemical grain refinement is advantageous to mechanical properties, particularly those that are sensitive to hot tearing and porosity.

The chemical grain refinement of aluminum and its alloys has been practiced for over 50 years, mostly by primary aluminum producers in ingot casting. The foundry industry has more or less borrowed the techniques developed by the primary producers. However, the researches showed that the best grain refiners for wrought alloys are not necessarily the best for foundry alloys [41].

2.2.4.1 Titanium grain refinement

As it is seen from Al-Ti phase diagram (Figure 2.19a), the peritectic reaction in this diagram is critical to the refinement of aluminum alloys. $TiAl_3$ particles will react with the liquid phase on cooling below 665 °C according to the peritectic reaction:

$$\text{Liquid} + TiAl_3 \rightarrow TiAl_3 + \alpha \text{ (solid)} \qquad (2.20)$$

Consider a $TiAl_3$ particle in contact with pure aluminum, or a commercial alloy of low titanium content. Shortly after the addition of a master alloy, a diffusion field will be established in the vicinity of the $TiAl_3$ crystal. At the surface of $TiAl_3$, the titanium content in the liquid metal is about 0.15% (the concentration away from the particle in the bulk of the metal phase is much lower). When the melt is cooled, because titanium raises the melting point of the metal, and because $TiAl_3$, is an extremely effective nucleant, solid aluminum will form at the surface of the $TiAl_3$ particle at temperatures above the melting

point of the bulk metal. Once solid has formed, however, the $TiAl_3$ particle becomes engulfed in the solid phase, and further growth becomes limited by the diffusion of Ti from $TiAl_3$ through the shell of solid aluminum. Normal dendritic growth can not occur because the solid metal nucleus is still above the growth temperature of the (low titanium content) bulk metal (Figure 2.19b) [42].

The α-Al phase is a dilute solid solution of titanium in aluminum. It has a face centered cubic (FCC) crystal structure, a lattice parameter close to that of pure aluminum and, therefore, is an ideal heterogeneous nucleant. As a result of this mechanism, the number of nuclei and hence the final as-cast grain size is related to the microstructure of the original master alloy.

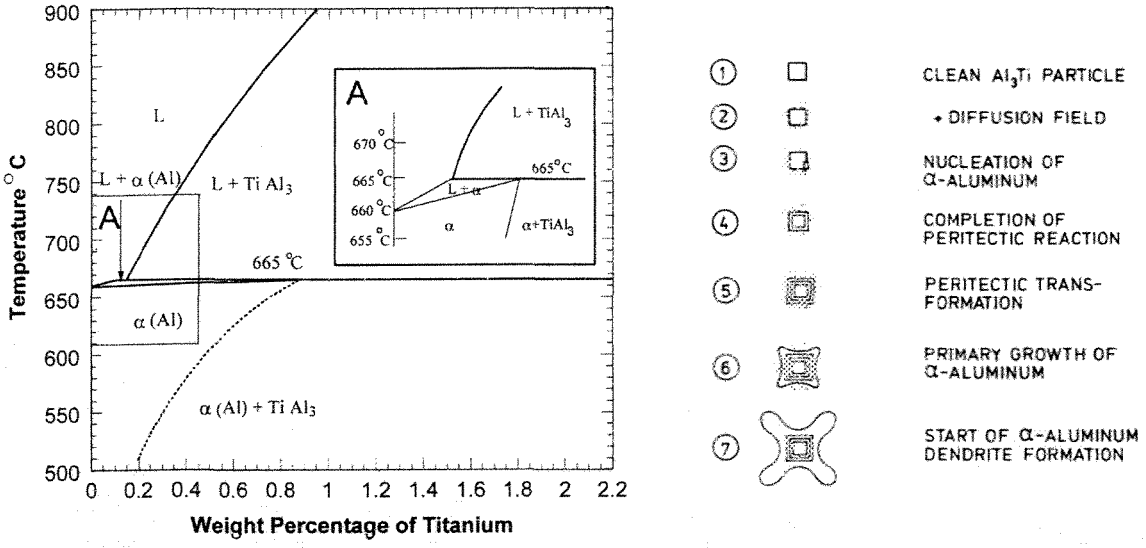

(a) (b)

Figure 2.19: Grain refinement mechanism due to Ti addition: (a) Al rich end of the Al-Ti phase diagram [43], (b) steps of α-Al rings formation on unreacted particles of $TiAl_3$ [24]

St.John and Hogan[44], Arnberg et al. [45-47], Blake and Smith[48], Hadlet et al.[49], McCartney [21,50], and Guzowski et al.[42] have all reported extensively on aluminide morphology using optical microscopy, SEM with deep etching and TEM of thin foils. They have found that $TiAl_3$ develops a minimum of 3 different morphologies, depending on the manner and the temperature history of the master alloy (Figure 2.20):

- Slow cooling from high temperature produces plates or "flakes" with a faceted dendritic growth form.
- Rapid cooling of a saturated solution from high temperature forms "petal" like shapes;
- If the master alloy is produced by salt reactions at a relatively low temperature, the faceted "blocky" aluminides form.

They found that the grain refining response of the alloy depends on the morphology of the titanium aluminide. Blocky crystals tend to act fast, but their effect fades quickly. Petal, and flake, or plate-like structures act more slowly, but their grain refining efficiency improves with time and lasts longer. The blocky structure is important for aluminum producers who add grain refiner in rod form. When furnace additions are made the longer-lasting plate-like structure is preferred.

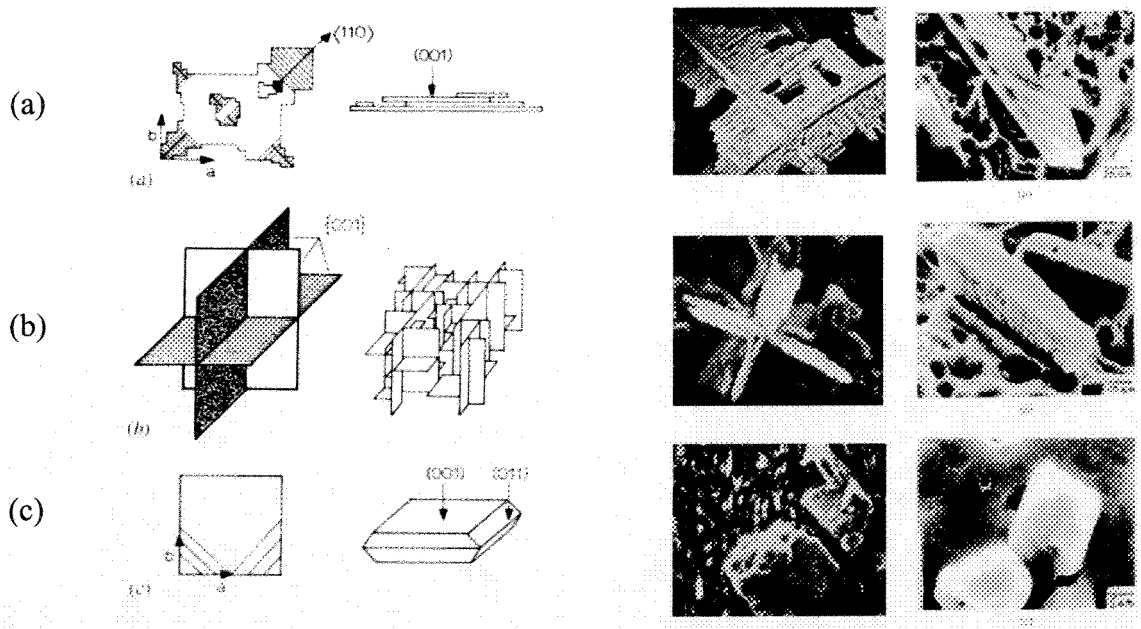

Figure 2.20: A: Schematic drawings of the different morphologies of $TiAl_3$ crystals: (a) flake-like crystals, (b) petal like crystals, and (c) blocky crystals [42,46]. B: SEM micrographs of deep etched samples showing different morphologies: (a) flaky aluminide (b) petal like aluminide (c) blocky aluminide [48-50]

Technically, an Al-Ti alloy which contains many small $TiAl_3$ particles will be a better grain refiner than one which contains fewer but larger $TiAl_3$ particles. In fact, this is one of the difficulties associated with the use of master alloys; the effectiveness depends on the microstructure of the alloy and can vary from batch to batch and from supplier to supplier. Al-Ti master alloys do not refine foundry alloys as efficiently as wrought alloys. Sigworth and Guzowski [41] suggested that the effectiveness of the $TiAl_3$ nuclei may be poisoned by a silicon titanium compound which will be described later.

2.2.4.2 Boron grain refinement

Many grain refiner manufacturers have introduced a series of Ti-based grain refiners such as Tital (Ti-Al), TiCAR (Ti, C, Al), TiBOR (Ti-B-Al), while neglecting Al-B alloys, although the effectiveness of Al-B as a grain refiner understood and reported as early as in 1980 [51]. Lu et al. [51] has reported the effect of different master alloys on the grain size of small castings made from 356 and Al-5%Si alloys. Their results for 356 alloy, which are reproduced in Figure 2.21 show that interestingly Al-B master alloy is more efficient grain refiner than both Al-Ti and Al-Ti-B alloys. As evident, boron addition tripled grain refinement. Such results were reproduced by Sigworth and Guzowski [41].

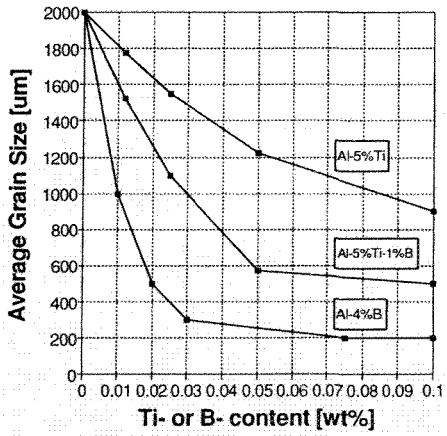

Figure 2.21: The beneficial effect of boron on the grain refinement of 356 alloys [reproduced from 51]

The reason for such efficient refining ability should be better understood by examining the Al-B binary diagram (Figure 2.22). As seen, eutectic reaction leads to the formation of the α-Al plus AlB_2, an active nucleant for the aluminum alloys:

$$\text{Liquid} \rightarrow AlB_2 + \alpha \text{ (solid)} \qquad (2.21)$$

The eutectic reaction takes place at temperature just below the equilibrium freezing temperature of pure aluminum (660.6°C) and the resulted AlB_2 particles could act as effective nucleants especially for Al-Si hypoeutectic alloys with melting points well below 660°C. It is important to note that this reaction will not be able to nucleate pure aluminum. In the case of the Al-Si alloys, these nucleants are efficient since the melting point for the hypoeutectic Al-Si alloys are much lower than 660°C [52]. Therefore, the most important factor for boron efficacy is the dissolved Si in the alloy; however in the absence of Si, it is not a refiner.

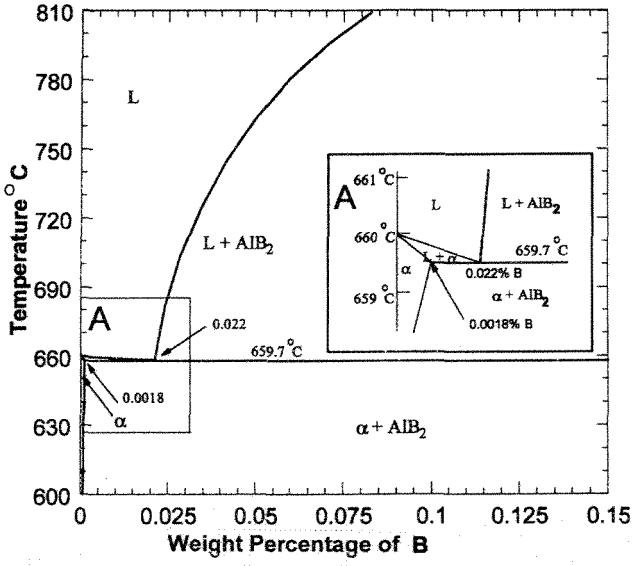

Figure 2.22: The Al rich end of the Al-B phase diagram [43]

Tøndel et al. [53] confirmed that boron is the most efficient grain refiner and introduced an alternative master alloy based on Si-B for the refining of the Al-Si foundry alloys. Silicon takes about 1%B in the solution which means that when silicon dissolves in the Al melt, B is uniformly dispersed at the same time. Moreover, the grain refining effects were claimed to be:

- independent of holding time (no fading)
- unaffected by remelting treatments (permanent effect)
- almost independent of cooling rate in the range of 0.5 to 15°Cs^{-1}
- efficient for Al-Si alloys with Si content between 5 and 11%

However, the procedure of introducing boron into the alloy is so important, i.e., size and shape of the boron particles. Some Al-B master alloys have large particles and sometimes form large agglomeration of AlB_2 or AlB_{12} particles which could not be dissolved quickly in the melt (considering the solubility limit) and the other reason is the impurities in the master alloy.

2.2.4.3 Titanium-boron refinement

Mondolfo et al. [54-56] have suggested that Al-Ti-B master alloys perform better due to the shift in the onset of peritectic towards lower Ti in the Al-Ti phase diagram in the presence of boron (0.01%B) and as a result ensuring the thermodynamic stability of $TiAl_3$ particles at low level of titanium addition (0.05%Ti).

The importance of a combination of boron and titanium in grain refining is well established with the application of LiMCA (Liquid Metal Cleanliness Analyzer) (Figure 2.23). It is clear from this figure that the highest and lowest particles counts belong to the addition of Al5Ti1B and Al6Ti master alloys respectively. When Al6Ti is present in the additive, the inclusion content remains almost constant till the nominal Ti level reaches 0.12%wt. An increase in Ti above this value changes the particle count drastically due to thermodynamically stabilizing of $TiAl_3$ and causing a linear increase in the count with increasing Ti content [57]. It is important to note that by addition of boron in the form of Al5Ti1B or Al5Ti0.6B, the critical titanium level shifts to lower titanium level.

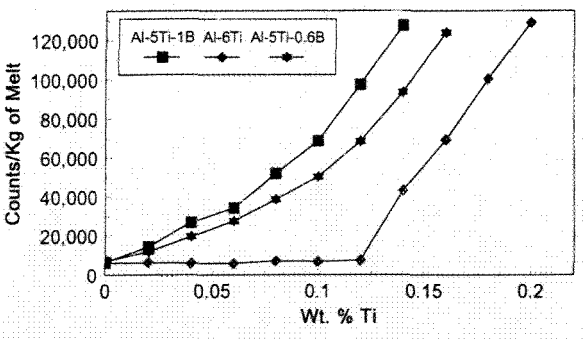

Figure 2.23: Particle counts vs Ti content for different master alloy [57]

The role of boron in the Al-Ti-B system is less clear. As discussed above, it has been suggested that boron acts to shift the onset of peritectic reaction to the lower titanium

level. Mohanty and co-workers [52,58], by introducing TiB_2 particles into 99.7%Al melts with a gas injection technique, found that TiB_2 particles on their own, do not nucleate α-Al and they proposed that in the absence of excess Ti, TiB_2 particles are pushed to the grain boundaries and are not found in the grain centers where nuclei would be expected. They suggested that TiB_2 particles only activate grain refining if there is Ti dissolved in the melt and that as little as 0.01%Ti is required for the TiB_2 particles to become potent nucleation sites. They have stated a hypothesis where at lower Ti levels than peritectic, Ti atoms diffuse towards the TiB_2 particles, and form a thin layer of $TiAl_3$ on the surface and this layer activates the nucleation mechanism.

Sigworth [59] disagreed with the above mentioned theory and remarked that the mechanism was thermodynamically impossible. Sigworth postulated that in pure aluminum, TiB_2 particles are not effective nucleants while Karantzalis [60] showed that TiB_2 particles are potent nucleants in Al-Cu, Al-Si and Al-Ti alloys. The enhanced grain refining action in Al-Si, Al-Cu, and Al-Ti alloy melts with TiB_2 particles was claimed to be a result of constitutional undercooling and GRF factor which enable the borides to become active nuclei. Since GRF is high in the Al-Ti system, small addition of Ti causes observation of $TiAl_3$ on the TiB_2 particle surfaces due to higher GRF and lower cooling of the casting.

As mentioned for the Al-Ti master alloys, the grain refining ability of AlTiB seems to depend on the microstructure of the master alloy as well, i.e., size, distribution, and morphology of the intermetallic phases [42,61,62]. Figure 2.24 shows the TiB_2 distribution in desirable and undesirable Al5Ti1B refiners. Figure 2.25 illustrates some typical morphologies found in different Al-Ti-B grain refiners. Poor grain refiners contain blocky $TiAl_3$ crystals (Figure 2.25a), similar to those found in binary Al-Ti master alloys and as a result, boron in the master alloy has not influenced the effectiveness of $TiAl_3$.

The samples which have the ability to give a very fine grain size at short holding times contain a variety of different aluminide structures. In this case the $TiAl_3$ surface was covered with boride particles presumably TiB_2 or $(Ti,Al)B_2$.

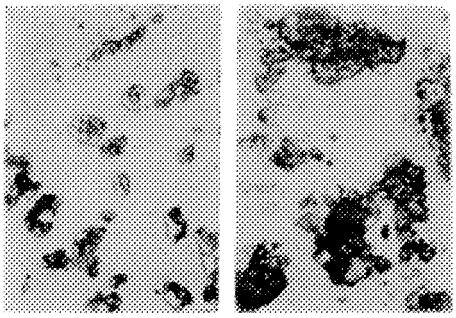

Figure 2.24: TiB_2 distribution in Class1 and Class2 Al5Ti1B rod [62]

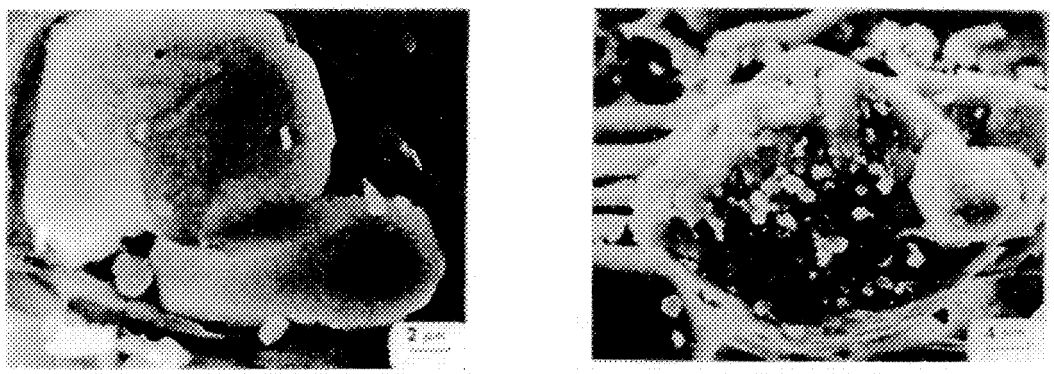

(a) (b)

Figure 2.25: Morphologies of some intermetallic phases found in AlTiB grain refiners
(a) blocky $TiAl_3$ crystals found in a poor master alloy,
(b) duplex aluminide consisting of $TiAl_3$ studded with borides [42]

It is clear that borides found on the surface of $TiAl_3$ crystals would be in an especially favorable situation to nucleate new grains of aluminum. At the surface of $TiAl_3$, the titanium content in the liquid should be near the peritectic solubility of 0.15 %. The boride-coated duplex particle should therefore be an extremely potent nucleant (combining the nucleating potential of $(Al,Ti)B_2$ at high dissolved Ti contents , and the ability of $TiAl_3$ to nucleate grains at a temperature 5° above the alloy liquidus). The refiners containing duplex particles are fast-acting and long-lasting. The $TiAl_3$ portion of the duplex particles would dissolve with time, thereby increasing the dissolved titanium content in the melt and

freeing boride crystals to become effective nuclei. The desired condition for the formation of the duplex particles in the master alloy, together with the $AlTi_3$ morphology, are dependent on the holding time of the liquid before casting (Figure 2.26) [42].

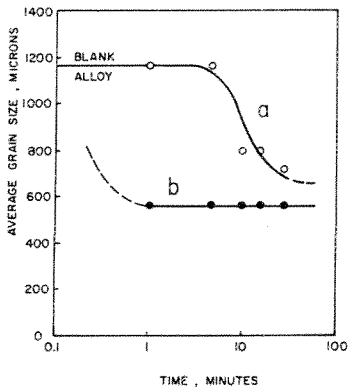

Figure 2.26: The effect of holding time on grain refining response (Al5Ti0.2B alloy added to 99.7% Al with 0.01% Ti addition level): (a) alloy at the end of the salt reaction, (b) alloy held 60 Min at 825 °C [42]

Although high boron containing grain refiners appear to offer many advantages, they have a number of drawbacks as given below [41,63]:

- The AlB_2 particle is designed to dissolve and react with Ti to form TiB_2 (density of 4.5 g/cm3), which settles to the bottom of the furnace and agglomerates. The long term use of B will cause boride sludge deposits to accumulate in the furnace. If very large agglomerates are allowed to form, these will be brought back into suspension and can cause filter blockage or inclusion problems in the casting.

  In some experiments, fading was investigated with various types of grain refiners and concluded that agitating the melt after holding period can activate the intermetallics and their count revert back to a value close to the original levels even after 6 hours especially for AlTiB master alloy. The particles settle on holding but was redispersed on subsequent agitation [57,64,65].

- The poisoning effect of the refiner is a more serious (though less common) problem since it can occur very quickly and can not generally be reversed. Chemical poisons (most notably Zr) are believed to work by substituting Ti in the $TiAl_3$ or TiB_2

structure, thus forming $(Zr,Ti)Al_3$ or $(Zr,Ti)B_2$. These have less favorable lattice registries with aluminum and thus the nucleation potential is reduced.

- Third, when the Sr content of the alloy is low (<0.010%) and when large B additions were made (0.02% or more), a partial or complete loss of refining and modification was observed. This may be caused by an interaction between Sr and B to form stable boride particles, SrB_6 .

Many experiments have been carried out to identify the best ratio of Ti:B in AlTiB master alloys and till now there is still confusion regarding the type and addition level of master alloy that is most suitable for grain refinement of hypoeutectic Al-Si alloys.

For refinement assessment, performed on A356 and Al-7Si alloys grain refined with Al5Ti1B and cast into a KB hockey puck mold, Apelian et al. [66] defined 500μm as a very fine grain size and 200-300μm as an extremely fine grain size (the influence of cooling rate makes it difficult to compare grain size obtained by different workers even for the same refiner addition level). Sigworth & Guzowski [41] concluded that the optimum results can be obtained for a ratio of unity (3Ti-3B) which is more effective than Al5Ti1B for alloy 356.

Boot et al. [67], in their experiments to identify the best grain refiner for wheel casting, found that Strobloy (5Sr1.5Ti1.3B) or TiB Alloy (1.6Ti1.4B) produced casting with minimum internal porosity and hot tearing defect. Bondhus et al. [68] with experiments on Al-Si hypoeutectic alloys have shown that TiBloy has many advantages compared to conventional grain refiners. Spittle & Keeble [64] examined a number of grain refiners and concluded that with increasing Ti:B ratio , the tendency to fade decreased and the grain sizes fell. Gruzleski [43] suggested that Ti/B ratio must be greater than 2.22. A Ti/B ratio exceeding 2.22 implies that the melt must contain free titanium for grain refinement to be effective.

2.2.5 Fading effect

Since only a small amount of titanium is added, it is obvious that the grain refiner particles will dissolve, and the grain refining ability will decrease with time. On the other hand, in foundries due to the furnace and production specifications, melt is often held for long periods of time without any agitation and this also leads to settling of the grain refiner particles. This phenomenon is known as fading. Hence, fading mostly relates to both dissolution and sedimentation of the nucleants due to the density dissimilarities. For example, densities of $TiAl_3$ and TiB_2 particles are 3.35 and 4.5 g/cm^3 respectively while for aluminum melt, it is 2.3 g/cm^3.

Figure 2.27a shows the chemical composition variation of Ti in the case of a 20-120min contact time [65]. The highest concentration of Ti is found at the bottom of the samples and at the longest contact time, e.g. 120min. The grain size analysis is displayed in Figure 2.27b. The average grain size increases with longer contact time and greater distance from the bottom of the samples. It is worth mentioning that by stirring the melt, grain refiner particles become active again.

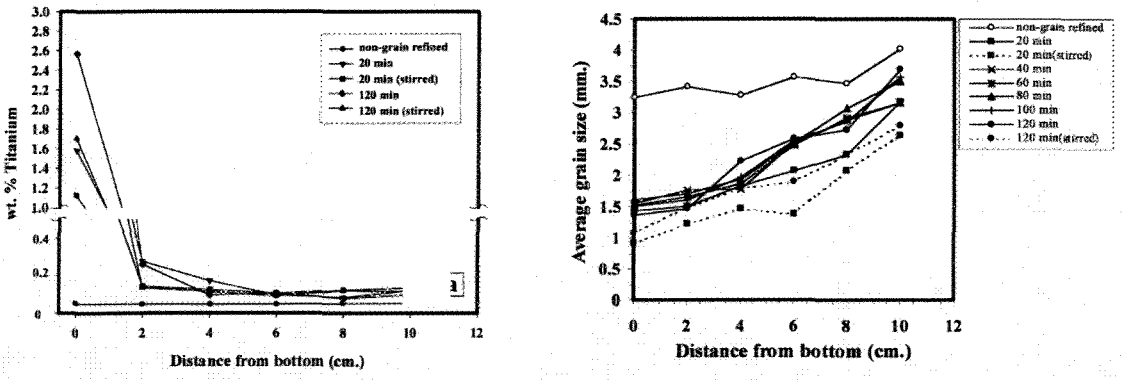

(a) (b)

Figure 2.27: (a) Ti variations of 356 alloy grain refined with 2% Al3Ti0.5B, (b) average grain size analysis [65]

Figure 2.28 shows the fading phenomenon in pure aluminum. Curve **a**, which shows the behavior of a binary Al-Ti master alloy addition, indicates that after holding for about 40 minutes, the grain size reverts to that of an untreated alloy. This figure also indicated that, if both Ti and B are used (curves **b** & **c**), not only the grain size is finer, but also the

fading time is significantly prolonged. This is particularly important in large furnaces which have relatively low rates of throughput.

Settling and thus fading are also dependant on the agglomeration of grain refining particles. For Ti & B containing grain refiner, agglomeration of TiB_2 particles is partly responsible for the fading effect. TiB_2 particle agglomerates are thought to be caused by a number of factors, including the presence of halides (e.g. chlorides), particle collision, attachment to oxide films, and surface adhesion by the aluminides and growth in filters [69]. Fading phenomenon was reported to be eliminated in the case of grain refining with boron due to AlB_2 particles [53] because of better distribution in the master alloy and lower density, 2.5-3.1 g/cm^3, compared to other grain refiners.

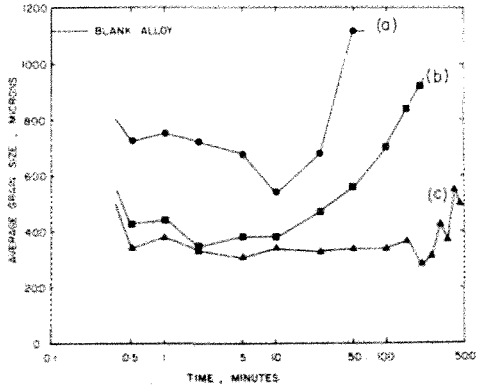

Figure 2.28: Grain refining ability in 99.7 %Al with time [42]:
(a) 0.01%Ti added as a 5.35% Ti master alloy, (b) 0.01%Ti added as a 5.4%Ti-0.034%B master alloy, (c) 0.01%Ti added as a 5.0% Ti-0.2%B master alloy

2.2.6 Effects of alloying elements on grain refinement

The chemistry of melt plays an important role in grain refining. Normally small additions of alloying or solute elements reduce the grain size. These are classified as "growth restricting elements" or growth hindering additions. This phenomenon could be explained in terms of constitutional undercooling which is a solute rich zone ahead of the growing solid in which the actual temperature is lower than the solidification temperature.

Kissling and Wallace [26] were the first to present the effect of alloying elements on the grain size of pure aluminum. They have shown that the most important alloying element for this purpose is Ti (Figure 2.29). Apelian [70] and Kori et al. [71] confirmed the effect of alloying elements on Al-7%Si alloy. As shown in Figure 2.30b, the growth restriction effect of alloying elements decreases with holding time and fades approximately after 10 minutes due to dissolution in matrix. However, the grain size with alloying elements is always lower than the original alloy.

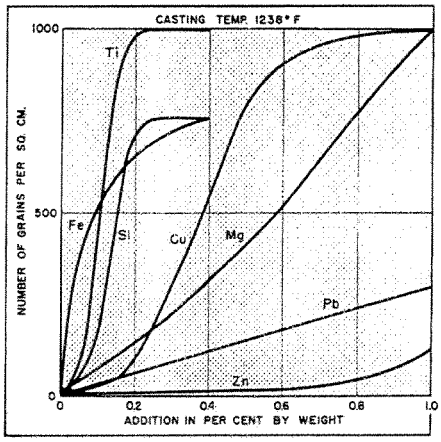

Figure 2.29: Effect of alloying elements on the grain size of aluminum [26]

Silicon has a remarkable effect on the effectiveness of Ti rich master alloys. It appears that the higher Si content found in foundry alloys somehow interferes with the grain refining effect of titanium and promotes that of boron (especially for %Ti/B ratios greater than three). By considering the Si-Ti phase diagram (Figure 2.31), it is possible that a titanium silicide ($TiSi_2$) coating forms on the surface of $TiAl_3$ crystals and thus poisoning the effectiveness of the nucleant [41]. In the ternary AlTiSi system, a peritectic reaction was proposed to exist with a complex stoichiometry of $Ti_XSi_YAl_{1-(X+Y)}$ [72].

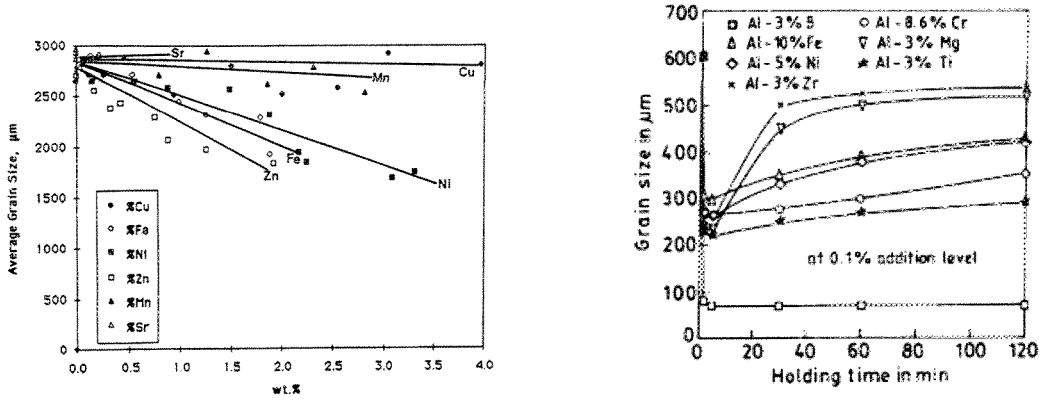

(a) (b)

Figure 2.30: Grain size analysis of Al7Si alloy: (a) with different addition levels [70], (b) grain refined with 0.1% of B, Cr, Fe, Mg, Ni, Ti and Zr [71]

This AlTiSi phase has been found in the center of α_{Al} grains and it is believed that for silicon contents of 6%, this reaction occurs at approximately 600°C just below the liquidus of 356 alloy. The grain size initially decreases with Si content up to 2-3%Si and thereafter continuously increases up to 8-9 % [64].

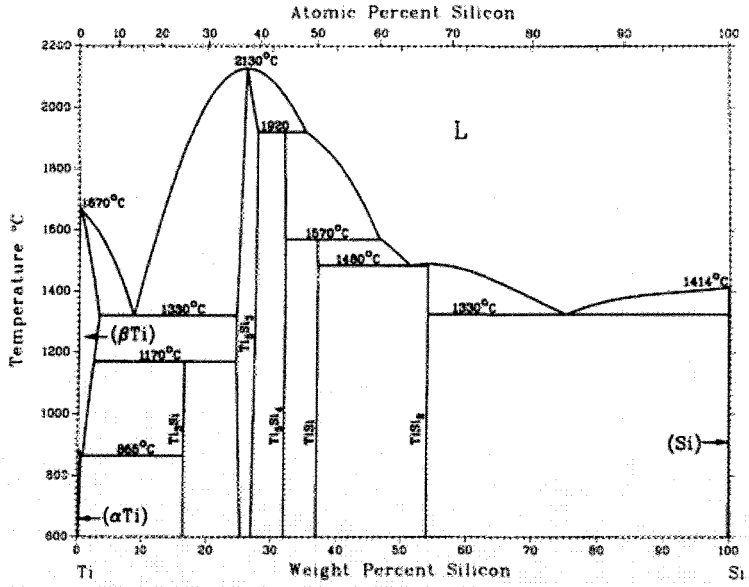

Figure 2.31: Phase diagram of the Si-Ti system [41]

By considering the solubility of Ti in aluminum, fading is virtually eliminated by adding Ti close to 0.15% (Figure 2.32). Industrial practice suggested that 0.1%Ti is required in foundry alloys to ensure good performance from master alloys. However,

excess addition can cause reduction of mechanical properties due to the formation of intermetallics [21,61-63,67].

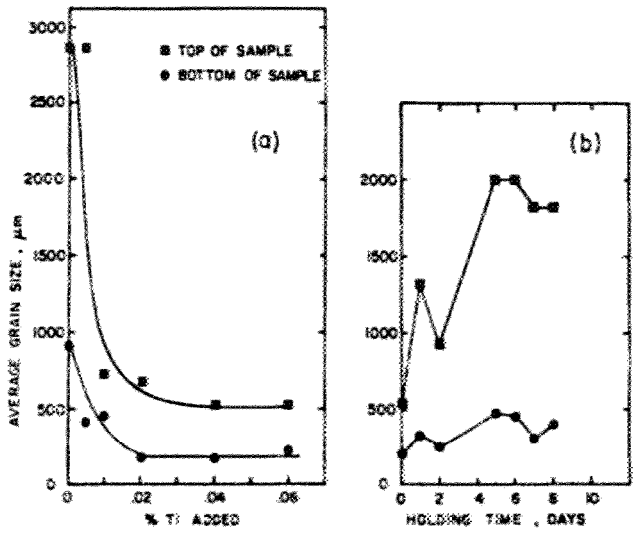

Figure 2.32: Grain refining response of an Al5Ti1B rod in a melt of secondary 319 alloy containing 0.15%Ti; (a) grain size five minutes after Ti addition; (b) grain size with holding after 0.06 % Ti addition (total %Ti in the alloy is 0.21 %) [41]

Figure 2.33 clearly shows the effect of alloying elements on the grain size reduction in aluminum alloys. As could be seen, Mg and Ti appear to promote a fine grained casting and this is in line with the GRF concept.

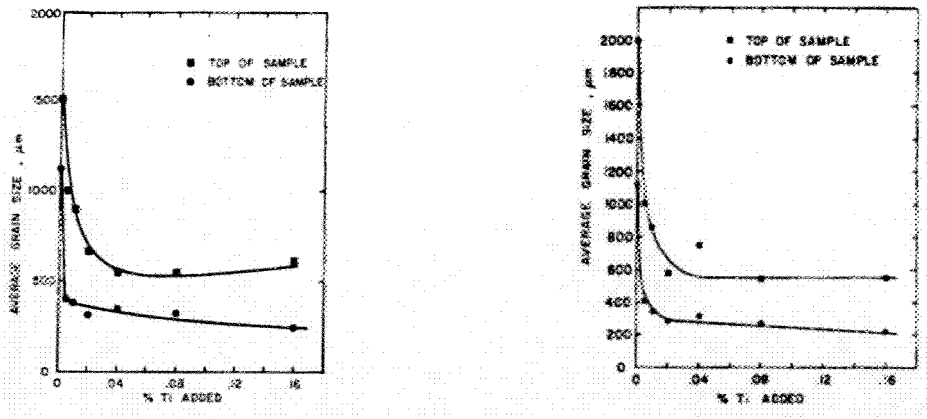

(a) (b)

Figure 2.33: Grain refining response of an Al5Ti1B master alloy rod in a melt of high purity Al7%Si alloy (a) and in a virgin 356 alloy (b) [41]

Sigworth et al. [41] concluded that silicon has a remarkable effect on the efficiency of Al-B (AlB_2 type) and B-rich Al-Ti-B master alloys. Boron does not refine the grains in wrought (low Si) Al-alloys, but is a powerful grain refiner when 5-7% Si is present. The presence of other elements in the Al-Si casting alloys (Cu, Zn, Fe, Mn, Ti, and Sr) seems to have little effect on the grain refining performance of the AlB_2, and $(Al,Ti)B_2$ crystals.

Cooper et al. [61] summarized the characteristics of a range of grain refining master alloys, Table 2.4. This has enabled a better understanding of the nucleation of α-Al, agglomeration behavior, poisoning tendency and fading characteristics.

Table 2.4: Some characteristics of grain refiners [61]

Particle	Density (gr/cm3)	Stability	Fading	Master alloy
TiB_2	4.52	Tm=2952°C high stability	Significant after several hours due to agglomeration	Al5Ti1B Al3Ti1B
$TiAl_3$	3.35	Dissolve rapidly depends on the Ti in solution	Not applicable as phase dissolve in the melt quickly	Al5Ti1B Al3Ti1B AlXTi
AlB_2	2.55	Tendency to form TiB_2 if Ti exists in solution	Only if Ti exists, it would be rapid and it changes to TiB_2	Al4B
$(Al,Ti)B_2$	2.55<X <4.52	Tendency to form TiB_2 if Ti exists in solution	Low fade due to small particle size and low density	TiBloy

2.2.7 Effects of grain refining on properties

Grain refining has been associated with the formation of casting defects. It is generally believed that an increase in the level of grain refinement is beneficial for castability. The advantages of effective grain refinement are [21,36]:

- Improvement in soundness
- Reduced hot tearing tendency
- Distribution of second phases and microporosity on a fine scale
- Improved machinability as a result of better phases distribution
- Reduction in solution treatment time

- Improved appearance following chemical, electrochemical, and mechanical finishing
- Improved mechanical properties (and even uniform properties)

Only very limited data is available for the above mentioned properties for Al-Si alloys. The majority of research activities appear to have been concentrated on Al-4%Cu and it would be applicable to 200 series alloys. The Al-4%Cu alloys are largely single phase materials containing a minimum of eutectic. Although the results may be useful for 200 series alloys, but not to Al-Si alloys as they are quite different to Al-4%Cu due to high eutectic content.

- Hot tearing tendency

Under normal solidification conditions, aluminum alloys without grain refiners exhibit coarse structures. The coarse columnar grain structure is less resistant to cracking during solidification and post solidification cooling than a well-refined grain structure of the same alloy. This is because of reduced resistance to tensile forces at elevated temperatures which may be expected as a result of increased sensitivity to grain-boundary formation in coarse-grained structures.

The principal reason in which reducing grain size increases resistance to hot tearing is the lowering of the dendrite coherency point (DCP) [73,78]. However, in Al-Si alloys the combination of a large volume fraction of eutectic liquid and a relatively low coherency temperature means that foundry alloys with a Si content greater than about 5% exhibit a low cracking tendency compared to the Al-4.5Cu alloy. In Figure 2.34, the susceptibility to cracking is indicated by a hot tearing index of less than 50. This occurs in an Al-4.5Cu alloy with a grain size of approximately 350 μm to a grain size of approximately 1300 μm in an Al-4.5Cu-5Si alloy [32].

In the case of A356 wheel cast part, Boot et al. [67] concluded that the degree of hot cracking observed at the junction of casting decreased with grain refiner addition.

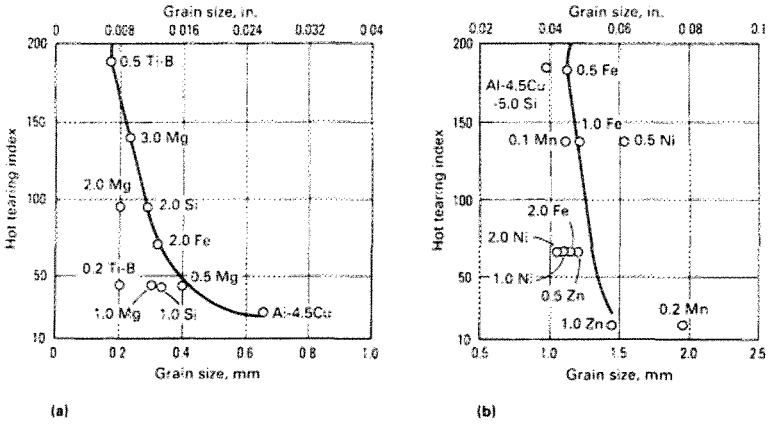

Figure 2.34: Effect of grain size on the hot tearing tendency of Al4.5Cu (a) and Al4.5Cu5Si (b) alloys with various additives [32]

- Porosity Distribution

As discussed, grain refinement delays the onset of coherency during solidification and allows easier mass feeding into shrinkage areas. In Al-Si alloys, the most direct and quantifiable impact of a reduction in grain size (and the accompanying increase in grain-boundary area) is a more uniform distribution of gas porosity and eutectic colonies. For the same hydrogen content, there is a measurable reduction in the volume of gas porosity in a grain-refined casting compared to a non refined casting. The reduced volume fraction of gas porosity is also reported to improve resistance to fatigue crack growth [32].

- Intermetallic distribution

A fine grain structure also minimizes the detrimental effects on the castability and properties associated with the intermetallics. Large, insoluble intermetallic particles that are present or form in the temperature range between liquidus and solidus lower the feeding distance. A finer grain size promotes the formation of finer and more evenly distributed intermetallic particles with corresponding improvements in feeding characteristics [32].

- Surface appearance

Large grains frequently emphasize different reflectance based on random crystal orientation, resulting in an orange peel or spangled appearance following chemical finishing, anodizing, or machining [32].

- Fluidity

Fluidity has been investigated by many researchers and is known to be affected by many factors such as superheat, mold temperature, solidification range, surface tension, melt treatment, etc. [2]. Mollard et al. [74] reported a reduction in fluidity of Al4.5%Cu alloy with 0.15%Ti addition using a vacuum fluidity test apparatus. The reason was associated to early nucleation caused by grain refinement resulted in slurry flow. Aslem et. al. [75] by fork shaped castings, have shown that under equal conditions, addition of Al5%Ti1%B and Al10%Sr enhances better mold filling. Figure 2.35 schematically illustrates their assumption on how the additions affect the filling behavior.

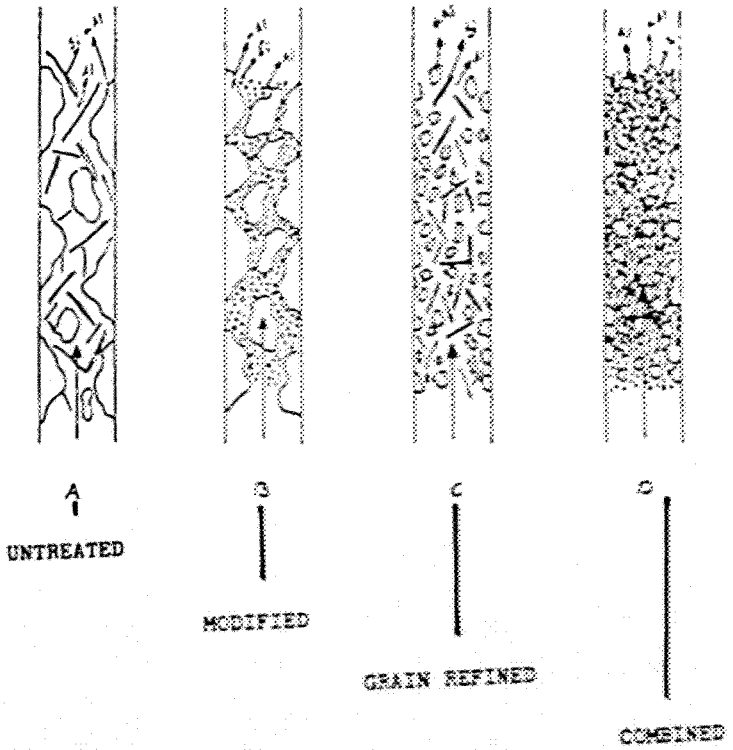

Figure 2.35: Model of the melt fluidity of Al7Si [75]

Dahle and Kwon [76,77] confirmed the above results. As mentioned by Chai et al. [78], increasing grain refinement and modifiers postpone dendrite coherency point. Thus a late coherency point is an indication of smaller interconnections between α-Al particles and improved flow comparing to non-refined alloy.

- Mechanical properties

Properties such as tensile strength and elongation are usually improved by grain refinement. In Al-Si alloys, this is mainly due to improvements in porosity distribution rather than to any decrease in grain size. The properties of Al-Si alloys are controlled by the eutectic and any influence of grain size is secondary [36]. Prasada et al. [79] investigated the wear behavior of Al and Al7%Si. Their results showed that the wear rate decreases with grain size and DAS reduction. It was shown that grain refinement improves the load bearing capacity of the alloy.

2.3 Modification of Al-Si alloys, a review

The modification of cast Al-Si alloys was discovered by accident 86 years ago [80] by introducing sodium fluoride to a flux and was subsequently developed to trace additions of sodium at levels around 0.01 wt% [81]. Since that time, the metallurgical literature has been abounded with contributions concerned with practical control of the process, with the use of alternative additions and, throughout, with attempts to explain the mechanisms involved.

To some extent, it was the knowledge of modification in this system that prompted the search for similar effects in cast irons, leading to the development of nodular ductile iron. Since the original discovery of modification, there have been many developments in its science and technology, although most of these have occurred since 1970.

2.3.1 Modification mechanism

In unmodified Al-Si alloys, the primary nonfaceted aluminum phase in hypoeutectic alloys is dendritic. The minor silicon phase forms as faceted flakes, either as the primary phase or as the finer eutectic constituent. The morphologies of silicon in the untreated alloys can be described in terms of facets on the close-packed {111} faces of the diamond cubic structure, generally combined with a few twins on the same planes.

A very important feature of silicon crystallization is that twins are easily formed. These crystallographic defects occur when large groups of atoms uniformly shift position across a plane in the crystal structure, known as a TPRE "Twin Plane Re-entrant Edge" (Figure 2.36).

Figure 2.36a shows a Si particle containing a single twin plane bound by {111} planes in the early stage of growth. The twin plane creates a 141° re-entrant angle and a 219° ridge at the edge of the particle. The energy required for the deposition of a new atomic layer at the re-entrant corner is approximately half of that required to deposit a new layer on an atomically smooth interface. Consequently, the re-entrant corner, 141°, is a favorable site for atomic additions, compared to the 219° ridge or the smooth <111>

interface. The particle in Figure 2.36a will continue to grow in this manner until it is bound by the {111} ridge at the growth front, when the growth rate will decrease because further growth can only occur by layer deposition on {111} planes. The existence of two parallel twin planes is the minimum requirement to ensure the continued presence of a re-entrant corner in the growth direction (Figure 2.36b,c). Each new atomic layer initiated at the 141° re-entrant corner (type I) results in the growth of a layer that covers the two adjacent {111} planes as shown in Figure 2.36c. When these layers reach a twin plane at a 219° ridge, a 109.5° re-entrant corner (type II) is created. This is an equally attractive site for atomic additions and growth from these corners preserves the original re-entrant system and permits continuous, unlimited propagation in the direction of the original 141° re-entrant grooves. Thus the TPRE system allows growth to proceed preferentially in any or all of the six <211> directions depending on the heat flow direction [82].

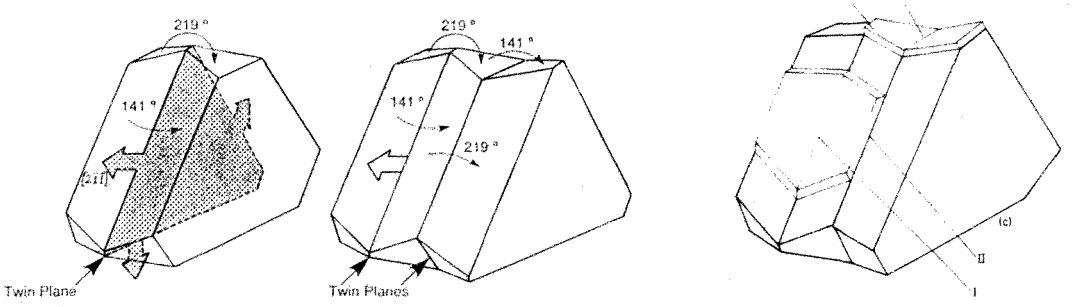

(a) (b) (c)

Figure 2.36: (a) A crystal of Si with one twin plane bound by {111} faces, (b) a crystal containing two twin planes, (c) re-entrant sizes I and II on the crystal [24,82]

Studies by transmission electron microscopy have revealed that modified silicon fibers contain orders of magnitude more twins than do the unmodified silicon plates (Figure 2.37). The surface of the fibers is micro faceted and rough as a consequence of the intersection of great number of twin planes with it. Silicon fibers are crystallographically imperfect, and each surface imperfection is a potential site for branching to occur should it be required by the solidification conditions. As a result, fibers in the chemically modified eutectic are able to bend, curve and split to create a fine microstructure; the plates of the unmodified structure are inhibited by their relative crystallographic perfection and form in a coarse acicular fashion.

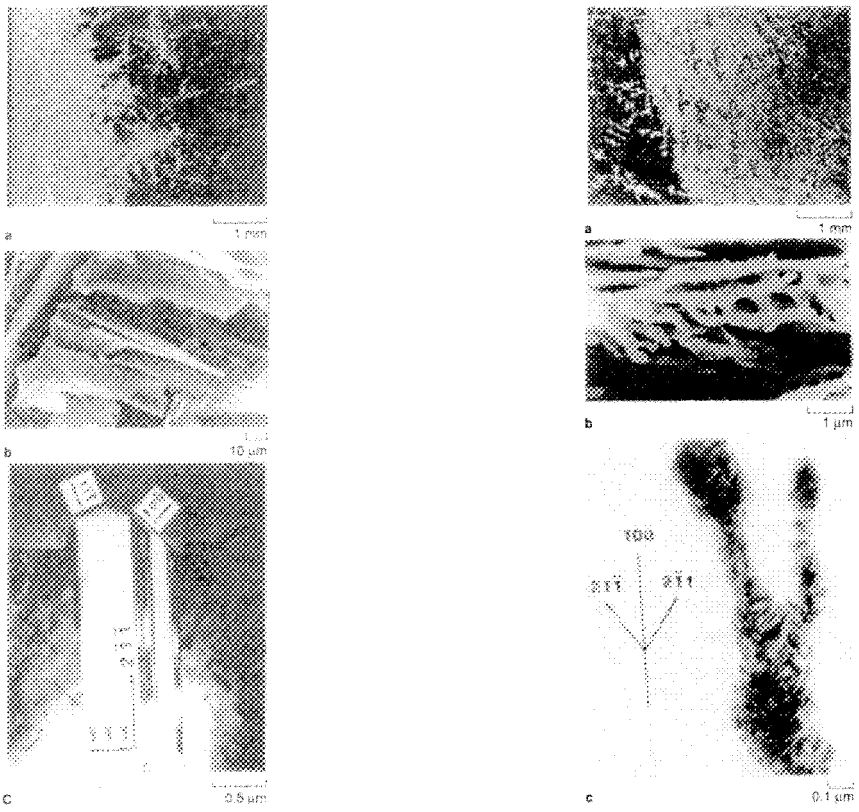

(A) (B)

Figure 2.37: A- Microstructure of Si flakes in unmodified Al-Si eutectic alloy:
(a) optical microscopy shows an irregular growth front, (b) SEM , deep-etched removing metal matrix,(c)TEM, shows a few {111} twins and growth orientation – B- microstructure of Si fibers in sodium modified Al-Si eutectic alloy:
(a) optical microscopy shows a near planar growth front, (b) SEM , deep-etched removing metal matrix, (c) TEM, showing a high density of multiple twinning and growth orientation [83]

In addition to the TPRE mechanism, Shu-Zu and Hellawell [83,84], Hogan and Shamsuzzoha [85,86] have proposed a theory for the development of the fibrous silicon structure, the so called "*Impurity Induced Twinning*" here after referred to as the IIT growth mechanism. They suggested that the atoms of the modifying element is adsorbed on and thereby disturb the growth step of the silicon crystals. This causes frequent twinning to occur, as depicted in Figures 2.38; the frequent twinning leads to the seaweed-like structure of silicon crystals actually observed. They further stated that the modifying element must

have an affinity to silicon and preferably form chemical compounds with this element. This will facilitate adsorption on the surface of silicon crystals growing in aluminum melt.

A certain size ratio of the ad-atoms to the silicon atoms of 1.6457 has been proposed as an optimum to induce a high degree of twinning [84]. Sodium comes close to this ratio, but strontium also fulfills this criterion reasonably well (Figure 2.39). It can be seen that an impurity atom of appropriate size would force a monolayer step to miss one regular close packed position and so fall into the next alternative stacking sequence, thereby creating a twin. The role of elements known to promote modification of silicon crystals (other than sodium), like calcium, strontium, and cerium, may be of a similar nature as that of sodium, i.e. removing the compound AlP and poisoning the TPRE step of growth, thereby lowering nucleation as well as growth temperature of the silicon crystals. Of these elements, Sr attracts special interest and it has become quite popular as a modifying agent [24,36,82-87].

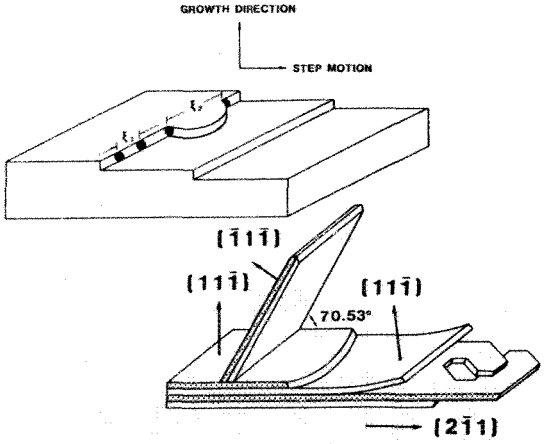

Figure 2.38: Model for adsorption of impurity atoms on growth steps of a silicon crystal resulting in twining to occur (twin configuration shaded) [84,87]

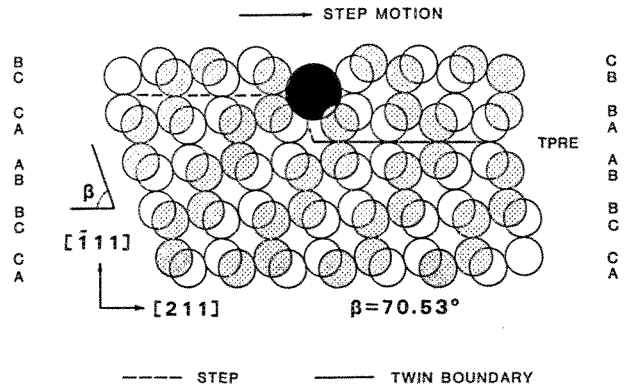

Figure 2.39: {011} plane projection of diamond cubic lattice to show how an impurity atom of a certain size could promote twinning by causing a growth step to assume the alternative {111} stacking sequence (model for "*Impurity Induced Twinning*") [84,87]

2.3.2 Chilling modification

A modified eutectic structure can be obtained in the absence of chemical modifiers by growth rates greater than $\geq 1 mms^{-1}$[84]. Fibers are quite smooth on external surfaces and TEM study has shown that the silicon fibers have smooth external surfaces and that many are twin free (Figure 2.40) [84]. These features are consistent with isotropic fibrous growth at an atomically rough interface, as shown in Figure (2.41). The transition in shape would seem to correspond to a gradual change from somewhat anisotropic growth of flakes to entirely isotropic growth by an intrinsic mechanism at higher undercooling. The quenched fibers are much finer than the slowly grown flakes and are also finer than the impurity modified fibers form at relatively low growth rates.

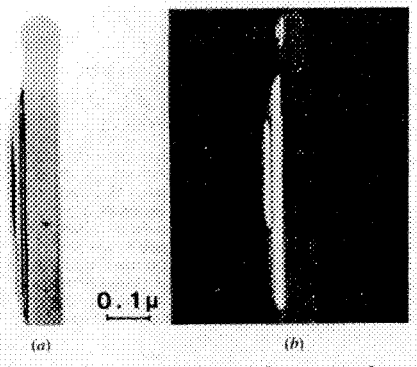

Figure 2.40: Quench modified silicon fiber with smooth surface and rare example of twinning, TEM images: (a) light field and (b) dark field [84,87]

It is worth mentioning that chemical modifiers are more effective at higher freezing rates. This is fundamentally different from quench modification. In the presence of a chemical modifier, both the twinning frequency and the angle of branching increase with freezing rate. Both of these promote modification and lead to finer structures [36,84,88].

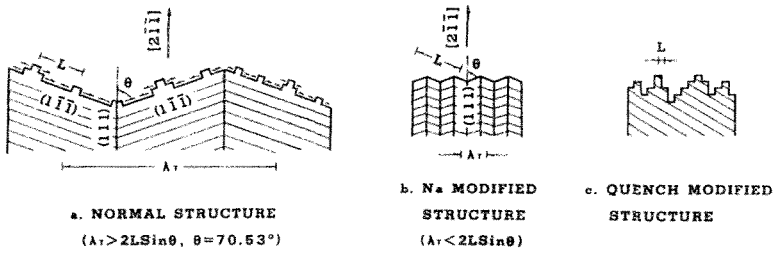

Figure 2.41: Schematic of the eutectic silicon growth interface: (a) unmodified flake silicon. Widely spaced {111} twins probably make the propagation of intrinsic steps across <111> interfaces the significant growth mechanism, (b) Impurity-modified fibrous silicon. Finely spaced {111} twins mean that TPRE is the major step source during silicon growth. If twinning occurs equally on four {111} systems, a <100> fiber growth direction results. (c) Quench-modified fibrous silicon. An atomically rough, twin-free eutectic silicon interface at which atomic additions are made randomly. Branching occurs readily by overgrowth [88]

2.3.3 Chemical modification

The addition of certain elements, such as calcium, sodium, strontium, and antimony, to hypoeutectic Al-Si alloys results in a finer lamellar or fibrous eutectic network. While a number of IA and IIA elements and several lanthanides produce a modified silicon eutectic, only Sr, Na, and Sb have found extensive commercial application during the last 3 decades. The amount of each element required depends on the alloy composition, impurities in the melt, and freezing rate.

As mentioned before, Lu and Hellawell [83,84] have demonstrated that substantial incorporation of foreign atoms of certain size into the silicon lattice enhances the formation of twins. A study on this ratio for elements that are known to modify to some extent, indicates that they all have a radius ratio in the vicinity of the ideal value; some are presented in Table 2.5. It is noticeable that the size of sodium atoms is closer to the ideal

value than strontium. In fact most of these elements that are either alkaline or rare earths elements have been reported to modify the alloy to some extent.

Table 2.5: Some properties of possible modifiers [89]

Element	Atomic radius (A°)	r/r_{Si}	Melting point	Vapor pressure (atm)	-ΔG oxide ($kJmol^{-1}$)	$K_{oxidation}$
Ba	2.18	1.85	725	$5*10^{-5}$	482	20
Sr	2.16	1.84	769	$1*10^{-3}$	480	15
Eu	2.02	1.72	822	$1.8*10^{-4}$	500	-
Ca	1.97	1.68	839	$2.6*10^{-4}$	509	400
Yb	1.93	1.65	824	$5.6*10^{-3}$	500	1500
La	1.87	1.59	926	10^{-6}	487	-
Na	1.86	1.58	98	0.2	367	$2.7*10^{-5}$
Ce	1.83	1.56	798	10^{-16}	497	-

Some other factors that are significant in determining the ability of any element to modify the silicon are listed in this table. The melting point is important because elements that melt at lower temperatures will presumably dissolve more readily in Al-Si melts that are typically held at higher temperatures. Thus, sodium dissolves easily but strontium has some difficulty and other elements on the list are even more difficult to dissolve.

The vapor pressure is of significance since elements with high vapor pressure tend to boil off the melt. The well known fading effect of Na is due to its high vapor pressure while Sr and all of the remaining elements in this table are much more stable in the melt. In addition to vaporization, effective modifiers may be lost through oxidation. The $K_{oxidation}$ values in Table 2.5 are the equilibrium constants for the following reaction:

$$X\ Al_2O_3 + Y\ Modifier \rightarrow 2x\ Al + 3\ Modifier_XO_Y \qquad (2.37)$$

Large values of this parameter are indicative of a high tendency to oxidation. Therefore while sodium vaporizes, it does not oxidize. Strontium, on the other hand is lost by slow oxidation and the oxidation of Ca and Yb is very severe [89].

2.3.3.1 Modifier addition

As discussed, several elements have been found to produce the modified structure. Some produce fibrous structure such as Na and Sr while the others produce a finer version of the coarse acicular structure (antimony , arsenic or selenium).There are several different elements which are capable of changing the morphology or size of eutectic silicon but only Na , Sr, and Sb have found significant industrial application. The chemical and physical properties of these agents are very different so they are added to the melt in quite different manners.

- *Sodium*

As early as 1920, it was found that very small addition of Na modifies the structure of Al-Si alloys, causing an increase in strength and an appreciable improvement in ductility. As time passed, Na addition became the established modification treatment for Al-Si alloys [80]. Sodium is usually added in metallic form, vacuumed and encapsulated in small aluminum cans to retard its natural burning in air. Sodium should be plunged into the melt and stirred gently for a short time to provide good dissolution and dispersion. The usual precautions apply regarding proper storage and the use of clean, dry tools. Fade, or loss of modification, increases with excessive agitation, degassing, prolonged holding periods, or excessively high temperatures. Sodium has a very low solubility in aluminum (about 0.01%) and because of that, manufacturing sodium master alloys is impossible (Figure 2.42).

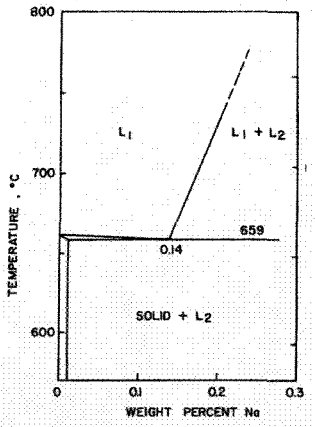

Figure 2.42: The solubility of sodium in aluminum [90]

In general, a sodium addition of 0.015 to 0.020% is required for adequate modification, which results in a residual level of Na in the casting of about 0.002%. Sodium should not be used with alloys containing more than 1% Mg, because of possible embrittlement effects [35].

- *Antimony*

Antimony is a modifier that is used predominantly in Europe and Japan. It is added in amounts of 0.1% and greater and serves as a permanent alloy constituent of the aluminum alloy. Antimony is commonly classed as a modifier though it is better classified as a silicon refiner because it reduces the size of eutectic silicon by improving nucleation and does not affect morphology. Antimony additions simply refine the Al-Si eutectic, causing a fine lamellar eutectic to form instead of the fibrous one produced by sodium or strontium. The microstructural differences that are apparent in Figure 2.43 are due to the inability of Sb to cause extensive twinning in silicon.

Antimony is a toxic material and in addition it can react with hydrogen dissolved in the liquid Al to form deadly stibine gas according to the reaction:

$$Sb + 3H \rightarrow SbH_3 \tag{2.38}$$

For these reasons, pure Sb is not added to melts in the foundry. Antimony treated alloy is purchased as pre-modified ingot from primary aluminum suppliers and is simply remelted and cast. Alloys modified with Sb are distinguished by lower gas susceptibilities than those containing Na or Sr. However Sb modified alloy is not recommended for food contact applications [35,36,89].

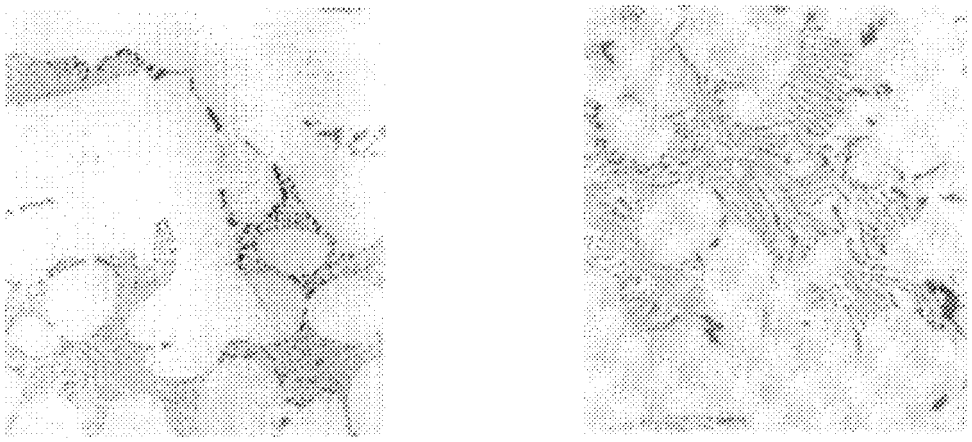

(a) (b)

Figure 2.43: Microstructural differences of:
(a) sodium-modified structure, and (b) antimony-refined structure [89]

- *Strontium*

In 1975, an aluminum master alloy containing 10% Sr and 14% Si was introduced for modifying the Al-Si alloys. It offered a convenient way of adding the modifier by eliminating the two major problems with sodium modification, namely: fume generation and uncertain modification. Unlike sodium, strontium presents no special storage or handling problems and manufacturing of Al-Sr master alloys is entirely feasible, since the Al-Sr phase diagram contains several intermetallic compounds (Figure 2.44).

Additions of 0.01 to 0.02% in foundry castings are sufficient, particularly when melting returns, where typical residual 0.008% Sr is available. Occasionally, pure Sr has been used as a modifier, but it is reactive with air and water vapor, and within a few minutes becomes covered with a mixture of SrO, SrO_2, $Sr(OH)_2$ and $(CaSr)NO_3$. This layer can completely prevent dissolution unless it is mechanically removed, and for this reason, pure metallic strontium is not the preferred way for addition to Al-Si alloys. Master alloys which contain less than about 45% Sr are not reactive in air, and no special precautions are necessary for their packaging and storage. Alloys with 20% to 60% Sr have melting points in excess of 900°C and while they are stable in air, they are of no practical use. The 90%Sr-10%Al alloy does contain some elemental strontium, and hence it is somewhat reactive in

air, although much less than pure strontium. For this reason, it is packaged in sealed containers as same as Na. They usually contain an inert gas rather than vacuum, reflecting the lesser reactivity of the Sr alloys compared to elemental Na [35,36].

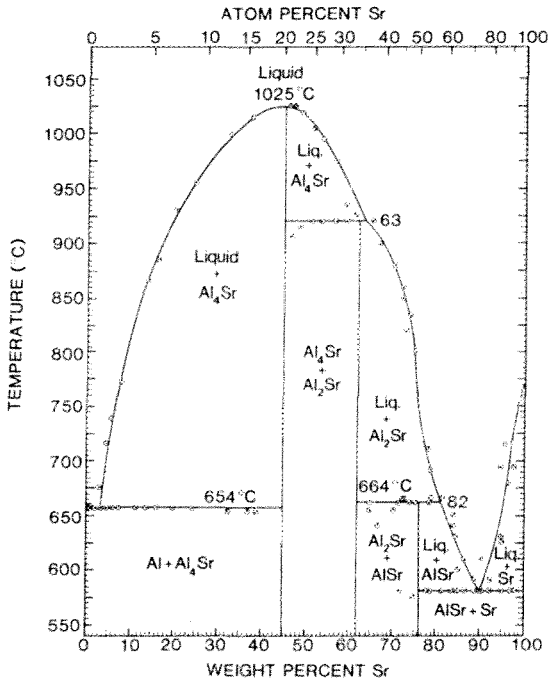

Figure 2.44: The Al-Sr phase diagram [91]

2.3.3.2 Modifier comparison and properties

2.3.3.2.1 Dissolution

Sodium dissolution occurs more simply and rapidly (with 98°C melting point), providing almost immediate optimal modification. As it was discussed, sodium has a very high vapor pressure (0.2atm at 727°C) and hence large amounts of the sodium which are added boil off almost immediately. Sodium recovery is therefore poor (20 to 30 % addition) and antimony appears to behave similarly.

Strontium addition could be performed at high levels (about 90%) and with very reproducible recovery but its dissolution characteristics are more complex than those of sodium. High Sr containing master alloys such as 90%Sr-10%Al dissolve by an exothermic process known as reactive dissolution. The elemental Sr reacts with the liquid Al-Si alloys and results in the formation of intermetallic compounds. The rate of this reaction, which is

temperature dependent, determines the effectiveness of Sr recovery and therefore the degree of modification achieved. It has been found that when elemental Sr is present, as in 90%Sr-10%Al master alloy, the exothermic reaction proceeds at about 725°C. However at lower temperatures, the reaction is slowed down, and an intermediate intermetallic compound, Al_2Si_2Sr, forms with good dissolution characteristics. Therefore, lower temperature provides better recovery than higher temperature (Figure 2.45a) [92,93].

On the other hand, lower strontium master alloys such as 10%Sr-90%Al dissolve by simple dissolution. The microstructure of this master alloy contains Al-Al_4Sr eutectic and large plates of Al_4Sr intermetallics. Thus most of the strontium is locked up in intermetallic compounds and the process of adding strontium to the melt is by dissolving these compounds. Therefore, recovery increases at higher temperatures (Figure 2.45b) because the dissolution rate is greater. The optimal recovery is achieved after a certain time, 10-20 minutes, depending on the temperature and the specific Sr alloy addition [92,93]. Such time is not only necessary for dissolution of Sr, but also helps it to interact with silicon particles to initiate morphological alternation, i.e., incubation period.

Furthermore, the rate and degree of modification depends on the kinetics of Sr-master alloys interaction with molten Al-Si alloy. They are [94,95];

- Dissolution rate of Al_4Sr particles in the melt
- Formation of a new phase , Al_2Si_2Sr
- Successive dissolution of this phase to give Sr in solution (Sr_L)
- Sr in solution affects the growth behavior of Si crystals and causes modification
- Partial reaction with phosphorus to form strontium phosphide , which leads to the fading of the modifying activity

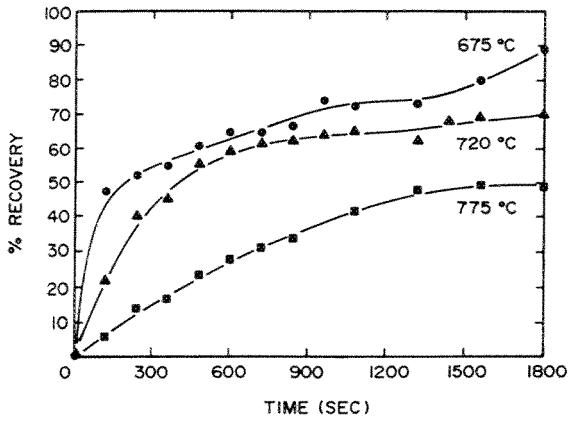

(a)

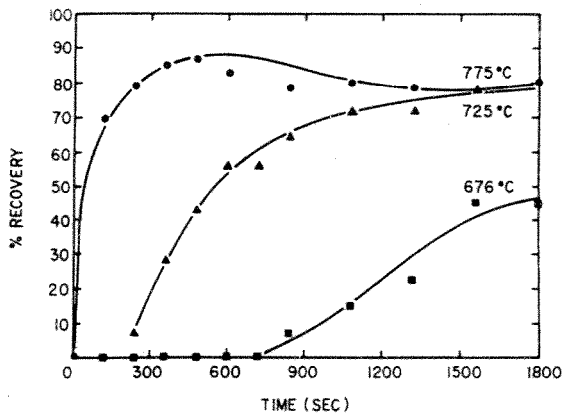

(b)

Figure 2.45: Comparison of dissolution rates for strontium additions made with: (a) 90%Sr-10%Al, (b) 10%Sr-90%Al master alloys [92,93]

2.3.3.2.2 Modifier fading

Of the three commercially available modifiers, Na, Sr and Sb, two are subject to fading. Antimony is chemically stable and is not known to undergo any fading effects. Basically three types of chemical reaction in the melt may cause modifier fading [32,36]:

- Modifier may vaporize due to a high vapor pressure at melt temperature
- It may oxidize due to an excessive chemical affinity for oxygen (Table 2.5)
- It possibly will react with other elements coming from the remelting of scrap (such as modifier interactions) or due to the especial refiner addition and consequent interaction with them such as what happens when B is added to the

Sr-modified sample. In the latter case, modifier is ineffective due to the chemically combined form.

- *Sodium*

One of the main disadvantages of sodium is its fading. As it can be seen from Table 2.5, sodium with a vapor pressure of 0.2 atm at typical melt temperatures can easily boil out of the melt, causing large losses. The data presented in Figure 2.46 is typical of sodium fade. As it is obvious, the loss of sodium content is very high and there is a subsequent loss over a period of 1-2 hours down to levels of 0.002%-0.005%. Fading strongly depends on many casting parameters such as dimension of casting, stirring of the melt, degassing condition, etc [32,36].

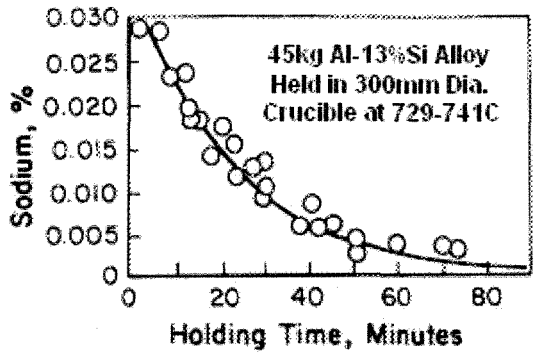

Figure 2.46: Loss of sodium during holding in a crucible [36]

- *Strontium*

Strontium fades more slowly than sodium and as it could be seen from Table 2.5, the vaporization of Sr is not an important factor for fading mechanism. Thus it appears that Sr losses from the melt are by oxidation, since the oxide of Sr is somewhat more stable than Al or Si [32,36].

2.3.3.2.3 Incubation time

Incubation period means the time the modifier needs to affect the structure. For example during the first 1-2 hours after Sr addition, the degree of modification is observed to improve [96]. At first this was thought to be due to slow dissolution of the strontium, but later several studies on the dissolution of Sr in Al-Si melts have shown that a minimum of

30 minutes is required to achieve the maximum melt Sr concentrations, even under the most favorable conditions [96]. Significantly shorter times are necessary if the optimum dissolution conditions are used. This appears to be related to the low dissolution rate of Al_4Sr and the time required for Sr to react with AlP present in the melt. Chai and Backerud [95] have shown that in Al-Sr master alloys, the size of Al_4Sr particles affects the degree of modification. A master alloy with fine Al_4Sr particles will reduce the incubation time.

With sodium, an incubation period may or may not exist. This phenomenon is not detectable because it is masked by the much more pronounced fading phenomenon. It is not known if an incubation period exists with Sb treatment. Antimony is virtually always used as pre-modified ingots containing 0.1-0.15% Sb. It is not added directly at the foundry level, and hence it is almost impossible to observe incubation effects [36,96,97].

2.3.3.2.4 Porosity formation

The influence of modification on porosity is a matter of considerable debate over the past 30 years. The effect is well illustrated in Figure 2.47. Jacob [98] studied cast bar treated with different modifiers in a mold arranged with a chill at one end and a riser at the other. As the Na or Sr content increased, the density of the bar was lowered due to enhanced porosity in the sections more distant from the chill. Because of different mechanism, Antimony does not increase porosity.

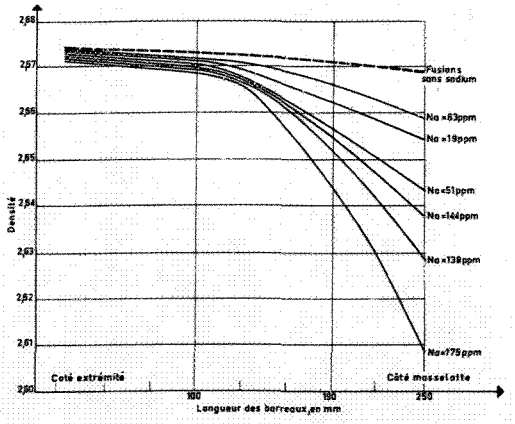

(a)

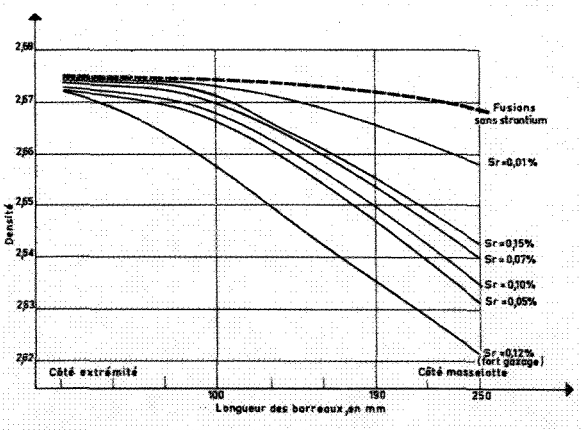

(b)

Continue

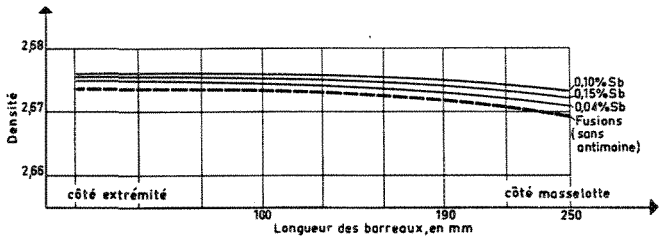

(c)

Figure 2.47: Density along the length of a bar solidified with a chill at one end and a riser at the other (X axis: Length of test piece in mm, Y axis: Specific Gravity):
(a) Na-modified, (b) Sr-modified, and (c) Sb-modified [98]

The increased porosity associated with modification may cancel any beneficial effects of structural refinement. It is now well accepted that modifiers disperse porosity throughout a casting causing an increase in microporosity and a decrease in macroporosity or piping. Argo and Gruzleski [99] have summed up the controversial situation and concluded that it is natural to attribute increased porosity in a modified casting to an increase in the hydrogen content and thus the modifier being thought to be somehow responsible in increasing the susceptibility of the melt to hydrogen pick up. However the other related works [100,101] have shown that this is not the case for Sr. They have carried out a controlled study on porosity in modified and unmodified A356 alloy, using the Tatur test to identify the differences in the distribution of porosity and shrinkage. Their radiographic and Tatur results have shown that modification leads to redistribution of porosity upon solidification, from primary pipe type into microporosity, appearing thereby to increase the porosity. An example of this is seen in the photograph of Figure 2.48. The unmodified casting contains large shrink porosity in the heavy section at each end. With Sodium modification, this is dispersed as microporosity throughout the part [102].

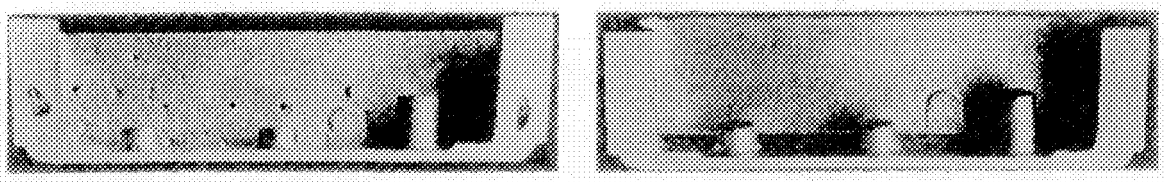

(a) (b)

Figure 2.48: Correlation between shrinkage and modification:
(a) large shrinks in the heavy sections, unmodified alloy; (b) by sodium modification, the macro-pores are replaced by micro-pores dispersed throughout the casting [102]

Another experiment [100] has shown that Sr additions do not increase the hydrogen level nor change the regassing rate of a previously degassed melt. If in fact there is no relationship between the dissolved hydrogen content of a melt and modifier concentration, then any increase in porosity must be due to some other effects such as [89]:

- A decrease in surface tension of the melt that would facilitate pore nucleation;
- Enhanced interdendritic feeding difficulties caused by the longer freezing range of modified alloys;
- Higher dirt (inclusion) levels in the modified melts that lead to easier pore nucleation.

Anson et al. [103], with different addition levels of Sr and by measuring pore size and density to distinguish between gas and shrinkage porosity, have shown that the porosity percentage increases with Sr concentration. The pore density (number of pores/cm^2) decreases as a function of the microstructural effect of Sr due to a decrease in the number of shrinkage pores. The average and maximum pore size increase with Sr concentration and these increases are greater than the decrease in pore density. Finally they have also reported that small addition of Sr (15-30ppm) produces a partially modified structure with more dispersed and spherical porosity.

2.3.3.2.5 Surface tension

Surface tension is a natural property of all liquids and it is due to an incomplete coordination of the atoms at the liquid-gas interface. Atoms in the bulk of the liquid are completely surrounded by the other atoms, while those at the surface are only in contact on the side and below. Interatomic attractions cause an uneven pull on the surface atoms, drawing them into the body of the liquid and resulting in a curvature of the surface as the liquid tries to assume a shape that has a minimum surface area.

As mentioned, the effect of Sr on the level of microporosity has been thoroughly studied by numerous workers such as [98-102]. It is generally claimed that the presence of modifier decreases the surface tension of the melt thus facilitating pore nucleation [104]. In

this part, considering the importance of surface tension in semi-solid processing, the correlation between modifier addition and surface tension will be reviewed.

Emadi et al. [104] by using sessile drop technique in an argon atmosphere have shown that at 685°C surface tension of A356 alloy changes from 0.79 to 0.64 N/m with Sr-addition and to 0.715N/m with Na addition. Anson et al. [105] continued the work on the sessile drop experiments but more precisely with and without atmospheric pressure and showed that at 630°C surface tension changes from 0.889 to 0.844 N/m with Sr-addition in the vacuum. They reached the point that addition of hydrogen gas has no significant effect on the surface tension of the unmodified A356 (0.874N/m), while it lowers the surface tension of the modified alloy to 0.801 N/m due to the formation of SrH_2.

In another series of experiments, Lee et al. [106] measured oxygen using an oxygen analyzer and the surface tension by measuring the force for pulling up a Pt-Rh ring from the liquid in the argon atmosphere at different temperatures. They have shown that with Sr and Na addition, the surface tension of the melt decreases. They used both oxygen analysis and surface tension measuring equipments. Figure 2.49 shows the surface tension and oxygen variation by sodium and strontium. In normal superheat, the surface tension of Na-treated samples are always smaller than Sr-treated ones. As the temperature increases, the surface tension also increases because of the increase of oxide amount (Figure 2.49b). Another conclusion is that Na-modification shows higher oxygen content comparing to Sr-modification and that is why Na-modified melt is so sensitive to superheat.

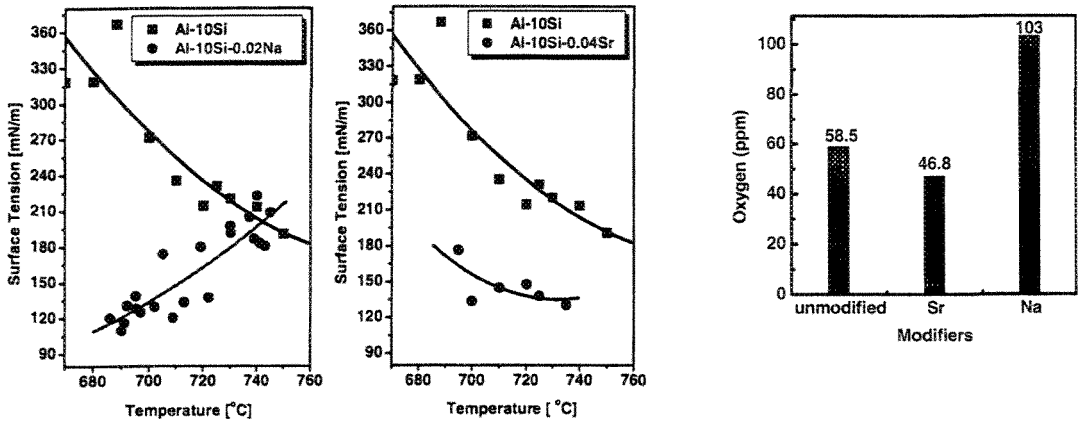

(a) (b)

Figure 2.49: (a) Surface tension, and (b) Oxygen content with Sr and Na additions [106]

2.3.3.3 Modifier interactions

The topic could be studied from two different points of view as follow:

- As it was described, Sr, Na, and Sb are the main modifiers used commercially to treat hypoeutectic Al-Si alloys. Table 2.6 illustrates the effects of various modifier additions to the melt. It is clear from this Table that single addition does not meet the entire requirement of a superior treatment. From this point, combining additions of modifiers have attracted attentions [110-113].
- From an industrial standpoint, scrap and returned parts may contain one or all of the three conventional modifiers and therefore this causes contamination of the original melt by these elements. The situation becomes worse if chemical analyzer has no detector for such elements.

2.3.3.3.1 Phosphorus reaction

Phosphorus interferes with modification by Na, Sr, or Sb and alloys with higher P levels require larger retained modifier concentrations in order to produce an acceptable cast structure. If the phosphorus concentration can be reduced to less than 1ppm, an Al-Si casting alloy will freeze with a lamellar structure without addition of any modifying agent [36,107]. Thus natural structure of these alloys is lamellar. It is only the higher P values associated with commercial alloys which cause the eutectic silicon to solidify in an acicular form. Thus the amount of modifier required depends on the P content.

Table 2.6: Summary of sole modifier additions

Element	Morphology	Advantages	Disadvantages
Sb	Fine lamellae	- Durable effect (no fading)	- Toxic gas formation - Not recommended for food industry
Na	Fiber	- No incubation period - Simple & rapid dissolution	- Storage problem - Rapid fading - Sensitive to degassing, prolong holding, high temperature - Fume generation during addition
Sr	Fiber	- More durable than sodium	- Incubation period - Porosity redistribution

Modifier/phosphorus interactions have been determined experimentally to some extent as seen from Figure 2.50. The more the phosphorus level decreases, the lesser quantity of each modifier is required. Also it was proved that increasing cooling rate, the acceptable phosphorus concentration increases [108,109]. In Al-Sr master alloys, it was shown clearly that P could increase the incubation period and it has little effect on the degree of modification during the first 10 minutes [95,96,108,109].

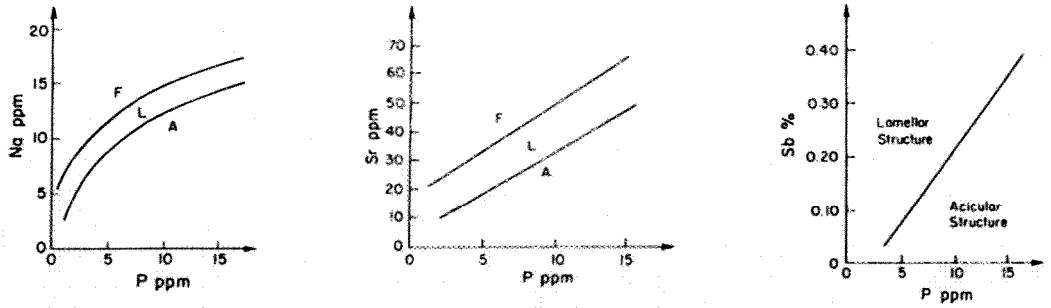

(a) (b) (c)

Figure 2.50: P-Modifier interactions in A356 alloy (solidification time of samples are 60s): (a) Na-P, (b) Sr-P, (c) Sb-P (F=fibrous; L=lamellar; A=acicular)[108,109]

2.3.3.3.2 Na / Sr-Sb interactions

The problem of Na/Sr-Sb interactions is shown in Figure 2.51. At the usual modifier levels (0.01-0.015%), poor modification is achieved if antimony is present and much higher treatment levels are required to reach reasonable modification ratings [110]. Thus the problem can be easily solved if one could distinguish antimony presence. Handiak et al.

[111] demonstrated that negative interaction between antimony and other modifiers is due to the following reaction:

$$Sb + Na \text{ or } Sr + \text{other elements} \rightarrow \text{Solid compounds} \qquad (2.39)$$

These solid compounds effectively remove the modifying agent from solution and thus prevent them to act as a modifier. Since the compounds contain antimony, a dense element, they tend to sink to the bottom of the furnace to form sludge.

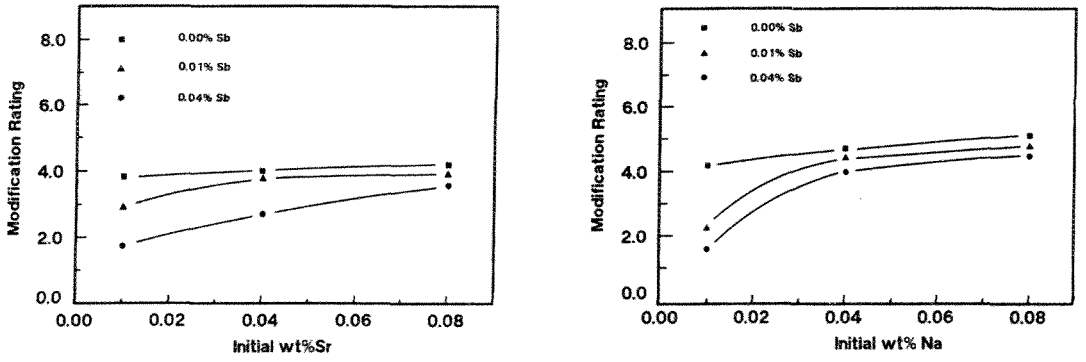

(a) (b)

Figure 2.51: Modification ratings of A356 alloy containing antimony [110]

2.3.3.3.3 Na-Sr interactions

The idea initiates from the fact that sodium has a rapid modification effect with short duration while strontium is associated with a lower acting but longer lasting effect. The first trial done by Wang and Gruzleski [110] has shown that in 356 alloy, the Na side of the combination yields modified structure in shortened incubation time in the first 40 minutes and an extended duration associated with Sr-modification. Lu et al. [113] with microstructural and thermal analyses on 356 alloy have shown that combined addition of Sr and Na does not appear to cause improvement of the modified structure even after a short period of time. Loss of modifying elements was believed to be responsible for the disappearance of the modification effect during holding. Na addition was claimed to accelerate Sr vaporization and/or oxidation kinetically, leading to a quicker loss of both modifier.

CHAPTER 3

LITERATURE REVIEW: PRINCIPLES OF SEMI-SOLID CASTING

CHAPTER 3

LITERATURE REVIEW: PRINCIPLES OF SEMI-SOLID CASTING

3.1 Semi-solid casting process, a review

Technologies for SSM processing can be generally divided into two basic groups (Figure 3.1):

1. Rheo- routes
2. Thixo-routes

The rheo-route involves the preparation of a SSM slurry from a liquid phase and its direct transfer into a die or mold for component shaping. The term "Slurry-on-Demand", SoD, has recently been coined in industry to describe slurry making operations that take place in the cast shops, thus provide a constant supply of slurry for shaping operations.

The thixo-route is basically a three step process, involving preparation of a feedstock material having an equiaxed or globular, non-dendritic structure or indeed having the potential to transform into equiaxed structure on further processing. The second step is reheating of the feedstock material to temperatures between solidus and liquidus (mushy zone) to generate a semi-solid structure. The final step is shaping of the mush that has thixotropic characteristics. The feedstock for thixo processes may include a variety of sources: rheocast billets, pellets or chips, spray formed solids, grain refined ingots, compacted powders, and mechanically deformed bars [7,8].

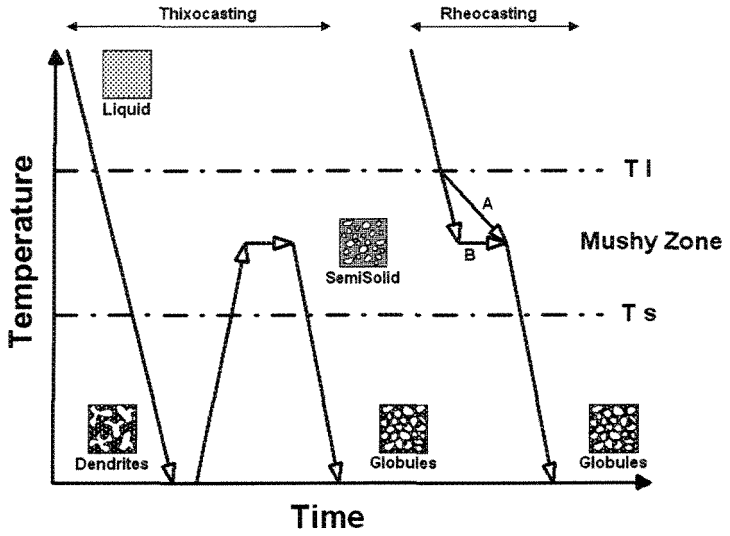

Figure 3.1: Schematic representation of two major categories of SSM processes

3.1.1 Rheo-route techniques

As mentioned before, there is a wide range of processes patented or under investigation within research and development centers worldwide. In spite of technical and technological differences amongst the available rheo-routes, they may be categorized within the following groups.

3.1.1.1 Mechanical stirring

The implication of stirring during solidification of alloys was initially originated at the Massachusetts Institute of Technology, MIT [114]. Melt agitation is commonly generated by means of augers or screw [115-118], impellers or some special kind of agitators [114,119-121]. Non-dendritic structures could be formed by applying shear forces exerted by stirrers during solidification. The process was developed from batch into a continuous process. In the simple continuous process, superheated liquid in the holding vessel flows down into a gap between the stirring rod and the outer cylinder where it is simultaneously stirred and cooled (Figure 3.2). Slurry flows from the bottom of the rheocaster either to be cast directly to shape (rheocasting) or to be solidified as feedstock material for subsequent reheating and thixoforming.

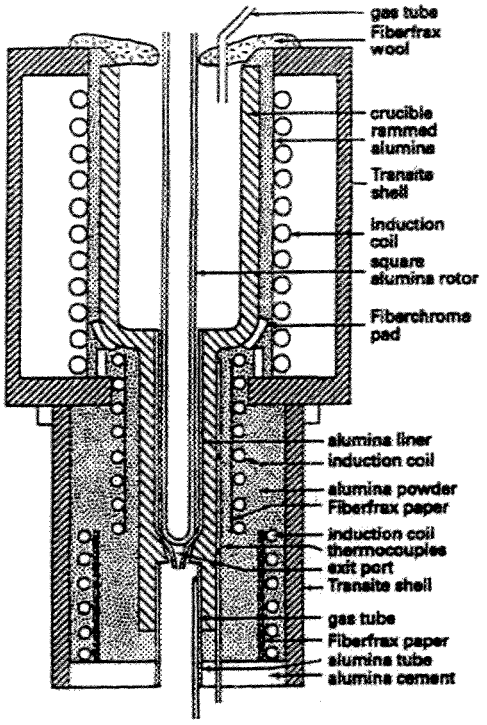

Figure 3.2: Schematic diagram of a primary rheocaster [114]

In spite of mechanical stirring being the first SSM processing route, it has found limited applications on industrial scale due to its drawbacks such as oxide contamination. Efforts were made to overcome its shortcomings which have resulted in introducing new processes using helicoidal screws and in most cases, shearing and solidification implemented in separate compartments [115-116]. The main reason for the modification seems to be the improvement in the microstructural uniformity of semi-solid billets. Figure 3.3 shows a new rheocasting method introduced in Japan. It is provided with two separate initial and stirring tanks. Liquid metal is transferred from the melt tank by a pump, sheared by water cooled stirrers and the resulting slurry is ejected out for further processing. This may be regarded as a SoD machine to provide the semi-solid slurry for high pressure die casting. Figure 3.4 illustrates a new design named "twin screw technology" [115].

The conventional mechanical stirring method has certain disadvantages, such as erosion of the stirrer (particularly with more chemically aggressive alloys), the contamination of the slurry by oxides and dross, gas entrainment, low productivity and the

difficulty in process control. In addition, slurries produced by such processes tend to contain larger, less ripened rosette particles and less homogeneity than other processes. Such morphologies immobilize and entrap more liquid, adversely affecting the rheological behavior of the slurry by reducing the effective liquid fraction [7,8,122].

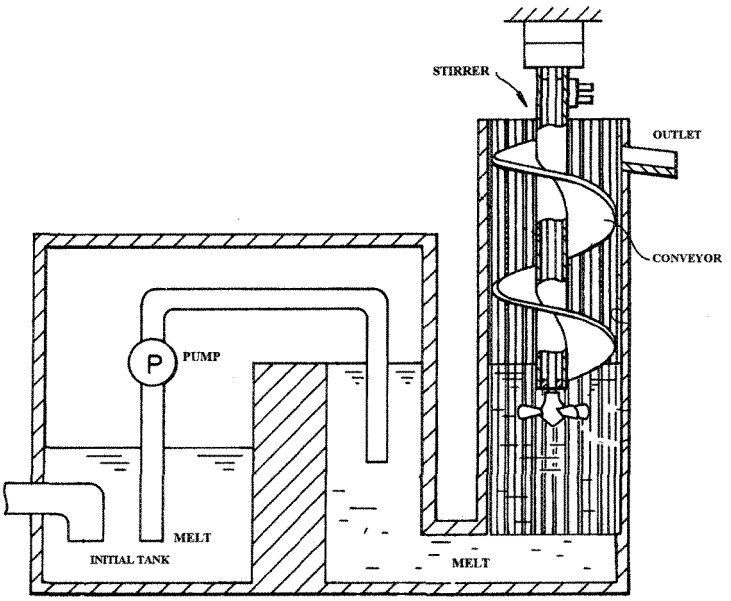

Figure 3.3: Schematic illustration of the single-screw rheocasting process [116]

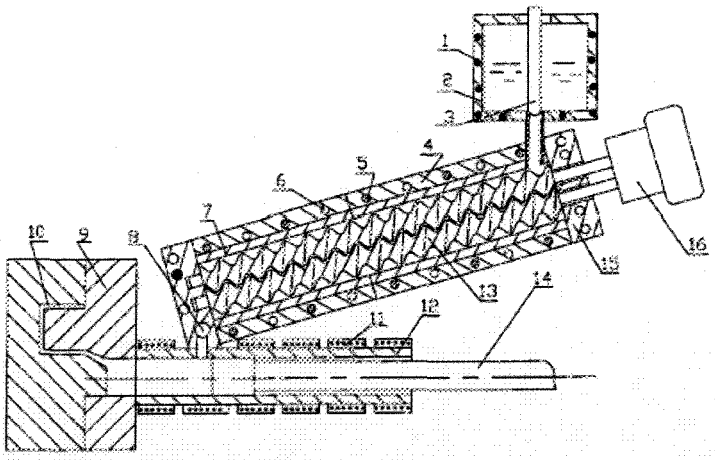

Figure 3.4: Schematic illustration of the twin-screw rheomolding process. 1)heating elements; 2)crucible; 3) stopping rod; 4)barrel; 5)heating elements; 6)cooling channels; 7)barrel liner; 8)transfer valve; 9)die; 10)mold cavity; 11)heating elements; 12)shot sleeve; 13)twin-screw; 14)piston; 15)end cup; 16)driving system [115]

3.1.1.2 Magneto Hydro Dynamic (MHD) stirring or Electro Magnetic Stirring (EMS)

It was claimed that MHD stirring process was developed by Young et al. [123,124] to overcome the associated problems with the direct mechanical stirring. In this technique, local shear is generated by a dynamic electromagnetic field. The solidifying metal acts as the rotor and the stirring action created by liquid movement shears the dendrites formed within the mushy zone, i.e. globules are created. The stirring is deep in the liquid which has previously been filtered and degassed, so that contamination is virtually eliminated. From the solidification point of view, such vigorous agitation breaks up the dendrites and transfers dendrite branches and newly formed grains into the bulk, improving distribution of particles and creating a uniform temperature through out the slurry. It has been reported [125] that MHD casting process could be able to deliver the desired solidified microstructure with a grain size that is normally about 30μm. This compares with the 100 to 400μm grain size produced by mechanical stirrers.

Electromagnetic stirring can be achieved through three different modes: vertical, horizontal, and helical flow. The helical mode is a combination of the vertical and horizontal modes. In the horizontal flow mode or rotational stirring the motion of the solid particles takes place in a quasi-isothermal plane so that mechanical shearing is probably the dominant mechanism for spheroidization (Figure 3.5a). In the case of vertical flow mode or linear stirring, dendrites are similarly fragmented at the solidification front but are recirculated to the hotter zone of the stirring chamber and partially remelt. Hence thermal processing is dominant over mechanical shearing (Figure 3.5b).

The continuous casting is made through either a vertical or horizontal arrangement, depending on the casting direction in relation to the gravity vector. While vertical stirring has so far been employed in vertical continuous casting only, horizontal stirring has been used in both vertical and horizontal casting systems. The microstructures produced from MHD feedstock are strongly affected by the design of the inductive coils. In addition,

electromagnetic force fields in the mushy zone are not uniform and this may result in billets with different degrees of structural modification in the radial direction.

According to Niedermaier et al. [126], the major advantages of horizontal MHD continuous casting include cost effectiveness and continuous production, but the quality of the billet is influenced by gravity. From a technological point of view, the essential difference between the two methods lies in the direction of gravity in relation to the casting direction. In contrast to horizontal MHD, the vertical MHD casting benefits from symmetrical solidification and with no limitation of the billet diameter. However, the vertical system suffers from drawbacks, such as discontinuous production, high investment and production costs. It is claimed that EMS application not only breaks down dendrites to encourage globularization, but also could have beneficial effects on secondary phases, such as intermetallic particles and eutectic silicon in Al-Si foundry alloys [127,128].

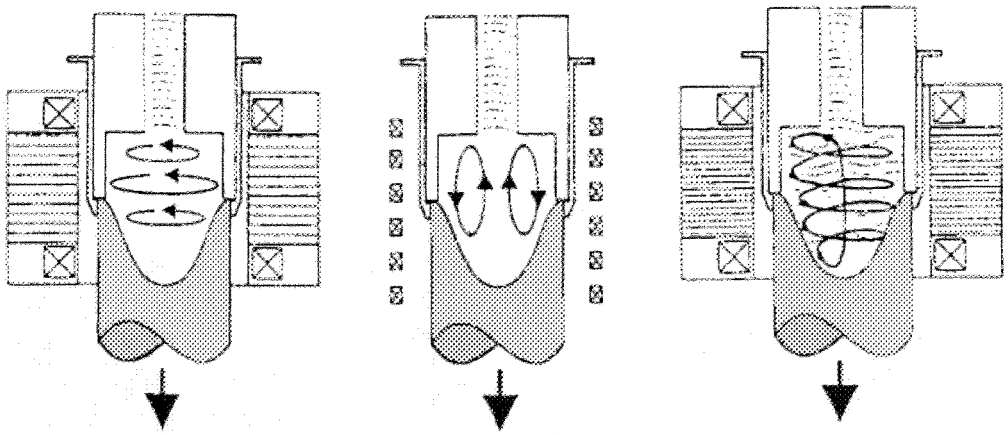

Figure 3.5: Schematic of electromagnetic coils for MHD stirring and solid particle flow pattern in the mushy zone (a) due to rotational inductive coils, (b) due to linear inductive coils, and (c) helicoidal stirring [126,129]

3.1.1.3 New RheoCasting NRC™ or UBE process

This process was developed in Japan by UBE industries [130] to produce SSM slurries of Al and Mg alloys. It is typically a SoD process and relies on thermal treatment of alloy melts. The sequence of processing steps leading to the formation of SSM slurries are (Figure 3.6) as follows:

- Molten alloy is prepared conventionally with a definite superheat depending on the case (step 1)
- The molten alloy prepared in step 1 is poured into a heat-insulated vessel. This transfer could be direct or by pouring through a jig (step 2). Here, the jig acts as a nuclei generator (It is important to note that grain refiner addition and also the amount of superheat in step 1 depend on the application of jig).
- In step 3, the alloy is held within the vessel for a period of time (5 second to 60 minutes) in the mushy zone to obtain a specific fraction of solid suitable for pressure forming. In this step and with a uniform temperature profile within the vessel very fine and isotropic dendritic primary crystals grow with a spherical shape as the fraction solid increases with decreasing temperature.
- In step 4, the obtained billet is pressure formed within a mold cavity to produce a shaped part

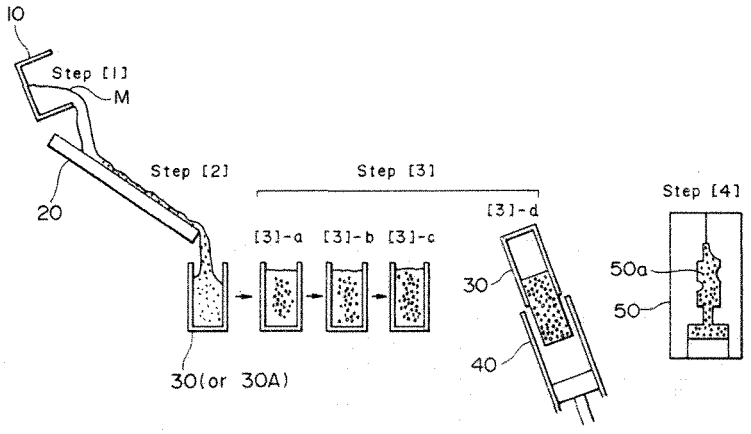

(a)

Continue ⟶

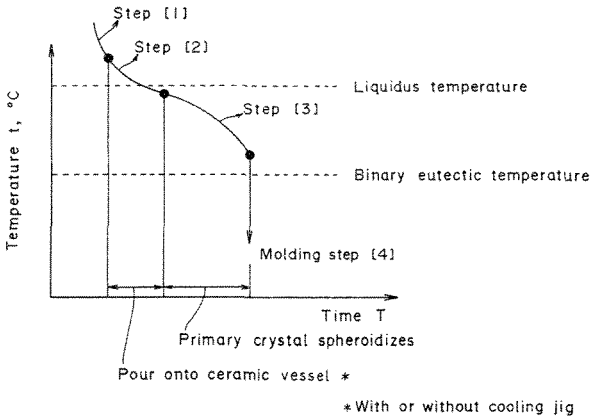

(b)

Figure 3.6: (a) Schematic representation of NRC process,
(b) diagram showing the process sequence for hypoeutectic Al-Si alloys [130]

3.1.1.4 Liquid mixing process

This process is based on the formation of a new alloy from a mixture of two molten alloys, either 2 hypo- or a hypo- and hyper-eutectic Al-Si alloy [131,132]. The rational for this process is based on the fact that if two or more molten alloys having different melting points that are held superheated are mixed either directly within an insulated vessel or indirectly with a first contact on cooling plates, they generate nuclei in the alloy melt. As mentioned [130], the superheat temperature, the melt refining process, the holding time within the insulating vessel, and the way of mixing are the main parameters that must be fully controlled, see Figure 3.7.

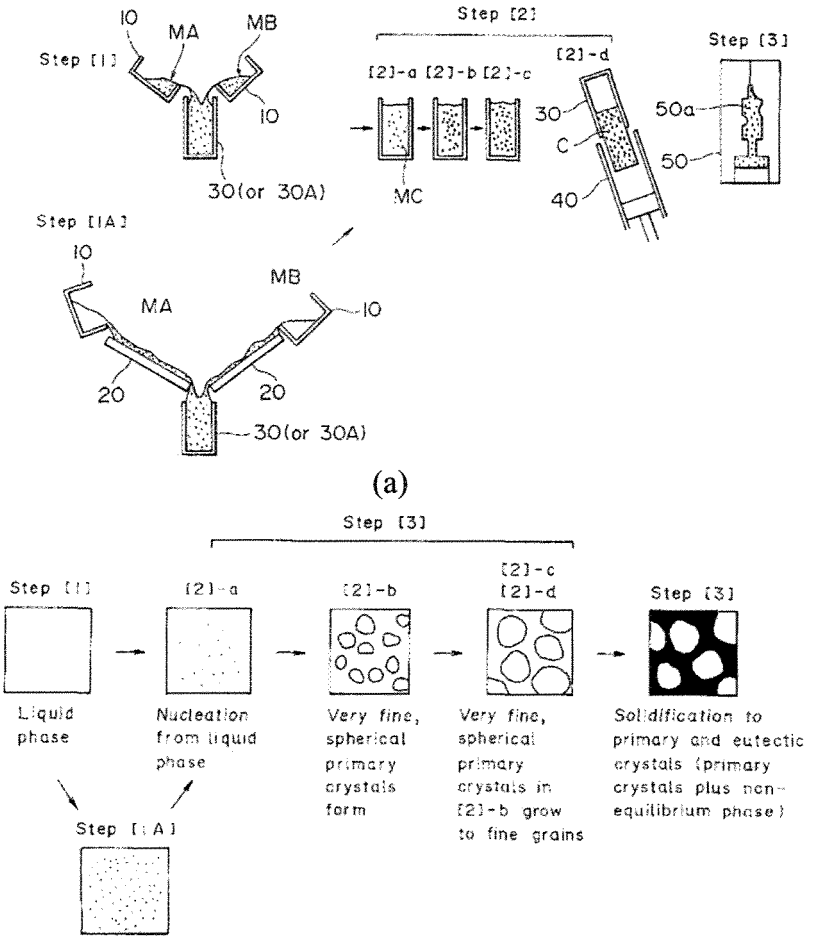

Figure 3.7: (a) Schematic representation of one mixing process;
(b) a diagrammatic representation showing the metallographic structure of a shaped part
10) ladle; 20) cooling jig; 30) ceramic container; 40) injection sleeve; 50) mold [130]

3.1.1.5 The new MIT process, Semi Solid Rheocasting SSR™

This is a process recently disclosed by a team at MIT [133-135]. The process has been claimed to produce fine SSM structures without entrapped liquid. This process, Figure 3.8a, consists of the following steps;

- Agitation over a very short time and just below the liquidus temperature with a copper or graphite rod, the so called "Spinning Cold Finger"
- Localized heat extraction, and
- A short period of slow cooling or isothermal holding in the semi-solid region

The combined stirring/cooling action at the liquidus temperature results in copious nucleation of primary α-Al particles in the melt. The SSR process is shown to be compatible to both low and high fraction solid castings. It is interesting that low fraction solid slurry could be handled like a liquid and there is no need for changing a conventional diecasting machine. Therefore, for example, the stroke of the machine does not need to be lengthened. Typical SSM structure produced by this method is shown in Figure 3.8b. This concept is under commercialization by IdraPrince as the SSR™ (Semi Solid Rheocasting) process [136].

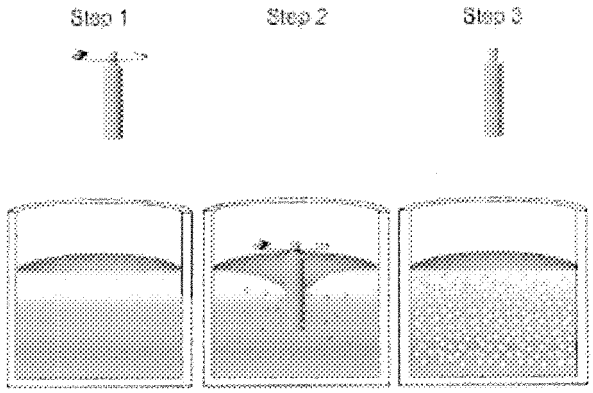

(a)

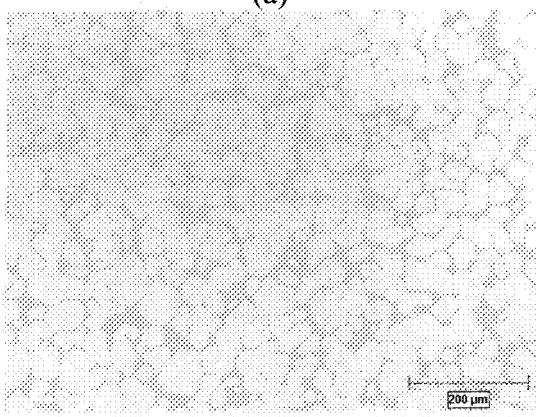

(b)

Figure 3.8: (a) Sequence of the SSR™ process, (b) micrograph for 356 cast alloy [136]

3.1.1.6 Ultrasonic treatment

Experimentally, it is well established that application of ultrasonic treatment to a cooling melt at a starting temperature just above its liquidus can produce effectively a fine and non-dendritic microstructure, which is suitable for subsequent reheating and thixoforming operations. Introduction of high power ultrasonic vibration into a liquid alloy can lead to two basic physical phenomena [137]: cavitations and acoustic streaming.

Cavitation involves the formation, growth, pulsation, and collapsing of tiny bubbles in the melt. The compression rate of these unsteady state bubbles can be so high that their collapsing generates hydraulic shock waves. Primary particles are broken up by these waves, thus producing artificial sources of nuclei. The propagation of high-intensity ultrasonic waves also involves the initiation of steady-state acoustic stream in the melt. The total effect of various kinds of streams is to mix the melt vigorously with consequent homogenizing.

Hydraulic and acoustic streams generate shock waves resulting from the collapse of cavitation bubbles to effectively break particles of the already solidified alloys and acoustic streams generate by ultrasonic treatment will homogeneously distribute these fine solid particles. When ultrasonic vibrations are coupled with the solidifying metal, structural changes occur including grain refinement, suppression of columnar grain structure, increased homogeneity and reduced segregation.

Abramov et al. [137-139], investigated the possibility of obtaining a thixotropic structure by an ultrasonic treatment in Al-Si based alloys and claimed that it is an effective way of treating major commercial Al-Si alloys. They concluded that the ultrasonic field provides nucleation sites and destroys the growing crystals. The reported mechanical properties have shown enhanced elongation values. It also reduces the size of primary silicon particles in hypereutectic Al-Si alloys. Figure 3.9 is an example of the resulting microstructures.

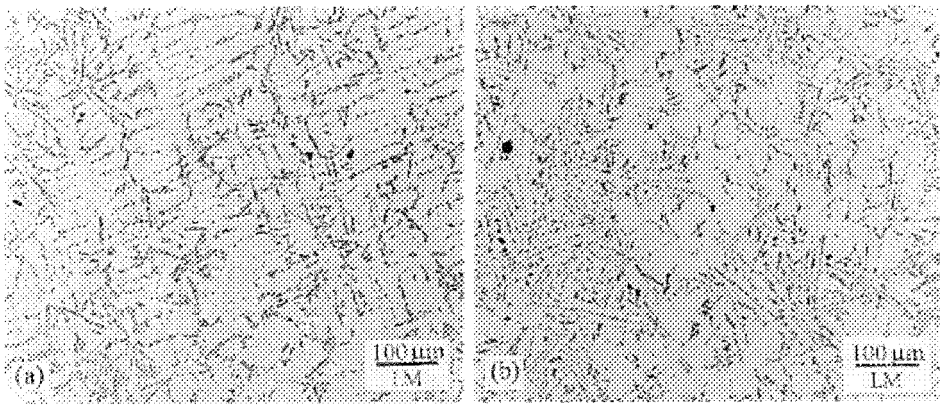

Figure 3.9: Microstructure of Al9Si alloys:
(a) conventional casting, (b) solidified with ultrasonic treatment [137]

3.1.1.7 Hitachi Process

Shibata et al. [140-141] described a new process to create slurry in the shot sleeve. In this process, Figure 3.10, liquid is transferred directly by an electromagnetic pump to the shot sleeve. In the next step, SSM is generated in the water cooled shot sleeve with EMS application. Because of cooling from shot sleeve and induction heating from electromagnetic field, it was claimed that the temperature of the liquid metal in the shot sleeve decrease almost uniformly. This process claims to have the following advantages:

- Direct casting from liquid state thus offering all the rheo-casting advantages
- With EMS application, uniform temperature distribution in the shot sleeve is assured
- With electromagnetic pumping, oxide inclusions are reduced and pouring weight is accurate
- Mechanical properties of the casting prepared by this process are better than those of squeeze casting and are almost the same as those of conventional SSM process

It seems that this process is extensively used by Hitachi Metals Inc [141].

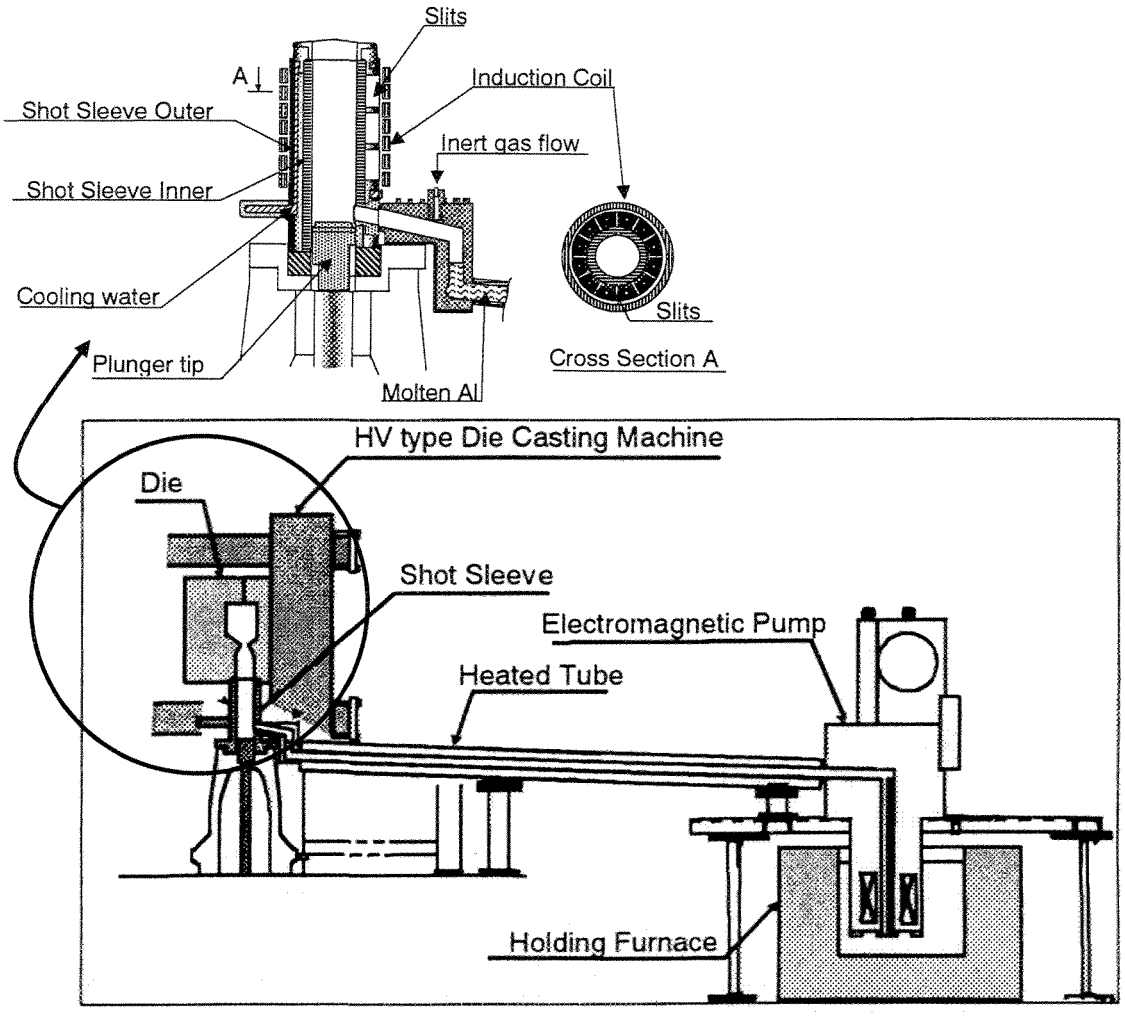

Figure 3.10: Hitachi process with focusing the electromagnetic stirring in the shot sleeve [141]

3.1.1.8 Low pouring or superheat casting

It has long been realized by foundrymen and ingot casters that low pouring temperature not only causes the formation of equiaxed grains, but also reduces casting defects, such as gas and shrinkage porosity. Shibata et al. [142] applied this concept for SSM processing, i.e., low pouring temperature. It is well understood that convection during mold filling is an important factor as solidification begins. For low pouring temperatures, the natural convection due to pouring redistributes the nuclei formed, while at high pouring temperatures, the convection subsides before solidification even begins and all the formed nuclei remelt leaving the solidification to start with a relatively motionless melt.

Shibata et al., have shown that spherical primary solid phase can be easily obtained by low pouring temperature method. Figure 3.11 shows schematic drawing of the semi-solid process in their study. The melt was poured into the shot sleeve and injected into the die cavity after a defined cooling period. Figure 3.11b shows the effect of pouring and sleeve temperatures on roundness of α-Al particles. Higher roundness of primary α-Al particles were obtained at the lower pouring and sleeve temperatures. This phenomenon appears to be based on equiaxed grain formation initiated by a copious nucleation mechanism.

Wang et al. [143-144], produced AlSi7Mg0.35 alloy with different pouring temperatures in a 50mm diameter mold. In their experiments, pouring temperature was decreased from 725 to 625°C. With decreasing pouring temperature, as-cast microstructures changed from coarse dendritic (725°C) to fine rosette-like (625°C). Also with reheating the billets at 580°C and quenching, particle size decreased with decreasing pouring temperature (Figure 3.12). Table 3.1 also summarizes their results. The variation of shear stress with displacement after isothermal holding at 580°C for 15 minutes is also reported. The 725°C cast samples show high shear strength in excess of 50kPa, while for the 675°C material the shear strength is reduced significantly to 20kPa. When the pouring temperature is reduced to 650°C, the shear resistance of the material is very low at about 5kPa and the shear stress does not drop significantly after the maximum (Figure 3.13).

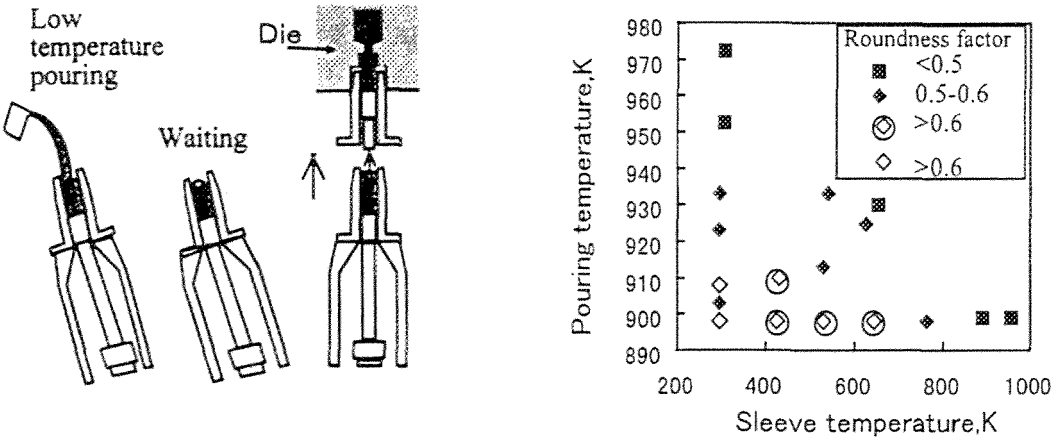

(a) (b)

Figure 3.11: (a) Schematic of casting method,
(b) effects of pouring and sleeve temperature on roundness factor [142]

Table 3.1: Summary of the microstructural parameters measured in the as cast and reheated billets at 580°C for 15 minutes [144]

As cast microstructure			Reheated microstructure	
Casting Condition	Structure	Grain Size (μm)	Particle Size (μm)	Morphology
725°C	Coarse- grained , dendritic	900	310	Solid network
675°C	Medium-grained, dendritic	350	160	Irregular globular
650°C	Fine-grained, dendritic	200	102	Spherical globular
625°C	Fine rosette-like	180	95	Spherical globular

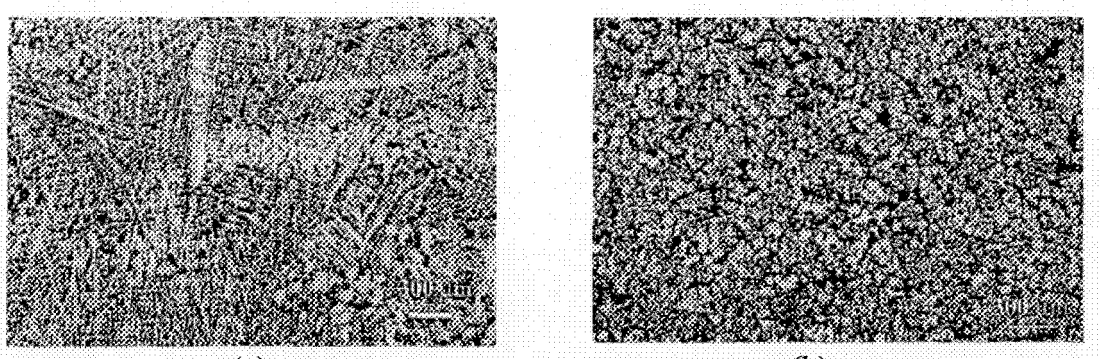

(a) (b)

Continue ⟶

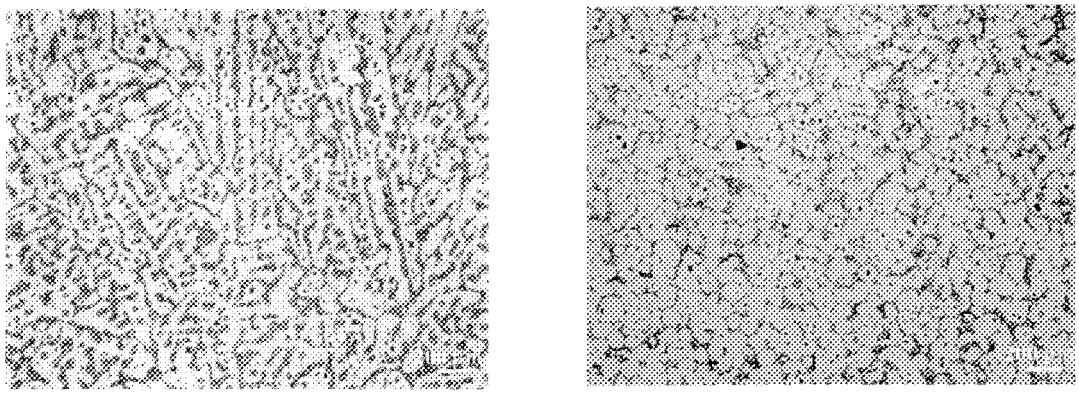

(c) (d)

Figure 3.12: Microstructures of: (a) as-cast at 725°C, (b) as-cast at 625°C , (c) and (d) partially remelted and isothermally held for 15min from specimens with initial microstructure exhibited in (a) and (b) respectively [144]

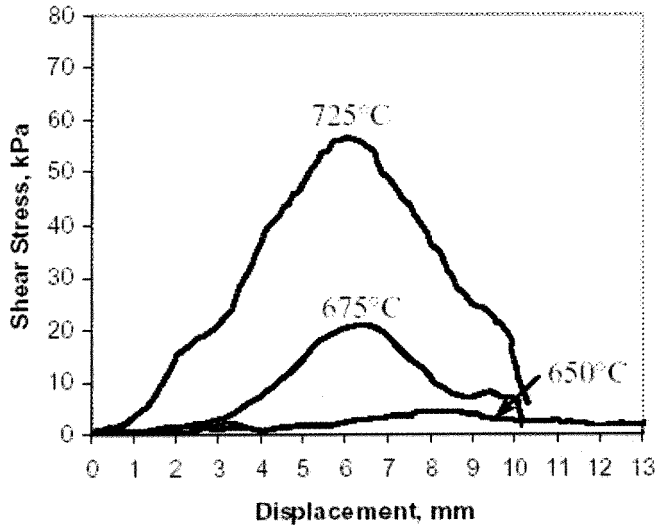

Figure 3.13: Variation of shear stress with displacement for the 356 cast at different temperatures and isothermally held at 580°C [reproduced from 145]

Interestingly, another important issue is the way of pouring which was shown for the first time by Chalmers [25]. Dahle et al. [146] have studied this phenomenon by using an experimental arrangement as shown in Figure 3.14. A thin cylinder of metal screen was placed into a mold and then molten metal was poured both from the wall and center of the mold. One can see that the grain size in the center is much finer when liquid is poured from the cold wall because of the large amount of nuclei produced in the first contacts.

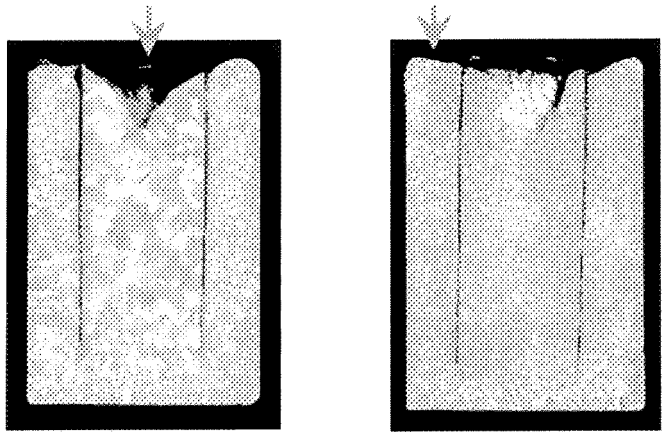

(a) (b)

Figure 3.14: Macrostructures produced by different pouring techniques: (a) central pouring, (b) wall pouring [146]

3.1.1.9 Sub Liquidus Casting (SLC®)

The SLC® process from THT Presses Inc considered another simple slurry production approach to SSM processing [147]. This process involves pouring grain refined or a super refined melt at very low or near liquidus temperatures into a vertical shot sleeve, controlled cooling of metal in the shot sleeve and injection into the die cavity, following formation of desired fraction solid and slurry ripening within the cold chamber (Figure 3.15). It has been reported to yield a globule size of approximately 75μm [147-148]. Unlike other SoD routes, the SLC® process requires no slug preparation equipment or processing time outside of the casting machine [149].

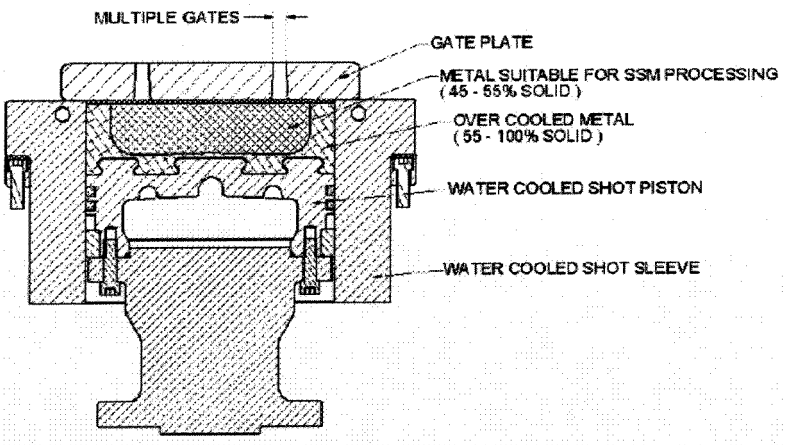

Figure 3.15: Schematic of SLC shot sleeve and gate plate [147]

3.1.1.10 Swirled Enthalpy Equilibration Device (SEED)

This is a new process patented by ALCAN International [16]. In the SEED process, a superheated alloy is poured into a cylindrical mold. The mold is then rotated at certain RPM. Duration of this stage depends on the dimension of the mold and the mass of charge, but typically between 30 and 60 seconds was reported [151]. In the next step the swirling motion is stopped, and after a brief pause of 5 to 10 second the bottom plug is removed to allow some remaining liquid to drain. The degree of superheat and the swirling and drainage time and speed are selected in such a way as to allow a solid fraction of 0.3-0.4 to form before drainage. This is based on heat exchange between the mold and molten alloy. After a specific time between 30 to 45 seconds, the prepared billet is unloaded and transferred into a high pressure diecasting machine to fabricate the finished products (Figure 3.16).

At the present time, this process is being commercialized and specific information on it is available in the open literature [150-152].

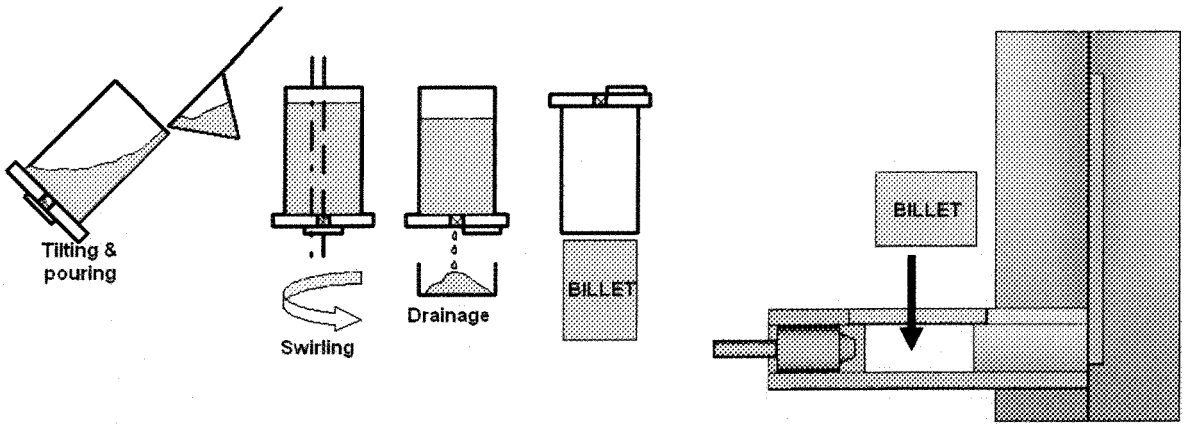

Figure 3.16: Preparation procedure of slug SEED process [152]

3.1.2 Thixo-route techniques

3.1.2.1 The Strain-Induced Melt Activation (SIMA) Process

It was the primary objective of the SIMA inventors [124] to devise a more flexible and economical process for providing small diameter feedstock for some wrought alloys. This process involves (Figure 3.17):

- Cold deformation or quenching of a hot extruded or rolled bar to induce sufficient strain,
- Reheating the cold worked billet to the semi-solid temperature range. In this step, following partial remelting, an extremely fine, uniform, and nondendritic spherical microstructure is generated (Figure 3.18),
- Thixoforming the billet

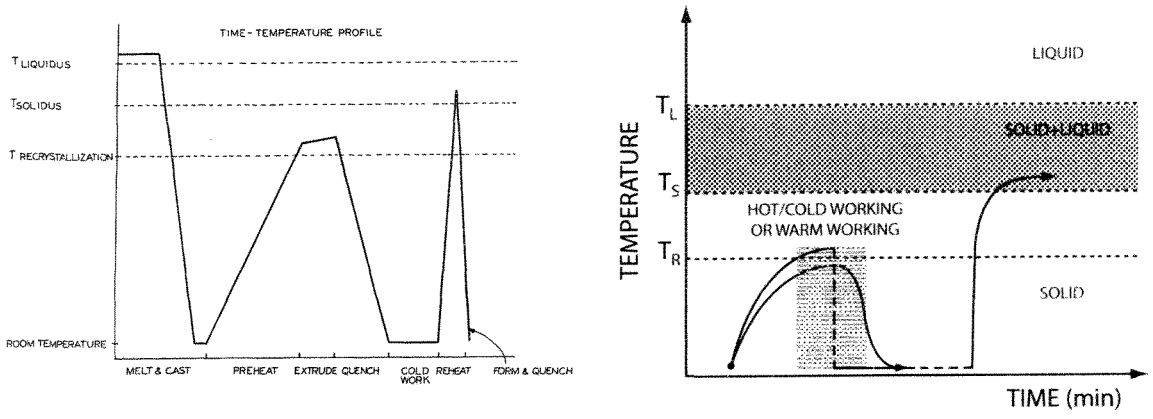

(a) (b)

Figure 3.17: (a) Original SIMA process, (b) SIMA procedures for pre-cast billets [122,124]

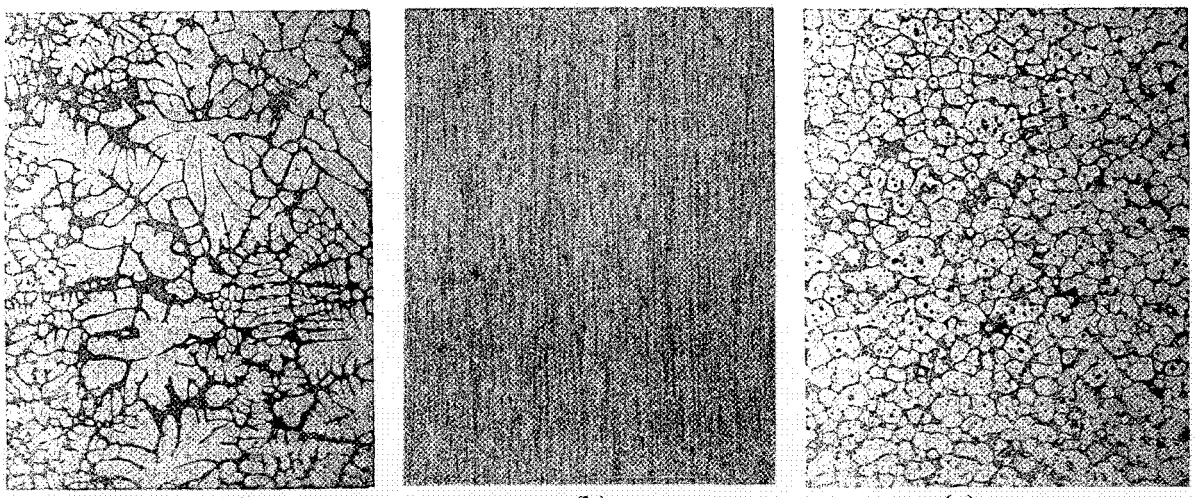

(a) (b) (c)

Figure 3.18: SIMA processing route for semi-solid forming, 357 alloy: (a) direct chill cast with 6 inch diameter, (b) longitudinal section of the extruded stretched bar, (c) cross section of the reheated and quenched sample [124]

Scientifically, if the material has been sufficiently deformed and recrystallized to generate a fine-grained microstructure, a partial remelting will then cause it to fragment generating an ideal slurry composed of rounded solid particles within a liquid matrix. The initial deformation may be carried out above the recrystallization temperature (hot working) followed by cold working at room temperature [124,125], or alternatively below the recrystallization temperature (warm working) to ensure the maximum strain hardening, as suggested by Kirkwood and co-workers [7,153].

Sufficient cold deformation induces recrystallization during subsequent heating when strain is larger than a critical value. Recrystallization leads to the formation of a large proportion of high angle grain boundaries, which are able to melt during partial remelting. Therefore, the larger the applied strain, the smaller the grain size becomes, i.e. finer globules will be generated when cold working is sufficient. This is shown in Figure 3.19 for Al7%Si alloy cold rolled with various thickness reductions [154].

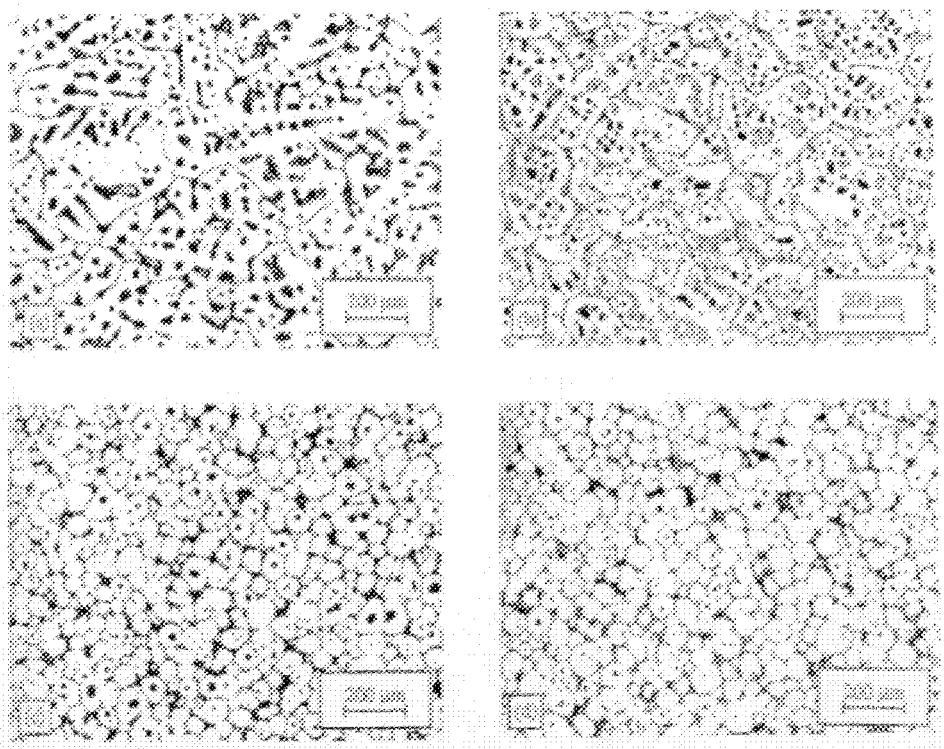

Figure 3.19: Microstructure of conventionally direct chill cast Al-Si7Mg0.6 after partial remelting at 580°C (fs~0.45), and cold rolling (a) 0%, (b) 10%, (c) 25% and (d) 40% prior to partial remelting. Isothermal held ~30seconds [154]

3.1.2.2 Spray Casting (Osprey)

This process with two different production methods is shown in Figure 3.20. Briefly, the alloy charge is induction melted in a crucible located on the top of the spray chamber (this melting unit could be directly linked to a tundish). The molten metal flow is directed through a nozzle into a gas atomizer (the flow rate varies for different alloys). This results in atomization of the liquid stream into different size droplets. The liquid droplets are cooled by the atomizing gas and interact with the substrate.

According to Mathur et al. [155], there are two distinct stages of the process: One is when the droplets are in flight and just interact with the atomizing gas, and the other is when they impact and interact with the substrate. In the first stage, the generated droplets are categorized as fully liquid, semi-solid, or completely solid. They are collected on a substrate and solidified to form a shaped casting (Figure 3.20b). In the next stage of the process, the droplets impinge, consolidate, and solidify on the substrate to form a homogenous structure.

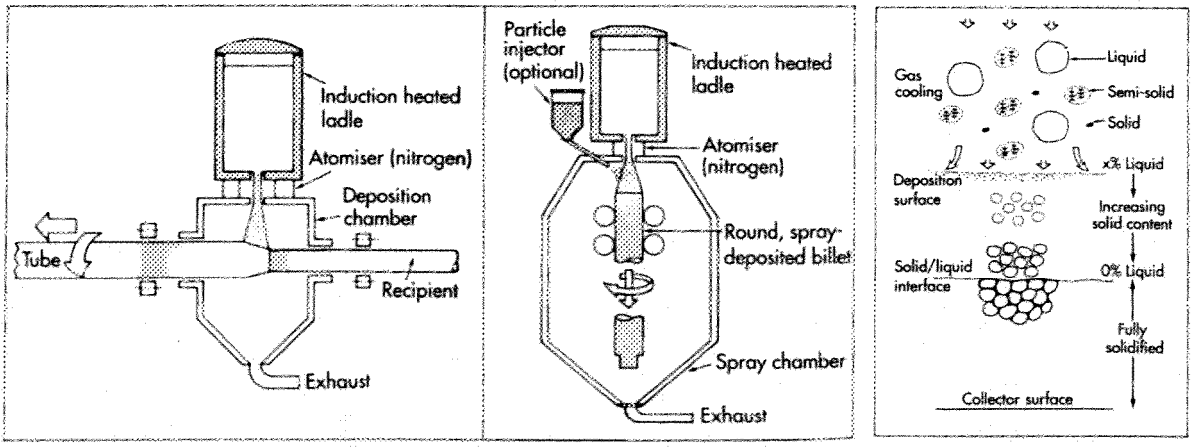

(a) (b)

Figure 3.20: (a) Two different arrangements for tube and billet production by Osprey process, (b) solidification mechanism of Osprey process [156]

The Osprey process has been applied to a wide range of alloys, such as aluminum and its SiC composites, and high temperature alloys such as high speed steel, and copper alloys [155,156].

3.1.2.3 Liquidus or low superheat casting

As it was described before, this process could be also a source for the thixocasting process. With low pouring temperature, the resulting microstructures are usually fine and non-dendritic. Partial remelting and isothermal holding of the sample will produce a globular structure suitable for thixoforming operations. This technique has been reported for both cast and wrought aluminum alloys.

Wang et al. [143], have performed experiments with AlSi7Mg0.35 alloy with different pouring temperatures in a 50mm diameter mold. Using a stepped die for squeeze casting and reheating the produced billets from different pouring temperatures, they have shown that the low temperature poured material filled completely the die with negligible porosity (Figure 3.21).This technique could be used for industrial application but the major obstacles may arise from difficulties related to accuracy and uniformity of temperature control, and consistency and uniformity of resulting microstructure in large scale production [8].

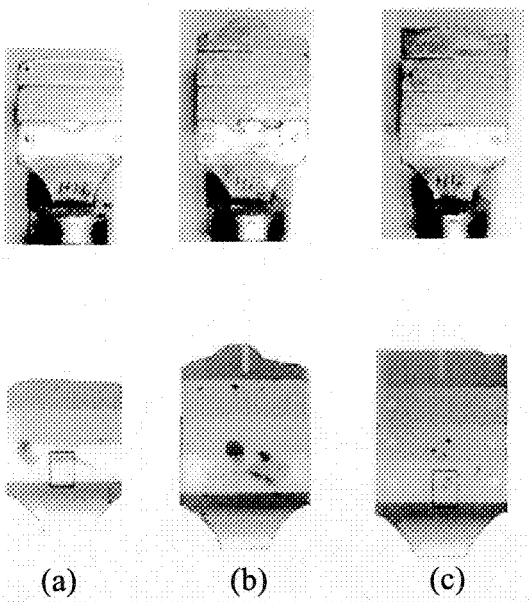

(a) (b) (c)

Figure 3.21: Cast pieces from different pouring temperatures (above) and their X-ray radiographs (below).
Pouring temperatures are (a) 725°C, (b) 675°C, and (c) 650°C [143]

3.1.2.4 Chemical grain refinement

Chemical grain refinement is a routine practice in continuous casting of aluminum alloys. This technique has also been considered for feedstock production [9-11,157]. In this method, globular SSM slurries can be obtained by simply reheating grain refined billets that could be purchased from cast houses or primary producers. It was claimed [158] that in this technique, the morphology of the primary α-Al particles is still globular or rosette-like, but the amount of liquid entrapped within the particles is significantly larger than MHD slurries.

In a recent work by Pan et al. [159], it was shown that the grain refinement approach is more flexible and cost effective compared to the EMS technique. They proved that the type of grain refiner is a critical parameter in the establishment of the final microstructure and by using a new trade mark grain refiner, named SiBloy, concluded that during reheating of grain refined billets, the B-refined billets have 4 times less entrapped liquid compared to TiB_2-refined billets (Figure 3.22).

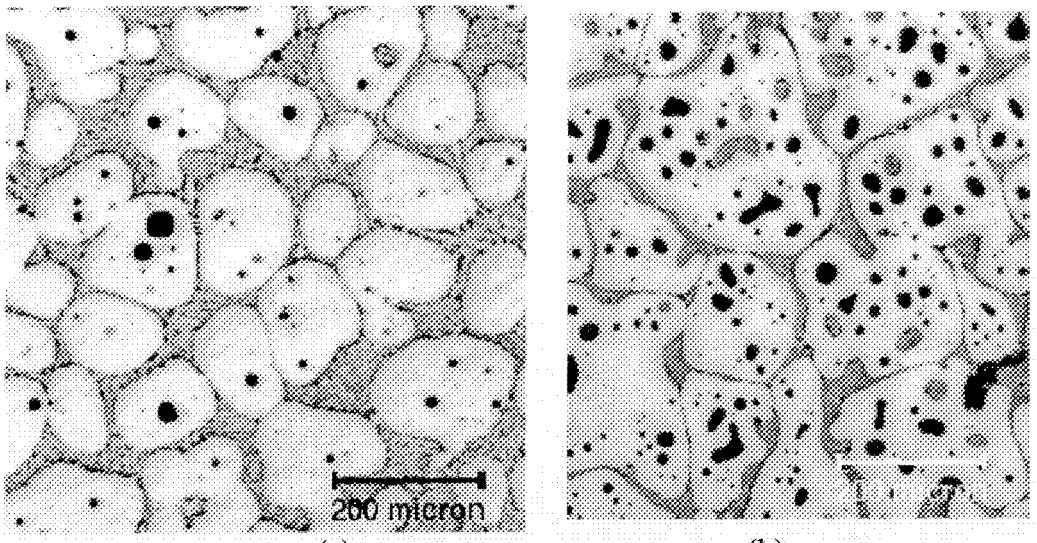

(a) (b)

Figure 3.22: A comparison of semi-solid structures of: (a) B-refined billets, (b) TiB_2 grain refined (Reheat temperature: 585 °C) [159]

3.1.2.5 Thixomolding

Thixomolding is a process that was developed especially for magnesium alloys (Figure 3.23). The raw material for the process is neither liquid (as in rheocasting) nor solid billet (as in thixocasting), but rather solid pellets or chips of 2-5mm in size obtained during machining or other metal working of the magnesium alloys. These chips are fed into a heated injection system where they are partially melted and transformed under continuous shear force into thixotropic slurry. The core of this unit is an Archimedean screw which performs both rotary and translational movement. To prevent the magnesium alloy from oxidizing, an argon atmosphere is maintained within the system. Two major advantages of this process are its effective slurry production and elimination of liquid metal handling. At the present it appears that this process is limited by relatively low solid fractions (~0.3), selection of the material for the screw, and oxide formation [8,122].

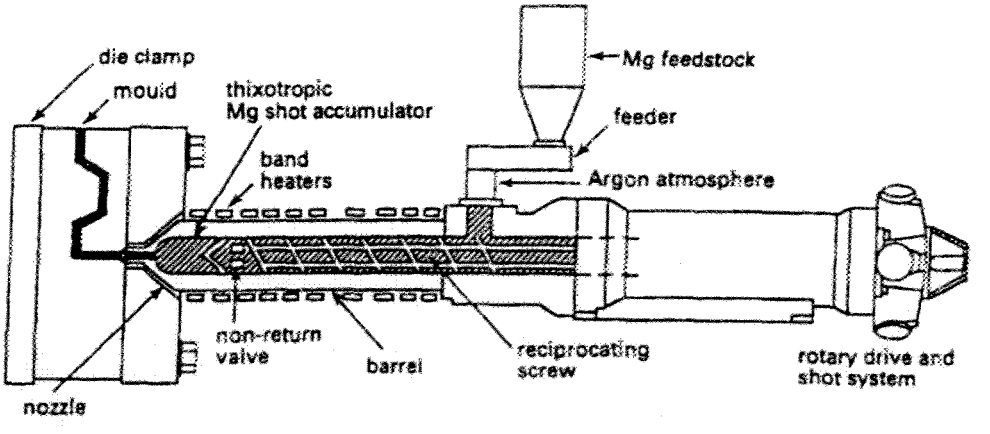

Figure 3.23: Schematic diagram for thixomolding process [8]

3.2 Grain refining and modification in the semi-solid casting, a review

3.2.1 Effects of grain refining on semi-solid structures

Addition of grain refining agents to molten aluminum is now a prerequisite for successful and economic casting. Grain refinement provides an equiaxed grain structure, uniform mechanical properties, and better machinability; it also eliminates shrinkage, increase resistance to hot tearing and improves feeding.

In the SSM processing of aluminum alloys, specially Al-Si alloys, the size of the primary α-Al particles play an important role in the final mechanical properties. Most of the alloying elements reduce the size of α-Al grains but as mentioned before, the effective method for reducing the size of grains is the application of grain refiner. It was reported that the best flow behavior for semi-solid metal processing is achieved if the raw material structure consists of finer and more rounded globular grains [10].

In the science of semi-solid, there is not much work reported on the direct incorporation of grain refiners during the processing and preparation of slurries and most of the works are related to the post thermal treatment of the cast billets [9-13]. As a result, the current section is to cover the research works on the two main groups of SSM processes; thixocasting and rheocasting.

3.2.1.1 Grain refining in the thixocasting

A typical grain refining curve shown in Figure 3.24 presents the grain size of primary phase in relation to the grain refiner addition rate. At lower addition level, the grain size decreases significantly with increasing addition rate. However above a definite titanium and/or boron addition level (C_1) only slight improvements in grain size are achieved. Due to technical and economical reasons, the usual addition level is therefore as low as possible, this is in the range of C_1 for cast alloys and even below C_1 for wrought alloys. If DC-cast bars of this type are reheated for SSM processing, the reheating times of up to several hours are required to produce globular grains by means of ripening and

coalescence [157]. Depending on the alloy system this may result in formation of very large grains. However some preliminary experiments indicated that higher addition levels of grain refining agents may promote the formation of globular grains during reheating, even though it does not significantly change the as cast structure [9,160].

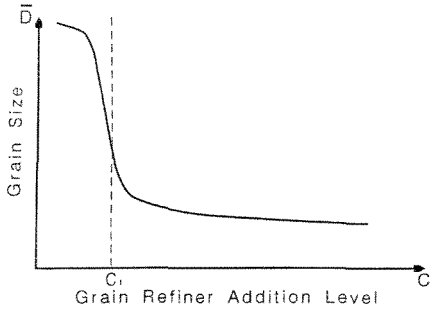

Figure 3.24: Grain refining of Al alloys with grain refiner containing Ti and B [9,160]

Gabathuler et al. [10] by using different grain refiners, EMS and ultrasonic SSM routes, and observing the microstructure and the forces needed to extrude SSM AlSi7Mg0.3 billets through a die (ingot with 75mm diameter), claimed that AlTi5B1 and AlTi2.5B2.5 master alloys are not efficient enough for the production of thixobillet because the desired grain size for an adequate thixotropic material is less than 150 μm and the measured grain sizes were never below 200 μm (Table 3.2).

Table 3.2: Influence of AlTiB grain refiner on the grain size and homogeneity of DC cast AlSi7Mg0.3 [10]

Grain refiner	Concentration [%]	Grain diameter [μm]		Homogeneity of grain size
		Near ingot surface	Ingot center	
Without	-	≈ 5000	≈ 2000	feather crystals
$AlTi_5B_1$	0.02	350	500	good
	0.1	300	500	good
	0.5	240	420	very good
$AlTi_{2.5}B_{2.5}$	0.02	400	450	good/poor
	0.1	300	350	good
	0.5	220	300	very good

Wan et al. [9,160] studied the effects of grain refining on the billet production. They added AlTi5B1 master alloy to the A356 and poured it in a water cooled conical brass mold

and a preheated steel mold to achieve different cooling rates. The samples were heated in a medium frequency induction furnace to a temperature 5°C above the eutectic/solidus temperature with varying heating rate and holding period and they were quenched after holding. The following results were concluded (Figure 3.25):

- At a given addition rate, the grain size both in the as-cast and subsequently reheated conditions decreases with increasing the cooling rate,
- Above approximately 0.025%Ti, the as-cast grain size is almost constant and the as-cast grains are equiaxed dendritic,
- The minimum reheating time for the formation of rounded globular grains decreases with increasing addition level of grain refiner,
- At an addition level of 0.26%Ti, the minimum reheating time is at a technologically acceptable level of 5 minutes and the reheated globular grain size is approximately 120μm.

Mertens et al. [11] have studied the aluminum wrought alloy AlMgSi1 (6082) with different feedstock manufacturing and feeding routes. With grain refinement, it was observed that in the as-cast structure, the material already has a globular dendritic matrix. Heating to 635°C and isothermal holding for 5 minutes, induces a structure suitable for thixoforming with a mean grain diameter of about 90μm approximately. After holding for 20 minutes at 640°C, the α-Al phase is present in an almost spherical form, but the structure is slightly coarser. An approximately 130μm mean grain diameter was reported (Figure 3.26).

Bergsma et al. [12,161] have observed the combination effects of high solidification rates and grain refining on 76.2mm dia. billets of A356 and A357. The average grain size before reheating was 120μm and samples were reheated to 588°C and then quenched. The results show that combination of grain refiner addition and semi-solid thermal transformation (SSTT) result in spherical particles formation. Also with increasing the holding time at 588°C, the particles tend to grow and the shape changes (Figure 3.27).

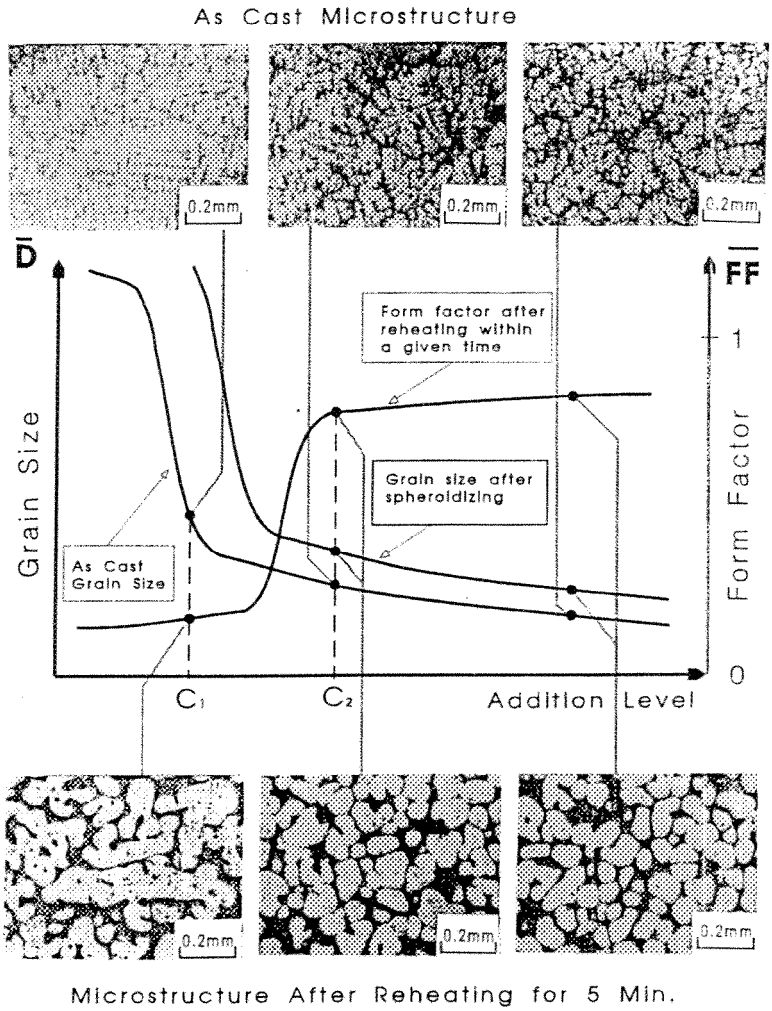

Figure 3.25: Results of grain refinement for thixotropic raw material. The microstructures of A356 are shown as example. C_1=conventional addition level and C_2=critical addition level [9,160]

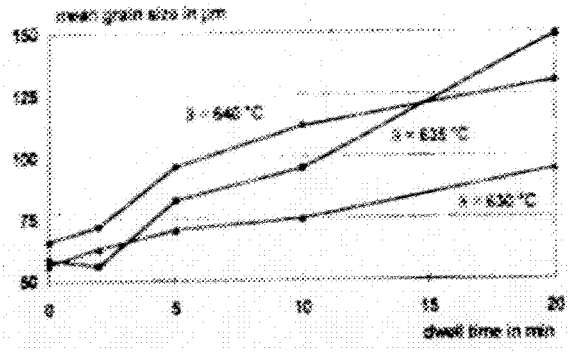

Figure 3.26: Structural development of the grain refined material as a function of the temperature and holding time [11]

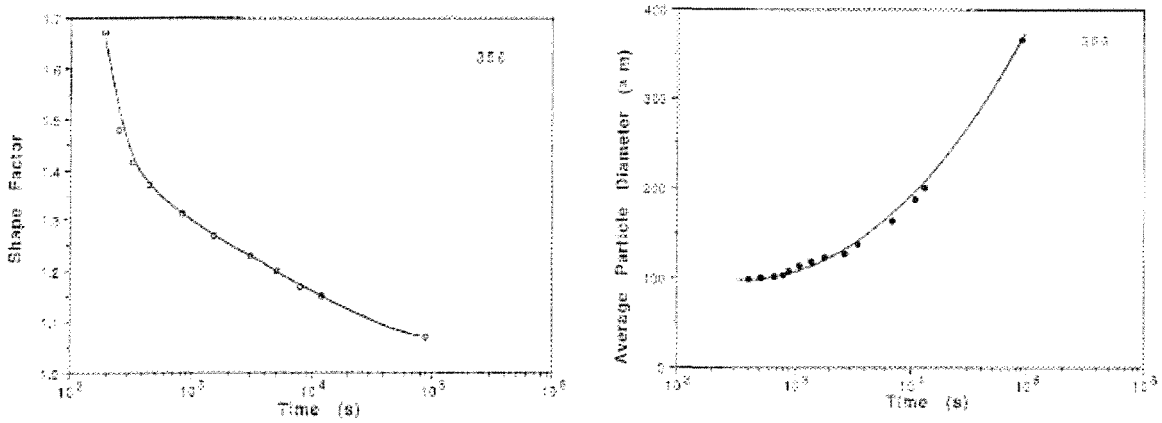

(a) (b)

Figure 3.27: (a) Shape factor as a function of holding time,
(b) average 3D particle diameter versus holding time [12]

Wang et al. [143-145] with experiments on Al7Si0.35Mg in 50 mm steel mold and with different pouring temperatures, have shown that using both low pouring temperature and grain refining could optimize the structure during billet casting, partial remelting, and injecting. They confirmed that the addition of grain refiner imparts little effect on grain size for the casting condition used in their work but after isothermal holding at 580°C, they concluded that the grain refined samples attained a globular structure faster than the non grain refined alloy because of the more rosette like structure of the grain refined sample.

Table 3.3 and Figure 3.28 show the variation of grain and globule size before and after refiner addition and/or reheating. As seen, grain refiner has an obvious effect on the structure both on the as-cast and reheated structures. Figure 3.29a shows stepped die cast pieces. Injecting of the reheated refined alloy led to the complete filling of the mold with the added bonus of defect free cast piece. Figure 3.29b is a good indication of reheating time which shows that smaller grain size could be reheated in lesser time during thixocasting.

Table 3.3: Selected parameters measured in the as-cast and reheated billets at 580°C for 15 minutes [144]

As-cast microstructure			Reheated microstructure	
Casting Condition	Structure	Grain Size(μm)	Particle size(μm)	Morphology
650°C	Fine-grained, dendritic	200	102	Spherical globular
650°C + GR	Fine globular	160	95	Spherical globular

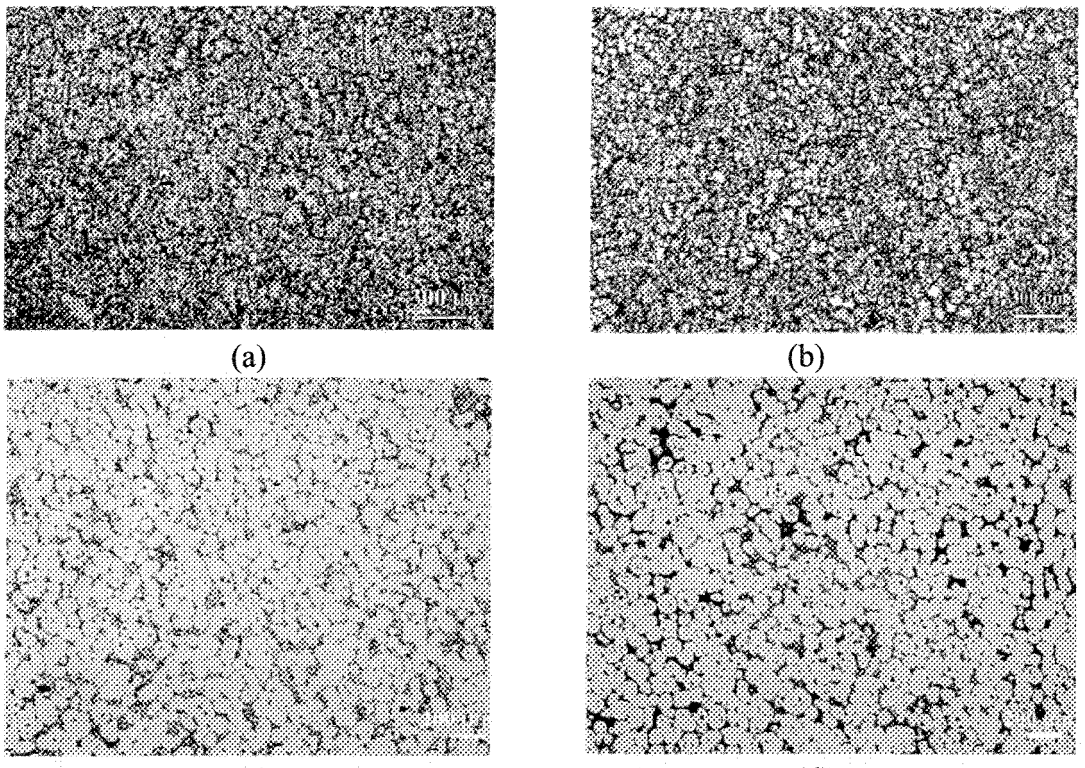

(a) (b) (c) (d)

Figure 3.28: Microstructures of: (a) as-cast 650°C, (b) as-cast grain refined 650°C, (c) and (d) partial remelted and isothermally held for 15minutes from the initial microstructure of a and b respectively [144]

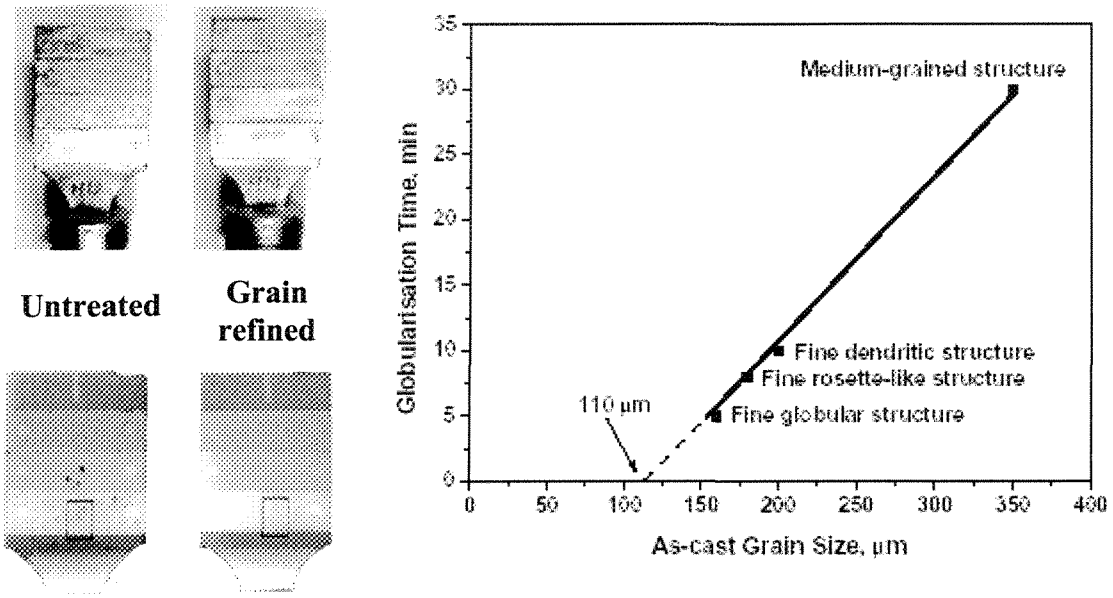

(a) (b)

Figure 3.29: (a) Cast pieces from grain refined (right) and non refined (left) samples and their X-ray radiographs [143], (b) globularization time for different microstructures isothermally held at 580°C [144]

Also they measured the shear behavior of the semi-solid material by a direct shear test. Figure 3.30 shows the shear results for different treatment and holding times. For longer holding times, more globules form which results in lower shear strength. The reduction in shear strength is achieved at longer times for non-grain refined samples; 6 minutes of reheating to reach to 10kPa shear strength in contrast to 3 minutes for the refined specimen to have the same shear. The difference in shear strength becomes negligible at longer reheating times [145].

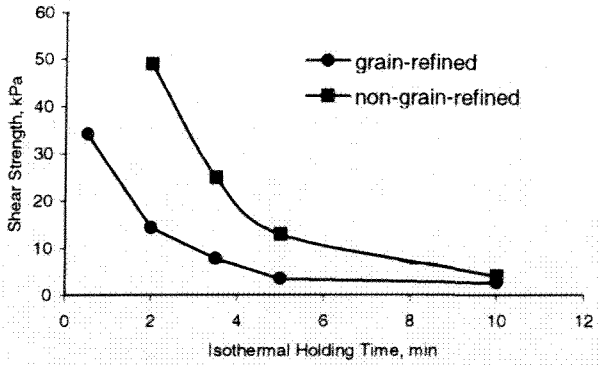

Figure 3.30: Variation of shear strength with isothermal holding time for the cast and EMS materials [reproduced from 145]

Pan et al. [159,162] have investigated the effect of melt treatment in different thixo-routes. They used boron grain refiners in the form of SiBloy trade mark and for comparison purpose, a commercial TiB_2 refined ingot was examined as well. It was found that in non reheated samples, boron grain refined billets have smaller grain size compared to TiB_2 grain refined sample (Figure 3.31a&b). Moreover, B-refined billets have more uniform grain size distribution on the billet cross section than commercial TiB refined samples. Figure 3.31 compares typical B-refined and TiB-refined billets before and after reheating. One can see that the structure of the latter has much more entrapped liquid content, larger α-Al particles and less spherical particles after reheating (comparing Figure 3.31c&d). Quantitative metallography has shown that the B-refined billets have 4 times less entrapped liquid. Figure 3.32 shows the difference between TiB and B-refined billets. They finally concluded that the optimized boron-refined alloy is an excellent candidate billet material for SSM processing.

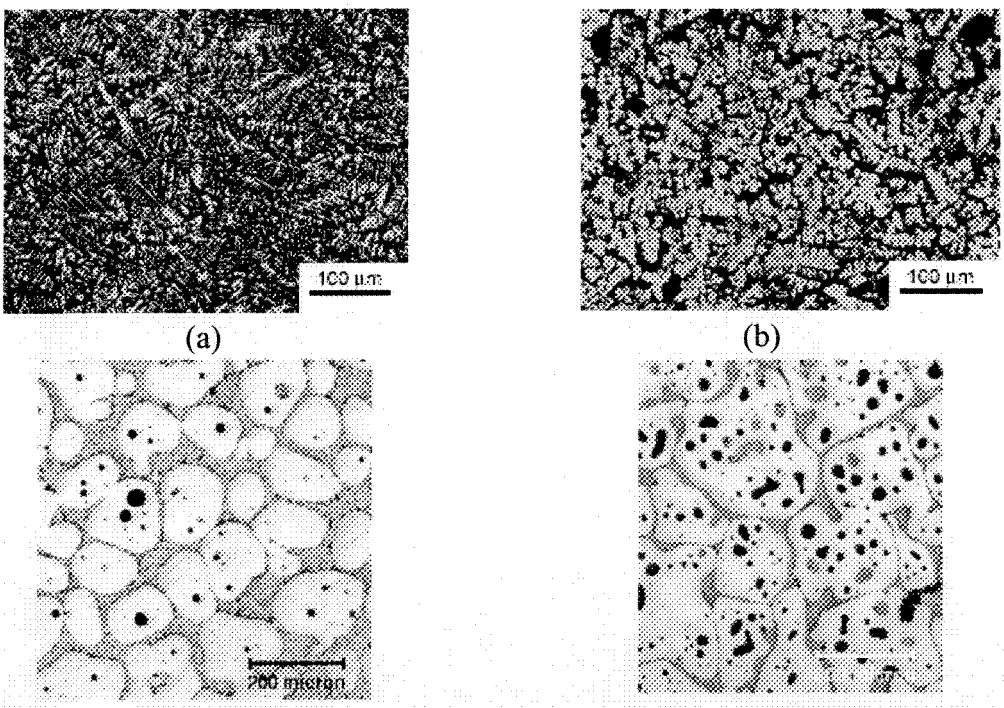

(a) (b)

(c) (d)

Figure 3.31: Typical grain structures of the alloys investigated,
(a) B-refined, (b) TiB_2-refined, followed by a comparison of semi-solid structures of B-refined billets (c) with those of commercial grain refined (d)
(Reheated Temperature: 585 °C) [159]

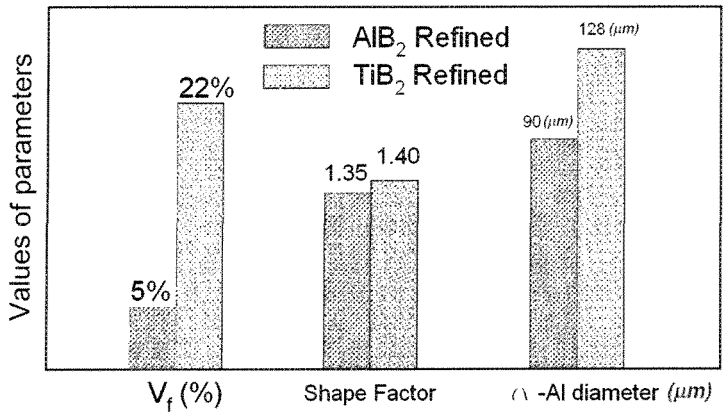

Figure 3.32: Image analysis results (V_f: entrapped liquid content, shape factor of the α-Al phase ($P^2/4\pi A$), and α-Al particle size) [159]

3.2.1.2 Grain refining in the rheocasting

Grimmig et al. [163] used grain refiner and modifier to investigate the effect of melt treatment on the final quenched microstructure on A356 alloy. For rheo-route, they used cooling slope process. It was claimed that the addition of grain refiner did not change the structure and just what supplier added was enough. However, it is clear from the optical micrographs in their paper, shown here in Figure 3.33, that the primary α-Al particles are finer, better distributed, and even α-Al percentage is increased.

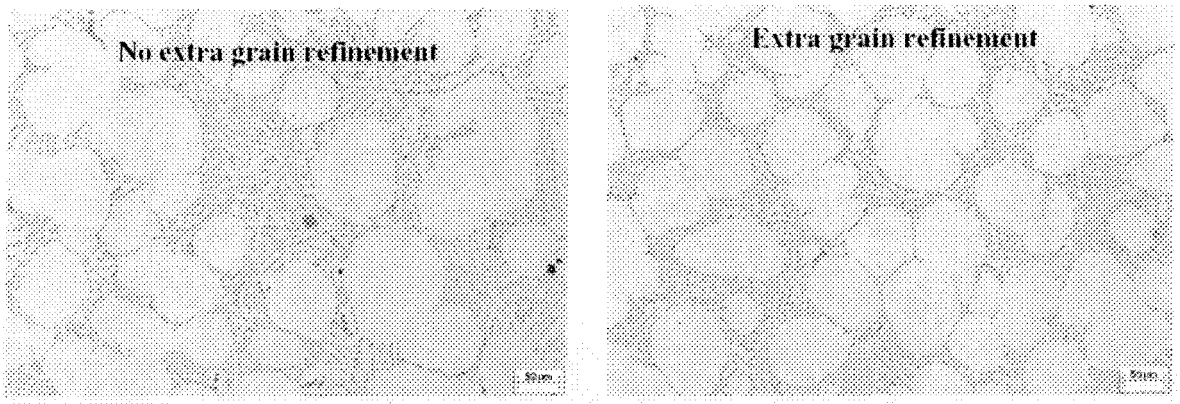

Figure 3.33: Microstructures with and without inoculation in the quenched billets [163]

Shibata et al. [142], by employing the low pouring rheocast technique, have shown that addition of grain refiner roughly raises the roundness factor of the α-Al particles. Also this increase is more for TiB_2 grain refiner (Figure 3.34).

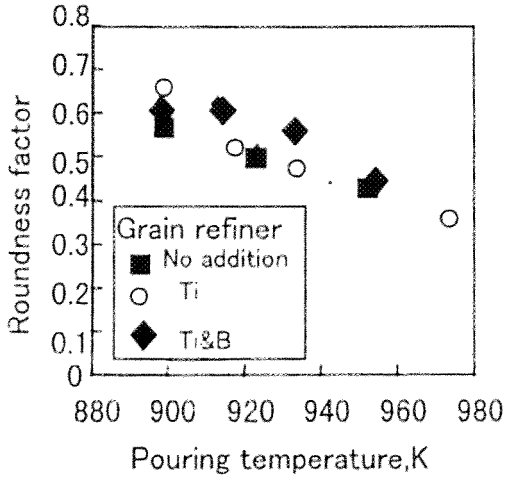

Figure 3.34: Roundness factor of test specimen [142]

In the support of the above mentioned observations, Sukumaran et al. [164] with isothermal rheocasting studies of Al5.2Si alloy have shown that the refiner addition (in the form of Al5Ti0.6B) prior to stirring has influence on the size and morphology of the primary α-Al phase . The effects of applied shear rate on the primary particle size of the non-refined and refined alloys are shown in Figure 3.35. The size of primary α-Al particles obtained with the refiner addition followed by stirring is comparatively smaller than that obtained without refiner. This has been proposed due to heterogeneous nucleation resulting in the formation of equiaxed grains suppressing the formation of dendritic/columnar structure.

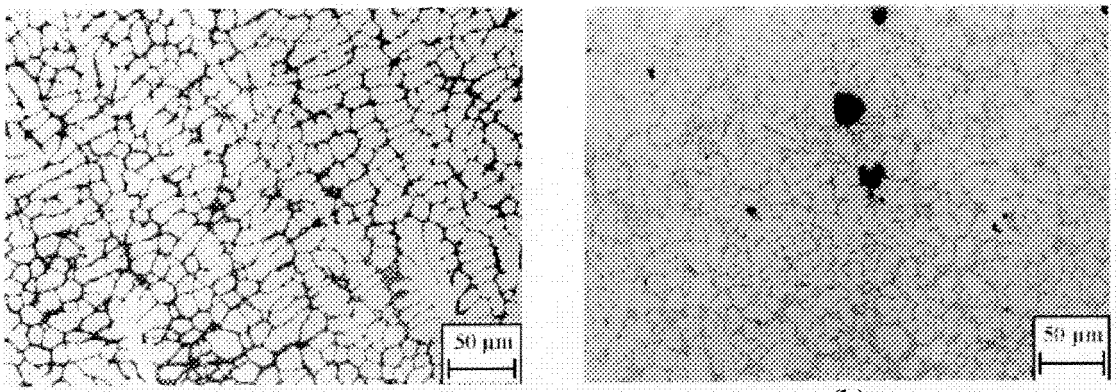

(a) (b)

Continue ⟶

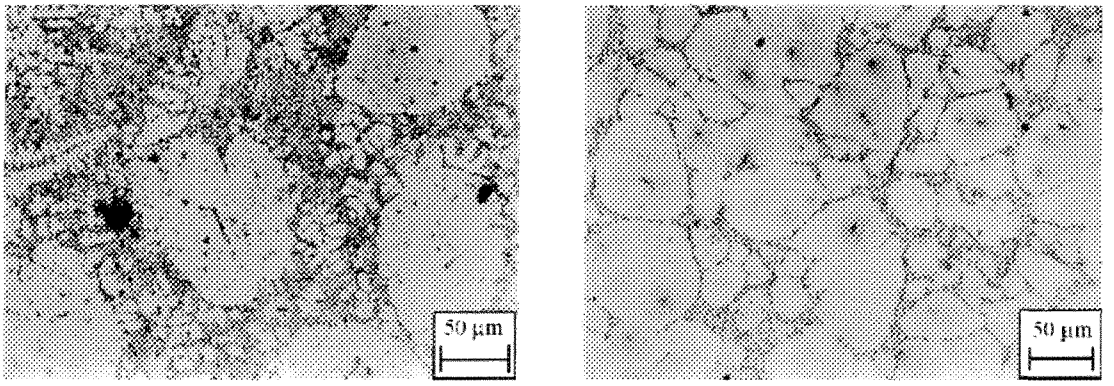

(c) (d)

Figure 3.35: Effects of shear rate and refiner addition on the primary α-Al size [164]: (a) and (b) with $210s^{-1}$, (c) and (d) $535s^{-1}$,(a) and (c) without refiner, (b) and (d) with refiner (duration of stirring 30minutes)

The effects of isothermal shearing time at a constant shear rate ($210s^{-1}$) on the mean particle size and intercept length are shown in Figure 3.36. As the isothermal shearing time increases, the particle size decreases initially, reaches a minimum value and increases again. In the case of grain-refined alloy, the time that was required to obtain minimum particle size is less than that for the non-refined one. In both figures, the addition of refiner reduces the size of the particles and improves the degree of their roundness.

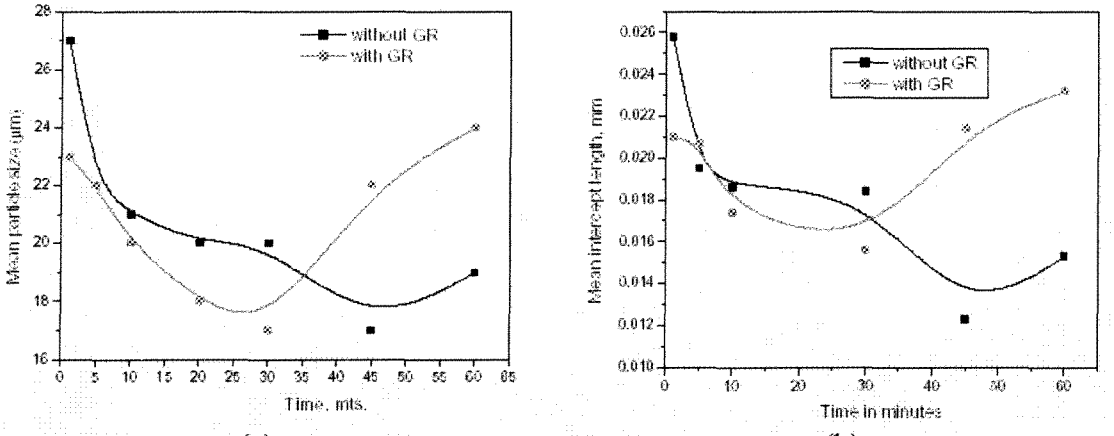

(a) (b)

Figure 3.36: Mean particle size (a) and mean intercept length (b) versus time for isothermal stirring at 615°C [164]

3.2.2 Effects of modification on semi-solid structures

It is well known that the irregular growth of the eutectic can be modified by the addition of modifiers such as Sr. In the presence of a modifying element, Si growth is interfered and its morphology changes to fibrous. In general, the structural modification is concluded to be the result of a change in the growth mechanism from layer to continuous growth. The morphological change of the Si phase results in improving mechanical properties, including higher strength and better ductility of the alloy.

One of the main aims of SSM processing, with specific emphasis on Al-alloys, is to obtain globular structure of the primary phase to improve mechanical properties and thixotropic behavior of the alloy. As a result, there is not much work reported on the other micro-constitutes that usually form during solidification of Al alloys such as silicon. Fat Halla [165] have studied the effect of modification on the stirring of commercial alloys A-S7G03 (7.1%Si, 0.3%Mg) and A-S4G (4.2%Si, 0.1%Mg). Some of their results are shown in Figure 3.37.

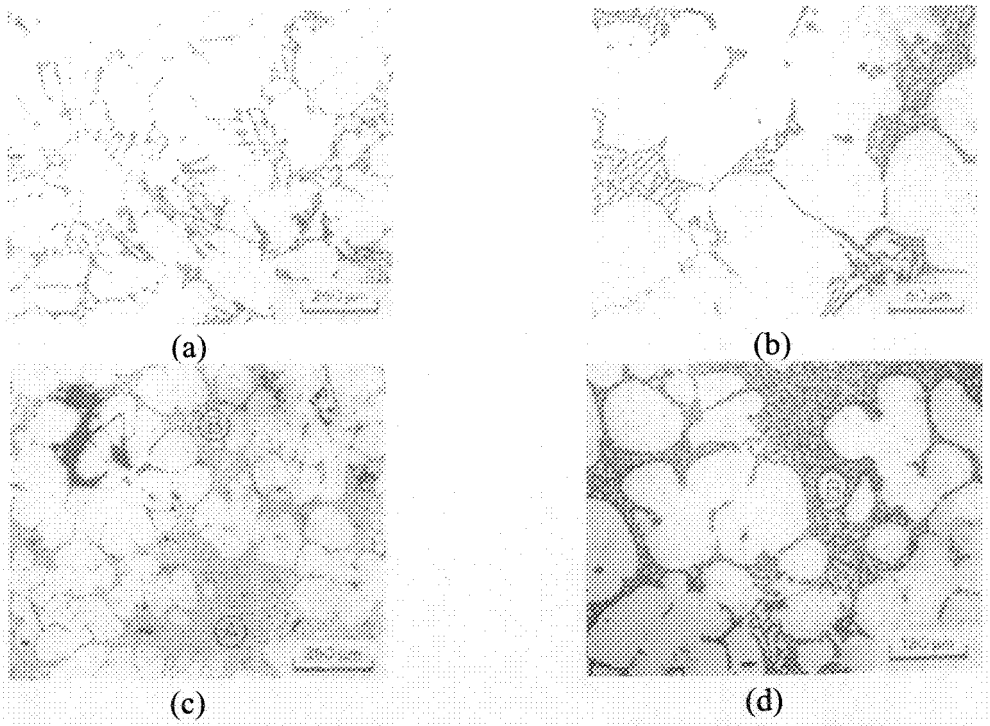

Figure 3.37: Alloy A-S7G03 (a) conventionally cast (b) stir cast (c) stir cast with 0.02%Sr (d) stir cast with 0.04%Sr [165]

As expected, the eutectic silicon in the conventionally cast sample has a flake morphology with relatively large size. With stirring, not only the α-Al particles transformed to rosettes and globules but also the eutectic silicon is broken into much smaller sizes. With Sr addition, the eutectic silicon becomes very fine and the optimum modification of stir-cast alloys was achieved at around 0.02%Sr. Higher amount of Sr addition, results in overmodification which could have detrimental effects on the mechanical properties [165].

Figure 3.38 shows stress-strain curves for the unmodified and modified stir-cast 356 alloy. The yield strength has almost the same value of 110MPa for both cases. The ultimate tensile strength (UTS) has significantly increased from 160MPa to 210MPa with modification. Moreover, the percent of elongation was increased remarkably from 2.75% for the nonmodified alloy to 15% for the modified one. Furthermore, the fracture surfaces, as examined by SEM, showed dimple and smooth ripple patterns, for the modified stir-cast alloys, reflecting the high ductility.

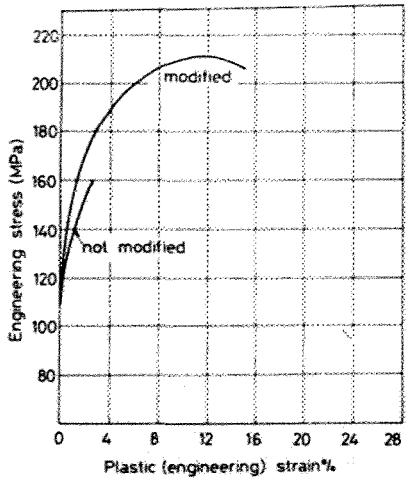

Figure 3.38: Stress-Strain diagram for stir-cast, modified and nonmodified A-S7G03 alloy [165]

Loue and Suery [14] have worked with AlSi7Mg thixocasting billets. They have done some experiments with direct chill and permanent mold casting using electromagnetic stirring, EMS, and addition of Sr for modification. They have investigated the effect of isothermal holding at 580°C on the resulting microstructure and claimed that with addition of Sr, the morphology of eutectic silicon has changed from lamellar to fibrous and the grain

size has decreased slightly. It was found that the kinetic of fusion of the eutectic phase during partial remelting was not altered by the Sr modification. Also the presence of Sr in the liquid phase does not change the coarsening characteristics of the solid phase.

Jung et al. [15] investigated the morphological changes of primary Al phase in A356 alloy by using EMS and Sr modification. They concluded that the optimum current for globalization is 15A. Also the optimum addition of Sr is 50ppm. Above this amount, the eutectic silicon was well modified but the average size of primary α-Al phase increased. It was suggested that the increase in the α-Al particle size is due to the extended mushy zone resulting from Sr addition. The average size of the eutectic Si for the stirred condition is slightly smaller than that of the non-stirred alloy. This is not directly related to electromagnetic stirring and is probably because of uniform distribution of the modifier due to the stirring (Figure 3.39) [15].

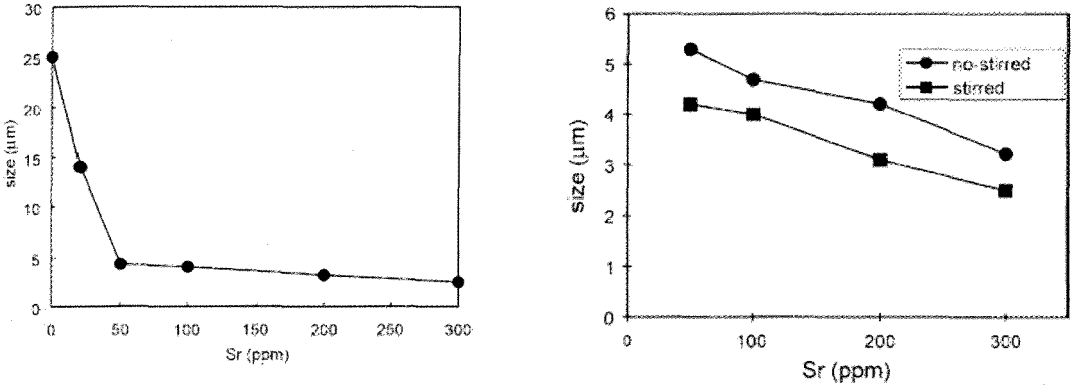

(a) (b)

Figure 3.39: (a) Variation of the average size of the eutectic Si stirred at 15A with the amount of Sr, (b) Effect of electromagnetic stirring on the average size of the eutectic Si [15]

In the recent work of Grimmig et al. [163] on A356 slurries produced by the cooling slope process, they have shown that 175ppm Sr addition changed the Si morphology from lamellar to fibrous and this effect fades during holding time (Figure 3.40).

(a) (b)

Figure 3.40: Microstructures of non-modified and modified A356 quenched billets [163]

3.3 Principles of rheology

The semi-solid materials exhibit both like solid and liquid depending on the applied shear stress. In the absence of external forces, the material maintains its integrity and therefore could be easily handled in the form of a billet. When shear is applied, the material flows like a liquid but with less turbulence and able to fill the die cavity in progressive steps.

As a two phase flow, the study of the flow behavior is more complicated and needs special knowledge of the so called "*rheology*". Rheology is the science of deformation and flow of matters and is regarded as a branch of physics concerned with the mechanics of deformable bodies [174]. The inter-relationship of rheology and mechanical properties of the materials is closely tide up with materials' viscosity within mushy state.

3.3.1 Newtonian and non-Newtonian fluids

Basically, Newtonian fluid is defined as a fluid between two parallel plates where the upper plate is stationary and lower one is set in motion with a velocity V_x at time zero. The fluids adjacent to the plates have the same velocity as the plates, i.e., the fluid adjacent to the lower plate moves with a velocity V_x. As time proceeds the fluid gains momentum, and after a sufficient time steady state condition is reached. At the steady state, for plates of area A, and laminar flow, the force is expressed by:

$$\frac{F}{A} = \mu \frac{V_x}{Y} \tag{3.1}$$

Where Y is distance between plates and μ is constant of proportionality or dynamic viscosity. The force per unit area is the shear stress and in steady state when the velocity profile is linear, shear stress may be expressed as:

$$\tau_{yx} = -\mu \frac{dV_x}{dy} \tag{3.2}$$

So, liquid metals are Newtonian fluids. This means that their shear stress (τ) is proportional to the shear rate ($\frac{dV_x}{dy} = \overset{o}{\gamma}$) at a given temperature. Any fluid that does not obey the Newtonian relationship is called non-Newtonian. The subject of "*rheology*" and "*thixotropic behavior*" is devoted to the study of the behavior of such fluids. In chemistry science, high molecular weight liquids which include polymer melts as well as liquids with fine suspended particles (slurries), and pastes are usually non-Newtonian. In this case, the slope of the shear stress versus shear rate curve will not be constant and depends to shear rate and physical conditions such as pressure, time, and temperature [167]. Different non-Newtonian fluids are categorized in Figure 3.41.

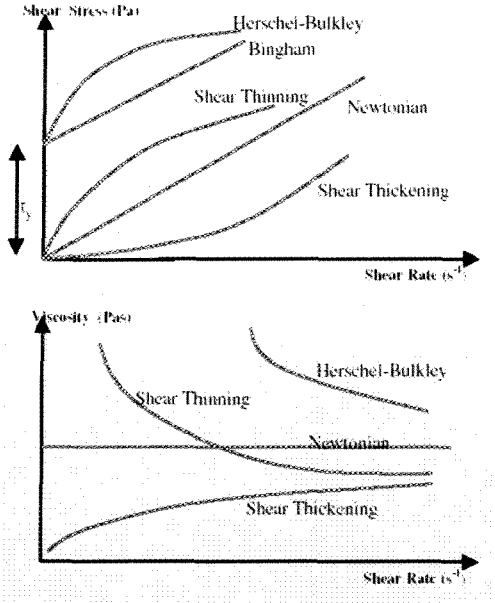

Figure 3.41: Shear stress versus shear rate and viscosity versus shear rate curves for different fluids [166]

3.3.1.1 Shear thinning and thickening fluids

When viscosity decreases with increasing shear rate, the fluid is called shear-thinning. Many paints which consist of pigment particles in polymer solutions exhibit this behavior. When the paint is applied on to a surface by brushing or spraying, its viscosity decreases. When the paint is on the wall, its viscosity increases and prevents it from flowing due to the gravity. In contrast to shear thinning, shear thickening fluids are those, where the viscosity increases as the fluid is subjected to a higher shear rate. Shear-thinning fluids are called "Pseudoplastic" fluids and in these fluids the shear stress τ is proportional to shear rate γ° as follow:

$$\tau = \mu \overset{0}{\gamma} \tag{3.3}$$

From non-Newtonian fluids, viscosity is termed the "apparent viscosity". Some shear-thinning fluids exhibit Newtonian behavior at extreme shear rates, both low and high. For such fluids, when the apparent viscosity is plotted against log shear rate, a curve similar to Figure 3.42 could be seen.

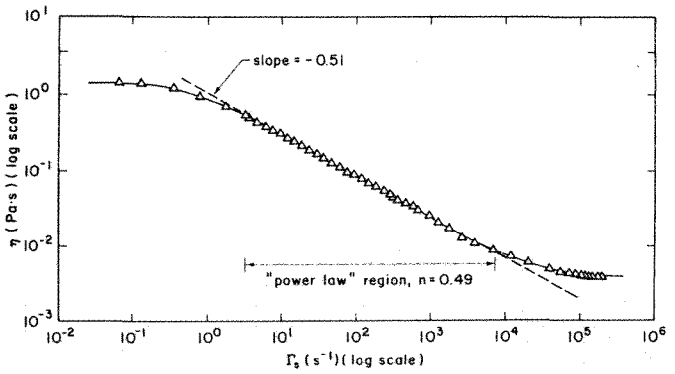

Figure 3.42: Relation between apparent viscosity and shear rate in a logarithmic scale, 0.4wt% poly acrylamide in water, room temperature [168]

The regions where the apparent viscosity is approximately constant are known as the Newtonian regions. The behavior of fluids falls between these regions can usually be approximated by a straight line, where the results are interpreted in terms of the power law. In this region, the behavior could be approximated by:

$$\log \mu = a + b * \log \overset{0}{\gamma} \tag{3.4}$$

This could be rewritten as:

$$\mu = K(\overset{0}{\gamma})^{b} \tag{3.5}$$

Where $k = \exp a$. Instead of b, n-1 is used for the exponent and as a result the apparent viscosity is as follow:

$$\mu = K(\overset{0}{\gamma})^{n-1} \tag{3.6}$$

Upon using the connection among the shear stress, apparent viscosity, and the shear rate the equation could be shown as:

$$\tau = K(\overset{0}{\gamma})^{n} \tag{3.8}$$

Where n is called the power law index. Note that n=1 corresponds to Newtonian behavior. Typically for shear thinning fluids, n lies between 1/3 and 1/2.

3.3.1.2 Viscoplastic or yield stress fluid

Another important type of non-Newtonian fluids is viscoplastic or "yield stress" fluids. This is a fluid which will not flow unless the applied shear stress exceeds a critical value known as the yield stress (τ_0). For example, when a tube of toothpaste is opened, it would be good if the paste does not flow at the slightest amount of shear stress. So viscoplastic fluids behave like solids when the applied shear stress is less than the yield stress. Once it exceeds the yield stress, the viscoplastic fluid will flow just like a fluid. Bingham plastics are a special class of viscoplastic fluids that exhibit a linear behavior of shear stress against shear rate. Nonlinear viscoplastic fluids are also exist in this group.

For certain class of fluids, the apparent viscosity continues to change as a function of time for which particular shear rate is applied. These are known as time dependent non-Newtonian materials. Fluids which become more pseudoplastic with time at a constant shear rate are known as thixotropic fluids. The viscosity of a thixotropic liquid will decrease with time under a constant applied shear stress and the structure breaks down

progressively with time at a constant shear rate. Eventually, a dynamic equilibrium is reached where the rate of the structural break down is balanced by the simultaneous rate of reformation. Thus a minimum value of the apparent viscosity is reached at any constant rate of shear.

Another important group of fluids exhibits viscoelastic behavior. This means that these fluids behave both as solids (elastic) and fluids (viscous). Viscoelastic fluids exhibit strange phenomena such as climbing up a rotating shaft, etc. An example of a common viscoelastic liquid is egg-white. When it flows out of a container, a quick jerking motion is enough to snap it back into the container [169].

3.3.2 Rheometers/Viscometers

In this section, the most widely known experimental techniques for measuring the fluid viscosity are described.

3.3.2.1 Rotational viscometery

This technique has been mostly used for rheological characterization. There are various rotational viscometers, i.e., spheres, disks, cones, and cups however the most common type is the coaxial-cylinder device. In this method, a cylinder of radius r_i is suspended in the sample fluid in a container of radius r_o. Basically two configurations exist, Searle [170-172] type in which the inner cylinder rotates and the outer one remains stationary, and the Couette [173] which has a rotating outer cylinder. The theory of rotational viscometery is based on a rotating body which is immersed in a liquid and experiences a viscous drag or rotating force. The amount of viscous drag is a function of the rotational speed and there is no difference whether the body rotates or the container. The main advantages of rotational viscometery is its continuous measurement at a given shear rate for a period of time [174].

In the metallurgical applications, the rheological tests are often performed in three different modes:

- Continuous cooling and shearing from a temperature above the liquidus
- Transient or steady state experiments from a specified starting condition under fixed solid fraction and shear rate [175]
- Shearing after partial solidification or remelting [6]

From a mechanical point of view, semi-solid slurry resists against deformation and thus induces a force which could be measured by a torque meter. This technique has high flexibility in operating modes and flow conditions. The main disadvantages are its limitation to low shear rates and relatively low solid fractions since high shear rate can cause flow instability and high fraction solid can lead to wall slippage.

3.3.2.2 Extrusion

This technique is divided into direct and indirect extrusion [176]. In this method, the flow is pressure driven and is characterized by a variation of shear rate along the cross section. Viscosity is visually calculated assuming linear viscous behavior which may not necessarily be true for all the cases. Disadvantages are unsteady state data and segregation due to the pressure gradient.

3.3.2.3 Indentation

This is another application of hardness test. Here, a constant pressure applied to a ball to penetrate the surface of the semi-solid slurries. Similar to hardness, it is simply applicable for different test conditions. It was claimed that this method works with fraction solid greater than 85% [177].

3.3.2.4 Parallel plates

The material to be tested is placed between two parallel plates. In the case of semi-solid, a cylindrical sample with low aspect ratio is compressed between plates at constant deformation rate or under constant load. The rheological behavior of the test material is determined from the measurement of the displacement of one plate with respect to the other as a function of time [177-179].

Generally, rheological characterization of SSM slurries with high fraction solid is difficult due to the high shear stresses requirement. For this reason, parallel plate test has been used for high fraction solid slurries (>0.5) [7]. It was claimed that the stress-strain field in this test is highly inhomogeneous due to the presence of friction. The flow conditions are complex and it is difficult to define the steady state and prevent solid/liquid segregation [8].

As it will be described in the next chapter, the entire rheological tests were performed using parallel plate test procedure; this technique is described in more details here. For semi-solid applications, parallel plate viscometer was first used by Laxmanan et al. [180]. Their compression apparatus consisted of a furnace with a tight control of temperature, linear voltage displacement transducer, and different compression loads from 10 to 3000gr. Test specimens were Sn15%Pb alloy with a small size of 12.5mm diameter and 6.25mm height. The tin-lead alloy slurries were selected due to their low working temperatures (~200°C) to allow better experimental conditions and thus more accurate data. With different fraction solids and forging pressures, they have shown that dendritic samples deformed differently from the non-dendritic ones. For high fraction solids (>0.4) only small strains were observed even at very long times while for lower fraction solids (<0.35), the strain increased very slowly at first but accelerated suddenly (Figure 3.43a) [180]. Moreover, they reported that the pressure required to achieve a given amount of deformation is much higher for the dendritic structure. The pressures required with the non-dendritic structure are approximately two orders of magnitude lower than those for the dendritic structure (Figure 3.43b).

Suery et al. [179] continued Laxmanan's work with parallel plates compression test. The difference was on applying various deformation rates, i.e., low deformation rates from $8.5*10^{-3}$ to 0.85 mms^{-1} and high deformation rates from 3.8 to $2.5*10^{3}$ mms^{-1}. Figure 3.44a shows a typical experimental result for the comparison of different morphologies in Sn15%Pb alloys. Samples with non-dendritic and fine dendritic structures deform differently from the ordinary dendritic ones and the force remains very low up to a strain of

one. A plot of the fraction of liquid within a non-dendritic billet is shown in Figure 3.44b. At strains greater than 0.6, the segregation begins to occur and becomes complete in the center by 0.85 compression. It is important to note that in their experiments, the morphology of fine dendritic samples after preheating changed to globules and that is why its behavior is the same as non-dendritic.

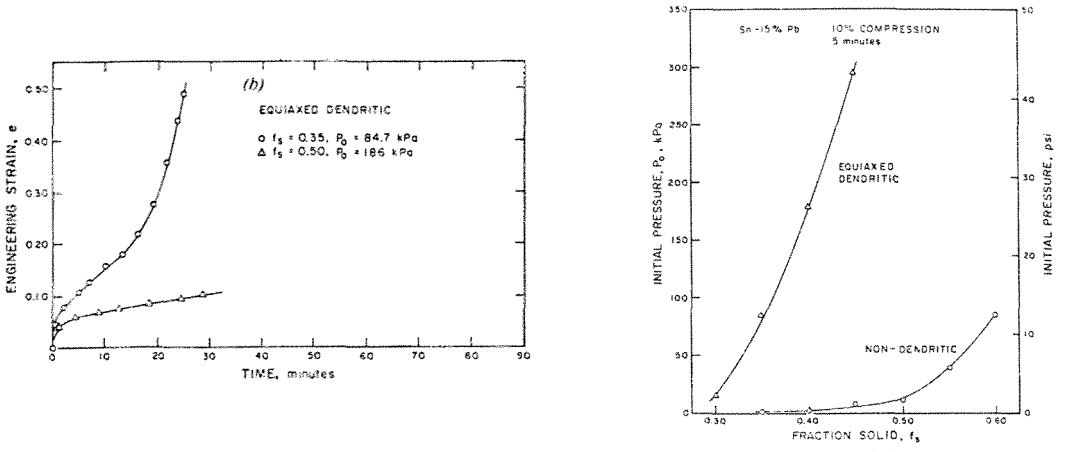

(a) (b)

Figure 3.43: (a) Typical strain-time curves for equiaxed-dendritic structures, (b) relation between initial pressure, morphology, and fraction solid [180]

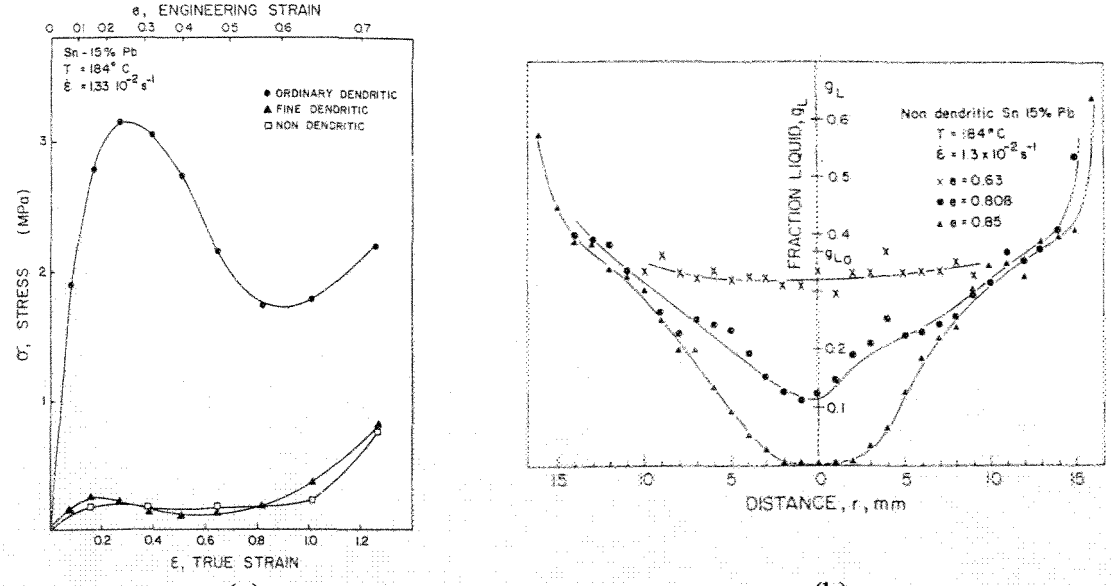

(a) (b)

Figure 3.44: (a) Stress vs. strain for specimens of different structures of Sn15%Pb, (b) fraction of liquid vs. distance along the radius of a non-dendritic specimen (deformed at a strain rate of $1.33*10^{-2}s^{-1}$) [179]

With applying higher velocities, liquid segregation minimized (Figure 3.45). As seen, the microstructure contains approximately the same amount of eutectic in the middle and near the edge. They claimed that in this deformation regime, homogenous distribution is related to the flow of the liquid through the channels of the solid which becomes more difficult and consequently the segregation becomes less [179].

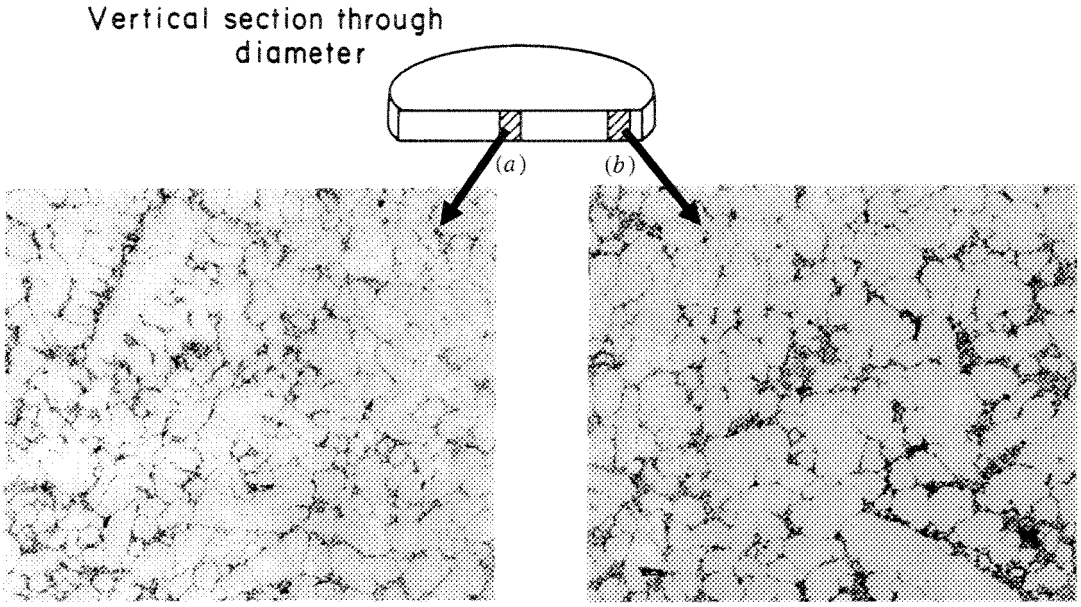

Figure 3.45: Microstructures of dendritic Sn-15%Pb alloy deformed to a strain of 0.65 by compression at a strain rate of $1.2*10^3$ s^{-1}: (a) middle, (b) edge, ~x120 [179]

CHAPTER 4

EXPERIMENTAL PROCEDURE

CHAPTER 4

EXPERIMENTAL PROCEDURE

4.1 Melt preparation

In order to investigate different parameters such as the effects of titanium in solution and silicon morphology, the alloys' chemical compositions were classified into three different groups, i.e., binary alloy Al7%Si, 356 alloys with and without Ti in solution (Table 4.1). Since various grain refiners and one modifier with different addition levels were used, melts were prepared separately in small silicon carbide crucibles.

In all experiments, about 2.2kg of each alloy was prepared in an electric resistance furnace. This amount was selected so that there was sufficient material for all the required experiments, i.e., chemical and thermal analyses, and SSM slurry preparation.

4.1.1 Base alloy preparation

Three different hypoeutectic Al-Si alloys were prepared: Al7%Si, commercial 356 alloy (with Ti in solution) which is named Com356, and 356 alloy without Ti in solution, named A356. Table 4.1 shows the compositions of these alloys. The alloy compositions given in the current document are in weight percentage unless otherwise specified.

Table 4.1: Chemical composition of the base alloys (wt. %)

	Si	Mg	Fe	Mn	Cu	Ti	B	Sr	Al
Binary Alloy	7.0-7.3	Nil	Max 0.09	Nil	Nil	Nil	Nil	Nil	bal.
A356	6.4-6.7	0.36-0.4	Max 0.08	Max 0.003	Max 0.001	Max 0.0058	Nil	Nil	bal.
Com356	6.8-7.0	0.33-0.36	Max 0.09	Max 0.003	Max 0.002	0.1-0.13	Nil	Nil	bal.

The binary alloy was prepared by mixing commercially pure aluminum (99.97%) and silicon (99.5%). Pure Argon (99.998%) was used for degassing of the alloys for 10 minutes at a flow rate of $5ft^3hr^{-1}$. Melting temperature was set at 720-730°C however was decreased to ~680-700°C due to degassing by cold argon.

4.1.2 Grain refiner and modifier additions

In this context, three grain refiners and one Sr-based modifier were used with the following specifications:

- Al5%Ti1%B, rod form, produced by KBAlloys Co.
- Al5%B, rod form, produced by KBAlloys Co.
- Al4%B, waffle form, produced by KBAlloys Co.
- Al10%Sr, rod form, produced by SMC Co. (Shieldalloy Metallurgical Corporation)

It should be noted that it was not the main objective of the current research to focus and establish a comparison between different refiners. However, during the experiments various observations were made on the effectiveness of each refiner. To achieve different degrees of refinement, modification, and combined effects, the above-mentioned master alloys were added to the melt to raise the titanium and/or boron and/or strontium levels in the alloy. Specified amounts of these master alloys, wrapped in aluminum foil, were added to the melt at 720-730°C using a preheated graphite bell. It is important to note that all the melts were degassed with argon after master alloys addition and the contact time for the first sampling was set to 20-30 minutes depending on the treatment (~30 minutes for modification due to incubation period and ~20mintues for sole grain refiner).

In order to reduce settling and agglomeration of the added master alloys, all the melts were stirred by a preheated graphite rod approximately 2 minutes before sampling.

4.1.3 Chemical analysis

Samples for chemical analysis were cast into a standard scissor mold. Disk shape samples having a 56mm diameter and 10mm thickness were prepared for chemical analysis by machining the surface to remove surface segregation. Finally, 6-8 point ablations (OES) were performed on the machined surface using ThermoARL-4460 and the results are presented by averaging all ablations. The measurement of the grain refiner and modifier elements concentrations is the most significant issue and therefore calibration of the device regarding these elements especially boron is so vital. All the tests were done at the ALCAN Arvida Research Center which is a worldwide producer of standards for such analysis. The two standards of 356.2-AN and 356.2-CAK especially produced for analysis of A356 Al-Si alloys were used with a 1% accuracy of the results.

4.2 Casting procedure

4.2.1 Conventional and semi-solid castings

In order to evaluate the effects of grain refining and modification on the semi-solid slurries, cast parts were prepared both conventionally and by rheocasting. For conventional method, i.e., static condition, graphite cups were used. The prepared charge was poured into graphite cups of 25mm inner diameter and 5mm wall thickness. Cups were held in the melt for approximately one minute to reach equilibrium condition and to ensure uniform temperature distribution across the sample at the beginning of solidification. Each cup with ~50g of alloy was transferred to the testing platform and two K-type thermocouples were quickly immersed into the melt near the center and wall of the mold and temperature readings were collected by a high speed high resolution National Instrument data logger system (SCXI-1102) with 10 per second sampling rate. The cooling rates for the graphite molds were between 1.5-2°Cs^{-1} above liquidus temperature.

For SSM processing, swirled enthalpy equilibration device, SEED technology, as a representative was used (Figure 4.1). About 2kg of the alloy was poured into a coated cylindrical steel mold of 75mm diameter and 250mm long. In all experiments, the mold

was tilted to reduce turbulence during pouring. The mold was then rotated at 150RPM or 2.5Hz. The duration of this stage depends on the mold dimension and the charge mass and for these series of experiments it was set to 60 seconds. In the next step, the swirling motion was stopped and after a brief pause of 5 to 10 seconds, the bottom plug was opened to allow a portion of the remaining liquid to drain. Before drainage, all process parameters were set to reach a fraction solid of 0.3-0.4. This is based on heat exchange between the mold and molten alloy. After a specific time of 20 seconds, the prepared billet was unloaded and transferred into the water-tank to be quenched to room temperature at about 20-25 seconds. In all experiments, two 0.8 mm diameter K-type thermocouples were inserted near the mold wall and also the center at a distance 80mm from the bottom of the mold to collect thermal data. The quenching temperatures for all the tests were 598.5±2.5°C.

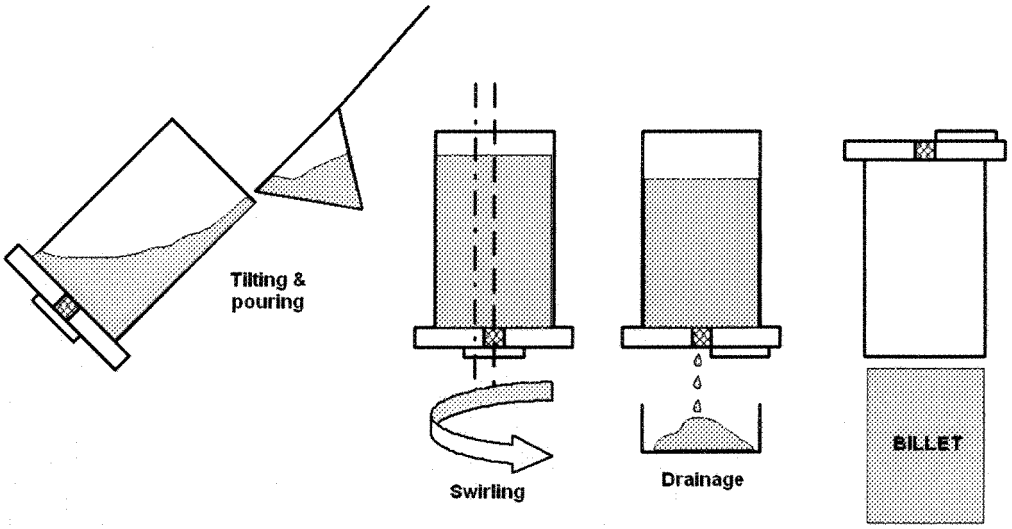

Figure 4.1: Schematic of SEED process

4.2.2 Thermal analysis (TA)

The cooling curve analyses were done for both conventional and SEED processes. In both methods, two K-type thermocouples were embedded into the center and near the mold wall at a distance of 10mm and 80mm from the bottom of graphite cup and steel mold respectively. A minimum of two thermal analysis runs were performed for each addition level.

Cooling rates were measured above the liquidus temperatures and it was between 1.5-2°C/s for the graphite cup and ~5°C/s for the SEED billets.

The analysis of thermal data was carried out based on the analysis of the Al-Si solidification data [24,181] and since there are some dissimilarities in definition of critical parameters in the literature, the following points would be defined and identified on a real cooling curve as shown in Figure 4.2 (for graphite cup samples only):

- $Tnuc_{Al}$: Start of primary α-Al dendrites nucleation
- $Tmin_{Al}$: Unsteady state growth temperature, the temperature beyond which the newly nucleated crystals grow to such extent that the latent heat liberated surpasses the heat extracted from the sample.
- Tg_{Al}: Recalescence of steady state growth temperature due to release of latent heat of primary α-Al dendrites
- ΔT_{Rec}: Temperature difference between unsteady ($Tmin_{Al}$) and steady (Tg_{Al}) state growth temperatures of primary α-Al particles (recalescence)
- $Tnuc_{eut}$: Start of eutectic nucleation
- $Tmin_{eut}$ and $Tmax_{eut}$: Minimum and maximum of eutectic temperatures
- $\Delta\theta$: Variation of eutectic recalescence ($Tmax_{eut}$ - $Tmin_{eut}$)
- T_{end} : Solidification termination
- ΔT_{α}: α-Al solidification range ($Tnuc_{Al}$ - $Tnuc_{eut}$)
- ΔT_{eut}: Eutectic solidification range ($Tnuc_{eut}$ - T_{end})

It is worth mentioning that the chemical composition of the melt plays an important role on the thermal analysis results. As for instance, the liquidus temperature of the Al-Si melts varies with Si% according to the following equation [182]:

$$T_l = 662.2 - 6.913*[\%Si] \quad (4.1)$$

So, by a simple calculation, it is obvious that a compositional difference of 0.1%Si between two samples means a difference of about 0.69°C.

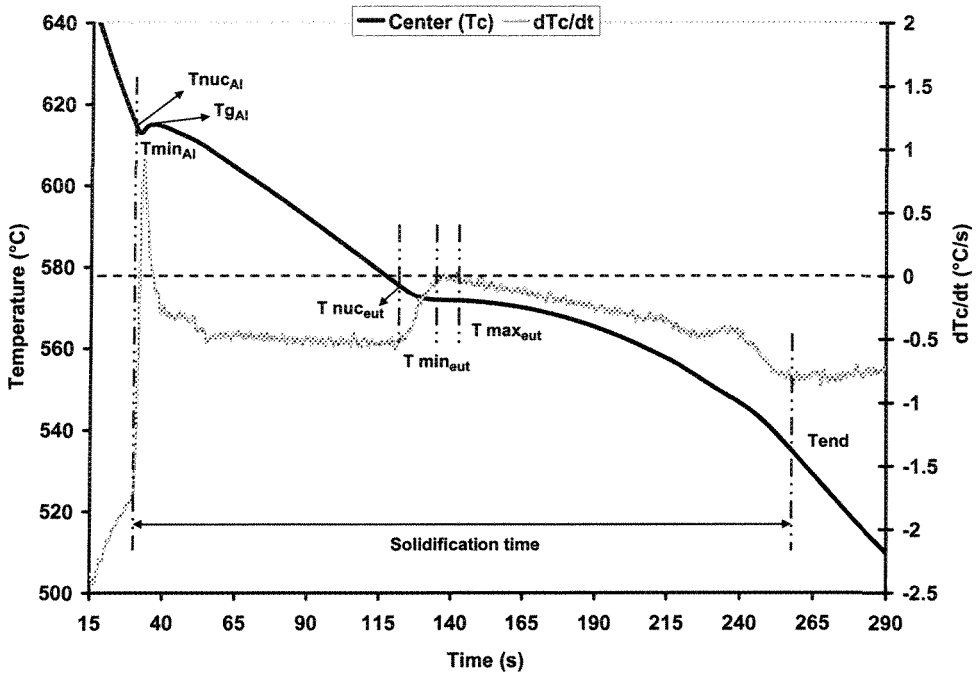

Figure 4.2: Cooling curve, first derivative, and reperesentation of important paramereters of 356 alloy

4.3 Rheological tests

In order to examine the rheological behavior of the billets, after drainage of the remaining molten metal, i.e. end of the SEED process, a few semi-solid slugs were taken out of the mold and compressed uniaxially in a simple parallel plate compression machine, *"the press"* (Figure 4.3). For the grain refiner and modifier investigations, a 2.2kg dead weight was applied by a pneumatic lifting system.

The applied force and resulting displacement are monitored using a load cell with a precision of 0.02% and a displacement transducer with ±0.1-0.2% full stroke precision. A cylindrical furnace was installed on the press bed to keep the billet temperature constant during the compression tests. The furnace is equipped with quartz heat resistant windows to view the billet. Two K-type thermocouples were positioned within the furnace to control the chamber temperature within a precision of 598±2°C. The overall time for pressing was 10 minutes and all compressed samples were quenched in water immediately after compression. Detailed information on the device was described elsewhere [183].

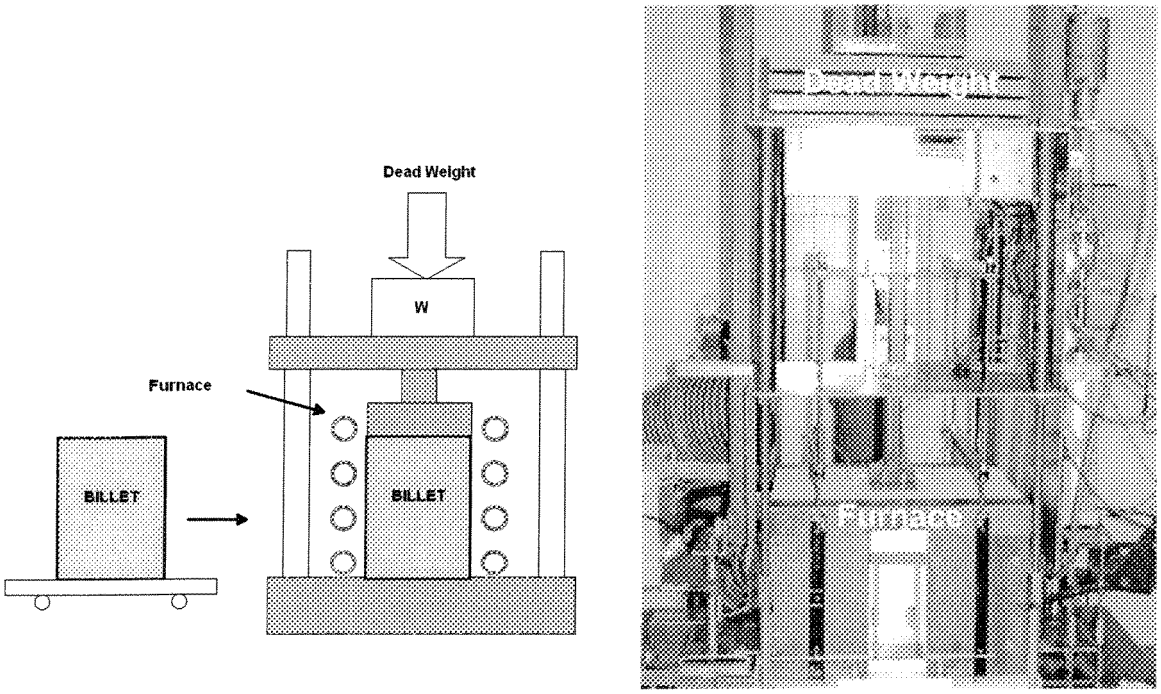

(a) (b)

Figure 4.3: (a) Schematic and (b) an actual overview of the press

By applying a constant load, the pressure decreases continuously during the compression test and the viscosity could be calculated from the strain-time graphs with the following equation:

$$\text{Engineering Strain } e = 1 - \frac{h}{h_o} \tag{4.2}$$

Where h_o and h are initial billet height (mm) and instantaneous height (mm) respectively. By the way, the raw data obtained from the data logger is shown in Figure 4.4.

For viscosity measurements, the resulting strain-time graphs could be further treated mathematically which are beyond the scope of this thesis. Nevertheless, for better clarification, it should be noted that the SSM slurries could be assumed as Newtonian fluids for low applied shear rates, i.e. less than 0.01 (s^{-1}) and small variation of shear rate within the samples [179,180,183-185]. After an initial rapid deformation, the billet deforms steadily at a constant rate and in this period viscosity measurement is valid. The steady state deformation behavior is attributed to the equal rate of agglomeration and de-agglomeration

of particles which will be discussed later. In the current study, the steady state period was between ~200-600 s after the commencement of deformation.

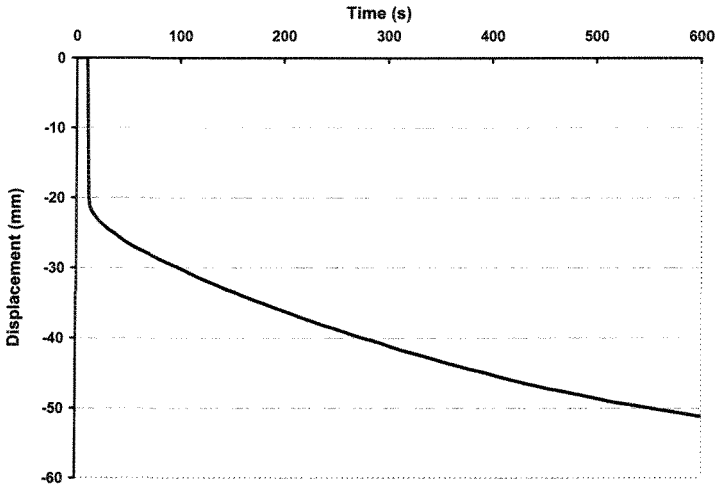

Figure 4.4: Typical displacement during compression test

In the literature for rheological tests, mostly small samples have been used, h<<R (height is much smaller than the radius of the billet). The reason for this size was mentioned on the importance of radial deformation [179,180,185]. Although, this is in contrary to the current work where actual billet is used. It should be stressed that the validity of rheological measurements for billet geometry of $\left(\frac{h}{R}\right) \geq 1$ was confirmed before [186].

4.4 Microstructural analysis

4.4.1 Optical microscopy

For the purpose of studying the structural evolution, samples were sectioned transversely near the tip of the thermocouples, i.e., 10mm and 80mm from the bottom for static and dynamic conditions respectively. All samples were mounted in bakelite, ground, and polished to 0.05μm colloidal silica.

Quantitative analyses were carried out using a Nikon optical microscope (Eclipse ME600) attached to a Clemex image analyzer. The outputs of the image system were classified according to the purpose of the study and for the following evaluations:

- Area fraction of primary α-Al particles or silicon particles
- Perimeter of primary α-Al or silicon particles
- Average circular diameter of primary α-Al particles based on the diameter of a circle having the same area as the measured object:

$$D = 2\sqrt{\frac{area}{\pi}} \tag{4.3}$$

where area is the primary α-Al or silicon particles area

- Count as the total number of primary α-Al or silicon particles in a defined area
- Number density as the total number of particles per unit area (mm^{-2})
- Length and width are the maximum and minimum distances between two pixel of the boundary respectively (Figure 4.5b)
- Aspect ratio is given by the ratio of the longest over the shortest feret diameter, i.e., length per width. Feret diameter is defined as the distance between two parallel tangents on each side of an object (Figure 4.5a)

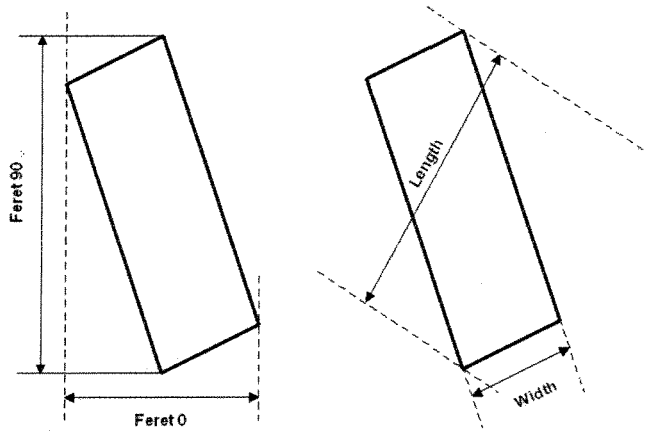

(a) (b)

Figure 4.5: Definitions of feret and aspect ratio

- Sphericity given by:

$$\text{Sphericity} = \frac{4\pi A}{P^2} \tag{4.4}$$

where A is the total area of primary α-Al particles and P represents perimeter of liquid-primary particles interface. The closer the sphericity to one, the higher is the globularity

of the α-Al particle. Since the average value of sphericity shows less sensitivity to the morphological evolution, the new parameter is defined as the percentage of particles having sphericity greater than 0.8. By this method, reasonable results are obtained.

- Area/Perimeter which is actually proportional to inverse of surface area per unit volume, S_V:

$$S_v = \frac{4}{\pi}\frac{P}{A} \tag{4.5}$$

Where, S_v is specific volume surface of the particles (an estimation of 3D)

A routine was written to clearly distinguish the color differences between eutectic and α-Al particles and for better distinction, etching with HF solution was used. For the reason of having a representative of the structure, all the data were obtained from image processing of the resulting microstructure between the center and the wall surface of the billet (Figure 4.6). For characterizing the α-Al particles in the SEED specimens, 85 fields with the total area of 255mm^2 were examined (Mag. x50). The number of fields examined renders statistically viable results with higher degree of confidence.

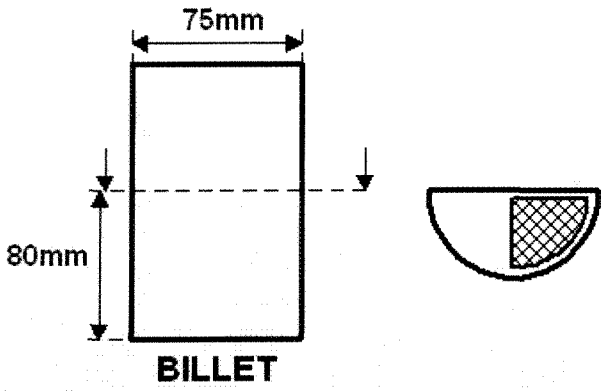

Figure 4.6: Area for quantitative analysis for SSM billets and applied scanning mode

In the case of rheological tests, the microstructure was studied on the longitudinal sections and regions with the highest deformation rate which is shown schematically in Figure 4.7.

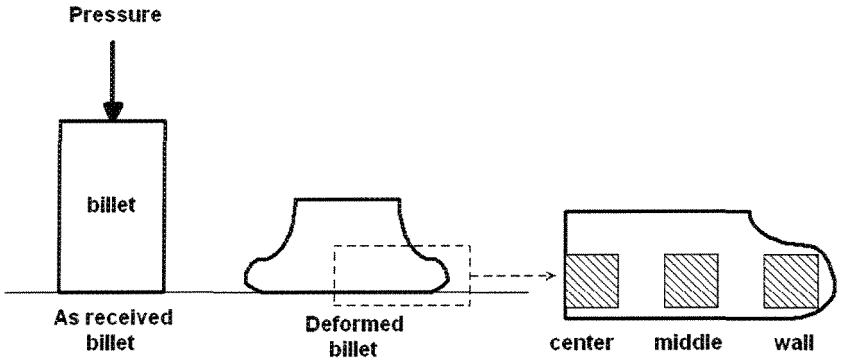

Figure 4.7: Area for optical micrographs observations for a typical deformation

4.4.2 Electron microscopy

Electron probe microanalysis (EPMA) was used to perform high quality elemental microanalysis for the following cases:

- Quantitative microanalyses of special microstructural feature and intermetallics' compositions
- X-ray mapping of special elements of interest

For this purpose, wavelength dispersive spectroscopy (WDS), was carried out using JEOL JXA-8900 microprobe.

The operating conditions were 10kV acceleration voltage, 20nA beam current, 1μm probe size, and 20s counting time on the peaks. Calibration was carried out with different natural and synthesized standards of Al, Si, Mg, Fe, Sr, Ti, and B. The calibration accuracy of the standards was carefully checked before the actual analysis after that by analyzing the standards as unknown and experiments started when the results of the calibration were 100±1%. For the best quantitative results, analyses are obtained on the polished and unetched metallographic samples to increase the precision of the quantitative analytical results. For better conductivity all the samples were coated with a thin layer of carbon.

In the case of investigation of silicon morphology, scanning electron microscopy (HITACHI S4700 and JEOL JSM 840A) was used for better characterization of the structure on the deep etched samples (10%HF, for 10 minutes).

CHAPTER 5

RESULTS AND DISCUSSION
GRAIN REFINING

CHAPTER 5

RESULTS AND DISCUSSION - GRAIN REFINING

5.1 Master alloys specifications

5.1.1 Al5%Ti1%B

Figure 5.1 shows the microstructures of transverse section and the backscattered electron micrographs and x-ray maps in Figure 5.2 elaborate on the chemistry of the intermetallic compounds in the as-cast master alloys. The microstructure of Al5Ti1B master alloy consists of $TiAl_3$ and TiB_2 particles embedded in aluminum matrix. The microstructure is almost homogeneous with small clusters of TiB_2 particles which were segregated within the aluminum matrix. The average length and width of $TiAl_3$ particles are 27±15 μm, 11±6 μm respectively. The presence of the TiB_2 particles is substantial because of the high boron content shown in the boron-map. Microprobe analysis of large particles confirmed the presence of blocky $TiAl_3$ particles (Table 5.1).

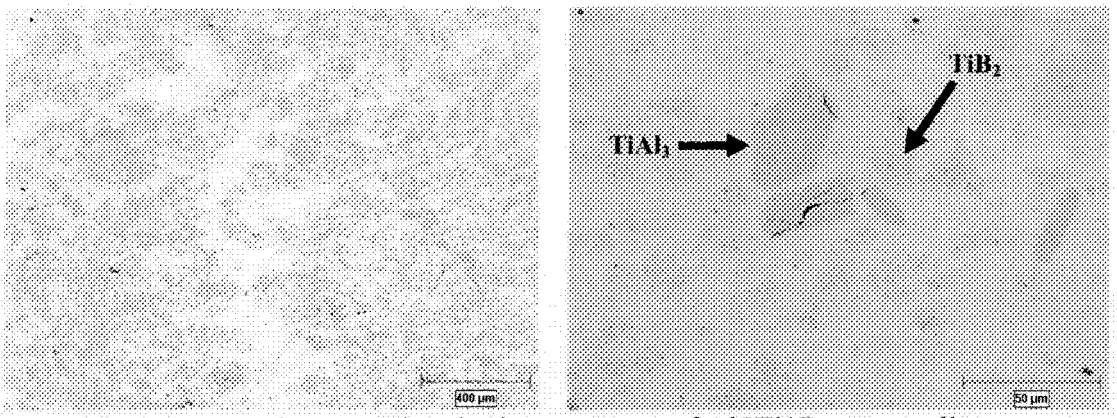

Figure 5.1: Cross sectional microstructure of Al5Ti1B master alloy

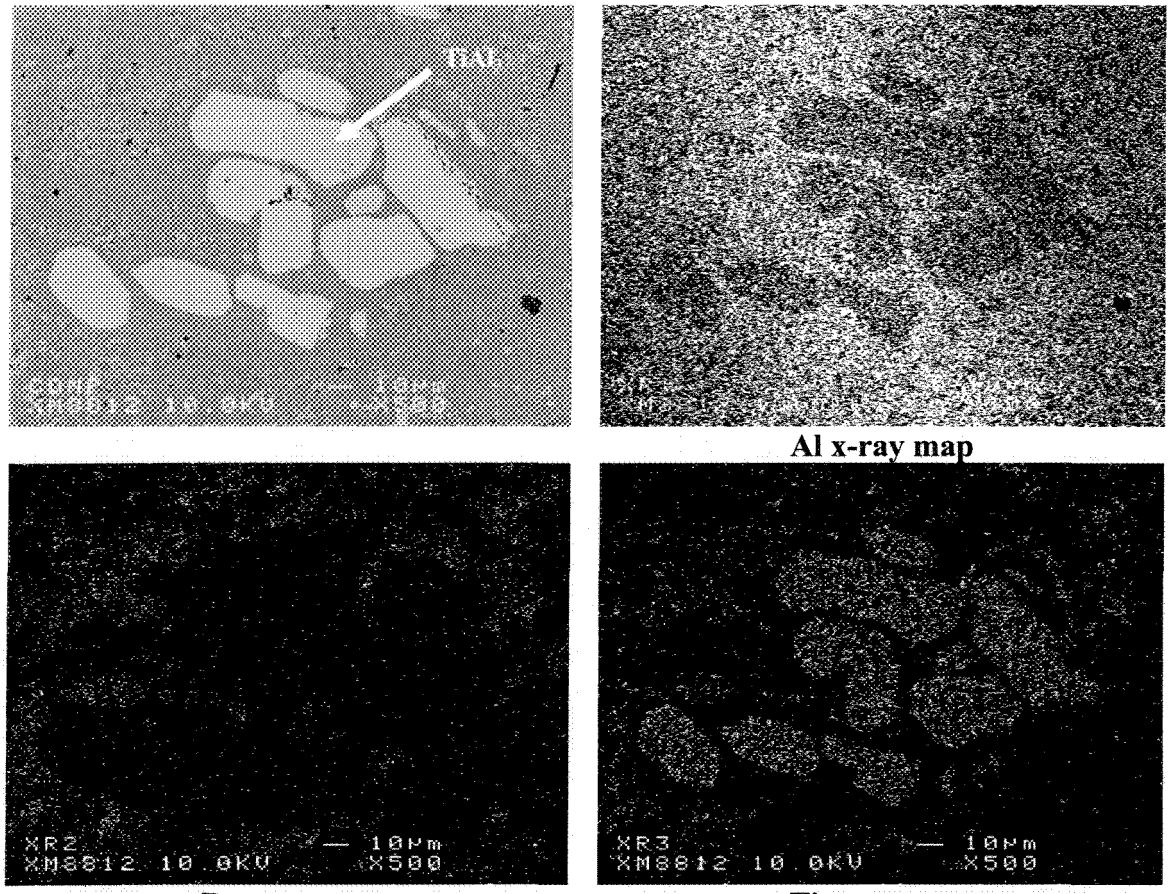

Figure 5.2: Back scattered electron micrograph together with x-ray maps of Al5Ti1B master alloy

Table 5.1: Chemical analysis of $TiAl_3$ particles in the Al5Ti1B master alloy (at. %)

Al	B	Ti	Si	Mg	Fe
73.09	2.06	24.69	0.14	0	0
74.59	0	25.12	0.29	0	0
73.39	1.34	25.22	0.01	0.03	0
73.50	1.22	25.25	0.007	0	0

5.1.2 Al4%B

The optical micrographs in Figure 5.3 show the cross sectional view of the commercially produced master alloy. Chemical analysis by microprobe and size measurement confirmed that the microstructure of the Al-4%B consists of AlB_{12} particles with the average size of 6 ± 3 µm. The AlB_{12} particles are not distributed well within the master alloy and different sizes of particle agglomeration could be seen in the structure.

Figure 5.4 shows backscattered electron micrograph plus x-ray maps for Al and B. The chemical analysis given in Table 5.2 confirms the AlB_{12} stoichiometry for the intermetallic particles in the master alloy.

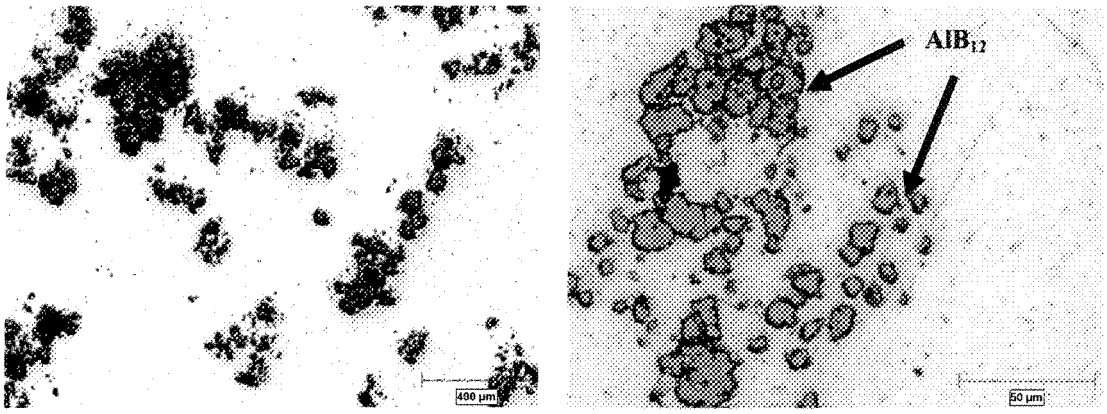

Figure 5.3: Cross sectional microstructure of the waffle form of Al4B master alloy

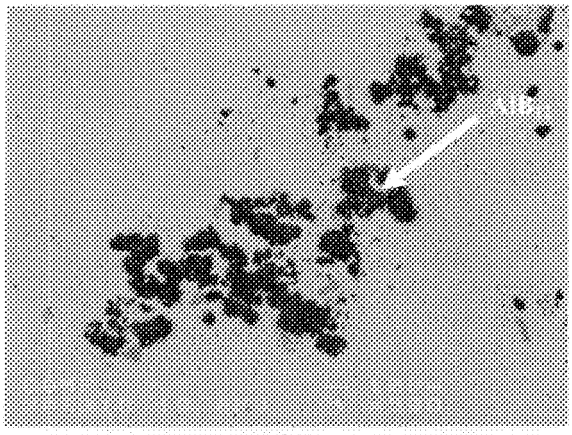

BSE

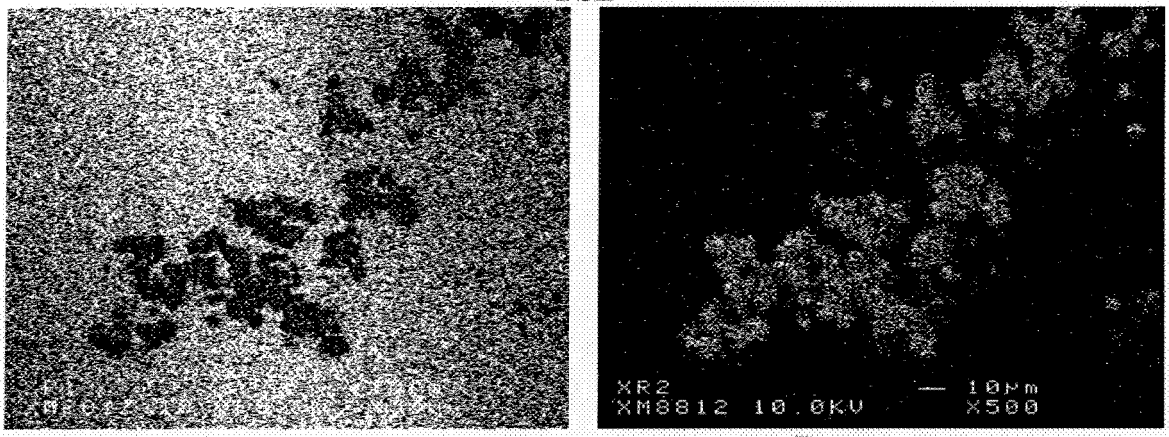

Al x-ray map **B x-ray map**

Figure 5.4: Back scattered electron micrograph and x-ray maps of Al4B master alloy

Table 5.2 : Atomic percentage of boride particles result in the Al4B master alloy

Al	B	Ti	Si	Mg	Sr	Fe
7.25	92.73	0.0027	0.0027	0.012	0.004	0
6.97	93.00	0.005	0	0.027	0	0

5.1.3 Al5%B

The microstructure of the commercially produced master alloy (Figure 5.5) comprises fine and nearly rectangular AlB_2 particles with the average length and width of 9±6 μm, 6±3 μm respectively. These particles are distributed within the matrix and some degree of agglomeration is obvious in the structure. Figure 5.6 shows backscattered electron micrograph plus x-ray maps for Al and B. With microprobe analysis, the presence of AlB_2 particles was confirmed (Table 5.3).

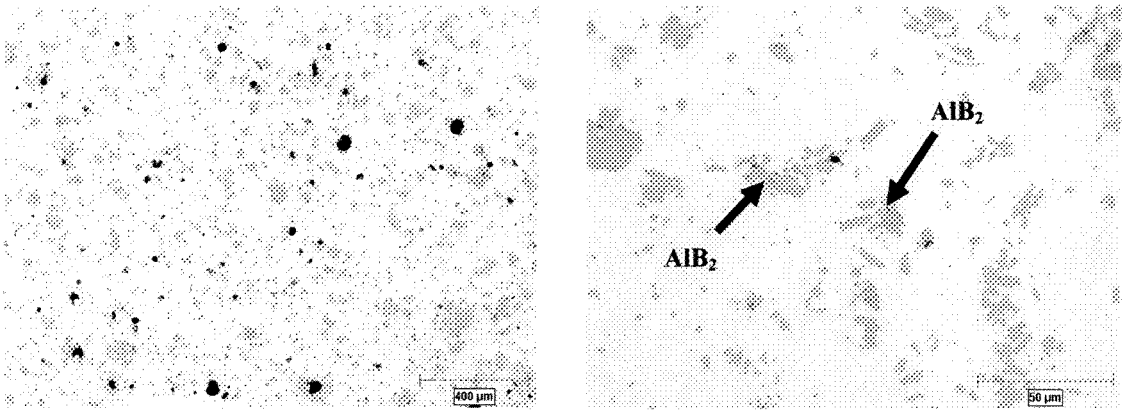

Figure 5.5: Cross sectional microstructure of the Al5B master alloy

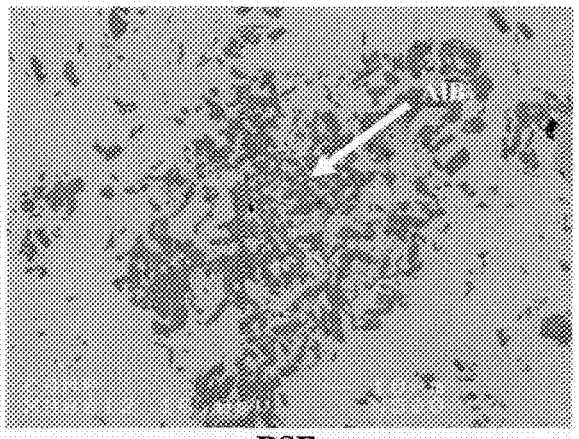

BSE

Continue ⟶

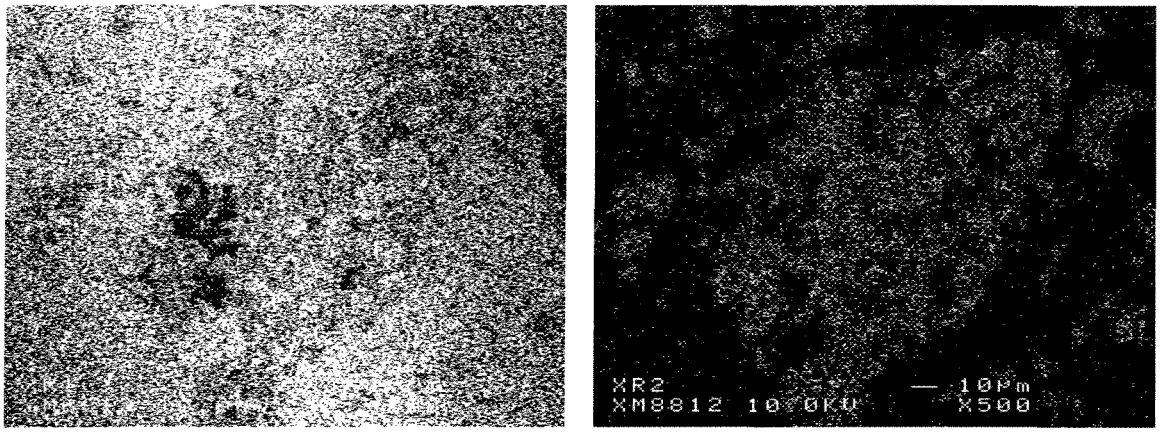

Al x-ray map **B x-ray map**

Figure 5.6: Back scattered electron micrograph together with x-ray maps of Al5B master alloy

Table 5.3: Atomic percentage of boride particles detected in the Al5B master alloy

Al	B	Ti	Si	Mg	Sr	Fe
31.90	68.08	0.004	0	0	0.007	0
30.797	69.19	0	0	0.004	0.009	0

5.2 Grain refining in A356 alloy

5.2.1 Addition of titanium and boron with Al5Ti1B

These series of tests were done by addition of Al5Ti1B as a grain refiner. Also the base alloy was free from titanium (maximum 58ppm Ti in solution) so the results are not affected by the dissolved titanium. The chemical compositions of the base alloys are listed in Table 5.4.

Table 5.4: Chemical analysis of the base alloy (wt. %)

Si	Mg	Fe	Mn	Cu	Ti	B	Sr	Al
6.44-6.53	0.36-0.39	Max 0.07	Max 0.003	Max 0.001	Max 0.0058	Nil	Nil	bal.

5.2.1.1 Conventional casting

5.2.1.1.1 Thermal analysis

The effect of Al5Ti1B grain refiner addition to the A356 alloy on the early stages of solidification is illustrated in Figure 5.7. The results are from the thermocouple at the center

of the graphite cups. As it is obvious, small additions of Ti-B shifted the cooling curves up and to the left with the recalescence decreasing with increasing master alloy content. The nucleation event takes place at higher temperatures and shorter times after pouring. As reported by other researchers [24,53,66], an effective grain refiner should not show any undercooling before the actual growth temperature and therefore the smaller the recalescence, the more effective the grain refiner. In these series of experiments, it is clearly shown that Al5Ti1B does not remove recalescence completely even at its optimum percentage. Therefore, it could not be rated as a perfect grain refiner for this alloy.

Thermo-Calc software was used as a useful tool for prediction of Ti effects on phase reactions of Al7Si1Mg alloy. In this case, an iso-pleth[1] diagram was constructed for Ti addition as shown in Figure 5.8. As it is evident from the iso-pleth and also confirmed before [21], the start of peritectic reaction shifts to lower Ti concentration of ~0.12% Ti for A356 alloy in contrast to ~0.15 Ti for Al-Ti binary alloys. This has a bearing on the nucleation of α-Al grains due to the formation of Al_3Ti particles. Furthermore, close examination of the iso-pleth, zoomed segment in Figure 5.8, reveals that Ti addition to A356 alloy increases liquidus temperature, i.e. nucleation starts at higher temperatures with Ti addition. This may have some effects on the semi-solid processing of the alloy since higher Ti content could enlarge the solidification range, i.e. greater freedom during SSM processing, and altering the directionality of solidification to enhance the formation of solid across the bulk liquid . In actual testing condition however, other parameters such as alloying and trace elements, cooling rate, and specially TiB_2 particles in the master alloy may increase solidification temperature even further and improve grain refining potency.

[1] An isopleth diagram is a pseudo binary diagram which may come from ternary or higher degree phase diagram where the phase relationship is identified for the elements of interest at different temperatures with variation of one element.

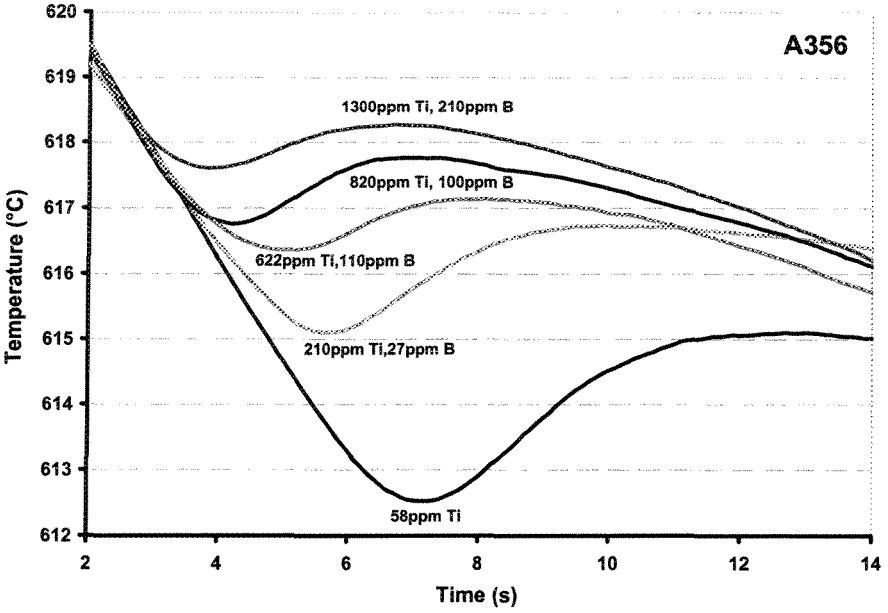

Figure 5.7: The initial section of cooling curves for the conventionally cast specimens. (central thermocouple)

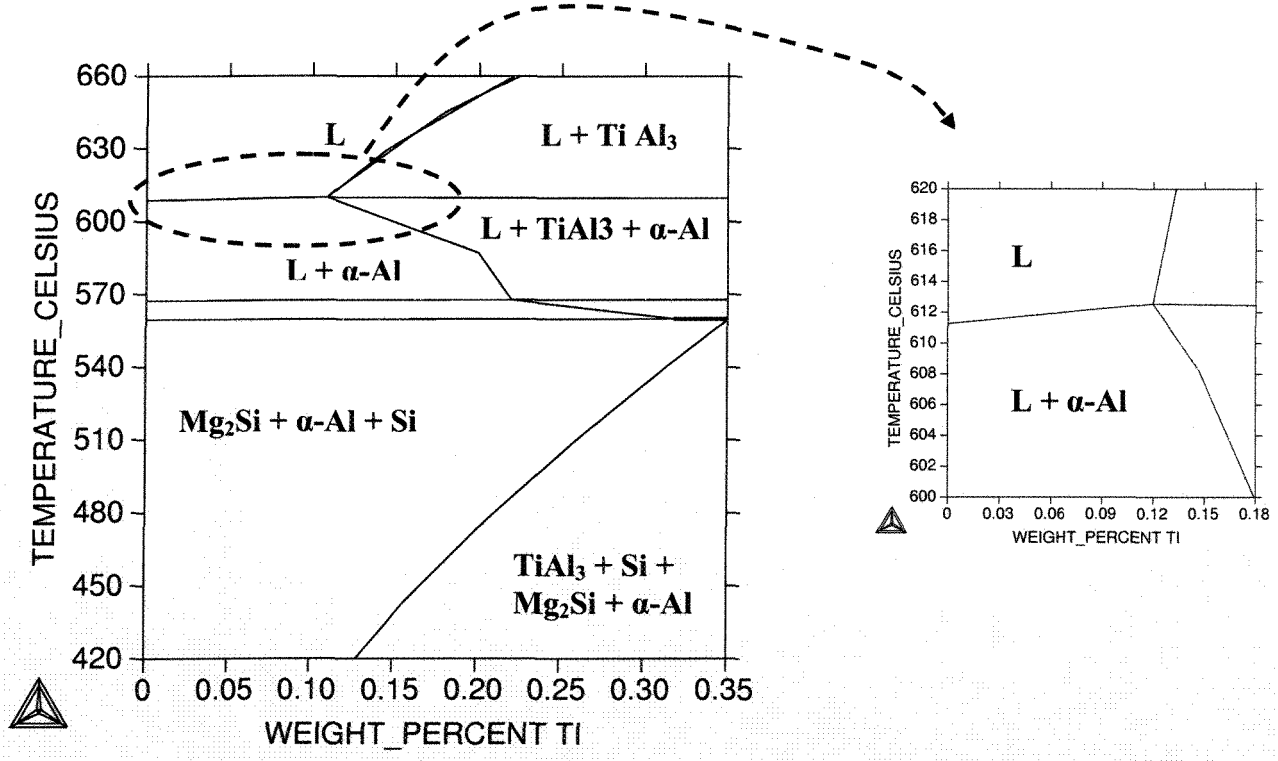

Figure 5.8: Pseudo-binary phase diagram, isopleth, for Al7Si1Mg with Ti (Thermo-Calc calculations)

Figure 5.9 shows nucleation and growth temperatures of α-Al particles including recalescence. With addition of grain refiner, both nucleation and growth temperatures increased. As it could be seen from Figure 5.9a, nucleation temperature increased by ~5°C while growth temperature increased by ~3°C with addition of Ti-B master alloy. The increasing nucleation temperature allows new crystals to form ahead of solidification front, rendering an equiaxed fine grained as-cast structure. Furthermore, the rate at which growth temperature increases is less than nucleation temperature rise. In other words, there are more nuclei with less potential for growth and thus effective grain refinement should be expected. This is one of the basic criteria for a grain refiner to be rated as effective.

Recalescence (ΔT_{Rec}) becomes approximately constant after ~600ppm Ti addition and therefore, from thermal analysis point of view, the critical Ti addition for this alloy appears to be about 600ppm (Figure 5.9b). Further addition may reduce grain size even further, but equally may form Ti-based intermetallics which are detrimental to the mechanical properties of the as-cast products as discussed later. Lowering the recalescence has a great influence on growth of primary α-Al particles. As defined before, minimum temperature at the beginning of solidification, $Tmin_{Al}$, shows the temperature where the rate of latent heat liberation is balanced out with the heat extracted from the sample. In untreated alloy, the existence of recalescence means the heat generated with the commencement of solidification could not be transferred out of the mold completely and therefore the heat balance leads to the appearance of recalescence. However this is not the case for the refined alloy. In refined alloy, as depicted in Figure 5.9a, nucleation temperature ($T_{nuc\ Al}$) increases and therefore in contrast to the untreated alloy, there are more primaries within the same time interval for the refined alloy. These solid α-Al particles can serve as heat sinks to absorb the heat released from surrounding liquid and therefore leads to lower recalescence compared to the untreated alloy.

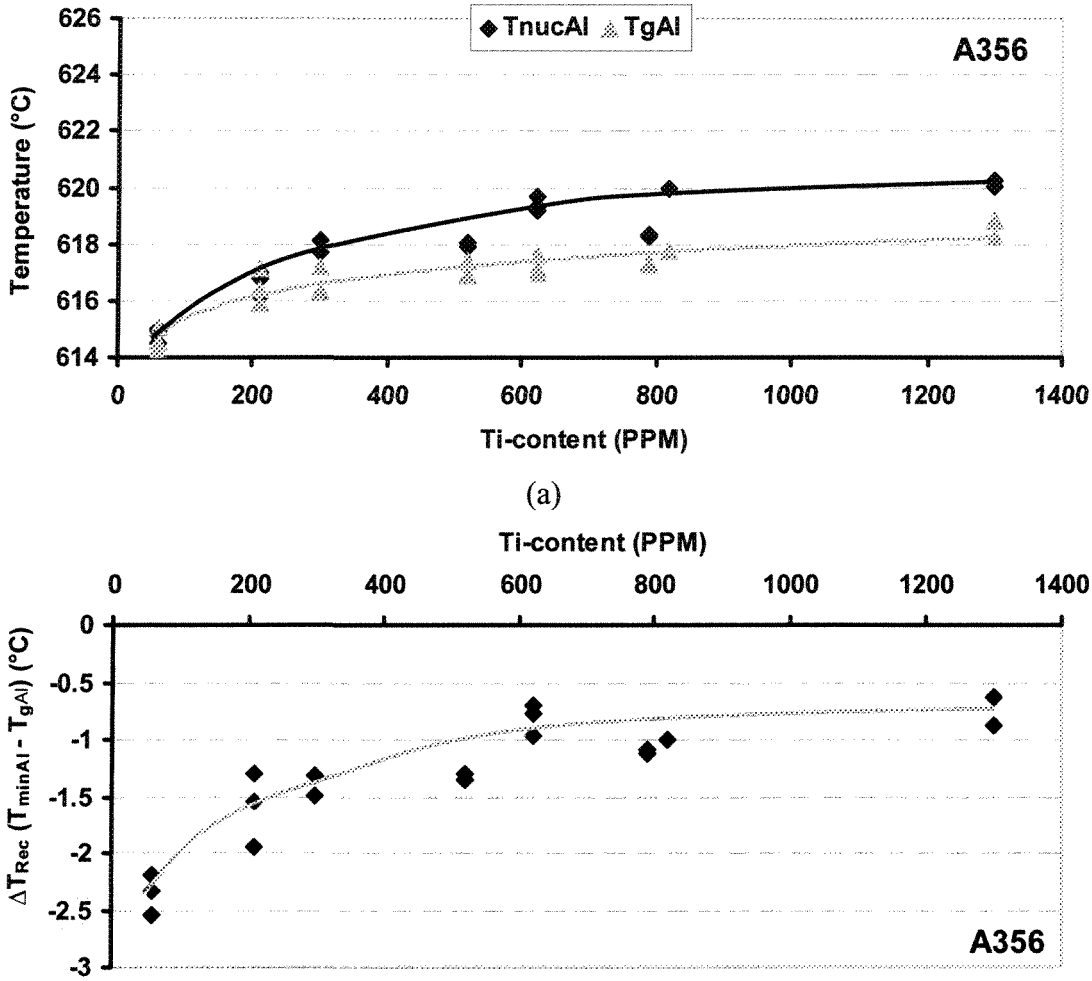

Figure 5.9: Effect of Ti & B addition on the: (a) nucleation and growth temperatures of primary α-Al, (b) ΔT_{Rec}(undercooling)

5.2.1.1.2 Structural analysis

Figure 5.10 shows the microstructural evolution by addition of Ti & B to the alloy. The microstructure without refiner is fully columnar (dendritic) and transforms to equiaxed (dendritic) morphology with increasing Ti and B (black areas are porosity). Moreover untreated alloy is completely dendritic and the branches of dendrites are obvious while by refiner, there is no directionality and the growth is multidirectional. The presence of more potent nuclei in the system is the main reason for this transformation. The incorporation of numerous nucleants due to grain refining encourages the formation of many α-Al particles

adjacent to each other with their boundary layers almost in contact. The result is lesser growth and multi-directional heat flow to eventually form equiaxed structure.

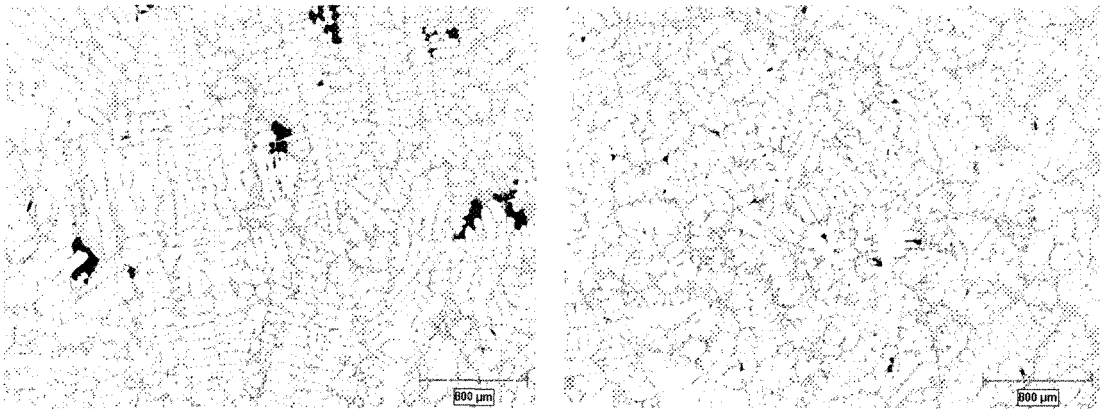

(a) (b)

Figure 5.10: Optical micrographs showing the addition effects in the conventional process: (a) without addition, (b) 520ppm Ti, 73ppm B

Finding nucleation sites is one of the most challenging steps in grain refiner investigation. The likelihood of finding grain refining nucleants would increase with increasing Ti & B concentration as it is the case for the specimen in Figure 5.11. A study of the microstructures in the samples by optical and electron microscopy has shown that most of the nucleation sites for α-Al are heterogeneous particles. Figure 5.11 shows a nucleus at the center of α-Al grain along with its x-ray maps. The particle is basically rich in Si, Ti and B with some Al. It may be suggested that on addition of Al-Ti-B master alloy, the fine TiB_2 particles in the master alloy, Figure 5.2, have acted as nucleation sites, not for α-Al primary phase but for Al_3Ti as the first new phase nucleating out of the melt. The Al_3Ti particles in A356 alloy, as reported [187], do not have the simple Al_3Ti stoichiometry but are a complex mixture of Al, Ti and Si. Therefore, the α-Al has nucleated on a compound of Ti, B, Al, and Si as confirmed by the x-ray maps in Figure 5.13. Table 5.5 gives a typical composition of these nucleants.

Table 5.5: Typical atomic percentage of Al,Ti,B,Si based-nucleant

Al	B	Ti	Si	Mg	Fe
9.82	68.63	13.26	5.8	0.015	2.47

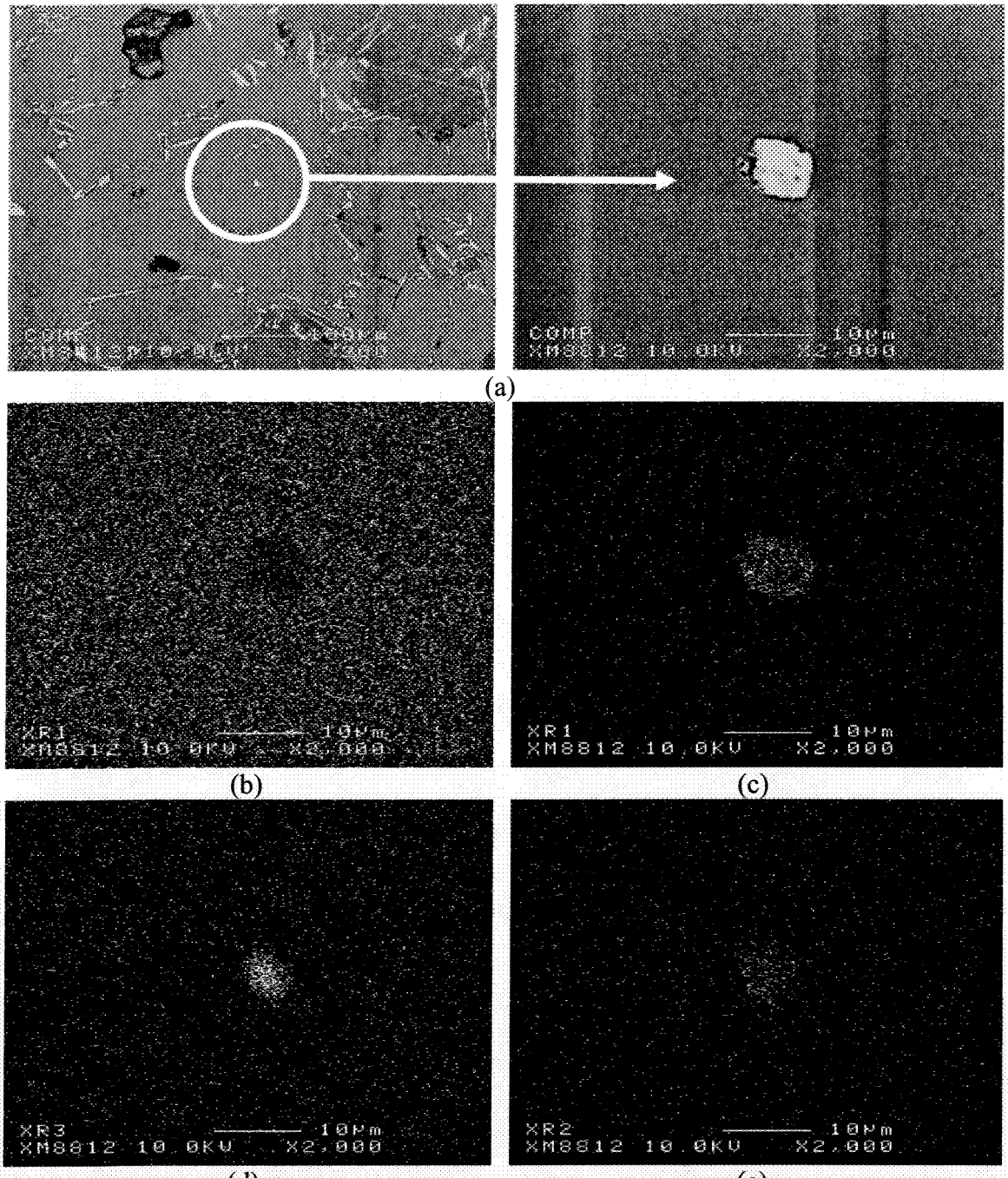

Figure 5.11: SEM micrographs of the nucleant in the sample with 1300ppm Ti & 210ppm B (a) backscattered micrographs, and x-ray maps of (b) Al, (c) Si, and (d) Ti, and (e) B

It is also worth mentioning that with higher percentages of master alloy addition, Ti-based intermetallics may form. The formation of intermetallic particles is an indication of

over refinement as shown in Figure 5.12. Figure 5.13 also shows x-ray mapping of the agglomerations which confirms the presence of Ti and boron based compounds (agglomeration is defined as a group of particles where the spacing is so small that they could not be detected as isolated particles).

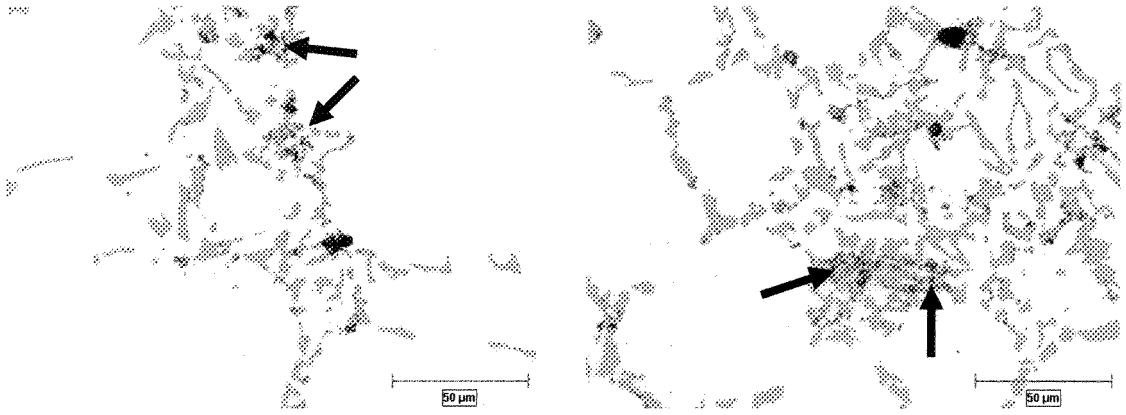

(a) (b)

Figure 5.12: Optical micrographs to show intermetallics agglomeration (arrowed) in the A356 samples for: (a) 820ppm Ti, 100ppm B and (b) 1300ppm Ti, 210ppm B

The ability of the Al5Ti1B master alloy to initiate refining depends on two parameters. First and the obvious one is the potency of the intermetallic particles in the master alloy such as $TiAl_3$ and TiB_2. Besides, after addition of grain refiner and by passing the time, due to the solubility of the master alloy within the melt, a portion of Ti should dissolve. This portion which may come from the $TiAl_3$ or the Ti in the α-Al matrix of the master alloy imparts its growth restriction tendencies to further improve the overall efficiency of the refiner.

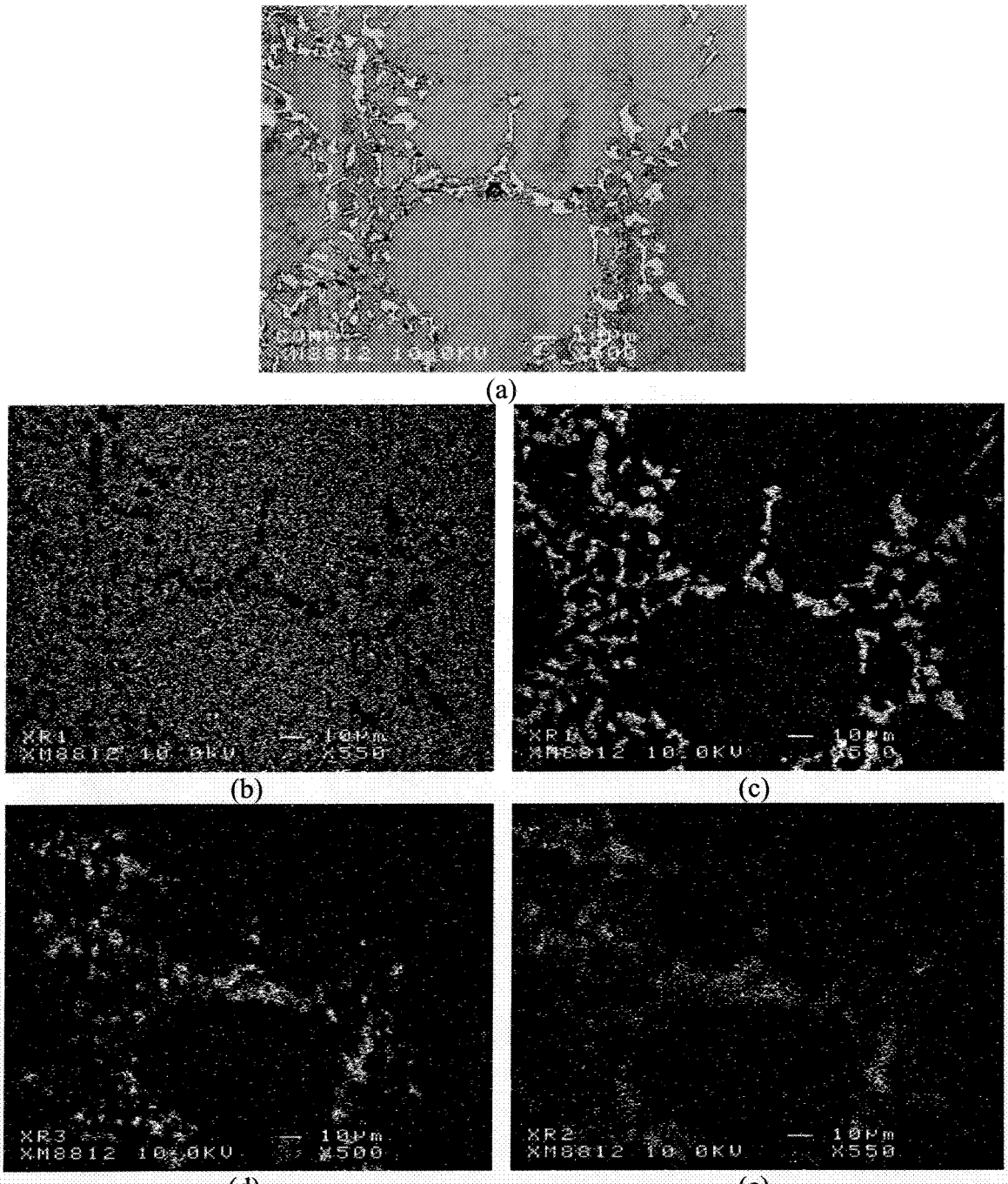

Figure 5.13: (a) Back scattered electron micrograph together with x-ray maps of the intermetallic particles formed due to Ti & B addition,
(b) Al, (c) Si, (d) Ti, and (e) B maps
(Graphite cup sample with 1300ppm Ti & 210ppm B)

5.2.1.2 Semi-solid processing

5.2.1.2.1 Structural analysis

The effectiveness of added grain refiner, Al5Ti1B master alloy, on the morphology of primary α-Al particles in the stirred alloy is well illustrated in Figure 5.14 (dark spots are porosities). At first glance, it is obvious that there is no entrapped eutectic within the primary α-Al particles. The eutectic encapsulation is one of the major defects in SSM processing due to decreasing the efficient liquid accessible for deformation. It appears that grain refiner addition has further reduced primary α-Al particles size and dispersed eutectic regions uniformly as an added bonus to the already refined structure resulted due to stirring. The percentage of primary α-Al phase is also increased slightly with grain refiner addition which is related to the higher nucleation temperature and existence of numerous nuclei, as already discussed for thermal analysis results (section 5.2.1.1.1).

By refiner addition, the quantity of active nucleants in the melt is increased and as a result, more α-Al particles can nucleate. These effective nucleation sites lead to more spherical particles and lesser growth ability of the primary particles. On the other hand, it may be argued that with the addition of Ti, grain growth is restricted due to constitutional supercooling where the primary α-Al dendrites reject Ti into the solid-liquid interface as they grow. As the concentration of Ti increases at the interface, it may reach the level where new nucleants of Al_3Ti could form within the interface layer. The presence of TiB_2 in the master alloy together with the newly formed Al_3Ti particles, encourage the formation of new α-Al nuclei within the interface. The newly formed α-Al particles are expected to reject Ti into the newly formed interfaces as they grow. The repetition of such mechanism ensures the formation of finer and more equiaxed particles as these globules could not grow much because of the neighboring globules and also higher growth restriction factor due to titanium addition.

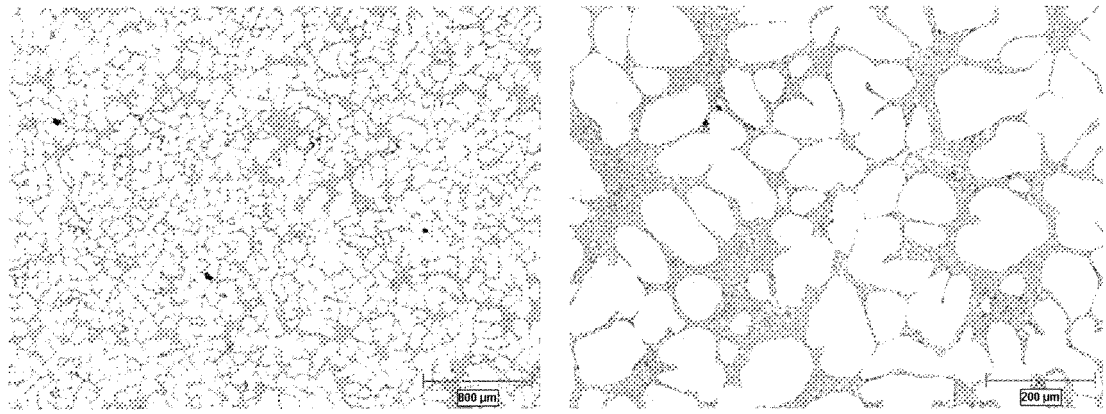

(a)

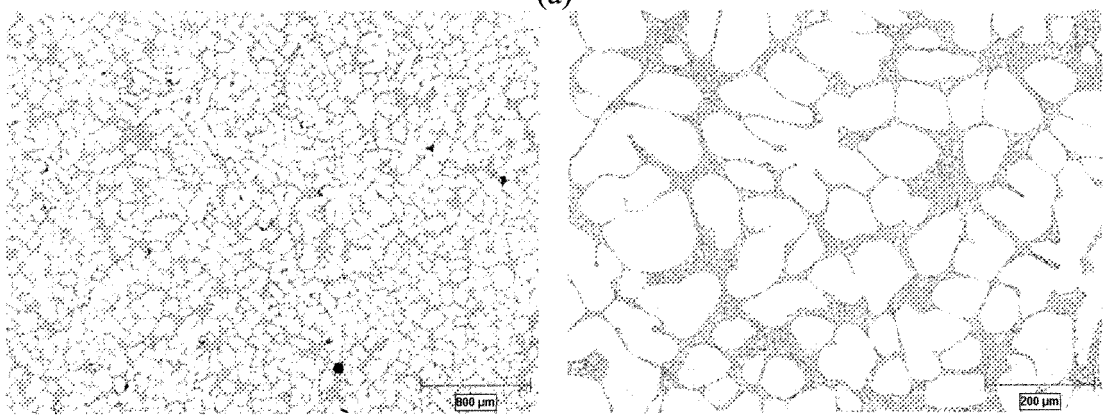

(b)

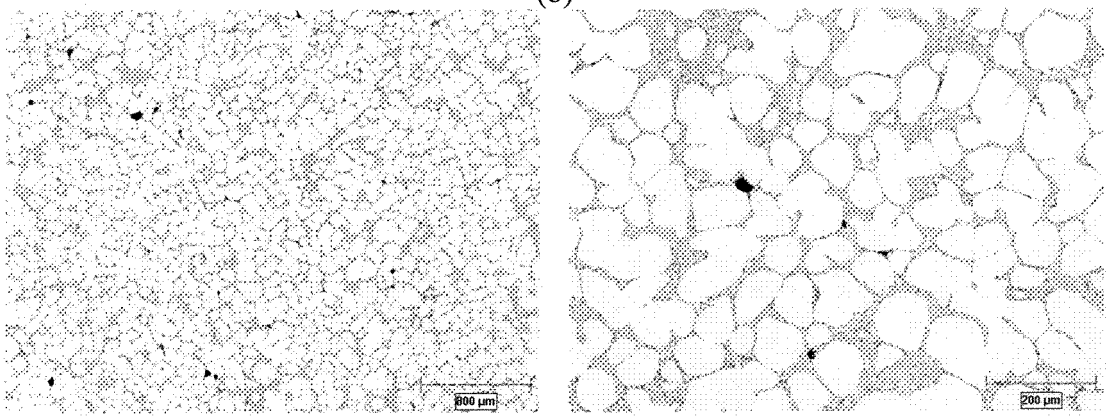

(c)

Continue ⟶

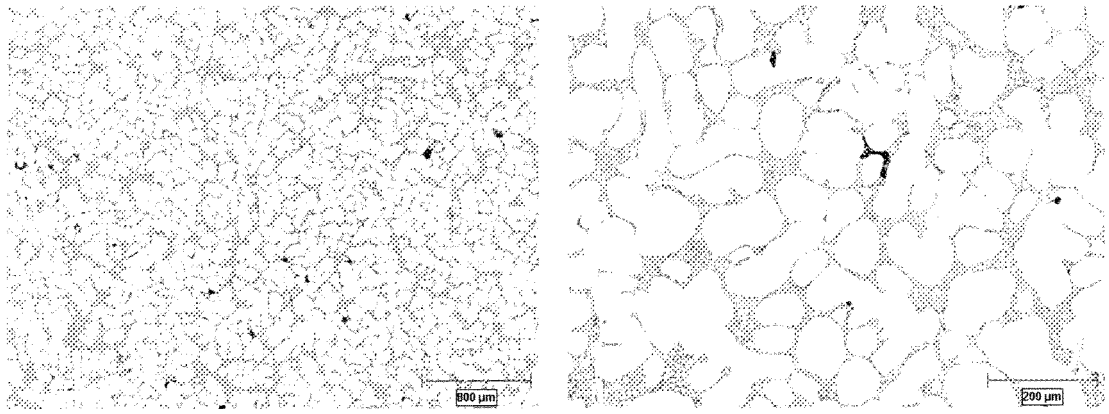

(d)

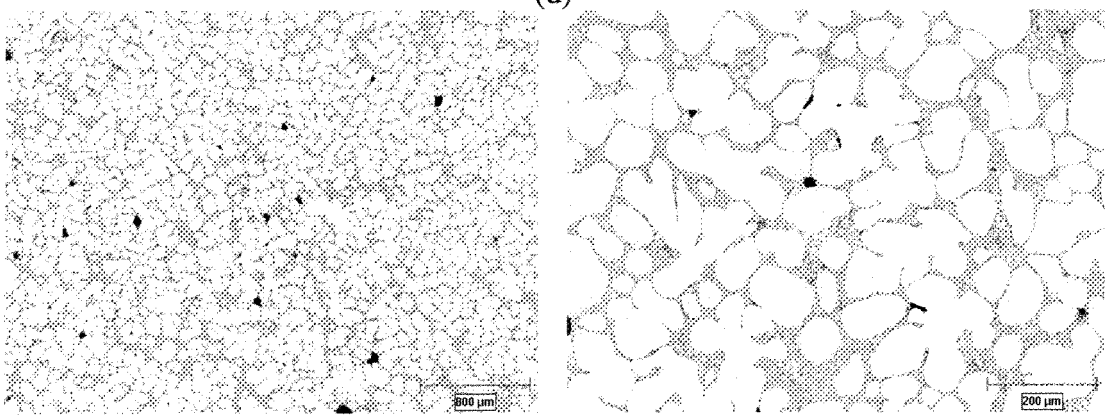

(e)

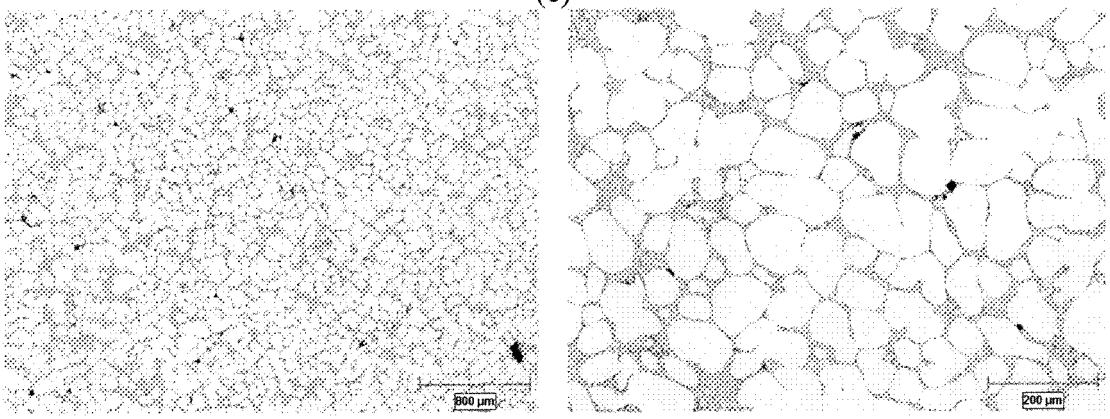

(f)

Figure 5.14: Optical micrographs showing the additional effects in the SEED process: (a) without addition, (b) 210ppm Ti, 27ppm B, (c) 300ppm Ti, 38ppm B, (d) 520ppm Ti, 73ppm B, (e) 820ppm Ti, 100ppm B, and (f) 1300ppm Ti, 210ppm B

The optical micrographs in Figure 5.14 show the effect of Ti-B on the primary α-Al phase in the nominated samples. As it could be seen, samples have been grain refined with increasing percentage of Ti-B and also the globularity of α-Al particles increased. However

it should be mentioned that the drawback here is the agglomeration of Ti-based compounds with increasing Ti content beyond approximately 1000ppm which degrades the potency of the heterogeneous nucleants as already mentioned before, i.e., Figures 5.15 and 5.16. Basically, the sources for agglomeration are;

1. The nature of grain refiner itself where some Ti-based particles may not have the potency to act as nucleation sites nor to go into solution and rejected at the interface to eventually segregate within the eutectic region as the last liquid to solidify. By ThermoCalc calculation it is confirmed that the solubility limit of titanium in Al7Si0.35Mg at 700 and 650°C are 0.38% and 0.2% respectively.
2. The other source may be attributed to the peritectic reaction. With reference to the Al-Ti binary phase diagram [21] and with computational thermodynamic using Thermo-Calc for approximately the same alloy, Figure 5.8, it could be possible for peritectic reaction to shift to lower Ti levels and as reported this shift is greater in the presence of Boron [55,58]. The resulted Al_3Ti particles may agglomerate before becoming active nucleants.

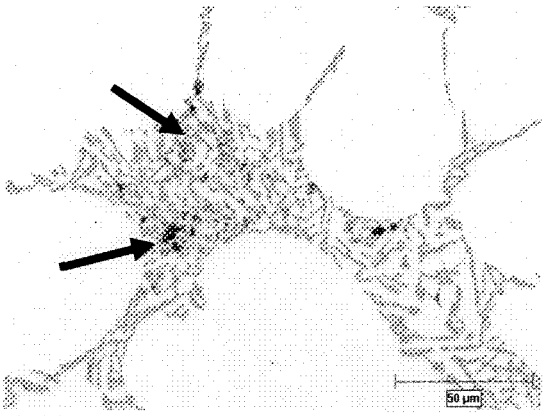

Figure 5.15: Ti based intermetallics (arrowed) in SEED sample with 1300ppm Ti, 210ppm B

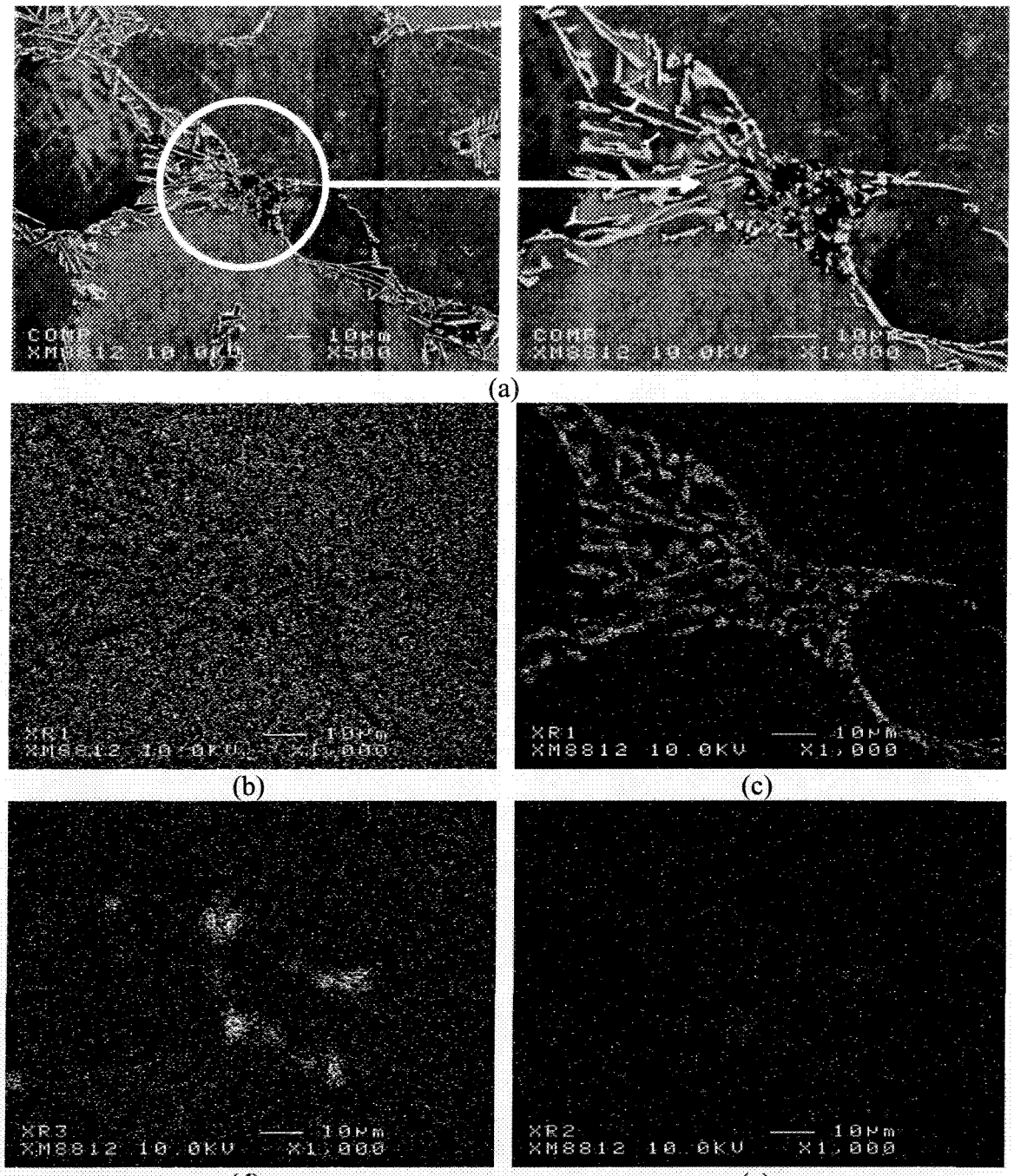

Figure 5.16: (a) Back scattered electron micrographs (different magnifications) together with x-ray maps of the intermetallic particles formed due to Ti & B addition, (b) Al, (c) Si, (d) Ti, and (e) B maps (SEED sample with 1300ppm Ti & 210ppm B)

As a solidification principal, the solidification range is defined as the difference in temperatures between the first and the last liquid to solidify. In binary Al-Si alloys, solidification range is easily defined as the zone for formation of α-Al dendrites while in ternary and multi-component Al-Si systems such as AlSiMg, solidification range consists of two main intervals, the temperature range for the formation and growth of α-Al dendrites (ΔT_α) and/or iron intermetallics and the temperature range for the eutectic and post-eutectic reactions including the formation of Mg_2Si and/or iron compounds (Figure 5.17).

For the 356 alloys, the solidification ranges for the formation of α-Al dendrites and eutectic reactions are plotted in Figure 5.18. It is shown that by increasing the Ti and B additions, α-Al solidification range increases by ~6°C and addition of grain refiner has almost no effect on the eutectic solidification range. This issue has a great influence on the rheo-processing since initiation and formation of α-Al globules totally depends on the SSM processing such as stirring in this region. The attention of the reader is also drawn to the fact that there is no intention to re-introduce the concept of solidification range, since the importance of solidification interval in SSM processing is well proven before [4,8]. However, the distinction of different parts of the solidification range is essential since the eutectic portion of the mush evolution has not a great bearing in slurry preparation and the key parameter is the primary particles formation.

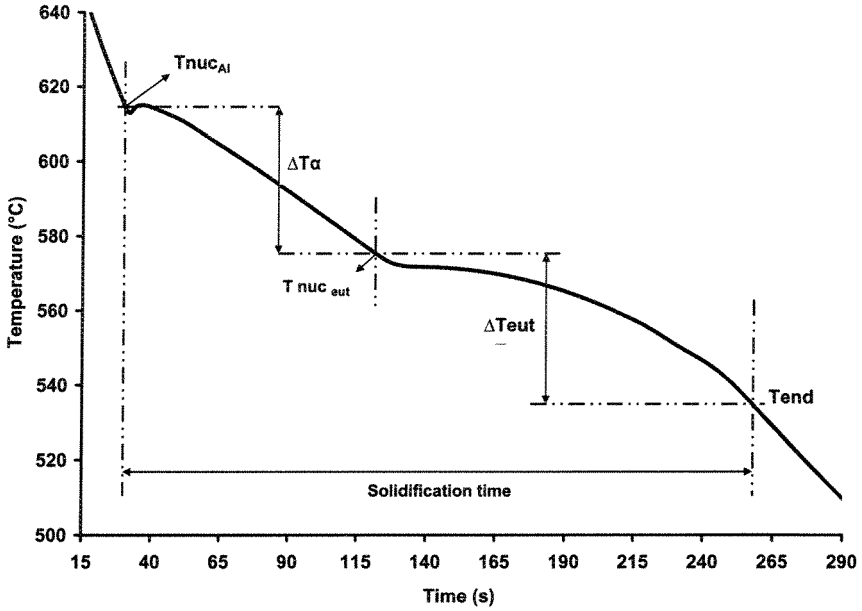

Figure 5.17: Cooling curve and definition of various solidification ranges

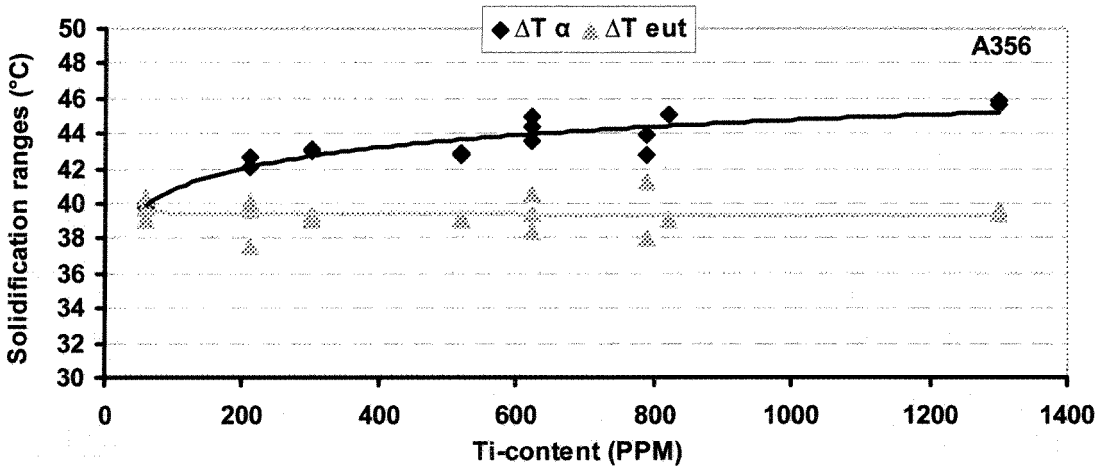

Figure 5.18: Effect of Ti and B on the solidification range of various phases

5.2.1.2.2 Image analysis

Figure 5.19 illustrates the quantitative results from image processing of the resulting microstructure. With refiner addition, the primary α-Al percentage appears to increase slightly (Figure 5.19a). This is due to higher number of effective nuclei for the primary α-Al particles and also shifting of liquidus temperature to higher values with eutectic temperature remaining unchanged.

On the other hand, due to the efficacy of refiner, the equivalent circular diameter decreases (Figure 5.19b). This parameter has a direct relation with number density, i.e., the quantity of primary particles per unit area (Figure 5.19c). More effective nucleation sites lead to better distribution of particles in the sample powered by limited growth which results in smaller particle size. Such increase in number density is in spite of the difficulty in image processing and differentiating between two adjacent α-Al particles especially when they coarsen or there is less eutectic in the structure; it is possible to under estimate α-Al number density.

Also as a marginal but critical result, the main criteria of SSM processing, i.e. fine primary phase particles, preferably less than 100μm diameter with globular or rosette structure [158], are easily achieved by SEED even in untreated alloy. The SEED process is an effective route to prepare billets for rheocasting applications. For better size distinction of the particles, aspect ratio is used and it was just calculated for ratios above 2 which is a representative of non globular structure. The average trend of area/perimeter and aspect ratio decreased which these factors are indications of having reduction in size. Such parameters are symbols of more isolated, finer, and more spherical α-Al particles (Figure 5.19d,e).

As it was described in the experimental procedure, the step before quenching is to drain the remaining liquid to have a self standing billet. As it could be seen, in Figure 5.19f, with more Ti addition, the percentage of liquid drainage increased. This is an interesting result, since it is expected to have less drainage due to slight increase in α-Al particles percentage due to grain refiner addition. However, since the globularity of α-Al particles is increased, it is expected to have smooth channels without interlocking pathways for liquid to flow. This may be attributed to dendrite coherency point, DCP, where both stirring and grain refiner addition postpone DCP. This phenomenon has been reported for conventional casting [78] where DCP point was postponed to lower temperatures with grain refiner addition, i.e. the formation of finer and more equiaxed structure. Greater values for liquid drainage due to grain refiner addition are therefore one of the reasons for greater and more globular α-Al particles in the billet.

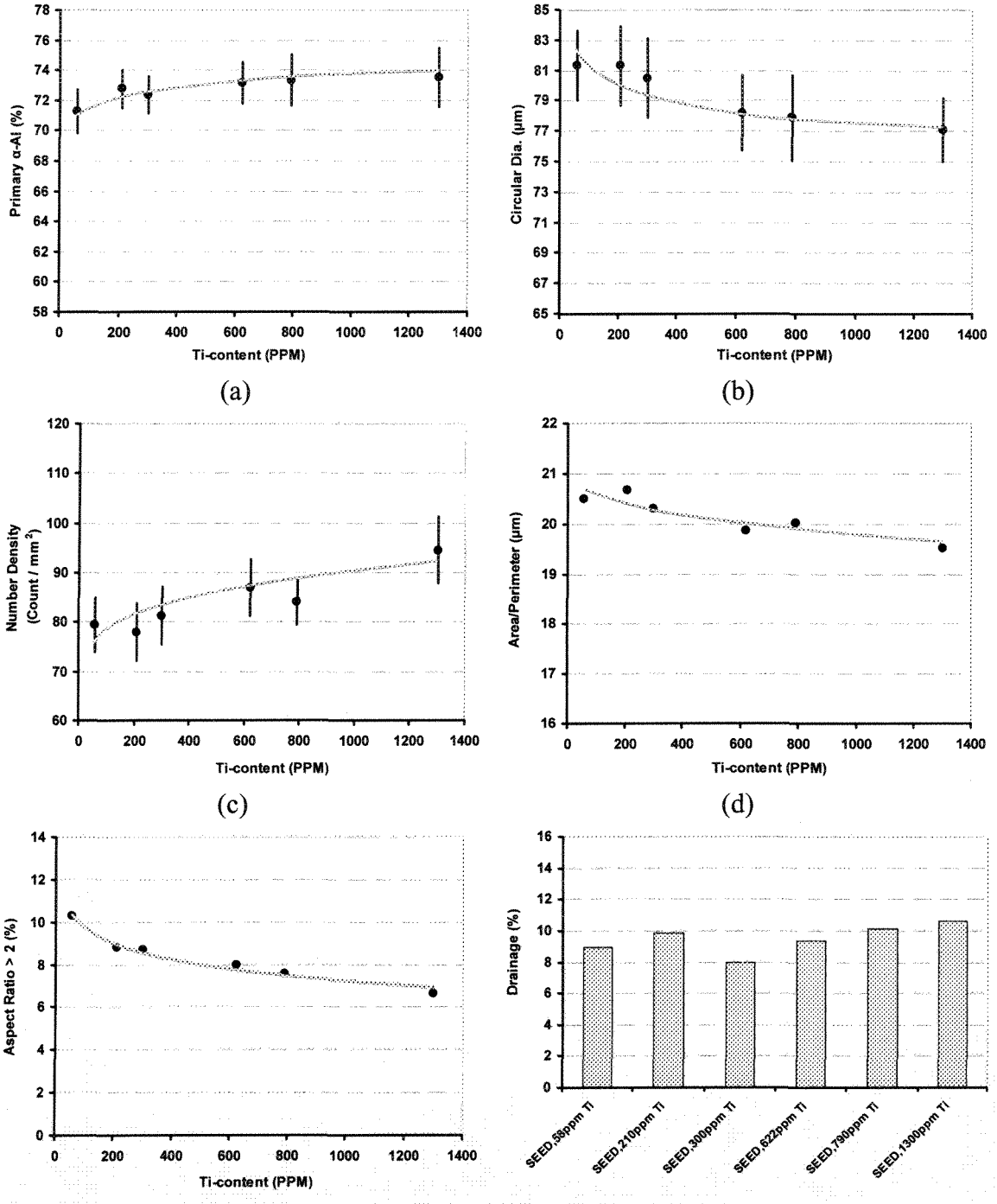

Figure 5.19: Image analysis parameters for A356 with Ti&B addition:
(a) primary α-Al percentage (b) average circular dia., (c) number density of α-Al particles, (d) area/perimeter, (e) percentage of α-Al particles having aspect ratio >2, and (f) drainage as a process parameter

By using the average value of sphericity, it was concluded that this parameter is not responsive to small variation of the morphology and in most cases due to the averaging; the maximum difference between sphericity values for the treated and untreated alloys is less than 0.1. Therefore a more sensitive parameter was chosen which is the percentage of particles having sphericity greater than 0.8. The histogram chart in Figure 5.20a shows the percentage of α-Al particles with sphericity >0.8 rises with increasing grain refiner addition. Figure 5.20b compares the sphericity numbers for the alloys without and with refining. Closer values to 1 show more spherical particles which these values are greater for refined alloy.

It is worth noting that image analysis technique is the reproduction of the microstructure which is not exactly the same being studied. Therefore, it should always be kept in mind that what image analysis can not do, for example it should be mentioned that the definition of diameter in the software is based on the equation ($2\sqrt{area/\pi}$), which area refers to the area of the object being measured. Such measurement makes the assumption that the examined object has a shape close to a circle and for instance, the more the particle is rectangular, the greater is the error in the calculation. Considering this point, it should be expected to detect small differences between the average circular diameter of a rosette and globule α-Al particle with the same area.

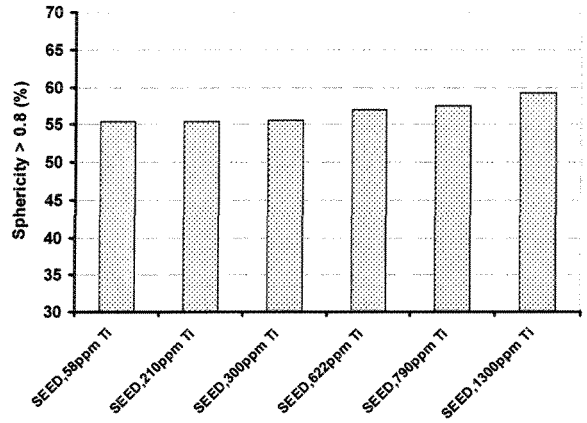

(a)

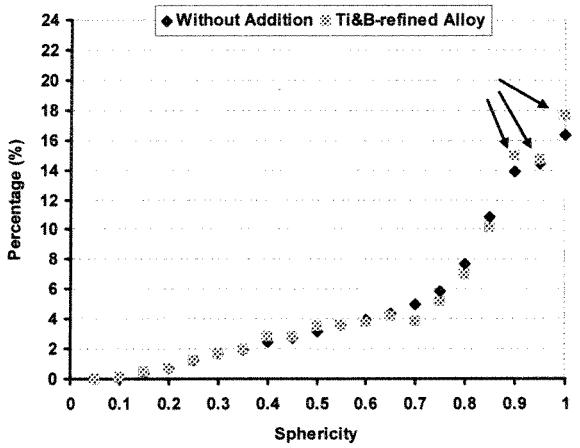

(b)

Figure 5.20: (a) The effect of refiner addition on the percentages of particles with sphericity>0.8, (b) effect of refiner on sphericity values (820ppm Ti & 100ppm B)

5.2.2 Addition of boron in the form of AlB_{12} with Al4%B

The addition of boron in the form of Al-4%B master alloy to the A356 alloy (without Ti in solution) was investigated. The experimental procedure was the same as described in chapter 4. The chemical compositions of the base alloy are listed in Table 5.6.

Table 5.6: Chemical analysis of the base alloy (wt. %)

Si	Mg	Fe	Mn	Cu	Ti	B	Sr	Al
6.42-6.6	0.36-0.39	Max 0.07	Max 0.003	Max 0.001	Max 0.0058	Nil	Nil	bal.

5.2.2.1 Conventional casting

5.2.2.1.1 Thermal analysis

The magnified region of the onset of solidification is presented in Figure 5.21. Boron addition in excess of 200ppm eliminates undercooling and interestingly there is not any recalescence where the temperature keeps falling continuously after nucleation.

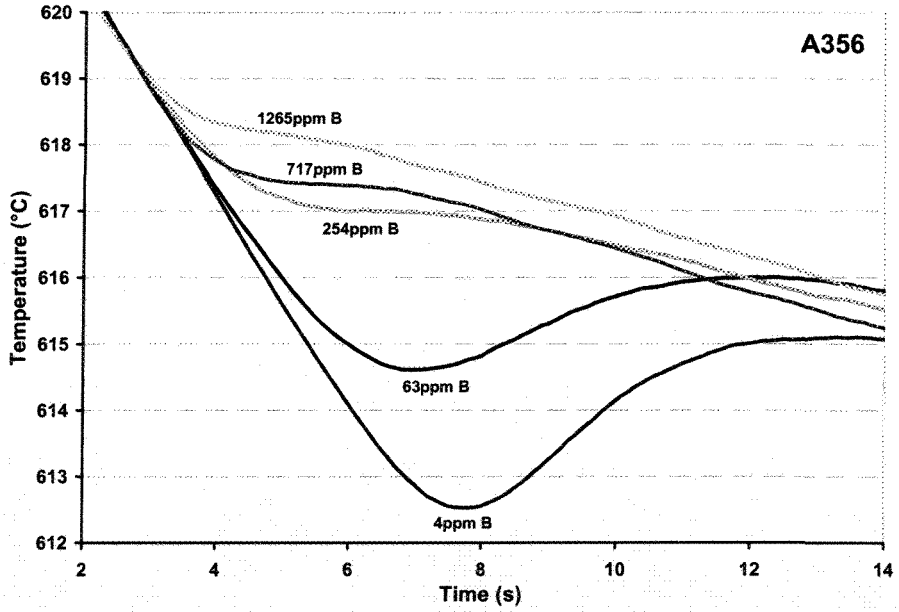

Figure 5.21: Start of the solidification for the typical central cooling curves

Thermo-Calc software was used as a predictive tool to examine as how the boron addition affects the ternary Al-Si-Mg alloy. For this purpose, an iso-pleth diagram was constructed for boron addition to the Al7Si1Mg alloy (Figure 5.22).

As seen, boron addition expanded the mushy zone and brings about the formation of a new, AlB_2, phase in A7SiMg alloy. This area is more visible in the iso-pleth diagram calculated for a constant value of boron, 0.02%, as shown in Figure 5.23. The formation of boron compound is expected to have marked effect on the nucleation of primary α-Al particles in the Al-Si alloys having more than ~4% silicon content. Furthermore by the formation of AlB_2, the liquidus shifts to higher temperature and that is to have sooner nucleation. It is worth mentioning that in real casting condition, this thermodynamic calculation would be slightly changed by non-equilibrium conditions such as higher cooling rate, existence of trace elements etc.

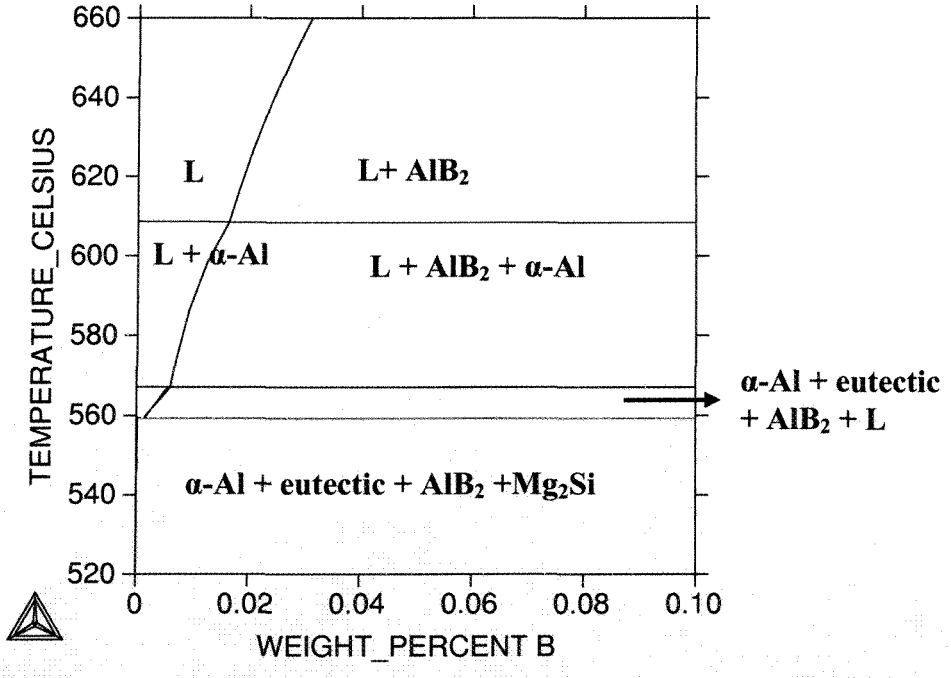

Figure 5.22: ThemoCalc calculation of the iso-pleth for Al7Si1Mg versus B

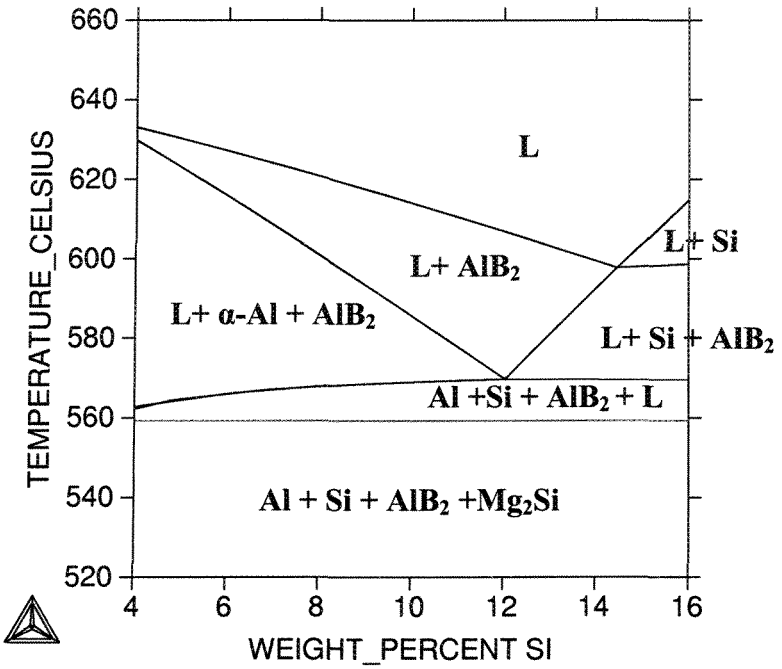

Figure 5.23: Iso-pleth of the AlSi1Mg0.02B versus Si

Thermal analysis data were determined by the principles of cooling curve analysis [24] and especially with the intention of identifying the nucleation ($Tnuc_{Al}$) and growth (Tg_{Al}) temperatures and the magnitude of recalescence (ΔT_{Rec}) (Figure 5.24). For boron concentrations up to 200ppm, an undercooling of ~ 2°C is registered but approaches zero and remains zero for all other additions above ~200ppm. It has to be emphasized that small changes in the chemical composition of the alloy have considerable effects on the critical points and should not vary too much, e.g. each 0.1%Si causes about ~0.7°C variation in the liquidus temperature, if the results to be compared with one another..

It is evident from Figure 5.24 that by boron addition the nucleation temperature of primary α-Al is increased by ~7°C while the growth temperature raised by only ~ 2°C; which means that the rate at which the nucleation temperature increases is higher. This is equivalent to more nuclei generation with less capacity for growth which leads to more equiaxed structure since the inter-nuclei spacing is reduced and the number of heat sinks increased almost everywhere in the melt to encourage multidirectional heat flow. This is one of the basic criteria for a refiner to be rated as efficient.

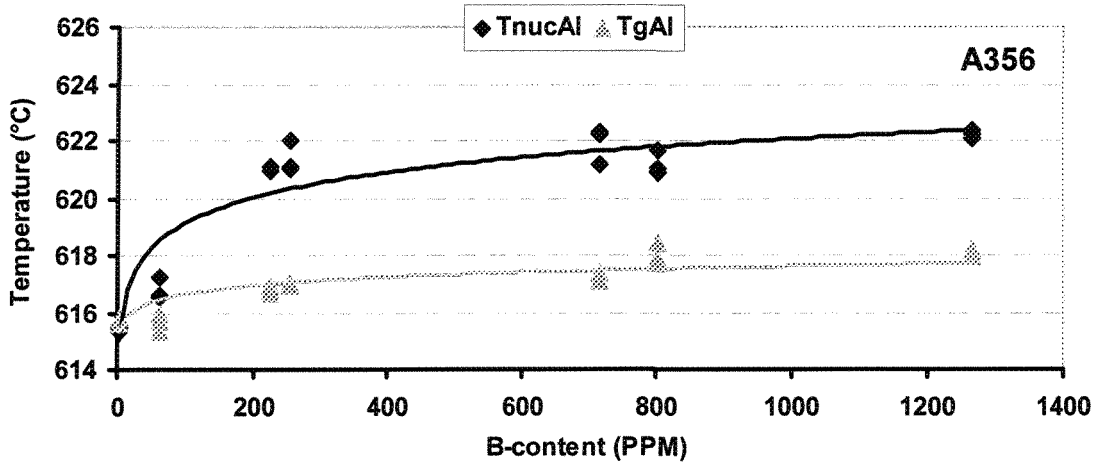

(a)

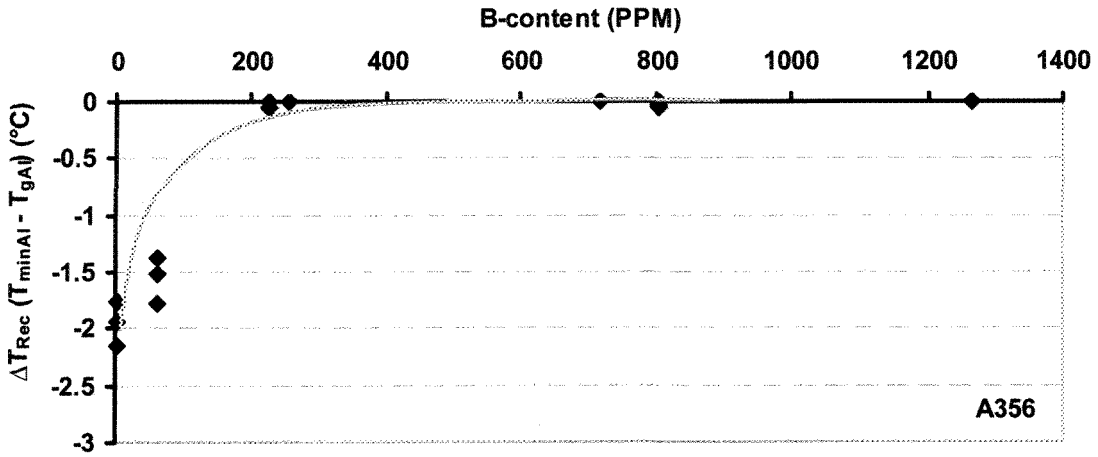

(b)

Figure 5.24: Effect of boron addition on the:
(a) α-Al nucleation and growth temperatures, (b) ΔT_{Rec}(undercooling)

5.2.2.1.2 Structural analysis

Figure 5.25 shows the microstructural evolution by addition of boron to the alloy. As seen, the microstructure in the grain refined sample is quite different from that of the non-grain refined. Grain refinement efficiency means that there are sufficient active nucleants to encourage the formation of smaller grains. At the beginning of solidification, if the mean distance between the nucleants/nuclei would be small, the resulting grains grow slowly due to limited transport of heat. In addition, each nucleus could act as heat sink for others to impose a localized multi-directional heat flow within the melt. Consequently this

should lead to globular grain structure. This is the case for boron grain refinement, where an equiaxed structure is formed with boron concentration in excess of 200ppm.

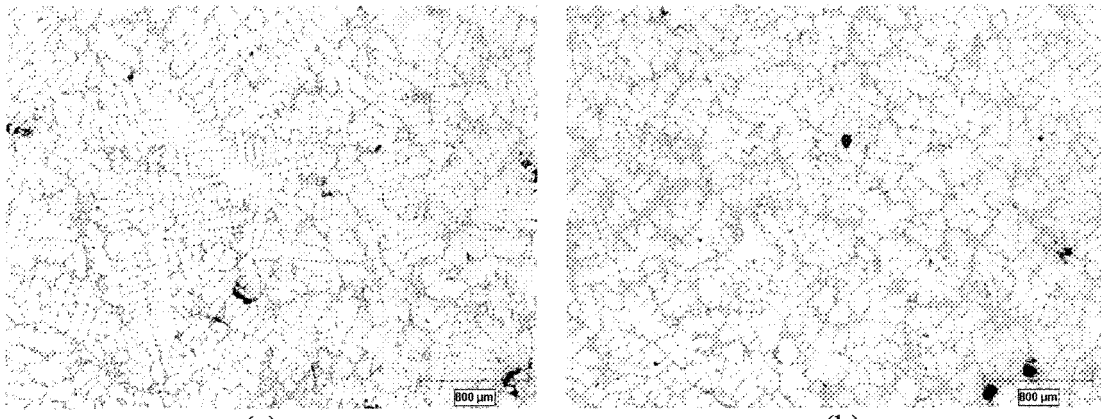

(a) (b)

Figure 5.25: Optical micrographs to show the effect of boron addition in the conventional process: (a) without addition, (b) with 254ppm B addition

The presence of agglomerated intermetallic particles is the main shortcoming of higher boron level. Figure 5.26 shows the segregated boron based intermetallics having different sizes depending on the boron content. The segregation of large agglomeration is partly due to the nature of the master alloy where as mentioned before the AlB_{12} particles are not distributed well within the master alloy and there are different sizes of particle agglomeration as well. This is exaggerated by the low solubility of AlB_{12} in the melt at the working temperature.

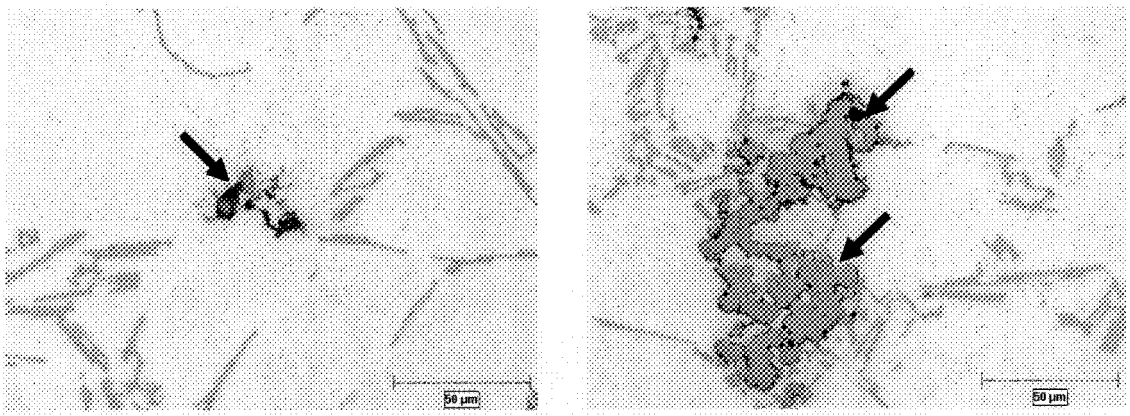

(a) (b)

Figure 5.26: Optical micrographs to show intermetallics agglomeration for: (a) 717ppm ,(b) 1265ppm boron addition

One of the main requirements for an efficient grain refiner is its small disregistry with the aluminum matrix and the lesser the disregistry, the better is the results. According to the data given in appendix A, the measured disregistry between AlB_{12} and the α-Al matrix is 151% and therefore it is rather unlikely for them to act as nucleants in the system. So, the question may arise as why and how the improved refinement efficiency of this master alloy around 200ppm B could have resulted. It is believed that the enhanced refinement efficiency is coming from the following sources;

- The presence of AlB_2 particles within the master alloy
- Dissolved boron in the alloy
- Transformation of AlB_{12} to AlB_2

By examining the master alloy structure more closely, it is clear that there are AlB_2 particles in the matrix hidden amongst the AlB_{12} agglomerates as shown in Figure 5.27a where another master alloy with mainly AlB_2 particles is shown to highlight this point (Figure 5.27b). It is believed that these particles play fundamental role on improving the refining efficiency of the master alloy.

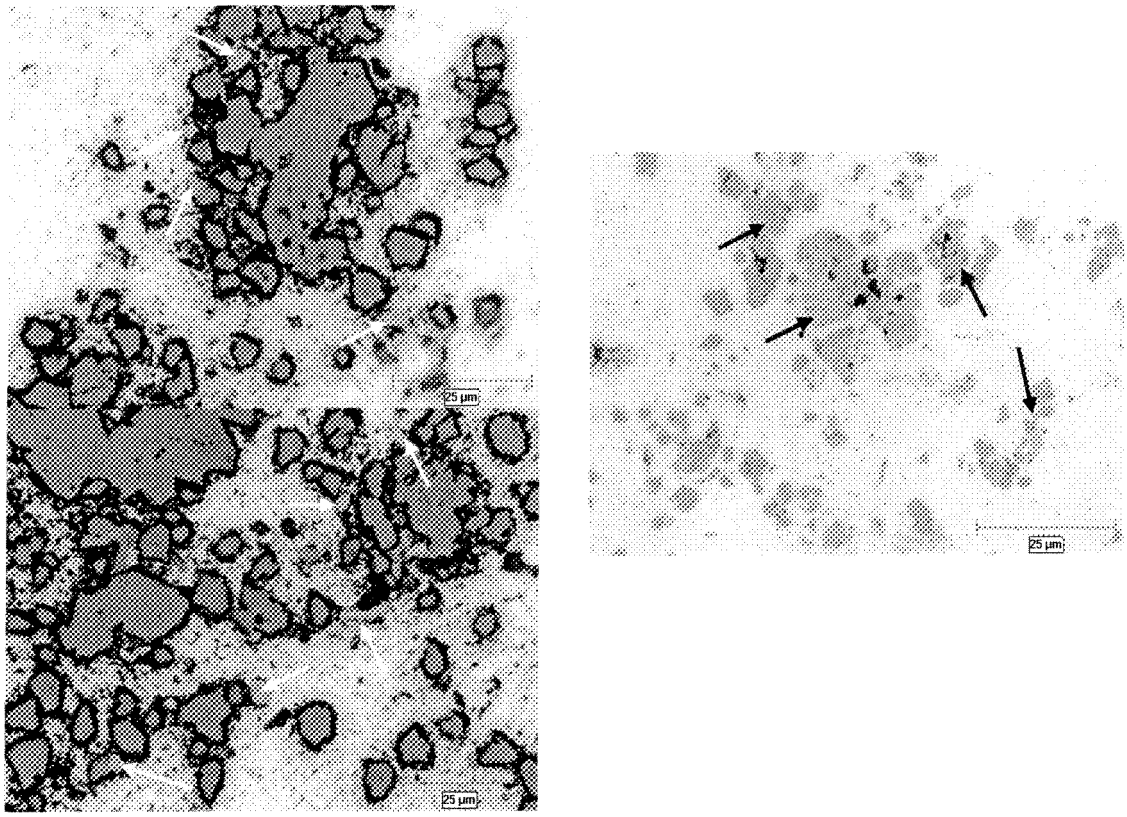

(a) (b)

Figure 5.27: AlB_2 particles in different master alloys:
(a) Al4B, waffle form, (b) Al5B, rod form (arrows show the AlB_2 particles)

Figure 5.28 shows the solubility limit of B in the melt at different temperatures. At 700°C, there is ~0.05% boron in the solution and this amount is quite enough to react with aluminum from the melt and form indigenous nucleants. Further, as it was shown in Figure 5.3, the majority of the boride particles in this master alloy are AlB_{12}. The aluminum rich side of the B-added A356 alloy phase diagram (Figure 5.28) shows that AlB_{12} transforms to AlB_2 at 975°C and moreover is only stable at B concentrations in excess of ~0.5%. However since there are localized agglomerations of AlB_{12} particles, it is logical to assume that the boron concentration is much higher locally than the nominally added value. As a result and according to the phase diagram, it is possible to have some degree of transformation of AlB_{12} to AlB_2, with the newly formed AlB_2 acting as nucleation sites for primary α-Al. In addition, there is a fourth possibility for this master alloy to be an efficient grain refiner and that is the dissolved Ti in the alloy and its high affinity for B to partially

transform the AlB_{12}/ AlB_2 particles to complex compound of AlTiB, suitable for acting as nucleation site for the primary α-Al.

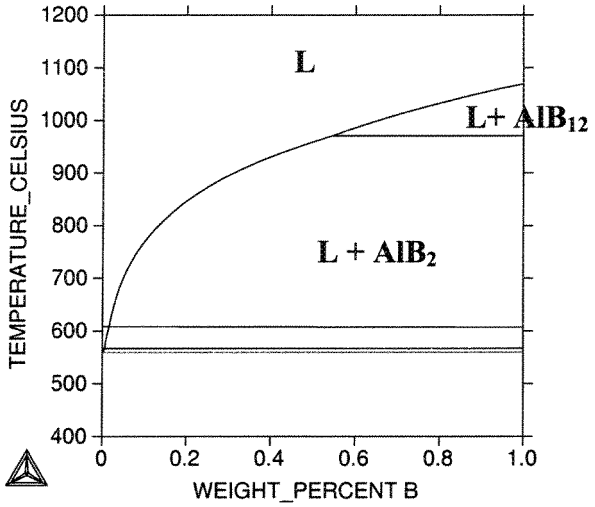

Figure 5.28: ThermoCalc calculation of iso-pleth for Al7Si1Mg versus B

5.2.2.2 Semi-solid processing

5.2.2.2.1 Structural analysis

The optical micrographs in Figure 5.29 show the effect of boron on the primary α-Al phase. With increasing the percentage of boron, the structure is not only refined but also the globularity of α-Al particles increased. In addition, better distribution of the eutectic regions due to inoculation improves gliding, rolling over, of the primary particles during injection of the billet into the mold.

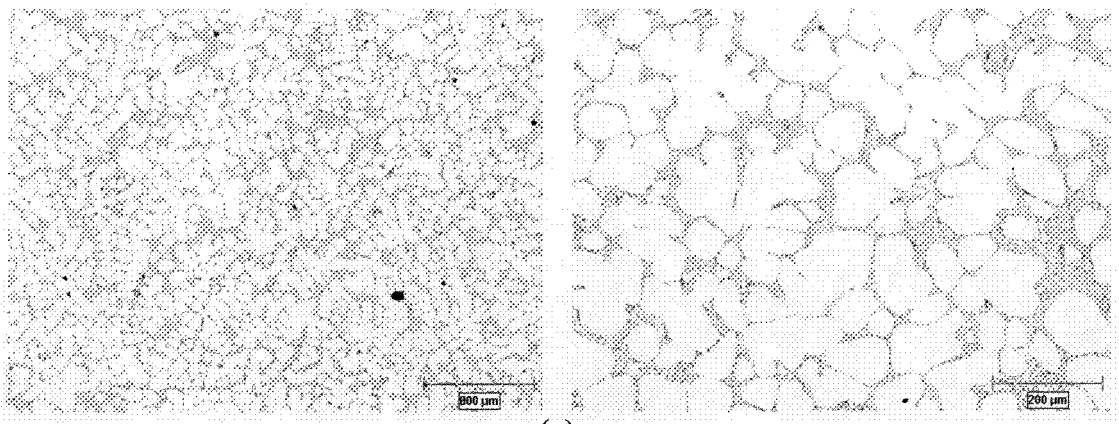

(a)

Continue ⟶

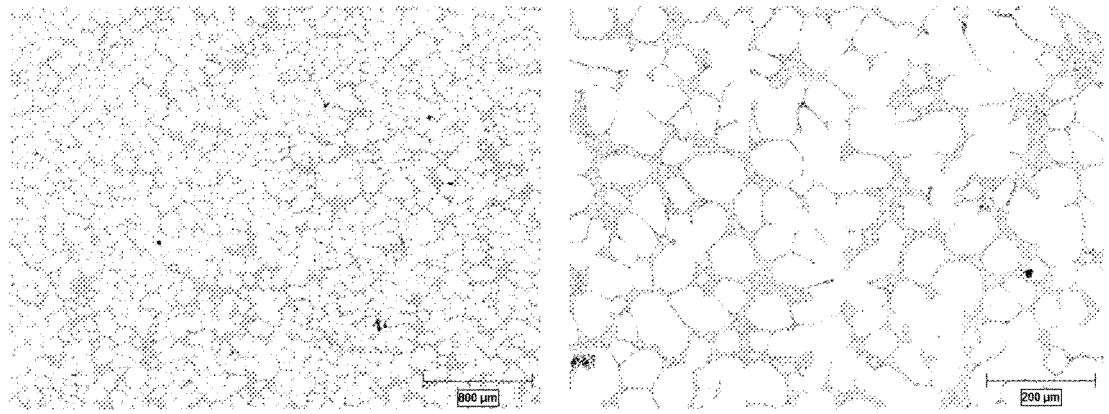

(b)

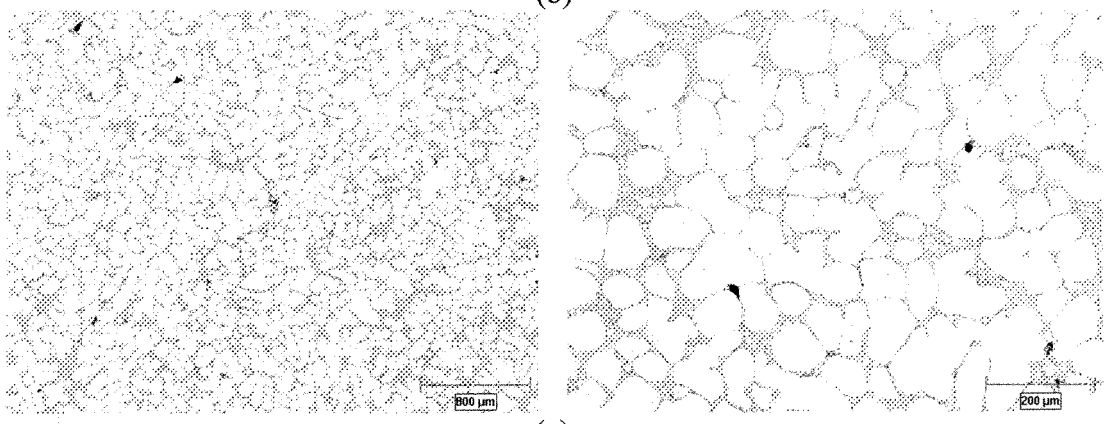

(c)

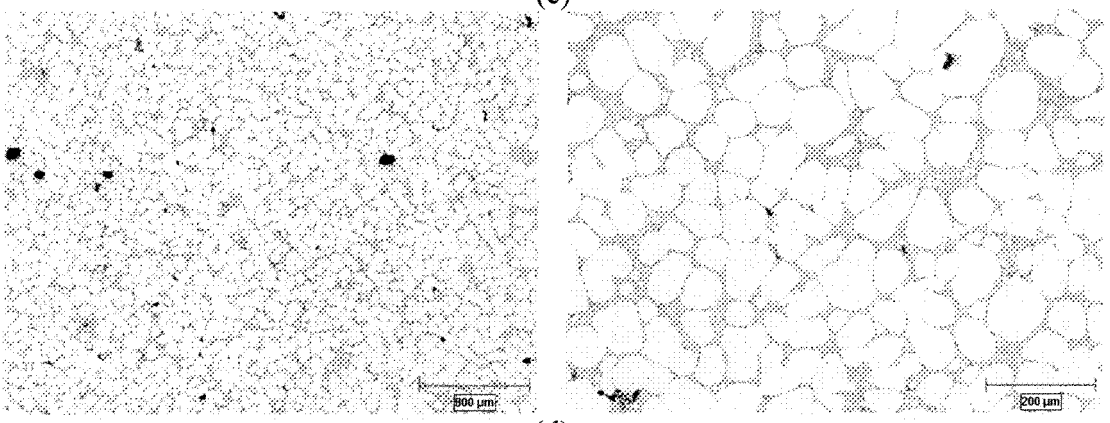

(d)

Continue ⟶

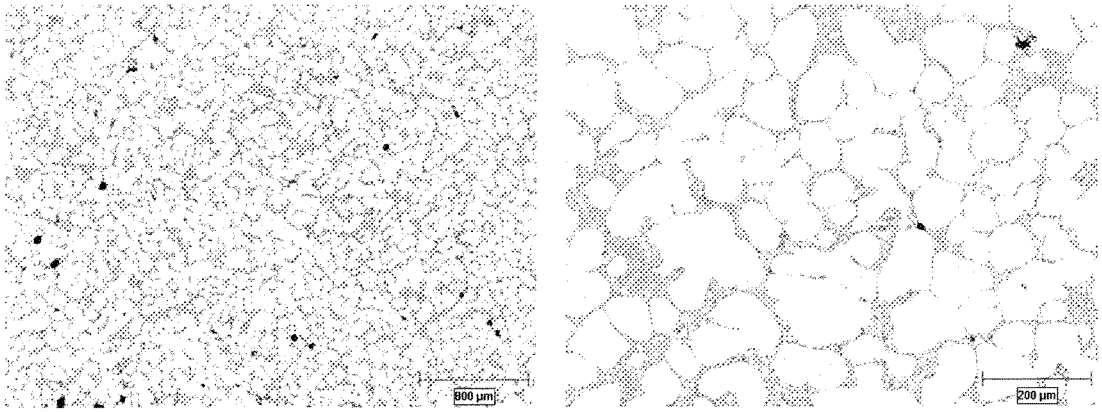

(e)

Figure 5.29: Microstructural variation due to different boron levels:
(a) without addition, (b)63ppm, (c) 254ppm, (d) 803ppm, and (e)1265ppm B

As mentioned earlier by refiner addition nucleation temperature of α-Al particles increases significantly. By increasing the nucleation temperature, it would be expected that solidification range of the system also increases. Figure 5.30 demonstrates the variations of the two distinct solidification ranges of primary α-Al (ΔT_α), and eutectic (ΔT_{eut}) for the A356 alloy with boron. By boron addition, ΔT_α increases by nearly 6-8°C with ~200ppm boron and remains almost constant up to 1200ppm. This is in contradiction with ThermoCalc prediction seen in Figure 5.22 where liquidus temperature increases by nearly 50°C when boron concentration increases from 200 to 300ppm.

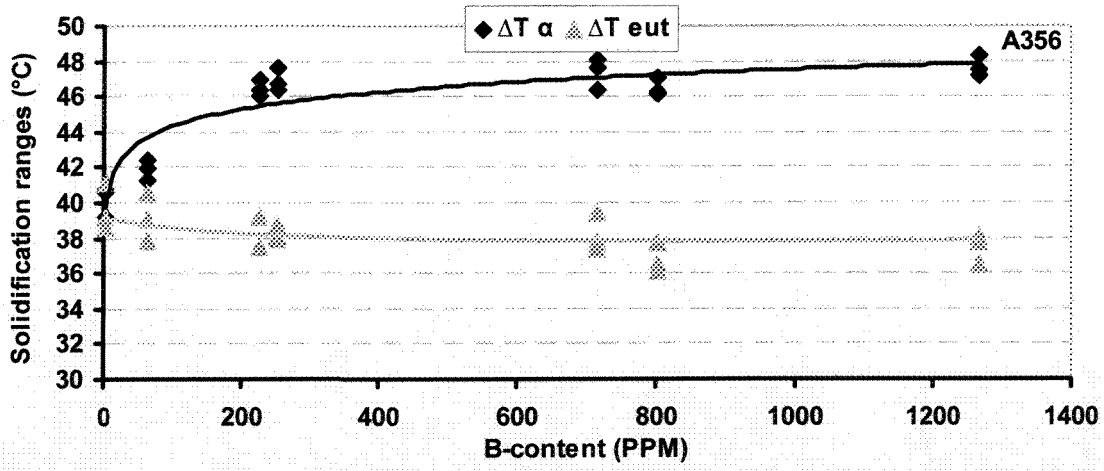

Figure 5.30: Effect of boron on the solidification range of various phases

This is expected since the phase diagram in Figure 5.22 is based on pure boron addition while in the current study, aluminum boron rich particles are introduced to the melt. Since these particles are stable and have almost no solubility at this temperature, therefore only act as nucleant not interfering on the thermodynamic of mixing of AlSiB as is the basis for the ThermoCalc prediction. It is also worth noting that boron influences the ΔT_{α} not ΔT_{eut}.

The main drawback here is the agglomeration of the boride compounds with increasing B content beyond 230ppm as shown in Figures 5.31 and 5.32. The x-ray maps and microprobe analyses (Table 5.7) confirm the segregation of AlB_{12} particles. Another interesting feature is the formation of Ti-based compounds which are dispersed around the AlB_{12} agglomerates. As it was shown in Table 5.6, Ti concentration is at trace level in the base alloy but has significant effect on the formation of Ti-based intermetallics. It is proposed that by boron addition to the melt and due to the high affinity of Ti for B, these elements react and form AlTiB compounds which after a short time transform to stable TiB_2 compound. These TiB_2 particles appear in an area with high concentration of boron such as AlB_{12} boundaries. X-ray maps in Figure 5.32e&f support the aforementioned hypothesis.

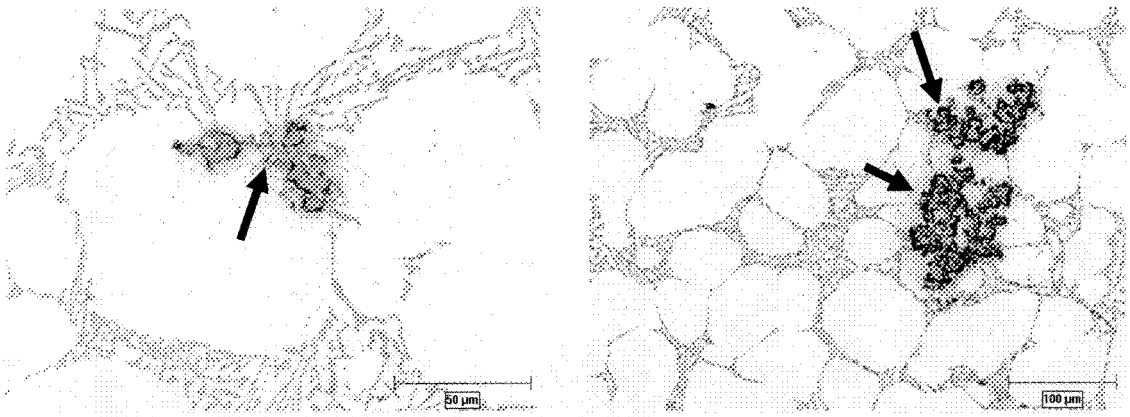

(a) (b)

Figure 5.31: Boron based intermetallics in two different SEED samples:
(a) 226ppm and (b) 717ppm boron addition

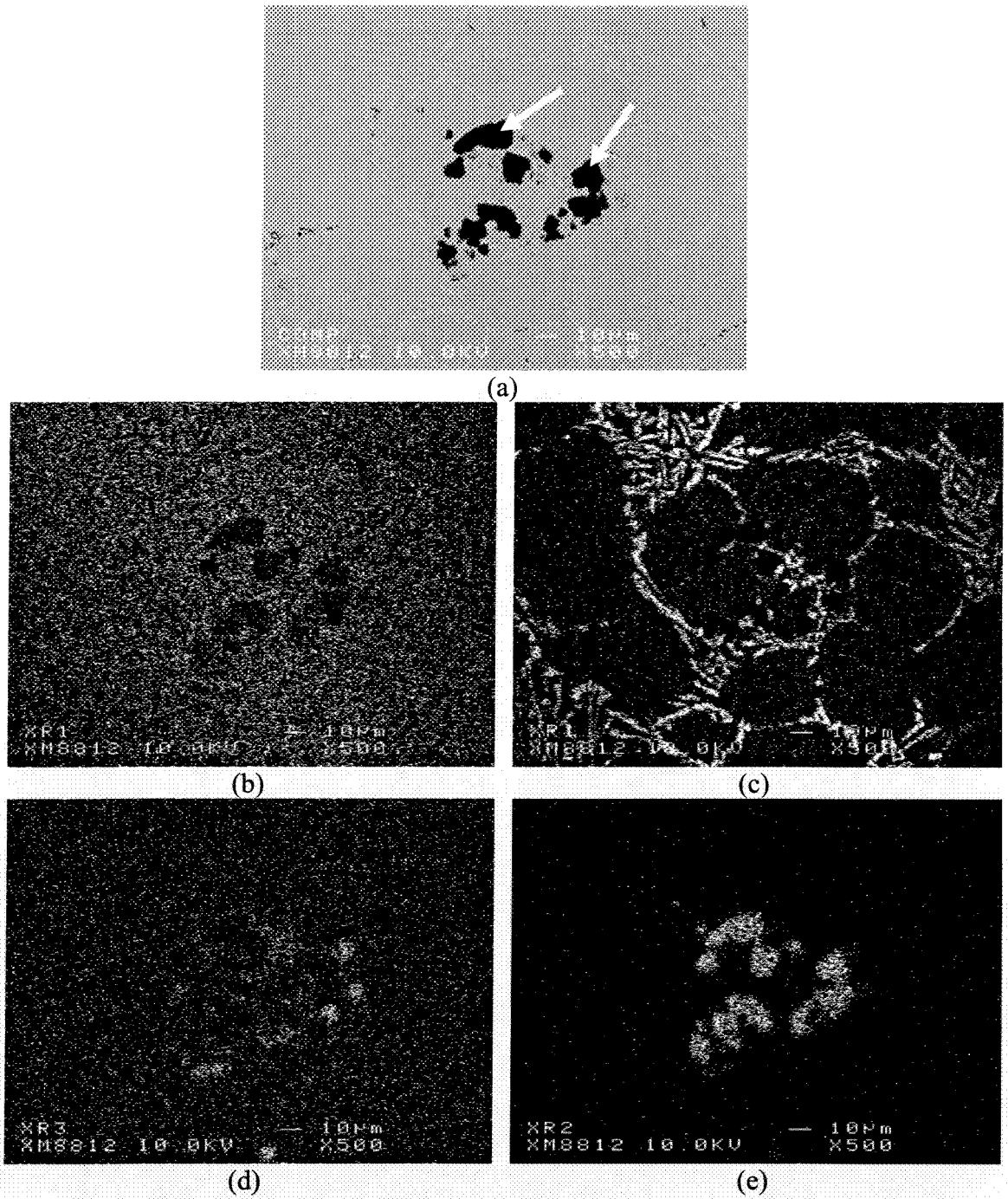

Figure 5.32: Results of electron probe microanalysis (EPMA):
(a) back scattered electron micrographs for intermetallic particles formed due to B addition and x-ray maps of:
(b) Al, (c) Si, (d) Ti, and (e) B map (SEED sample with 803ppm B)

Table 5.7: Microprobe analysis of the agglomerations (at. %)

Al	B	Ti	Si	Mg	Sr	Fe
7.305	92.68	0	0	0.01	0.001	0
7.65	92.31	0.002	0.009	0.02	0	0

One of the most complicated issues to analyze refinement treatment is the nucleant compounds. Finding these types of nucleants is a prolonged process which directly relates to the sectioning of the samples. Figure 5.34 shows a nucleant in the B-refined billet. Microprobe analysis was impossible due to the size of this particle but x-ray maps of the nucleant confirms its AlB stoichiometry and knowing the inability of AlB_{12} to act as a nucleant, it may be true to conclude this particle being AlB_2.

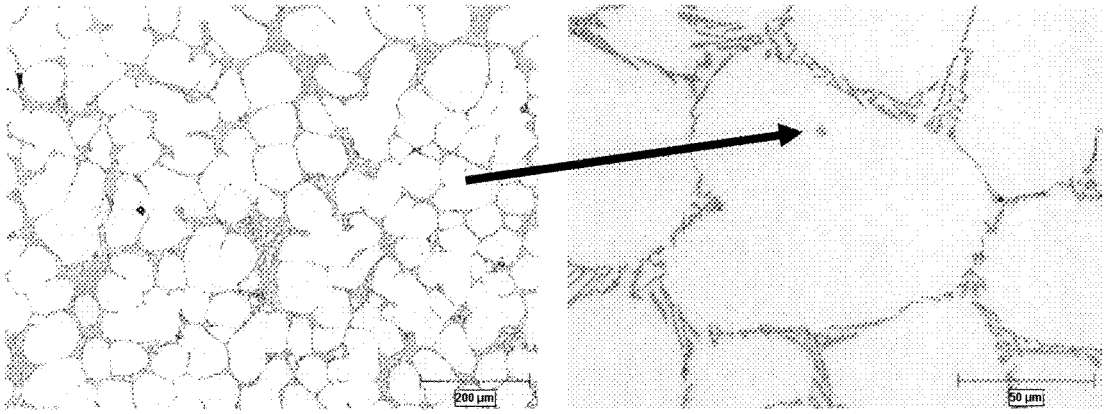

(a) (b)

Figure 5.33: Optical micrographs to show a boride based nucleus in the center of an α-Al rosette in the alloy with 254ppm boron

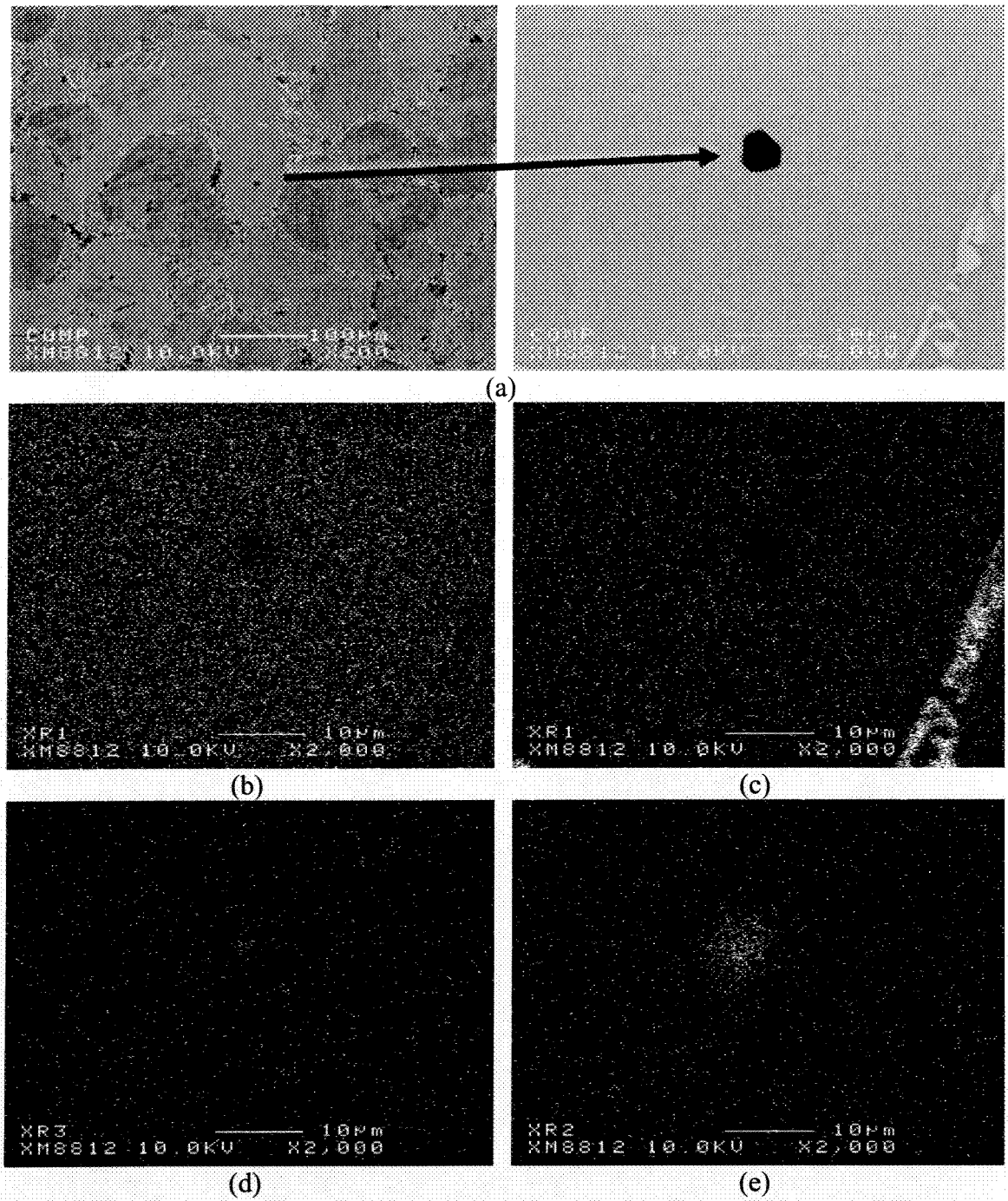

Figure 5.34: (a) Backscatered micrographs of the nuclei in the sample with 803ppm B, and x-ray maps of: (b) Al, (c) Si, (d) Ti, and (e) B

5.2.2.2.2 Image analysis

The results of the quantitative metallography are illustrated in Figure 5.35. The percentage of primary α-Al increased slightly with boron. This is due the higher number of effective nuclei and shifting the onset of nucleation to higher temperature as discussed in detail before.

In contrast to Al5Ti1B addition, boron proved to be more efficient and this efficiency is seen in more globule size reduction and sharp increase in the number of α-Al particles per unit area, i.e., density. The reduction of A/P and percentage of α-Al particles having aspect ratio >2 do also confirm the formation of smaller and rounder primary particles.

With addition of boron, the amount of drainage increased. The formations of liquid droplets during transferring of billet were also an indication of more fluidity compare to the non-grain refined samples.

As discussed earlier, an effective grain refiner results in the morphological evolution of the primary phases during solidification; the dendritic and columnar structures transform to rosette and equiaxed morphologies in conventional casting and increasing the number of globules and globularity factor in rheocasting. This evolution causes a late coherency point. An early coherency point is related to a highly branched structure with the dendrites interconnected; while a late coherency point indicates that there exists more globular structure and there are small interconnections between them. As a result, with addition of boron grain refiner, the fluidity[1] increases up to around 226ppm, while after that, it is approaching a certain state and has small decrease due to the agglomerated particles. This phenomenon probably is related to increase of B-based intermetallics with increasing the amount of grain refiner. This is in accordance with the pervious findings [75-77] where the addition of grain refiner increased the flowability of the liquid.

[1] The term fluidity employed here does not have the same meaning as the traditional definition. It is defined as the greater volume of alloy flowing out of the billet during the drainage stage.

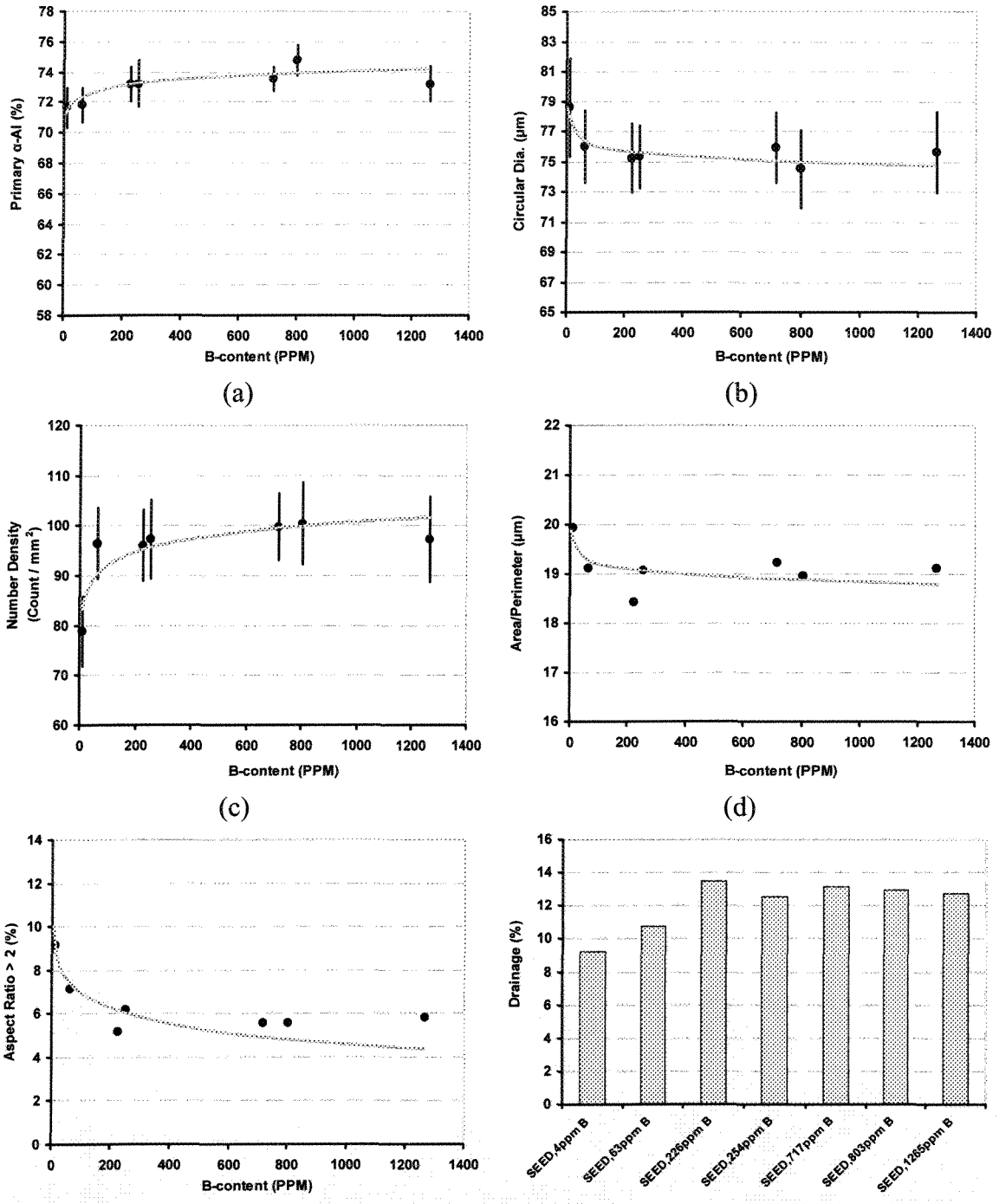

Figure 5.35: Image analysis parameters for A356 with boron addition (a) α-Al percentage, (b) circular diameter, (c) number density of α-Al particles, (d) area/perimeter, (e) percentage of α-Al particles having aspect ratio >2, and (f) drainage as a process parameter

Figure 5.36a shows the percentage of the particles with sphericity greater than 0.8. The greater the sphericity, the more globular the primary α-Al particles are in the structure. Figure 5.36b compares statistical significance of sphericity for A356 alloy with and without B-addition. With grain refining, cumulative data is more concentrated on larger values of sphericity, i.e., near 1.

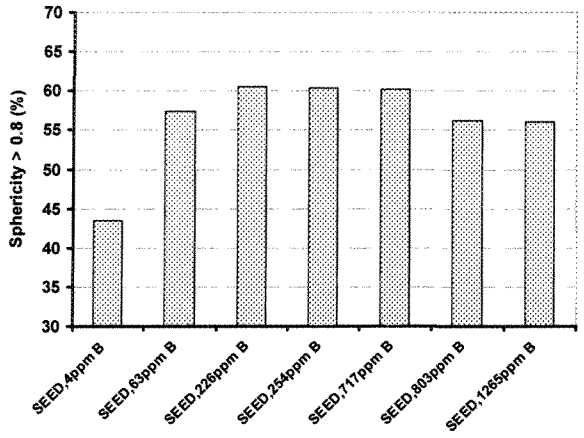

(a)

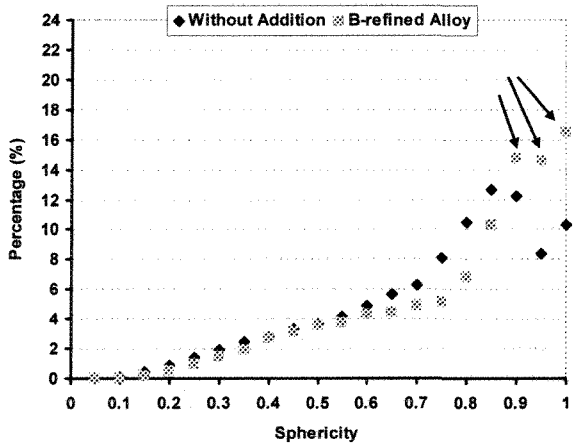

(b)

Figure 5.36: (a) variation of sphericity percentage with boron additon, (b) data ranking without boron and with 254ppm B

5.2.3 Addition of boron in the form of AlB_2 with Al5B

Addition of boron in the form of Al-5%B master alloy to the A356 alloy (without Ti in solution) was investigated. Due to the previous results from Al4%B master alloy, higher additional rates were not attempted. The experimental procedure was described in chapter 4. The chemical compositions are listed in Table 5.8.

Table 5.8: Chemical analysis of the base alloy (wt. %)

Si	Mg	Fe	Mn	Cu	Ti	B	Sr	Al
6.5-6.7	0.36-0.4	Max 0.07	Max 0.003	Max 0.001	Max 0.0057	Nil	Nil	bal.

5.2.3.1 Conventional casting

5.2.3.1.1 Thermal analysis

The effect of Al5B grain refiner addition to the alloy on the early stage of solidification is illustrated in Figure 5.37. One representative center thermocouple was selected for each experiment. As shown, small addition of boron has a remarkable effect on the solidification of the alloy. The growth temperature is raised about ~2°C by adding 159ppm boron and beyond that it remains relatively constant. Furthermore, the addition of boron eliminates the undercooling and recalescence resulting in continuous temperature reduction after nucleation. From a thermal analysis point of view, the critical boron content for this alloy seems to be more than 159ppm boron but higher values should be treated cautiously due to the agglomeration and formation of insoluble boride particles.

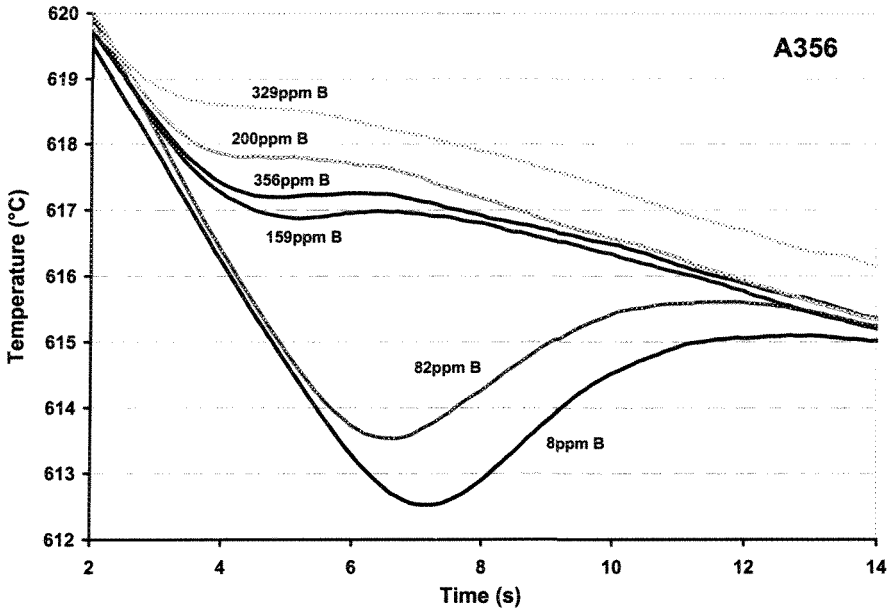

Figure 5.37: The onset of solidification at the center of cups having different concentrations of boron (with Al5B master alloy addition)

For each sample, the nucleation ($Tnuc_{Al}$), growth (Tg_{Al}), and recalescence (ΔT_{Rec}) temperatures were calculated and plotted in Figure 5.38. For boron content up to 200ppm, an undercooling of ~ 2°C exists however approaches and remains zero for all other additional levels. The nucleation temperature increases by ~7°C while the growth temperature increases by ~3°C (Figure 5.38a). As it is evident, the rate of the nucleation temperature ascending is higher than the growth temperature. However, the difference between these two temperatures widens with more boron additions.

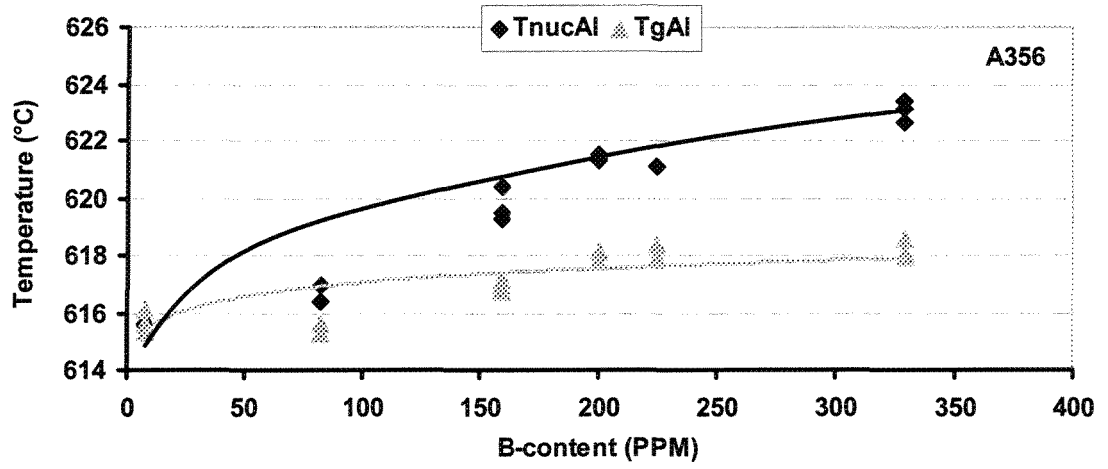

(a)

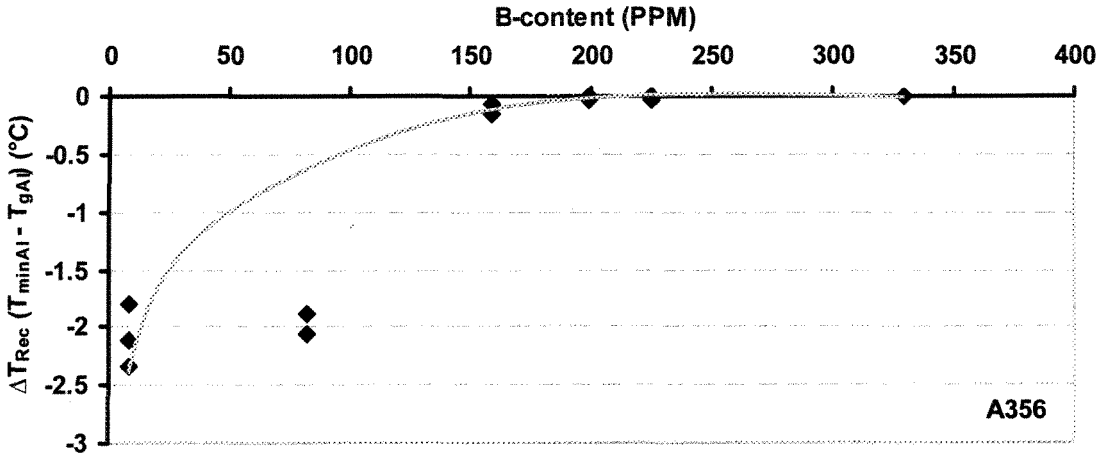

(b)

Figure 5.38: Effect of boron addition on the:
(a) nucleation and growth temperatures of primary α-Al, (b) ΔT_{Rec}(undercooling)

5.2.3.1.2 Structural analysis

Figure 5.39 shows the microstructural evolution of the alloy due to the addition of boron. As it could be seen, the microstructure of the refined sample is quite different from the non-refined one. Such transition may be attributed to the higher density of nucleants due to the refiner addition as explained below. When there is a high density of nuclei growing in the melt the boundary layers around each respective nucleus may interfere with each other which eventually restrict the particle growth and also by assuming the spherical boundary layer, the outcome would be fine rosette or spherical particles.

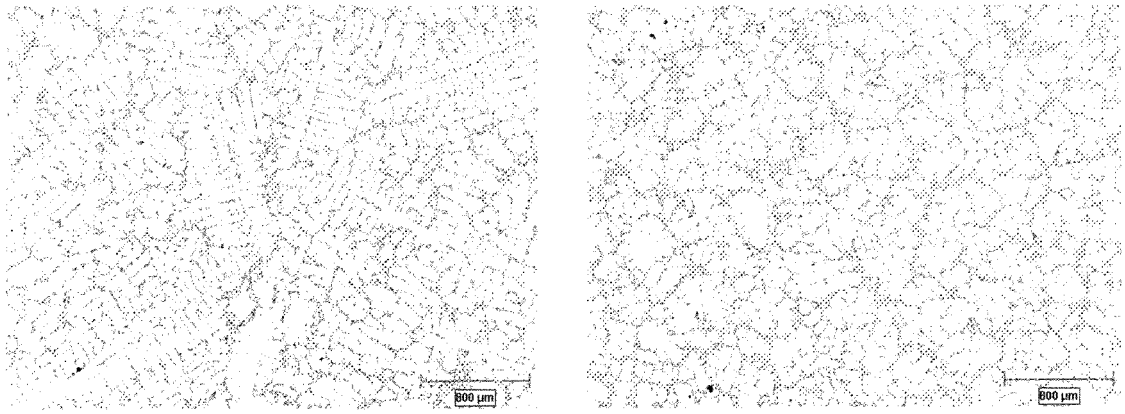

(a) (b)

Figure 5.39: The effect of boron level on the microstructure:
(a) without addition, (b) 225ppm B

The presence of intermetallic particles is an indication of over addition of boron to the melt as shown in Figure 5.40. As the boron concentration increases, not all the boride particles could act as nucleation sites for aluminum. Furthermore, the limited solubility of these particles in α-Al may lead to the formation of agglomerates within the matrix. This is clearly indicated in Figure 5.40 where boron concentration is in excess of optimum value around 200-250ppm boron. By ThermoCalc calculation, it becomes clear that boron solubility limits are 0.048% and 0.027% at 700, 650°C respectively and it becomes less than 0.0018% after eutectic reaction.

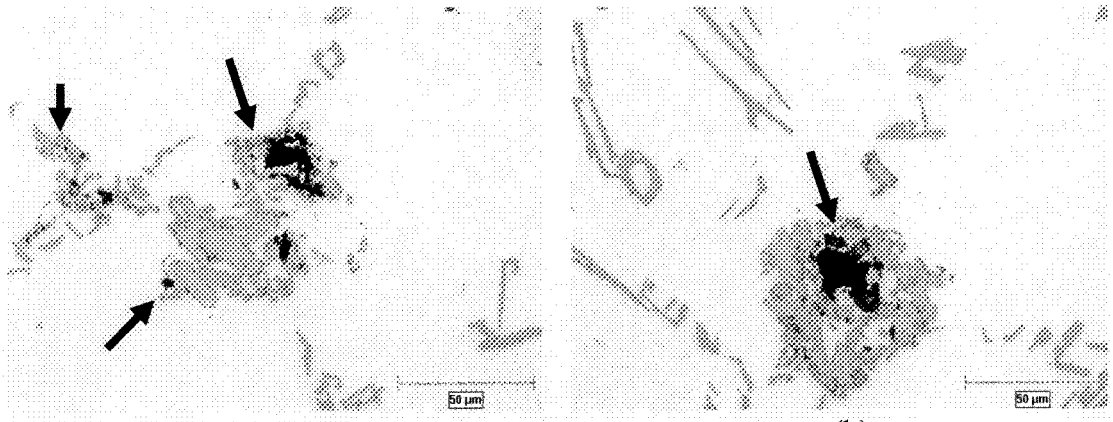

(a) (b)

Figure 5.40: Optical micrographs showing agglomerated AlB_2 particles for boron additions of: (a) 329ppm, and (b) 356ppm boron addition

5.2.3.2 Semi-solid processing

5.2.3.2.1 Structural analysis

The optical micrographs in Figure 5.41 show the effect of boron on the primary α-Al phase. As it could be seen, there is no entrapped eutectic within the α-Al primary particles and the samples have been refined and even have better globularity with boron addition. The drawback here is the formation/agglomeration of boron based intermetallics compound with increasing boron content beyond 300ppm as it is shown in Figure 5.42 and 5.43. Microprobe analysis confirmed that these particles are AlB_2 (Table 5.9).

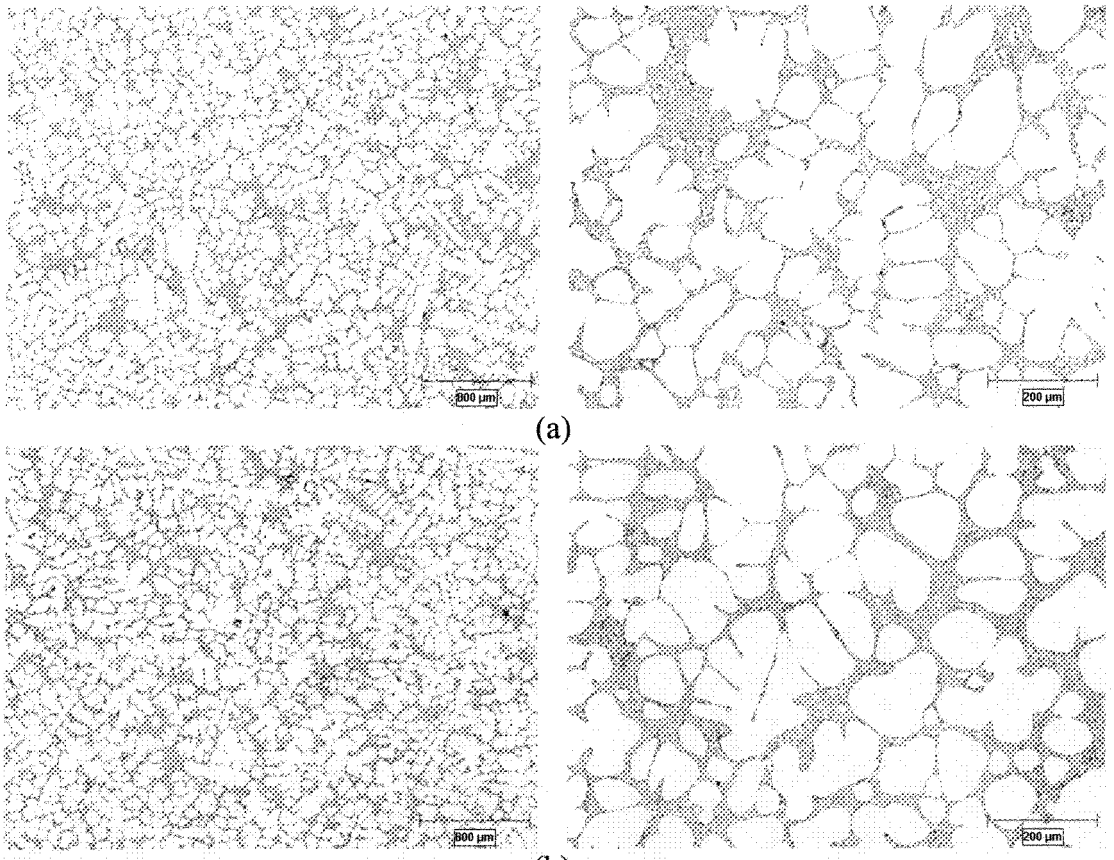

Continue ⟶

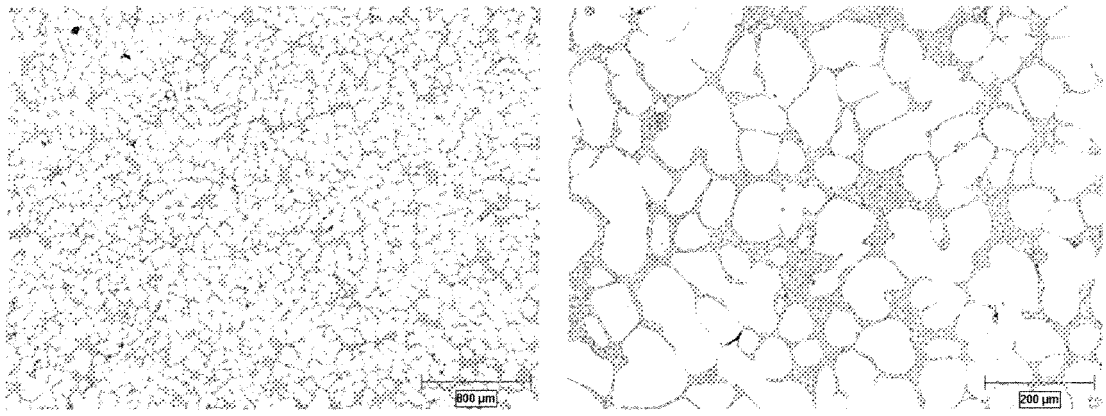

(c)

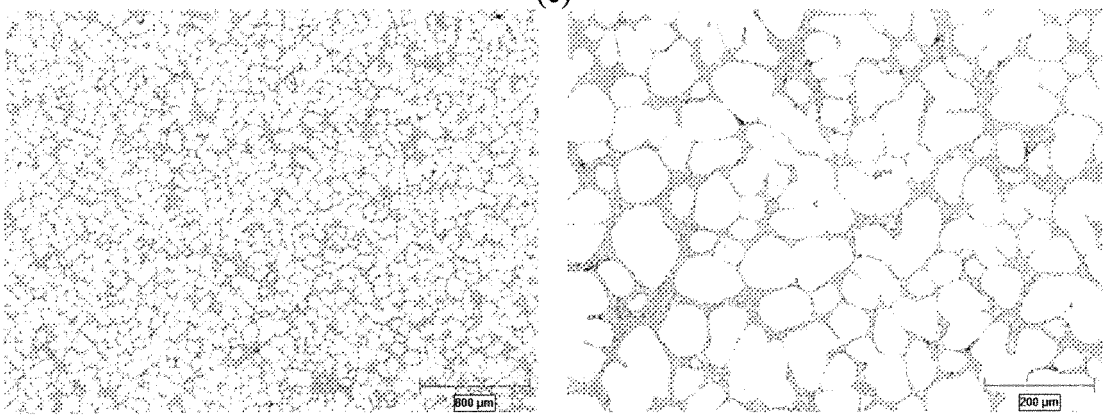

(d)

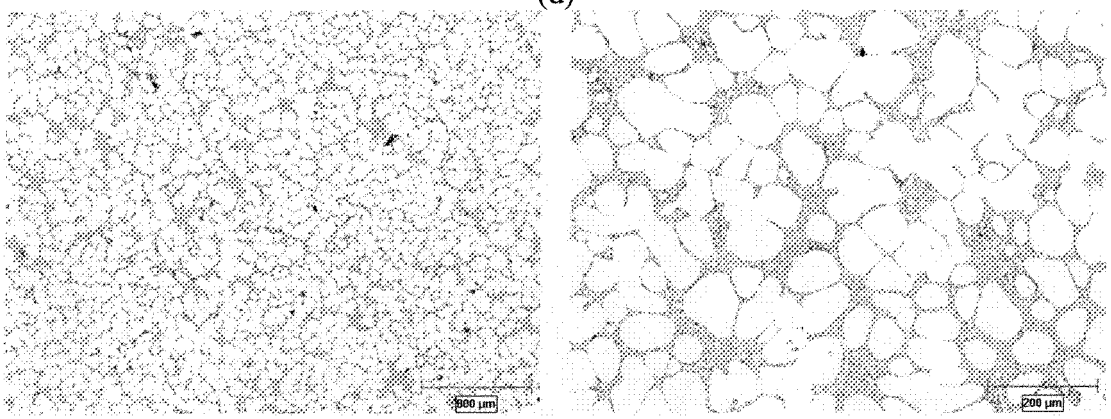

(e)

Figure 5.41: Optical micrographs to show the additional effects in the SEED process: (a) without addition, (b)82ppm, (c) 159ppm, (d) 225ppm, and (e)329ppm B

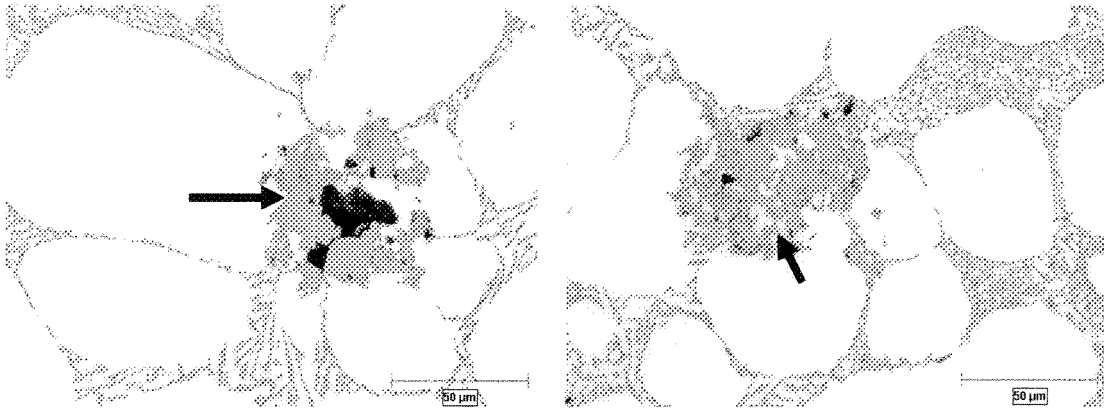

Figure 5.42: Boron based intermetallics with 329ppm boron addition in SEED samples

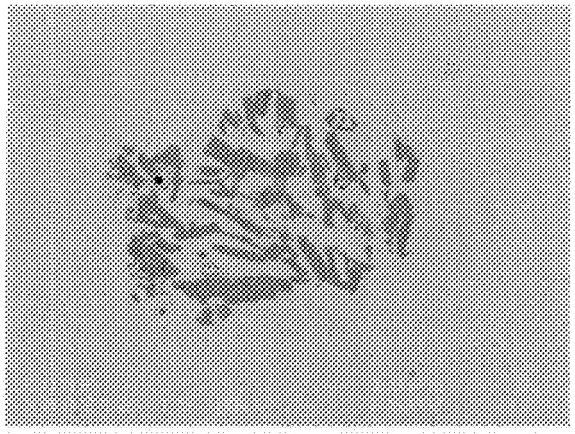

(a)

(b)

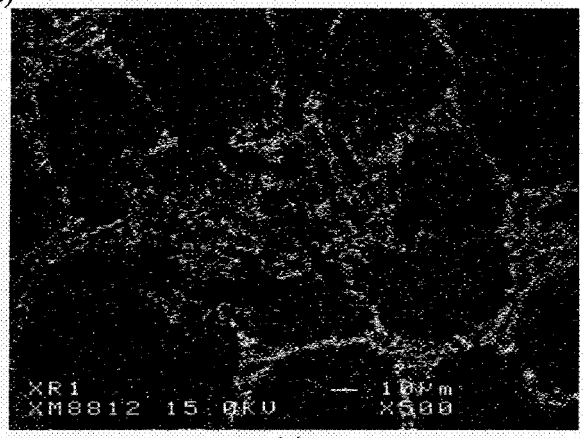

(c)

Continue ⟶

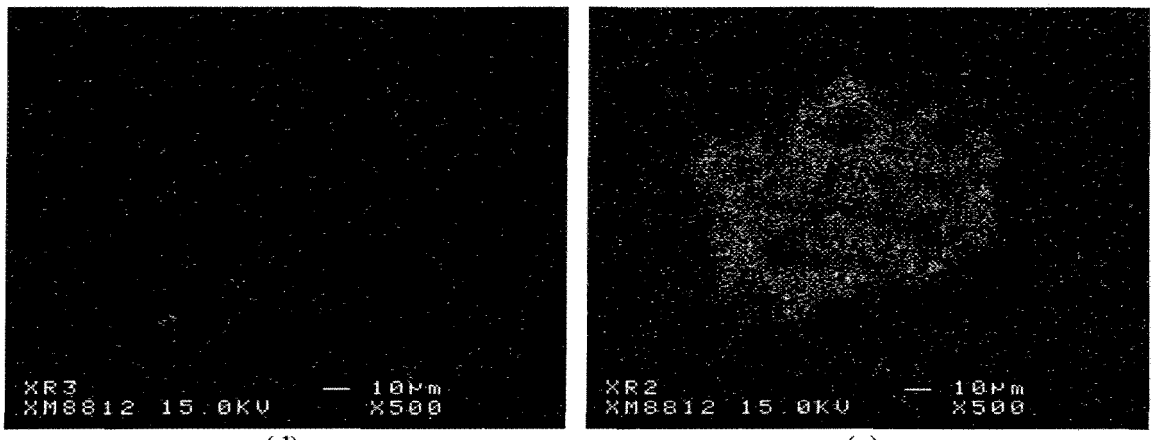

(d) (e)

Figure 5.43: (a) back scattered electron micrograph showing the agglomration of boride particles and x-ray maps for:
(b) Al, (c) Si, (d) Ti, and (e) B map (SEED sample with 329ppm B)

Table 5.9: Atomic percentages of agglomerations by microprobe analysis

Al	B	Ti	Si	Mg	Sr	Fe
29.11	68.40	0	0.012	2.47	0	0
30.40	69.53	0.01	0	0.06	0	0

The concurrent presence of liquid and primary solid particles is the principal requirement for SSM processing. As it was described earlier, in addition to the temperature sensitivity of the solid fraction and the SSM temperature process window, partitioning of the solidification range is essential. Figure 5.44 shows the influence of boron on the solidification range. Comparing different solidification ranges for A356 alloy with boron addition, it is obvious that there are changes in α-Al solidification range (ΔT_α) which increase with boron addition up to 200ppm and remains almost constant afterwards. For eutectic solidification range, it appears that there is a slight reducing trend with increasing boron. However it is believed that such decreasing trend may be attributed to the experimental errors and the results are supported by other cases which are reported in Figures 5.18 and 5.30.

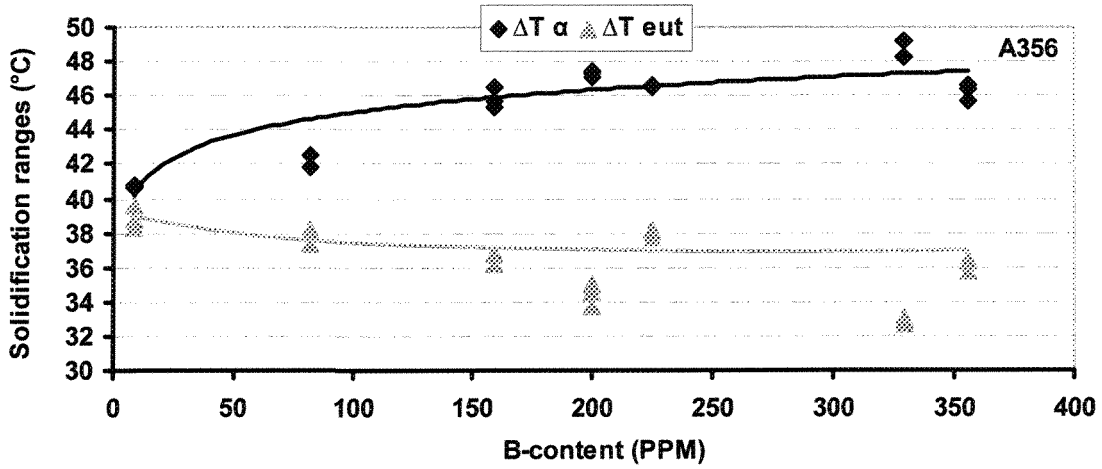

Figure 5.44: The effect of boron addition on the primary α-Al and eutectic solidification ranges

Fundamentally, refiners should act as nucleants for primary particles formation. Identification of nucleants in the as-cast billets is time consuming since the detection probability depends on the polished surface and whether it intersects the nucleant or not. Figure 5.45 shows the optical micrographs of a nucleant and Figure 5.46 shows another nucleant which has been characterized by the backscattered electron micrograph and the x-ray maps of the particle. From Table 5.10 it becomes clear that the nucleant has a stoichiometry close to AlB_2.

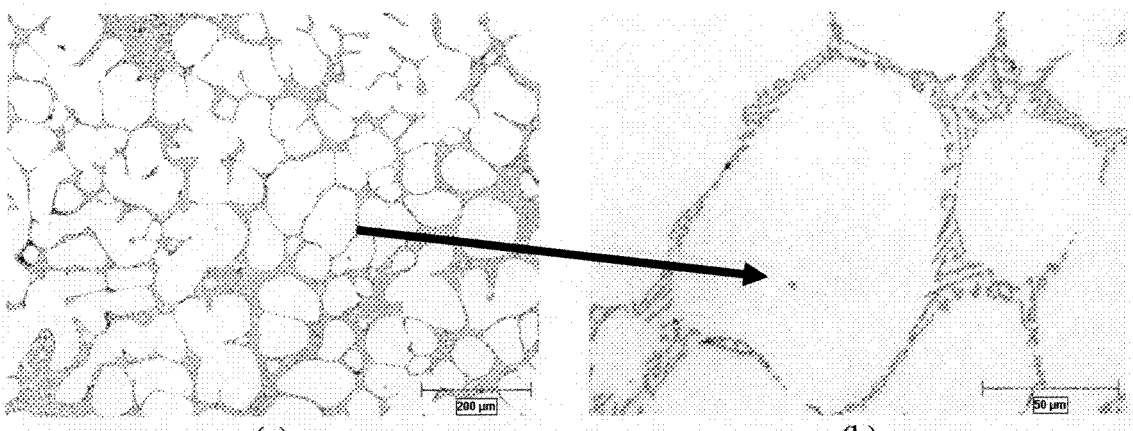

(a) (b)

Figure 5.45: An AlB_2 nucleant in the center of an α-Al particle (329ppm boron)

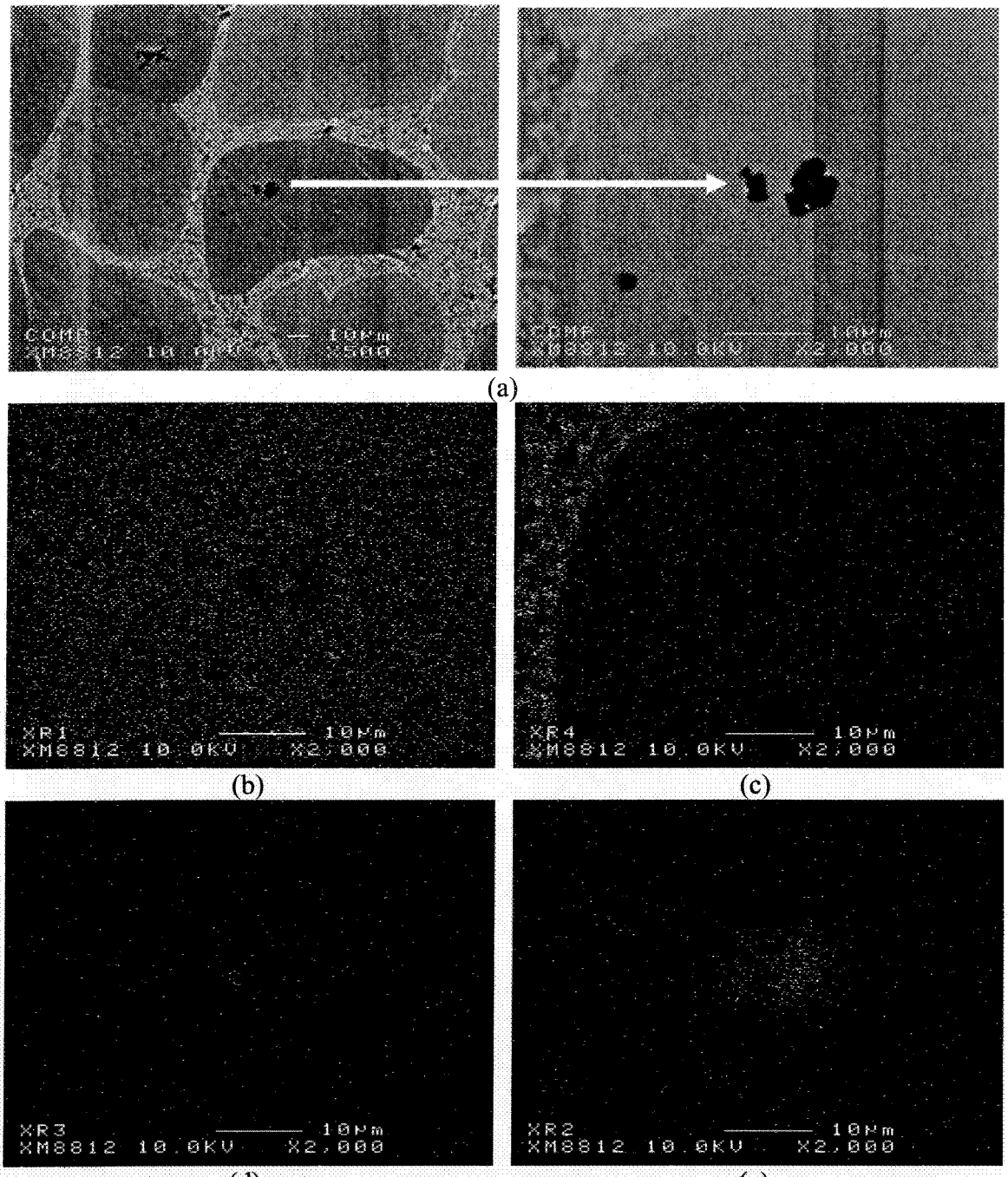

Figure 5.46: (a) Backscatered micrographs of the nucleus in sample with 329ppm B; and x-ray maps of (b) Al, (c) Si, (d) Ti, and (e) B

Table 5.10: Atomic percentages of nucleus by microprobe analysis

Al	B	Ti	Si	Mg	Sr	Fe
27.21	61.59	0.07	0.105	11.017	0	0

5.2.3.2.2 Image analysis

In order to fully characterize the microstructure of semi-solid slugs, it is necessary to quantify the percentage, size, shape, and morphology of primary particles. For this purpose, image analysis was employed and Figure 5.47 and 5.48 illustrate the results.

Increasing the percentage of primary α-Al is noticeable since not only numerous nucleation sites are injected into the system but also liquidus line is shifted to higher temperatures. Increasing the number of globules in a unit area and decreasing the average circular diameter, A/P ratio, and percentage of α-Al particles having aspect ratio >2, all confirm that globule size is reduced.

As it was discussed earlier, an effective grain refiner causes the morphological evolution during solidification from dendritic and columnar to rosette and equiaxed growth in conventional casting, and increasing the number of globules and globularity factor in rheocasting. This evolution causes a late coherency point. An early coherency point is related to a branched structure and all the dendrites interconnected easily; while a late coherency point indicates that there exists more globular structure and there are less interconnections between them. So, with addition of boron grain refiner, the fluidity increases up to around 200ppm, while after that, it is approaching a constant value and has small decrease. This phenomenon probably is related to increase of B-based intermetallics with increasing the amount of grain refiner. This is in accordance with the previous findings [75-77] where the addition of grain refiner increased the flowability of the liquid.

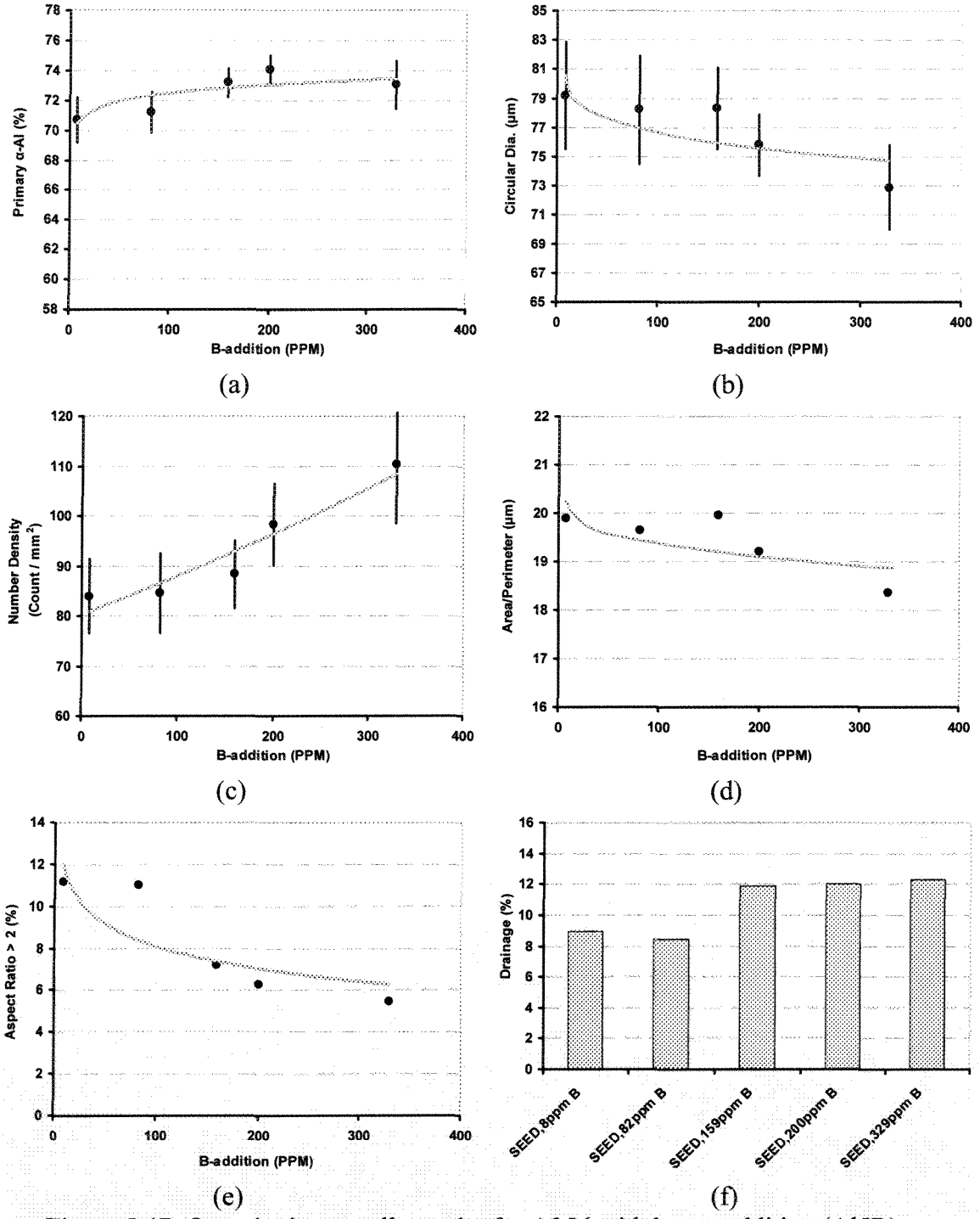

Figure 5.47: Quantitative metallography for A356 with boron addition (Al5B): (a) primary α-Al percentage (b) circular diameter, (c) number density of α-Al particles, (d) area/perimeter ratio, (e) percentage of α-Al particles having aspect ratio >2, and (f) drainage as a process parameter

Figure 5.48a shows the percentage of the particles with sphericity greater than 0.8. The more the sphericity, the more globular particles are in the structure. Figure 5.48b compares statistical significance of sphericity. With grain refining, data is more concentrated on larger values of sphericity, i.e., near 1. As it will be shown in rheological experiments, chapter 8, this parameter has a great influence on the flowability of slurries.

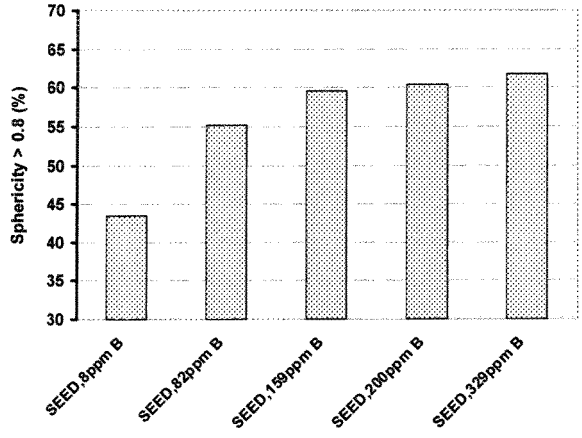

(a)

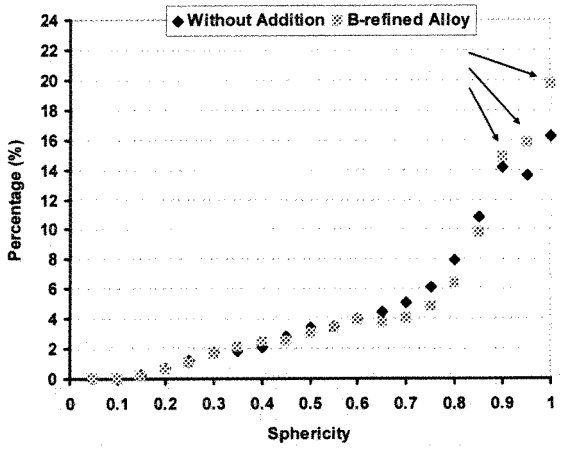

(b)

Figure 5.48: (a) Variation of sphericity percentage with boron addition (Al5B), (b) data sorting without and with 225ppm B

5.3 Grain refining in Commercial 356 alloy

5.3.1 Addition of titanium & boron with Al5Ti1B

The objective of these series of tests was to understand the effect of refiner addition to what is usually employed in the foundries as commercial alloy. As per ASTM standard [188], commercial 356 contains maximum 0.25%Ti. The added Ti has two advantages: first, as a refiner, it could act as nucleation sites for primary α-Al and secondly as a solute element in aluminum, it has the uppermost growth restriction factor (GRF) in suppressing the grain growth. The experimental procedure is exactly the same as described in chapter 4. The chemical composition of the base alloy is listed in Table 5.11.

Table 5.11: Chemical analysis of the base alloy (wt. %)

Si	Mg	Fe	Mn	Cu	Ti	B	Sr	Al
6.8-6.9	0.33-0.35	Max 0.09	Max 0.002	Max 0.002	0.13-0.131	Nil	Nil	bal.

5.3.1.1 Conventional casting

5.3.1.1.1 Thermal analysis

Figure 5.49 illustrates the influence of inoculation on the early stages of commercial 356 alloy solidification. As mentioned, these series of 356 alloys originally contain Ti in solution before addition of the refiner. With this amount of Ti in solution before any addition, liquidus temperature shifts up according to the pseudo-binary phase diagram of Al7Si1Mg versus Ti (Figure 5.8) and it is identifiable by comparing the cooling curves of A356 and Com356 where in the commercial alloy the commencement of solidification is already shifted up.

Figure 5.50 shows the two most important TA parameters for α-Al formation. By Ti addition, α-Al nucleation temperature increases as it was reported earlier. By comparing the results with these of A356 alloy, the liquidus temperature of the base alloy is slightly higher than that for A356 alloy; where $Tnuc_{Al}$ is about 617°C for base alloy and 615°C for the A356 (Figure 5.50a). Another interesting conclusion is coming from the comparison

between Figure 5.50a and 5.9a. As seen, it seems that addition of grain refiner is not as effective as what is seen in A356 alloy. This is due to the effect of dissolved Ti already present in the as-received commercial alloy and therefore the added Ti is less effective than the one added to Ti-free A356 alloy.

The liquidus portion of the cooling curves in Figure 5.49 and the calculated recalescence values show that the recalescence temperature decreases with Ti and B addition reaching to less than -0.5°C after about 300ppm (Figure 5.50b). Thus according to the concept of grain refining efficiency, the optimum concentration of grain refiner is around 300ppm Ti, since greater values may result in segregation of Ti-based intermetallics as will be discussed later.

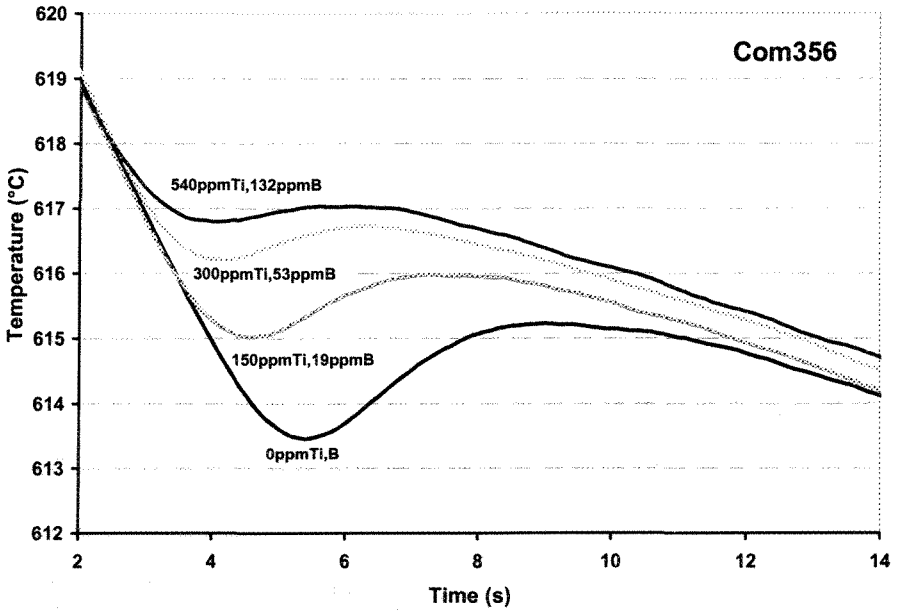

Figure 5.49: The early stages of solidification (cooling curves) for commercial 356 alloys with refiner addition (numbers are just additional Ti&B)

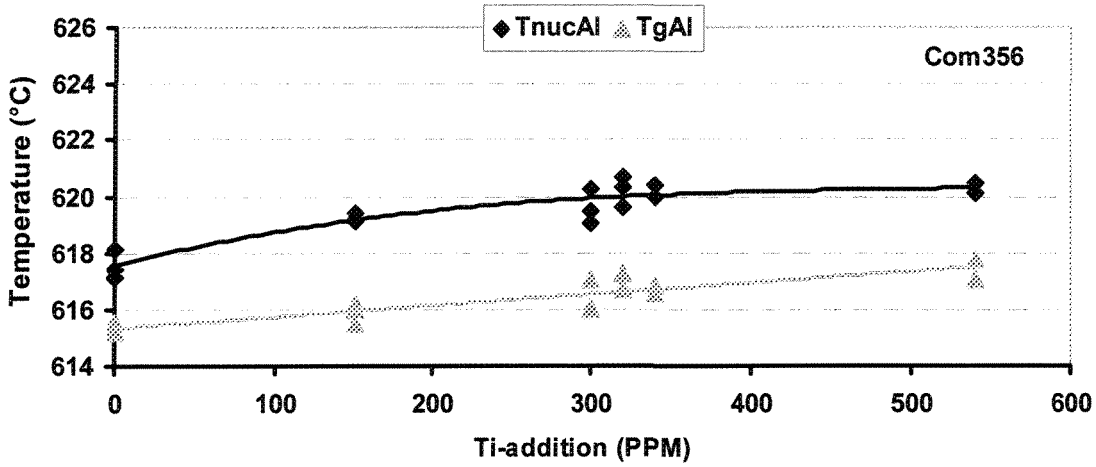

(a)

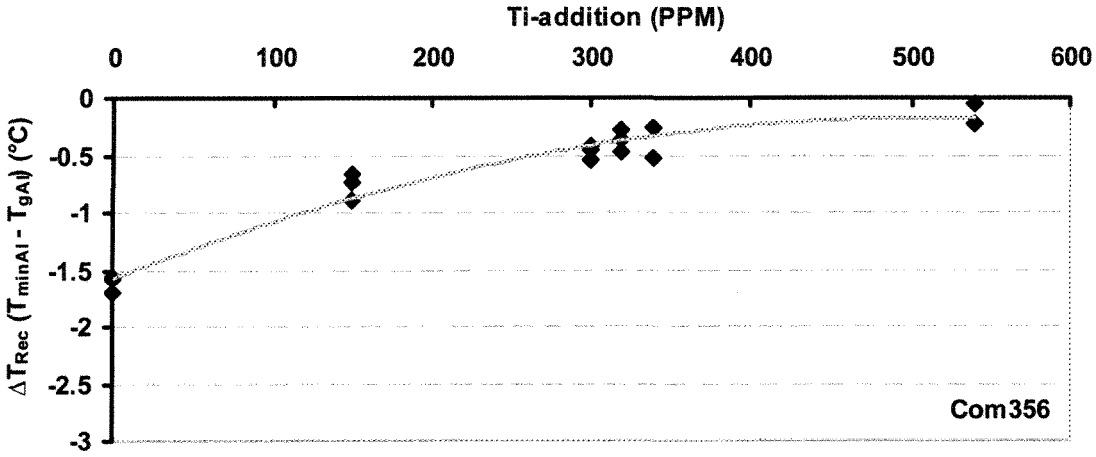

(b)

Figure 5.50: Effect of Ti and B additional rate on the: (a) primary α-Al nucleation and growth temperatures, (b) recalescence temperature range

5.3.1.1.2 Structural analysis

Figure 5.51 shows the microstructural evolution by addition of Ti & B to the alloy (dark areas are porosities). As it could be seen, the morphology of primary α-Al particles changes from dendrites to the desirable rosette with higher amount of Ti & B addition. Although greater values of the refiner causes enhanced morphological changes in α-Al particles, over refining addition may be detrimental due to segregation of Ti-based intermetallics in the eutectic region.

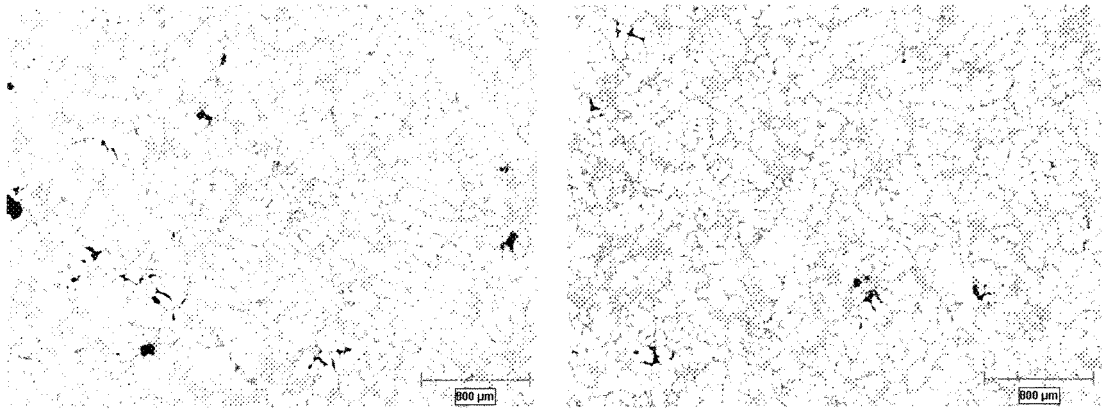

(a) (b)

Figure 5.51: Optical micrographs showing the refiner addition:
(a) without addition, (b) 300ppm Ti, 53ppm B

As shown in Figure 5.51, addition of Ti leads to the morphological evolution of primary particles from dendritic to equiaxed structure. This evolution has a great advantage to the as-cast structure but it should be considered that with higher addition, it is more possibility to have Ti-based intermetallics in the eutectic region. As it was shown in table 5.11, the original alloy contained ~0.13%Ti. By looking at the phase diagram of Al-Ti (Figure 2.19) or the iso-pleth of Al7Si1Mg (Figure 5.8), it is apparent that the peritectic reaction occurs at 0.12%Ti and as a result greater addition of Ti by means of refiner could cause the formation of Al_3Ti particles or kinetically lowers the dissolution rate of these particles into the melt. Therefore, the presence of intermetallic particles is an indication of increasing the Ti content beyond its optimum value. Figure 5.52 shows Ti-based intermetallics with two different sizes with more addition of Ti & B.

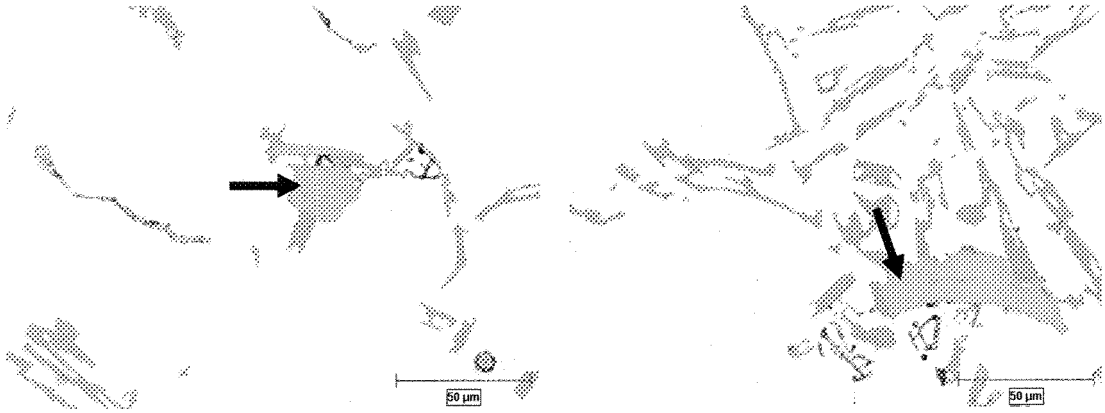

(a) (b)

Figure 5.52: Optical micrographs showing Ti-based intermetallics:
(a) 0.153%Ti, 0.0087%B and (b) 0.184%Ti, 0.0132%B
(percentage is total Ti and B levels in the alloy, not the addition)

5.3.1.2 Semi-solid processing

5.3.1.2.1 Structural analysis

The optical micrographs in Figure 5.53 give an overall view of the effect of Ti&B on the primary α-Al phase. The microstructure is refined with increasing the percentage of Ti&B and the degree of globularity of α-Al particles has improved. This is obvious by comparing the first and the last micrographs, Figure 5.53a&d. The added bonus is an increase in the α-Al percentage in the refined alloy associated with the greater number of nucleation sites and higher nucleation temperature of the primary phase.

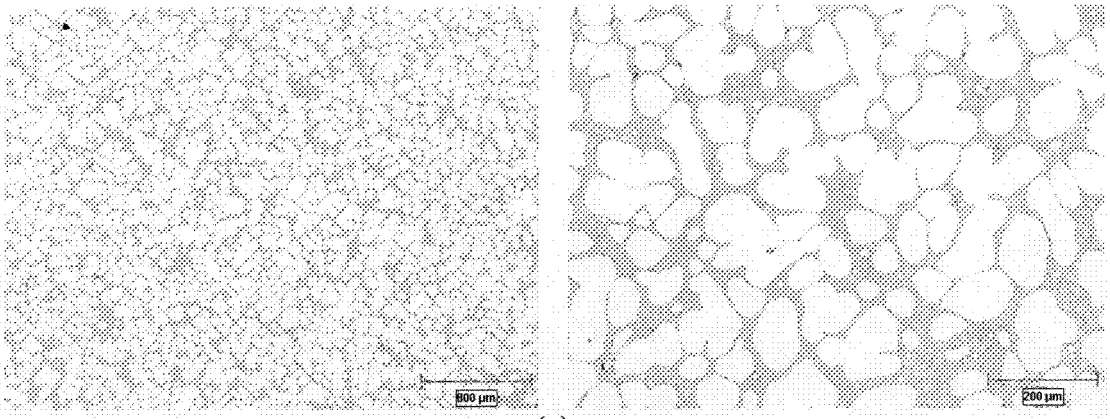

(a)

Continue ⟶

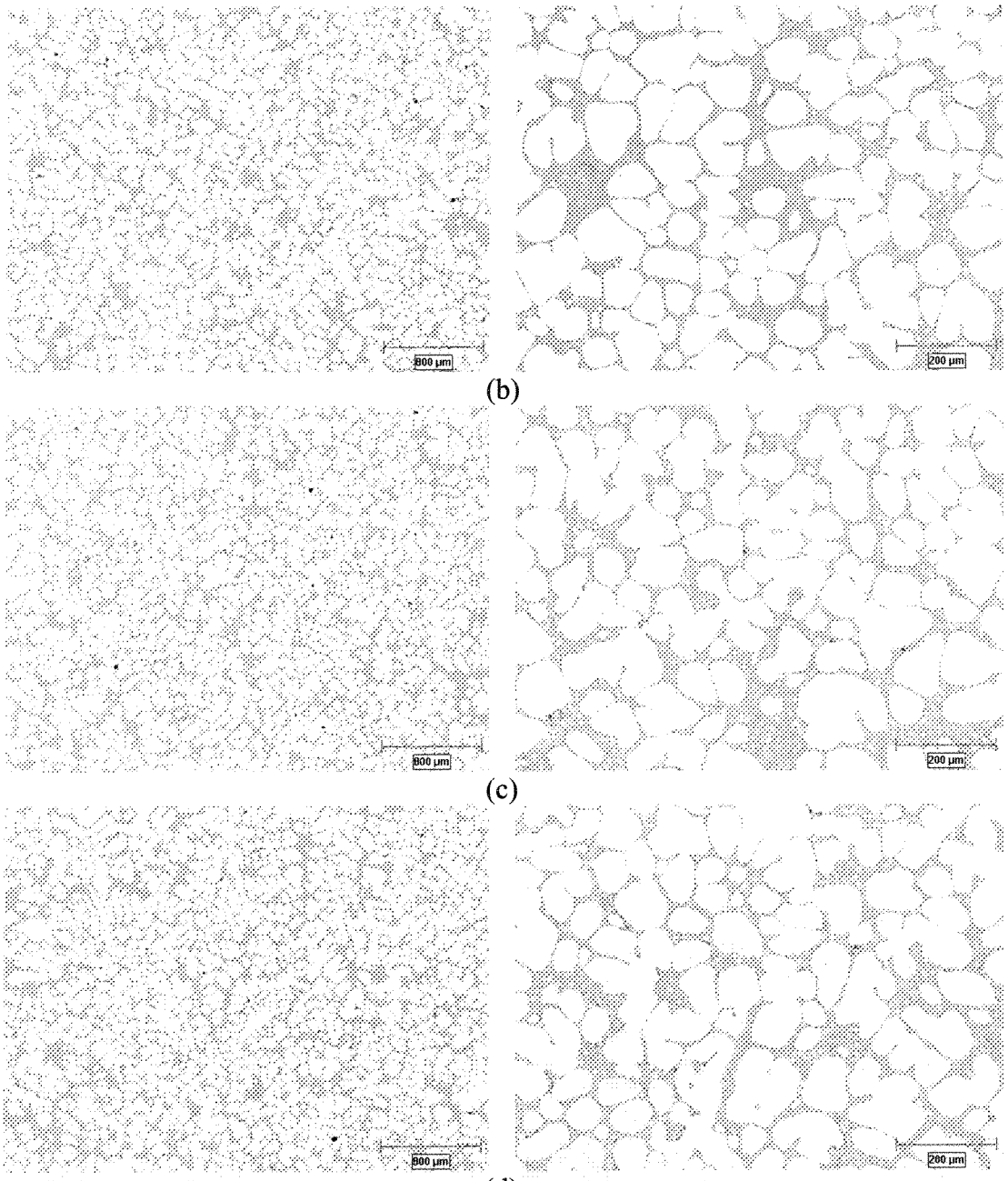

Figure 5.53: Microstructural changes associated to refiner addition in the quenched SEED billets: (a) without addition, (b) 150ppm Ti, 19ppm B, (c) 300ppm Ti, 53ppm B, and (d) 540ppm Ti, 132ppm B

Two distinct parts of the solidification range is shown in Figure 5.54. The primary α-Al solidification range, and that of the eutectic reactions, ΔT_{α} and ΔT_{eut}, have the same trend as the previous results, e.g. Figure 5.18. The α-Al solidification range increases by

refiner addition but the eutectic solidification range is approximately constant. The increasing rate here is slightly less than that found for A356 alloy, maximum 4°C.

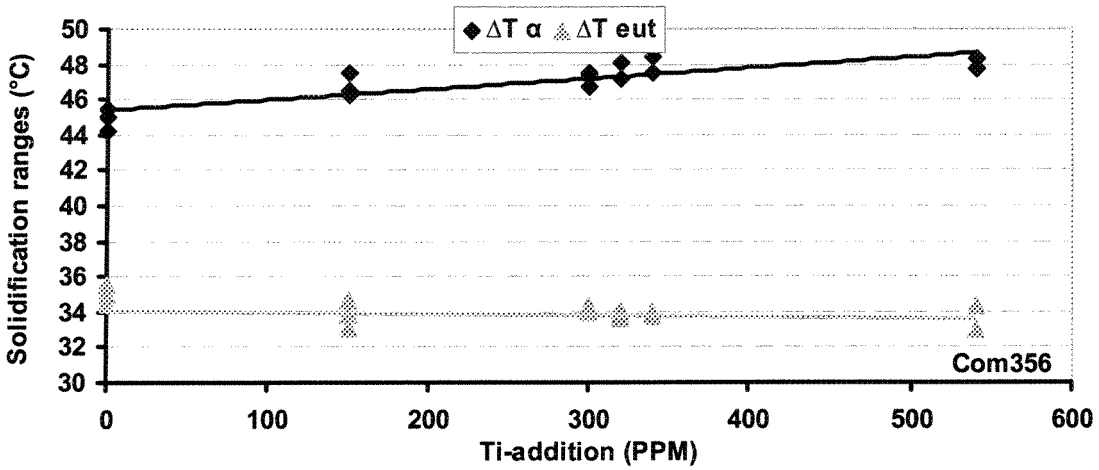

Figure 5.54: Variation of solidification ranges due to the Ti and B addition

By looking for the nucleation sites of α-Al particles, Figure 5.55 and 5.56, it was specified that this nucleant is not a compound of Ti and B but it is a compound of AlTiSi. This could be a proof that nucleation sites may be a combination of Al,Ti,B, and Si elements.

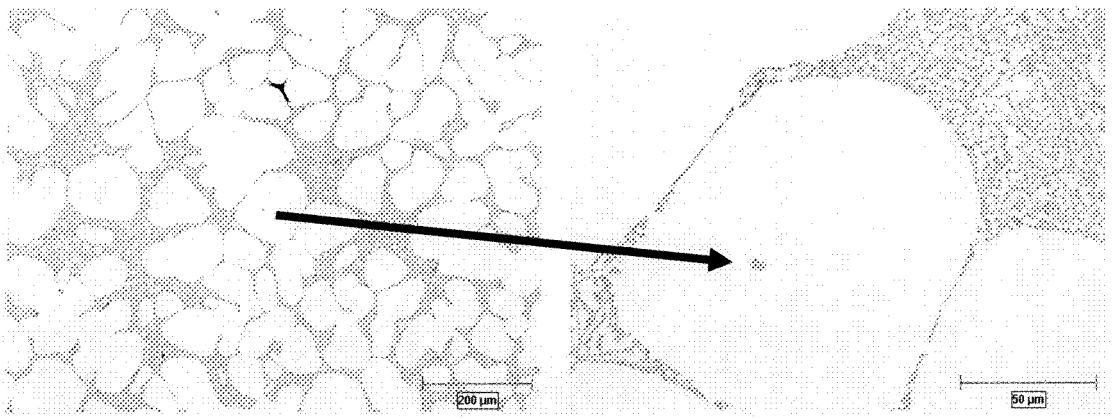

(a) (b)

Figure 5.55: Optical micrographs showing the presence of nucleant at the center of an α-Al particle, with 0.16%Ti, 0.0053%B addition

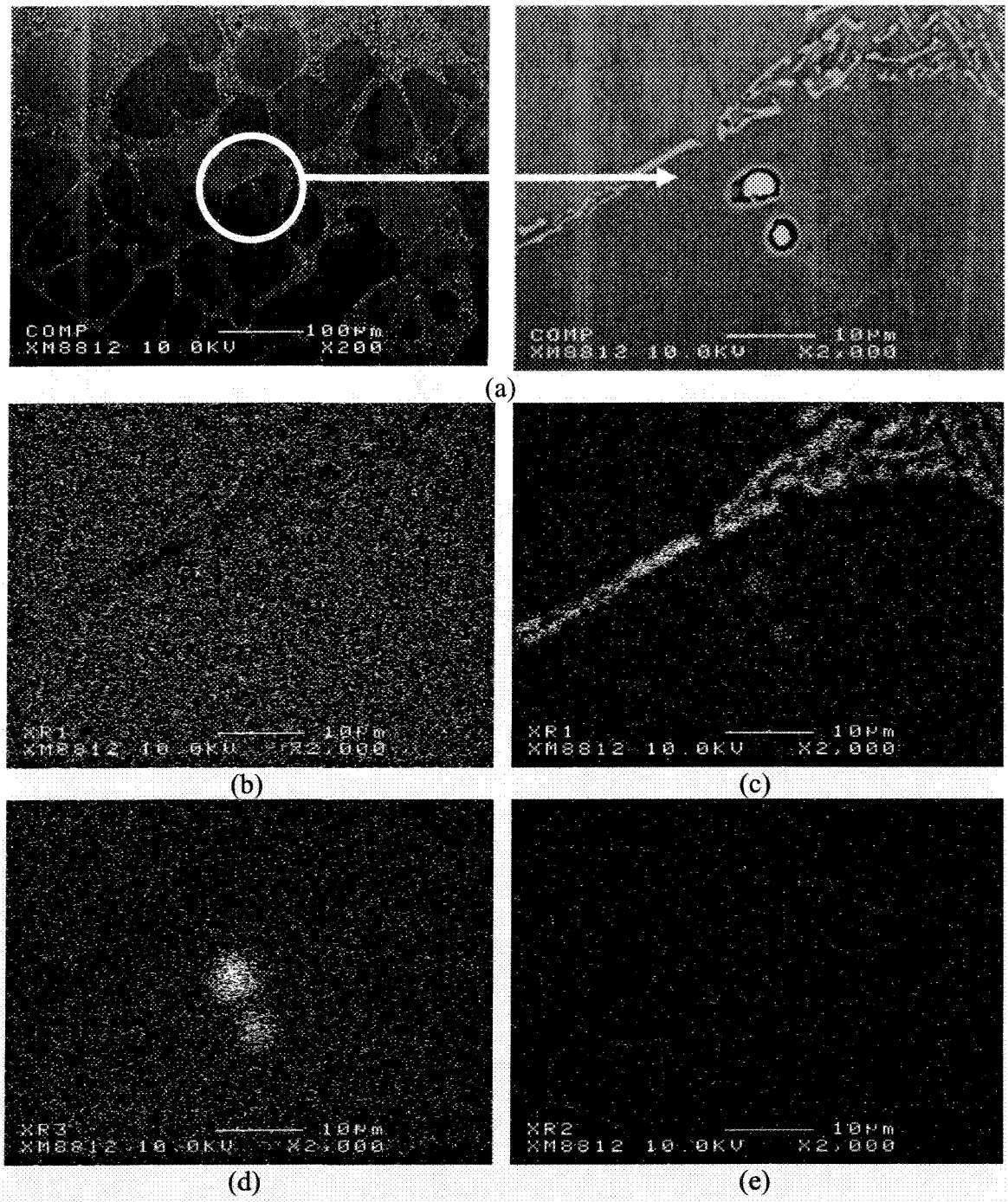

Figure 5.56: Backscatered electron micrographs of the nucleaus in billet treated with 540ppm Ti and 132ppm B (a) and x-ray maps of (b) Al, (c) Si, (d) Ti, and (e) B

The drawback however is the segregation and agglomeration of Ti based intermetallic compounds with increasing Ti content beyond 500ppm as illustrated in Figure

5.57 and 5.58. The microprobe results (Table 5.12), confirm the stoichiometry of these large particles as Al_5Ti_2Si. By looking at the x-ray maps of Ti and B in Figure 5.58, it is proposed that the small clusters of particles attached to the large Ti-based intermetallics are TiB_2 although the point chemical analysis is impossible because of their small sizes and limit of detection. The TiB_2 particles which are shown by the arrows in Figure 5.57 probably coming directly from the master alloy where they could not act as effective nucleants.

Figure 5.57: Optical micrographs showing the formation of Ti based intermetallics in the SEED billets with: (a) 0.153%Ti, 0.0087%B , (b) 0.184%Ti, 0.0132%B (arrows show clusters of TiB_2)

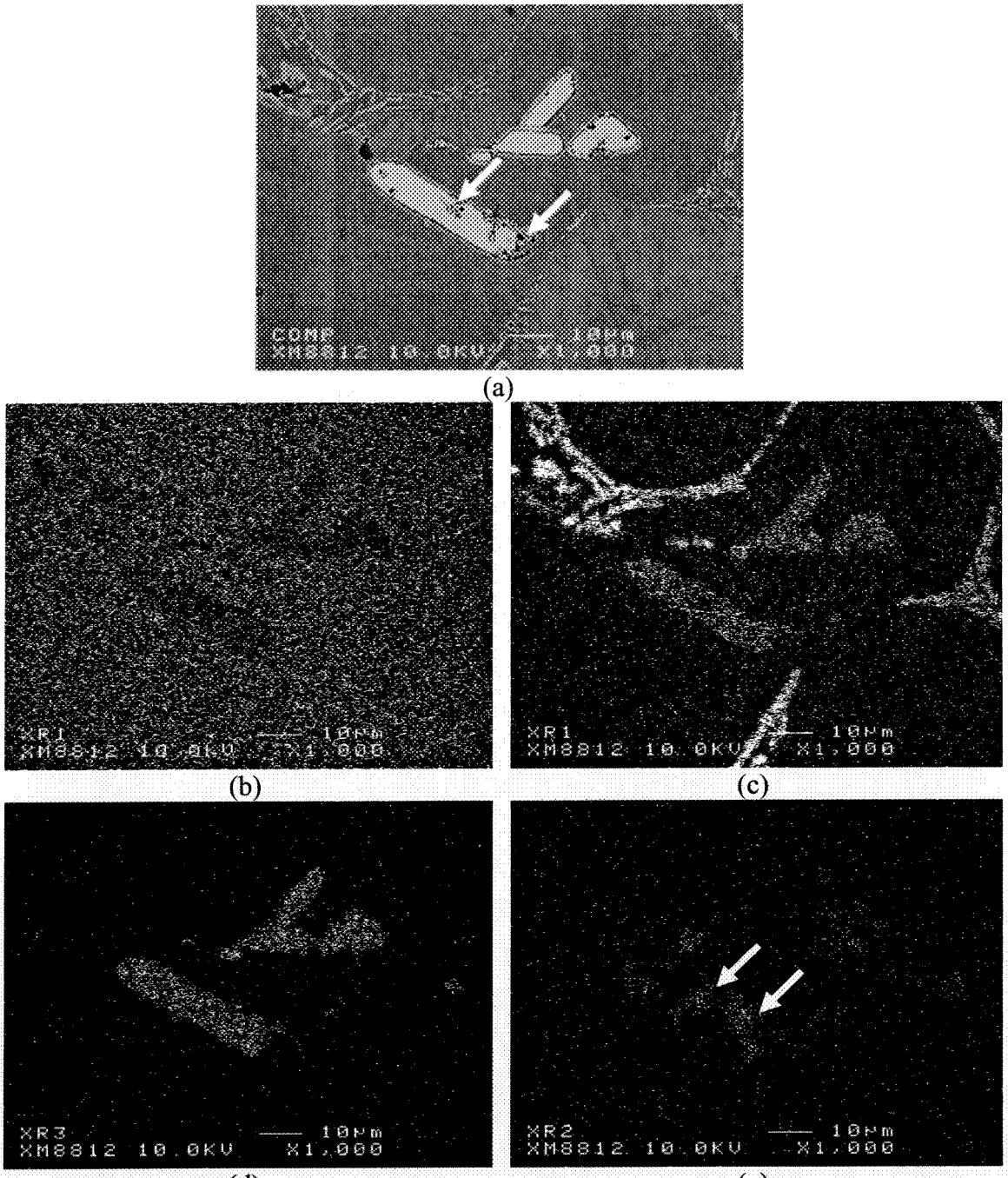

Figure 5.58: (a) Back scattered electron micrographs of the intermetallic particles formed due to Ti and B addition, together with x-ray maps (b) Al, (c) Si, (d) Ti, and (e) B maps (SEED cast billets with 540ppm Ti and 132ppm B)
(arrow shows a large cluster of TiB_2)

Table 5.12: Atomic percentage of the titanium compounds

Al	B	Ti	Si	Mg	Sr	Fe
62.40	0	25.02	12.57	0	0	0
62.11	1.85	24.91	11.12	0	0.008	0

5.3.1.2.2 Image analysis

The data obtained by image processing is shown in Figure 5.59. By refiner addition the percentages of primary particles appear to have increased slightly. This is attributed to expanding of α-Al solidification range by refiner addition and greater number of nucleants. Furthermore, more nucleation possibilities may restrict growth to render finer primary α-Al particles. This is evident when the average circular diameter of globules is plotted against Ti addition, Figure 5.59b where there is a decreasing trend in particle size with increasing Ti%. This is further supported by particle counts, number density which also increased, i.e. finer particles. The overall particle size is less than 100μm. There is not much variation in the A/P factor but the percentage of α-Al particles with aspect ratio greater than 2 decreases which confirm more globularity.

As it was discussed previously, drainage may be regarded as an indication of fluidity and by Al5Ti1B addition, the amount of drainage decreased. It is believed that the main reason is the formation of Ti-based intermetallics with additions in excess of ~ 0.1%. On cooling and also due to non-equilibrium solidification condition more complex intermetallics such as Al_5Ti_2Si could form to block the flow of the remaining liquid during drainage (Figure 5.59f).

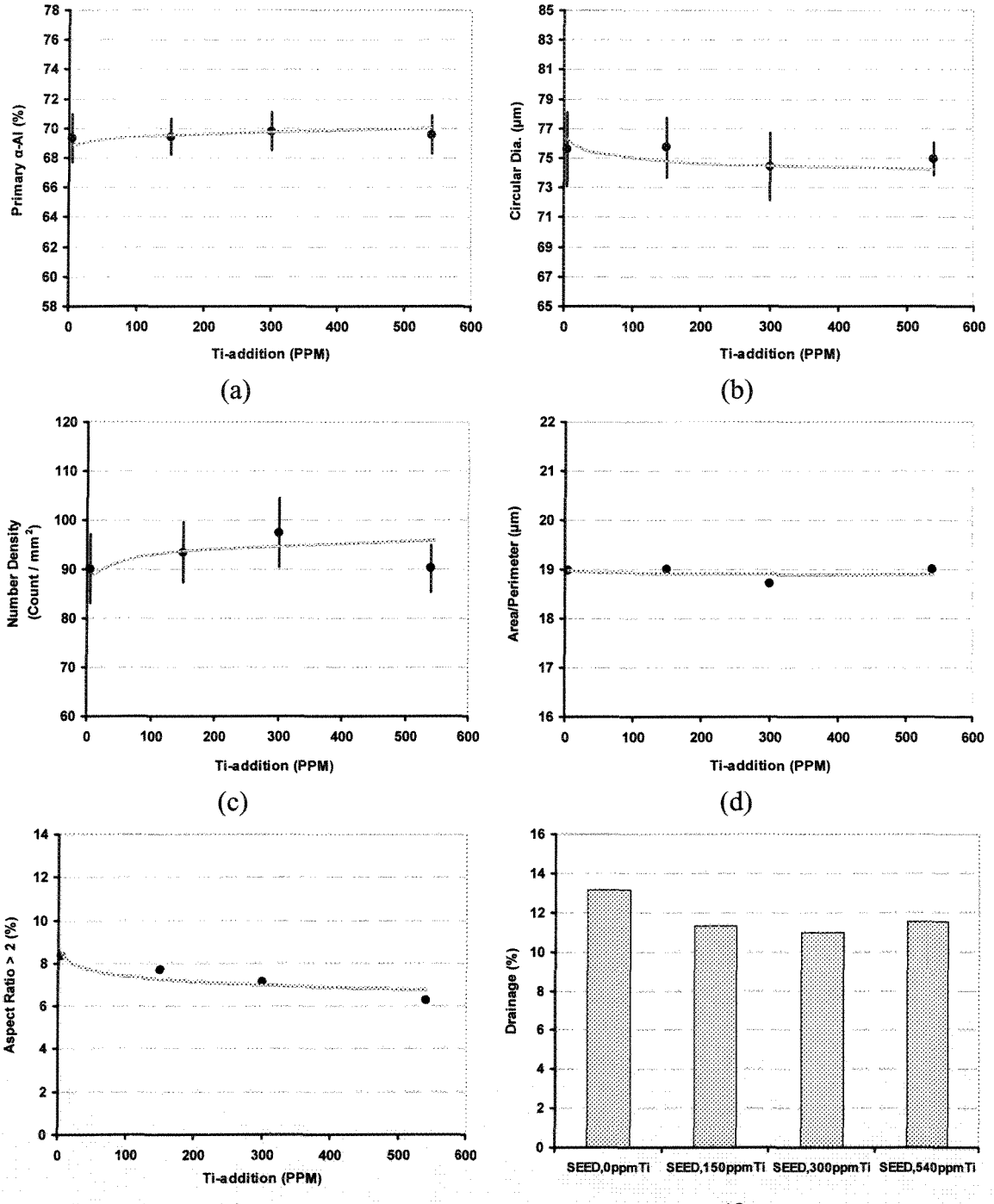

Figure 5.59: (a-e) Quantitative metallography for Com356, and (f) drainage as a process parameter

Figure 5.60 confirms that addition of Ti to the commercial 356 alloy does not alter the globularity of α-Al particles as much as those for A356 and the sphericity numbers are almost the same before and after the addition. As a conclusion it should be mentioned that in commercial alloy, the effect of refiner addition is masked by the GRF factor which associated to the Ti in solution and image analysis almost have the same results obtained before and after the treatment and this confirms the benefits of commercial alloy which is used in the majority of the casting plants.

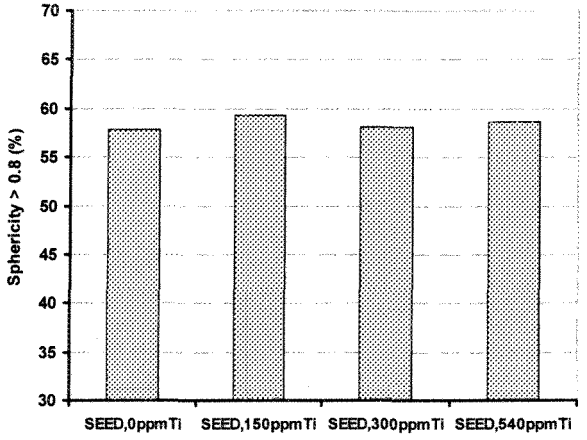

(a)

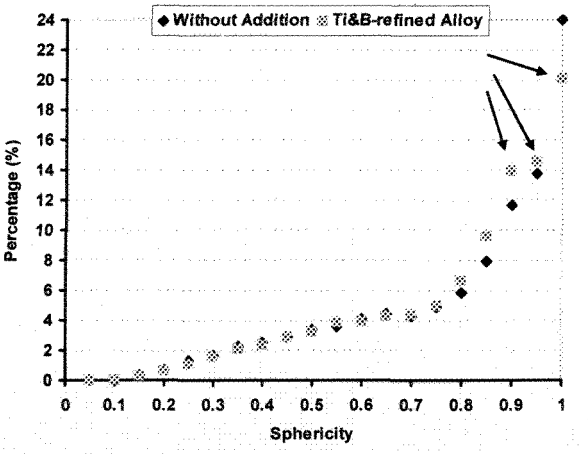

(b)

Figure 5.60: (a) Variation of sphericity percentage with refiner addition, (b) categorized sphericity data without Ti and with 300ppm Ti & 57ppm B

CHAPTER 6

RESULTS AND DISCUSSION MODIFICATION

CHAPTER 6

RESULTS AND DISCUSSION - MODIFICATION

6.1 Master alloy specification

6.1.1 Al10Sr

The optical (Figure 6.1) and backscattered electron micrographs (Figures 6.2) together with the associated x-ray maps show the microstructure of the commercially produced master alloy. As it is evident, the structure of Al-10Sr master alloy consists of blocky Sr-rich particles, Figure 6.2 - Sr map, distributed within Al matrix. The average particle size is about 16 ± 8 μm and the chemical composition, given in Table 6.1, suggests the Al_4Sr stoichiometry.

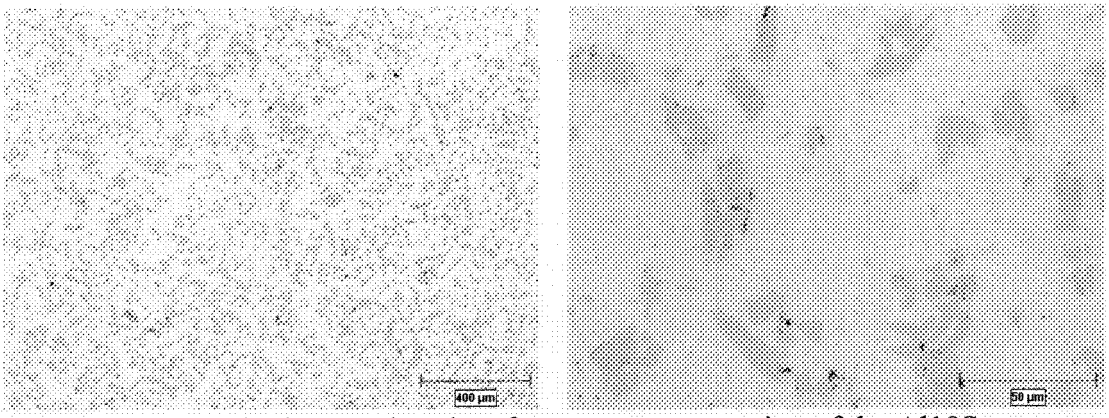

Figure 6.1: Optical micrographs taken from transverse section of the Al10Sr master alloy

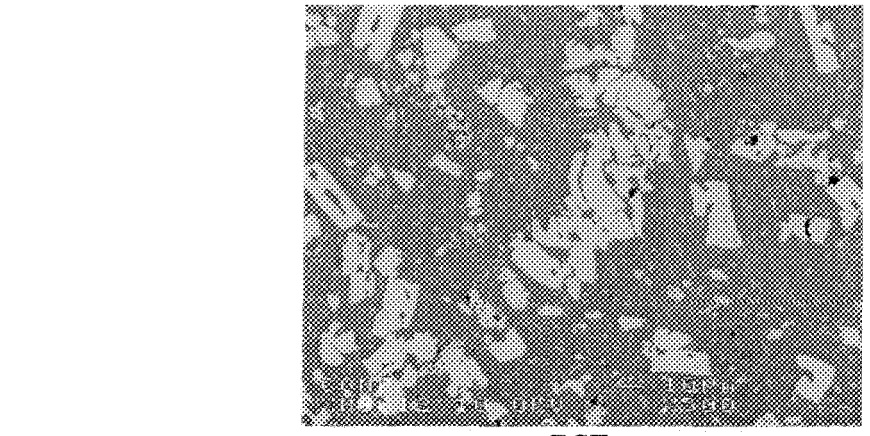

BSE

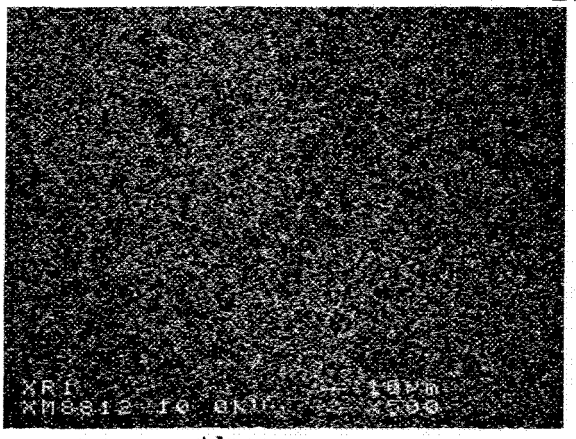

Al x-ray map

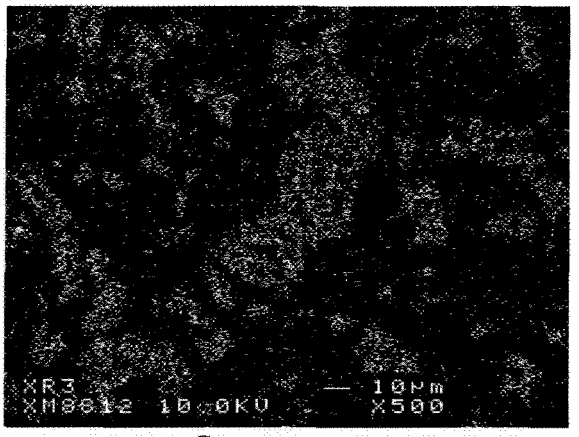

Sr x-ray map

Figure 6.2: Back scattered electron micrograph together with x-ray maps for Al10Sr master alloy

Table 6.1: Chemical analysis of the intermetallic particles in the Al10%Sr (at. %)

Al	B	Ti	Si	Mg	Sr	Fe
79.53	0.69	0	0	0	19.77	0
80.18	0.23	0	0	0	19.59	0

6.2 Modification in Al7%Si alloy

The purpose of these series of tests is to investigate the effect of Sr-modification on the binary Al7%Si since in commercial alloys, size and compactness of eutectic silicon would be different to that of the binary system. Furthermore, the presence of alloying elements and minor/trace elements may overshadow the effect of Sr as will be described in section 6.3. The initial chemical compositions are listed in Table 6.2.

Table 6.2: Initial chemical composition (wt. %)

	Si	Mg	Fe	Mn	Cu	Ti	B	P	Sr	Al
Modified	7.0-7.3	Nil	Max 0.09	Nil	Nil	Nil	Nil	Max 0.0003	Nil	bal.

6.2.1 Conventional casting

6.2.1.1 Thermal analysis

The effect of Al10Sr modifier addition on the eutectic reaction is illustrated in Figure 6.3 for a selection of samples. One central thermocouple was selected for each experiment. Small addition of strontium has a considerable effect on the eutectic plateau of the alloy where the eutectic temperature decreased by ~3°C by adding just 54ppm Sr.

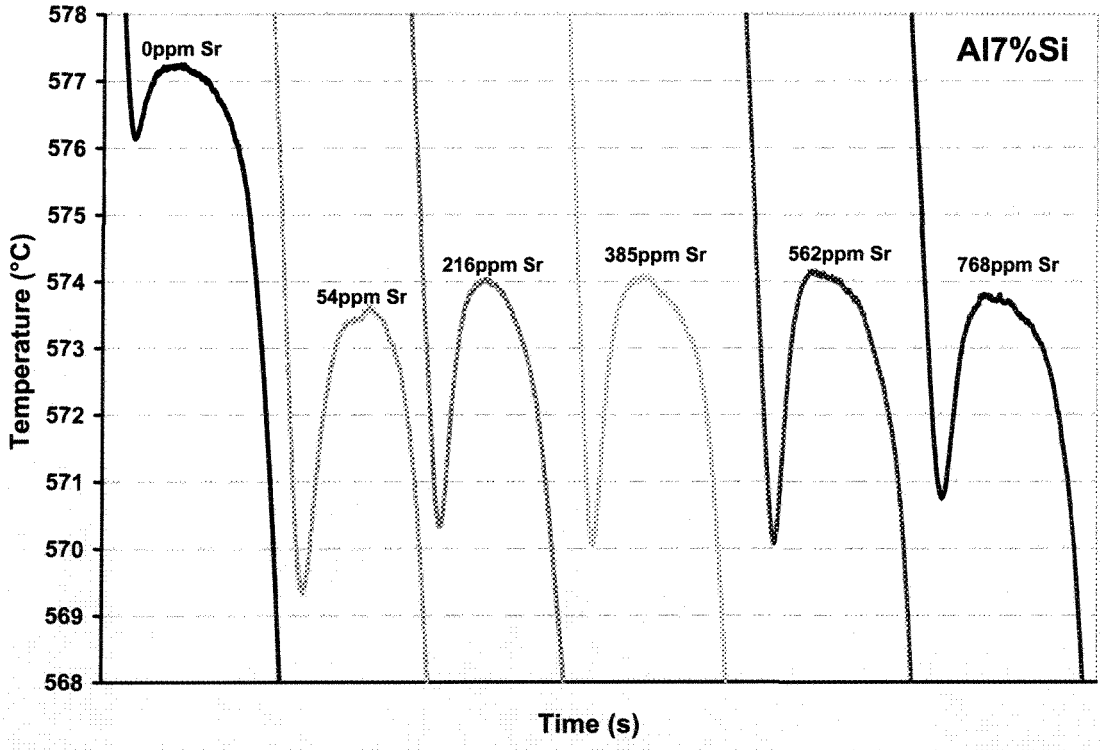

Figure 6.3: Eutectic plateau of the central thermocouples for different Sr-level

For each sample, the nucleation and maximum temperatures of eutectic ($Tmin_{eut}$, $Tmax_{eut}$) and eutectic recalescence variation ($\Delta\Theta$) were measured on the cooling curves (Figure 6.4). As seen in Figure 6.4a, nucleation temperature of the eutectic, $Tnuc_{eut}$,

decreases to a minimum level around 50-100 ppm and increases slightly ~200-300 ppm before becoming constant at ~574°C, for higher Sr addition. The same trend is also observed for the eutectic maximum temperature, $Tmax_{eut}$. Eutectic recalescence ($\Delta\Theta$) also increases to a maximum value and then decreases with further Sr addition (Figure 6.4b).

There is a direct relationship between the nucleation temperature and the number of potent nuclei in the melt. The rise in the nucleation temperature increases the number of potent nuclei and therefore reduces the barrier for the eutectic reaction commencement. As it was proved [189,190], AlP and iron particles are the most appropriate sites for silicon nucleation. By modification, the majority of such sites are deactivated and as a result, the nucleation temperature drops, i.e., the barrier for nucleation is interfered and the density of eutectic silicon nucleation decreases. This is shown in Figure 6.4b where recalescence explains the barrier for nucleation and the more the recalescence, the more is the obstacle to the nucleation, harder to nucleate. The lack of adequate nucleation sites for silicon is compensated during silicon growth where branching enables Si to keep up with Al. This is the origin for flake to fibrous transformation.

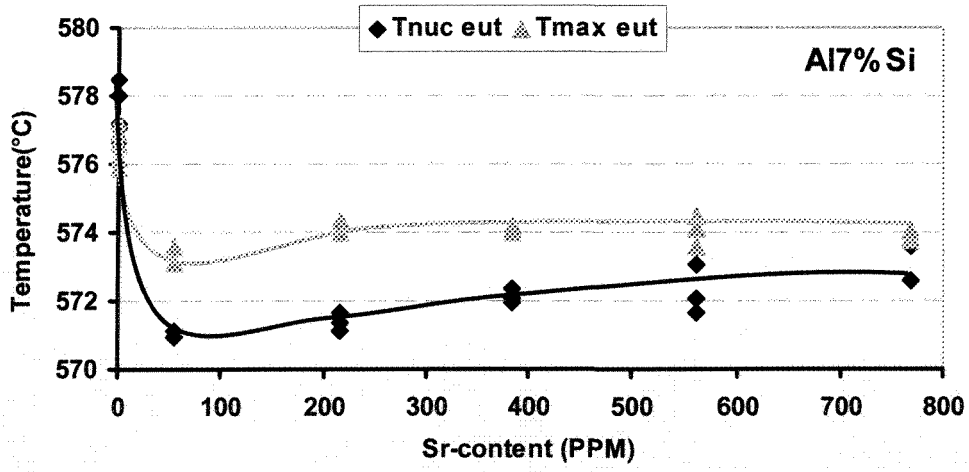

(a)

Continue ⟶

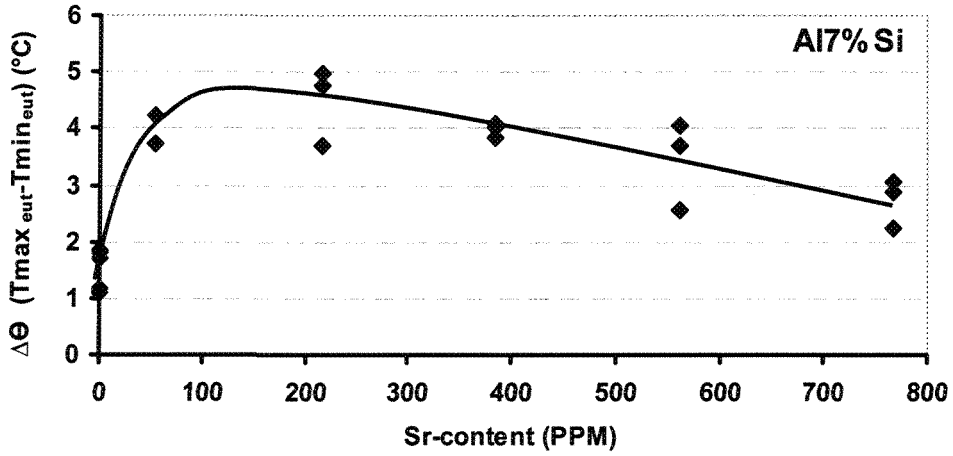

(b)

Figure 6.4: Effect of Sr addition on the: (a) $Tnuc_{eut}$, $Tmax_{eut}$, (b) $\Delta\theta$

6.2.1.2 Structural analysis

The effect of changing the amount of Sr in the alloy on the morphology of the primary α-Al phase and the eutectic structure is shown in Figure 6.5. The microstructure in the modified samples is quite different from the non-modified one. In the non-modified samples, silicon plates up to 130μm long could be detected in the structure and the boundaries of primary α-Al cells are not clear in the solidified alloy. By addition of Sr, silicon morphology changed from coarse acicular and lamellar to the fibrous. In the commercial binary alloy, small amount of the modifier has a great influence on the structure and so the intermediate procedures, i.e., lamellar and partially modified structures were almost omitted.

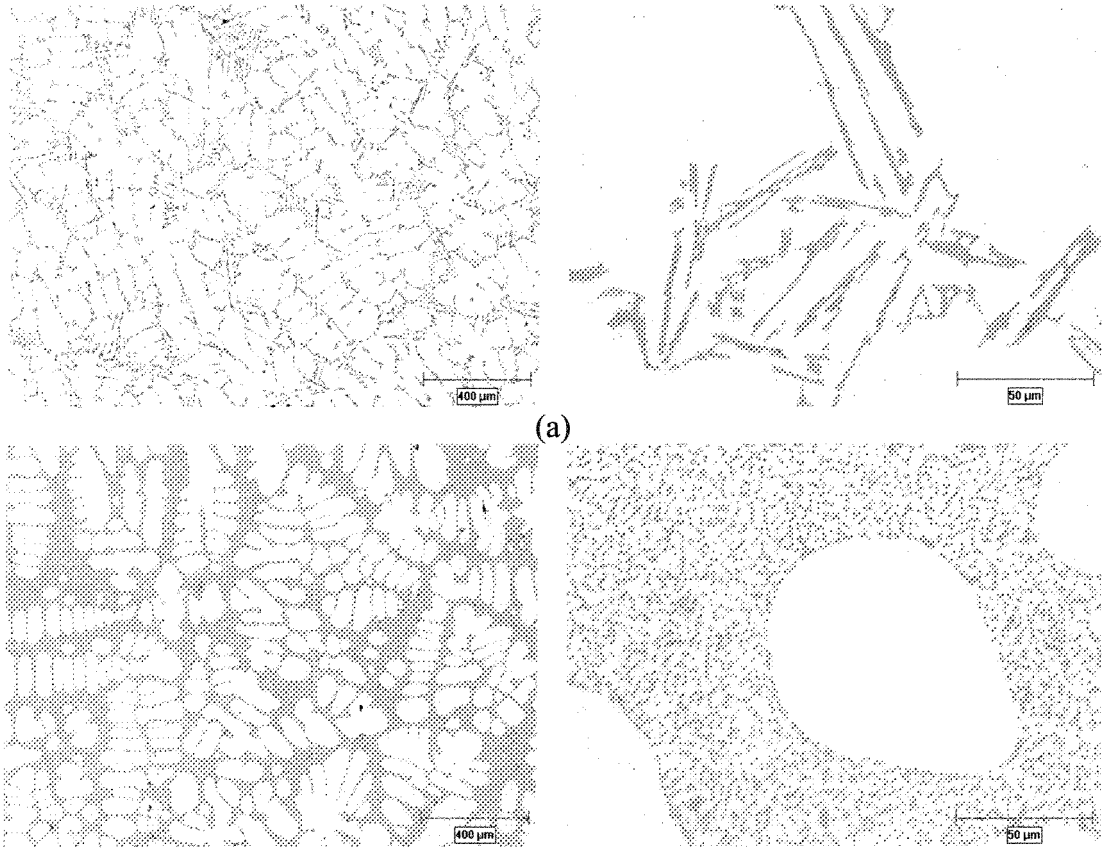

Figure 6.5: Optical micrographs showing the effect of Sr addition on the conventionally cast Al7%Si: (a) without Sr, (b) 54ppm Sr

It is interesting to note that simultaneous to the morphological evolution of eutectic silicon particles from acicular to fibrous structure, the amount and morphology of the primary α-Al phase changes too. Comparing Figure 6.5a and b, it is shown quite clearly that in the unmodified alloy, there is no special orientation of primary α-Al and they grow randomly. With increasing the Sr content, the solidification behavior of the α-Al particles changed and it becomes fully columnar. It seems that Sr changes the solidification mode of the alloy. As a proof for this observation, by using electron backscattered diffraction (EBSD) method, it was reported that there was no orientational differences between the primary α-Al phase and eutectic aluminum at the vicinity of the eutectic pools [191]. However, this point is beyond the scope of this research and it needs more investigation.

6.2.1.3 SEM analysis

Figure 6.6 shows the scanning electron micrographs of the specimens cast in graphite molds. As it could be seen, without modifier addition, the silicon morphology is accicular and flakes are quite large even at x500 magnification. With Sr-modification, the silicon morphology changes to fibrous with a seaweed like appearance. SEM analysis showed that overmodification causes the formation of complex morphologies where fibrous Si contains some flake type branches as seen in Figure 6.7.

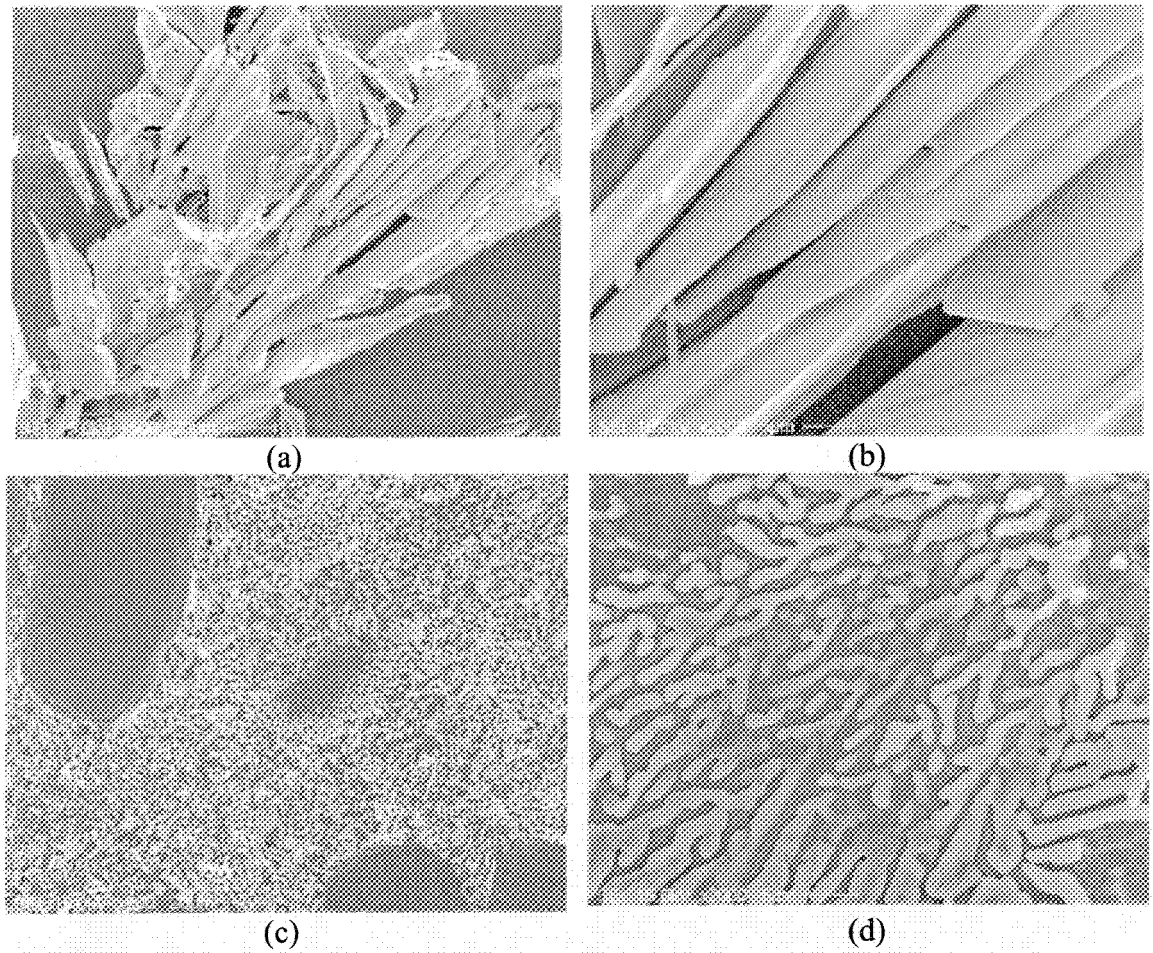

Figure 6.6: Secondary electron images of the conventionally cast specimens, deep etched in 10%HF, (a & b) without Sr (c & d) 54ppm Sr

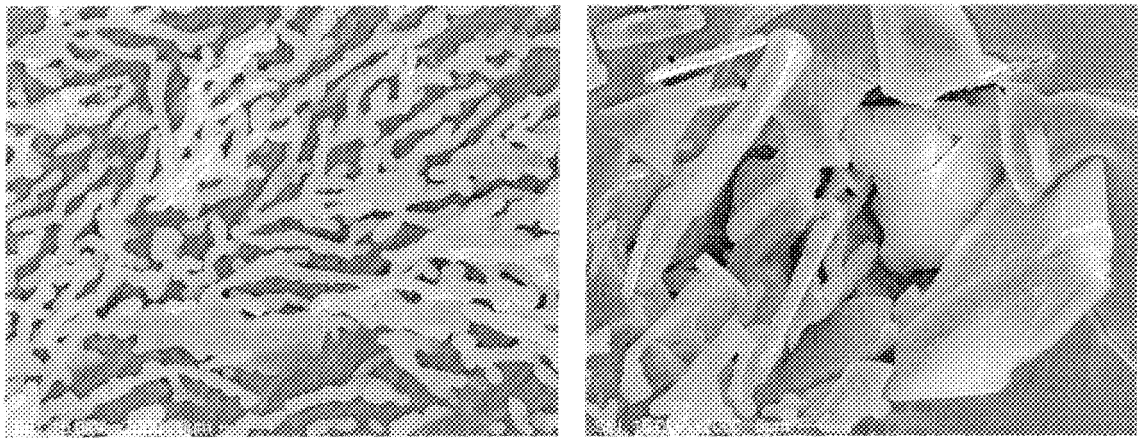

Figure 6.7: SEM micorgraphs showing the overmodification phenomenon (768ppm Sr) , deep etched in HF

6.2.2 Semi-solid processing

6.2.2.1 Structural analysis

The optical micrographs in Figure 6.8a&b highlight the distinct morphological differences of primary α-Al and eutectic silicon morphologies in conventional and SEED quenched billets (conventional billet is prepared in the same mold without agitation and drainage). The SEED process appears to be quite effective in transforming the primary α-Al dendrites into rosette and globular morphologies. Another advantage of the SEED process is its stirring function. Stirring not only leads to thermal and solutal homogenization but also by applying forced convection to the remained liquid results in the better fluid flow and changing the solidification pattern to multidirectional case and therefore this effect finally directs to enhanced refining of the silicon flakes which will be discussed in section 9.3. It is worth mentioning that this alteration does not mean any modification of eutectic silicons and stirring only causes smaller flakes in the structure.

Figure 6.9 shows the micrographs of quenched samples with different levels of strontium. By Sr addition, silicon morphology changes directly from lamellar to fibrous structure without any intermediate evolution with the added bonus of more spherical primary particles. As mentioned for conventional cast specimens, effect of overmodification could easily be detected by coarsening and increasing inter-lamellar/inter-rod spacing of the eutectic silicon and the formation of Sr-based intermetallic phases. It is

noticeable from Figure 6.10 that Sr compounds may segregate in two distinct morphologies of cuboidal and flake/plate. As it will be shown in the next section, microprobe analysis revealed these particles are Al_2Si_2Sr compounds in confirmation of results reported before [24,96]. These particles were found to form in castings with Sr addition in excess of 390ppm.

As seen in Figure 6.10, the silicon particles in the Sr-modified structures are quite small which almost makes the quantitative analysis impossible. However optical microscopy confirms that overmodification occurs in excess of ~200ppm. Therefore it could be concluded that the optimum additional level of Sr is between 50-200ppm. It is interesting to note that with modification, the distance between Si particles decreased while the reverse is true when Sr addition is beyond the optimum level.

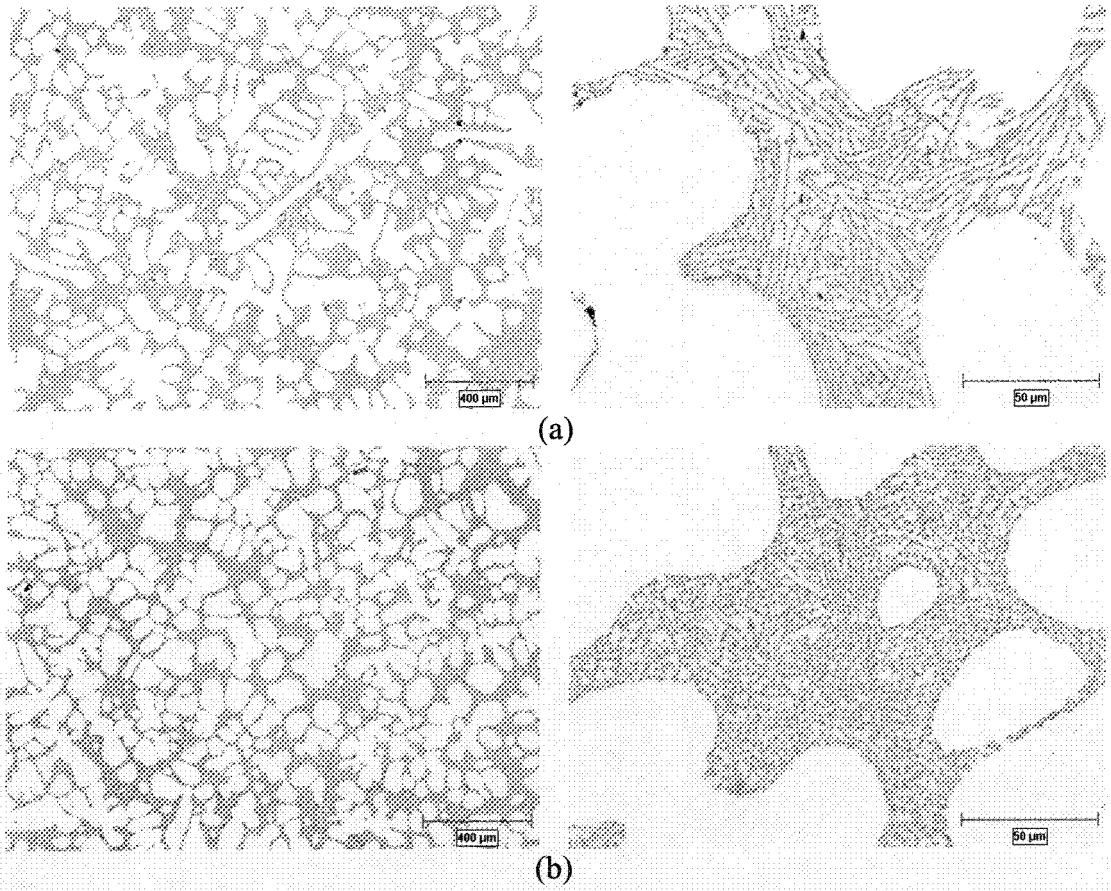

Figure 6.8: Optical micrographs in: (a) conventional and (b) SEED quenched samples, without Sr (both quenched from 598.5±2.5°C)

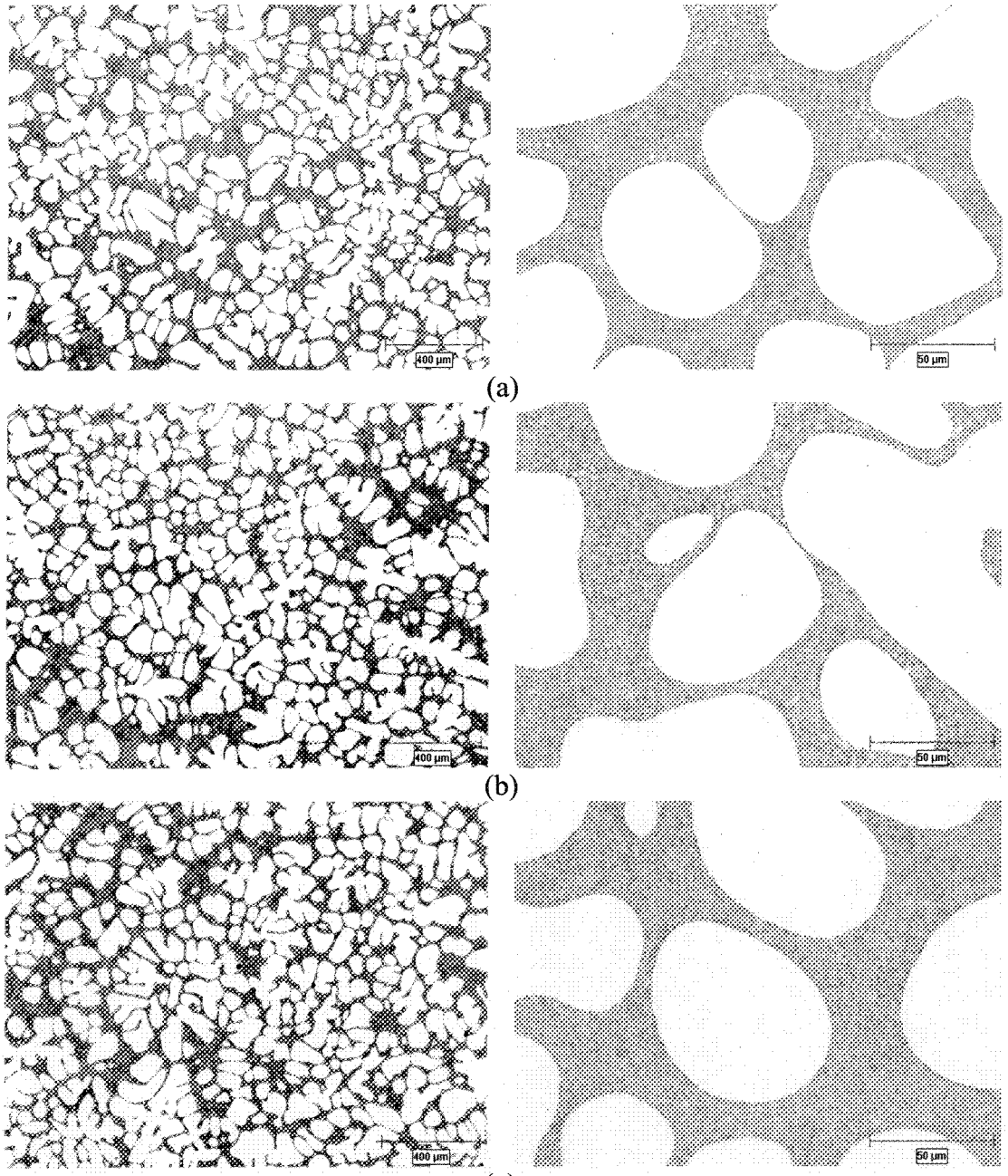

Continue ⟶

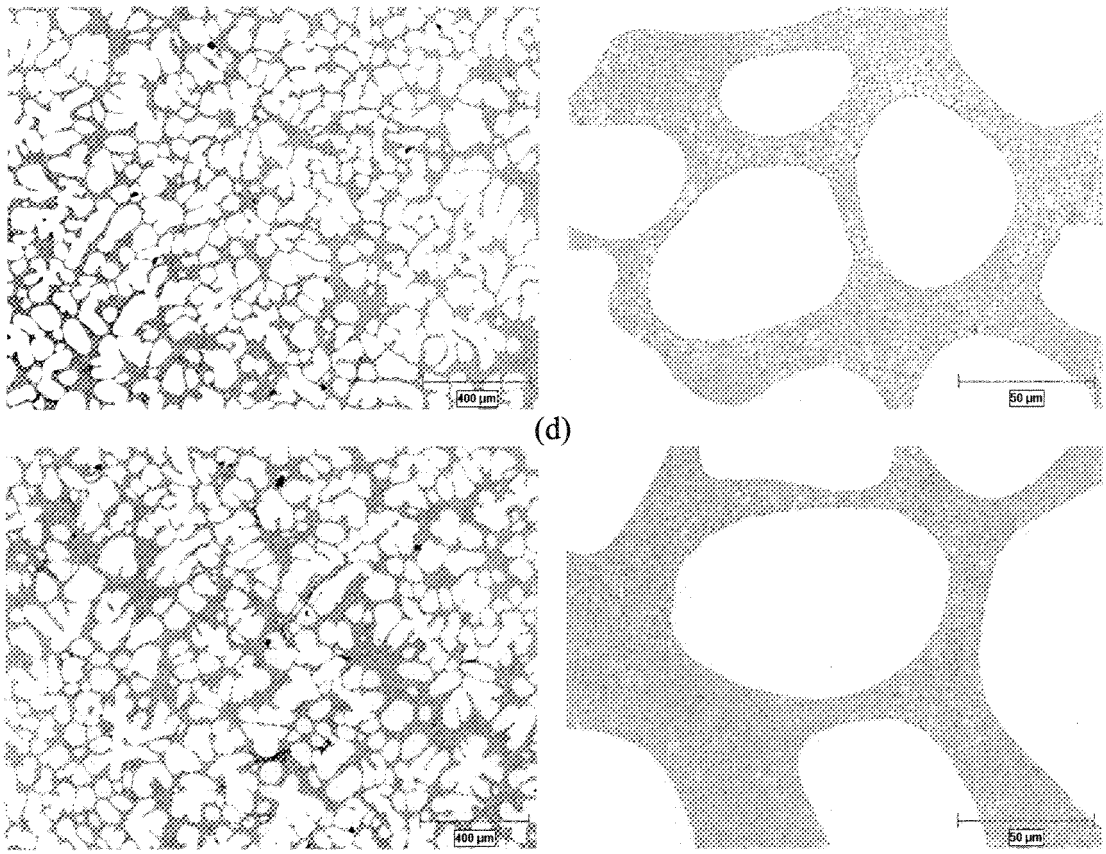

Figure 6.9: Optical micrographs showing the microstructural evolution regarding Sr addition: (a) 54ppm Sr, (b) 216ppm Sr, (c) 385ppm Sr, (d) 562ppm Sr, and (e) 768ppm Sr

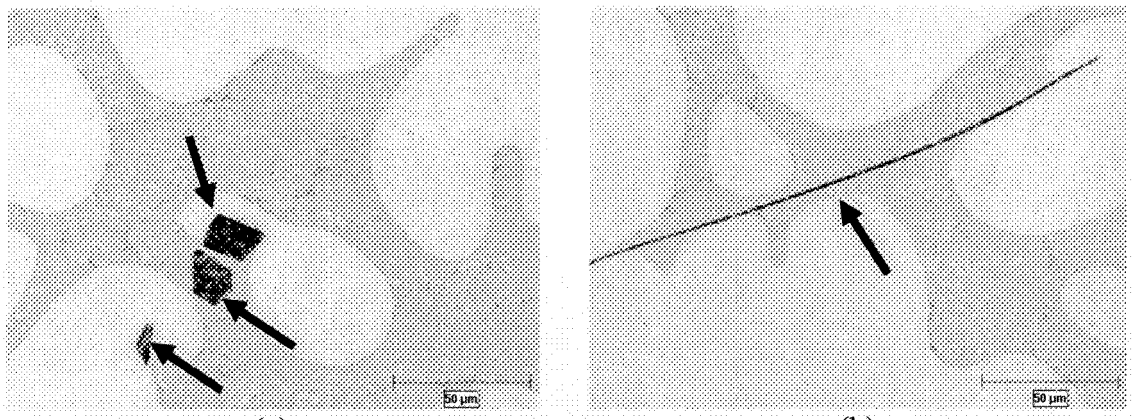

(a) (b)

Figure 6.10: Optical micrographs showing Sr-based intermetallic compounds formed in the SEED processed Al7%Si alloy (768ppm Sr): (a) cuboidal, (b) flake/plate

The importance of mush partitioning was reported in chapter 5 and the effects of refiner were well described. As mentioned, α-Al solidification range increases with grain refiner since the onset of α-Al nucleation temperature shifts to higher values. The variation of solidification ranges with strontium addition is shown in Figure 6.11. There is a significant rise in the ΔT_{α} value with strontium addition, i.e. nearly 7.5°C and interestingly ΔT_{eut} decreases. Increasing of the ΔT_{α} is due to the main eutectic reaction shifting down by Sr addition while decreasing of the ΔT_{eut} is due to the constant value of total solidification range.

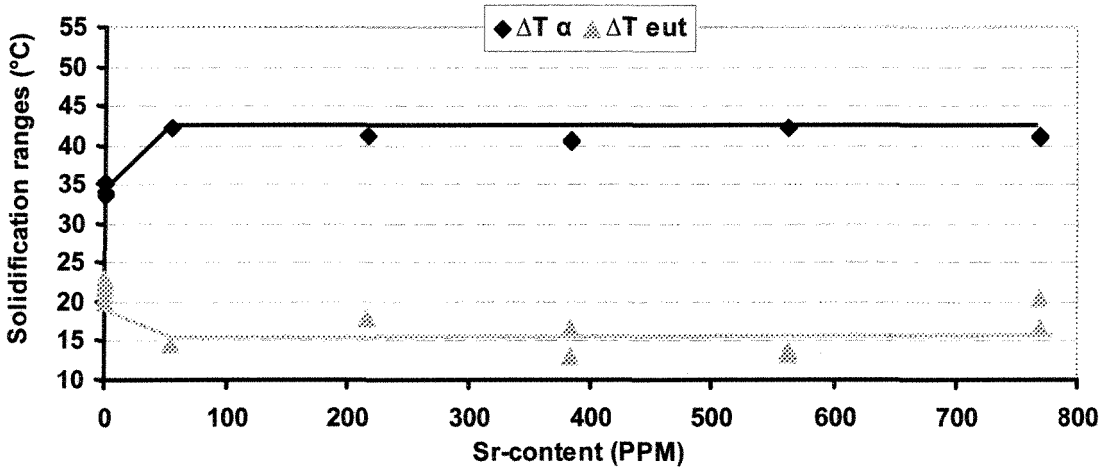

Figure 6.11: Effect of Sr on the solidification range of various phases

6.2.2.2 SEM analysis

Figure 6.12 shows the scanning electron micrographs of the non-modified and modified SEED samples. The use of deep etched specimens reveals the true morphology of the silicon particles. The silicon crystals are interconnected plate-fan like structure appearing to have grown out of numerous nucleation sites; while modified structure consists of highly branched fibers of silicon. A small number of nucleation sites are obvious in Figure 6.12c and d which accompanied by bulky fibrous growing from few sites. From modification stand point, it was shown that highly twined nature of modified silicon causes bending and branching of silicon crystals and form seaweed like structure in the modified samples [84,89].

One of the interesting points of SEM investigation is the difference between the fibrous structures in quenched billet (Figure 6.12c) and conventionally cast piece (Figure 6.6d). As it could be seen, the fibrous structure in SSM billet is denser and finer comparing to the conventional cast specimens. The key reason for this alternation is the quenching procedure which was applied at the last stage of SSM processing and the other one is attributed to the force convection flow. Furthermore if Figures 6.12c&d are compared with 6.12e&f, it is clear that the distance between silicon fibers in modified samples is lesser than overmodified samples. This conclusion is in line with optical micrographs and image results.

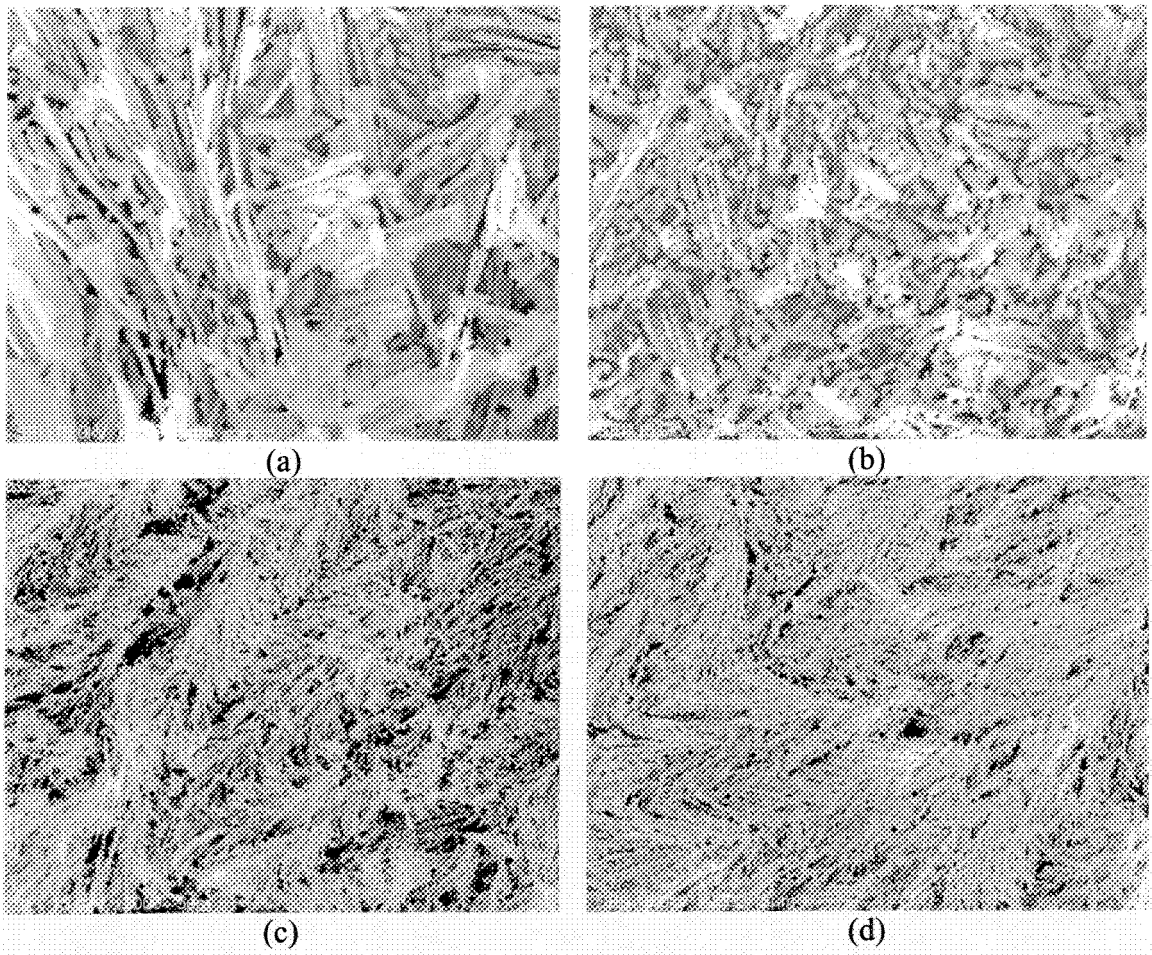

(a) (b)

(c) (d)

Continue ⟶

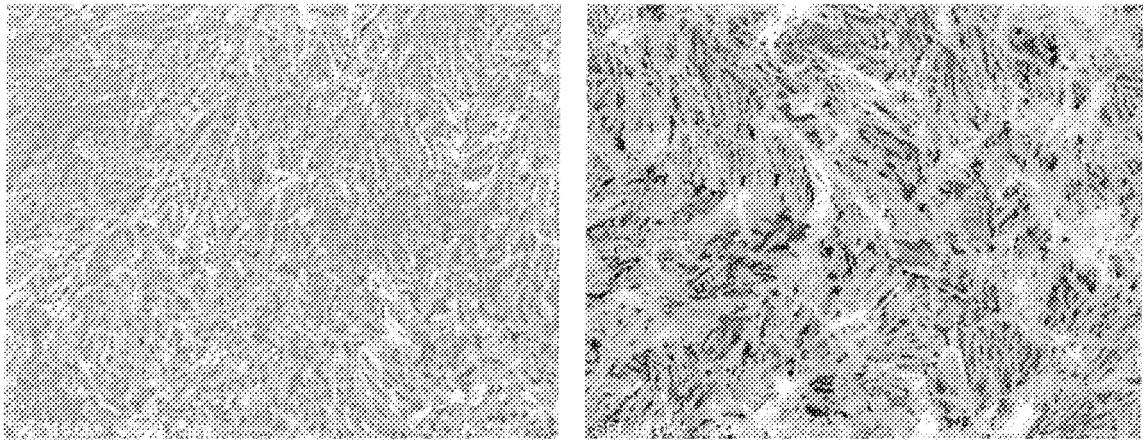

(e) (f)

Figure 6.12: SEM micrographs of:
(a) Conventional cast, without Sr, (b) SEED, without Sr, (c) SEED, 54ppm Sr, (d) SEED, 216ppm Sr, (e) SEED, 562ppm Sr, and (f) SEED 768ppm Sr

6.2.2.3 Image analysis

Results from image processing of SSM microstructures are shown in Figure 6.13. As discussed earlier, the silicon particles are so small that they could not be analyzed by the image system and thus only the results for the primary α-Al particles are given here. By addition of Sr, primary α-Al percentage increases slightly. As reported before [89,192], with Sr addition, the eutectic line is pushed downward and to the right to increase the freezing range of α-Al primary phase. This should render the α–Al percentage which could be confirmed with lever rule calculation.

Circular diameter of primary α-Al particles increases slightly with Sr addition. It is interesting to note that with increasing Sr concentration, the primary α-Al percentage is increased while the number density is approximately constant. Therefore, the equivalent circular diameter should increase to have always the balance between all the equations.

The amount of drainage increased with Sr about 216 ppm and it confirmed Sr ability to increase the flow of the remained liquid in the billet [75]. From dendrite coherency point of view, with Sr addition, solid fraction at the coherency point increases to induce less restriction toward the movement of the remaining liquid. In other words, modification

suppresses the DCP and consequently causes better flowability [193]. However, higher addition of Sr decreases the drainage for the reason of Sr-based intermetallic formation.

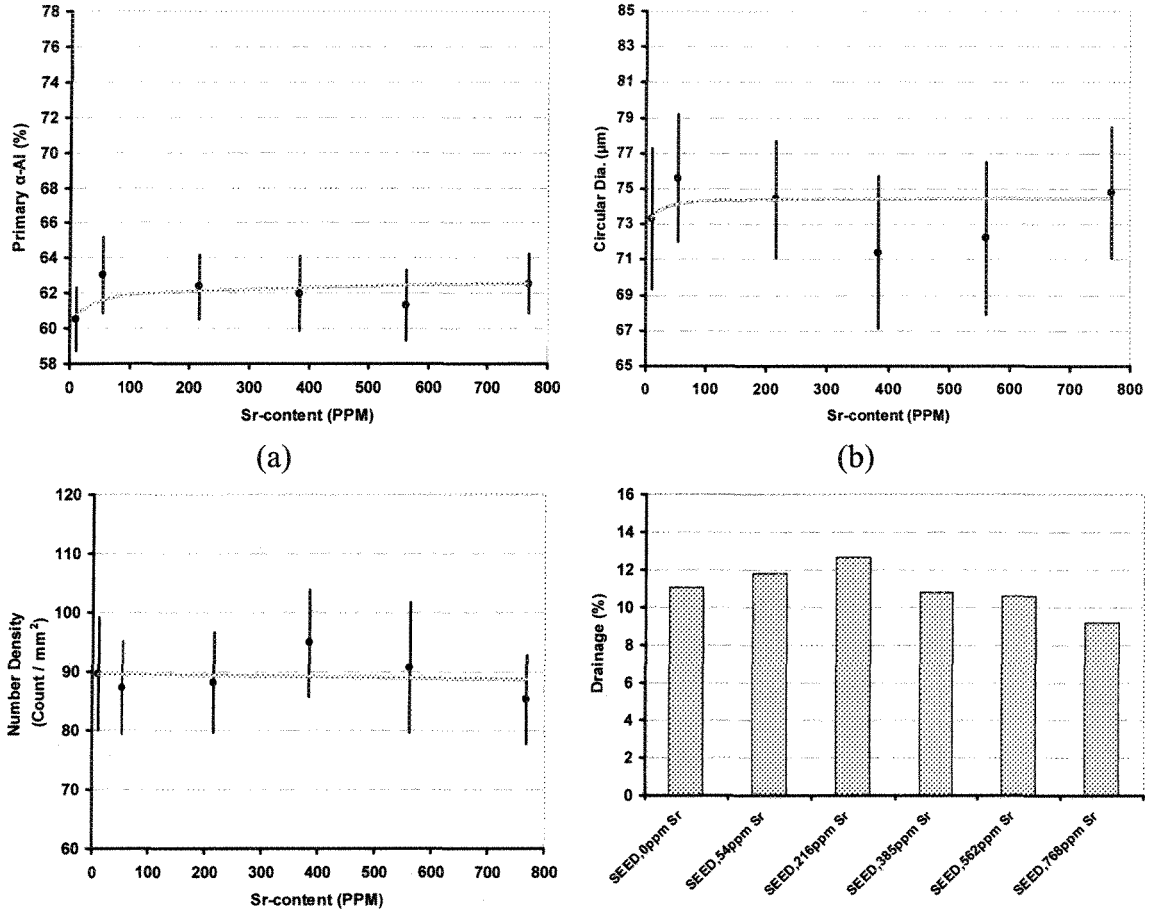

Figure 6.13: (a-c) Quantitative results for Al7%Si with Sr addition, and (f) drainage percentage

The sphericity values are presented in Figure 6.14. By modification, the sphericity of primary α-Al globules increases and this variation may be easily verified by distribution graph which shows greater values for particles having sphericity number closer to one i.e., more spherical particles.

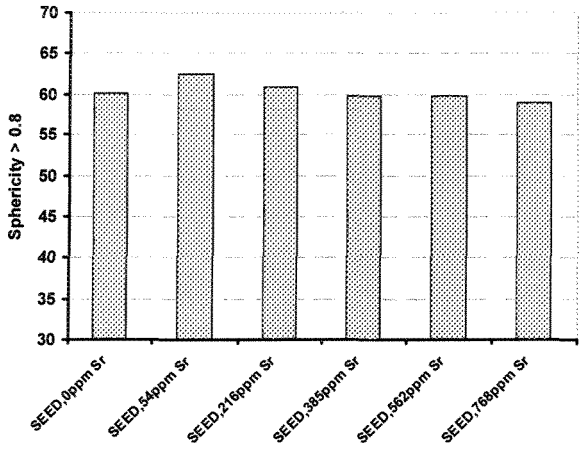

(a)

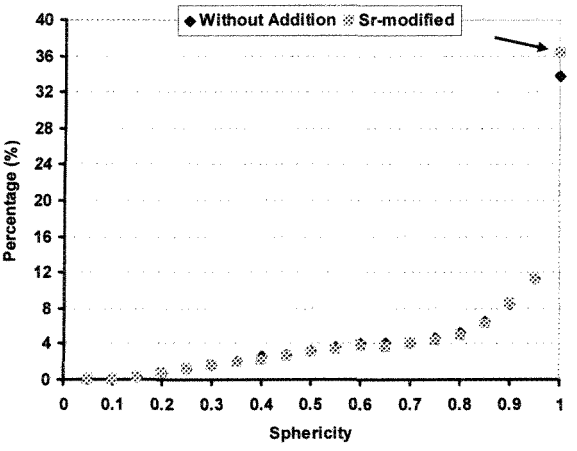

(b)

Figure 6.14: (a) variation of sphericity percentage with Sr additon, (b) data categorization without and with 54ppm Sr

6.3 Modification in A356 alloy

These series of tests were done by addition of Al10%Sr as a modifier. All the experimental procedure is exactly as same as what was described in chapter 4. The base compositions are listed in Table 6.3.

Table 6.3: Chemical analysis of the base alloy (wt. %)

Si	Mg	Fe	Mn	Cu	Ti	B	P	Sr	Al
6.62-6.81	0.36-0.4	Max 0.08	Max0.003	Nil	Max 0.0058	Nil	Max 0.0003	Nil	bal.

6.3.1 Conventional casting

6.3.1.1 Thermal analysis

Figure 6.15 shows the eutectic segment of the cooling curves for a selection of samples after Sr addition. The addition of small percentage of strontium, 47ppm, has depressed the eutectic plateau by as much as nearly 6°C. After the initial sharp drop in the eutectic temperature, further increase in the modifier concentration could only lift up the eutectic temperature slightly (~2°C).

Figure 6.16 illustrates the changes in the cooling curve parameters due to the Sr addition. The eutectic nucleation temperature, $Tnuc_{eut}$, decreased to its minimum value at about 50-100ppm Sr and increased slightly before becoming constant at Sr concentrations of about 300ppm and more. A similar trend is observed for the eutectic maximum temperature, $Tmax_{eut}$, Figure 6.16a.

Eutectic recalescence (Figure 6.16b) also increased to its maximum value at about 50-100 ppm Sr and decreased slightly before becoming constant with further addition of Sr. These are indications of greater barriers for eutectic nucleation due to Sr addition. The reduction in eutectic temperature and the fact that the alloy liquidus remained unchanged have caused the primary α-Al solidification range to increase as clearly shown in Figure 6.17. It is therefore anticipated to have an increase in the percentage of primary α-Al phase as will be discussed later. From SSM point of view, the primary α-Al solidification range is of great importance since an expanded α-Al solidification range improves the likelihood of

having more globular semi-solid slurries and gives a wider working temperature with lower sensitivity to temperature variation. However, the larger the mushy zone, the greater is the risk of hot tearing and porosity formation in the cast product, but this may be compensated when the SSM billets are shaped under adequate external pressure.

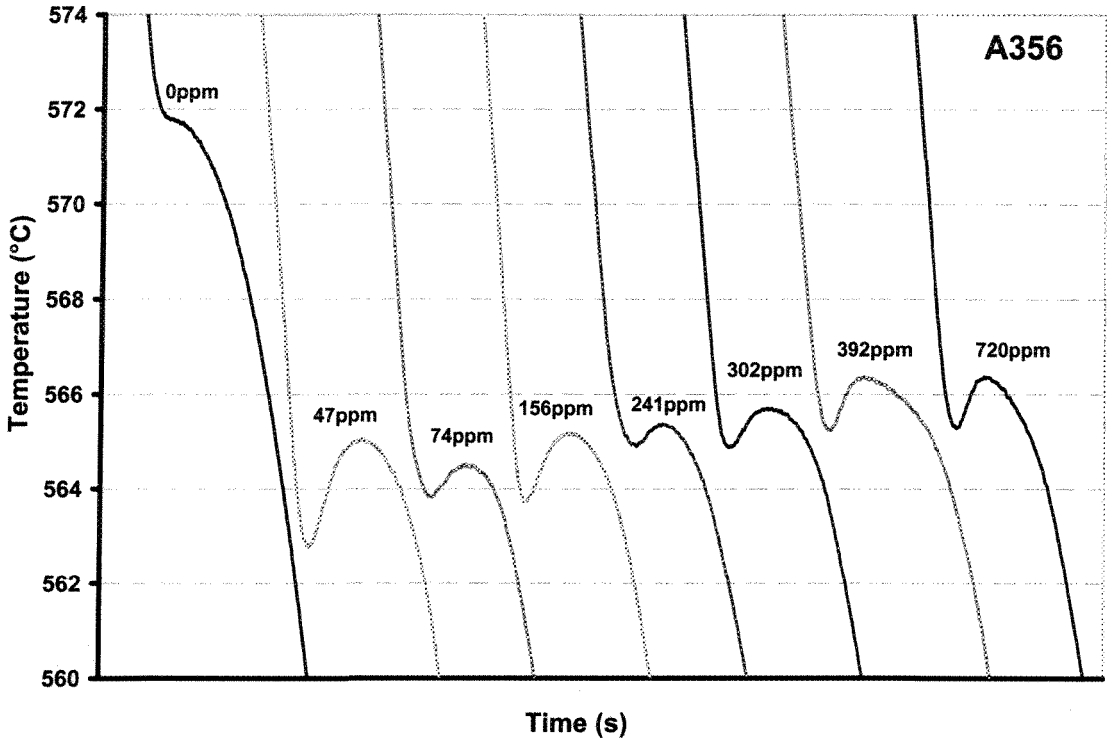

Figure 6.15: The eutectic segment of the cooling curves taken from the thermocouples at the center of graphite cups

Eutectic nucleation temperature (Figure 6.16a) has a direct effect on the number of potential nuclei found in the melt. In other words, there are fewer barriers for nucleation with increasing nucleation temperature and thus greater number of isolated eutectic Si particles may form, i.e. this is the case for flake morphology. The highest value for eutectic nucleation temperature before modification may be attributed to the trace phosphorus and iron contents in the alloy used in this study. As confirmed before [189,190], AlP particles and iron compounds are favorite nucleation sites for silicon. Nafisi et al. [192] reported both liquidus and eutectic temperatures increase with addition of phosphorus to the Al-Si eutectic alloy. With modifier such as Sr, such potential nucleation sites are deactivated by

fewer nucleation sites and consequently nucleation barrier increases and as a result the nucleation temperature decreases. The variation of eutectic recalescence ($\Delta\Theta$), Figure 6.16b, shows that small Sr addition (47ppm) resulting in an increase of $\Delta\Theta$ up to ~ 2°C. This is a nucleation barrier equivalent to having a reduction in the number of active nucleation sites which forces Si to branch out to form a three dimensional interconnected morphology, fibrous, to keep up with the growing aluminum phase.

Furthermore from growth point of view, Sr is reported to poison the re-entrant edge growth steps in silicon crystals [84,85], thus deactivating the "TPRE" (Twin Plane Re-entrant Edge) growth. Consequently, due to interruption in the effective growth mechanism for Si, high degree of $\Delta\Theta$ is needed to drive an alternative growth mechanism for the development of the fibrous silicon structure which is "Impurity Induced Twinning - IIT" mechanism [84].

In conclusion, Sr addition affects both nucleation and growth behavior of eutectic Si to transform silicon morphology from flake to fibrous. Furthermore, the overall results of thermal analysis for this study are in line with the previous reports [24,194-196].

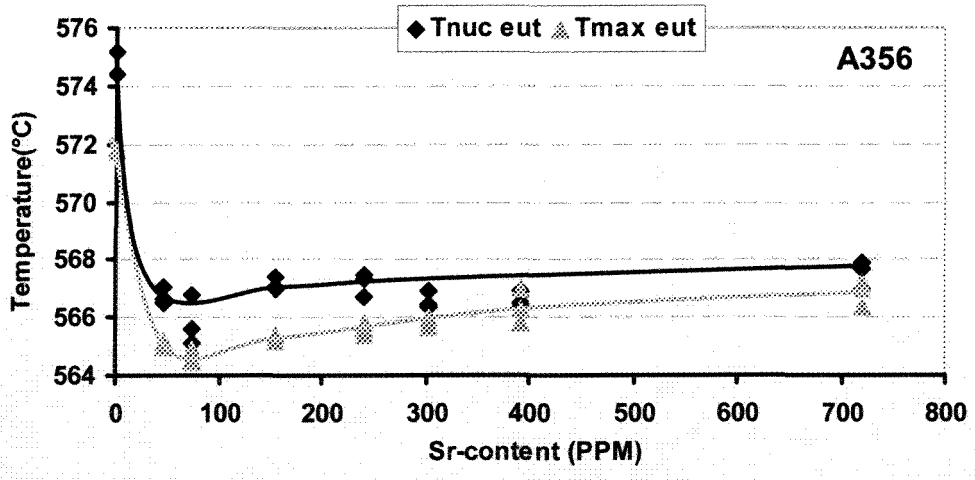

(a)

Continue

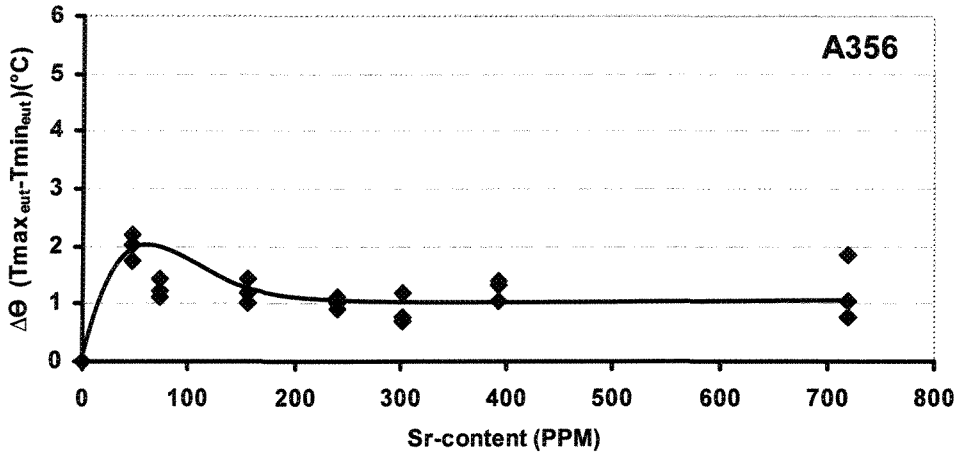

(b)

Figure 6.16: Effect of Sr addition on the:
(a) nucleation and maximum temperatures of the eutectic, ($Tnuc_{eut}$, $Tmax_{eut}$),
(b) eutectic recalescence, $\Delta\Theta$

By calculating different solidification ranges, it becomes obvious that ΔT_{α} increases by Sr addition due to the lowering of the main eutectic reaction and since the total solidification range is constant, ΔT_{eut} decreases (Figure 6.17). By increasing the α-Al solidification range, there is more chance for having better semi-solid slurries due to wider working temperature range.

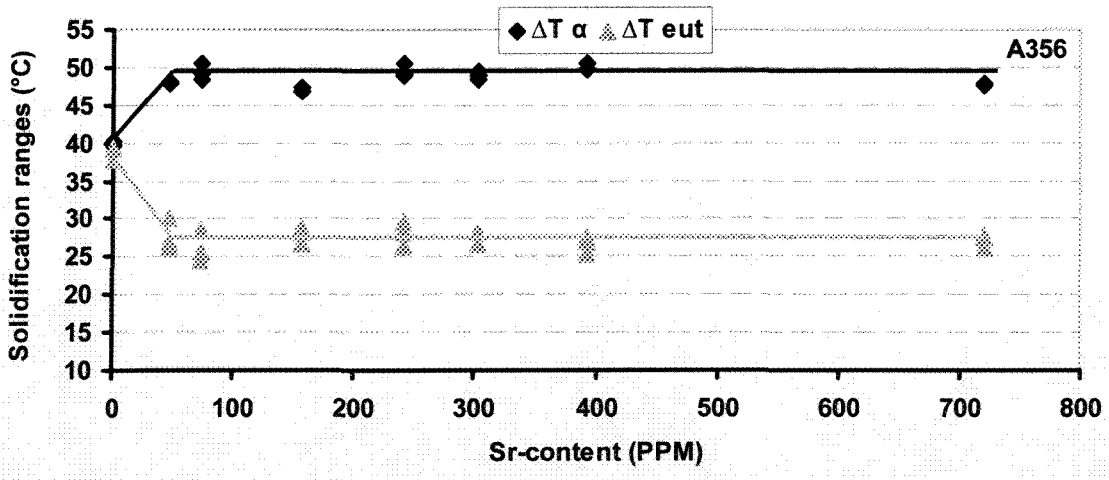

Figure 6.17: Effect of Sr on the solidification range of various phases

6.3.1.2 Structural analysis

The morphology of primary α-Al phase appears to be somewhat different to that of non-modified alloy as seen in Figure 6.18. If the micrographs are examined closely, it is evident that the eutectic regions within the modified alloy appear to have boxed-in the primary α-Al phase, while this is not the case for non-modified structure. In other words, eutectic regions within modified alloy are continuous and interconnected while there are isolated individual patches of eutectic regions for the non-modified alloy. Such distinct difference may be attributed to the fibrous morphology of Si and the fact that each individual Si nucleus grows through branching and expanding three dimensionally rather than as an isolated flake for non-modified alloy. It is beyond the scope of the current study to report on the effect of Sr addition or the presence of the Al_4Sr compound within the master alloy, Figure 6.2 and Table 6.1, on the solidification mode (nucleation and growth) of the primary α-Al phase.

The concept of "boxing-in" of the primary α-Al particles by the eutectic mixture in the modified alloy is well illustrated in Figure 6.18 along with the changes related to the silicon morphology. In the non-modified samples, silicon plates up to 120μm long could be seen in the Al matrix with the boundaries of primary α-Al dendrites being not clear. It may be true to say that in non-modified alloy, the remaining liquid does not solidify as a duplex mixture of Al and Si, but there is an overshoot of primary α-Al dendrites, due to difficulty of nucleation of Si, to take with them the Al content of eutectic mixture. Employing electron backscattered diffraction (EBSD), Nogita, and Dahle [191] reported that in non-modified alloys there is not any difference in the crystallographic orientation between the primary α-Al phase and the eutectic aluminum at the vicinity of the eutectic pools.

With modification however, the eutectic melt solidifies as a duplex mixture due to the changes in the silicon morphology. The addition of 47ppm Sr is sufficient to transform the flake Si to fibrous morphology and with further addition of Sr, the structure becomes fully modified and eventually overmodified. Overmodification can easily be detected by the coarsening of silicon particles and increasing their inter-particle spacing and the

segregation of Sr-based compounds (Figure 6.19). Electron probe microanalysis (EPMA) has confirmed Al_2Si_2Sr stoichometry for the segregated Sr-based compounds.

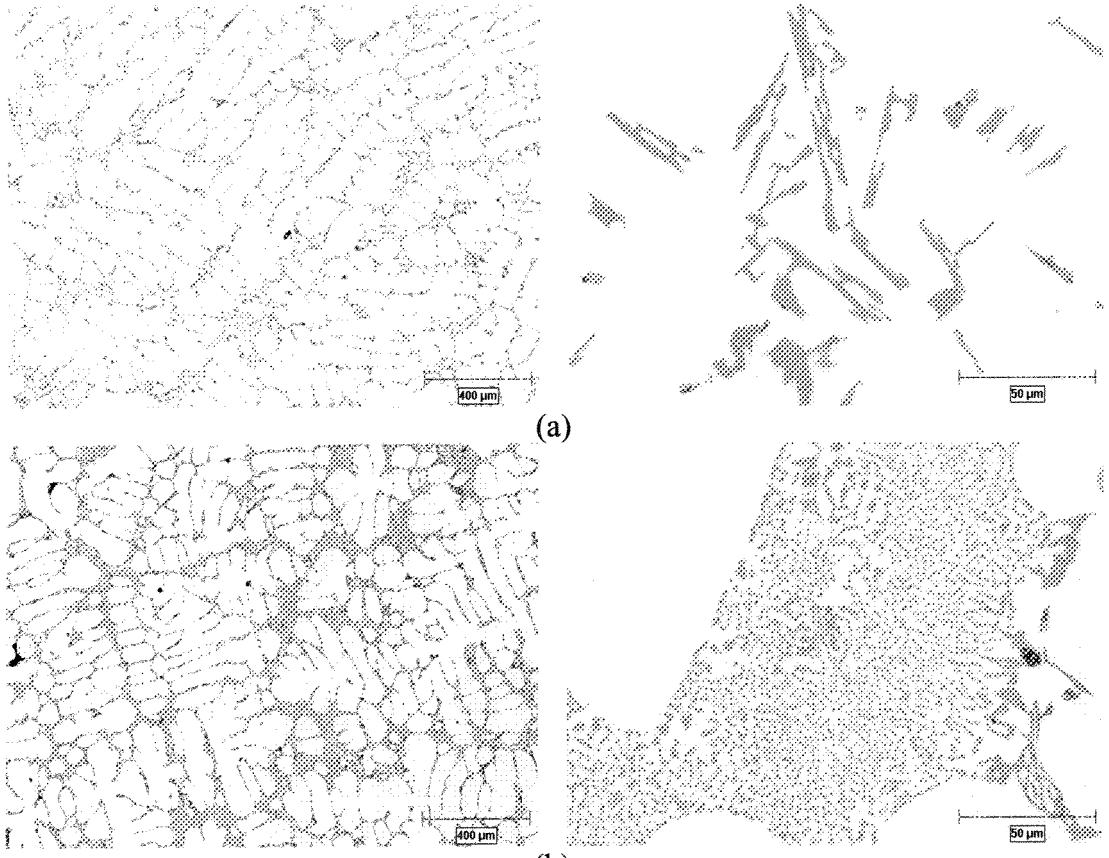

Figure 6.18: Optical micrographs showing the effect of Sr addition in the conventional casting: (a) without Sr, (b) 156ppm Sr

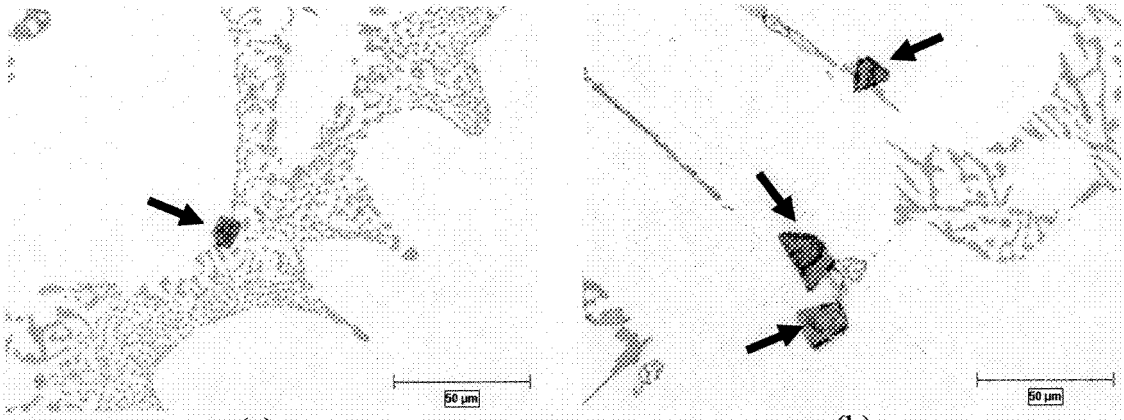

Figure 6.19: Sr-based intermetallic compounds (arrowed) formed in the overmodified specimens; (a) 302ppm Sr, and (b) 720ppm Sr

6.3.1.3 SEM analysis

In order to further characterize the morphological changes of the eutectic Si due to Sr modification, deep etched graphite mold samples were examined by SEM, see Figure 6.20. The flake silicon particles of the non-modified alloy are quite coarse even at such low magnification, Figure 6.20a. With Sr-modification, silicon morphology changes to fibrous with seaweed appearance, Figure 6.20c&d. SEM analysis showed that overmodification may initiate some discontinuity in the fibrous structure by forming pseudo flake silicons as it is evident in Figure 6.21 (arrowed).

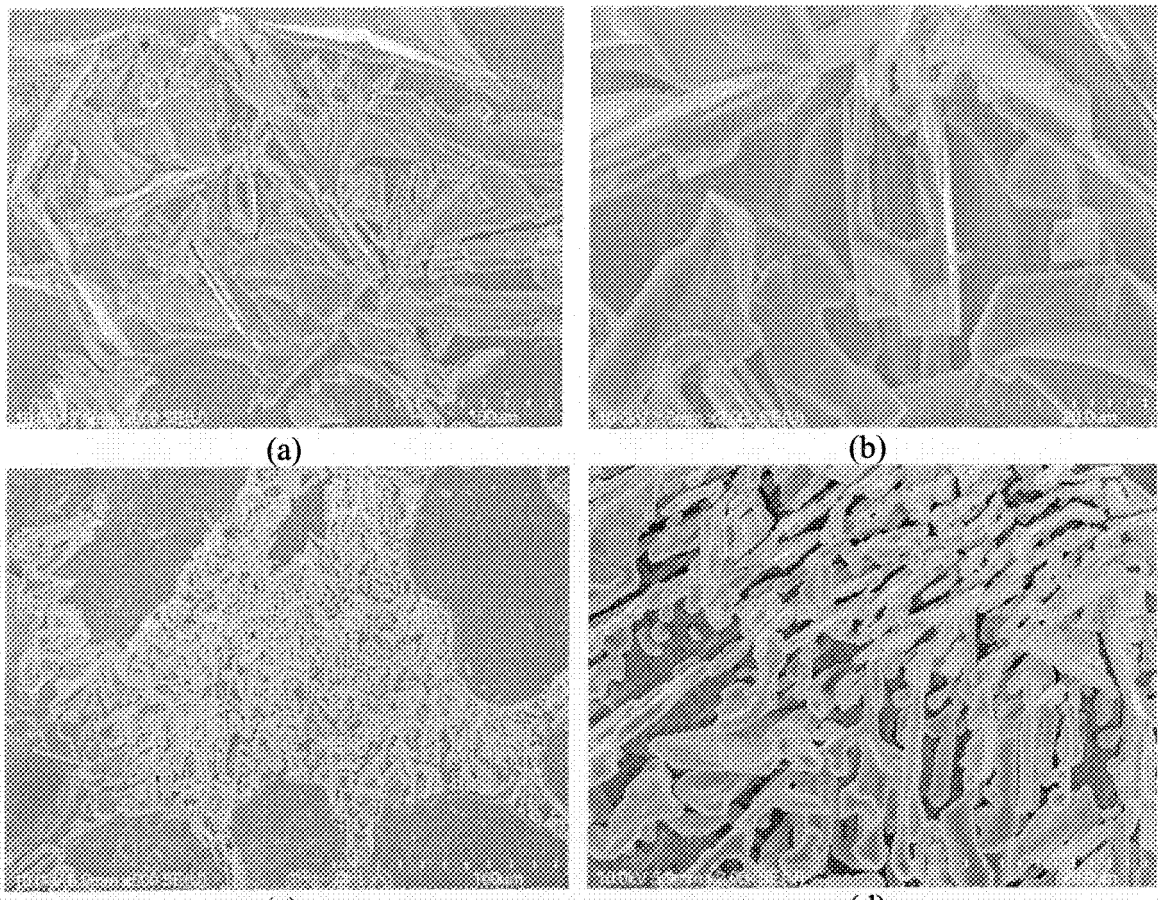

Figure 6.20: SEM micrographs of the deep etched (10%HF) graphite mold samples, (a & b) without Sr (c & d) 156ppm Sr

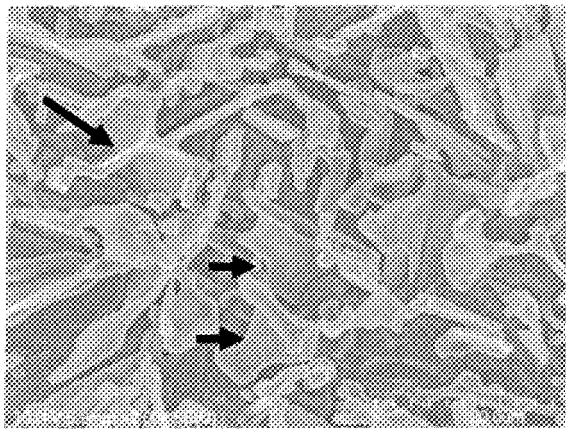

Figure 6.21: SEM micrograph showing the formation of pseudo flake Si particles (arrowed) due to overmodification (720ppm Sr)

6.3.2 Semi-solid processing

6.3.2.1 Structural analysis

The left hand sides' optical micrographs in Figures 6.22 show the effect of Sr addition on the morphology of the primary α-Al particles. The Sr-treated structure appears to have more globular characteristics with isolated primary α-Al particles dispersed in a refined eutectic matrix. As discussed for the conventional cast structure, the eutectic regions within the modified alloy appear to have boxed-in the primary α-Al phase.

The Si morphology, Figure 6.22 right hand sides, however is fully fibrous as expected with modification treatment but denser and finer than those of conventionally air-cooled casting of Figure 6.18. This is, mainly due to the higher cooling rate of the quenched SEED billets, and partly due to the SSM process itself. The SEED process is a rheocasting route based on the stirring of the melt within the mushy zone. As reported before [128], stirring not only leads to the formation of globule structure in the slurry but also imparts forced convection onto the remaining liquid resulting in better fluid flow and smaller silicon particles. As a result the Si morphological changes of the SEED processed billets could not be resolved and characterized by image processing.

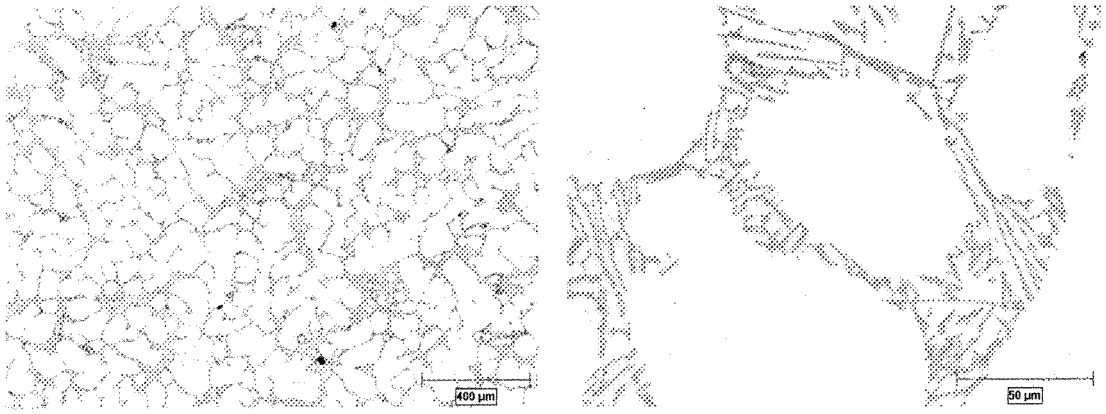

(a)

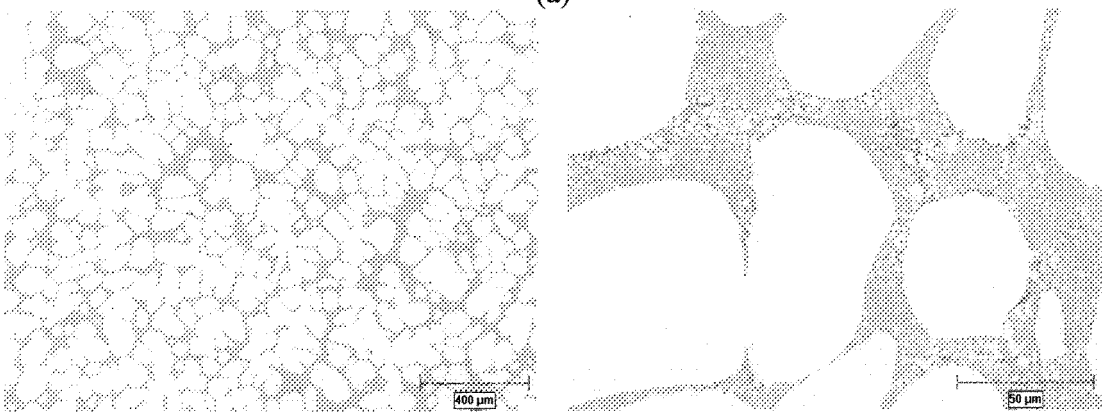

(b)

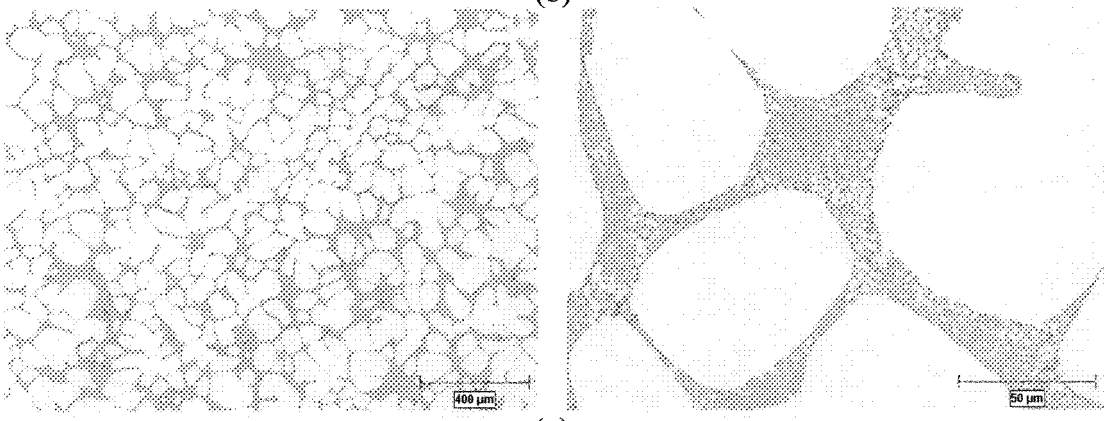

(c)

Continue

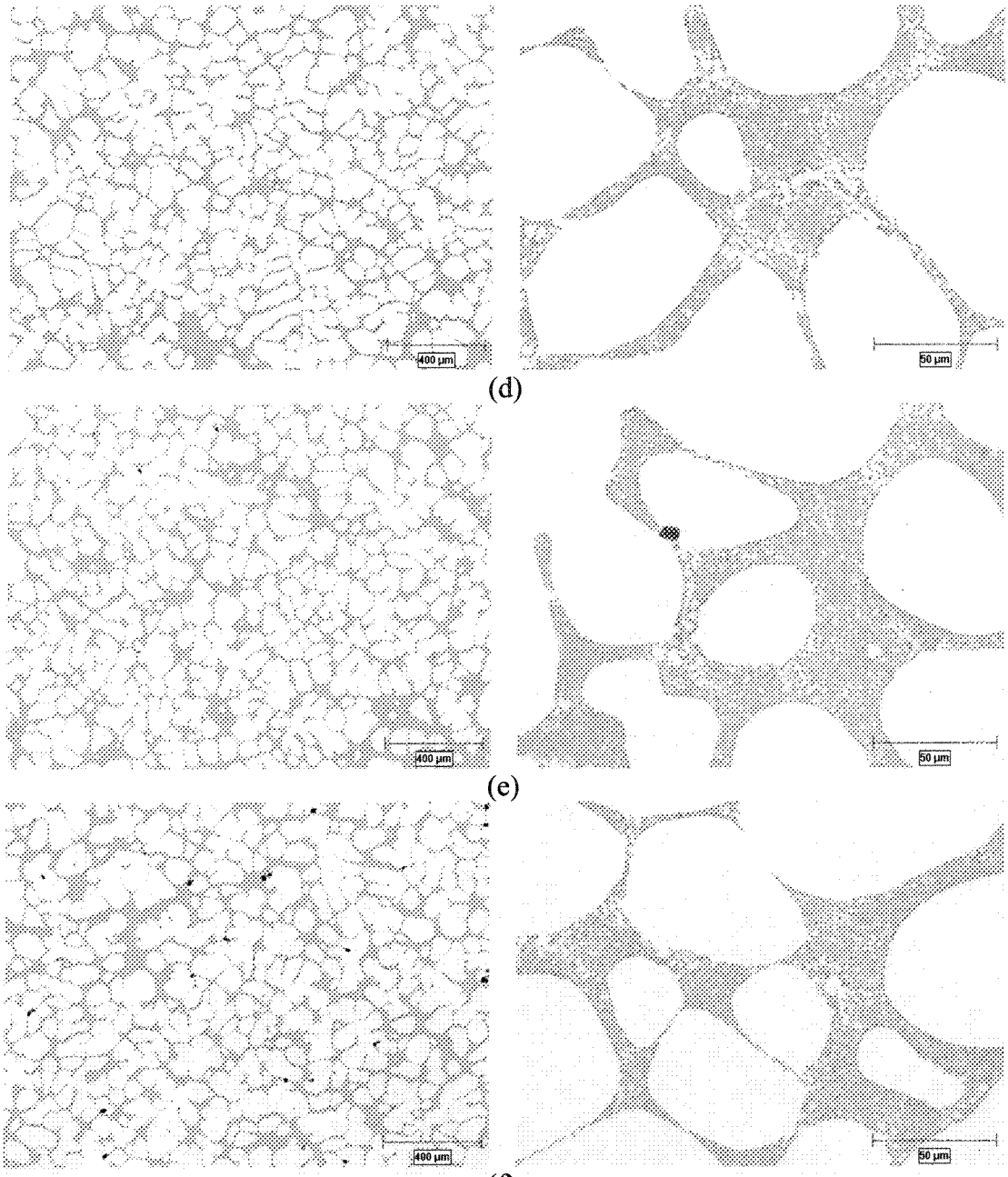

Figure 6.22: Optical micrographs to show the additional effects in the SEED process:
(a) without Sr, Conventional process, (b) 47ppm Sr,
(c) 74ppm Sr, (d) 156ppm Sr, (e) 302ppm Sr, and (f) 720ppm Sr

As mentioned for the conventional cast specimens, the effect of overmodification could easily be detected by the coarsening and increasing of the intersilicon spacing and the formation of Sr-based intermetallic phases within the eutectic pools. It is noticeable from

Figure 6.23 and 6.24 that Sr compounds may segregate in two distinct morphologies of cuboidal and flake/plate.

The microprobe analysis of the Sr-based compounds, x-ray maps in Figure 6.24 and Table 6.4, suggests Al_2Si_2Sr stoichiometry in confirmation of the results reported before [24,96]. These particles were found to form in castings with Sr additions in excess of 390ppm. It should be emphasized that no chemical variation was detected between these two morphologies. Therefore the optimum percentage for Sr addition appears to be between 50-200ppm.

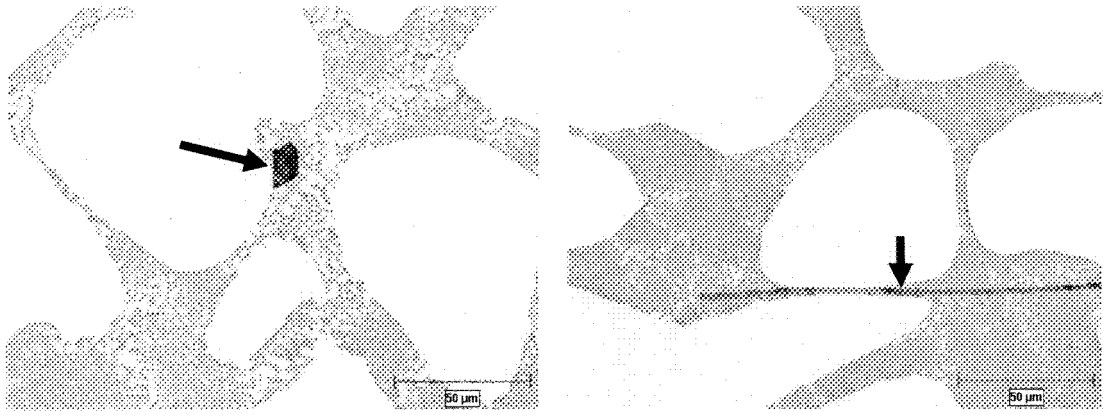

(a) (b)

Figure 6.23: The formation of Sr-based intermetallic compounds, (arrowed), due to overmodification of the SEED billets: (a) 302ppm Sr, (b) 720ppm Sr

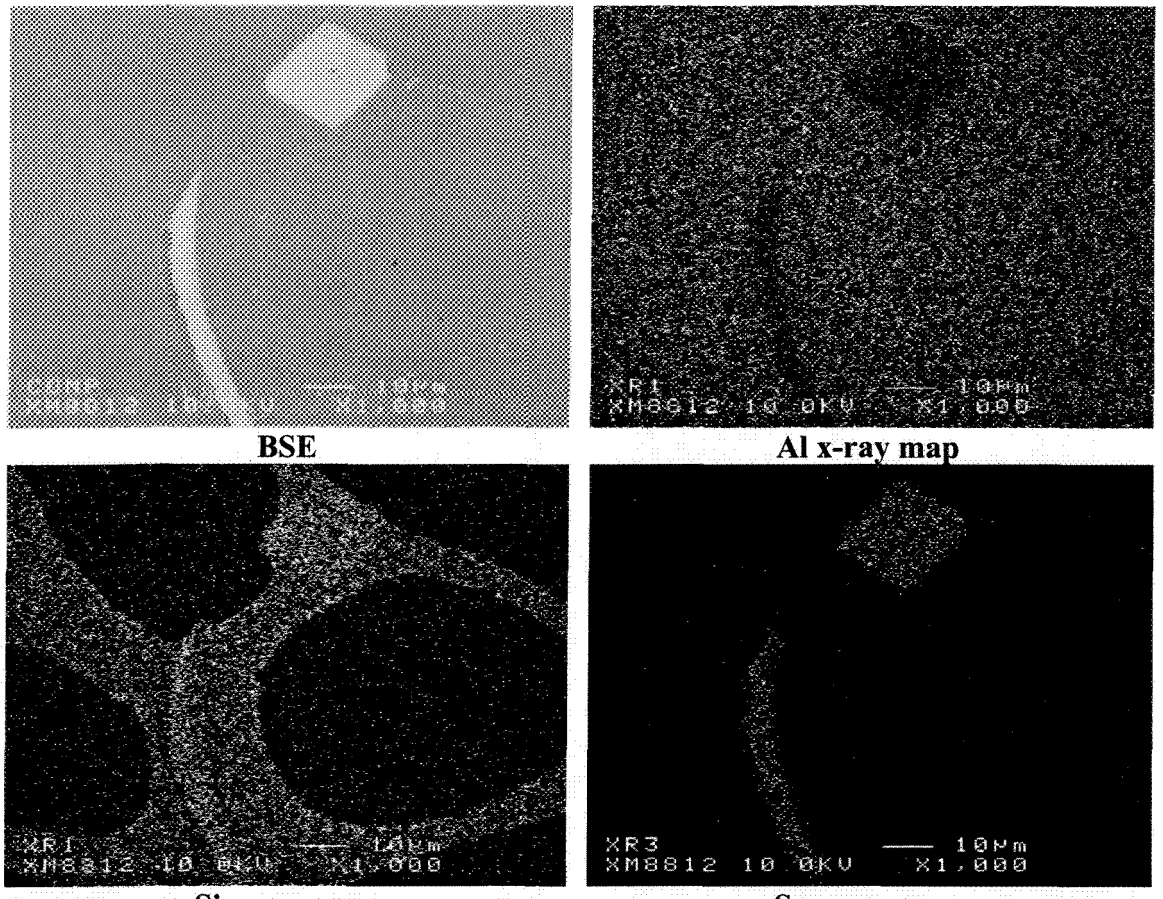

Figure 6.24: Back scattered electron micrograph and respected x-ray maps of the intermetallic particles formed due to Sr addition (768ppm Sr)

Table 6.4: Microprobe analysis of the Sr-based intermetallics, (at. %)

Al	B	Ti	Si	Mg	Sr	Fe
39.90	2.97	0	39.13	0.01	17.98	0
40.56	0	0	40.71	0	18.73	0
39.24	0	0	42.46	0	18.29	0

6.3.2.2 SEM analysis

The SEM analysis of the non-modified deep-etched SEED billets, Figure 6.25a, suggests the plate like silicon crystals to have grown out of individual nucleation sites, while the modified structure consist of highly branched silicon fibers, but with much lower number of isolated fibers. As for instance, the Si in Figure 6.25b mainly consists of one highly branched fiber with its origin, nucleation point, arrowed.

The inter-lamellar/inter-rod spacing appears to have decreased in the SEED billets when Figures 6.20 and 6.25 are compared. Such refinement is partly due to the quenching of SSM slurries from the mushy zone and partly due to the fluid flow and thermal uniformity within the SSM mold. This means that the branching of Si fiber is not hindered and it can branch in any direction, since there is not any directional heat flow within the mold. From the modification mechanism point of view, in the presence of chemical modifier, both the twining frequency and the angle of branching increase with freezing rate, both of which promote modification and formation of finer structures [84]. The high frequency for branching with Sr addition requires a new terminology for the fibrous growth morphology as proposed here, *"pine-like growth"* as well depicted in Figure 6.26.

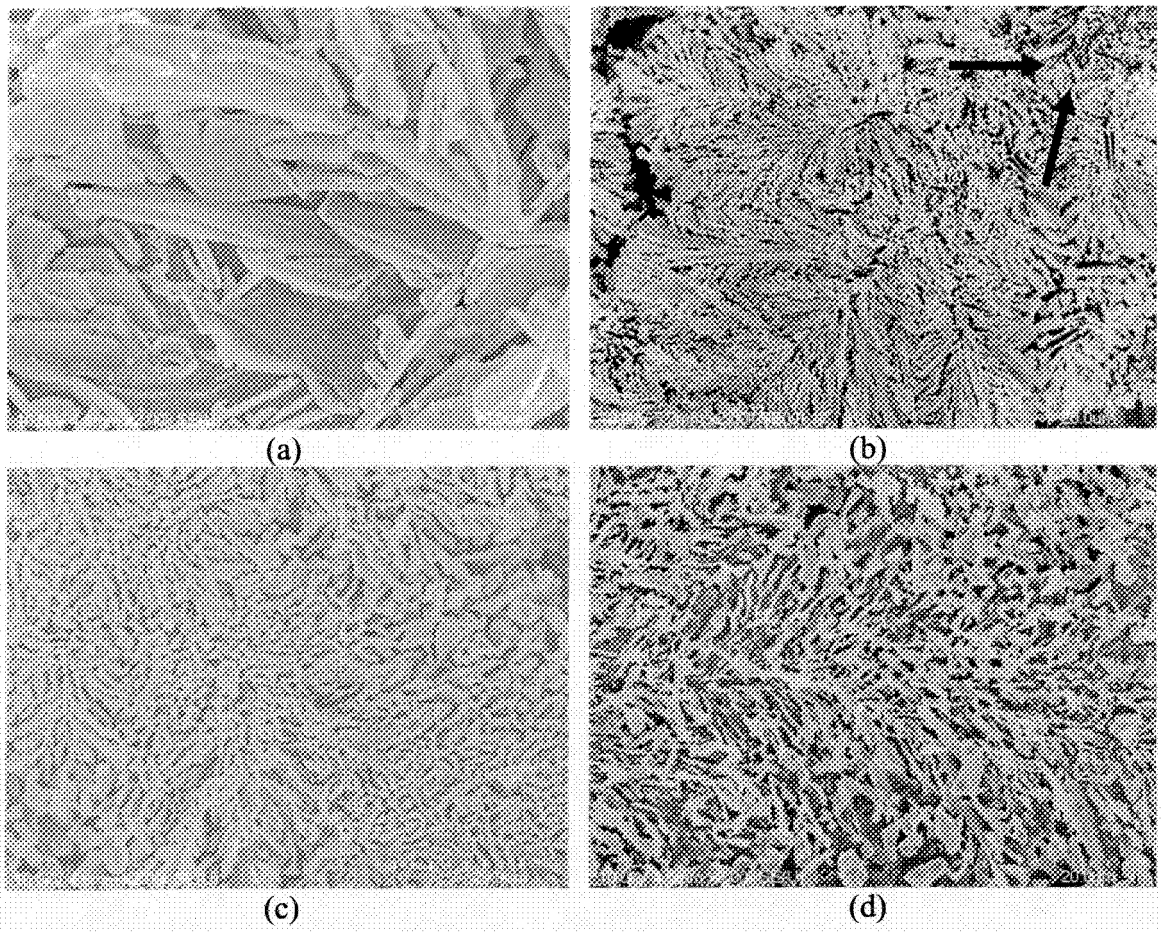

Continue ⟶

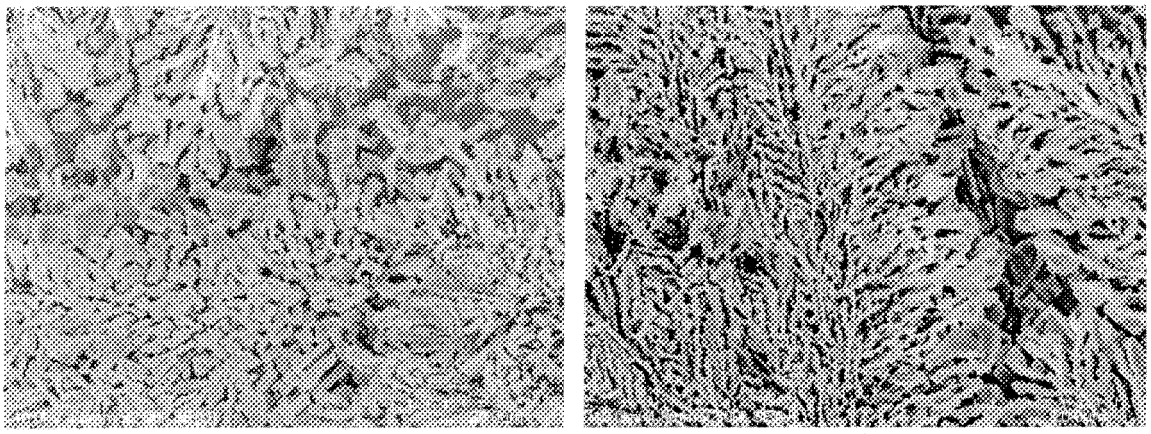

(e) (f)

Figure 6.25: Scanning electron micrographs of the deep etched (10%HF) SEED billets to show morphological changes of eutectic Si with Sr addition; (a) without Sr, (b) 47ppm Sr, (c) 74ppm Sr, (d) 156ppm Sr, (e) 302ppm Sr, and (f) 768ppm Sr

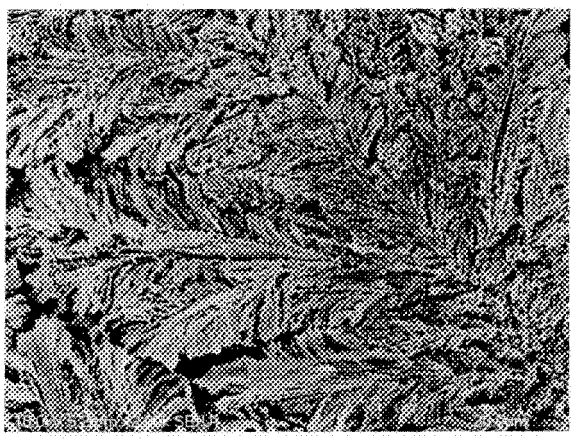

Figure 6.26: Scanning electron micrograph showing the pine-like Si morphology and its frequent branching for the SEED billet modified with 47ppm Sr

6.3.2.3 Image analysis

As shown in Figure 6.22, the Sr-modified silicon particles are too small to be resolved by optical microscopy and therefore the quantitative results are only given for the primary α-Al particles.

The percentage of the primary α-Al particles increases slightly with the addition of Sr (Figure 6.27a). As mentioned before, with addition of Sr, the eutectic line moves downward with the eutectic point shifting to the right, thus expanding the α-Al freezing range of the alloy and increasing the fraction of primary α-Al. This is of great importance in

the SSM processing since a wider solidification range renders more flexibility in SSM processing especially when the commercialization of the process is intended.

The average circular diameter increases with Sr addition while the number density remains approximately constant (Figures 6.27b,c). This is in line with the increase in the primary α-Al percentage since the equivalent circular diameter should increase to preserve the balance between all the equations. The area/perimeter ratio also increases with Sr addition in support of the findings for the average circular diameter (Figure 6.27d).

In order to further highlight the globularization effect of the SEED process with Sr addition, the percentage of primary α-Al particles having aspect ratio above 2 was measured and presented in Figure 6.27e. The reducing trend in this figure is an indication of better globularization of the primary α-Al particles with Sr addition. The percentage of sphericity values greater than 0.8 also confirm such conclusion, see Figure 6.28a. With modification, the percentage of particle having sphericity closer to one increases which is an indication of the particles approaching to spherical morphology.

The drainage of the remaining liquid increases with Sr addition to further confirm previous finding where Sr improves the flowability of the alloy [75]. From dendrite coherency point (DCP) of view, it was reported [78] that modification postpones the DCP point in conventional casting in spite of increasing α-Al percentage. For SSM processes, the concept of DCP is different since there is no dendrite formation and therefore, dendrite interlocking is prevented. Therefore, better flowability may be attributed to the formation of more continuous and smooth liquid channels in the semi-solid structure. However higher values of strontium decreases the flowability of the remaining liquid due to the formation of Sr-based intermetallics.

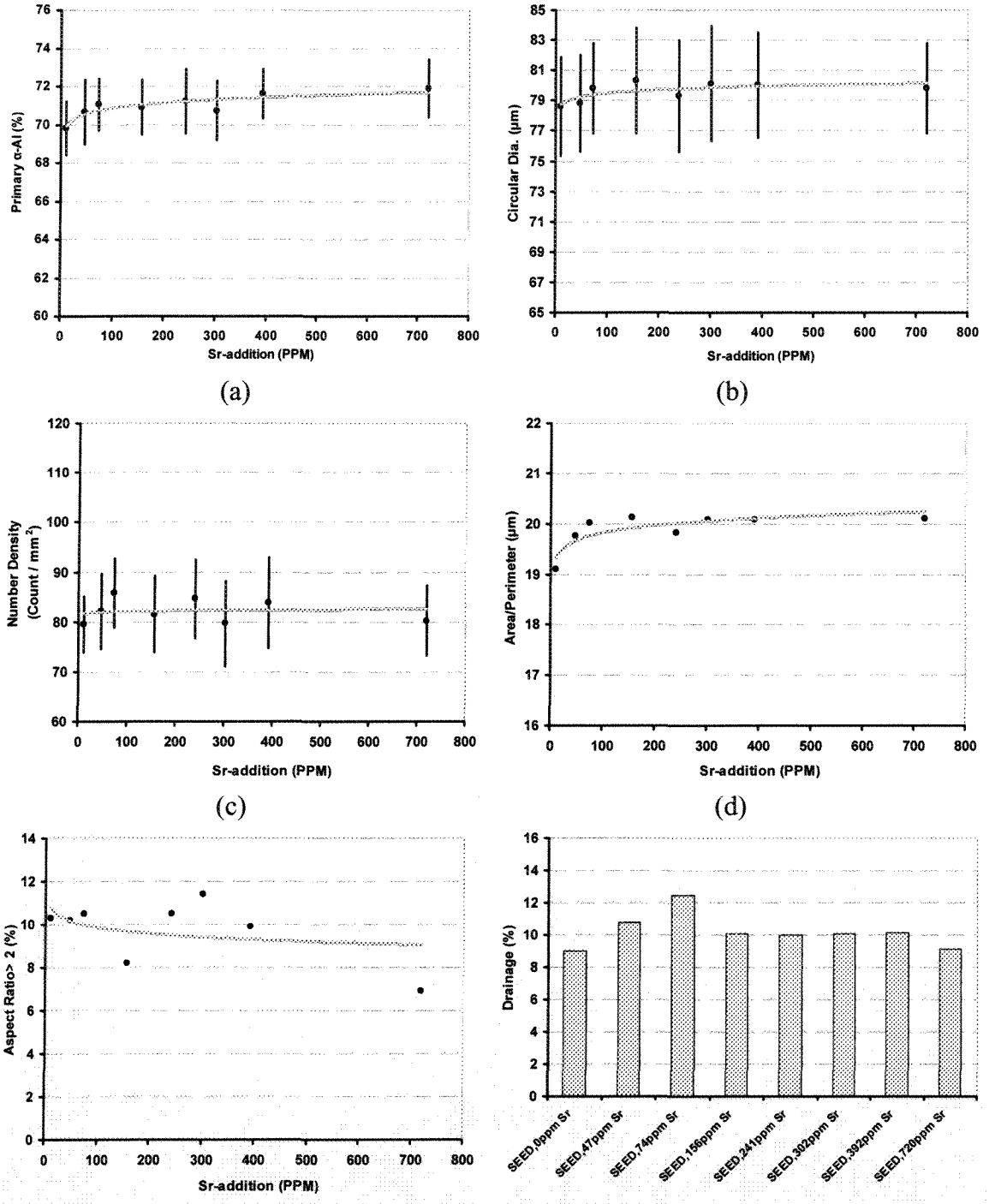

Figure 6.27: The image processing data of the primary α-Al particles in the Sr-modified A356; (a) primaryα-Al percentage, (b) average circular diameter, (c) number density, (d) area/perimeter, (e) percentage of particles having aspect ratio > 2 and (f) drainage percentage of the remaining liquid

The concept of sphericity was used to better understand the role of modification on the morphology of the primary α-Al particles. Figure 6.28 shows the percentage of α-Al particles with sphericity greater than 0.8. With modification, the percentage of particles having sphericity values closer to one increased with Sr.

During SSM processing, the globules form in the mushy zone where there is neither any eutectic silicon nor other compounds present. Therefore the question may arise as "why should modification have any influence on the primary α-Al morphology?". It is believed that any variation in the surface tension of the alloy plays an important role on the globularization of α-Al particles. Previously, it was reported that Sr and Na decrease the surface tension of the melt [103,104]. By decreasing the surface tension, wetability of primary α-Al particles by the remaining liquid is improved. This is equivalent to having more contact between the remaining liquid and primary α-Al. Decreasing the surface tension causes more flow around the α-Al particles and consequently renders enhanced shaving and trimming of these particles and therefore causes the formation of more spherical and rounder particles.

During stirring, thermal and solutal homogenization takes place and with consideration of better fluidity due to lower surface tension and better wetability, it may be true to conclude that the flow around particles could smooth off primary α-Al particles better and thus rounder particles are obtained.

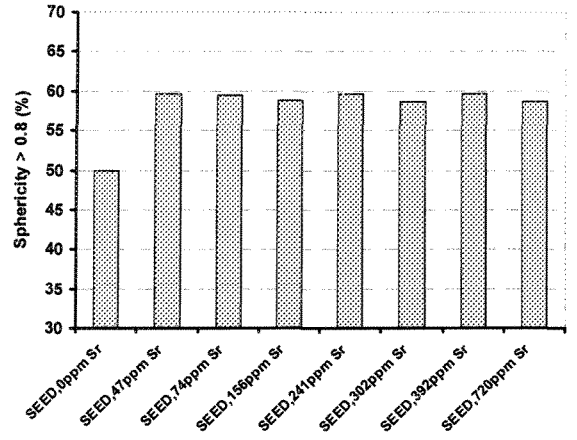

(a)

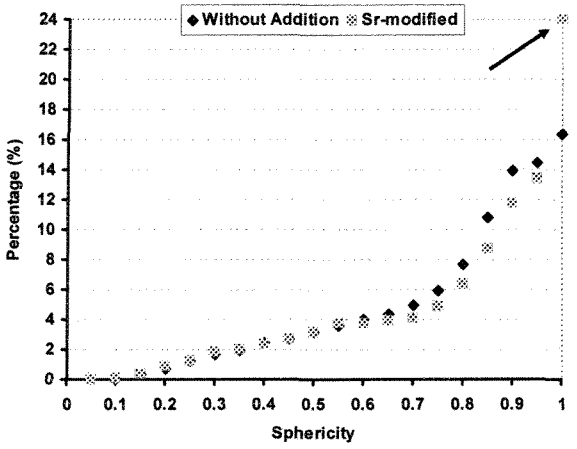

(b)

Figure 6.28: (a) Variation of sphericity with Sr addition, (b) data classification without and with 156ppm Sr

CHAPTER 7

RESULTS AND DISCUSSION
COMBINED EFFECT

CHAPTER 7

RESULTS AND DISCUSSION – COMBINED EFFECT

7.1 Combined effect in A356 alloy

7.1.1 Addition of titanium, boron, and strontium

The aim of these series of tests is to reach a conclusion in a simultaneous addition of refiner and modifier to the alloy, i.e., the combined effect. The optimum additional level was measured from the previous experiments and the final chemical compositions are listed in Table 7.1.

Table 7.1: Chemical analysis for before and after treatment (wt. %)

	Si	Mg	Fe	Mn	Cu	Ti	B	P	Sr	Al
Base alloy	6.68	0.4	0.07	0.003	0.001	0.0058	0.0001	0.0003	0.000	bal.
Treated alloy	6.68	0.39	0.08	0.003	0.001	0.058	0.0098	0.0003	0.014	bal.

7.1.1.1 Conventional casting

7.1.1.1.1 Thermal analysis

Figure 7.1 is the nucleation and growth segments of typical cooling curves for primary α-Al formation and eutectic reaction of both untreated and treated alloys. As it is evident, the nucleation and growth temperatures have shifted up for primary α-Al, while the eutectic reaction has been suppressed to lower temperatures as a result of grain refiner and modifier co-addition.

From solidification point of view, Figure 7.1a, at a given cooling rate, as the temperature falls below the nucleation temperature $Tnuc_{Al}$, nucleation rate rises exponentially to such an extent that compensates heat extraction and eventually overrides it after the minimum temperature, $Tmin_{Al}$. In other words, the evolution of latent heat retards the cooling rate up to the minimum and thereafter the melt is reheated to Tg_{Al} due to mainly growth of primary nuclei. It is quite important to note that by the time recalescence is completed, all nucleation opportunities are ceased and the final grain density is predictable.

The effects of separate sole additions of refiner and modifier to A356 Al-Si alloy are reported before in sections 5.2.1 and 6.2. Sole addition of grain refiner lifted up nucleation temperature by as much as 4-5°C, while sole addition of Sr-based modifier depressed eutectic temperature by almost 7-8°C. In other words, if both additives performed the same way for the combined case, the solidification range should increase by 11-13°C which is the case for combined addition. Although widening solidification range may not be regarded important for conventional casting or even be a drawback due to increasing the incident of porosity, but surely it is quite crucial for SSM processes. Furthermore, development of wider freezing range slows down directional solidification which is again a positive point in SSM processing.

As mentioned before, small addition of Ti and B shifted the curves up and recalescence decreased. In other word, addition of grain refiner has catalyzed the nucleation of primary α-Al sooner and with more nuclei in the melt. Furthermore, both nucleation and growth temperatures of α-Al particles increased but the temperature rise is greater for $Tnuc_{Al}$ as clearly seen in Figure 7.2a. This means that there are more nuclei with lower chance of growth at any one time during nucleation and early growth of primary phase.

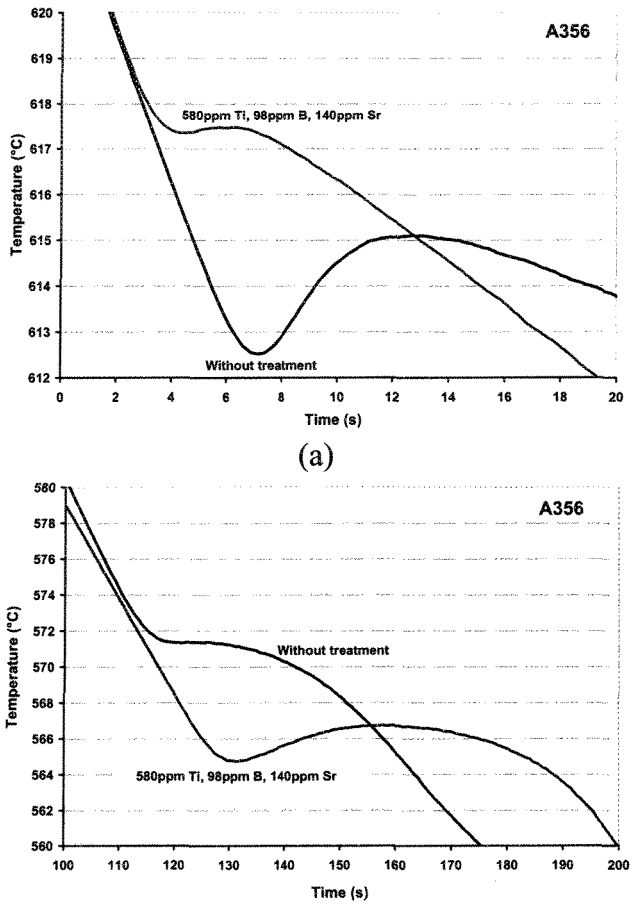

(a)

(b)

Figure 7.1: Cooling curves before and after additions:
(a) beginning of solidification, (b) eutectic reaction zone

Figure 7.2b presents the variations in $Tnuc_{eut}$, $Tmax_{eut}$, $\Delta\Theta$, and ΔT_α due to combined treatment. As mentioned before, the changes in eutectic TA parameters are the same for sole and combined treatments which may confirm the independent function of grain refiner and modification during solidification. In other words, the strong affinity of B for Ti to form TiB_2 nucleants impedes any reaction between Sr and B to form SrB_6 compounds and thus inactivate Sr as a modifier. It is evident from Figure 7.2b that the eutectic nucleation temperature and eutectic maximum temperature decrease with Sr addition. The eutectic recalescence, $\Delta\Theta$, also increased by ~2°C with 140ppm Sr. Also depression of the eutectic temperature causes larger α-Al solidification range and consequently more α-Al formation. The interesting point here is that increasing in ΔT_α is a

bit more here comparing the Sr addition alone since with refiner addition, nucleation temperature of α-Al particles increased and it causes greater solidification range.

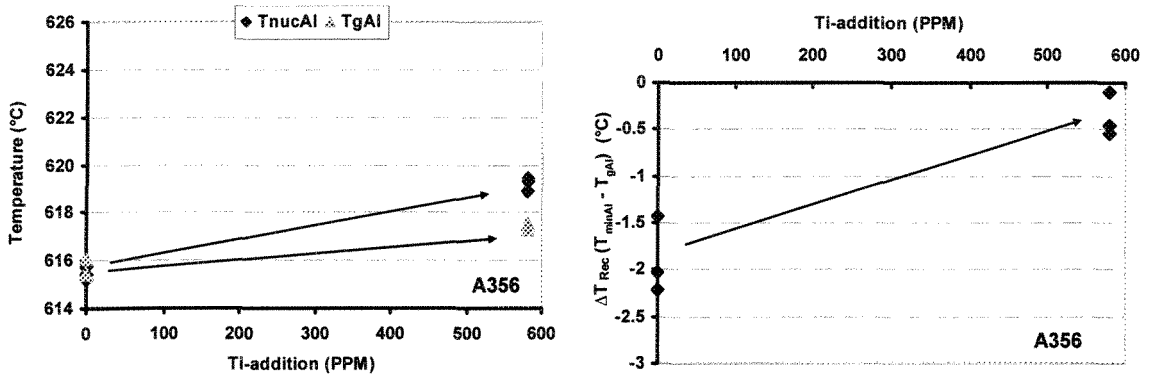

(a)

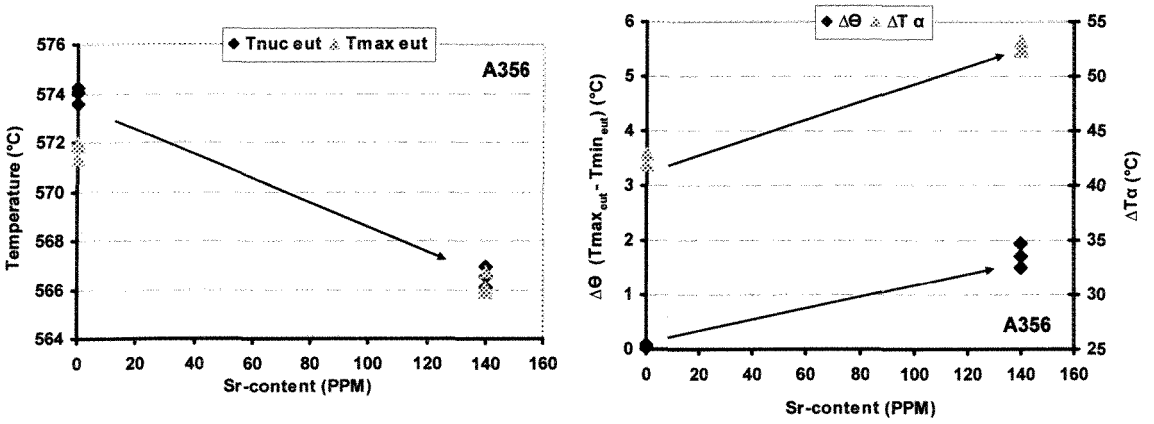

(b)

Figure 7.2: Variation of: (a) nucleation and growth temperature of α-Al particles due to grain refiner effect, (b) nucleation, maximum, and recalescence of eutectic and ΔT_α due to modifier effect

7.1.1.1.2 Structural analysis

The optical micrographs in Figure 7.3 depict microstructural changes due to combined treatment. The primary α-Al phase has a fully columnar (dendritic) structure in the untreated specimen but transforms to equiaxed morphology with combined addition. Such effect is believed to be solely due to grain refiner segment of combined treatment (dark areas are porosities). The eutectic mixture is also affected by this treatment where the flake silicon in Figure 7.3a has fully transformed to fibrous, Figure 7.3b, due to Sr content.

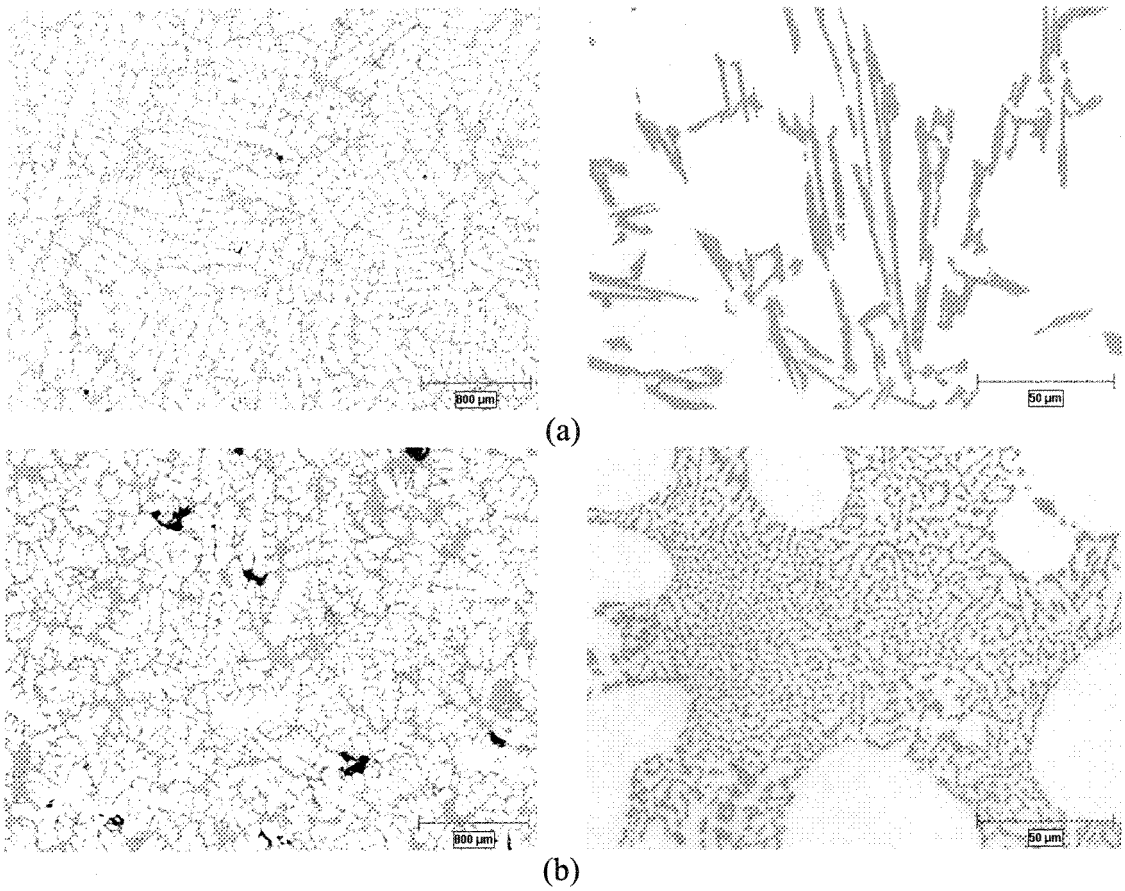

Figure 7.3: Optical micrographs for showing the effect of simultaneous melt treatment: (a) Without addition, (b) 580ppm Ti, 98ppm B, 140ppm Sr

7.1.1.1.3 SEM analysis

The Sr content of the combined treatment modifies the morphology of eutectic Si as shown by the two SEM micrographs in Figure 7.4 where the flaky structure of silicon changes to fibrous and the seaweed like structure is visible.

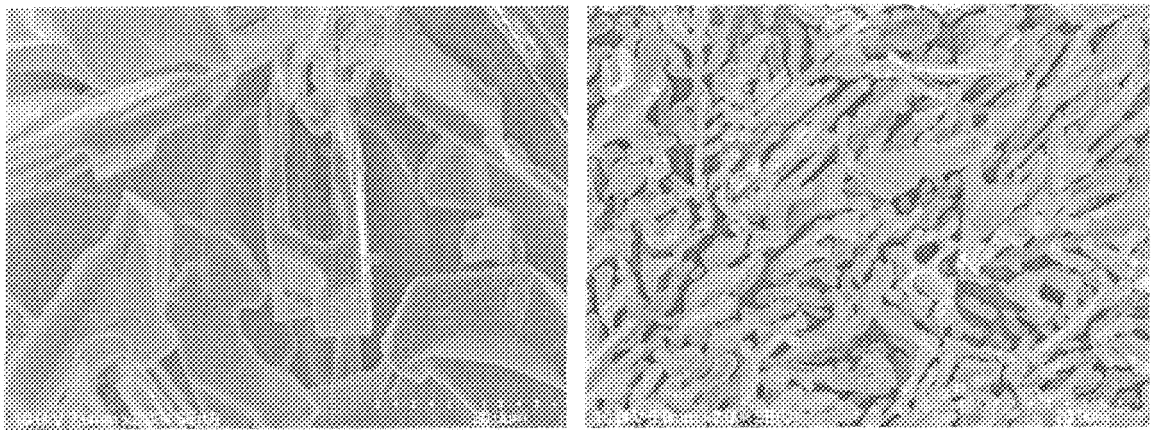

(a) (b)

Figure 7.4: Scanning electron micrographs of the selected samples, deep etched in 10%HF: (a) without addition, (b) 580ppm Ti, 98ppm B, 140ppm Sr addition

7.1.1.2 Semi-solid processing

7.1.1.2.1 Structural analysis

The optical micrographs in Figure 7.5 show the effect of combined treatment. Grain refining efficiency is obvious through globules size reduction and more primary particles, while modification effect could be seen at higher magnification by morphological changing of silicon particles from lamellar to fibrous (Figure 7.6).

The effect of combined treatment on rendering better globularity of primary α-Al particles could also be explained in terms of the modifier and its effect on silicon morphological changes. This is due to the growth nature of the fibrous structure of Si in the eutectic mixture which encompasses the primary α-Al phase without being a continuation of it. Therefore, the globules are indeed true globules when Sr is added. As shown by Dahle et al. [197], in unmodified alloy, the eutectic grows from the primary phase, while for Sr-modification eutectic grains nucleate and grow separately from the primary dendrites.

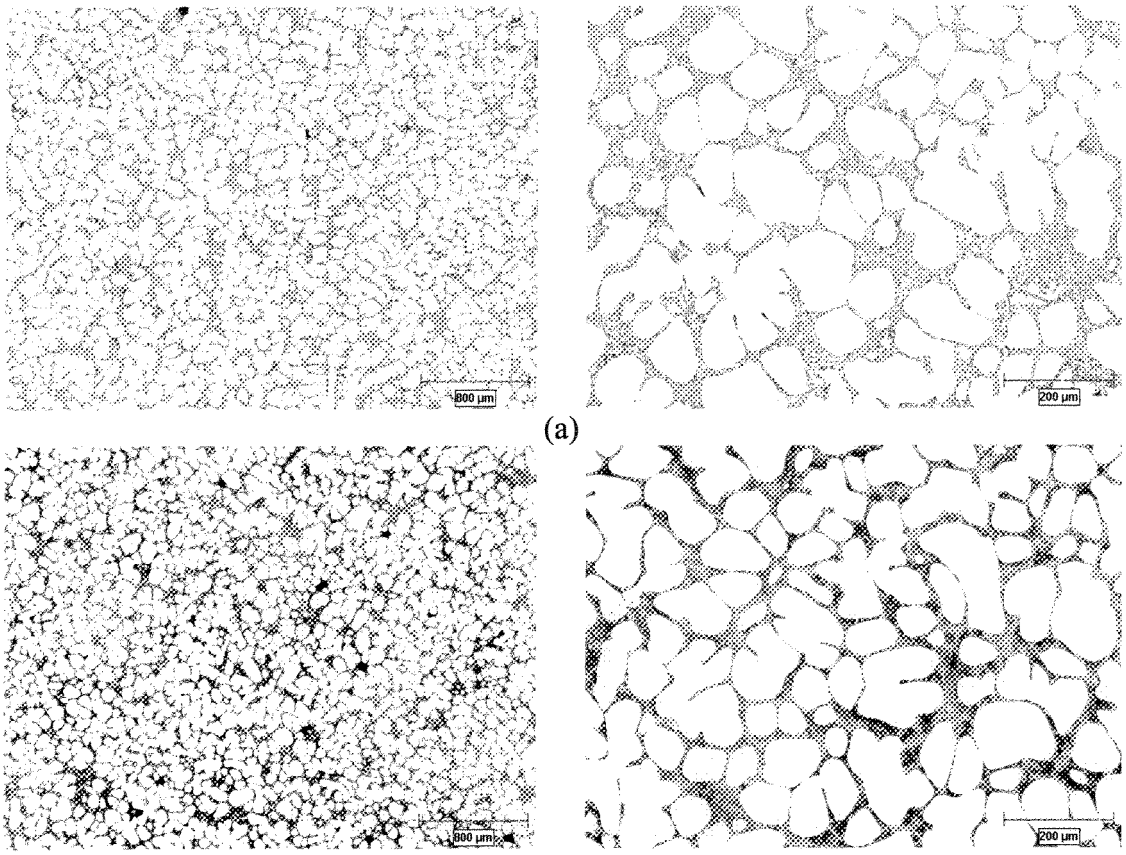

Figure 7.5: Optical micrographs presenting the effect of simultaneous melt treatment: (a) Without addition, (b) 580ppm Ti, 98ppm B, 140ppm Sr

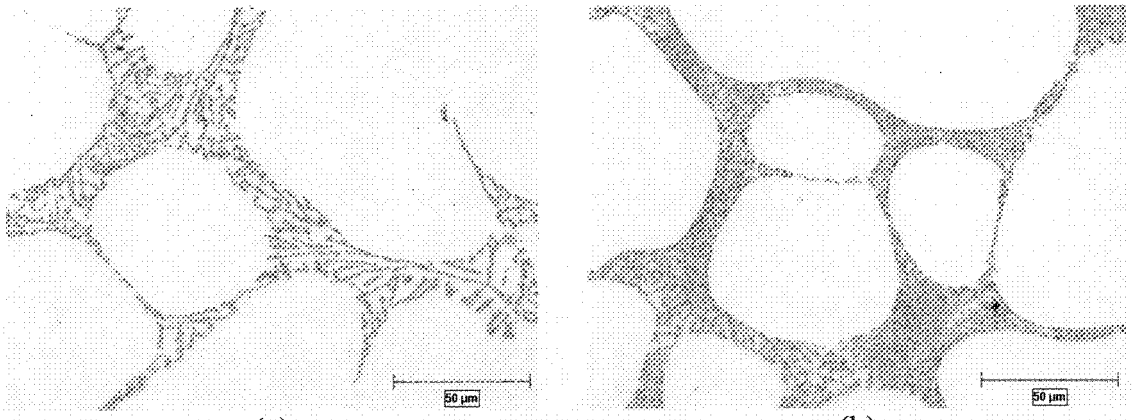

(a) (b)

Figure 7.6: Variation of silicon morphology due to Sr addition: (a) without Sr (b) 140ppm Sr

One of the key parameters in alloy design for SSM processing is the solidification range. That is why pure metals and eutectic alloys are not suitable for the SSM processes. This is quite important both scientifically and technologically since the formation of spherical solid particles, as the most desired form, depends on the temperature range where morphological evolution, i.e., dendritic to globule transition, may take place if appropriate conditions are met. As shown in sections 5.2.1.2 and 6.3.1.1, by individual refiner addition, ΔT_α increases by ~6°C while by sole modification, α-Al solidification range raises by ~10°C. Figure 7.7 shows variation of ΔT_α and ΔT_{eut} due to the combined addition. As seen, combined addition enlarges the ΔT_α by more than ~12°C.

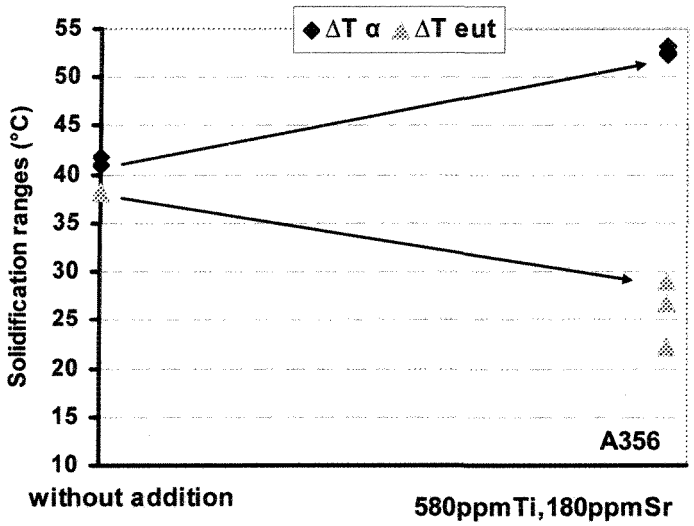

Figure 7.7: Effect of combined addition on the solidification range

7.1.1.2.2 SEM analysis

The morphological changes of silicon due to the combined treatment are illustrated by the SEM micrographs in Figure 7.8. The flaky structure of silicon has changed to fibrous morphology having seaweed like characteristic. Furthermore, in contrast to the conventional cast specimens, Figure 7.4, extra refinement of the structure is attributed partly to the quenching of SSM slurries from mushy zone and partly to fluid flow and thermal uniformity within the SSM mold. This means that the branching of Si fiber is not hindered and it can branch in any direction, since there is not directional heat flow in the mold.

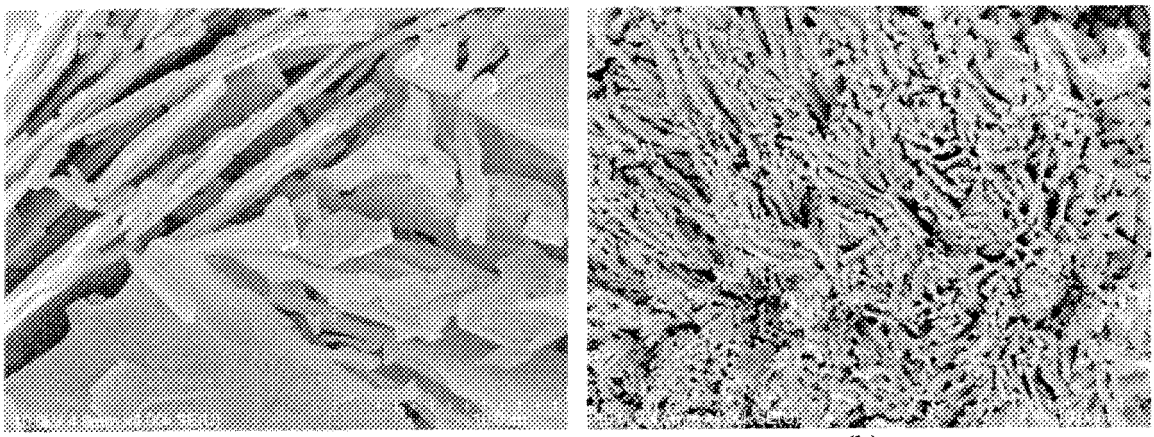

(a) (b)

Figure 7.8: SEM photos of the selected SEED samples, deep etched in 10%HF, (a) Without addition, (b) 580ppm Ti, 98ppm B, 140ppm Sr addition

By comparing Figure 7.4 and 7.8, it is obvious that interlamellar spacing decreased by higher cooling rate. Decreasing both flake and fibrous inter-lamellar/inter-rod spacing and size could also be interpreted according to the eutectic growth calculation. As it was shown [23], interlamellar spacing, λ, has an inverse relation with the rate of interface movement, v, as follow:

$$\lambda^2 v = \text{constant} \qquad (7.1)$$

This equation indicates that increasing the rate of interface movement by mean of higher cooling rate could lead to small interlamellar spacing as shown by comparing Figures 7.4 and 7.8 or 7.3 and 7.6.

7.1.1.2.3 Image analysis

As discussed in the previous sections, the scale of structure is quite fine in the SSM billets and optical quantitative metallography was not possible for the eutectic silicon. Therefore, the results as presented in Figure 7.9 are solely concentrated on the primary α - Al phase.

The primary α-Al percentage appears to have increased which is due to higher number of effective nuclei from the refining side plus increasing the α-Al solidification

range due to Sr, Ti, and B additions. It was given before that combined treatment increased the α-Al solidification range by 11-13°C.

It was shown that by sole modification, the number density of primary α-Al particles remained unchanged while its quantity increased and hence the average circular diameter rose. This is not the case for combined treatment as shown in 7.9b, where the average circular diameter decreased slightly but the raise in number density is more pronounced. This is attributed to grain refining effect in shifting the nucleation temperature to higher values and rendering more nuclei to form per unit volume. The greater number of nuclei compensates the enlargement of solidification range due to combined treatment. Furthermore, the average A/P ratio is approximately constant while the percentage of α-Al particles with aspect ratio >2 decreases. Such finding coupled with the increasing of sphericity values as shown in Figure 7.9d, is an indication of improving globularity of the structure.

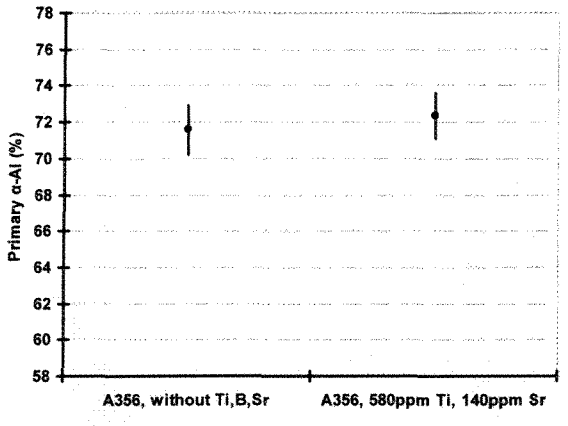

(a)

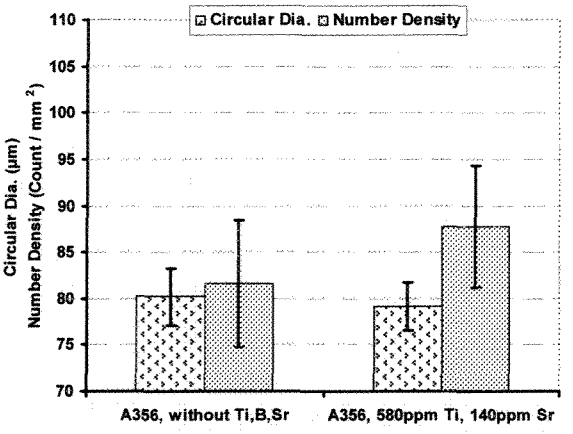

(b)

Continue ⟶

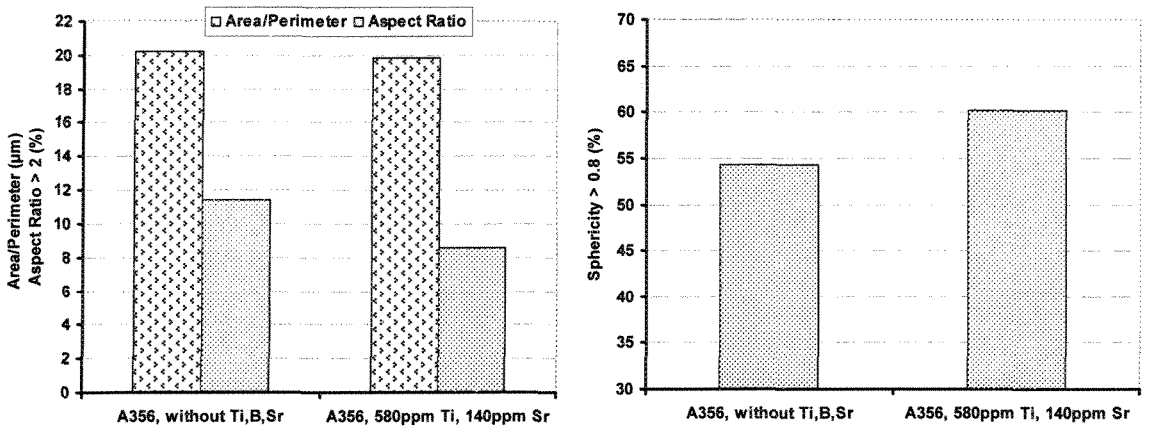

(c) (d)

Figure 7.9: Different parameters of SEED samples:
(a) primary α-Al percentage (b) circular diameter and number density of α-Al particles, (c) Area/perimeter and percentage of α-Al particles having aspect ratio >2, and (d) % of particles having sphericity > 0.8

As mentioned in the experimental procedure, drainage is a part of SEED process to provide a self standing billet, but it is believed that it can also be an indication of fluidity of the alloy. Here it has to be noticed that this may be contradictory to classical meaning of fluidity which is normally defined as the distance to which a metal will run before solidification. The drainage percentage increased with combined treatment as seen in Figure 7.10. Such finding may look contradictory to the fact that by increasing primary α-Al percentages drainage should decrease due to the agglomeration and blockage of the mold bottom orifice.

Drainage augmentation could be explained from different aspects. According to the literature on conventional casting [78], dendrite coherency point, DCP, has a direct relationship with the fluidity concept where a postponed DCP improves fluidity, i.e. smooth channels without interlocking pathways for liquid flow. While on the other hand, from modification point of view, Sr postpones the DCP and it means that in spite of increasing α-Al percentage, more flow exists in the slug. This is supported by better sphericity numbers where more globular particles are formed with the combined treatment. That is to say there are smoother inter-particle channels for liquid to flow. These are in line with increasing of fluidity of modified and refined alloys [75-77].

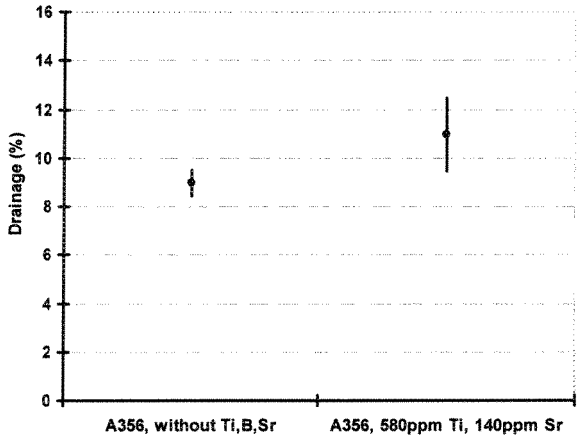

Figure 7.10: Drainage of liquid from closure during SEED process

7.1.2 Addition of boron and strontium

The optimum additional levels of boron were reported in sections 5.2.2. and 5.2.3 and for the strontium in section 6.3. The selected chemical composition of the mixed addition is therefore based on these findings and given in Table 7.2.

Table 7.2: Chemical analysis of A356 alloy before and after treatment (wt. %)

	Si	Mg	Fe	Mn	Cu	Ti	B	P	Sr	Al
Base alloy	6.66	0.4	0.07	0.002	0.001	0.0057	0.0001	0.0003	0.000	bal.
Treated alloy	6.6-6.8	0.38-0.4	Max0.07	Max0.003	Max0.001	Max0.004	0.02	0.0003	0.01-0.014	bal.

7.1.2.1 Conventional casting

7.1.2.1.1 Thermal analysis

The effect of sole refiner and modifier additions to the A356 alloy was illustrated previously, see sections 5.2.3 and 6.3. Figure 7.11a compares the cooling curves at the early stages of solidification for both untreated and B+Sr treated alloys. The combined melt treatment appears to be quite effective in decreasing the recalescence in the bulk liquid with the added bonus of lowering the eutectic reaction due to the strontium addition as shown in Figure 7.11b. The resulting thermal data extracted from further analysis of the cooling curves are plotted in Figure 7.12. In the untreated alloy, the recalescence is about 2°C and nucleation and growth temperatures of the primary phase are ~ 615-616°C (Figure 7.12a) while with the refiner effect, both temperatures increased and recalescence decreased. In the eutectic reaction zone, Figure 7.12b, Sr-modification causes lower eutectic nucleation temperature and the related recalescence also increased.

Comparing the results with the sole boron addition indicates that increasing of nucleation and growth temperatures of primary α-Al particles is slightly greater in the sole B-treated alloy and the recalescence for combined treatment could not reach zero. This is the main explanation for larger grain size in B-Sr treated alloys as will be described later.

From modification point of view, Sr decreases the nucleation and maximum temperatures of the eutectic and thus increasing the α-Al solidification range (Figure 7.13).

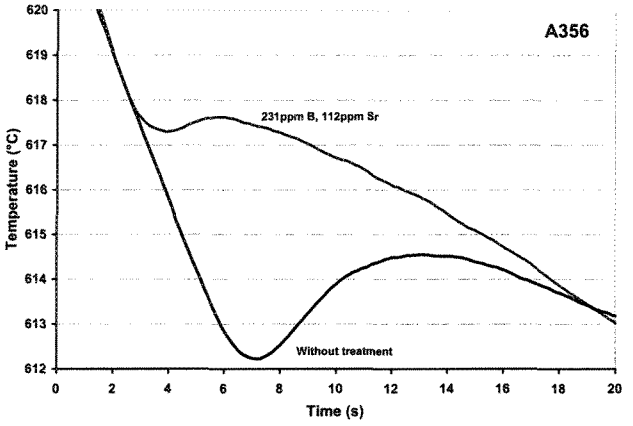

(a)

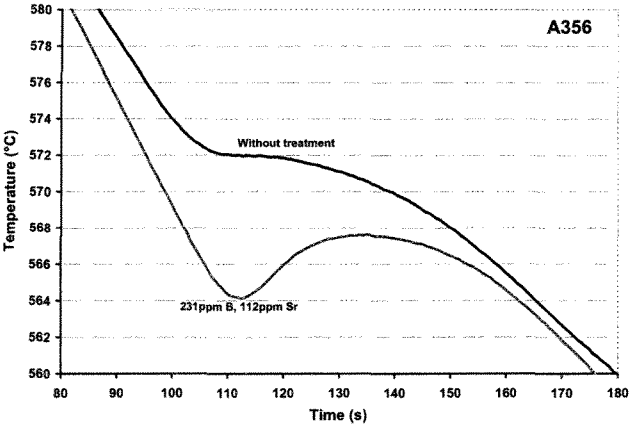

(b)

Figure 7.11: (a) Commencement of solidification with combined B-Sr treatment, (b) eutectic reactions

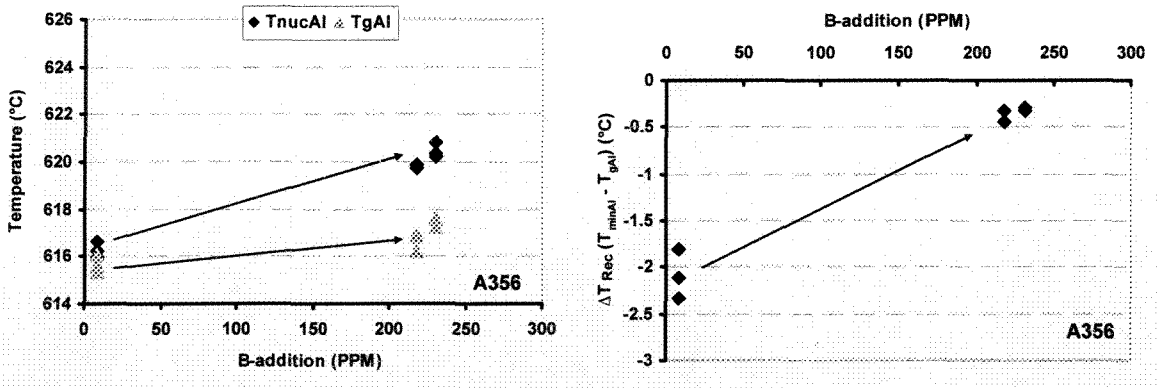

(a)

Continue

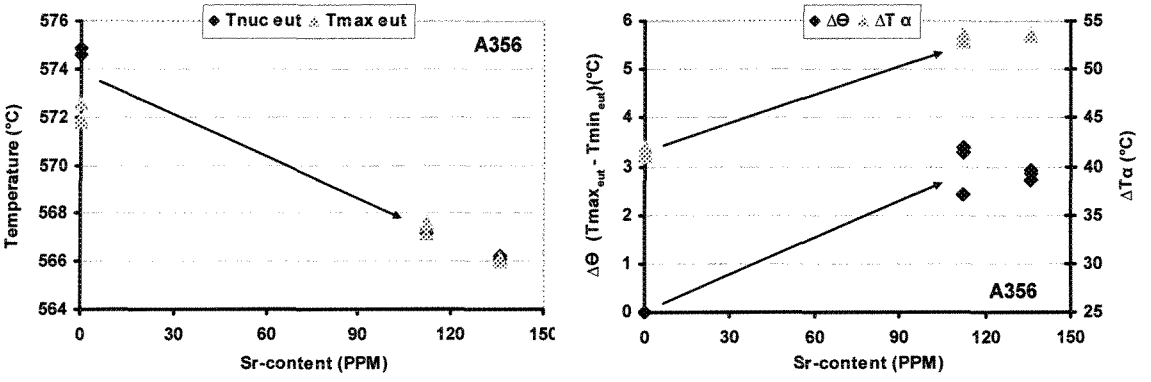

(b)

Figure 7.12: Variation of: (a) $Tnuc_{Al}$, Tg_{Al}, and ΔT_{Rec} due to the refiner, (b) $Tnuc_{eut}$, $Tmax_{eut}$, $\Delta\theta$, and ΔT_{α} due to modifier addition

As discussed in sections 5.2.2 and 5.2.3, boron is the most effective refiner for A356 alloy. With Sr addition and its reaction with B, the overall percentages of Sr and B to act as refiner and modifier respectively decrease and thus could not be as effective as those of sole addition (Figure 7.13). As it will be discussed later, Sr and B react and form SrB_6 compounds according to following reaction:

$$Sr + 6B \rightarrow SrB_6 \qquad (7.2)$$

This reaction shows that each Sr atom could react with six B atoms and form SrB_6 compound. According to appendix A and the disregistry values, both SrB_6 and TiB_2 could act as nucleant but it should be considered that boron consumption in the compound is one of the key parameters. It means that AlB_2 consumes less amount of boron comparing to SrB_6 and as a result by considering a constant amount of boron, the density of nucleant particles is much higher in the case of AlB_2 as lower number of boron atoms are associated with this compound. Therefore by greater number of potent nucleants, the probability of having lower grain size is increased.

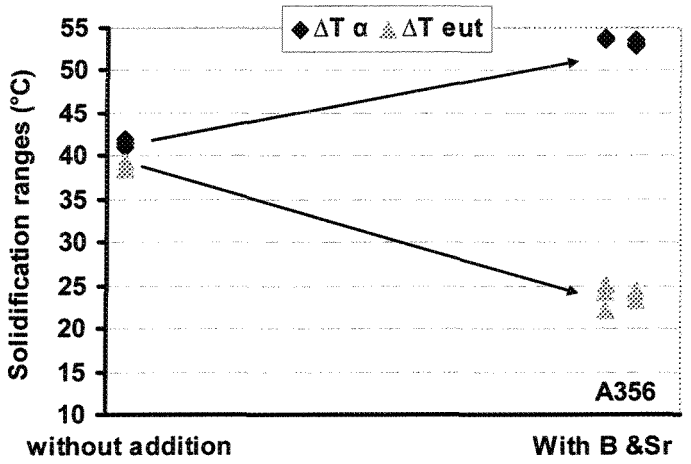

Figure 7.13: Effect of combined addition to the solidification range

7.1.2.1.2 Structural analysis

The microstructural transformation due to the combined addition is shown in Figure 7.14. From a refiner stand point, the microstructure obviously changes from columnar to equiaxed. This is attributed to the large number of nucleants dispersed within the bulk liquid to initiate nucleation and coupled with multidirectional growth to end up with an equiaxed structure. As mentioned, the formation of boron-based compound particles is the main reason for structural refinement. Interestingly, by formation of SrB_6 compounds and decreasing of the free Sr atoms in the liquid, the remaining Sr atoms are not capable of altering the morphology of the eutectic silicon to fibrous and as a result the acicular silicon morphology only changes to flakes.

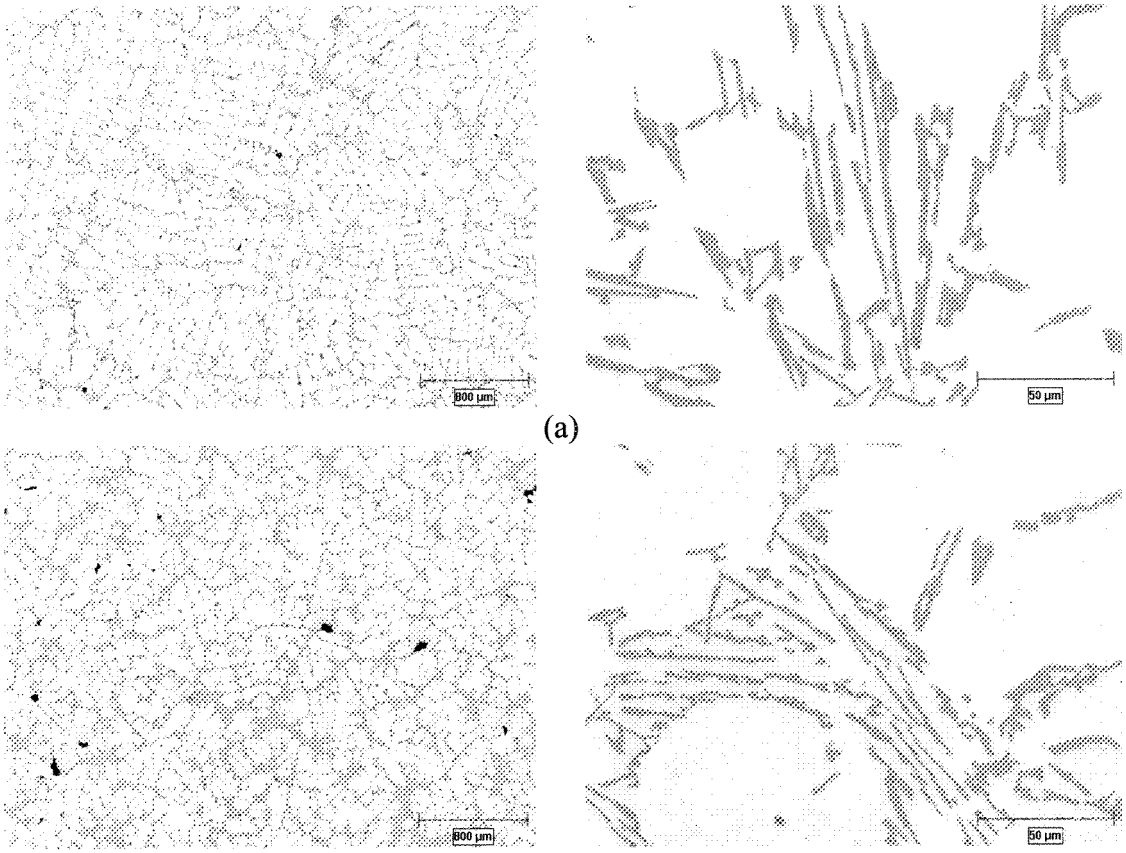

Figure 7.14: Micrographs representing the effect of simultaneous melt treatment: (a) Without addition, (b) 231ppm B, 112ppm Sr

As mentioned before, there is a strong affinity between Sr and B and following addition to the alloy these elements react and form SrB_6. Therefore, most of the boron atoms which should be utilized for refining purposes are consumed to form this compound. As it will be shown in the appendix A, SrB_6 has a low disregistry with the matrix but its boron consumption is high (six atoms) and that is why effective and full refining failed. On the other hand, due to this reaction, Sr is also removed from the melt and hence there is less strontium available for modification. The result is partial refining and modification. Figure 7.15 shows boron-based intermetallics at different addition levels.

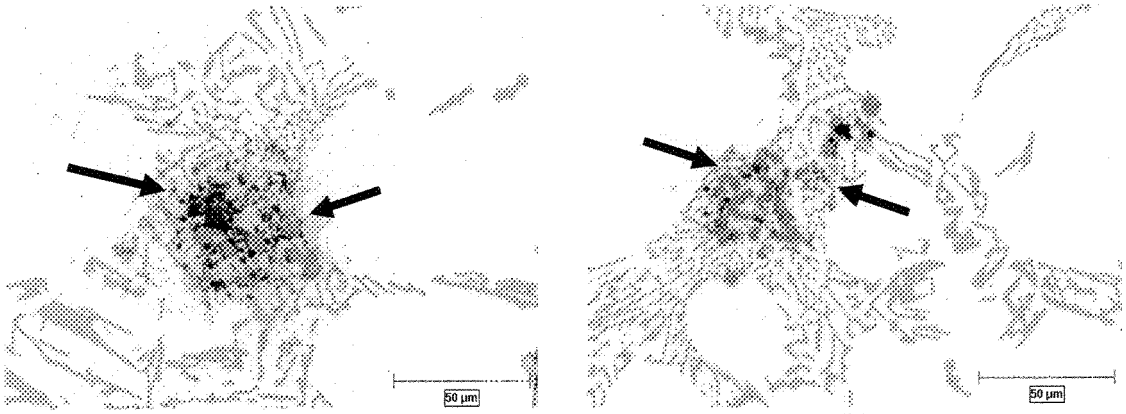

(a) (b)

Figure 7.15: Intermetallics formation and agglomeration due to:
(a) 231ppm B, 112ppm Sr, (b) 218ppm B, 136ppm Sr

7.1.2.1.3 SEM analysis

Figure 7.16 shows the scanning electron micrographs of selected graphite mold samples. It is evident that with Sr addition, the flaky structure of silicon still remains.

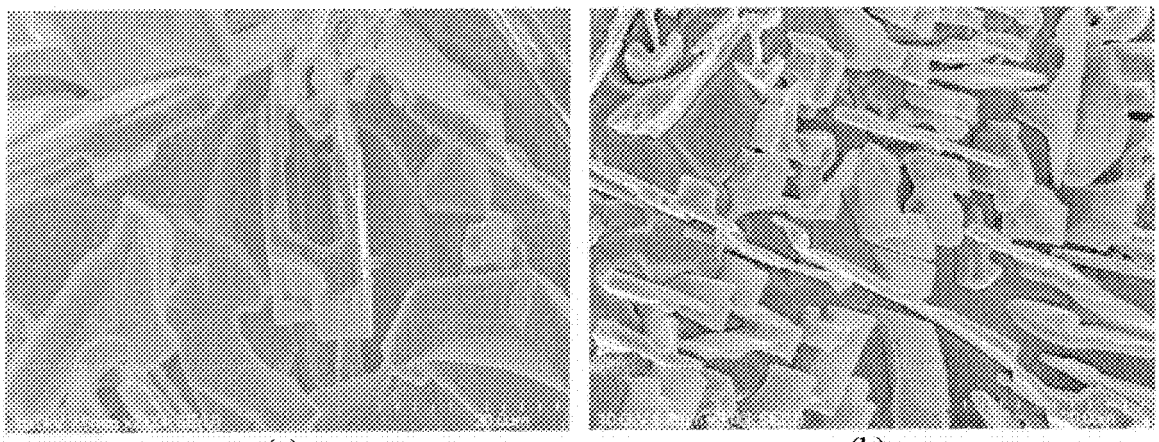

(a) (b)

Figure 7.16: Scanning electron micrographs of the selected samples, deep etched in 10%HF, (a) Without addition, (b) 218ppm B, 136ppm Sr addition

7.1.2.2 Semi-solid processing

7.1.2.2.1 Structural analysis

The optical micrographs in Figure 7.17 show the effect of combined melt treatment with B and Sr. The addition of inoculant means having more nucleants in the system and by considering of higher $Tnuc_{Al}$ which was shown in 7.12a, higher percentage of α-Al particles is expected. Moreover, Sr addition increased the percentage of primary phase due to the

depressing of the eutectic temperature and thus widening the solidification range for primary α-Al phase formation. Such qualitative remarks will be supported when the quantitative results are discussed in the section on image analysis.

The effect of modification is recognizable by the formation of rounder globules plus morphological evolution of silicon flakes to fibrous (Figure 7.18). As seen in Figure 7.18, the evolution of eutectic silicon is not homogenous in the sample and a mixture of partial/fibrous structure is seen through the examined surface. However, if Figure 7.18 is compared with that of Figure 7.14, the question may arise as why there is not any change in the silicon morphology in the conventionally cast billets. As shown in conventionally cast sample, Figure 7.14b, Sr addition in combined format resulted in minor changes of acicular to smaller flakes silicon particles. This result is in contradiction with the quenched billet microstructure where the quenched structure is fully fibrous (Figure 7.18b). For better explanation of this result, it is necessary to consider two distinct effects. By quenching the billets, the silicon flake size decreases due to the higher cooling rate with the added bonus of forced convection which is clearly shown by comparing Figure 7.14a and 7.18a. From a kinetics point of view, the reaction of Sr and B in this system is time dependent and in conventional air cooled samples, there is enough time for SrB_6 formation prior to the main eutectic reaction and therefore the remaining Sr is inadequate to cause morphological evolution of silicon flakes. In quenched billets the story is different since the billets were quenched from 598°C and this would result in lesser time for SrB_6 reaction to proceed and therefore the remaining and unreacted Sr in the system is increased; this amount of Sr is quite enough to alter the morphology as seen in the combined SEED treated sample.

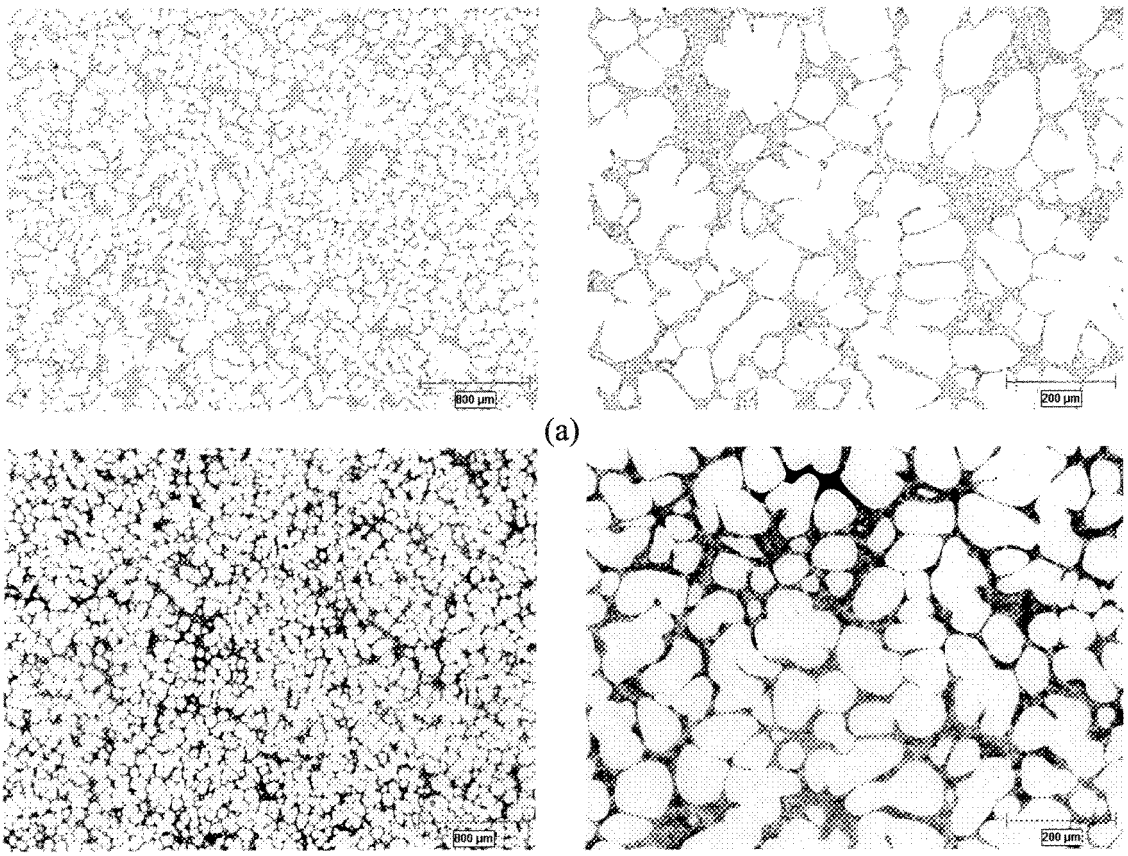

Figure 7.17: Optical micrographs to show the effect of combined treatment:
(a) Without addition, (b) 218ppm B, 136ppm Sr

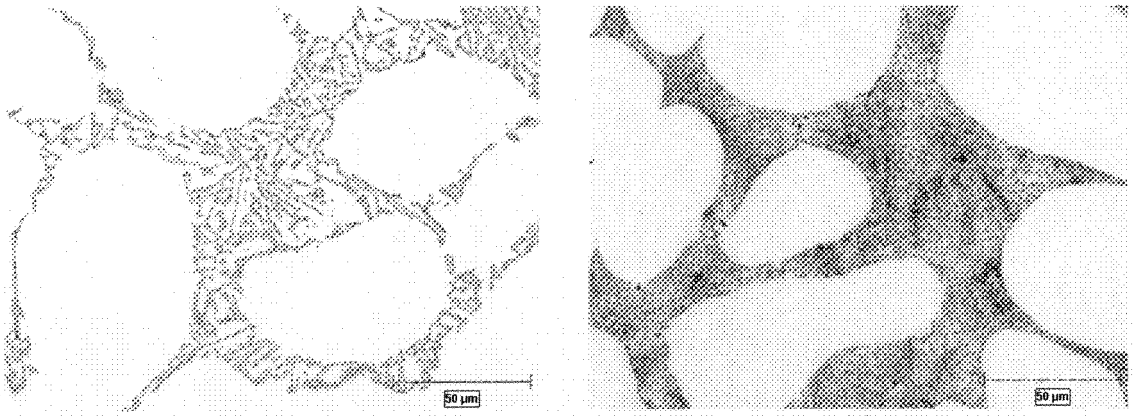

(a) (b)

Figure 7.18: Variation of silicon morphology:
(a) without Sr, (b) 218 ppm B, 136ppm Sr

As it was shown in conventional samples, Figure 7.15, combined addition of Sr and B has the disadvantage of intermetallic formation in the eutectic regions due to their high affinity. Figure 7.19 shows typical agglomeration in the SEED billets. Electron microprobe analysis of these particles confirmed SrB_6, (Table 7.3), stoichiometry.

The potential nucleation sites for the primary α-Al particles were searched as a routine procedure during the course of the current research. The backscattered electron micrograph and corresponding x-ray maps in Figure 7.20 and Table 7.4, confirms SrB_6 as a potential nucleation site for the primary α-Al particles but again the shortcoming of simultaneous addition is the reduction of both refining and modifying effects due to agglomeration and decreasing the potential sites for both treatments.

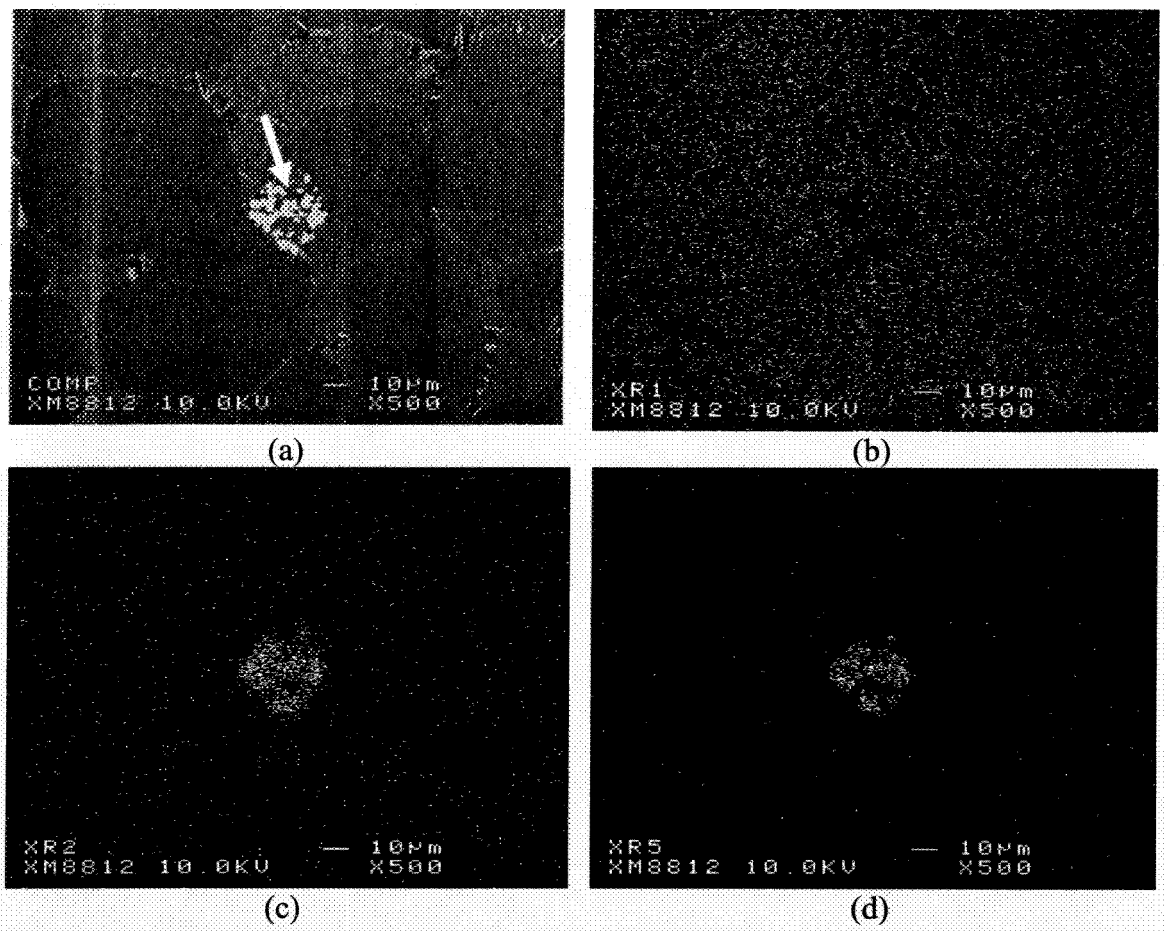

Figure 7.19: (a) back scattered electron micrograph of agglomorations, and x-ray maps for: (b) Al, (c) B, and (d) Sr (SEED sample with 231ppm B, 112ppm Sr)

Table 7.3: Atomic percentages of boride particle

Al	B	Ti	Si	Mg	Sr	Fe
0.77	86.20	0	0.4	0.10	12.53	0

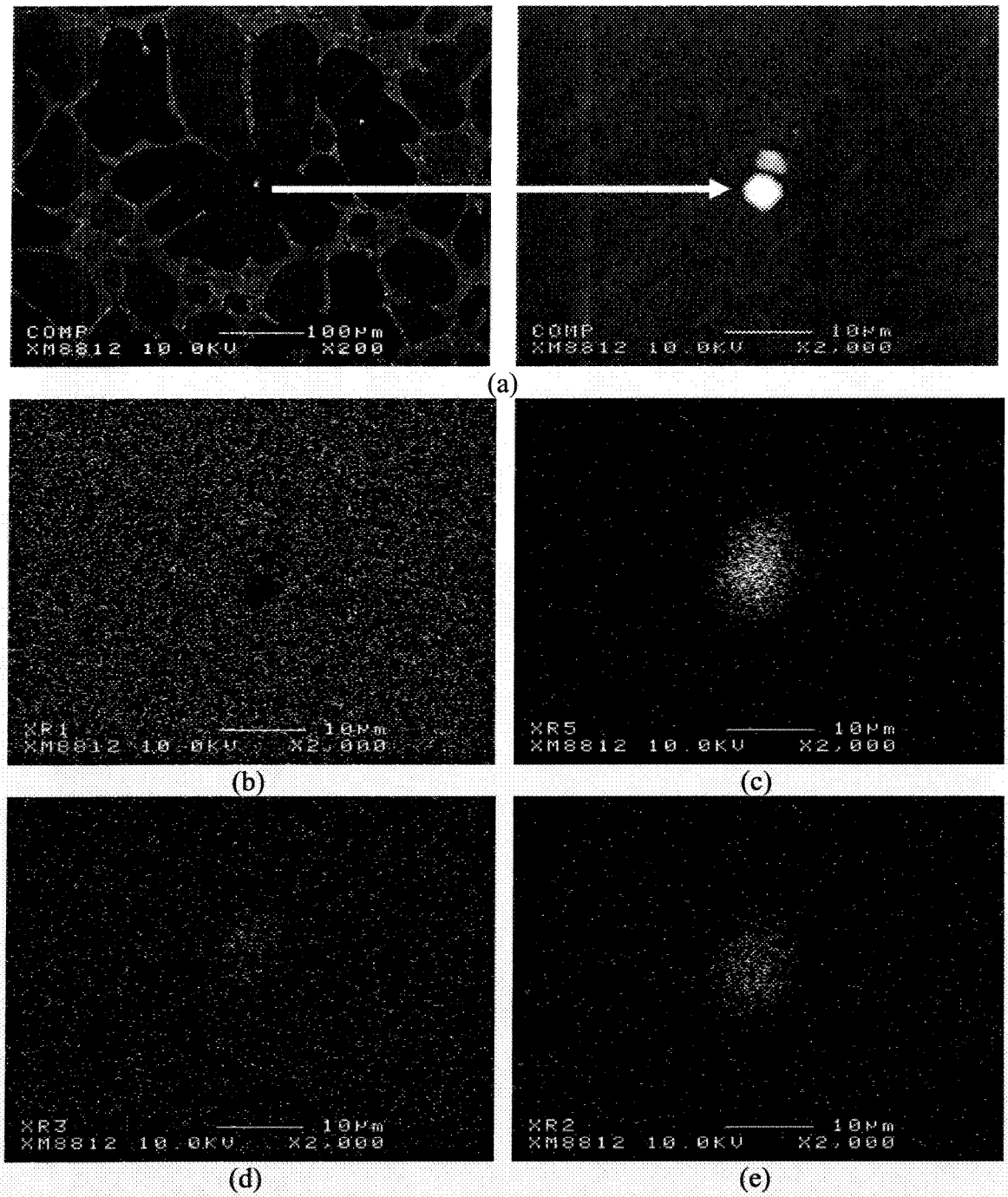

Figure 7.20: (a) backscattered micrographs of a nucleaus in the sample with 231ppm B, and x-ray maps of (b) Al, (c) Sr, (d) Ti, and (e) B

Table 7.4: Atomic percentages of nucleus by microprobe analysis

Al	B	Ti	Si	Mg	Sr	Fe
2.69	83.16	0.03	1.46	0.9	11.75	0

7.1.2.2.2 SEM analysis

Figure 7.21 shows the SEM micrographs of selected SEED samples. Comparing to the conventional cast specimens, finer and fibrous structure in these samples is obvious. With modifier addition, the flaky structure of silicon changes to fibrous and the seaweed like structure is visible but its distribution is not uniform in the sample and some parts with partial modification could be seen.

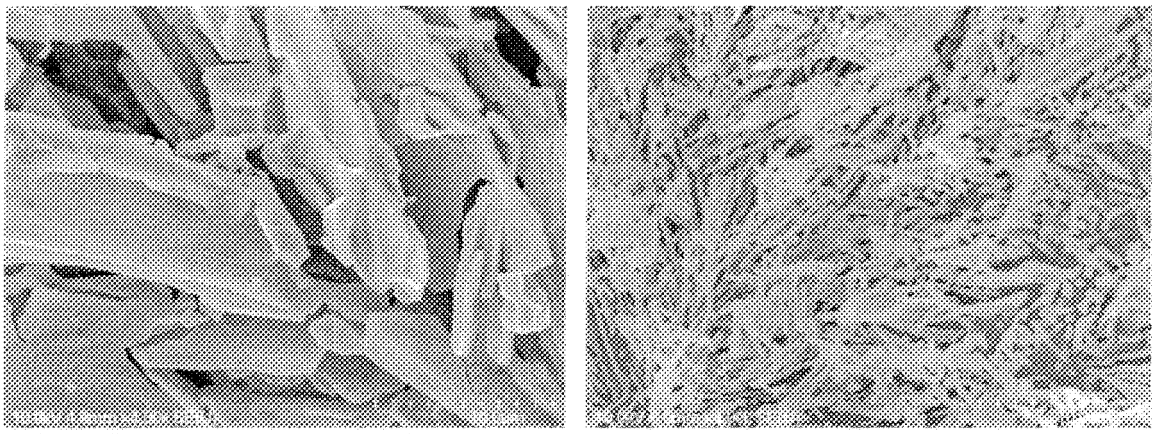

(a) (b)

Figure 7.21: SEM photos of the selected SEED samples, deep etched in 10%HF, (a) without addition, (b) 218ppm B, 136ppm Sr addition

7.1.2.2.3 Image analysis

The results of image processing for B-Sr treated slurries are shown in Figure 7.22. The primary α-Al percentage increased which is mainly associated to the numerous nucleation sites as discussed before, i.e. shifting up the solidification temperature due to the B addition and the benefit of lowering the eutectic reaction due to the Sr addition. Globule size reduction is seen through different parameters such as decreasing of circular diameter, the percentage of α-Al particles having aspect ratio >2, and the area to perimeter ratio and increasing of particles density. Also, the percentage of particles having sphericity greater than 0.8 increases which is an indication of higher degree of globularity

Furthermore, it should be emphasized that the refiner part of addition always dominates the modifier side. As shown in Figure 6.27c, by modification, number density of the primary particles is unchanged since there are no new nuclei introduces into the system while, refiner side increases the quantity of primary particles.

Higher percentage of sphericity coupled with lower surface tension due to the Sr addition results in smoother channels and easier flow of the remaining liquid could be achieved. Higher amount of the extracted liquid from the bottom orifice is an indication of better fluidity of the treated alloy (Figure 7.23).

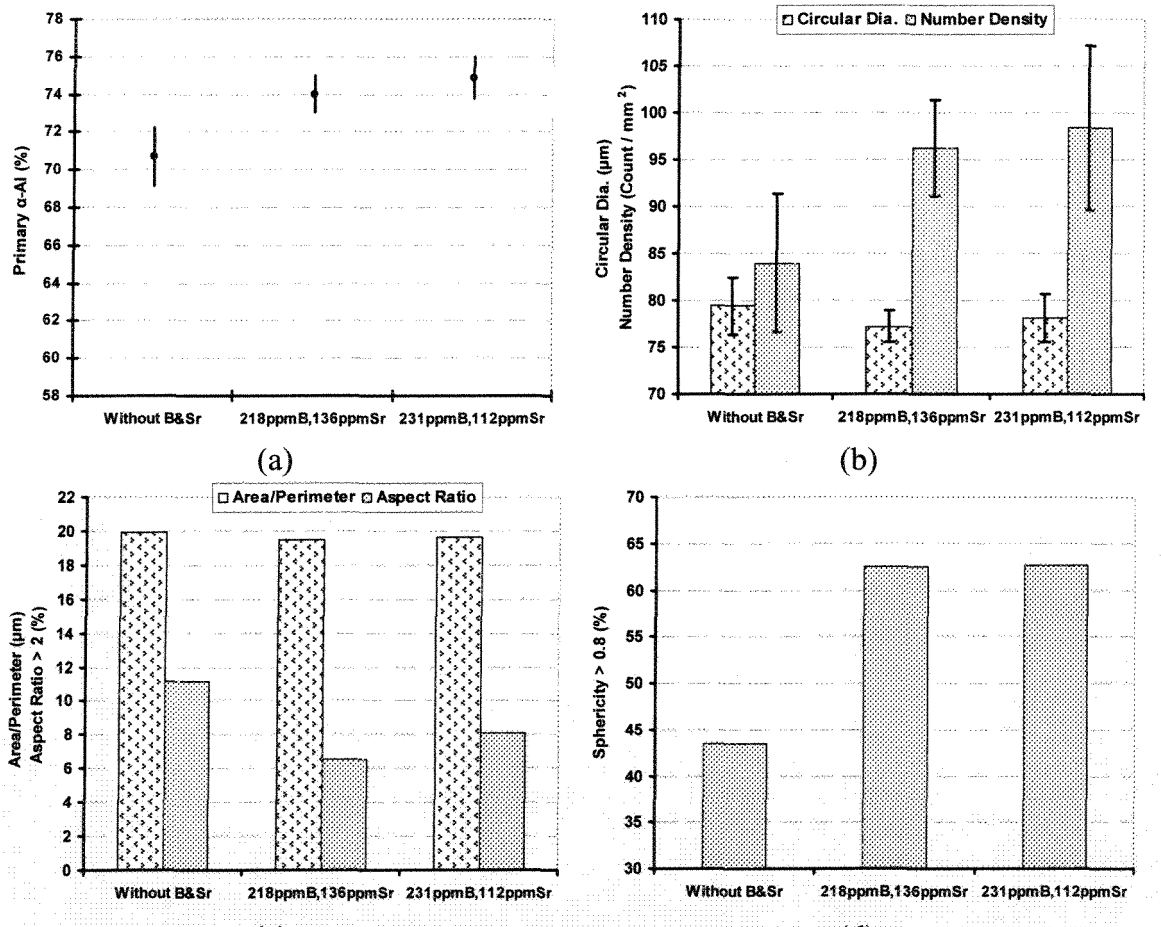

Figure 7.22: Image analysis parameters for B-Sr treated A356:
(a) primary α-Al percentage (b) circular dia. and number density of α-Al particles, (c) A/P ratio and percentage of α-Al particles having aspect ratio >2, (d) % of particles having sphericity > 0.8

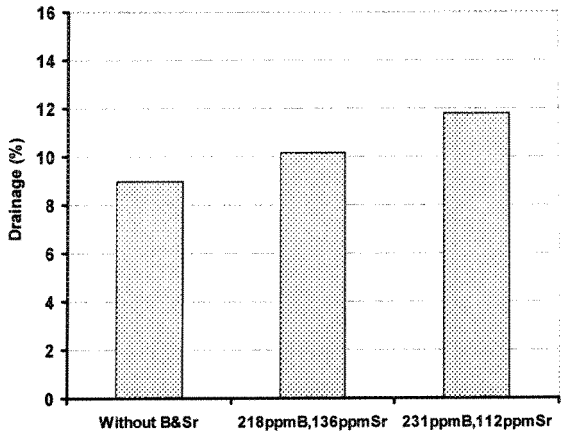

Figure 7.23: Drainage as a process parameter

7.2 Combined effect in Commercial 356 alloy

The effects of sole grain refiner and modifier additions were reported before. With the knowledge acquired for the optimum additional level, a series of melts were prepared to study the effect of combined addition with chemical compositions given in Table 7.5.

Table 7.5: Chemical analysis for the base alloy and combined treatment (wt. %)

	Si	Mg	Fe	Mn	Cu	Ti	B	P	Sr	Al
Base alloy	7.11	0.35	0.09	0.002	0.002	0.135	0.0008	0.0002	0.000	bal.
Treated alloy	7.06	0.35	0.09	0.002	0.002	0.153	0.0047	0.0002	0.014	bal.

7.2.1 Addition of titanium, boron, and strontium

7.2.1.1 Conventional casting

7.2.1.1.1 Thermal analysis

The effect of combined addition of refiner and modifier on the solidification behavior of commercial 356 alloy is shown in Figure 7.24. Small addition of Ti&B shifted the cooling curves to higher temperatures and decreased recalescence (Figure 7.24a). For commercial alloy, the addition of refiner elements leads to the same behavior as it was discussed in section 5.3. The results of analysis of the cooling curve have confirmed that with grain refiner addition, both nucleation and growth temperatures of the primary α-Al particles increase but the increasing rate is greater for $Tnuc_{Al}$ (Figure 7.25). In other words, more nucleation sites could neutralize dendritic solidification by reducing the growing space. Recalescence varied between -0.3 and zero and so it shows that refining process is efficient.

By Sr addition, Figure 7.24b, there is an apparent reduction in the eutectic reaction temperature and an increase in the recalescence value is obvious. Eutectic nucleation temperature, $Tnuc_{eut}$, and maximum temperature of the eutectic decrease with Sr addition as described previously (Figure 7.25b). The variation of eutectic recalescence, shows that $\Delta\Theta$ increased by ~2°C due to addition of 150ppm Sr. Also depression of the eutectic

temperature causes larger α-Al solidification range and as a result more α-Al formation. The results are in line with those reported for sole Sr addition in section 6.3. Comparing to the sole modifier addition, increasing of the α-Al solidification range is more in the case of joint addition due to the higher liquidus temperature.

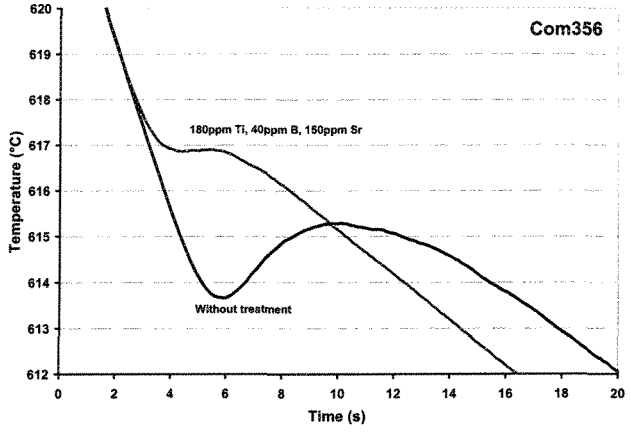

(a)

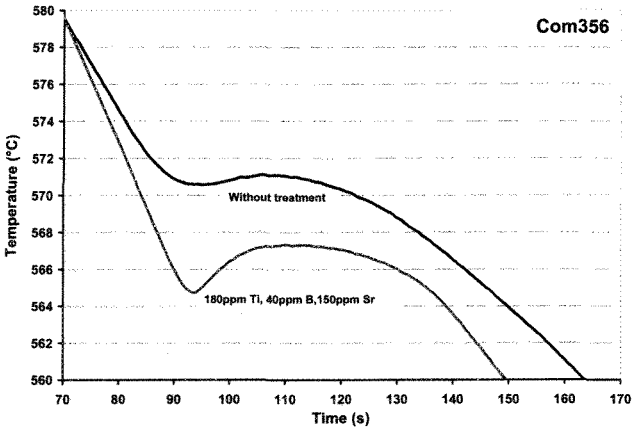

(b)

Figure 7.24: Cooling curves before and after additions:
(a) commencement of solidification, (b) eutectic reaction zone

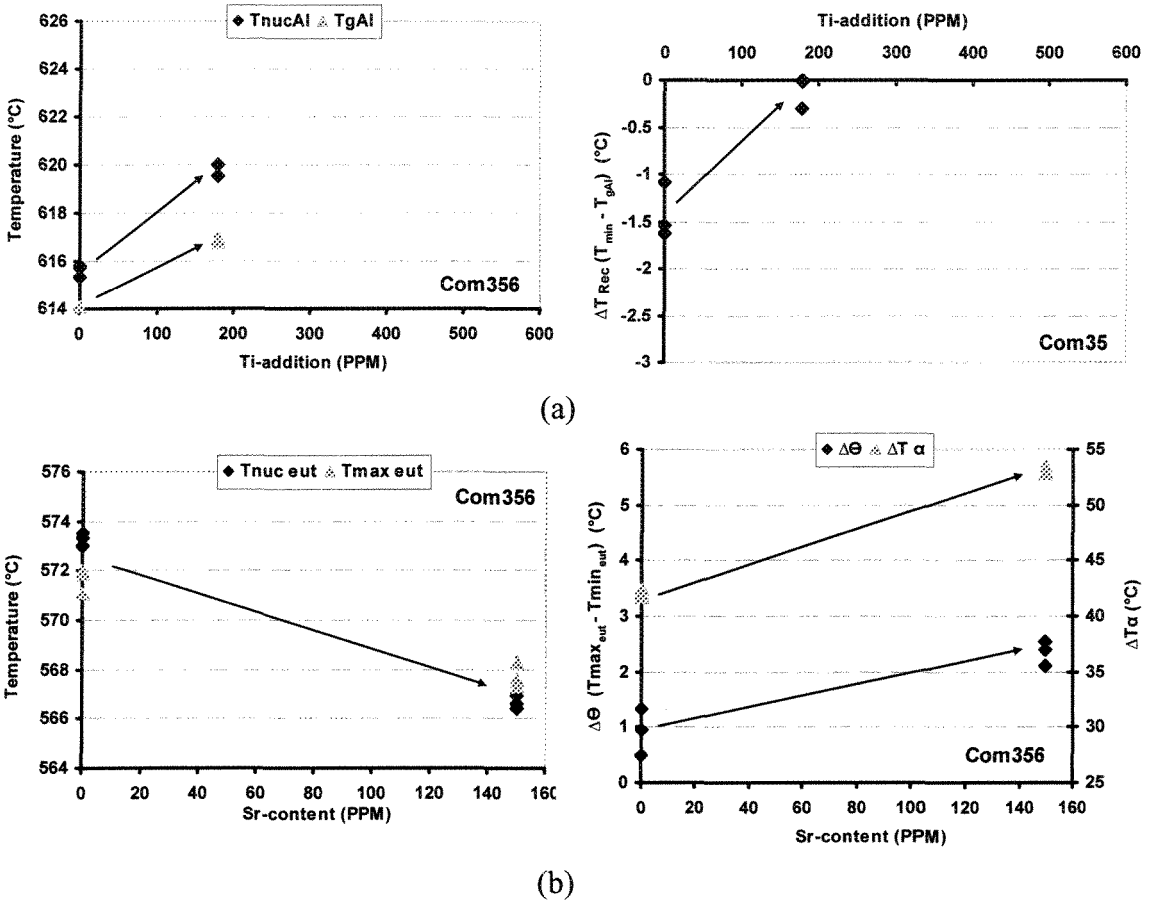

Figure 7.25: Variation of thermal analysis parameters: (a) $Tnuc_{Al}$, Tg_{Al}, and ΔT_{Rec} due to the refiner, (b) $Tnuc_{eut}$, $Tmax_{eut}$, $\Delta\theta$, and ΔT_{α} due to modifier addition

While refining increases the α-Al solidification range by ~4°C, the combined addition expands it by ~11°C which is almost three times that of sole addition of refiner (Figure 7.26). This is coming from the fact that the combined addition has an additional benefit of ascending the α-Al nucleation temperature plus lowering the eutectic nucleation temperature due to the Sr addition and therefore rendering an extended ΔT_{α}. It is worth noting that an expansion in the mushy zone temperature range has important implications in SSM processing since it causes wider operational range for slurries preparation.

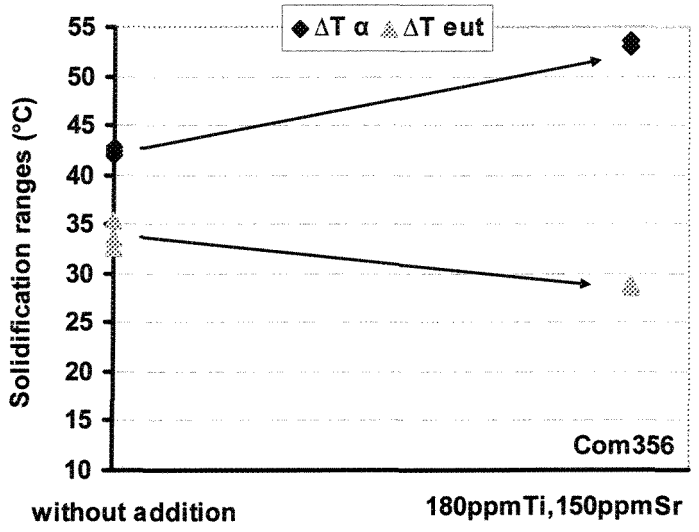

Figure 7.26: Influence of melt treatment on the solidification range of Com356

7.2.1.1.2 Structural analysis

The effect of combined addition on the microstructure of commercial 356 alloy is given in Figure 7.27. As it could be seen:

- The microstructure is no longer dendritic and the formation of an equiaxed morphology is evident with grain refiner addition.
- With Sr addition, silicon morphology changes from acicular and lamellar to fibrous. As mentioned in section 6.3, it seems that the eutectic regions in the modified alloy have boxed in the primary α-Al phase comparing to the unmodified alloy which shows isolated silicon flakes. It is believed that this is originated from growing of fibrous Si from limited number of nucleants and expanding three dimensionally.

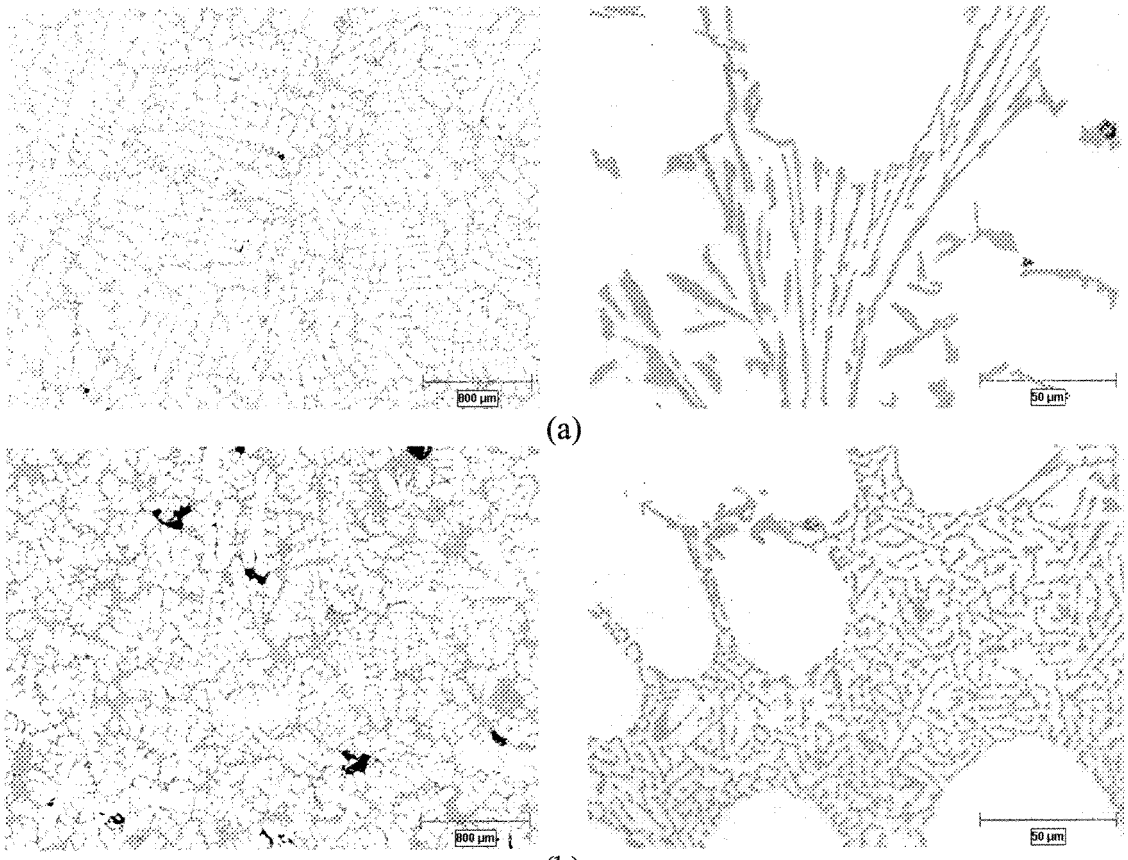

Figure 7.27: Microstructural variation due to the simultaneous melt treatment: (a) without addition, (b) addition of 180ppm Ti, 40ppm B, 150ppm Sr

7.2.1.2 Semi-solid processing

7.2.1.2.1 Structural analysis

The optical micrographs in Figure 7.28 show the effect of combined treatment. Grain refining efficiency is obvious through higher percentage and more globular and compacted primary particles, while modification effect could be seen at higher magnification by morphological changing of silicon particles from lamellar to fibrous (Figure 7.29).

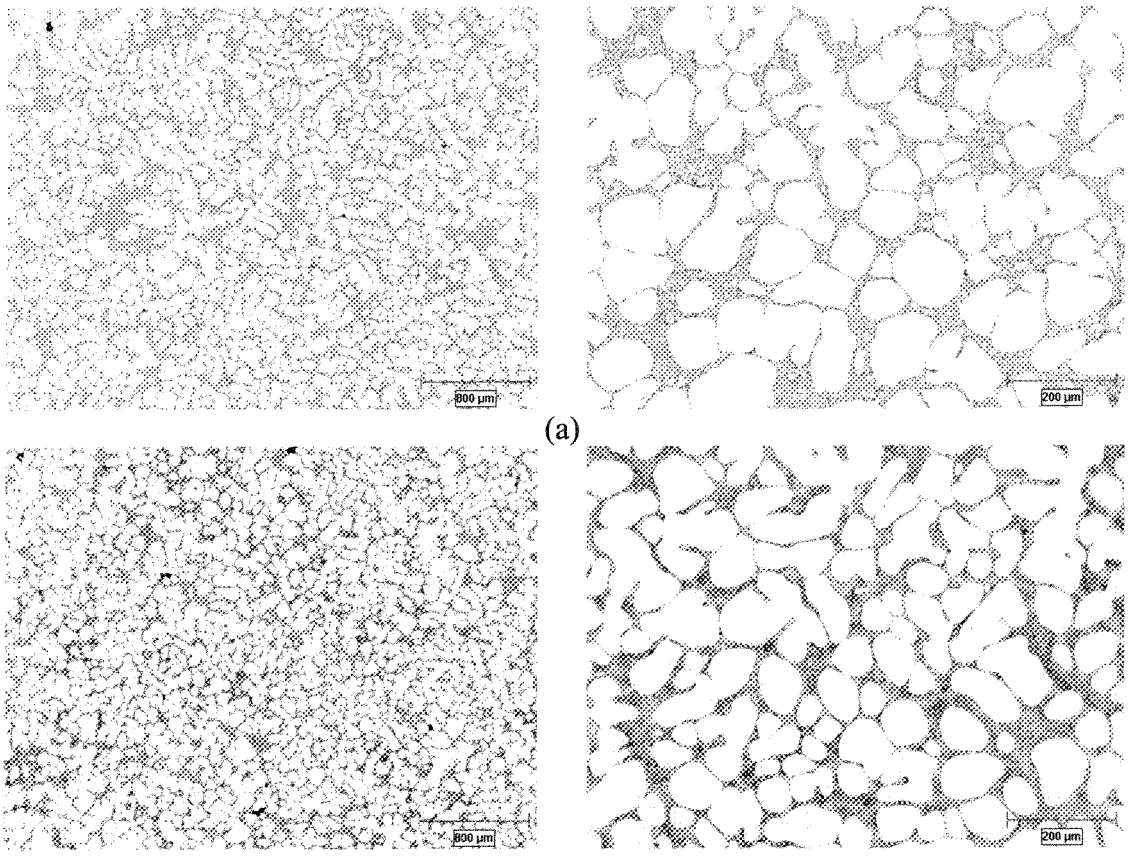

Figure 7.28: Effect of combined treatment on the α-Al particles:
(a) without addition, (b) 180ppm Ti, 40ppm B, 150ppm Sr

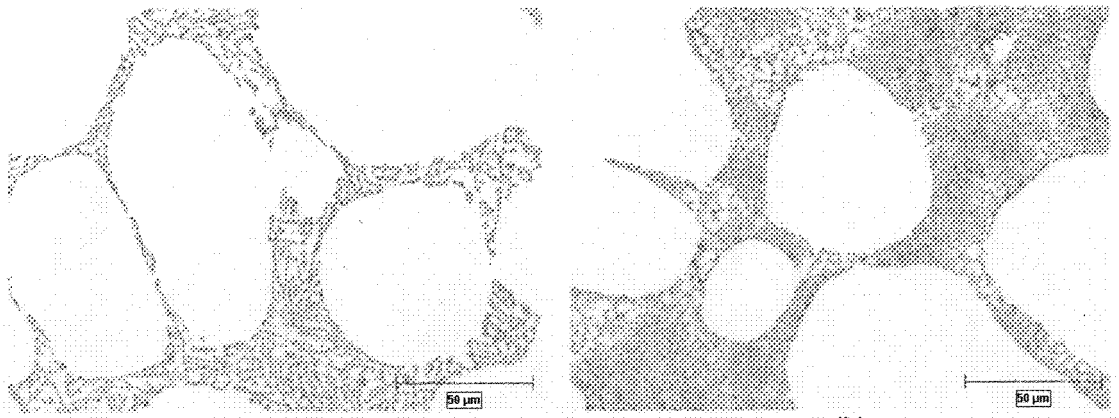

Figure 7.29: Variation of silicon morphology in SEED quenched billets:
(a) untreated alloy, (b) 180ppm Ti, 40ppm B, 150ppm Sr

7.2.1.2.2 Image analysis

The results from image analyzing are shown in Figure 7.30. The percentage of primary phase increases due to the existence of more nuclei from Ti and B addition and shifting of the main eutectic reaction (L → α-Al + Si) to lower temperatures as a result of Sr addition. Particles density slightly increases which is an indication of more individual primary particles in a unit area. There is almost no difference in the average circular diameter after treatment which is associated with the effectiveness of Ti in solution in suppressing the growth of primary particles.

The area to perimeter, percentage of α-Al particles having aspect ratio >2, and percentage of particles having sphericity > 0.8 appears to be less sensitive to the treatment. As mentioned before, as-recived ingots had Ti in solution and this amount of Ti is sufficient to suppress the additional growth of primary particles. Insignificant variation of image analysis parameters all confirm that combined addition is effective in increasing the density of primary particles plus forming slightly rounder particles.

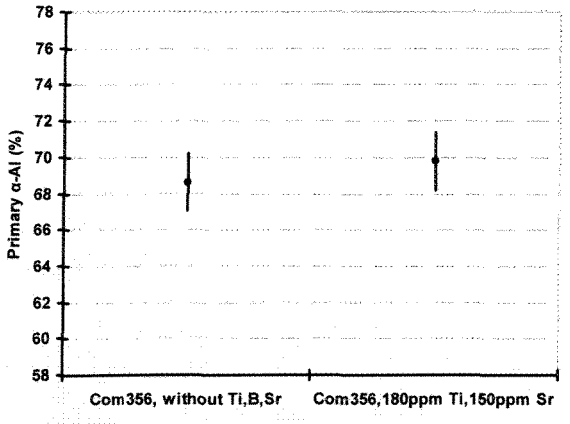

(a)

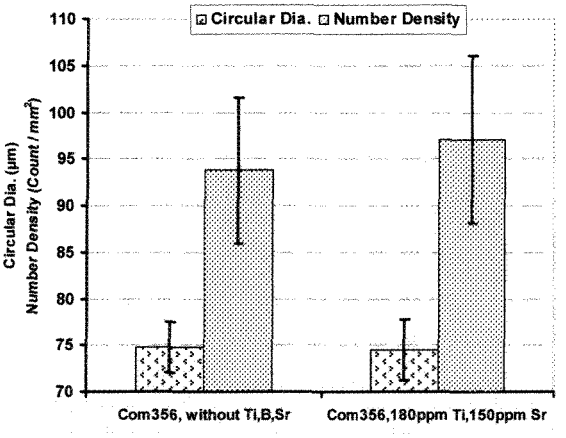

(b)

Continue →

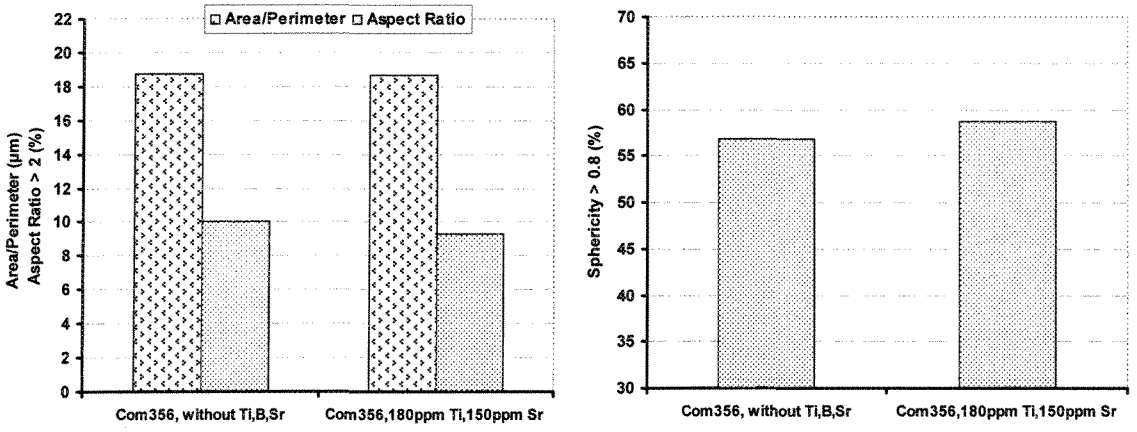

(c) (d)

Figure 7.30: Image analysis parameters for Com356: (a) primary α-Al percentage, (b) circular dia. and number density of α-Al particles, (c) A/P ratio and percentage of α-Al particles having aspect ratio >2 and (d) % of particles having sphericity > 0.8

From casting point of view, the drainage which is the flow of the remianing liquid through the solid network, may be regarded as a tool to define the fluidity concept, although it is fundamentally different to its classical definition. By combined treatment, the extracted liquid from the bottom orifice in a definite time increased (Figure 7.31). Lower dendrite coherency point and the postponment of the formation of 3-D solid network, due to the refiner and modifer agents may be an issue for consideration. This factor is complemented by stirring associated with the SEED process. In fact, more globular strucutre plus a lower DCP point should create smoother channels within the slurries and thus improves the fluidity.

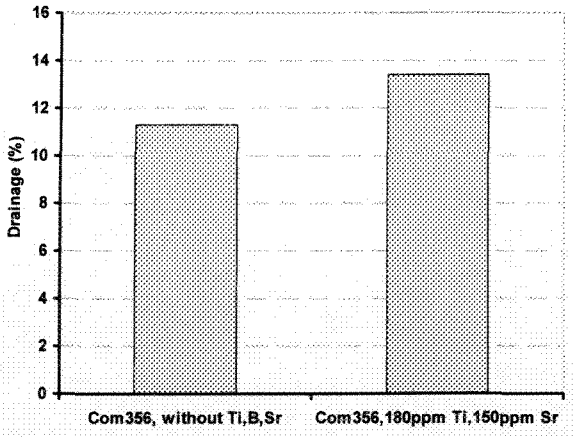

Figure 7.31: Drainage as a process parameter

CHAPTER 8

RESULTS AND DISCUSSION
RHEOLOGICAL BEHAVIOUR

CHAPTER 8

RESULTS AND DISCUSSION – RHEOLOGICAL BEHAVIOUR

8.1 Rheological tests for A356 alloy

8.1.1 Addition of titanium, boron, and strontium

8.1.1.1 Chemical analysis

The scope of this part of the work is to perform limited rheological tests on the SEED billets with the optimum addition level of refiner and/or modifier with Al5Ti1B and Al10Sr master alloys. The optimum rates were obtained from the previous sections (5.2.1, 6.3, and 7.1) and the final chemical compositions are listed in Table 8.1.

Table 8.1: Chemical analysis of the melts (wt. %)

	Si	Mg	Fe	Mn	Cu	Ti	B	Sr	Al
Original	6.5-6.75	0.36-0.4	0.07-0.08	0.002-0.003	0.001	0.0058	Nil	Nil	bal.
Grain Refined						0.06-0.07	0.010-0.014	Nil	
Modified						0.0058	Nil	0.017-0.018	
Combined						0.06-0.07	0.010-0.014	0.015-0.018	

8.1.1.2 Structural analysis

The optical micrographs in Figure 8.1 show the microstructural evolution of the untreated and treated billets before and after deformation. All specimens were quenched in water from 598 ±2°C. The micrographs in the first row, (Figures 8.1a, b, c), illustrate the

structure of the billets at the end of casting and just before the rheology tests, while the second row, (Figures 8.1d,e,f), shows the structure of the same billets after isothermal compression tests, (10 minutes at 598 ±2°C).

In contrast to untreated alloy, Figure 8.1a, the addition of refiner in the form of Al5Ti1B master alloy, Figure 8.1b, appears to have refined and increased the percentage of α-Al particles slightly. The concentration of the primary α-Al particles in the combined treatment, Figure 8.1c, has also increased almost to the same level as that of the sole refiner addition. The degree of globularity is also increased by melt treatment. Such qualitative remarks are confirmed with the quantitative image analysis results plotted in Figure 8.2 which is a conclusion from the previous works in sections 5.2.1, 6.3, and 7.1. The percentage of primary α-Al particles increases in all cases but the enhanced value is greatest in the refined and combined billets. Likewise, the quantity of particles in the unit area, particle density, shows the highest values for refined and combined treatments.

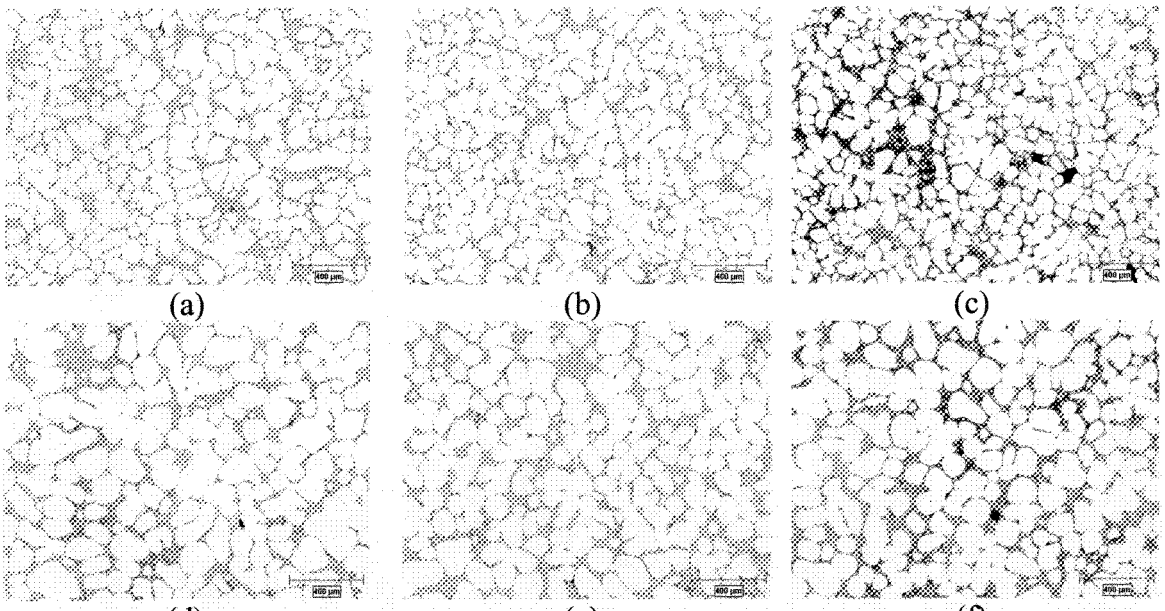

Figure 8.1: Microstrucutral evolution of quenched samples (a to c):
(a) base alloy, (b) grain refined with 620ppmTi, 110ppm B, (c) combined treatment, 610ppmTi, 100ppm B, 160ppm Sr ,
and after pressing (d to f): (d) sample "a", (e) sample "b", (f) sample "c"

The increase in the percentage of the primary α-Al particles due to melt treatment is because of the changes in the Al-Si phase diagram with the liquidus shifted up with inoculation and eutectic temperature lowered with Sr modification, i.e. expanded solidification range. Furthermore, the formation of numerous nucleants due to refiner addition is expected to reduce inter-α-Al particle spacing and thus to limit globules growth due to overlapping of solute rich boundary layers formed around growing phases during solidification. In addition, the refinement is also due to the titanium growth restriction capability of the dissolved Ti in α-Al. It is worth noting that there is a specific limit of grain refiner addition beyond which segregation and agglomeration of Ti-based intermetallic compounds are inevitable as shown in Figure 8.3.

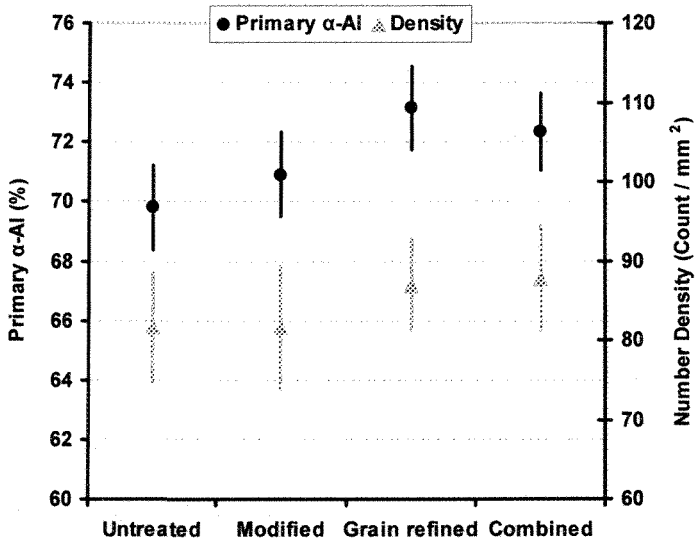

Figure 8.2: Variation of α-Al percentage and quantity of the particles with different treatments

Figure 8.3: Ti-based intermetallics in over-refined sample,
1000ppm Ti, 130ppm B addition, deformed billet

For the deformed billets, Figures 8.2d, e, f, there is general coarsening irrespective of melt treatment. This is expected, since the billets were held isothermally at 598°C±2 for 10 minutes under pressure which not only induced better contact between particle-particle, but also improved wetting between particle-liquid. In other words, the diffusion and transport of constituent elements as the pre-requisite for coarsening were improved. The disappearance of finer particles in the deformed billets is a clear indication of Ostwald ripening as the dominant mechanism for coarsening. The coarsening of the primary α-Al particles has also been treated quantitatively by image analysis and measurement of its average circular diameter. The primary α-Al particles have grown approximately 58% after 10 minutes isothermal deformation at 598°C±2, Figure 8.4. It should be noted that the average circular diameter is defined as the diameter of a circle having the same area as the measured object in the software, ($2\sqrt{area/\pi}$).

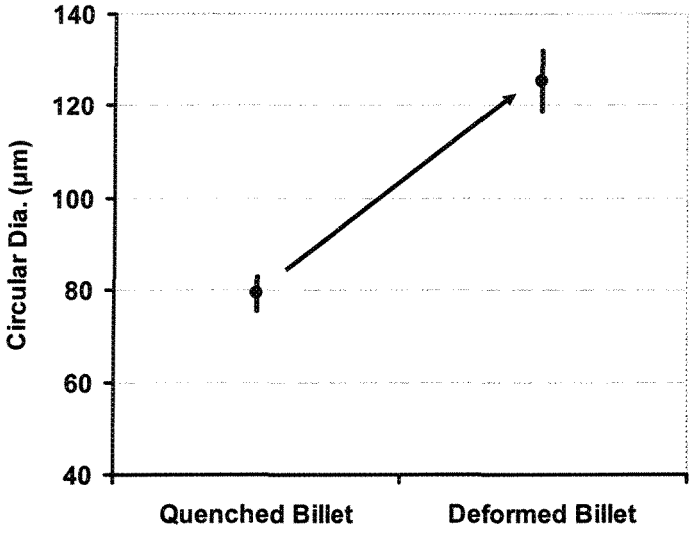

Figure 8.4 : Growth factor in the form of average circular diameter, untreated sample

The optical micrographs in Figure 8.5 show the combined effect of refiner and modifier. There are two distinct features detectable when Sr is added as part of melt treatment; the nature of the primary α-Al particles and the eutectic silicon morphology. As seen in Figure 8.5, some primary α-Al particles appear to have been boxed-in by the eutectic regions. This is due to the nature of the eutectic pools in the modified alloy, where there is much lower number of individual eutectic silicon particles in contrast to the un-modified alloy. This is due to the effect of Sr in restricting the number of nucleation sites for the eutectic silicon and eventual transforming the flake silicon to a fibrous morphology with highly branched silicon which grows three dimensionally around the existing primary α-Al particles.

In conclusion, melt treatment is beneficial during SSM processing of Al-Si alloys and improves morphological characteristics of the primary α-Al phase. As reported before in sections 5.2.1 and 6.3 in much more details and also partly shown in Figure 8.2, with the addition of refiner element(s), the average size of primary particles reduces and their quantity increases while modification results in larger primaries and keeps density value almost constant. Furthermore, both treatments result in higher sphericity values, which is quite important for the flowability of slurries.

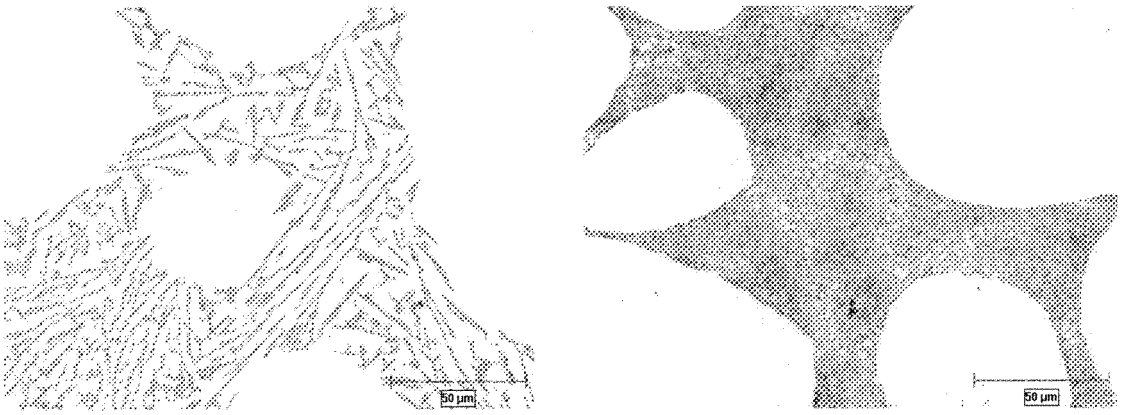

(a) (b)

Figure 8.5: Optical micrographs showing the effect of Sr addition in deformed billets: (a) untreated alloy , (b) combined treatment, 610ppmTi, 100ppm B, 160ppm Sr

8.1.1.3 Strain-time graphs

An engineering strain-time graph (e-t) is a basic graph to evaluate the deformation behavior of SSM billets and obtained from the initial height-time variation data. Figure 8.6 shows a typical deformation-time curve.

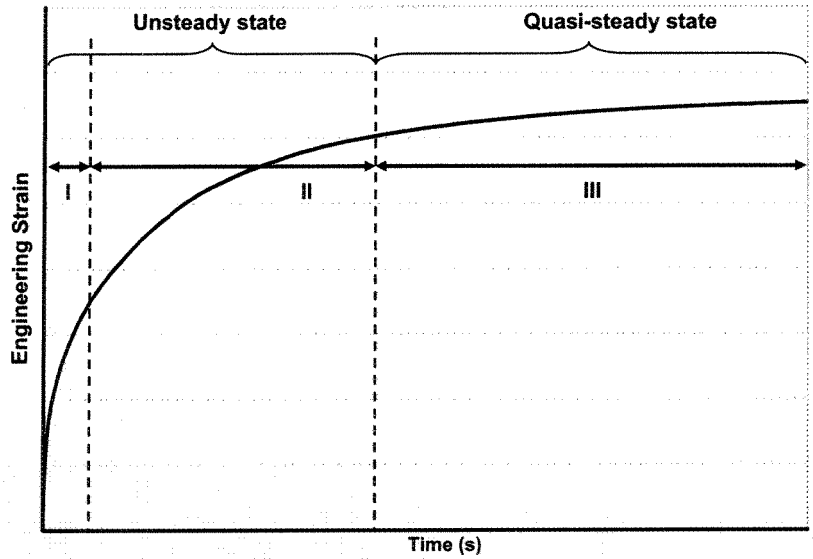

Figure 8.6: A typical graph for different deforamtion stages during parallel plate compression test

Such graph normally comprises three deformation stages of [184];

1. **Stage-I, unsteady-state,** where the billet flows almost without any resistance to applied pressure. This behavior is attributed to the easy movement of the primary

α-Al particles within the residual liquid and without appreciable collision. The extent of this region is dependent on the particle size and applied pressure where it is greater at smaller particle size or higher applied pressure.

2. **Stage-II, unsteady-state,** where there is some degree of resistance to flow due to the collision of solid particles and formation of α-Al agglomerates. The agglomerated chunks are the resisting constituents to billet flow.

Both stages I and II are regarded as non-steady states, since the slope of the graph varies with time, i.e. there is mainly agglomeration. That's why the first two regions are classified as unsteady state segment in Figure 8.6.

3. **Stage-III, Quasi steady-state,** where the billet deforms steadily with a constant slope. It is believed the solid-liquid mixture, "the mush", has reached a state where it deforms as a single phase. The processes of agglomeration and de-agglomeration establish a quasi steady state equilibrium condition in the mush at this stage of deformation.

Figure 8.7 shows the effect of various melt treatments on the deformation behavior of the SSM billets. The change in the billets deformability due to α-Al particles size and distribution is clearly visible on the graphs. The untreated alloy (base alloy) shows the lowest strain values while the grain refined and combined treated alloys deform at much higher range due to smaller globule size as indicated in the previous section. It has to be emphasized that the flow characteristics of the grain refined and combined treatment alloys are almost the same and only one deformation band is presented for both alloys. There is not much difference between the two sets of treatments, if only an improved rheological behavior of the alloy is the objective. However, it has to bear in mind that the treated alloy is eventually transformed into engineering components where mechanical properties are important. The mechanical properties are not only dependent on the primary α-Al phase, but also on the morphology of silicon which is even more critical. Therefore the combined

treatment is the preferred choice for melt treatment resulting in better die filling and superior mechanical properties. The modified alloy lies somewhere between the refined/combined and the base alloy.

The actual as-deformed billets, sectioned longitudinally, are shown in Figure 8.8, corresponding to the strain-time graphs in Figure 8.7, where the untreated billet (Figure 8.8a) shows the lowest deformation in contrast to the refined and combined treated billets. It has to be pointed out that the billets were of the same original height and diameter and the reduction of height is a clear indication of the billet capability to flow under applied constant pressure. The slight width differences in the three treated billets is due to longitudinal sectioning which may have been somewhat off-center for the combined treated billet.

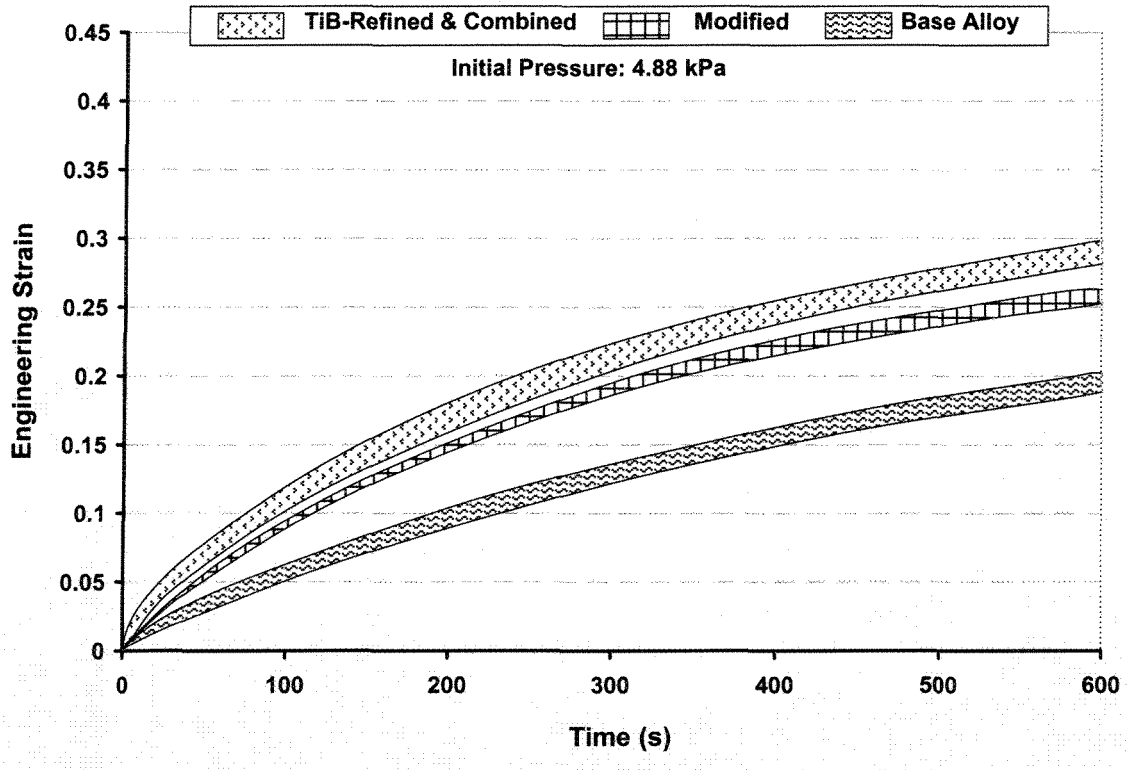

Figure 8.7: Strain-time graphs for melt treatment

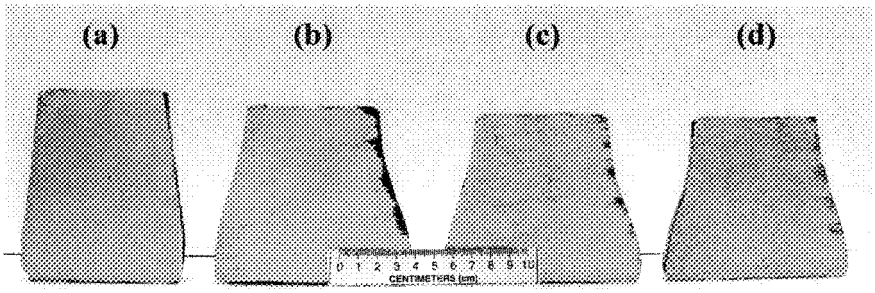

Figure 8.8: Deformed billets under 4.88kPa pressure;
base alloy (a), refined (b) ,modified (c), and combined (d)

To better understanding the particle size effect during deformation, several tests were performed on the over-refined billets and typical strain-time graphs are given in Figure 8.9. Over-refinement is defined as the addition of inoculant in excess of the optimum percentages of ~ 0.06-0.08% Ti, and ~0.01-0.02% B respectively. With over-addition, the average circular diameter of the primary α-Al particles in the quenched billets was reduced by ~5% and the number density increased by ~20% (section 5.2.1). The lower resistance to flow for the over-refined billet shown in Figure 8.9 is solely due to the smaller particle size of the primary α-Al phase. The deformation in the over-refined billet is even higher than that of the billet with optimum grain refiner addition throughout the compression test. However, the drawback of over-refined billets is the formation of Ti-based intermetallic compounds, as shown in Figure 8.3. It is important to note that the formation of Ti-based intermetallics in the over-refined condition did not impede the flow during rheological test. The main negative result of these intermetallics is on the mechanical properties of the finished product, once the billet is die-cast or forged. They may act as potential crack initiation sites for the finished product.

The optical photomicrograph in Figure 8.10 compares the deformability of the base alloy with that of the refined and over-refined billets to further confirm the strain-time graphs presented in Figure 8.9.

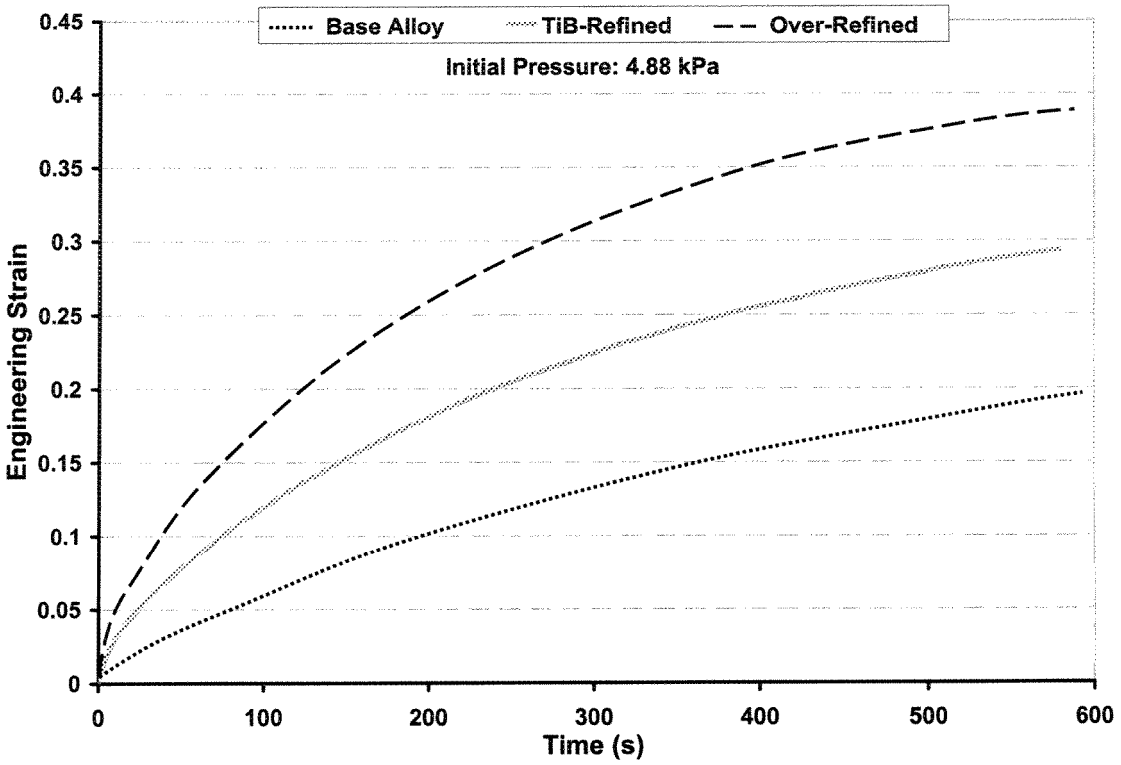

Figure 8.9: Comparison of the typical strain-time graphs for the untreated, refined and over-refined alloys

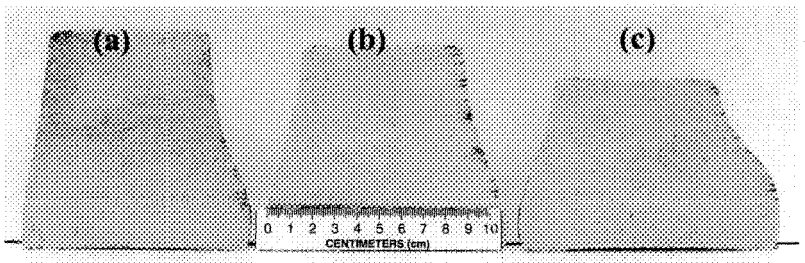

Figure 8.10: Deformed billets under 4.88 kPa pressure;
(a) base alloy, (b) refined and (c)over-refined

The superior flow characteristics of the grain-refined billets are attributed to the reduction of primary α-Al particle size and lower dendrite coherency point (DCP). For conventionally cast alloys, it is reported that grain refining and modification reduces the DCP to lower temperatures and thus induces less restriction to liquid mass flow [78]. For SSM alloys, the fact that dendrites are no longer the dominant morphology reduces the tendency to form a three dimensional interconnect solid network. Furthermore the grain-

refined alloy results in finer and more spherical primary α-Al particles with greater amount of solid-liquid interfacial area where the inter-particle liquid film could assist solid particles gliding over one another. The finer the particles, the greater the interfacial area which tends to facilitate the particle slipping and thus easier particle glide should be expected. For particle to particle contact, firstly the smaller particle size increases the magnitude of contact area between particles and therefore the applied pressure is better transferred from particle to particle resulting in easier movement of particles and better flow. Secondly, if it is assumed the particles slip over one another, the energy required to push smaller particles over each other is smaller than that required for larger ones.

For the case of Sr-modification, it is proposed that the reduction in the surface tension of the remaining liquid and lower DCP is the determining factors that improve flow characteristic of the SSM billets. It has been reported that strontium reduces surface tension of the melt [104,105], and hence decreases the viscosity to induce better flow within the SSM billets. By decreasing the surface tension, the wettability of the primary α-Al particles by the remaining liquid is improved. This is equivalent to having more contact between the remaining liquid and primary α-Al.

During stirring, thermal and solutal homogenization takes place in the bulk liquid leading to better fluidity due to the lower surface tension and better wettability. It may be concluded that the flow around particles could smooth off primary α-Al particles better producing rounder particles.

8.1.1.4 Liquid segregation

As described before, the billets were compressed uniaxially. The rapid initial vertical descent of the top plate causes lateral liquid separation in the billet while the solid particles are compacted and may collide to form agglomerated particles at the center of billets. The magnitude of segregated liquid zone depends on the deformation rate, temperature, and particle size and morphology [197].

Micrographs taken from the center, middle, and wall sections of the billets deformed at 4.88kPa are shown in Figure 8.11. The microstructures of the central zone are homogenous regardless of melt treatment. The eutectic liquid (dark regions) appears to have accumulated mainly at regions near the mold wall. This was expected, since the applied pressure displaces the residual liquid laterally towards the walls. This phenomenon is exaggerated during the injection of semi-solid billets in high pressure die casting due to greater magnitude of applied pressure [152]. The formation of segregated liquid regions is due to the differences in the density and flowability of the residual liquid and the primary α-Al particles.

Non-refined, modified, and refined samples show some degree of liquid segregation in the outer layers near the mold wall, while the combined and over-refined cases show the least segregation. The absence of liquid segregation for the latter cases may be attributed to better distribution of primary particles, and finer and more spherical α-Al in the billets. Fine α-Al solid particles move with liquid without excessive collision and bring about homogenous distribution of primary α-Al phase. The micrographs presented in Figure 8.11 confirm such hypothesis and show almost no segregation of liquid for the billets with the combined treatment.

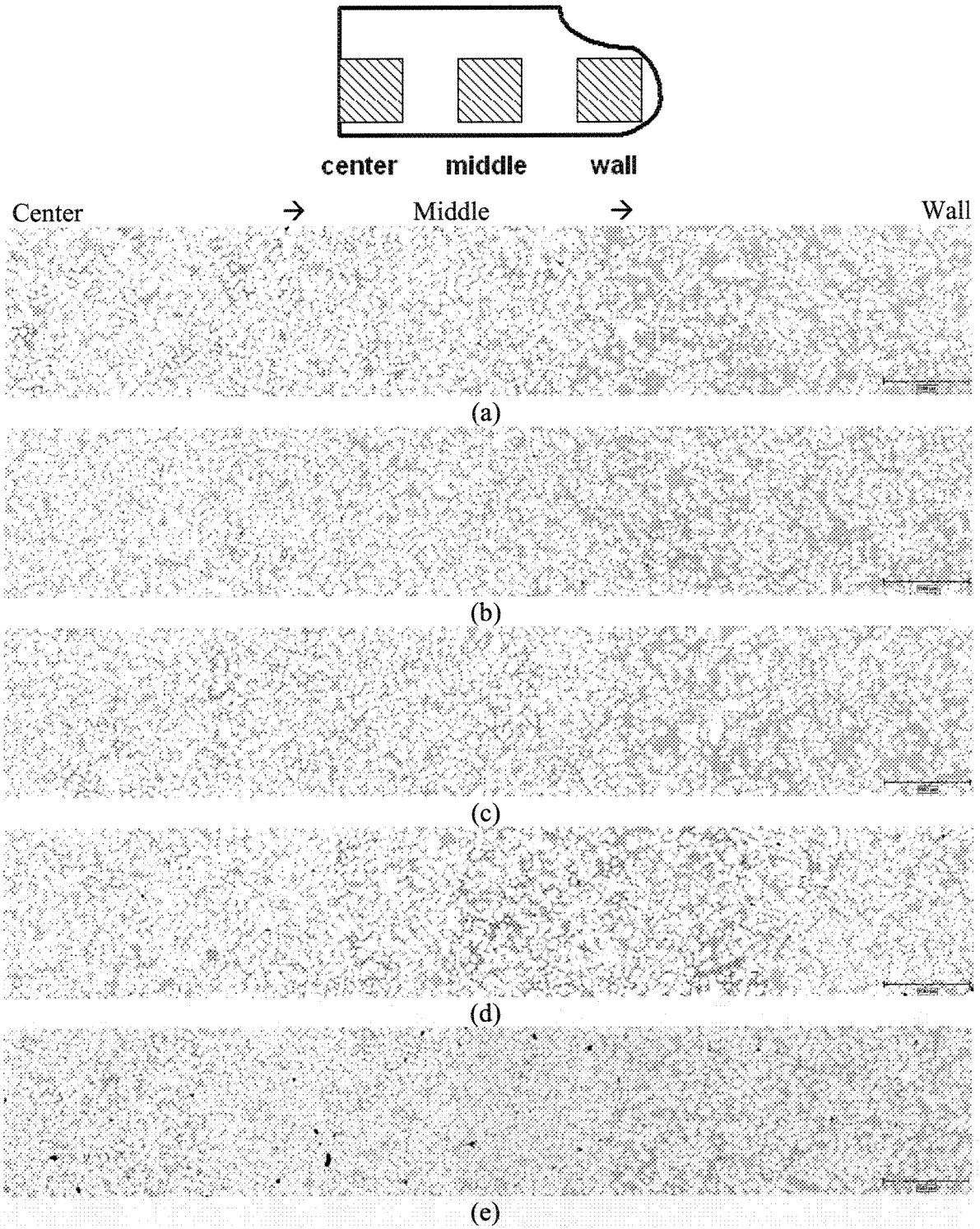

Figure 8.11: Microstructure of deformed SSM billets from center to the wall; (a) base alloy, (b) refined,(c) modified, (d) combined, and (e) over-refined billet

8.1.2 Addition of strontium and boron in the form of AlB_{12}

8.1.2.1 Chemical analysis

The optimum additional levels were obtained from the previous trials in sections 5.2.2 and 7.1.2. Table 8.2 shows the final chemical compositions.

Table 8.2: Chemical analysis of A356 alloy (wt. %)

	Si	Mg	Fe	Mn	Cu	Ti	B	Sr	Al
Original	6.6-6.75	0.36-0.4	Max 0.08	Max 0.003	Max 0.001	Max 0.0058	Nil	Nil	bal.
Grain Refined							0.02-0.03	Nil	
Combined							0.02	0.01	

8.1.2.2 Structural analysis

Figure 8.12 shows the refining and combined effects of B and Sr additions. As it was proved in section 5.2.2, boron is a superior refiner and with its addition, average circular diameter of the primary α-Al particles reduced ~4.2% and number density increased by ~23%. The smaller and more spherical primary α-Al particles with overall higher amount are obvious in the structure as seen in Figure 8.12b. Smaller primary particles play an important role on the flowability of the slurries and as it will be shown later, refined alloy has better flowability.

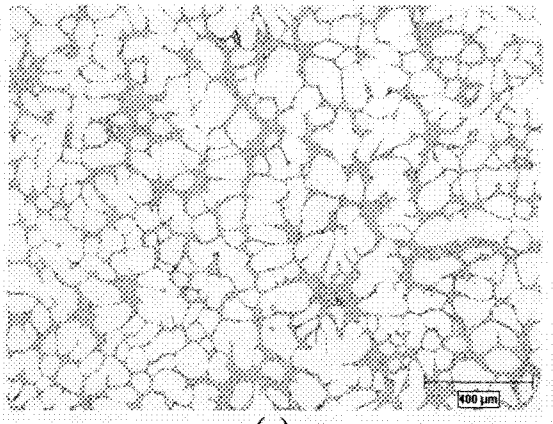

(a)

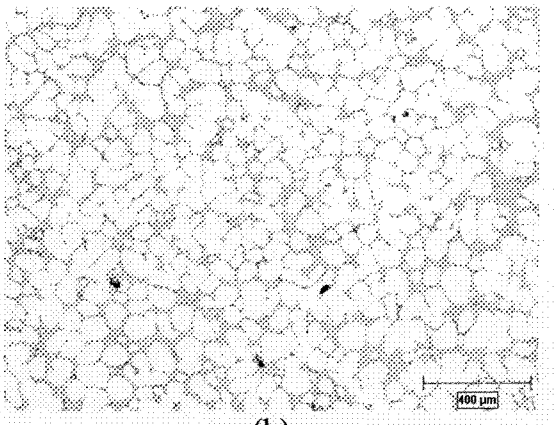

(b)

Continue ⟶

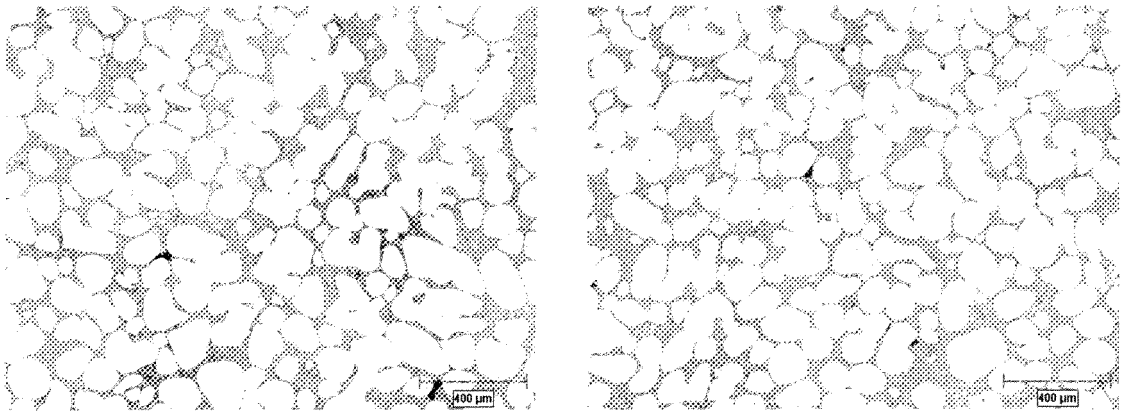

(c) (d)

Figure 8.12: Microstrucutral evolution of as-quenched SEED samples (from 598.5±2.5°C) (a to b): (a) original alloy, (b) grain refined with 210ppm B, and after compression tests (c & d): (c) deformed "a", (d) deformed "b"

By Sr and B combination, it is expected to have fibrous morphology of eutectic silicon but as it was discussed in section 7.1.2, this evolution is not uniform and homogenous through out the billets. It means that some parts are fully modified while others are partially modified as noticeable in Figure 8.13b.

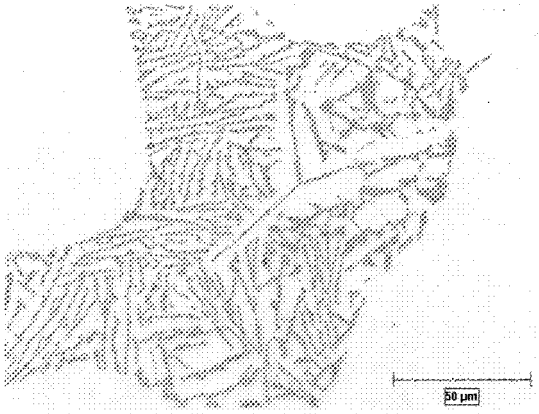

(a)

Continue ⟶

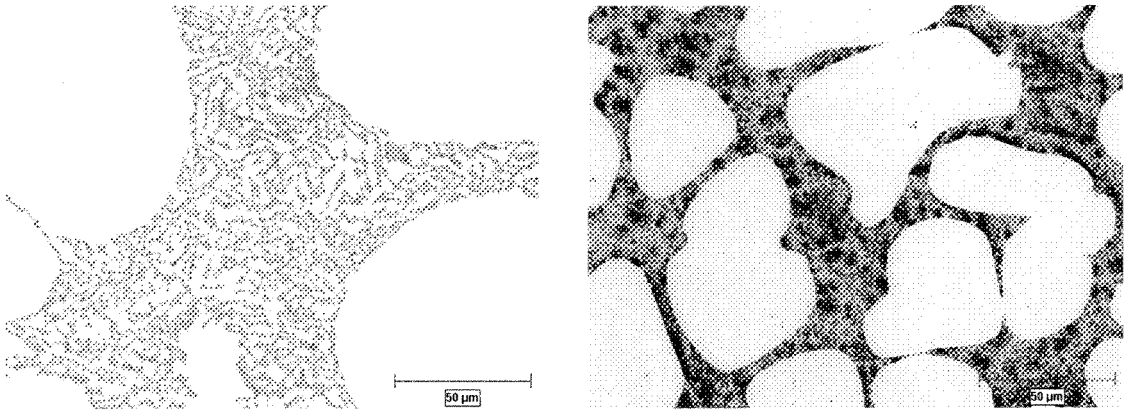

(b)

Figure 8.13: Optical micrographs showing the effect of strontium addition to the refined billet: (a) 290ppm B , (b) 170ppm B and 100ppm Sr

8.1.2.3 Strain-time graphs

The formability of the alloys with B-refining and combined treatment (B and Sr) was also studied as shown in Figure 8.14. The superior formability of the boron-treated alloy as an enhanced refiner is clear in the strain-time graphs with the highest strain at any time belonging to the B-refined slurries. Comparing the deformed billets also verifies the superior flow characteristics of the sole boron treated billets (Figure 8.15). As mentioned in chapter 5, by refiner the size of the primary particles decreases which is associated with more potent nuclei in the system, and results in improved flow behavior. With simultaneous treatment, i.e., Sr and B, the ability of boron to refine the alloy decreases since the high affinity of boron for strontium leads to the formation of SrB_6 compound. The remaining B is therefore not adequate to reduce particle size as in the case of sole B addition. Hence, the primary particles size are not as small as sole B addition and finally lead to less deformation as shown in Figure 8.14. Another disadvantage of combined treatment is the non-homogenous structure of the silicon eutectic which leads to non-uniform mechanical properties and premature failure.

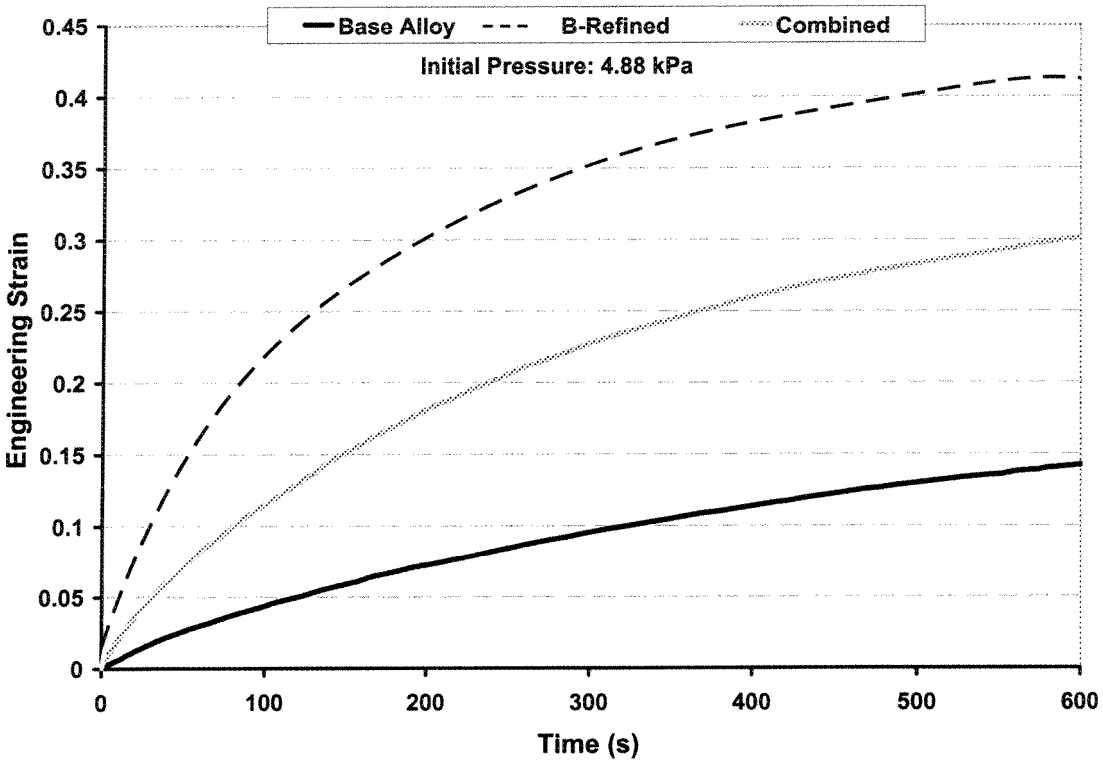

Figure 8.14: Strain-time graphs showing the effect of sole boron and combined B&Sr additions on the flow characteristics of the SEED billets

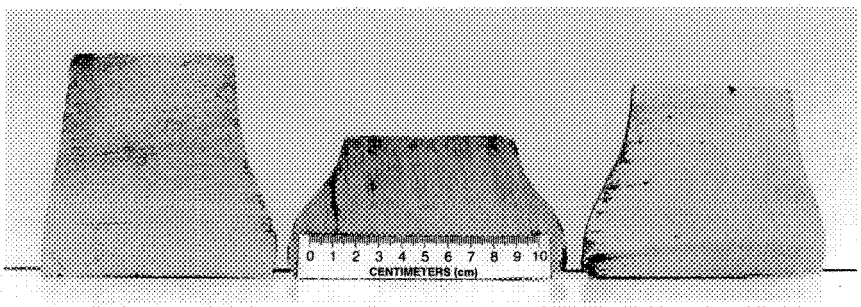

Figure 8.15: Deformed billets under 4.88kPa pressure
(base alloy, B-refined, and combined from left to right)

8.1.2.4 Liquid segregation

With deformation, liquid separates laterally and causes liquid segregation. It is worth mentioning that this effect is always a combination of liquid escaping due to the application of pressure and also tendency of liquid to migrate to lower billet extremes, i.e., "*elephant footing defect*" [122]. By comparing Figure 8.11e which shows the best condition

of TiB master alloy addition with Figure 8.16b, it could be deduced that boron-refinement eliminate liquid segregation by superior distribution of primary particles and consequent enhanced flowability due to smaller particle size. In the case of the combined addition, there is almost no segregation.

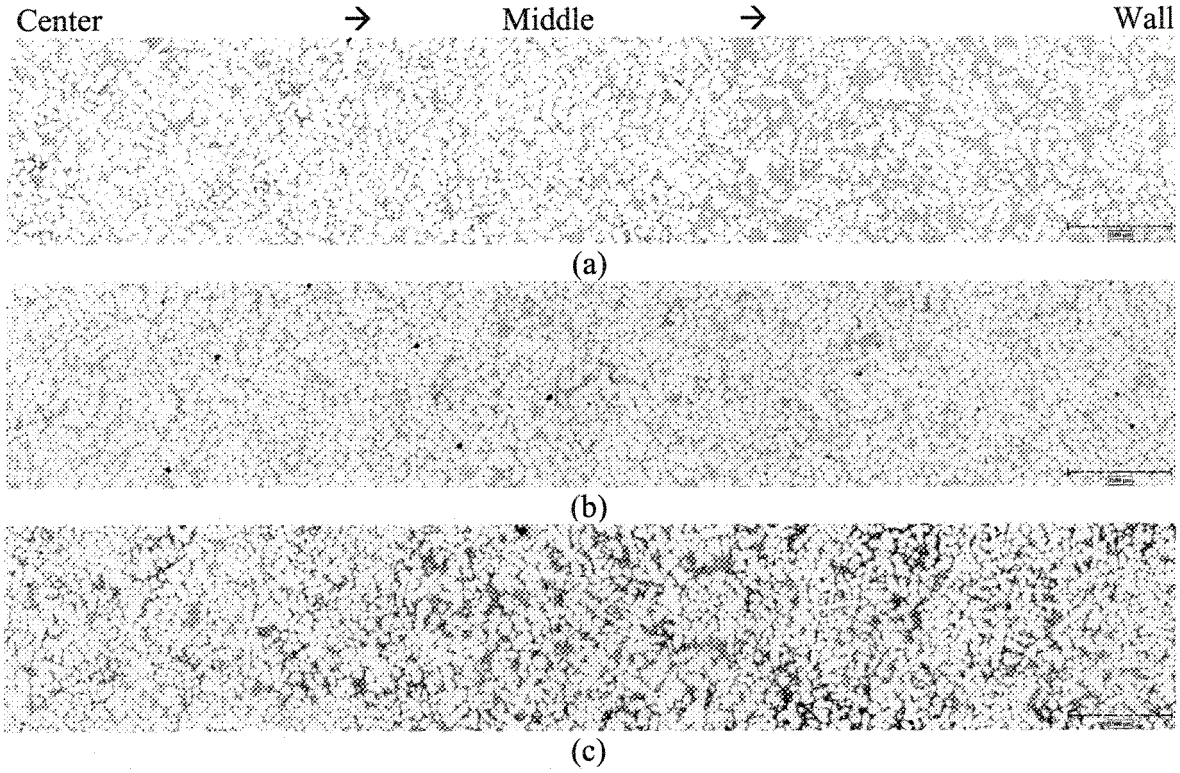

Figure 8.16: Microstructure of deformed SSM billets from center to the wall;
(a) base alloy, (b) refined, and (c) combined

8.1.3 Addition of strontium and boron in the form of AlB_2

8.1.3.1 Chemical analysis

The optimum addition levels were measured in sections 5.2.3 and 7.1.2. The final chemical compositions are shown in Table 8.3.

Table 8.3: Chemical analysis of A356 alloy (wt. %)

	Si	Mg	Fe	Mn	Cu	Ti	B	Sr	Al
Original	6.5-6.75	0.36-0.4	Max 0.08	Max 0.003	Max 0.001	Max 0.0058	Nil	Nil	bal.
Grain Refined							0.02-0.03	Nil	
Combined							0.02-0.03	0.012-0.016	

8.1.3.2 Structural analysis

Figure 8.17 shows the sole and combined (Sr and B) treatments of the A356 alloy. Refineability of the alloy could be seen through comparing Figure 8.1a and 8.17a. With boron refining, circular diameter of the globules decreased by ~5% while number density increased by ~18%.

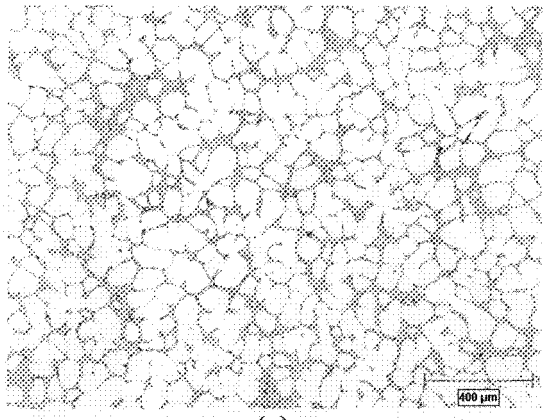

(a)

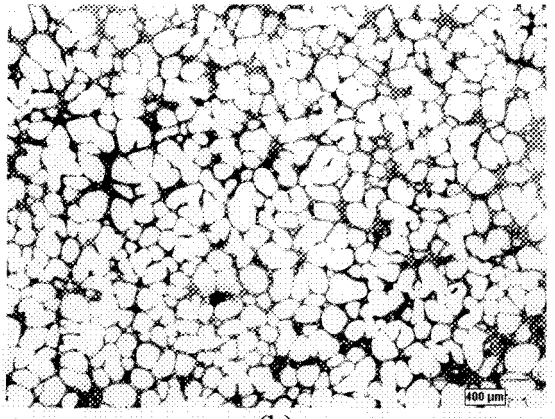

(b)

Continue ⟶

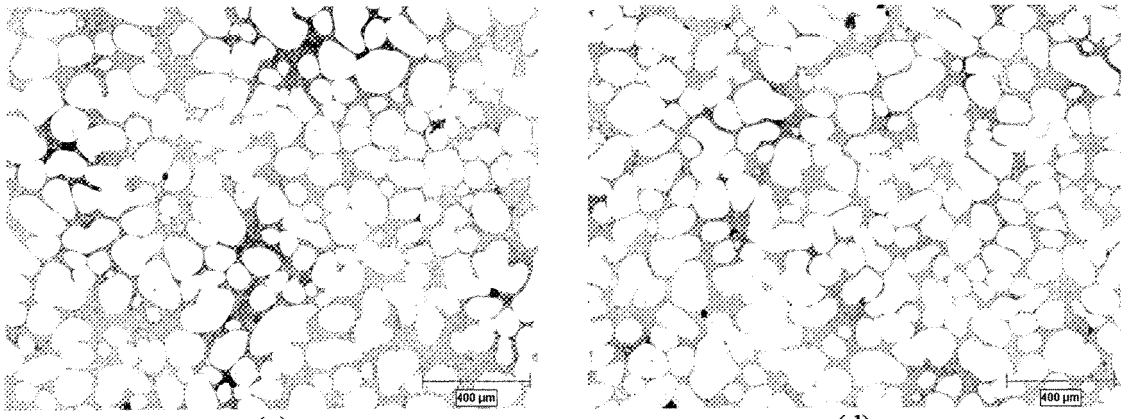

(c) (d)

Figure 8.17: Optical micrographs of quenched samples (a & b):
(a) grain refined with 225ppm B, (b) combined treatment, 230ppm B, 112ppm Sr , and after compression (c & d): (c) sample "a", (d) sample "b"

As discussed in section 8.1.2, with combined additions of B and Sr, non-homogenous modification will be observed which is shown in Figure 8.18. Inconsistent modification levels are obvious in these micrographs.

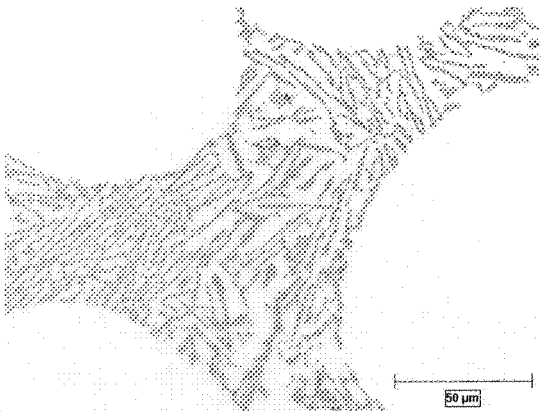

(a)

Continue ⟶

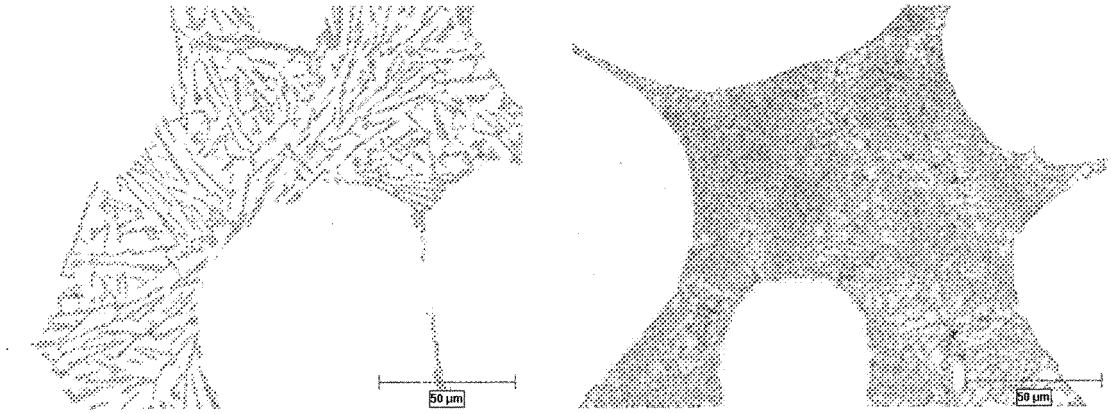

(b)

Figure 8.18: Effect of Sr addition on the deformed billets:
(a) 288ppm B , (b) 313ppm B and 160ppm Sr

With isothermal holding, an interesting phenomenon which is normally seen in thixocasting is observed; namely "entrapped eutectic". With holding the samples at a constant temperature, α-Al particles grow as elaborated in section 8.1.1.2 and with increasing in size and sintering the primary particles, liquid encapsulated to form entrapped areas (later this liquid transforms to eutectic mixture during quenching process). This process of liquid entrapment may also be assisted by agglomeration mechanism related to the application of external forces.

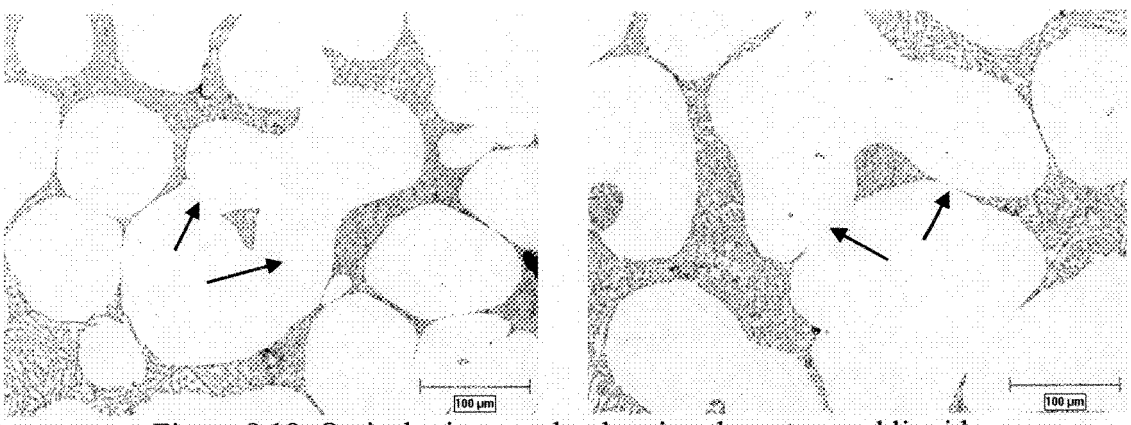

Figure 8.19: Optical micrographs showing the entrapped liquid:
(a) refined with 288ppm B , (b) with 313ppm B and 160ppm Sr addition

8.1.3.3 Strain-time graphs

It was demonstrated in section 8.1.2.3 that the formability of the sole B-refined alloy was better than the initial and combined treated slurries. As discussed in section 5.2.2.1, both master alloys are capable of enhanced refinement which is contributed to the presence of AlB_2 particles, dissolved boron in the aluminum matrix, and transformation of AlB_{12} to AlB_2 particles. As a result, this effect is not related to the type of the boron master alloy used and it is the same for both. While untreated alloy has the lowest deformation, the strain rate increases rapidly and strain shows the highest value by boron inoculation. The combined effect has the moderate value which confirms the interaction of B and Sr followed by formation of SrB_6 (Figure 8.20). Better deformability of the boron treated billet is also clear in Figure 8.21.

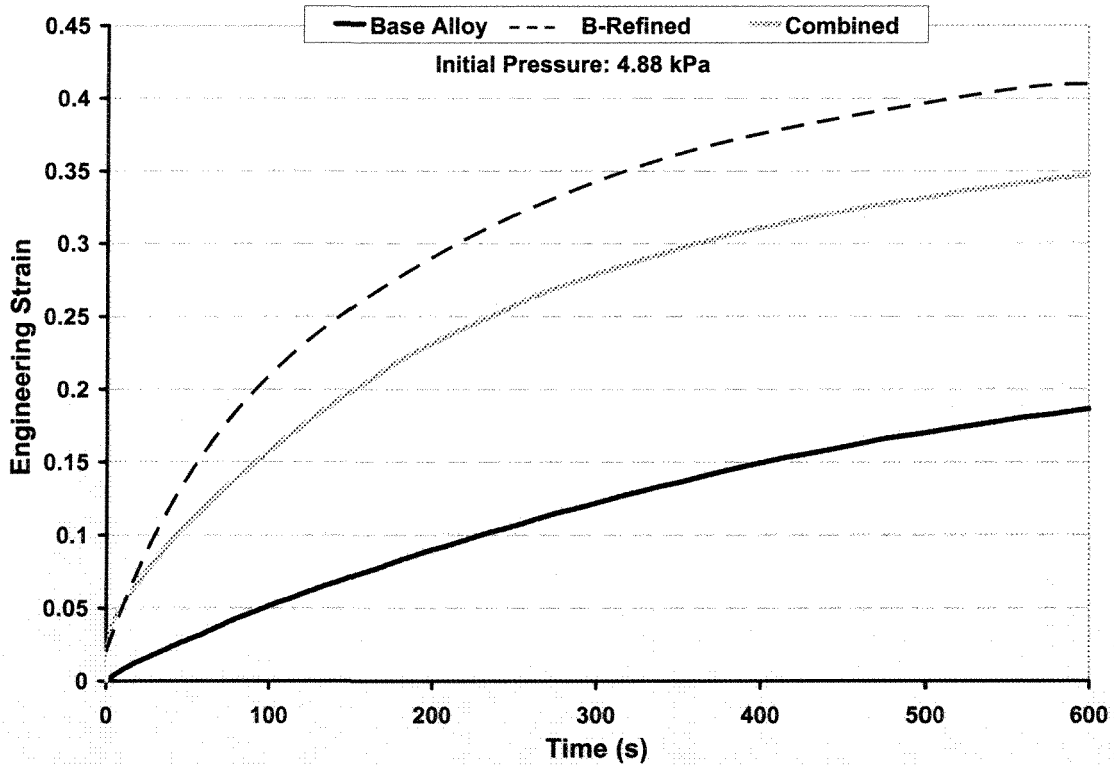

Figure 8.20: Strain-time graphs for B and B-Sr additions

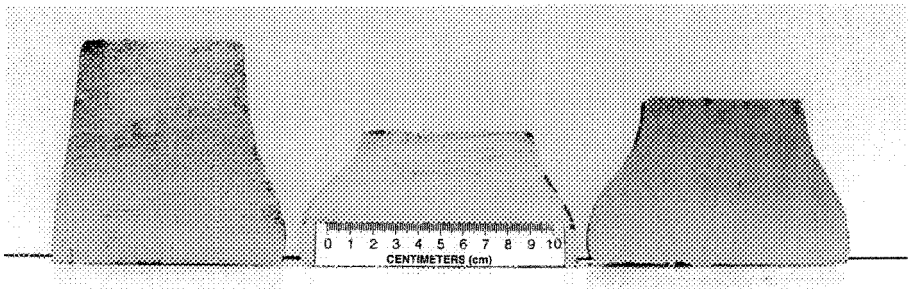

Figure 8.21: Deformed billets under 4.88kPa pressure
(base alloy, B-refined, and combined from left to right)

8.1.3.4 Liquid segregation

Liquid and solid redistribution pattern after deformation process is shown in Figure 8.22. Untreated alloy, Figure 8.22a, has a large liquid segregation area while by boron addition, homogenous distribution of primaries along the entire section of billet is clear. Liquid segregation in the case of combined treatment is also decreased but not as much as the refined alloy (Figure 8.22c).

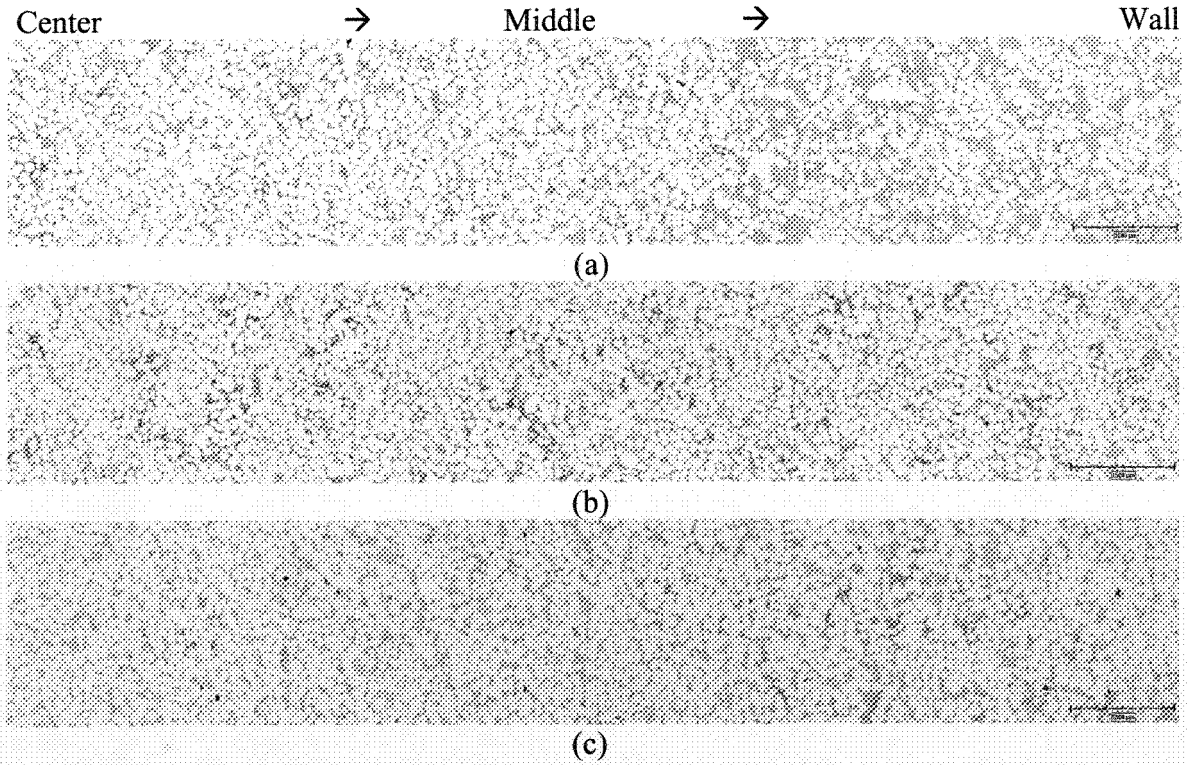

Figure 8.22: Microstructure of deformed SSM billets from center to the wall;
(a) original alloy, (b) refined, and (c)combined

8.2 Rheological tests for Com356 alloy

8.2.1 Addition of titanium, boron, and strontium

8.2.1.1 Chemical analysis

Finding a correlation between structural development and deformability of the alloy is the main concern in this chapter. In this section, the comparison is made for commercial alloy, with Ti content in the original ingots. The optimum additional level was measured from the previous experiments and the final chemical compositions are listed in Table 8.4.

Table 8.4: Chemical analysis of Com356 alloy (wt. %)

	Si	Mg	Fe	Mn	Cu	Ti	B	Sr	Al
Original	7.0-7.2	0.35-0.36	0.07-0.08	0.012	0.002	0.09-0.1	Nil	Nil	bal.
Grain Refined						0.12-0.13	0.006	Nil	
Modified						0.09-0.1	Nil	0.015-0.017	
Combined						0.12-0.13	0.006	0.011-0.012	

8.2.1.2 Structural analysis

As proved in section 5.3.1, due to the pre-existed Ti in the alloy, the resulting melts have higher values of GRF and hence the dendritic growth is restricted as far as possible. Figure 8.23 shows the microstructural evolution due to the refined and combined treatments. With refining, the primary α-Al percentage and its quantity increase slightly. These augmentations are not as much as the A356 alloy since the original titanium level in the commercial alloy could overshadow the refiner effect.

Figure 8.23 d, e, and f also show the usual coarsening effect of isothermal compression tests. It has been shown quite clearly that by isothermal holding at 598 ±2°C, the particles not only grow and become larger, but also contacts between the primary α-Al particles increases. These higher contacts are due to the compression force and diffusion at higher temperatures.

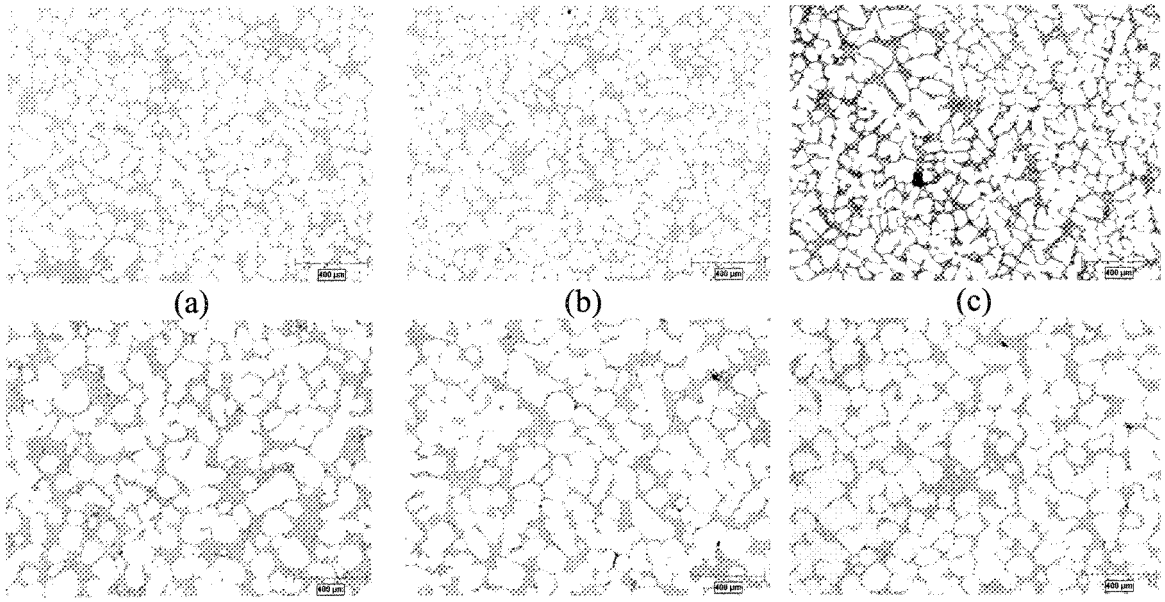

Figure 8.23: Microstrucutral evolution of Com356 quenched samples (a to c):
(a) base alloy, (b) grain refined, (c) combined treatment
and after pressing (d to f): (d) sample "a", (e) sample "b", (f) sample "c"

In the modified and combined cases, not only the percentage of the primary phase increases, but also the eutectic silicon morphology is changed. As seen in the deformed micrographs, Figure 8.24, the Sr addition causes morphological evolution of eutectic silicon from lamellar to fibrous structure. Also it seems that the primary α-Al particles are encapsulated by the eutectic regions.

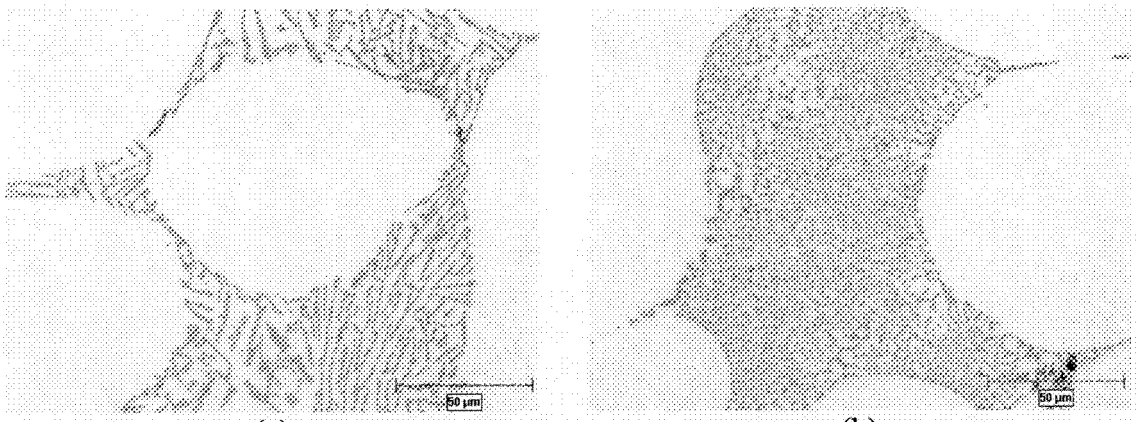

Figure 8.24: Effect of Sr addition in the deformed billets:
(a) non modified , (b) 164ppm Sr addition

8.2.1.3 Strain-time graphs

Effects of different treatment on the formability of billets are shown in Figure 8.25. Higher strain or better flowability is always related to the refined alloy treated by TiB master alloy. By strontium addition, surface tension of the liquid decreases and this is believed to be the main reason for improving in the slope of the modified curve. Combined treatment shows itself as a lower limit of the refined curve in the strain-time graphs.

Comparing the results here with A356 alloy, Figure 8.7, it appears that both alloying systems have the same trend in strain values before and after melt treatment. However it should be emphasized that the strain values for untreated alloy are higher in the case of commercial 356 alloy which is associated to the pre-dissolved titanium in the alloy and its role on increasing the GRF value. This topic will be elaborated more in section 9.1.

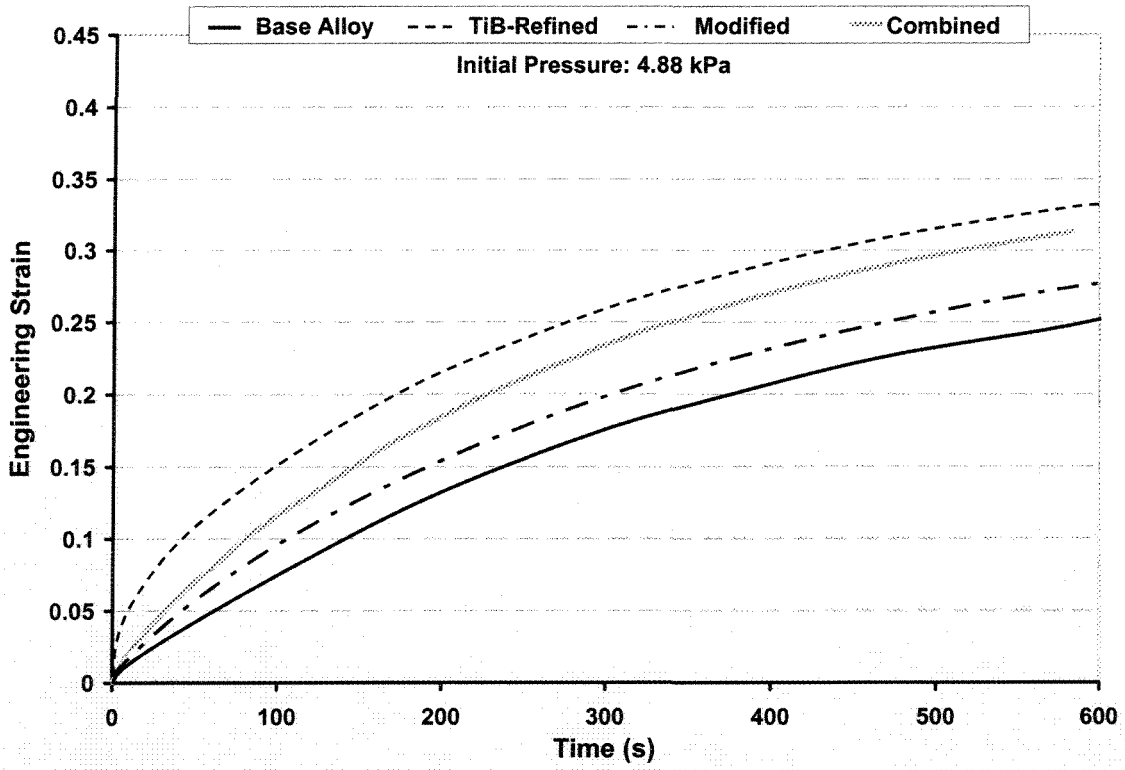

Figure 8.25: Strain-time graphs for entire treatments

Figure 8.26 compares longitudinal sections of the pressed billets with different deformation under 4.88kPa pressure.

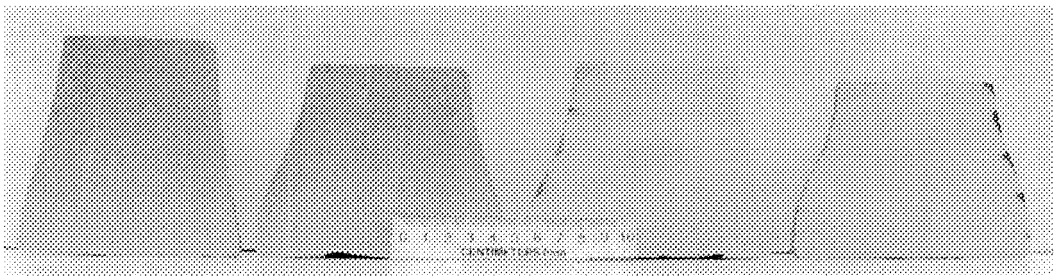

Figure 8.26: Sectional view of the ddeformed billets under 4.88kPa pressure (base alloy, refined, modified, and combined from left to right)

8.2.1.4 Liquid segregation

The microstructural changes from center to the wall of the deformed zones of the billets are shown Figure 8.27. As seen, the central parts are almost unchanged and there is no difference regardless the melt treatment. In the deformed billets, the liquid segregated adjacent to the wall due to the application of vertical force. Liquid segregation is unavoidable for the base alloys both in A356 and Com356 groups. This zone in the refined case appears to have the same segregation pattern as the base alloy with slightly more uniform pattern which is believed relates to the overshadowing of the refiner effect by the pre-dissolved titanium in the melt. The same pattern also exists for the modified sample however in the combined case; the segregation pattern is disappeared to some extent.

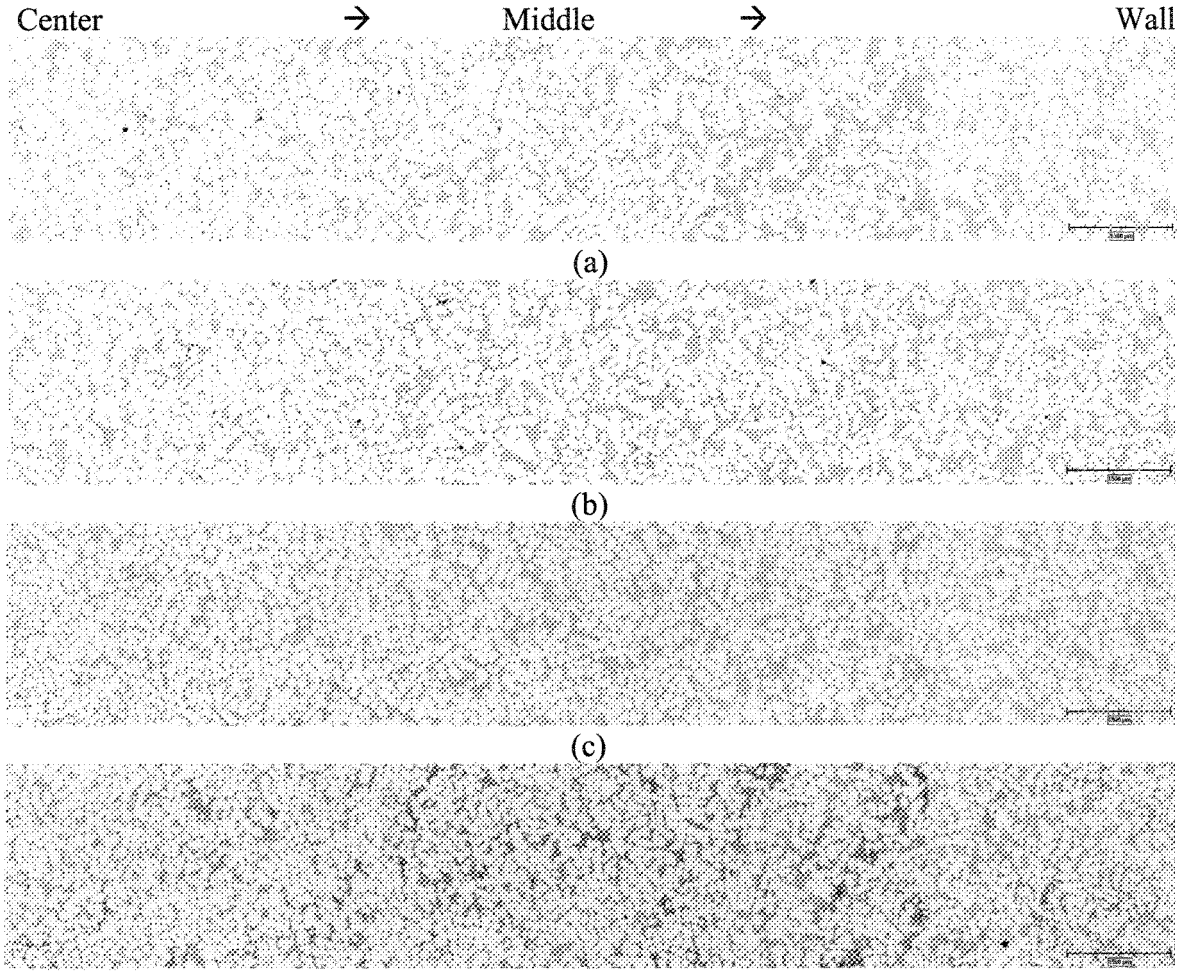

Figure 8.27: Microstructure of deformed SSM billets from center to the wall;
(a) base alloy, (b) refined,(c) modified, and (d) combined

CHAPTER 9

COMPLEMENTARY RESULTS

CHAPTER 9

COMPLEMENTARY RESULTS

9.1 Effect of dissolved Ti on the α-Al grain and globule size

As mentioned in sections 2.2.7 and 2.1.2.2, the chemistry of the melt plays an important role in the grain refining. Small additions of the alloying elements reduce more or less the grain size of the solidified structure depending on their efficiency. Amongst different alloying elements, Ti is the most important one and as it was shown in Table 2.3, it has the largest GRF value and apparently the highest growth restriction effect on aluminum. In this part of the research, effect of Ti-content has been studied in different casting processes, i.e., conventional and semi-solid casting. The final chemical compositions are listed in Table 9.1.

Table 9.1: Chemical analysis of the melts (wt. %)

	Si	Mg	Fe	Mn	Cu	Ti	B	Al
356 without Ti	6.5-6.8	0.35-0.39	0.07-0.08	0.002-0.012	0.001	Max 0.0058	Nil	bal.
356 with Ti						0.1-0.13		

9.1.1 Conventional casting

9.1.1.1 Thermal analysis

Figure 9.1 illustrates the effect of Ti in solution on the early stages of solidification for two different Ti concentrations in 356 alloys. As it is evident, titanium increased the nucleation temperature of the melt. According to thermodynamic calculations, by using ThermoCalc for approximately the same alloy composition, Figure 5.8, it is confirmed that

the liquidus temperature for this alloy is ~ 611°C and the solubility limit of Ti is ~ 0.12%wt. With increasing Ti, solidification starts at higher temperatures. It has to be emphasized that there may be some discrepancies between Figure 5.8, the ThermoCalc calculation, and the results presented in Figures 9.1 and 9.2, regarding the nucleation of primary α–Al. This is purely attributed to ThermoCalc calculation being under equilibrium condition while the current study is under non-equilibrium condition including higher cooling rate and presence of other alloying or trace elements.

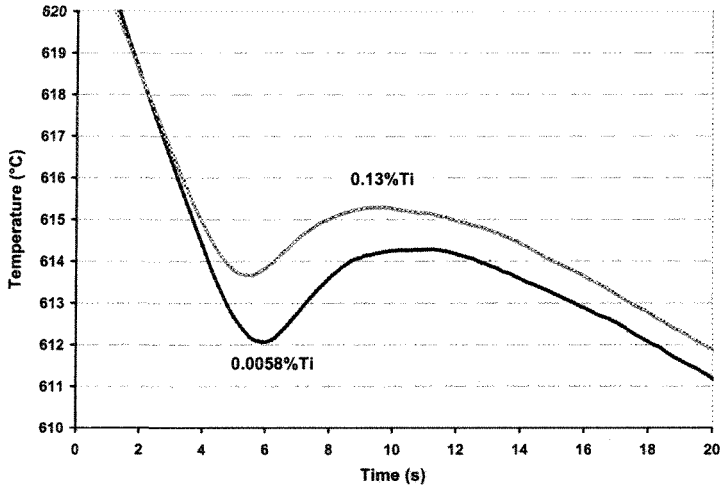

Figure 9.1: Typical cooling curves for a selection of samples (central thermocouple) of 356 alloys with different Ti levels

Figure 9.2 shows nucleation ($Tnuc_{Al}$) and recalescence temperatures of the primary α-Al particles. The concept of increasing the liquidus temperature could easily be seen in Figure 9.2 where $Tnuc_{Al}$ is increased by 2-3°C to about 617°C by alloying with Ti. This augmentation is shown by ThermoCalc calculation in Figure 5.8 but with lower rate due to the equilibrium condition. The solidification undercooling is also decreased by ~1°C with Ti addition. The greater reduction in solidification undercooling is expected to render finer structure. Such conclusion is based on the fact that the lower undercooling is an indication of easier nucleation of primary α-Al particles and thus more nuclei are expected to form, i.e. the nuclei density increases, with final structure becoming finer. The mechanism of refinement is further discussed in the next section.

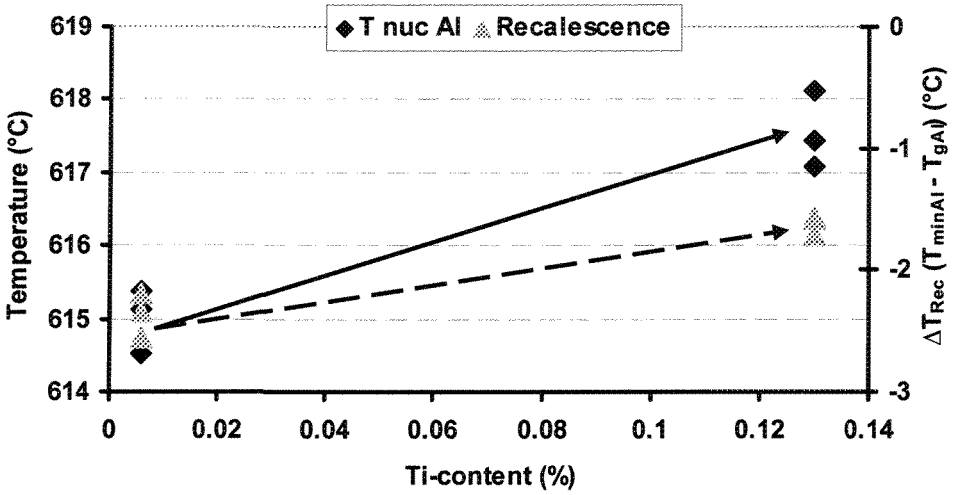

Figure 9.2: Effect of Ti in solution on the nucleation temperature and ΔT recalescence (undercooling) of primary α-Al particles

9.1.1.2 Structural analysis

Figure 9.3 shows the microstructural differences between the 0.0058% and 0.13% Ti containing alloys. As it is evident, the alloy with 0.13% Ti has finer dendritic structure, and the grain growth appears to have been restricted, i.e. the number of grains per unit area has increased.

It may be argued that such refinement is due to the more effective nucleation, not the growth restriction capability of Ti. In order to clarify this issue, it is helpful to define the two concepts of "grain refining" and "grain growth restriction". The former is dependent primarily on the presence and then the size, population, and morphology of nucleants, i.e. independent Ti-based compounds, while the latter is about the dissolved Ti in the α-Al matrix and its diffusion across solid-liquid interface. It is believed at this level of Ti concentration, it is rather unlikely and remote to have independent Ti-based particles since the formation of Ti-based compounds begin only at Ti%>0.12. Therefore, the concerning issue should be the diffusion of Ti at the solidification interface and its rate controlling role on the primary α-Al growth. The growth restriction concept is thus more acceptable than the formation of Ti-based nucleants to render more effective nucleation, especially at the early stages of solidification. However, it may be true to assume that in a

localized volume such diffusion of Ti may eventually lead to the formation of Ti-based nucleants, but this is a time dependent event and surely not at the beginning of solidification, i.e. the diffusion of Ti is a pre-requisite for such mechanism.

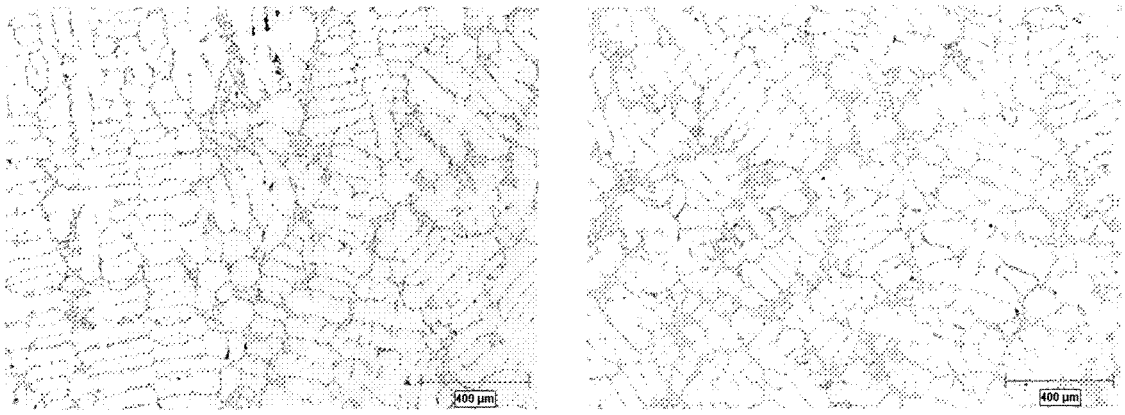

(a) (b)

Figure 9.3: Effect of Ti in solution on the microstructure:
(a) with 0.0058%Ti, (b) 0.13%Ti

9.1.2 Semi-solid processing

9.1.2.1 Structural analysis

Optical micrographs in Figure 9.4 show the resulted microstructure in the SEED process. As it is evident, the primary α-Al particles in both samples are almost fully globular. The fine eutectic structures in both figures are due to the quenching of billets in cold water which also prevented further coarsening of primary α-Al particles.

Although the microstructure of 356 alloy containing 0.13% Ti appears to be slightly refined, Figure 9.4, the effect of dissolved Ti on the microstructure is better realized if it is characterized quantitatively. Therefore, both quantitative metallography and rheological tests were carried out on different Ti-containing alloys, to highlight grain growth restriction which will be described later.

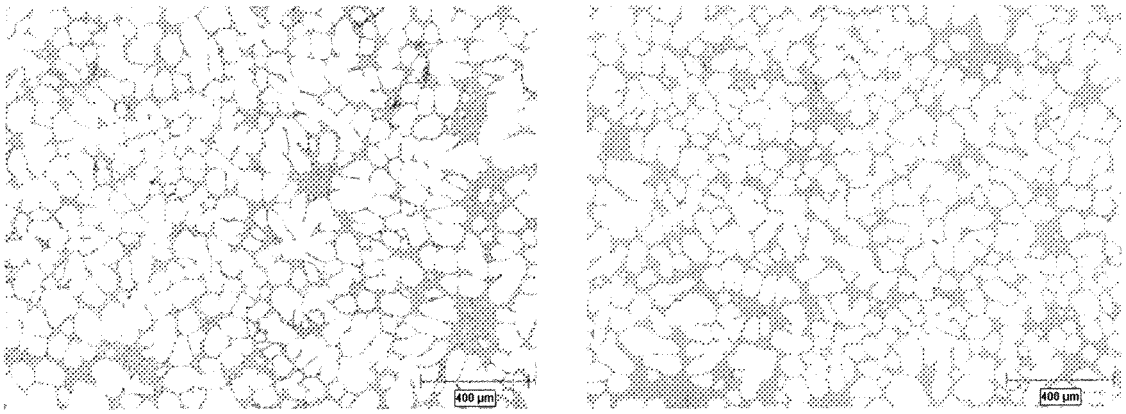

(a) (b)

Figure 9.4: Optical micrographs in the SEED process: (a) 0.0058%Ti, (b) 0.13%Ti

The concept of structural refining with dissolved Ti may be explained with reference to constitutional supercooling where the growing primary α-Al dendrites reject Ti into the solid-liquid interface as they grow. The rejected Ti atoms build up ahead of the solidification interface and form a Ti-enriched boundary layer. This is graphically illustrated in Figure 9.5 where the concentration of Ti at the boundary layer varies for different Ti concentrations due to differences in the diffusion fluxes for different Ti contents. The value of diffusion flux, $\frac{\partial c}{\partial x}$, is greater for 0.13%Ti than that of 0.0058. Therefore, the degree of constitutional supercooling is much greater for 0.13% Ti than that of 0.0058% Ti. Equally, the boundary layer thickness is greater for higher Ti content alloy as schematically illustrated in Figure 9.5. As pointed out by Kurz and Fisher [23], the equivalent boundary layer thickness (δ_c) is inversely proportional to growth rate, (V), for an alloy solidified at different growth rates, as given in equation 9.1. Since higher growth rates are equivalent to lesser diffusion and rejection of solute element into the boundary layer (lower $\frac{\partial c}{\partial t}$), it may be acceptable to consider higher concentration of solute element within the boundary layer is equivalent to that of lower growth velocity or greater thickness of this layer. This is indeed the concept of growth restriction discussed earlier.

$$\delta_C = \frac{2D}{V} \tag{9.1}$$

Where D is the diffusion coefficient for dissolved titanium. Furthermore, as the concentration of Ti increases at the interface, it may reach the level where new nucleants of Al_3Ti could form within the interface layer. The presence of such particles encourages the formation of new α-Al nuclei within the interface. This is in line with the cooling curves in Figure 9.1 where solidification undercooling decreased with higher Ti addition. The newly formed α-Al particles are expected to reject Ti into the newly formed interfaces as they grow. The repetition of such mechanism ensures the formation of finer and more equiaxed and spherical particles as observed in 0.13%Ti added 356 alloy, Figure 9.3. and 9.5.

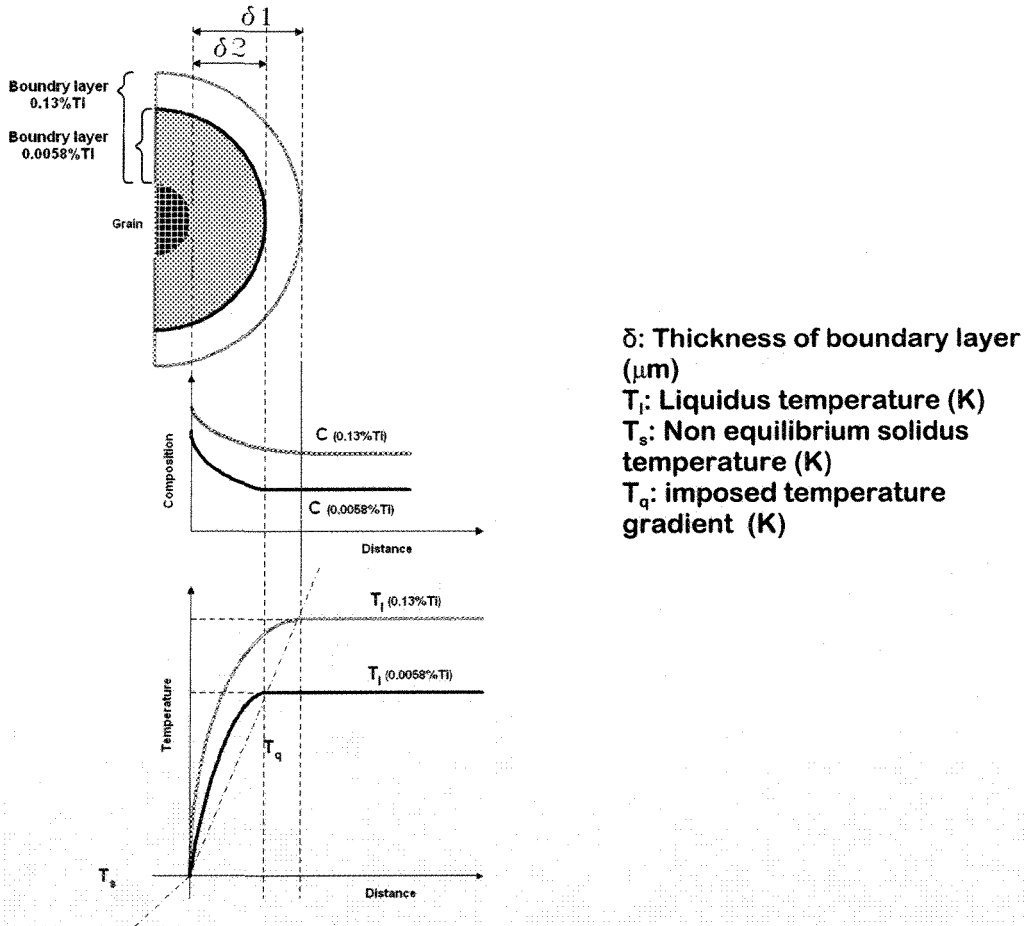

Figure 9.5: Schematic of constitutional undercooling in different solute buildup (higher and lower Ti are indications for ~0.1-0.2%Ti and ~0.01%Ti respectively)

The results of quantitative metallography are presented in Figure 9.6. The mean globule size, average circular diameter, appears to have decreased with increasing Ti

content. Nevertheless, the globule size was always less than 100μm regardless of Ti concentration which is an indication of the process capability in producing high quality rheocast billets [158].

The rise in the number of α-Al particles per unit area (mm^2), number density, coupled with the reduction of area to perimeter ratio, A/P, indicate microstructural refinement leading to the formation of more isolated and finer particles in the Ti-content billets.

From solidification point of view, with the addition of growth restricting elements such as Ti, dendrite growth tends to slow down in direction opposite to heat flow approaching those of the lateral growth. The overall growth therefore tends to be more radial and the resulting structure should be more globular., The formation of spheroidal particles are critical on the rheological behavior of the slurries as discussed later in this article. This is clearly shown by the reduction in percentage of the primary α-Al particles with aspect ratio greater than 2. The formation of more spherical particles is further supported by the rise in the percentage of particles with sphericity number greater than 0.8 with increasing Ti content (Figure 9.6b&c).

As pointed out before, the final stage in the SEED process is draining a portion of the remaining liquid from the system to have a self standing billet. The quantity of drainage may be regarded as an indication of fluidity in micro scale, micro-fluidity. It has to be emphasized that this may be contradictory to the classical meaning of fluidity which is normally defined as the distance to which a metal will run before solidification. That is why the concept of "micro-fluidity" is employed, *"the flow of molten alloy through a network of primary α-Al particles"*. Figure 9.6d illustrates more drainage of the remaining liquid with higher Ti in solution. This may be due to the formation of spherical particles within alloy having higher Ti and thus the ease of liquid flow through the less complex inter-particle channels. This concept could be compared to that of the dendrite coherency point (DCP) in the conventional casting and the fact that mass flow persists further, i.e. postponement of DCP to lower temperatures, with grain refining [78].

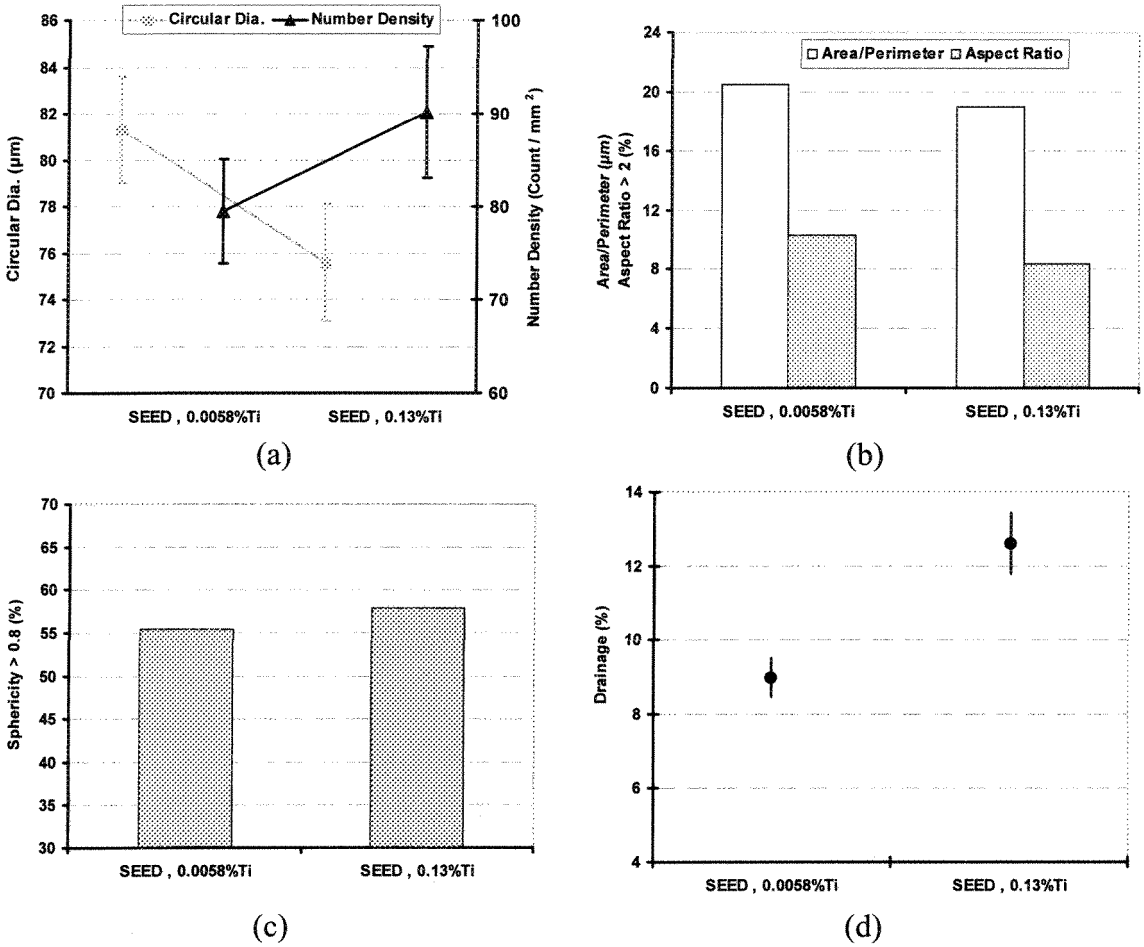

Figure 9.6: Image analysis parameters for 356 alloys: (a) circular diameter & number density of α-Al particles, (b) area/perimeter & percentage of α-Al partciles having aspect ration >2, (c) sphericity percentage, and (d) drainage

9.1.2.2 Strain-time graphs

The effect of α-Al morphology on the ability of billets to deform is clearly detectable in the strain-time graphs presented in Figure 9.7. Three distinct regions may be recognized on these graphs as reported before [186]:

- Stage I, where the billet flows almost without any resistance to applied pressure. It may be attributed to easy movement of the primary α-Al particles within the residual liquid and without appreciable collision. The extent of this region is dependent on the degree of globularity of the primary α-Al particles.

This is in agreement with Chen et al. results [199] where they proposed lateral liquid flow coupled with solid particles movement towards each other in the vertical direction as the main cause of easy flow during step-I. They also pointed out that step-I brings about solid/liquid segregation within the deformed billet. As it is evident, the extent of this region appears to be dependent on Ti concentration where less resistance to deformation is shown for higher Ti content.

- Stage II, where there is some degree of resistance to flow. This is due to the collision of solid particles and formation of α-Al agglomerates. The agglomerated chunks are the resisting constituents to billet flow.

This is also similar to what has been reported by Chen et al., where cooperative movement of solid and liquid phases is responsible for billet deformation. This is accompanied by some degree of resistance to flow where solid particles not only move vertically but also laterally. For constant force, the slope of the curve should decrease due to this resistance. As for the stage I, the ability of billets to deform increases with increasing Ti content.

Both stages I and II are regarded as non-steady state, since the slope of the graphs vary with time. The reducing trend in the slope may be attributed to mainly the collision and agglomeration of the primary α-Al particles.

- Stage III, where the billet flows almost steadily with a constant slope. It is believed the two processes of agglomeration and de-agglomeration have reached an equilibrium state, i.e. quasi steady state equilibrium.

This is the stage which is believed to have been neglected by Chen et al. [199]. They have defined step III as the section that the deformation force increases sharply since it should overcome the friction generated from the sliding between solid particles and also affecting by surrounding particles. This is believed to be stage IV according to the current study, where the deformation force for this step should be larger than the last steps.

As for the stages I and II, the ability of billets to deform in stage III increases with increasing Ti content.

The changes in the billets deformability due to the primary α-Al particles size and distribution are clearly detectable on the graphs in Figure 9.7. The alloy with almost no Ti shows the lowest strain values while the commercial 356 billet deforms at much higher range due to smaller globule size as already discussed. As mentioned in section 8.1.1.3, the billets with more globular and finer microstructure yield greater engineering strain and result in better flow. In other words, the superior flow of the alloy with higher Ti content is due to its structure having more globular and finer grains which enables it to flow better. Furthermore, the parameters from Figure 9.6, especially average circular diameter and number density of α-Al particles, clearly support the conclusion that the billet with higher dissolved Ti has more globules with smaller size.

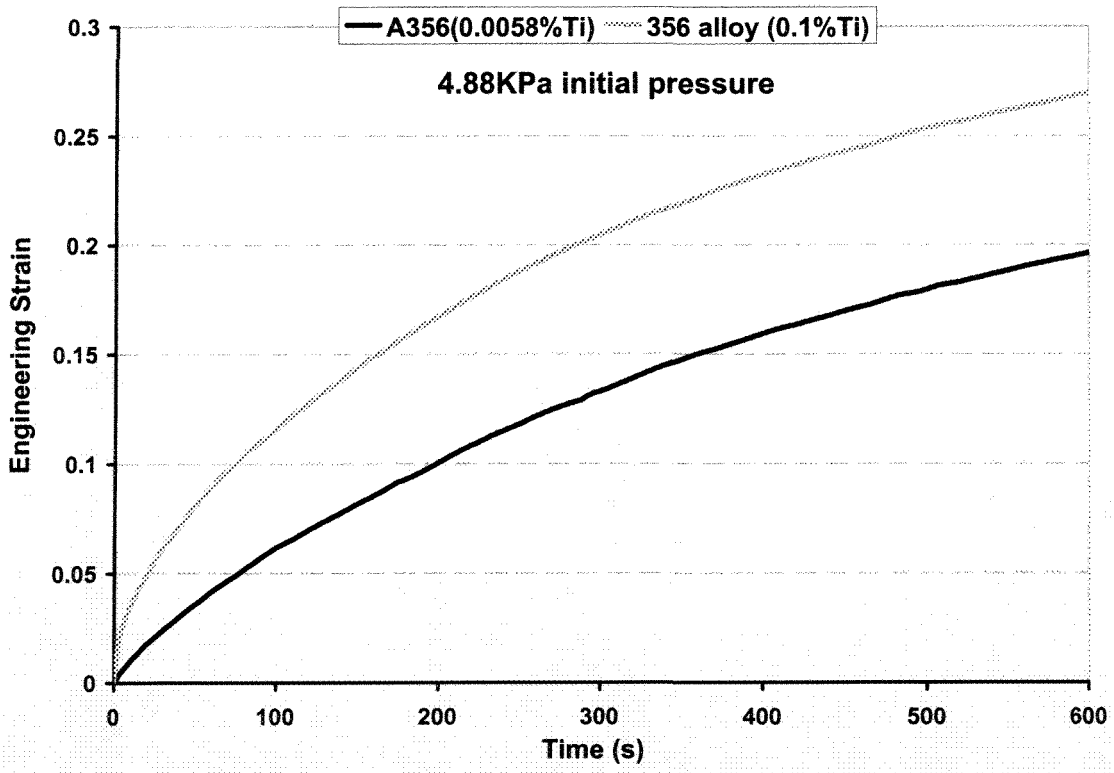

Figure 9.7: Strain-time graphs for different Ti in solution

9.2 Effects of pouring temperature on the structural evolution

Solidification is governed by *nucleation and growth* of primary crystals from the melt, where nucleation controls the size of grains formed and growth determines the grain morphology and the distribution of alloying elements within the matrix. The driving force for nucleation is the degree of undercooling created during solidification and growth is controlled by the temperature gradient in liquid. Both are however affected by the rate of heat extraction from the melt. The final structure is therefore dependent on the nucleation density, growth morphology, fluid flow, and diffusion of solutes. The latter two control refining, i.e. mechanical or thermal remelting, and coarsening of the as-cast structures, i.e. ripening. Therefore close control of casting conditions, such as pouring temperature, rate of heat extraction from the melt (cooling rate), nucleation sites (employment of grain refiners) and temperature distribution within the melt (temperature gradient), may result in formation of the desired as-cast structure. The above mentioned approach could easily be employed for semi-solid products through application of low pouring temperature as a SSM technique which was described in section 3.1.1.8

9.2.1 Experimental procedure

Melt preparation in this study was the same as mentioned in chapter 4. A similar casting procedure was employed to cast billets with the same setup but without any mold stirring and drainage. The sample with no stirring will be referred as "*conventional*". Pre-alloyed ingots of 356 with the chemical composition given in Table 9.2, was poured in the same steel mold of 75 mm diameter and 250 mm long at different superheats, ~ 0 - 80°C. In all experiments, the mold was tilted to reduce turbulence during pouring. Figure 9.8 shows schematically the actual experimental setup. The billets were taken out of the mold while still in the mushy zone and quenched quickly in cold water. The quenching temperature was registered within 592-597°C in all trials.

In all cases, two K-type thermocouples were installed at the mold center and near the wall with their tips at 80 mm from the bottom of the mold to monitor temperature

distribution of the bulk liquid during solidification. The cooling rate during solidification above the liquidus temperature was ~4 $°Cs^{-1}$.

Table 9.2: Chemical analysis of the melts (wt. %)

Si	Mg	Fe	Mn	Cu	Ti	B	Al
6.9-7.1	0.3-0.31	0.09	0.001	0.001	0.13	Nil	bal.

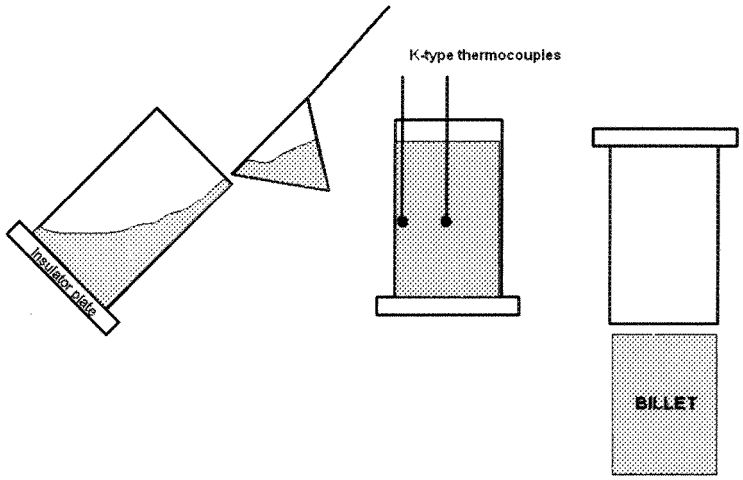

Figure 9.8: Experimental set up for pouring process tests

9.2.2 Thermal analysis

The cooling curves of Figure 9.9 represent temperature variations of the liquid near the mold wall and the center. It is noticeable that there are two different cooling regimes for the wall and central areas at the beginning of each trial, but an almost uniform cooling rate is reached later on during the test. The melt temperature is always higher at the centre of the mold immediately after pouring, which is contributed to the mold wall chill effect. There are three distinct regions identified on the cooling curves of Figure 9.9 as follow:

- Segment-I; the maximum temperature difference between the wall and center of the cast billet, seen at the beginning of solidification.
- Segment-II; the solidification time which extends between the maximum temperature difference between the wall and center of the billet up to the point where a uniform cooling rate is established within the bulk liquid. This is labeled

the *"metastability period"*, since the bulk liquid has not yet reached thermal equilibrium.

- Segment-III; the time between the beginning of uniform cooling rate and quenching. This is labeled as the *"stability period"*, due to uniform cooling rate through out the bulk liquid.

It is evident from Figure 9.9 that the melt temperature near the mold wall is different for three pouring temperatures of 615, 645, and 695°C with 615°C being heavily undercooled. Furthermore, the rise in the wall temperature following pouring is greatest, ~10°C, for the lowest pouring temperature of 615°C. Such temperature rise can only be justified by either a rapid phase transformation, released latent heat of fusion, or rapid heat flow from the central regions towards the wall due to large temperature difference, segment I, established at the beginning of solidification. It is also noticeable that the magnitude of segment-I decreases with increasing pouring temperature as plotted in Figure 9.10. It has to be mentioned that the segment-I is regarded as the driving force for the heat flow across the bulk liquid, so its reduction must prolong the time where uniform cooling rates are established within the mold. This should be evident in the duration of the metastability period, the time where the molten metal cooling rates near the wall and center of the mold approach a uniform value. The extent of metastability period increases with increasing pouring temperature, Figure 9.10. The optical micrographs shown in Figure 9.11 clearly illustrate the effect of pouring temperature on the resulting microstructure.

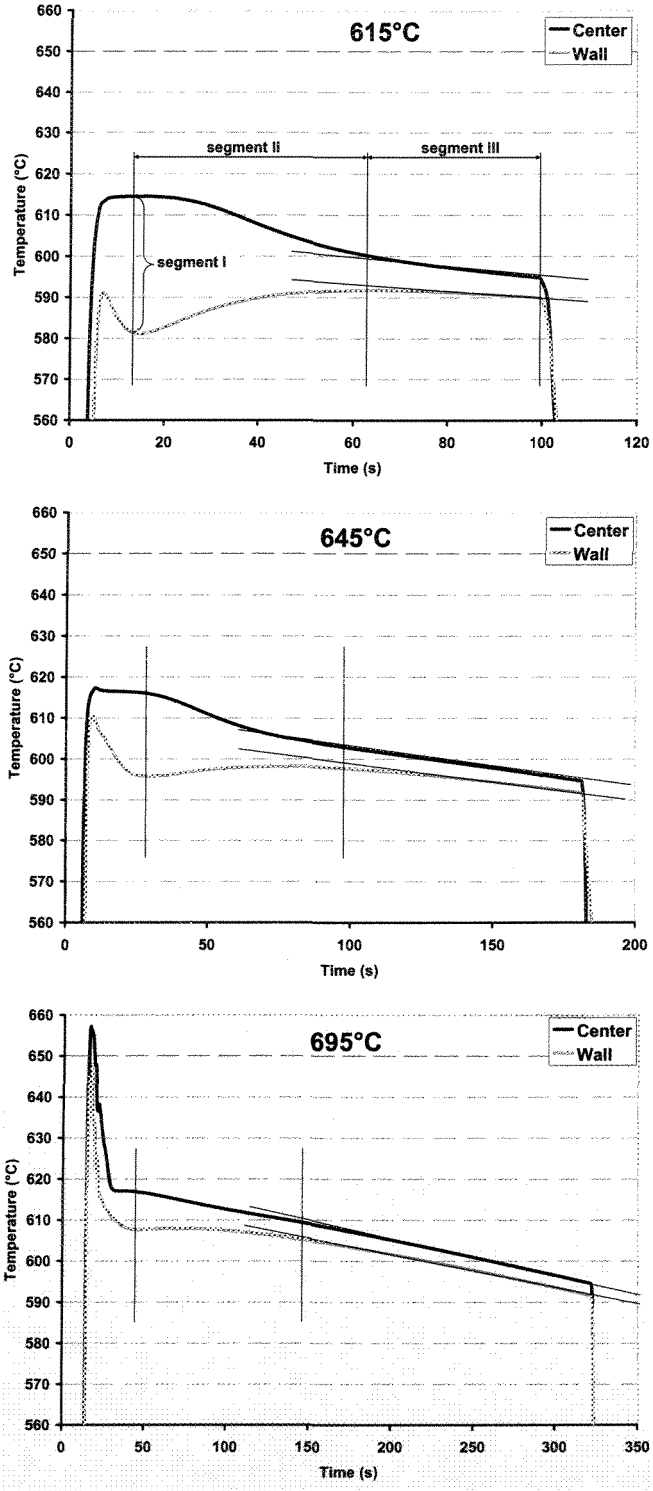

Figure 9.9: Typical wall and center cooling curves for 615, 645, and 695°C pouring temperatures

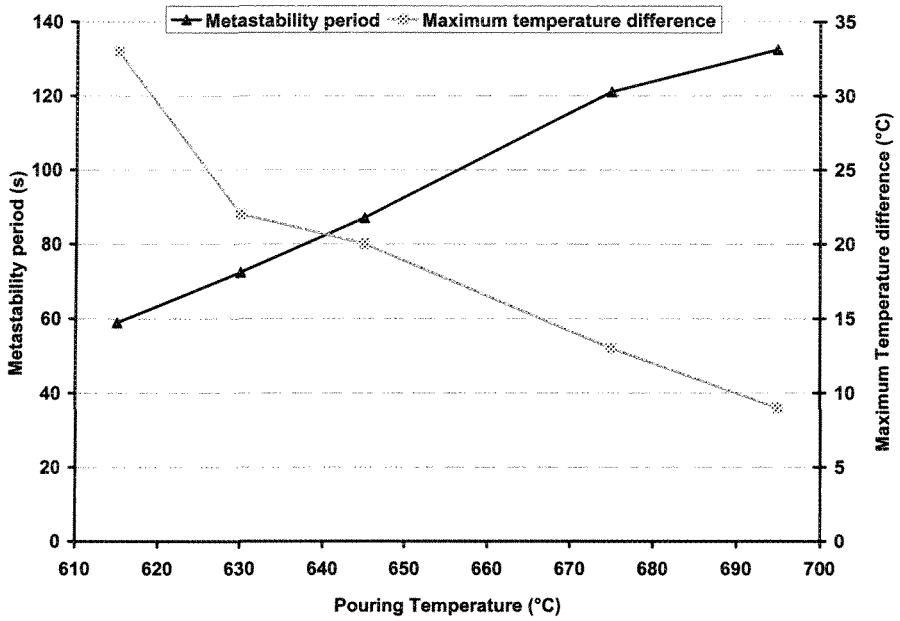

Figure 9.10: Effect of pouring temperature on the metastability period and temperature variation across the bulk liquid

Accordingly, based on the aforementioned observations, two hypotheses put forward to explain the fine grained globular structure seen in Figure 9.11. They are based on either nucleation or growth processes as the domineering factor on the formation of the primary α-Al particles. However, it is believed that both hypotheses are active, but in order to clearly identify the dominant mechanism, further solidification tests are required which is beyond the defined aims of the current research program.

- *Nucleation-based hypothesis*

The highly undercooled melt near the wall at low pouring temperature explodes with a large number of nuclei, big bang or copious nucleation, to lift up melt temperature with the released latent heat of fusion. However, as seen in Figure 9.9, the temperature rise near the mold wall is not sufficient enough to pose any threat to solidification by remelting the nuclei even for the lowest pouring temperature, nor the total heat content of the melt. The rate of temperature rise near the wall is greater for lower pouring temperature due to higher nucleation frequency and thus shorter times for the metastability period. The central parts however solidify in normal manner, but assisted by the floating nuclei, due to fluid

flow during pouring and natural convection from the wall region to eventually establish a uniform cooling rate. The probability of such nuclei to survive is much greater at lower pouring temperature and the uniform and multi-directional cooling, due to the geometry of the mold, promotes the formation of fine grained equiaxed as-cast structure as clearly seen in Figure 9.11 for 615°C pouring temperature.

- *Growth-based hypothesis*

The formation of fine grained equiaxed structure at lower pouring temperatures is also dependent on the growth characteristics of the nuclei. The very large temperature gap between the wall and center during the early stages of solidification, Figure 9.9 at 615°C, encourages faster heat flow towards the mold wall. As a result, the molten alloy near the mold wall acts as a heat sink. However the mold coating coupled with resulting air gap and assisted by the mold thin wall reduces the rate of heat dissipation through the mold wall into the surrounding environment to increase the melt temperature near the wall. In other words, a uniform temperature distribution is established within the bulk liquid which occurs at much shorter time at the lower pouring temperature of 615°C. This is supported with its shortest *"metastability period"*. As a result, the rate of heat flow towards the mold wall diminishes and the growth rate is reduced much sooner for the 615°C pouring temperature. This is coupled with multi-directional heat flow due to the mold geometry and promotes the formation of equiaxed and globular structure as shown in Figure 9.11, i.e. 615°C.

As pouring temperature increases, the mechanism of copious nucleation is less pronounced and there are fewer nuclei exist in the bulk liquid which eventually lead to the formation of a coarser structure. The severity of recalescence also decreases with increasing pouring temperature which supports the hypothesis of lower nucleation frequency. It is important to re-emphasize again the fact that there is longer metastability period at higher temperature, e.g. 695°C, which encourages better development of primary α-Al particles and the formation of more classical dendritic morphology as illustrated in Figure 9.11.

9.2.3 Structural analysis

The optical micrographs in Figure 9.11 show the microstructural changes for the conventional quenched billets. As it is evident with increasing the pouring temperature, increasing the superheat, the morphology of primary α-Al particles becomes more dendritic. As the superheat is reduced, lower pouring temperatures, the morphology changes to rosette and equiaxed and eventually with ripening process, i.e. remelting of thinner arms and growth of thicker arms, they become globular. The process of ripening which is analogous to Ostwald ripening for precipitates in solids, is clearly detectable in Figure 9.11 (675°C, arrowed). Furthermore, as the pouring temperature approaches 615°C, the melt is no longer superheated. As it was described, the mold itself reduces the rate of heat extraction from the mold wall and thus establishes a shallow temperature gradient within the molten alloy. Such low temperature gradient (G), encourages the wide spread nucleation of primary α-Al particles within the melt and consequently the formation of equiaxed and eventually globular structure as shown in Figure 9.11 (625 and 615°C).

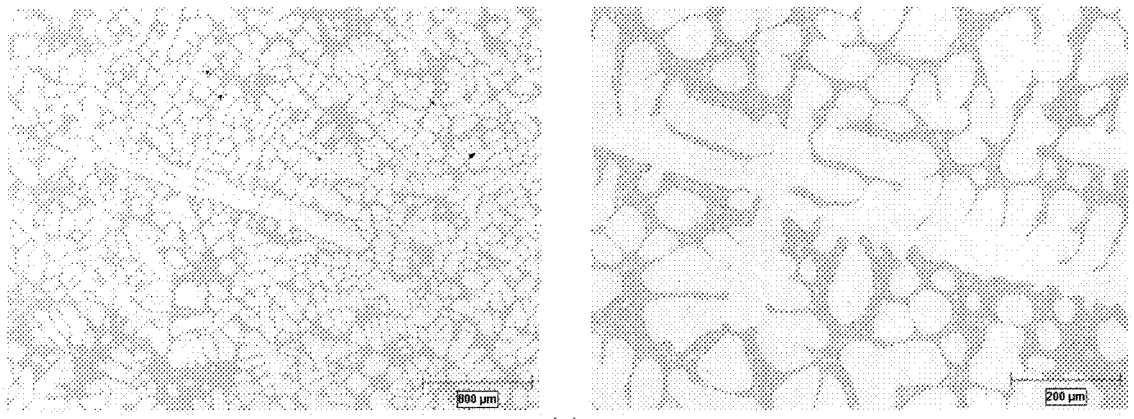

(a)

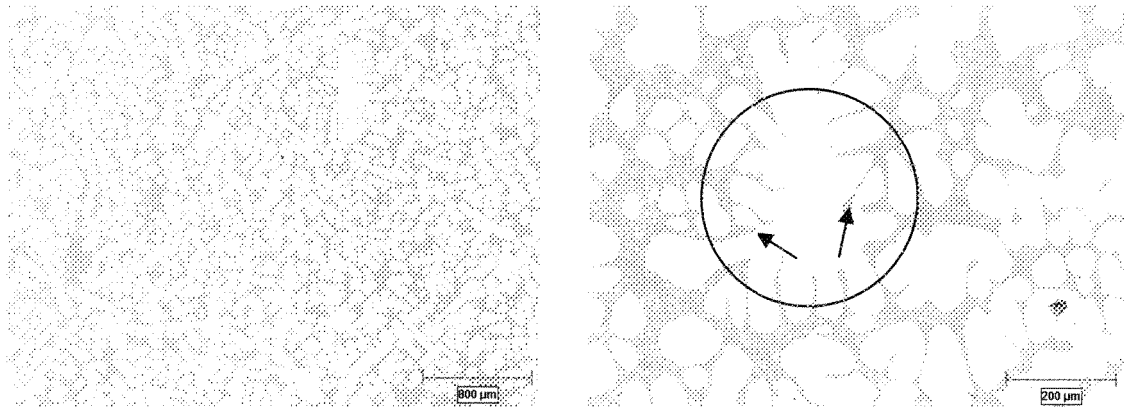

(b)

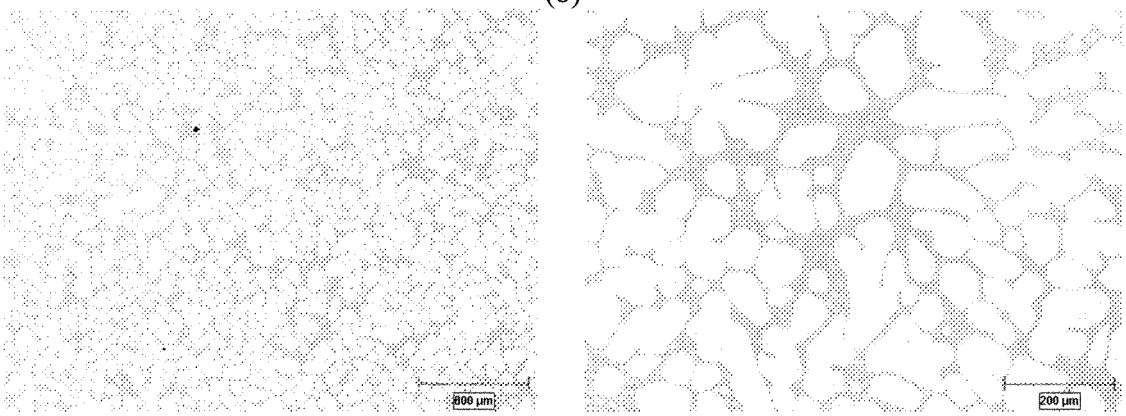

(c)

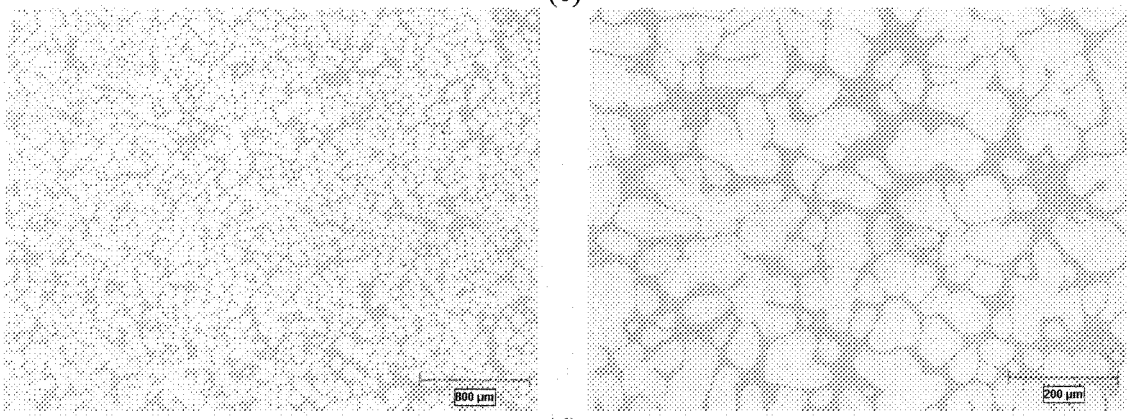

(d)

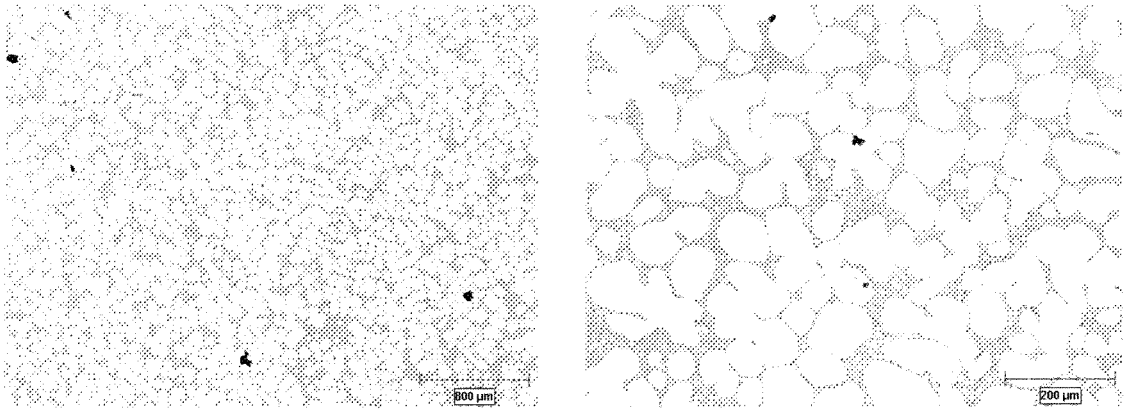

(e)

Figure 9.11: Morphological evolution within different pouring temperatures: (a) 695, (b) 675, (c) 645, (d) 625, and (e) 615°C

9.2.4 Image analysis

Image analyzing was done as described in the experimental procedure and the results are shown in Figure 9.12. The image processing results may be summarized as follows;

- With decreasing pouring temperature, average circular diameter decreased while number density increased. This finding is supported by decreasing the A/P ratio and is in line with optical micrographs presented in Figure 9.11, where as pouring temperature decreased, the morphology of primary α-Al phase becomes finer and less dendritic.

It is emphasized again that image analysis technique is the reproduction of the microstructure which is not exactly the same being studied. Therefore, it should always be kept in mind that what image analysis can not do, for example in the quenched conventional billets; it could not differentiate between the branches of dendrites and globules, Figure 9.13. As it could be seen, image analysis only detects the differences between individual particles and ignoring the origin of isolated particles. It means that the way dendrites intersect the polish surface may generate individual isolated particles. However, even with considering this point, data shows good correlation with changing pouring temperature.

- With decreasing pouring temperature, equiaxed solidification appears to be dominant and growth is in all directions, so globularity and sphericity increased (Figure 9.12d). For better observation, the distribution of particles with different sphericity is shown in percentage scale in Figure 9.14. It could be seen that the percentage of sphericity greater than 0.9 is abruptly shifted to higher level for 615°C which is an indication of more globular particles within such billets.

- For better interpretation, the aspect ratio was divided into two series of data, i.e., the average and the percentage of aspect ratio greater than 2. Both graphs prove that with increasing the pouring temperature, the formation of dendrites is promoted, i.e. the aspect ratio increased.

- The overall conclusion is that controlling of pouring temperature is an effective way to change the morphology of the primary α-Al phase.

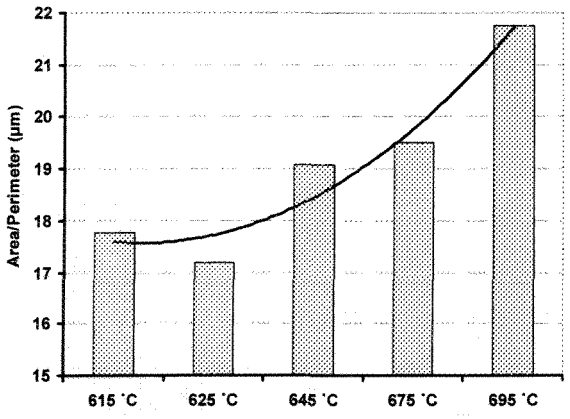

(a)

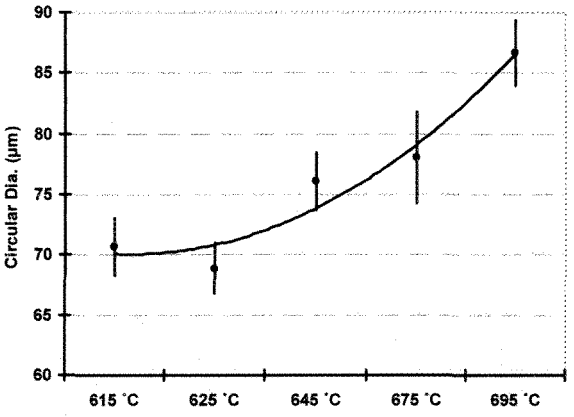

(b)

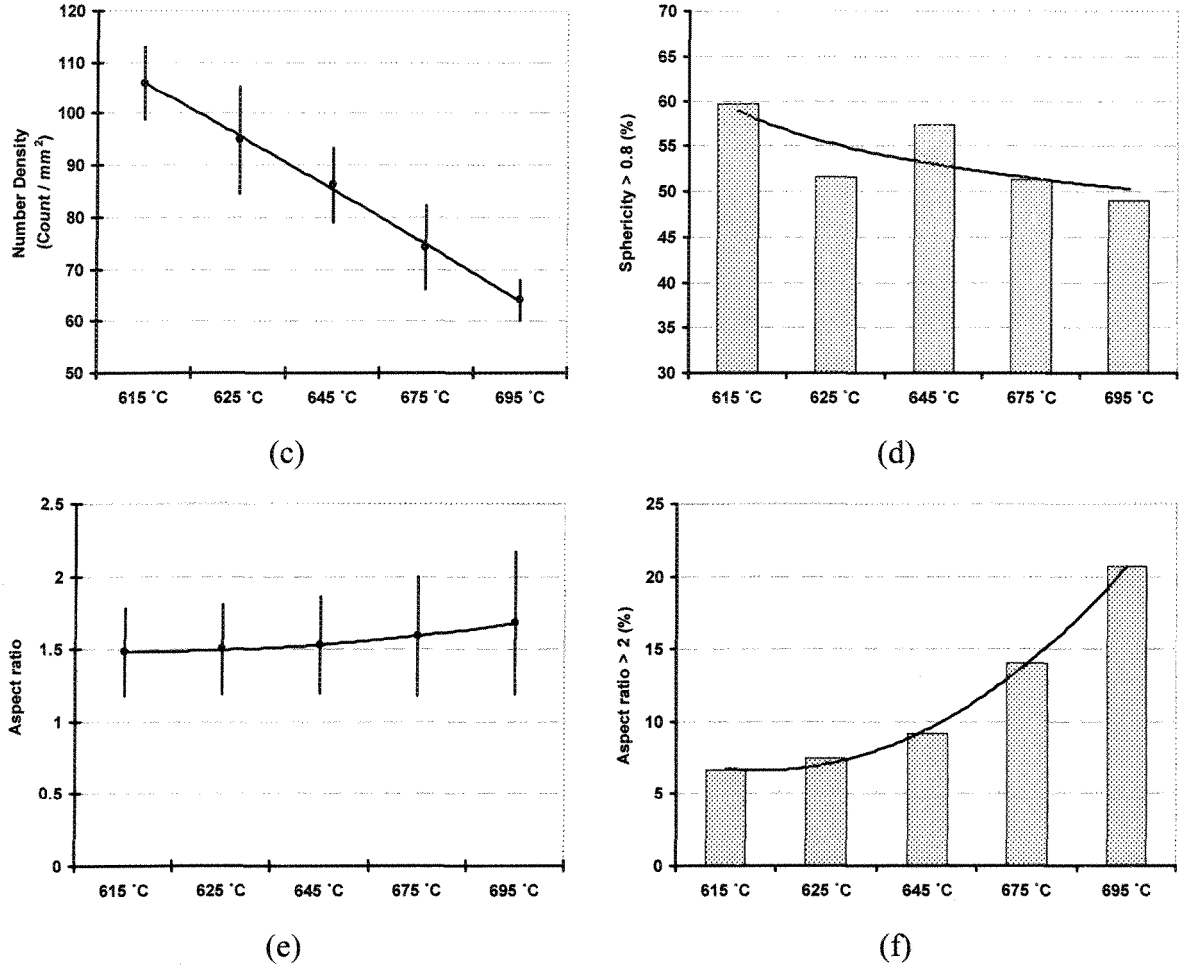

Figure 9.12: Image analysis data obtained from the conventional cast slugs

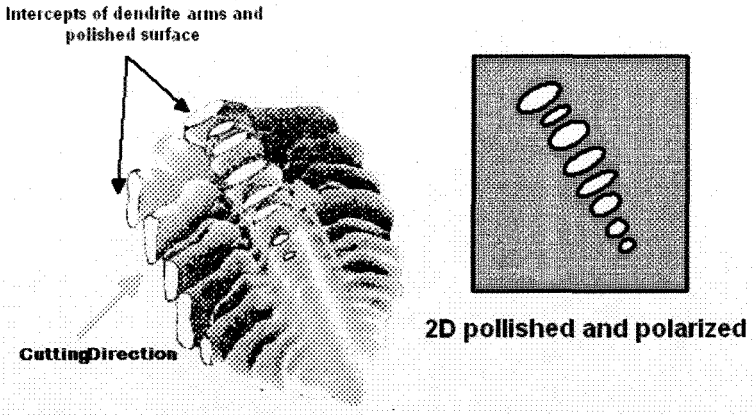

Figure 9.13: 3-D view of dendrite-polished surface intersection showing the dendrites branches

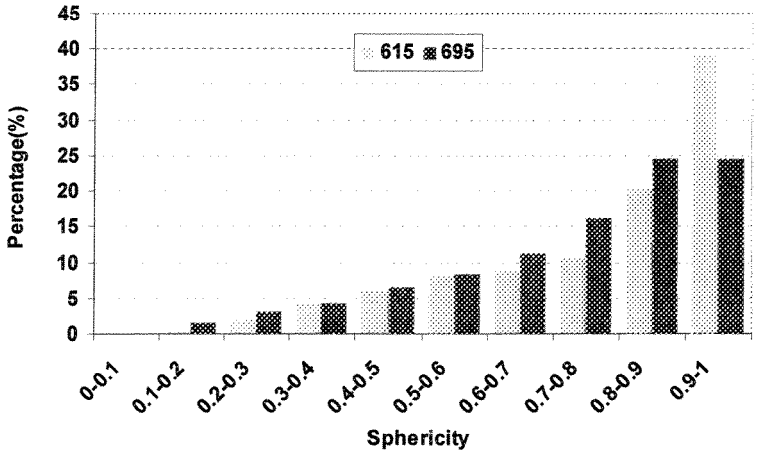

Figure 9.14: Statistical graphs showing the variation of sphericity percentage for 695 and 615°C

9.3 Effects of stirring on silicon distribution

For SSM processing of Al-Si alloys, there are two important microstructural features which influence the properties of the finished products. These are size, shape, and volume fraction of the primary α-Al phase and the morphology of silicon within the eutectic regions, eutectic silicon. It is well known that the irregular growth mode of eutectic Si can be modified by the addition of modifiers such as Sr or Na as the results of the current comprehensive study are shown in chapter 6.

The stirring technique is known to control the morphology and size of the primary α-Al particles and the modification process is to alter the morphology of the eutectic silicon. The classic morphology of silicon is flaky or acicular which is quite susceptible to cracking too. Special thermal treatment or addition of modifying agents such as Sr or Na could change the morphology of these flakes and improve mechanical properties. In this section, attempts are made to show that stirring not only generates a globular structure, but also decreases the size of the flakes in unmodified and stirred Al-Si hypoeutectic alloy.

In these series of experiments, binary Al-7%Si alloys with the chemical composition given in Table 9.3 were prepared according to the experimental procedure given in chapter 4.

Table 9.3: Chemical analysis of the melts (wt. %)

	Si	Fe	P	Sr	Al
Al7Si, no Stirring (Conventional)	7.29	0.08	0.0002	Nil	bal.
Al7Si, SEED	7.12	0.08	0.0002	Nil	bal.

It is important to note that for the experiments with no stirring, the liquid was poured in the same mold without stirring. In both processes, billets were water quenched from 591±2 °C. The quenched billets with no stirring are referred as "conventional".

9.3.1 Structural analysis

Figure 9.15 compares the billets microstructure cast by conventional and SEED processes. The application of stirring in the SEED process leads to morphological evolution of the primary α-Al phase from dendritic to globular and rosette structure. The average area percentage of the primary α-Al phase is ~60% for both SEED and conventional processes. This is higher than that expected from the Al-Si equilibrium phase diagram which can be attributed to:

- Inefficient quenching method; formation of eutectic colonies confirms the ineffectiveness of water quenching in preventing further liquid → solid transformation from the quenching temperature. This could be due to vapor formation around the billet which prevents effective quenching,
- Growth of the primary particles is another possibility for inaccuracy in the measurement. During transferring and quenching period, remained liquid may also precipitate on the pre-quench primary solid phase.
- Depressing eutectic line to lower temperatures due to quenching
- The drainage of liquid in the SEED process which results in higher percentage of primary α-Al phase within the mold.

On the other hand, with application of stirring, the silicon morphology becomes finer as seen in Figure 9.15. In unstirred sample, the eutectic silicon has long flaky

morphology while in the stirred condition, the morphology is still the same but much shorter and interestingly, they appear to have bent probably due to the flow. The changes in Si particles are easier to detect in the inverted photo micrographs presented in Figure 9.16.

(a) (b)

Figure 9.15: Optical micrographs showing the effect of SEED process on the formation of silicon particles; (a) unstirred, conventional, (b) SEED process

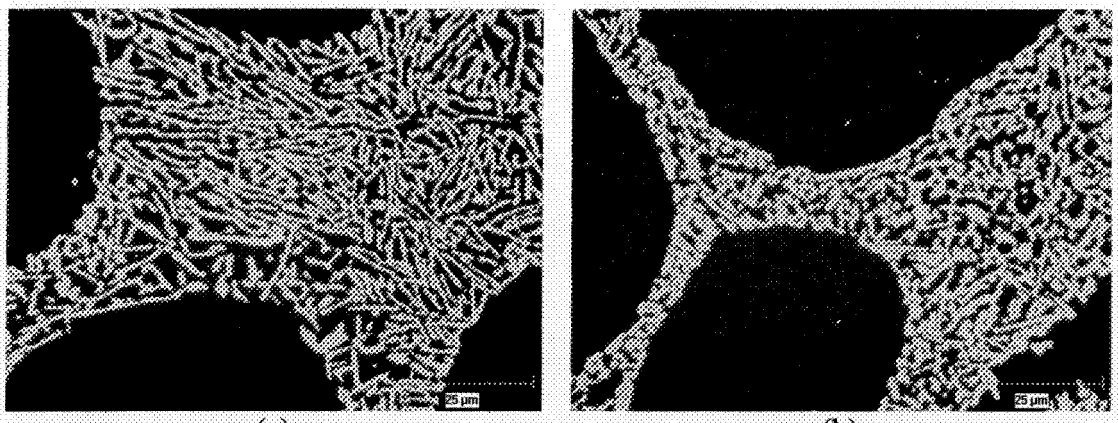

(a) (b)

Figure 9.16: Inverted images of the eutectic region;
(a) unstirred, conventional, (b) SEED process

The finer and more compacted Si is more desirable than acicular morphology as it improves mechanical properties. In conventional foundry practice, Sr is added to modify Si morphology, but Sr addition increases the porosity formation, which is detrimental to properties. As a result, the modification of Si particles achieved by stirring is of great importance as porosity is no longer an issue.

SEM micrographs of conventional and SEED quenched billets are shown in Figure 9.17. Flake morphology is clear in both samples and inter-silicon spacing in both cases is small which is due to the high cooling rate. The more compacted lamellar structure in the SEED billet is due to the fluid flow and thermal uniformity within the SSM billets.

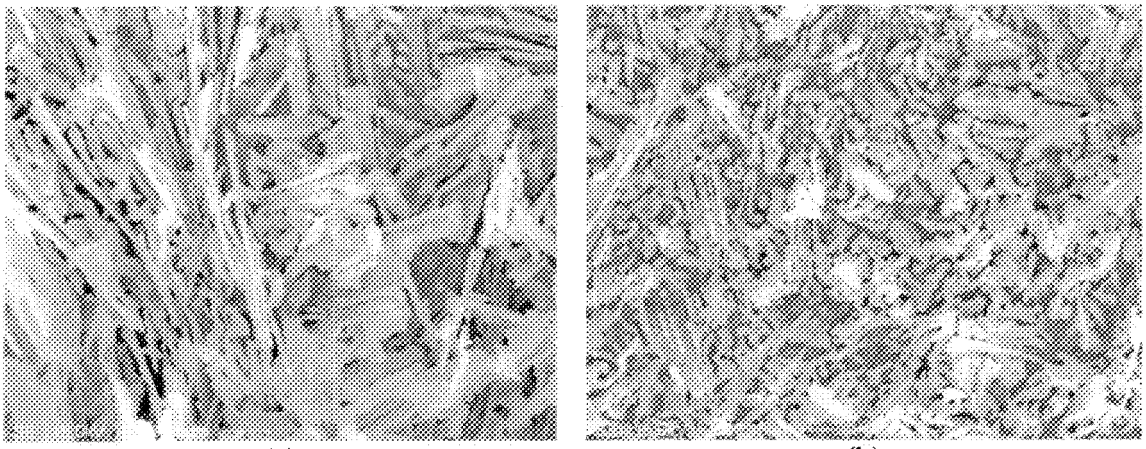

(a) (b)

Figure 9.17: SEM micrographs of quenched non-modified samples:
(a) conventional, (b) SEED

Comparing conventional and SSM quenched Al7Si billets has shown that the size of the flakes is altered by stirring, i.e., flake length is decreased and it seems that most of them are bent. This phenomenon could be explained from two different aspects;

- By stirring, the distribution of the remaining liquid in the bulk of the material is improved. The enhanced distribution of liquid pools and the fact that the α-Al particles act as heat sink for the small pools of eutectic liquid, the final silicon flakes are smaller in the stirred condition.

- On the other hand, the forced convention applied during stirring has a paramount role on the solute distribution. In the unstirred case, the distribution of solutes in the remaining liquid is such that it leads to the routine growth of eutectic silicon while with stirring the solute distribution is more uniform and the solidification pattern is multidirectional, since heat is no longer dissipated directionally. In this case the size of eutectic pools is also decreased leading to the formation of smaller silicon flakes. Bending of the flakes is a good indication of the forced convection effectiveness.

9.3.2 Image analysis

The results of image analysis for eutectic silicon are shown in Figure 9.18, and summarized as follows;

- With changing the process from conventional to the SEED, the percentage of Si particles with aspect ratio greater than 2 decreased. It means that the length of the silicon particles is reduced (Figure 9.18a) and particles are shorter. Figure 9.18b also shows the average length of silicon particles decreased while its width is almost constant.
- Number density of silicon particles remains almost constant and the difference is within the range of standard deviation (Figure 9.18c). Decreasing of the error bars are indications of silicon particles having better distribution within the structure.

  Some of the lamellar silicon particles in the SEED specimens, Figure 9.16b, seem to be touching and appear connected. Hence, the image processing software can not count them as separate particles and this may be the reason for the small difference in number density values.

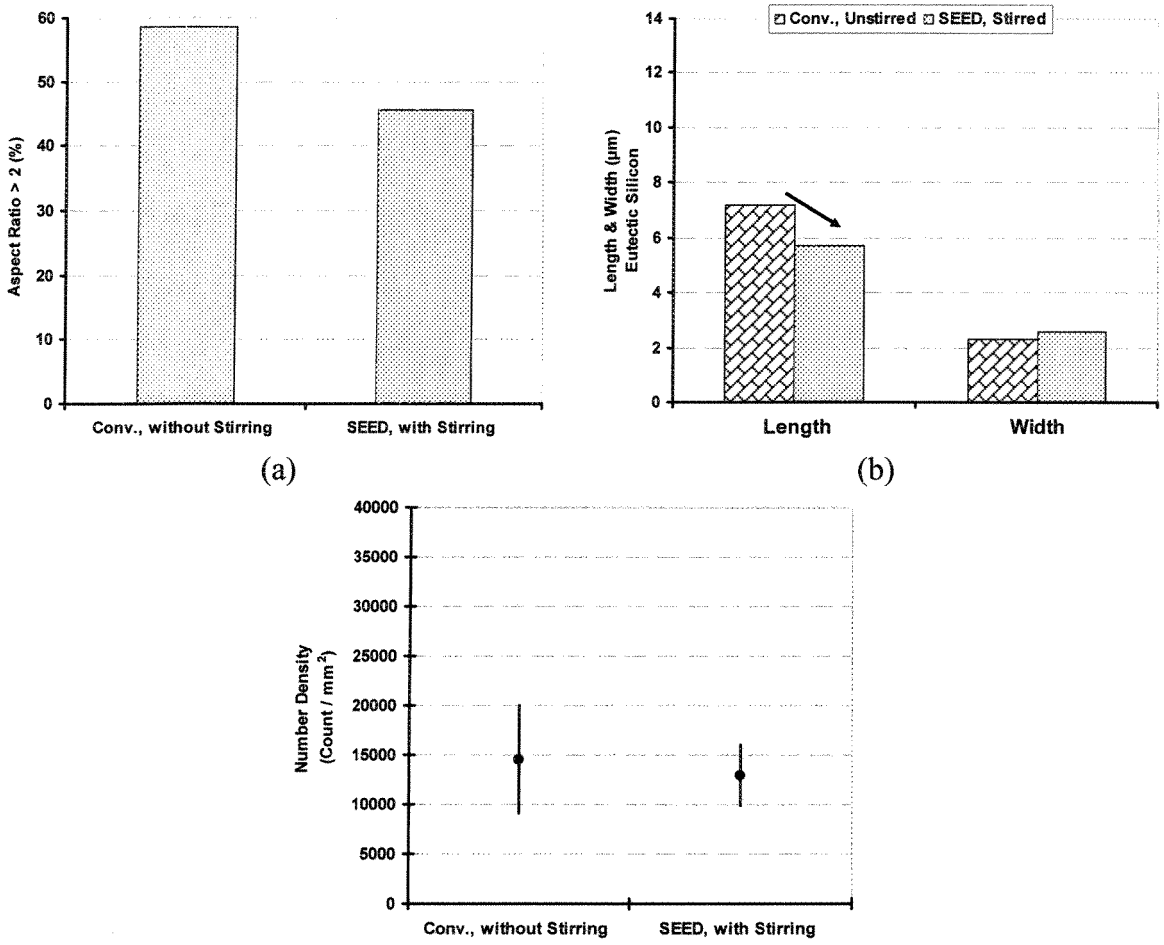

Figure 9.18: Image analysis results for eutectic silicon particles:
(a) aspect ratio, (b) length & width, and (c) number density of silicon particles

CHAPTER 10

CONCLUSIONS
&
SUGGESTIONS FOR FURTHER WORK

CHAPTER 10

CONCLUSIONS

The current comprehensive research program concentrated on melt treatment during semi-solid casting of Al-Si foundry alloys. The effects of grain refiner and modifier additions on the microstructure of Al-7%Si binary and A356 alloys were studied. It further examined the rheological behaviour of as-treated alloys to establish the importance of the primary phase morphology on the viscosity of SSM billets.

The conclusions are categorized in the following format to clearly highlight the main findings in each subgroup of the experiments.

Effects of grain refining

- Based on the semi-solid metal processing research, it is proposed that solidification range could be partitioned into two main intervals; the temperature range for the formation and growth of the primary α-Al dendrites (ΔT_α) and/or iron intermetallics and the temperature range for the Al-Si eutectic and the secondary eutectic reactions including the formation of Mg_2Si and/or iron compounds (ΔT_{eut}). Although such concept is not new, the formation of primary particles could be divided into three segments of α-Al nucleation, dendrite to rosette and globular transformation, and coarsening of the primary α-Al particles which is a new approach in SSM alloy design and treatment.
- Experiments have shown that inoculation shifts the cooling curve up while decreasing the recalescence. An ideal refiner should have no recalescence and be

able to increase nucleation temperature. From the SSM standpoint by refiner addition, α-Al solidification range increases and it has almost no effect on the remaining solidification range. A wider α-Al solidification range gives more freedom during SSM processing but side issues such as risk of hot tearing, more porosity, and micro/macro segregation should be considered.

- Different grain refiner additions have been tested in this work. It was found that generally refiners increase the nucleation and growth temperatures of primary phase but the rate at which growth temperature increases is less than that for nucleation temperature. In other words, refiner causes more nuclei with less potential for growth. It is quite important to note that these rates depend on the refiner type and increase with refiner efficiency.
- By using different techniques such as thermal analysis and quantitative metallography, it has been shown that amongst various refiners, Al5Ti1B is not as effective as expected and high additional levels are necessary for improving the efficiency with the disadvantage of Ti-based intermetallic formation.
- In SSM processing, refiner increases the α-Al percentage, reduces globule size, and disperses eutectic regions uniformly. Improvement of sphericity and size reduction of globules are the main advantages of refiner addition since the smaller and rounder particles give better slurry flowability.
- According to the results, the optimum percentage of TiB master alloy addition for the A356 is approximately between 0.06% Ti, 0.01% B and 0.08% Ti, 0.02%B. In the case of boron master alloys, ~0.02-0.025%B could be enough. For commercial 356 alloy with Ti in solution, most favorable percentage is laid around 0.03% Ti, and 0.005%B. Higher additions of Ti and/or B resulted in the agglomeration of intermetallic compounds within the eutectic region.
- Drainage is the final step of the SEED process before quenching which extract a portion of the remaining liquid to have a self standing billet. With refiner, the percentage of liquid drainage increased. It is expected to have less drainage due to the slight increase in α-Al particles percentage. However, since the degree of α-Al

particles globularity increases, it is supposed to have smooth channels without interlocking pathways for liquid flow. Furthermore dendrite coherency point, DCP may play a part, where both stirring and grain refiner addition postpone DCP and thus mass flow can proceed better and even for longer period. On the other hand, the greater value for liquid drainage due to grain refiner addition is one of the reasons for higher α-Al percentage in the billet.

- Minimum efficiency of refiner addition relates to the commercial 356. This is due to the higher dissolved Ti which results in greater "Growth Restriction Factor"-GRF values and consequently lesser particles size.
- Higher additional levels of each refiner lead to the agglomeration of the primary intermetallic particles in the refiner associated to two reasons. One is coming from the master alloys themselves having limited solubility in the melt at the temperatures used. This is evident from their respective iso-pleth diagrams (the solubility limits of individually added titanium and boron at 700°C are 0.38%Ti and 0.048%B and at 650°C are 0.2%Ti and 0.027%B) and thus the remaining elements rejected at the interface. In the titanium case, another reason is coming from the peritectic reaction which causes the formation of Al_3Ti intermetallics for the values above ~0.12%Ti.

Effects of modification

- It has been shown that a small addition of Sr, i.e. 150-200ppm, is quite adequate in changing the silicon morphology from flake to fibrous. Furthermore due to the higher cooling rate and better thermal balance in the SEED process, silicon morphology in Sr-modified billets is even finer and more compacted than that of the conventionally cast Sr-modified billets.
- By measuring different solidification ranges, it becomes obvious that ΔT_α increases by Sr addition due to the lowering of the main eutectic reaction temperature and as a result constant value for the total solidification range, ΔT_{eut} decreases.

- Quantitative metallography has proved that by modification, the primary α-Al percentage rises and since the density of particles (number per unit area) is constant, the average globule diameter increases. The improved globularity of the Sr-modified particles could be realized by increasing the percentage of particles having higher sphericity numbers, particularly those closer to one.
- The higher sphericity number in the modified case could be attributed to the lowering of surface tension by Sr. By decreasing the surface tension, the wettability of the primary α-Al particles by the remaining liquid is improved. This is equivalent to having more contact between remaining liquid and primary α-Al. Lowering the surface tension causes more flow around the α-Al particles and consequently better shaving and trimming that causes more spherical and rounder particles.
- Drainage increases with Sr addition and it confirms better flowability of the alloy. From dendrite coherency point of view, modification postpones the DCP point and it means that in spite of increasing α-Al percentage, the more continuous liquid channels exist in the semi-solid structure. However higher values of Sr cause the formation of Sr-based intermetallics which decreases the flowability of the remaining liquid.

Effects of combined addition

- By combined addition, α-Al solidification range increases more than sole treatments. This is due to the shifting of liquidus to the higher values by refiner addition plus lowering the main eutectic reaction temperature due to the modification.
- Combined treatment also takes advantages from both treatments. Grain refining efficacy is obvious through size reduction of globules and more primary particles, while modification effect could be detected at higher magnification by morphological changing of silicon particles from lamellar to fibrous. Therefore, combined addition not only replicates both effects, but also gives the added bonus of better globularity in the SSM process.

- SSM quantitative analysis has also confirmed that the combined treatment benefits from both sides. It was shown that with modification alone the number density of primary α-Al particles remained unchanged while its percentage increased and hence the average circular diameter increased. This is not the case for combined treatment, where the average circular diameter decreased slightly but the change in number density is more pronounced. This is attributed to the grain refining effect in shifting the nucleation temperature to higher values and rendering more nuclei to form per unit volume, overshadowing the modification result.

Rheological behavior

- Basic rheological tests were carried out to characterize microstructural evolution of the grain refined and modified A356 Al-Si billets in semi-solid state by using a compressive flow viscometer. It was concluded that grain refining and modification treatments improve flow characteristics of SSM billets and improve the viscosity.

- Grain refinement results in formation of smaller particles having better and uniform distribution with more spherically shaped primary α-Al particles within the "mush". The resulting material exhibits lower viscosity and better flow.

- The refinement of the grains has been identified as the main reason for better deformability of billets after grain refining. Modification also plays an important role through reduction of the residual liquid surface tension which improves the flow of SSM billets. Combined treatment has the added bonus of smaller particle size, more globularity, and lesser surface tension.

- Microstructural study of deformed zones showed less segregation of liquid adjacent to the mold walls for the combined and over refined SSM billets. This is attributed to the smaller particles size and easier flow within the billets.

Comparison of grain refiner

- By thermal analysis and optical microscopy, it was proved that boron based refiner could be an ideal substitute for the common AlTiB refiner group. Boron results in higher α-Al nucleation temperature and almost no recalescence observed in the onset of solidification. Higher nucleation temperature leads to wider α-Al solidification range due to the unchanged main eutectic reaction temperature. A wider solidification range gives more freedom during SSM processing but it should be noted that wider solidification range may induce greater risk for hot tearing and more porosity formation in the structure.

- In the SSM casting, quantitative metallography has shown that boron refiner leads to the formation of the smallest primary α-Al globules with the highest density number. Better sphericity and globularity of boron added billets lead to enhanced deformability in comparison to those of the untreated and Ti-B-refined billets. On the other hand, untreated slurry has the lowest slope in the strain-time graphs and boron addition results in the highest rate of strain which means the easier flow. This matter plus much less liquid segregation in the deformed billet has great importance in the die filling.

Effects of dissolved Ti on the structural evolution

- The effect of small addition of Ti to refine the commercial 356 alloy grain size is further highlighted for both conventional and semi-solid castings. Primary α-Al nucleation temperature increased by 2-3 ^{o}C and solidification undercooling decreased about 1 ^{o}C due to minor addition of Ti. For the rheocasting operation, the size of globules decreased and globularity increased by Ti in solution. This is equivalent to improved rheological properties especially flow properties which is of great importance during high pressure die casting of semi-solid billets.

Effects of pouring temperature on the structural evolution

There are two hypotheses put forward to justify the effect of pouring temperature on the morphology of primary α-Al particles in hypoeutectic SSM Al-Si alloys;

- The highly undercooled melt near the wall explodes with a large number of nuclei, big bang or copious nucleation, to lift up melt temperature with the released latent heat of fusion near the wall. The floating of these nuclei towards the central regions establishes a uniform cooling rate through out the mold. The uniform cooling rate coupled with multi-directional cooling, promotes the formation of fine grained equiaxed as-cast structure.

- The very large temperature gap between the wall and central region of the mold during the early stage of solidification encourages faster heat flow towards the mold wall at lower pouring temperatures. The mold coating, air gap and mold thickness, reduce the rate of heat dissipation from the mold wall to establish a shallow temperature gradient within shorter time. Such low temperature gradient (G), coupled with multi-directional heat flow, encourages multi-directional growth of primary α-Al nuclei within the melt, i.e. formation of equiaxed and eventually globular structure.

Effects of Stirring on Silicon Distribution

- Silicon morphology was changed by stirring used in the SEED process. Stirring reduces the length of the eutectic silicon particles but no change was detected in number density.
- The modification of Si particles achieved by stirring is of great importance as porosity is not an issue in contrast to the modification of Si by Sr addition which is usually accompanied by increasing the porosity content, i.e. adversely affects mechanical properties.

OVERALL CONCLUSIONS

A detailed, thorough, and comprehensive research was done to survey the effects of melt treatment on the structural and rheological properties of semi-solid billets with the main emphasize on the SEED technology. For this objective and parallel to SSM processing, conventionally cast samples were prepared. This procedure was accompanied by application of computer aided cooling curve analysis (CA-CCA) to reveal the critical points during the solidification process.

Conclusions were divided into different sections according to the results obtained during the entire trials; however it seemed necessary to wrap up the whole thesis with general conclusions as follows:

➢ Solidification range

One of the prerequisites for an alloy to be employed in SSM processing is to solidify across a temperature range, mushy zone. This is an essential requirement since the dendritic to globular evolution is taken place in this thermal range. In the case of hypoeutectic Al-Si alloys which are the most popular SSM alloys, the whole SSM evolution is occurred in the temperature window of about 580-595°C. By considering multi alloying systems such as commercial alloys and existence of wider solidification range due to the eutectic and post eutectic reactions, it is proposed that the solidification range should be partitioned into two main sections: ΔT_{α} and ΔT_{eut} which has already been explained. Figure 10.1 is a conclusion of variation in A356 solidification ranges with different treatments.

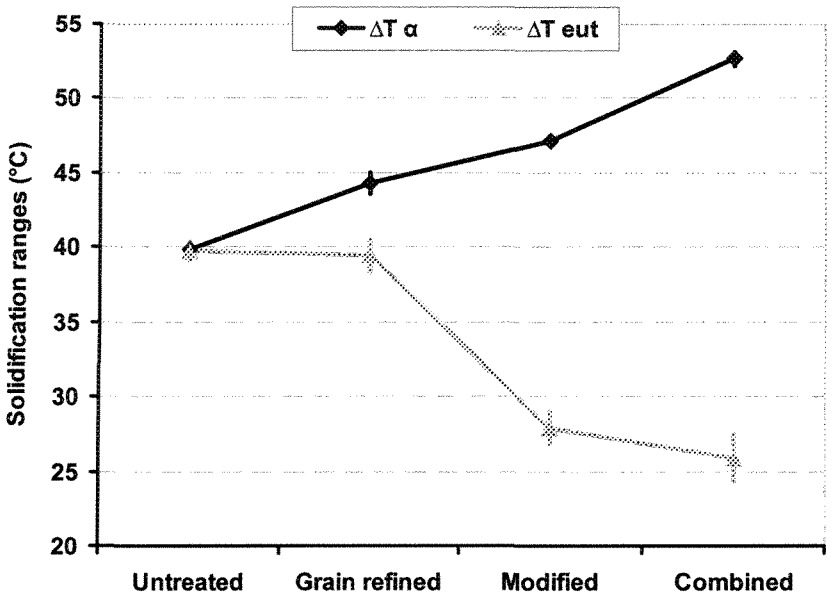

Figure 10.1: Variation of ΔT_{α} and ΔT_{eut} with melt treatment, A356 alloy, master alloys: Al5Ti1B, Al10Sr

As mentioned, refiner addition leads to higher nucleation temperature and consequently ΔT_{α} increases. By modification, eutectic temperature shifts down and this is the main reason for increasing the α-Al solidification range. It is worth mentioning that by Sr-addition, total solidification range is constant while this is not the case for refining where an increase in the mush is observed. Combined treatment has bilateral effect. It means that refiner side increases the liquidus temperature while modifier side decreases the eutectic temperature and finally the results are combination of both treatments.

➢ Correlation between thermal analysis, image analysis, and rheological data

Chapters 5, 6, and 7 represent complete results of melt treatment. These chapters are summarized with individual conclusions as given early in this chapter while the overall conclusion is tabulated in Table 7.1 and presented in Figure 10.2. As proved before and shown in Figure 10.2, modification process results in slight increase in the average circular diameter. This is initiated from the fact that fundamentally, Sr by itself does not have any effect on the α-Al nucleation temperature and besides by increasing the α-Al mush, it has better chance for primary particles to grow.

Table 10.1: Selected image and thermal analyses results, A356 alloy, master alloys: Al5Ti1B, Al10Sr

	Circular Dia. (μm)	Number density (count/mm^2)	Primary α-Al (%)	Sphericity greater than 0.8 (%)	T nuc $_{Al}$ (°C)
Untreated	81.3±2.3	81.6±6.81	69.8±1.43	55.4	614.8±0.26
Grain refined	78.2±2.5	86.9±5.78	73.15±1.39	57	619.39±0.26
Over refined	77.1±2.1	94.5±6.7	73.51±1.97	59.2	620.15±0.18
Modified	80.3±3.5	81.54±7.71	70.9±1.44	58.74	614.26±0.5
Combined	79.1±2.6	87.76±6.5	72.34±1.27	60.14	619.21±0.28

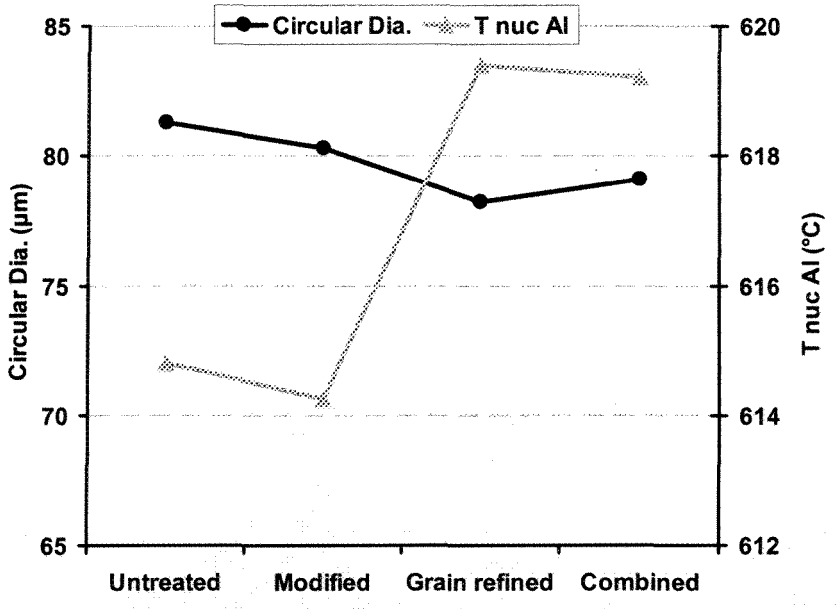

Figure 10.2: Correlation between globule size and α-Al nucleation temperature, A356 alloys, master alloys: Al5Ti1B and Al10Sr

In the case of refiner and combined treatments, the average circular diameter decreases and there is a strong relationship between the results of image analysis and that of the cooling curve analysis, i.e. thermal analysis. It was proved that by refiner addition, α-Al nucleation temperature shifts up and there are more potent nucleants within the system

which leads to lower particle size. It is interesting to note that the effectiveness of refining process depends on the refiner type and the best results were obtained with sole boron addition.

Parallel to image and thermal analyses results, the rheological tests have shown the same trend and in general untreated billet has the lowest deformability while the refined and combined treated billets have the highest engineering strains. This phenomenon is in line with other results and initiate from lower particle size with enhanced globularity of refined/combined slurries.

SUGGESTIONS FOR FURTHER WORK

A comprehensive study was done on the effects of melt treatment in SSM processing of 356 alloys. For further clarification and better understanding on the related matters, the following points could be suggested:

- High pressure diecasting of the treated slurries. This investigation has two main advantages. By producing cast pieces, it is possible to compare the mechanical properties as another important factor to support the commercialization of the process. Furthermore by pressure forming, the globule deformation pattern and specific phenomena such as liquid segregation could be studied in more details.
- Extensive work on the observation and characterization of the nucleants in the refined samples to comprehend the exact chemical compositions and crystallographic orientations which could be done by transmission electron microscopy, TEM
- Determining the rheological behaviour of the alloy by other methods such as back extrusion
- Efforts on refining and modifying of the other suitable semi-solid Al-Si alloying systems such as 319 and 357
- Investigation on the heat treatability of cast pieces regarding the melt treatment procedure and comparison of their mechanical properties with those of untreated alloy.

Appendix A: Lattice disregistry between solid Al and inoculant particle

As it was mentioned in chapter 2.2.1, one of the principals for a particle to be a refiner is its atomic match with the matrix and lattice disregistry is a controller for the effectiveness of a substrate for heterogeneous nucleation. Aluminum is fcc metal having a unit cell with a=4.0494A° at 25°C. So, all the grain refiners should match with this lattice parameter. Table A1 shows some physical characteristics for the most common grain refiners and their lattice disregistry. Lattice disregistry was defined as:

$$\delta = \frac{d_p - d_m}{d_m} * 100 \qquad (10.1)$$

Where d_p and d_m are the interatomic spacings of the particles and matrix respectively. Porter and Easterling [22] divided the interfacial boundary conditions into three classes: coherent, semi-coherent, and incoherent. A coherent interface arises when the two crystals match perfectly at the interface plane so that the two lattices are continuous across the interface (Figure A1). With sufficient atomic misfit or interfacial area, it becomes more favorable to replace the interface with a semi-coherent interface with a specified lattice disregistry (Figure A2). The last case occurs when the interfacial plane has a very different configuration in the interface. This condition happens when the patterns are totally different or interatomic distances differ more than 25% (Figure A3).

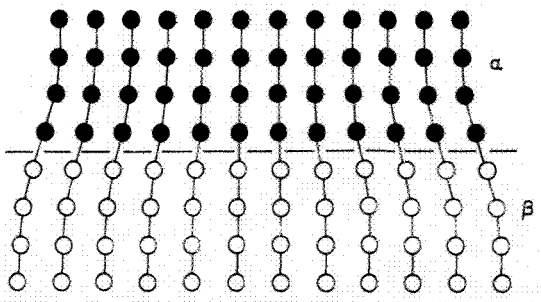

Figure A1: A coherent interface with slight mismatch leads to coherency in the adjoining lattices [22]

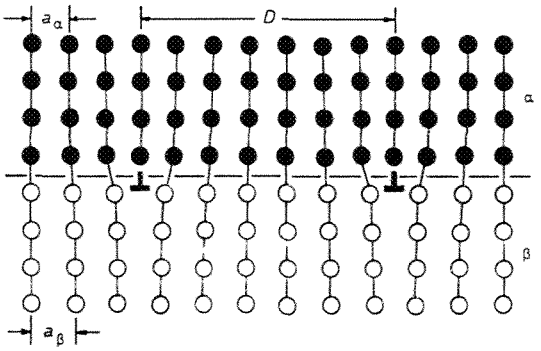

Figure A2: A semi coherent interface. The misfit parallel to the interface is accommodated by a series of edge dislocations [22]

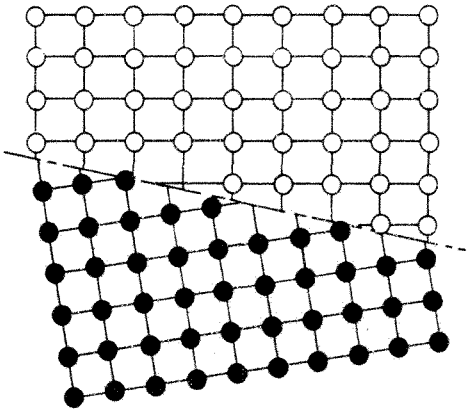

Figure A3: An incoherent interface [22]

Table A1: Some physical properties of grain refiner particles [200]

Particle	Lattice parameter (A°)	Density (g/cm3)	Bravais system	Disregistry at 25°C (%)
Al	a = 4.049	2.697	fcc	0
TiB_2	a = 3.030 c = 3.229	4.495	hcp	5.8
$TiAl_3$	a = 3.846 c = 8.594	3.35	tetragonal	5.02
AlB_2	a = 3.005 c = 3.25	3.1	hcp	4.96
AlB_{12}	a = 10.17 c = 14.28	2.55	tetragonal	151
SrB_6	a = 4.193	3.43	cubic	3.546

REFERENCES

REFERENCES

1.The Canadian Aluminum Industry Technological Roadmap, An initiative of The Government of Canada, 2000

2.Flemings,M.C., "Solidification Processing", McGraw-Hill, New York, 1974

3.Campbell,J., "Castings", Butterworth-Heinemann Ltd., London, UK, 1991

4.Flemings,M.C., "Behavior of metal alloys in the semi-solid state", Metal. Trans. A, vol.22A, May 1991, pp.952-981

5.Ghomashchi,R., Vikhrov,A., "Squeeze Casting: An Overview", J.Mat.Proc.&Tech., vol.101, 2000, pp.1-9

6.Spencer,D.B. - PhD Thesis, Massachusetts Institute of Technology, Cambridge, March 1971

7.Kirkwood,D.H., "Semi-Solid Metal Processing", International Materials Reviews, vol.39, No.5, 1994, pp.173-189

8.Fan,Z., "Semisolid Metal Processing", International Materials Reviews, vol.47, No.2, 2002, pp.49-85

9.Wan,G., Witulski,T., Hirt,G., "Thixoforming of Al alloys using Modified Chemical Grain Refinement for Billet Production", La Metallurgia Italiana,vol.86, 1994, pp.29-36

10. Gabathuler,J.P., Barras,D., Krahenbuhl,Y., " Evaluation of Various Processes for the Production of Billet with Thixotropic Properties", 2nd International Conference on Semi-Solid Processing of Alloys and Composites", MIT, Cambridge, USA, 1992, pp.33-46

11. Mertens,H.P., Kopp,R., Bremer,T., Neudenberger,D., Hirt,G., Witulski,T., Ward,P., Kirkwood,D.H., "Comparison of Different Feedstock Materials for Thixocasting", EUROMAT 97, Proceedings of the 5th European Conference on Advanced Materials and Processes and Applications,1997, pp.439-444

12. Bergsma,S.C., Tolle,M.C., Kassner,M.E., Li,X., Evangelista,E., "Semi-Solid Thermal Transformations of Al-Si Alloys and the Resulting Mechanical Properties", Materials Science and Engineering, A237, 1997, pp.24-34

13. Brusethaug,S., Voje,J., "Manufacturing of Feedstock for Semi-Solid Processing by Chemical Grain Refinement", 6th International Conference on Semi-Solid Processing of Alloys and Composites, Turin, Italy, 2000, pp.451-456

14. Loue,W.R., Suery,M., "Microstructural Evolution during Partial Remelting of Al-Si7Mg Alloys", Material Science and Engineering A, vol.A203, 1995, pp.1-13

15. Jung,B.I, Jung,C.H., Han,T.K., Kim,Y.H., "Electromagnetic Stirring and Sr modification in A356 alloy", Journal of Material Processing Technology, vol.111, 2001, pp.69-73

16. Doutre,D., Hay,G., Wales,P., "Semi-Solid Concentration Processing of Metallic Alloys", United States Patent no.6428636, Aug.6,2002

17. Lashkari,O., Nafisi,S., Ghomashchi,R., "Microstructural Evolution of 356 Al-Si Alloy in ALCAN Patented SSM Processing route – SEED; Part I: Effect of Pouring Temperature, Part II: Effect of Fluid Flow", Industrial report, Submitted to ALCAN Arvida Research Center, Report 1, Jan.2004

18. Nafisi,S., Lashkari,O., Ghomashchi,R., "Microstructural Evolution of 356 Al-Si Alloy in ALCAN Patented SSM Processing route – SEED; Part III: The Effects of Pouring Temperature and Swirling speed on the Microstructure of SEED-Cast Billets", Submitted to ALCAN Arvida Research Center, Report 2, Mar.2004
19. Nafisi,S., Lashkari,O., Ghomashchi,R., "Microstructural Evolution of 356 Al-Si Alloy in ALCAN Patented SSM Processing route – SEED; Part IV: Investigation on Morphological Variation from Top to the Bottom of the Billet, Part V: Investigation on optimizing the process parameters (Process Time), ts(Swirling), tr(Resting), td(Drainage)", Report 3, Submitted to ALCAN Arvida Research Center, May.2004
20. Nafisi,S., Lashkari,O., Ghomashchi,R., "Microstructural Evolution of 356 Al-Si Alloy in ALCAN Patented SSM Processing route – SEED; Part VI: Chemical Distribution on Top, Middle and Bottom positions of a SEED billet", Submitted to ALCAN Arvida Research Center, Report 4, May.2004
21. McCartney,D.G., "Grain Refining of Aluminum and its alloys using inoculants", International Materials Reviews , vol.34, No.5, 1989, pp.247-260
22. Porter,D.A., Easterling,K.E., "Phase Transformations in Metals and Alloys", Van Nostrand Reinhold publication, England, 1981
23. Kurz,W., Fisher,D.J., "Fundamental of Solidification" , Trans Tech Publication, Switzerland, 1989
24. Backerud,L., Chai,G., Tamminen,J., "Solidification Characteristics of Aluminum Alloys, Volume 2,Foundry Alloys" , American Foundry Society, Des Plaines, IL, 1990
25. Chalmers, B., "Principles of Solidification", John Wiley & Sons Inc., New York, 1964
26. Kissling,R.J., Wallace,J.F., "Grain Refinement of Aluminum Castings", Foundry, June1963, pp.78-82
27. Quested,T.E., Dinsdale,A.T., Greer,A.L., "Thermodynamic Modeling of Growth Restriction Effects in Aluminum Alloys", Acta Materialia, vol.53, 2005, pp.1323-1334
28. Johnsson,M. and Backerud,L., Z. Metallkde., vol.87, 1996, pp.216-220
29. Maxwell.I, Hellawell.A, "A Simple Model for Grain Refinement during Solidification", ACTA Metal., Feb1975, 23, pp.229-237
30. Backerud,L., Johnsson,M., "The Relative Importance of Nucleation and Growth Mechanisms to Control Grain Size in Various Aluminum Alloys", in Light Metals, ed.W.Hale, TMS, Anaheim, CA, 1996, pp.679-685
31. Easton,M.A., StJohn,D.H., "A Model of Grain Refinement Incorporating Alloy Constitution and Potency of Heterogeneous Nucleant Particles", Acta Materialia, vol.49, 2001, pp.1867-1878
32. Metal Handbook, Volume 15, "Casting", ASM Publication, Copyright 2002
33. Fredriksson,H., Olsson,A., "Mechanism of Transition from Columnar to Equiaxed Zone in Ingots", Materials Science & Technology, vol.2, 1986,P.P.508-516
34. Hunt,J.D., "Steady State Columnar and Equiaxed Growth of Dendrites and Eutectic", Material science and engineering, vol.65, 1984, pp.75-83
35. "Aluminum Casting Technology", AFS Publication, Des Plaines, IL,1986
36. Gruzleski,J.E., Closset,B.M., "The Treatment of Liquid Aluminum-Silicon Alloys", AFS Publication, Des Plaines, IL,1990

37. Yen,C.M., Evans,W.J., Nowicki,R.M., Cole,G.S., "Measuring the Quality of Aluminum Casting Alloys with Microprocessor-Aided Thermal Analysis", AFS Trans., vol.93, 1985, pp.199-204
38. Radhakrishna,K., Seshan,S., Seshardi,M.R., "Dendrite Arm Spacing in Aluminum Alloy Casting", AFS Trans., vol.88, 1980 , pp.695-702
39. Miguelucci,E.W., "The Aluminum Association Cast Alloy Test Program :Interim Report", AFS Trans., vol.93, 1985, pp.913-916
40. Vorren,O., Evensen,J.E., Pedersen,T.B., "Microstructure and Mechanical Properties of AlSi(Mg) Casting Alloys", AFS Trans., vol.92, 1984, pp.459-466
41. Sigworth,G.K., Guzowski,M.M., "Grain Refining of Hypoeutectic Al-Si Alloys", AFS Trans., vol.93, 1985, pp.907-912
42. Guzowski,M.M., Sigworth,G.K., Sentner,D.A., "The Role of Boron in the Grain Refinement of Aluminum with Titanium", Met.Trans.A ,vol.18A , 1987,pp.603-619
43. Gruzleski,J.E., "Microstructure Development During Metal Casting", AFS Publication, Des Plaines, IL, 2000
44. St.John,D.H., Hogan,L.M., "Metallography and Growth Crystallography of Al3Ti in Al-Ti Alloys up to 5% wt% Ti", Journal of Crystal Growth, vol.46, 1979, pp.387-398
45. Arnberg,L., Beckerud,L., Klang,H., "Grain refinement of aluminum 1: Production and properties of master alloys of Al-Ti-B type and their ability to grain refine aluminum", Metals Technology, vol.9, 1982, pp.1-6
46. Arnberg,L., Beckrud,L., Klang,H., "Grain refinement of aluminum 2: Intermetallic particles in Al-Ti-B type master alloys for grain refinement of aluminum", Metals Technology, vol.9, 1982, pp.7-13
47. Arnberg,L., Beckerud,L., Klang,H., "Grain Refinement of Aluminum by Addition of Master Alloys of the Al-Ti-B type", Solidification Technology in the Foundry and Cast House, London, The Metals Society, 1983, pp.89-92
48. Blake,N.W., Smith,R.W., "Grain Refining of Aluminum by Addition of Commercial Master Alloys", Solidification Technology in the Foundry and Cast House, London, The Metals Society, 1983, pp.83-88
49. Hadlet,D., McCartney,D.G., Thistlethwaite,S.R., "Grain Refinement of Commercial Purity Aluminum Using Al-Ti Master Alloys", Solidification Processing 1987, London, The Institute of Metals, 1988, pp.141-144
50. McCartney,D.G., "Discussion of The Rule of Boron in the Grain Refinement of Aluminum with Titanium", Met.Trans.A, vol.19A., 1988, pp.385-387
51. Lu,H.T., Wang,L.C., Kung,S.K., "Grain Refining of Hypoeutectic Al-Si Alloys", Journal of Chinese Foundryman's Association, vol.29, 1981, pp.10-18
52. Mohanty,P.S., Gruzleski,J.E., "Grain Refinement Mechanisms of Hypoeutectic Al-Si Alloys" , Acta Materialia, vol. 44, No.9, 1996, pp.3749-3760
53. Tøndel,P.A., Halvorsen,G., Arnberg,L., "Grain Refinement of Hypoeutectic Al-Si Foundry Alloys by Addition of Boron Containing Silicon Metal", in Light Metals, ed.S.K.Das, TMS, Denver, CO, 1993, pp.783-790
54. Mondolfo,L.F., "Aluminum Alloys – Structure and Properties", London, Butterworths, 1976

55. Marcantonio,J.A., Mondolfo,L.F., "Grain Refinement in Aluminum Alloyed with Titanium and Boron", Metallurgical Transactions, vol.2, Feb.1971, pp.465-471
56. Mondolfo,L.F., Farooq,Sh., Chikai,TSE, "Grain Refinement of Aluminum Alloys by Titanium and Boron", Solidification Technology in the Foundry and Cast House, London, The Metals Society, 1983, pp.133-136
57. Mohanty,P.S., Guthrie,R.I.L. , Gruzleski,J.E., "Studies on the Fading Behavior of Al-Ti-B Master Alloys and Grain Refinement Mechanism Using LiMCA" , in Light Metals, ed.J.W.Evans, TMS, Las Vegas, NV, 1995, pp.859-868
58. Mohanty,P.S., Gruzleski,J.E., "Mechanism of Grain Refinement in Aluminum" , Acta Materialia, vol. 43, No.5, 1995, pp.2001-2012
59. Sigworth,G.K., "Communication on Mechanism of Grain Refinement in Aluminum", Scripta Materialia, vol.34, 1996, pp.919-922
60. Karantzalis,A.E., Kennedy,A.R., "Nucleation Behavior of TiB2 Particles in Pure Al and Effect of Elemental Additions", Materials Science and Technology, vol.14, Nov.1998, pp.1092-1096
61. Cooper,P., Hardman,A., Boot,D., Burhop,E., "Characterization of a New Generation of Grain Refiners For the Foundry Industry", in Light Metals, ed.P.N.Crepeau, TMS, San Diego, CA, 2003, pp.923-928
62. Campo,J.J.D., Martin,M., Galan,L., "Correlation Between Grain Refining Efficiency and Microstructure in Ti-B-Al Master Alloys" , in Light Metals, ed.C.E.Eckert, TMS, San Diego, CA,1999, pp.797-802
63. Boone,W., Rodney,F., Carver,F., Seese,G.R., "Optimizing Grain Refiners and Modifiers in Al-Si Alloys", Modern Casting , January1998, pp.52-54
64. Spittle,J.A., Keeble,J.M., "The Grain Refinement of Al7Si Alloys with Boron Containing Refiners", in Light Metals, ed.C.E.Eckert, TMS, San Diego, CA,1999, pp.673-677
65. Limmaneevichitr,C., Eidhed,W., "Fading mechanism of Grain Refinement of Aluminum-Silicon Alloy with Al-Ti-B Grain Refiners", Materials Science & Engineering A349, 2003, pp.197-206
66. Apelian,D., Sigworth,G.K., Whaler,K.R., "Assessment of Grain Refinement and Modification of Al-Si Foundry Alloys by Thermal Analysis", AFS Trans., vol.92 1984, pp.297-307
67. Boot,D., Cooper,P., StJohn,D.H., Dahle,A.K., "A Comparison of Grain Refiner Master Alloys for the Foundry", in Light Metals, ed.W.Schneider, TMS, Seattle, WA, 2002, pp.909-915
68. Bondhus,E., Sagstad,T., Dahle,N., "Grain Refinement of Hypoeutectic Al-Si Foundry Alloys with TiBloy", in Light Metals, ed.C.E.Eckert, TMS, San Diego, CA,1999, pp.693-697
69. Detomi,A.M., Messias,A.J., Majer,S., Cooper,P.S., "The Imact of TiCAl and TiBAl Grain Refiners on Cast house Processing", in Light Metals, ed.J.L.Anjier, TMS, New Orleans, LA, 2001, pp.919-925
70. Apelian,D., Cheng,J.J.A., "Al-Si Processing Variables: Effect on Grain Refinement and Eutectic Modification", AFS Trans., vol.94, 1986, pp.797-808

71. Kori,S.A., Murty,B.S., Chakraborty,M., "Development of an Efficient Grain Refiner for Al-7%Si Alloy and its Modification with Strontium", Materials Science and Engineering A283, 2000, pp.94-104
72. Mohanty,P.S., "Studies on the Mechanisms of Heterogeneous Nucleation of Grains and Pores in Aluminum Castings", PhD Thesis, Department of Mining and Metallurgical Eng., McGill University, Montreal, Canada, Feb.1994
73. Flemings,M.C., Metz,S.A., "A Fundamental Study of Hot Tearing", AFS Trans., vol.78, 1970, pp.453-460
74. Mollard,F.R., Flemings,M.C., Niyama,E.F., "Aluminum Fluidity in Casting", Journal of Metals, Nov.1987, pp.34-37
75. Alsem,W.H.M., VanWiggen,P.C., Vader,M., "The Combined Effect of Grain Refinement and Modification in Aluminum Alloys", in Light Metals, ed.E.R.Cutshall, TMS, San Diego, CA, 1992, pp.821-829
76. Dahle, A.K., Tondel,P.A., Paradies,C.J., Arnberg,L., "Effect of Grain Refinement on the Fluidity of Two Commercial Al-Si Foundry Alloys", Met.Trans.A., 27A, 1996, pp.2305-2313
77. Kwon,Y.D., Lee,Z.H., "The Effect of Grain Refining and Oxide Inclusion on the Fluidity of Al-4.5Cu-0.6Mn and A356 Alloys", Mater.Sci.Eng. ,A360 ,2003, pp.372-376
78. Chai,G., Rolland,T., Arnberg,L., Backerud,L., "Studies of Dendrite Coherency in Solidifying Aluminum Alloy Melts by Rheological Measurements", 2nd International Conference on Semi-Solid Processing of Alloys and Composites, Cambridge, Massachusetts, 1992, pp.193-201
79. Prasada,A.K., Karabi,D., Murty,B.S., Chakraborty,M., "Effect of Grain Refinement on Wear Properties of Al and Al-7%Si Alloy", Wear, vol.257, 2004, pp.148-153
80. Pacz,A., US Patent No.1387900,1920
81. Edwards,J.D., Frary,F.C., Churchill,H.V., US Patent No.1410461,1920
82. Elliot,R., "Eutectic Solidification Process", Butterworth, London, 1983
83. Shu-Zu,Lu, Hellawell,A., "Modification of Al-Si Alloys: Microstructure ,Thermal Analysis, and Mechanisms", JOM, Feb1995, pp.38-40
84. Shu-Zu,Lu, Hellawell,A., "The Mechanism of Silicon Modification in Aluminum-Silicon Alloys: Impurity Induced Twinning", Met.Trans.A, vol.18A., 1987, pp.1721-1733
85. Hogan,L.M., Shamsuzzoha,M., "Crystallography of the Flake-Fiber Transition in the Al-Si Eutectic", materials forum, vol.10, 1987, pp.270-277
86. Hogan,L.M., Shamsuzzoha,M., "Crystallography of the Flake-Fiber Transition in the Al-Si Eutectic", Solidification Processing, 1987, Sheffield, The Institute of Metal, 1987, pp.40-43
87. Shu-Zu,Lu, Hellawell,A., "Impurity Induced Twinning and Modification of Silicon in Al-Si Alloys", Solidification Processing, 1987, Sheffield, The Institute of Metal, 1987, pp.44-47
88. Shu-Zu,Lu, Hellawell,A., "Growth Mechanisms of Silicon in Al-Si Alloys", Journal of Crystal Growth, vol.73,1985, pp.316-328
89. Gruzleski,J.E., "The Art and Science of Modification:25 Years of Progress", AFS Trans., vol.100, 1992, pp.673-683

90. Ransley,C.E., Neufeld,H., "The Solubility Relationships in the Aluminum-Sodium and Aluminum-Silicon-Sodium Systems", Journal of the Institute of Metals , vol.78 ,1950, pp.25-46
91. Closset,B. , Dugas,H. , Pekguleryuz,M.O., Gruzleski,J.E., "The Aluminum-Strontium Phase Diagram", Met.Trans.A, vol.17A., 1986, pp.1250-1253
92. Pekguleryuz,M.O., Gruzleski,J.E., "Conditions for Strontium Master Alloy Addition to A356 Melts", AFS Trans., vol.96, 1988, pp.55-64
93. Pekguleryuz,M.O., Gruzleski,J.E., "Dissolution of Non-Reactive Strontium Containing master Alloys in Liquid Aluminum and A356 Melts", Canadian Metallurgical Quarterly, vol.28, 1989, pp.55-65
94. Katgerman,L., F.Sluiter,M.H., "Development of Al-Sr Alloys Suitable for in-line Modification", Solidification Processing, Sheffield, The Institute of Metal, 1987, pp.482-484
95. Chai,G., Backerud,L., "Factors Affecting Modification of Al-Si Alloys by Adding Sr-Containing Master Alloys", AFS Trans., vol.100, 1992, pp.847-854
96. Sigworth,G.K., "Theoretical and Practical Aspects of the Modification of Al-Si Alloys", AFS Trans., vol.91, 1983, pp.7-16
97. Hess,P.D., Blackmun,E.V., "Strontium as a Modifying Agent for Hypoeutectic Aluminum-Silicon Alloys" , AFS Trans., vol.83, 1975, pp.87-90
98. Jacob,S., "Modification de l'AS7G06 par le sodium,l'Antimoine et le Strontium", Fonderie ,No.363,1977, pp.13-25
99. Argo,D., Gruzleski,J.E., "Porosity in Modified Aluminum Alloy Casting", AFS Trans., vol.96,1988, pp.65-74
100. Gruzleski,J.E., Handiak,N., Campbell,H., Closset,B., "Hydrogen Measurement by Telegas in Strontium Treated A356 Melts", AFS Trans., vol.94, 1986, pp.147-154
101. Dimayuga,F., Handiak,N., Gruzleski,J.E., "The Degassing and Regassing of Strontium Modified A356 Melts", AFS Trans., vol.96, 1988, pp.83-88
102. Arbenz H.V., "Lunkerneigung von Aluminium-Guslegierungen", Giesserei, vol.49, 1962, pp.105-110
103. Anson,J.P., Gruzleski,J.E., Stucky,M., "Effect of Strontium Concentration on Microporosity in A356 Aluminum Alloy", AFS Trans., vol.108, 2001, 01-009
104. Emadi,D., Gruzleski,J.E., Toguri,J.M., "The Effect of Na and Sr Modification on Surface Tension and Volumetric Shrinkage of A356 Alloy and Their Influence on Porosity Formation", Met.Trans.B, vol.24B, 1993, pp.1055-1063
105. Anson,J.P., Drew,R.A.L., Gruzleski, J., "The Surface Tension of Molten Aluminum and Al-Si-Mg Alloy under Vacuum and Hydrogen Atmosphere", Met.Trans.B, vol.30B, Dec1999, pp.1027-1032
106. Lee,J., Kim,M., Hong,Y., "The Effect of Sc on the Modification of Eutectic Si in Al-Si Alloys", 66th World Foundry Congress, Turkey, 2004, pp.103-114
107. McDonald,S.D., Nogita,K., Dahle,A.k., "Eutectic Nucleation in Al-Si Alloys", Acta Materialia, 2004, pp.4273-4280
108. Garat,M., Scalliet,R., "A Review of Recent French Casting Alloy Developments", AFS Trans., vol.86, 1978, pp.549-562

109. Nagel,G., Portalier,R., "Structural Modification of Aluminum Silicon Alloys by Antimony Treatment", AFS International Cast Metals Journal, Dec.1980, pp.2-6
110. Wang,W., Gruzleski,J.E., "Sodium and Strontium Modification in the Presence of Antimony", Materials Science and Technology, vol.5,1989, pp.471-475
111. Handiak,N., Gruzleski,J.E., Argo,D., "Sodium, Strontium and Antimony Interactions During Modification of AS7G03 (A356) Alloys", AFS Trans., vol.95, 1987, pp.31-38
112. McIntyre,H.R., Looij,J., Kral,M.V., "Effects of Simultaneous Na and Sr Additions in Eutectic Al-Si Casting Alloy", in the proceeding of "Solidification of Aluminum Alloys", edited by Chu,M.G., Granger,D.A., Han,Q., TMS publication, Warrendale,P.A., USA, 2004, pp.111-120
113. Lu,L., Nogita,K., Dahle, A.K., "Combining Sr and Na additions in Hypoeutectic Al-Si Foundry Alloys", Mater.Sci.Eng.A., vol.399, June 2005, pp.244-253
114. Mehrabian,R., Flemings,M.C., "Die Castings of Partially Solidified Alloys", AFS Trans., vol.80, 1972, pp.173-182
115. Ji,S., Fan,Z., Bevis,M.J., "Semi Solid Processing of Engineering Alloys by a Twin Screw Rheomoulding Process", Materials Science and Engineering, A229, 2001, pp.210-217
116. Asuke,F., "Rheocasting Method and Apparatus", United States Patent no.5865240, Feb.2,1999
117. Uetani,Y., Takagi,H., Matsuda,K., Ikeno,S., "Semi-continuous casting of mechanically stirred A2014 and A390 aluminum alloy billets", Light metals 2001 conf., Toronto, pp.509-520
118. Prasad,P.R., Ray,S., Gaindhar,L., Kapoor,M.L., "Relation between processing, microstructure and mechanical properties of rheocast Al-Cu alloys", J. Mater. Sci. vol.23, 1988, pp.823-829
119. Ichikawa,K., Kinoshita,Y., "Stirring condition and grain refinement in Al-Cu alloys by rheocasting", J. I. M. Trans., vol.28, No.2, 1987, pp.135-144
120. Hirai,M., Takebayashi,K., Yoshikawa,Y., Yamaguchi,R., "Apparent viscosity of Al-10% Cu semi solid alloys", ISIJ Inter, vol.33, No.3, 1993, pp.405-412
121. Lee,H.I., Doherty,R.D., Feest,E.A., Titchmarsh,J.M., "Structure and segregation of stir-cast aluminum alloys", Proceeding Inter. Conf. of Solidification, Warwick, U.K., 1983, pp.119-125
122. Figueredo,A., "Science and Technology of Semi-Solid Metal Processing", North American Die Casting Association, Rosemont publication, IL, 2001
123. Young,K.P., Tyler,D.E., Cheskis,H.P., Watson,W.G., "Process and Apparatus for Continuous Slurry Casting", United States Patent no.4482012, Nov.13,1984
124. Young,K.P., Kyonka,C.P., Courtois,F., "Fine Grained Metal Composition", United States Patent no.4415374, Nov.15,1983
125. Kenney,M.P., Courtois,J.A., Evans,R.D., Farrior,G.M., Kyonka,C.P., Koch,A.A., Young,K.P., "Semisolid Metal Casting and Forging", in the Metal Handbook, vol.15, "Casting", ASM Publication, Copyright 2002
126. Niedermaier,F., Langgartner,J., Hirt,G., Niedick,I., "Horizontal Continuous Casting of SSM Billets", 5th International Conference on Semi-Solid Processing of Alloys and Composites, MIT, Cambridge, USA, 1998, pp.407-414

127. Nafisi,S., Emadi,D., Shehata,M., Ghomashchi,R., Charette,A., "Semi-Solid Processing of Al-Si Alloys: Effect of Stirring on Iron-Based Intermetallics", 8th International Conference on Semi-Solid Processing of Alloys and Composites, Limassol, Cyprus, 2004
128. Nafisi,S., Ghomashchi,R., Emadi,D., Shehata,M., "Effects of Stirring on the Silicon Morphological Evolution in Hypoeutectic Al-Si Alloys", in Light Metals, ed.H.Kvande, TMS, San Francisco, CA, 2005, pp.1111-1116
129. Zillgen,M., Hirt,G., "Microstructural Effects of Electromagnetic Stirring in Continuous Casting of Various Aluminum Alloys", 4th International Conference on Semi-Solid Processing of Alloys and Composites, Sheffield, England, 1996, pp.180-186
130. Adachi,M., Sasaki,H, Harada,Y., "Methods and Apparatus for Shaping SemiSolidMetlas", UBE Industries, European Patent EP 0 745 694 A1, Dec. 4, 1996
131. Findon,M., de Figueredo,A.M., Apelian,D., Makhlouf,M.M., "Melt Mixing Approaches for the Formation of Thixotropic SemiSolid Metal Structure", 7th International Conference on Semi-Solid Processing of Alloys and Composites, Tsukuba, Japan, 2002, pp.557-562
132. Saha,D., Apelian,D., Dasgupta,R.,"SSM Processing of Hypereutectic Al-Si Alloy via Diffusion Solidification", 7th International Conference on Semi-Solid Processing of Alloys and Composites, Tsukuba, Japan, 2002, pp.323-328
133. Martinez,R., Figueredo,A., Yurko,J.A., Flemings,M.C., " Efficient Formation of Structures Siutable for Semi-Solid Forming", Transactions of the 21st International Die Casting Congress, 2001, pp.47-54
134. Flemings,M.C., Martinez,R., Figueredo,A., Yurko,J.A., "Metal Alloy Compositions and Process", United States Patent no.6645323, Nov.11,2003
135. Yurko,J.A., Martinez,R.A., Flemings,M.C., "Commercial Development of the Semi-Solid Rheocasting (SSR)", Transactions of the International Die Casting Congress, 2003, pp.379-384
136. Yurko,J.A., Martinez,R.A., Flemings,M.C., "SSRTM: The Spheroidal Growth Route to Semi-Solid Forming", 8th International Conference on Semi-Solid Processing of Alloys and Composites, Limassol, Cyprus, 2004
137. Abramov,V., Abramov,O., Bulgakov,V., Sommer,F., "Solidification of aluminium alloys under ultrasonic irradiation using water-cooled resonator", Materials Letters, vol.37, 1998, pp.27-34
138. Abramov,V.O., Abramov,O.V., Straumal,B.B., Gust,W., "Hypereutectic Al–Si based alloys with a thixotropic microstructure produced by ultrasonic treatment", Materials & Design, vol.18, 1997, pp.323-326
139. Abramov,O.V., "Action of High Intensity Ultrasound on Solidifying Metal", Ultrasonics, vol.25, 1987, pp.73-82
140. Shibata,R., Kaneuchi,T., Souda,T., Iizuka,Y., "New Semi Solid Metal Casting Process", 4th International Conference on Semi-Solid Processing of Alloys and Composites, Sheffield, England, 1996, pp.296-300

141. Kaneuchi,T., Shibata,R., Ozawa,M., "Development of New Semi-Solid Metal Casting Process for Automotive Suspension Parts", 7th International Conference on Semi-Solid Processing of Alloys and Composites, Tsukuba, Japan, 2002, pp.145-150
142. Shibata,R., Kaneuchi,T., Souda,T., Yamane,H., "Formation of Spherical Solid Phase in Die Casting Shot Sleeve Without Any Agitation", 5th International Conference on Semi-Solid Processing of Alloys and Composites, MIT, Cambridge, USA, 1998, pp.465-469
143. Wang,H., Davidson,C.J., Taylor,J.A., StJohn,D.H., "Semisolid Casting of AlSi7Mg0.35 Alloy Produced by Low-Temperature Pouring", Material Science Forum, vol.396-402, 2002, pp.143-148
144. Wang,H., Davidson,C.J., StJohn,D.H., "Semisolid Microstructural Evolution of AlSi7Mg Alloy during Partial Remelting", Material Science and Engineering, vol.A368, 2004, pp.159-167
145. Wang,H., StJohn,D.H., Davidson,C.J., Couper,M.J., "Characterization and Shear Behavior of Semisolid Al-7Si-0.35Mg Alloy Microstructures", Aluminum Transactions, vol.2, 2000, pp.56-66
146. Dahle,A.K., Hutt,J.E.C., Lee,Y.C., StJohn,D.H., "Grain Formation in Hypoeutectic Al-Si Alloys", AFS Trans., vol.107, 1999
147. Jorstad, J.L., Thieman, M., Kamm, R., "SLC, the Newest and Most Economical Approach to Semi-Solid Metal (SSM) Casting", 7th International Conference on Semi-Solid Processing of Alloys and Composites, Tsukuba, Japan, 2002, pp.701-706
148. Jorstad, J.L., Thieman, M., Kamm, R., Loughman, M., Woehlke, T., "Sub Liquidus Casting: Process Concept and Product Properties", AFS Trans., vol.80, 2003, paper 03-162
149. Kamm,R., Jorstad,J.L., "Semi-Solid Molding Method", United States Patent no.6808004, Oct.6,2004
150. Doutre,D., Hay,G., Wales,P., "SEED: A new process for semi solid forming", light Metals Conference, CIM, Vancouver, Canada, 2003, pp.293-306
151. Doutre,D., Langlais,J., Roy,S., "The SEED Process for Semi-Solid Forming", 8th International Conference on Semi-Solid Processing of Alloys and Composites, Limassol, Cyprus, 2004
152. Nafisi,S., Lashkari,O., Ghomashchi,R., Langlais,J., Kulunk,B., "The SEED Technology: A New Generation in Rheocasting", Light Metals, CIM publication 2005, pp.359-371
153. Kirkwood,D.H., Kapranos,P., "Semi-Solid Processing of Alloys", Metals and Materials, vol.5, Jan.1989, pp.16-19
154. Loué.W.R., Suéry,M., "Microstructural Evolution During Partial Remelting of Al-Si7Mg Alloys", Mater.Sci.Eng., A203 , 1995, pp.1-13
155. Mathur,P., Apelian,D., Lawley,A., "Analysis of the Spray Deposition Process", Acta Metallurgy, vol.37, No.2, 1989, pp.429-443
156. Leatham,A., Ogilvy,A., Chesney,P., Wood,J.V., "Osprey Process-Production Flexibility in Material Manufacture", Metals and Materials, March 1989, 140-143
157. Wan,G., Sahm,P.R., "Particle Growth by Coalescence and Ostwald Ripening in Rheocasting of Pb-Sn", Acta Metall. Mater, vol.38, No.11, 1990, pp.2367-2373

158. Apelian,D., "Semi-Solid Processing Routes and Microstructure Evolution", 7th International Conference on Semi-Solid Processing of Alloys and Composites, Tsukuba, Japan, 2002, pp.25-30
159. Pan,Q.Y., Arsenault,M., Apelian,D., Makhlouf,M.M. "SSM Processing of AlB2 Grain Refined Al-Si Alloys", AFS Trans., vol.112, 2004, Paper 04-053
160. Wan,G., Witulski,T., Hirt,G., "Thixoforming of Al alloys using Modified Chemical Grain Refinement for Billet Production", Conference on Aluminum Alloys: New Process Technologies, Italy, June 1993, pp.129-141
161. Bergsma,S.C., "Casting, Thermal Transforming and Semi-Solid Forming Aluminum Alloys", United States Patent no.5571346, Nov.5,1996
162. Pan,Q.Y., Apelian,D., Makhlouf,M.M. "AlB2 Grain Refined Al-Si Alloys: Rheocasting/Thixocasting Applications", 8th International Conference on Semi-Solid Processing of Alloys and Composites, Limassol, Cyprus, 2004
163. Grimmig,T., Aguilar,J., Fehlbier,M., Bührig-Polaczek,A., "Optimization of the Rheocasting Process under Consideration of the Main Influence Parameters on the Microstructure", 8th International Conference on Semi-Solid Processing of Alloys and Composites", Limassol, Cyprus, 2004
164. Sukumaran,K., Pai,B.C., Chakraborty,M., "The Effect of Isothermal Stirring on an Al-Si Alloy in the SemiSolid Condition", Mater.Sci.Eng.A., A369, 2004, pp.275-283
165. Fat-Halla,N., "Microstructure and Mechanical Properties of Modified and Nonmodified Stir-Cast Al-Si Hypoeutectic Alloys", Journal of Material Science, vol.23, 1988, pp.2419-2423
166. Atkinson,H.V., "Modeling the Semisolid Processing of Metallic Alloys", J. Progress in Materials Science, vol.50, 2005, pp.341-412
167. Wilkes,J.O., Bike,S.G., "Fluid Mechanics for Chemical Engineers", Prentice-Hall PTR, New Jersey, 1999
168. Denn,M.M., "Process Fluid Mechanics", Prentice-Hall Inc., New Jersey, USA, 1980
169. Holland,F.A., Bragg,R., "Fluid Flow for Chemical Engineers", Edward Arnold Publishers, London, 1995
170. Brabazon,D., Browne,D.J., Carr,A.J., "Mechanical Stir Casting of Aluminum Alloys from the Mushy State: Process, Microstructure and Mechanical Properties", Material Science and Engineering , vol.A326, 2002, pp.370-381
171. Ichikawa,K., Kinoshita,Y., "Rheocasting Techniques Applied to Intermetallic TiAl Alloys and Composites", Material Science and Engineering , vol.A239, 1997, pp.493-502
172. Jeng,S.C., Chen,S.W., "The Solidification Characteristics of 6061 and A356 Aluminum Alloys and their Ceramic Particle-Reinforced Composites", Acta Metallurgia, vol.45, No.12, 1997, pp.4887-4899
173. Martin,L.M., Brown,S.B., Favier,D., Suery,M., "Shear Deformation of High Solid Fraction (>0.60) Semi-Solid Sn-Pb under Various Structures", Material Science and Engineering , vol.A202, 1995, pp.112-122
174. Van Wazer,J.R., Lyons,J.W., Kim,K.Y., Colwell,R.E., "Viscosity and Flow Measurement", John Wiley & Sons Inc., New York, 1963

175. Joly,P.A., Mehrabian,R., "The Rheology of a Partially Solid Alloy", Journal of Materials Science, vol.11, 1976, pp.1393-1418
176. Vieira,E.A., Kliauga,A.M., Ferrante,M., "Microstructural Evolution and Rheological Behavior of Aluminum Alloys A356, and A356+0.5%Sn Designed for Thixocasting", J. Mater. Proc. Tech., vol.155-156, 2004, pp.1623-1628
177. Ferrante,M., Freitas,E., Bonilha,M., Sinka,V., "Rheological Properties and Microstructural Evolution of Semi-Solid Aluminum Alloys Inoculated with Mischmetal and with Titanium", 5th International Conference on Semi-Solid Processing of Alloys and Composites, MIT, Cambridge, USA, 1998, pp.35-42
178. Kapranos,P., Liu,T.Y., Atkinson,H.V., Kirkwood,D.H., "Investigation into the Rapid Compression of Semi-Solid Slugs", Journal of Materials Processing Technology, vol.111, 2001, pp.31-36
179. Suery,M., Flemings,M.C., "Effect of Strain Rate on Deformation Behavior of Semi-Solid Dendritic Alloys", J. Metal. Trans. A, vol.13A, 1982, pp.1809-1819
180. Laxmanan,V., Flemings,M.C., "Deformation of Semi-Solid Sn-15 Pct Pb Alloy", J. of Metal. Trans. A., vol.11A, 1980, pp.1927-1937
181. Tuttle,B.L., "Definitions in Thermal Analysis", Modern casting, Nov.1985, pp.39-41
182. Yang,B.J., Stefanescu,D., Leon-Torres,J., "Modeling of Microstructural Evolution with Tracking of Equiaxed Grain Movement for Multicomponent Al-Si Alloy", J.Met.Mater.Trans.A, 2001, vol32, pp.3065-3076
183. Lashkari,O., Ghomashchi,R., "Fabrication of A Simple Compression Parallel Plate Test Machine to Study the Rheological Behavior of SSM Slugs Prepared by SEED", Industrial report, ALCAN Inter., August 2004
184. Lashkari,O., Ghomashchi,R., Adjersch,F., "Rheological Study of 356 Al-Si Foundry Alloy Prepared by a New Innovative SSM Process", Extraction and Processing Division (EPD) congress, Feb.2005, San Francisco, USA, pp.149-156
185. Azzi,L., Ajersch,F., "Development of aluminum-base alloys for forming in semi solid state", TransAl conference, June 2002, Lyon, France, pp.23-33
186. Lashkari,O., Ghomashchi,R., "The implication of rheological principals for characterization of semi solid Al-Si cast billets", Submitted for publication in J. Mater.Sci., 2005
187. Jafarnia,A., Ghomashchi,R., Chen,X.G., Charette,A., "Dissolution of AlTiSi intermetallic compounds in A356 Al-Si alloy", Light Metals, CIM publication 2004, pp.322- 331
188. ASTM International Standard Worldwide, Volume 02.02, Aluminum & Magnesium Alloys, 2004, pp.78-92
189. Bates,A.P., Calvert,D.S., "Refinement and Foundry Characteristics of Hypereutectic Aluminum-Silicon Alloys", British Foundry man, vol.59, 1966, pp.113-119
190. Shankar,S., Riddle,Y.W., Makhlouf,M.M., "Nucleation Mechanism of the Eutectic Phases in Aluminum-Silicon Hypoeutectic Alloys", Acta Mater., vol.52, 2004, pp.4447-4460
191. Nogita,K., Dahle,A.K., "Eutectic Solidification in Hypoeutectic Al–Si Alloys: Electron Backscatter Diffraction Analysis", Materials Characterization, vol.46 ,2001, pp.305-310

192. Nafisi, S., Ghomashchi,R., Boutorabi,S.M.A., Hedjazi,J., "New Approaches to Melt Treatment of Al-Si Alloys: Application of Thermal Analysis Technique", AFS Trans., vol.112, 2004, Paper 04-018
193. Arnberg,L, Backerud,L. , Chai,G., "Solidification Characteristics of Aluminum Alloys, Volume 3,Dendrite Coherency" , American Foundry Society Inc., Des Plaines, IL, 1996
194. Argyropoulos, S., Closset, B., Gruzleski, J.E., Oger, H., "The Quantitative Control of Modification of Al-Si Foundry Alloys Using a Thermal Analysis Technique", AFS Trans., vol.91, 1983, pp.351-357
195. Charbonnier, J.,"Microprocessor Assisted Thermal Analysis of Aluminum Alloys Structure", AFS Trans., vol.92, 1984, pp.907-922
196. DasGupta,R., Brown,C.G., Marek,S., "Analysis of Overmodified 356 Aluminum Alloy", AFS Trans., vol.92, 1984, pp.297-310
197. Dahle,A.K., Nogita,K., Zindel,J.W., McDonald,S.D., Hogan,L.M., "Eutectic Nucleation and Growth in Hypoeutectic Al-Si Alloys at Different Strontium Levels", Met.Trans.A, vol.32A, 2001, pp.949-960
198. Beaulieu,A., Azzi,L., Ajersch,F., Turenne,S., "Numerical Modeling and Experimental Analysis of Die Cast Semi-Solid A356 Alloy", Proceeding of M. C. Flemings, TMS, 2001, pp.261-265
199. Chen,C.P., Tsao,C.Y.A., "Semi-Solid Deformation of Non-Dendritic Structures-I. Phenomenological Behavior", Acta Metal., vol.45, No.5, 1997, pp.1955-1968
200. International Center of Diffraction Data, www.ICDD.com